Part I

ENANTIOSPECIFIC TOTAL SYNTHESIS OF UNNATURAL ENANTIOMERS OF C-19 METHYLATED SARPAGINE/MACROLINE/AJMALINE-TYPE BIOLOGICALLY ACTIVE INDOLE ALKALOIDS VIA THE PICTET-SPENGLER REACTION/DIECKMANN CYCLIZATION PROCESS.

Part II

DESIGN, SYNTHESIS, AND CHARACTERIZATION OF NOVEL GAMMA-AMINOBUTYRIC ACID TYPE A ($GABA_A$) RECEPTOR LIGANDS FOR THE TREATMENT OF NEUROLOGICAL DISORDERS INCLUDING EPILEPSY, DEPRESSION, ANXIETY, PAIN, AND THE SYNTHESIS OF BACK UP COMPOUNDS FOR THE CLINICALLY PROGRESSING KRM-II-81 FOR THE TREATMENT OF PHARMACO-RESISTANT EPILEPSY AND DRAVET SYNDROME.

by

Kamal Prasad Pandey

A Dissertation Submitted in

Partial Fulfillment of the

Requirements for the Degree of

Doctor of Philosophy

in Chemistry

at

The University of Wisconsin-Milwaukee

May 2023

ABSTRACT

Part I

ENANTIOSPECIFIC TOTAL SYNTHESIS OF UNNATURAL ENANTIOMERS OF C-19 METHYLATED SARPAGINE/MACROLINE/AJMALINE-TYPE BIOLOGICALLY ACTIVE INDOLE ALKALOIDS VIA THE PICTET-SPENGLER REACTION/DIECKMANN CYCLIZATION PROCESS.

Part II

DESIGN, SYNTHESIS, AND CHARACTERIZATION OF NOVEL GAMMA-AMINOBUTYRIC ACID TYPE A ($GABA_A$) RECEPTOR LIGANDS FOR THE TREATMENT OF NEUROLOGICAL DISORDERS INCLUDING EPILEPSY, DEPRESSION, ANXIETY, PAIN, AND THE SYNTHESIS OF BACK UP COMPOUNDS FOR THE CLINICALLY PROGRESSING KRM-II-81 FOR THE TREATMENT OF PHARMACO-RESISTANT EPILEPSY AND DRAVET SYNDROME.

by

Kamal Prasad Pandey

The University of Wisconsin-Milwaukee, 2023
Under the Supervision of Professor James M. Cook

Abstract-Part I

Nature has been an extensive and sustainable pool of biologically active compounds. Many molecules from nature are secondary metabolites, which are, presumably, used in the defense mechanisms of plants or organisms. These biologically active molecules have been a major source of medications including treatment of cancer, malaria, and antiarrhythmic agents for centuries. It is not a surprise that many clinical drugs are either directly inspired or derived from natural products. The natural bioactive alkaloids such as morphine, vincristine and reserpine exhibit biological activity, and contain their particular stereochemistry. Plants or organisms have evolved to produce, ordinarily, only one of the enantiomers. As a result, it is possible to isolate

and screen for biological activity only one of the enantiomers, i.e., the natural enantiomer. Unnatural enantiomers might also be as good as the natural enantiomer or even better in activity, as well as in their toxicity profile depending on the metabolic pathway. For example, an unnatural L-nucleoside-based drug, lamivudine, has been saving millions of lives, and it is also listed in WHO's essential drugs. The Indole scaffold is one of the few 'privileged structures' in modern medicinal chemistry because it has a structural similarity with the molecules of life such as tryptamine and serotonin. The Milwaukee group have developed an efficient and practical method for the total synthesis of a number of sarpagine/macroline/ajmaline- related bioactive natural products (indole alkaloids). Moreover, the ambidextrous Pictet-Splenger reaction/Dieckmann-cyclization process allows the synthesis of natural and unnatural enantiomers of sarpagine/macroline/ajmaline-type indole alkaloids either from D or L-tryptophan. However, the total synthesis of unnatural enantiomers of the C-19 methyl substituted sarpagine/macroline/ajmaline indole alkaloids was not previously executed. By employing the Pictet-Spengler reaction/Dieckmann-cyclization strategy on large scale, the total synthesis of C-19 methylated macroline-type indole alkaloid, (+)-talcarpine, was completed for the first time. The opposite absolute stereochemistry for the unnatural enantiomer was successfully controlled in each step of the synthetic pathway. The desired stereochemistry was confirmed by data from X-ray crystallography of key intermediates (tetracyclic ketone core and pentacyclic ketone core), as well as by comparison of the optical rotation values to that reported for the natural enantiomer. In conclusion, both strategies developed in Milwaukee: the unified Pictet-Spengler reaction/Dieckmann cyclization process, and the ambidextrous Pictet-Spengler reaction/Dieckmann cyclization process work for the synthesis of both natural, as well as unnatural C-19 methylated sarpagine/macroline/ajmaline-type indole alkaloids.

Abstract-Part-II.

Epilepsy is one of the most commonly occurring neurological conditions and the ultimate cause of neurological disability. It affects 1-2 % of the total the population and among those patients, about 33% suffer from refractory epilepsy. Many drugs including the highly prescribed benzodiazepine class (such as Valium and Xanax) are available on the market for the treatment of neurological disorders such as epilepsy and anxiety. Unfortunately, the patients develop tolerance to the benzodiazepines, and they are useful in status epilepticus for about 3 days and are then no longer effective. It is well understood that the benzodiazepine class of drugs bind to the α and γ interface of the gamma-aminobutyric acid type A ($GABA_A$) receptor without selectivity at the subtypes. This non-selectivity results in adverse effects, and thus these drugs contain a plethora of side effects such as tolerance, addiction, sedation, ataxia, somnolence, and confusion. For the first time, agents such as HZ-166 (**6**) and XHe-II-053 (**5**) (developed in Milwaukee) were found to be α2/ α3 receptor subtype-selective ligands with anxiolytic and anticonvulsive activity, importantly, devoid of unwanted side effects including sedation and ataxia. However, the ester function in XHe-II-053 (**5**) and HZ-166 (**6**) could undergo metabolism into the less active corresponding carboxylic acid. This result in poor exposure, high clearance, and low blood brain barrier penetration. The replacement of the ester with heterocycles (oxazoles and oxadiazoles) improved metabolic stability and pharmacokinetics, and this led to the clinically progressing non-sedating anticonvulsant KRM-II-81 (**7**). As back-up compounds, analogs were designed and synthesized in this work based on the structure of KRM-II-81 (**7**). After docking in the human full-length heteromeric α1β3γ2 $GABA_A$ receptor subtype CryroEM structure (6HUO) [1], by following the published procedures by Masiulis *et* al. *Nature*, 2019, we tested their biological activity. Importantly, several novel oxazole and oxazoline

analogs exhibited potent anticonvulsant activity with improved *in-vivo* and *in-vitro* stability in the absence of cytotoxicity, sedation, ataxia, and loss of righting response. Among many novel KRM-II-81 (**7**) bioisosteres designed and synthesized, KPP-III-34 (**9**) (8-bromo substituted imidazodiazepine) exhibited an improved target site (brain) exposure, as well as metabolic stability in plasma and brain. This improved oral bioavailability as exactly as desired for pre-clinical studies. This KPP-III-34 (**9**) demonstrated exceptional efficacy (anticonvulsant activity) in many epilepsy models including the pentylenetetrazole (metrazole) induced clonic and tonic seizure models (in mice), two acute seizure models (6 Hz and maximal electroshock seizure model), corneal kindled seizure models (in mice), and it antagonized convulsions in the mesial temporal lobe epilepsy model (in mice). More importantly, KPP-III-34 (**9**), was found fully potent in the therapy (Lamotrigine)-resistant seizure model (in rats), non-convulsive status epilepticus model (in mice), and chronic seizure model (in rats). KPP-III-34 (**9**) exhibited very potent anticonvulsant activity either via intraperitoneal (i.p.), or oral administration in animals (mice or rats). This 1, 4-oxazole also showed impressively clean results in a toxicity profile. In addition, in the PDSP (UNC) screens, out of the 46 receptor and ion channel panel, it selectively bound to the rat brain benzodiazepine receptor site (homogenate) with >92 mean % inhibition in the primary screen, and without undesired binding to the other receptors including HERG. The KPP-III-34 (**9**) did not show sedation, ataxia, and loss of rightening response (up to 120 mg/kg), and it was non-toxic in the HEK-293 cell line (Dr. Arnold group, UWM). There were no tremors observed in this mouse model, whereas in KRM-II-81 (**7**) in mice, tremors were observed at 100 mg/kg dose. This is indirect evidence that mouse metabolism affected the ethynyl function, but not in rats, and this was the source of tremors. Moreover, no behavioral effects were seen up to the very high oral dose of 500 mg/kg in rats. **The facile synthesis of KPP-III-34 (9) was**

explored and executed successfully on large scale in 28.7% overall yield without employing column chromatography in any synthetic step and required no toxic and expensive palladium. Also, the intermediates and product were either crystallized or precipitated out to facilitate scale up. The synthesis of KPP-III-34 (**9**) is one step shorter than the synthesis of KRM-II-81 (**7**). And thus, the large-scale synthesis of KPP-III-34 (**9**) can be executed easier and quicker than KRM-II-81 (**7**). Thus, $GABA_A$ potentiator and $\alpha2$/ $\alpha3$ receptor subtype-selective (presumably), KPP-III-34 (**9**) is undoubtedly a potent and safe back up anticonvulsant agent of the clinically progressing KRM-II-81 (**7**) for the treatment of epilepsy (ETSP, NINDS).

To my loving parents (late),

parents-in-law

brothers, sisters,

sisters-in-law

and especially my wife Sapana Paudel

TABLE OF CONTENTS

LIST OF FIGURES xiv

LIST OF TABLES xviii

LIST OF SCHEMES xx

LIST OF ABBREVIATIONS xxiii

ACKNOWLEDGEMENTS xxv

Chapter 1. 1

Bisindoles and indole alkaloids from *Alstonia* species 1

1. Introduction 1

2. Occurrence and isolation of bisindoles from *Alstonia* species. 4

3. Bioactivity of bisindole alkaloids from *Alstonia* species. 19

4. Biosynthesis. 25

4.1. Proposed biogenetic pathway toward angustilongines (**6–9**) 25

4.2. Plausible biogenetic pathway to (-)-lumusidines A-D (**14–17**). 27

4.3. Proposed biogenetic pathway to lumutinines A–D (**16–19**). 29

4.4. Possible alternative mechanism of bisindole formation of (+)-lumutinine A (**16**) and (+)-macralstonine (**24**) as representative examples via a Friedel–Crafts alkylation process, as suggested by Fukuyama. 30

4.5. Proposed biogenetic pathway to (-)-macrocarpamine (**31**). 32

5. Synthesis of representative monomeric units of bisindole alkaloids from *Alstonia* species discussed herein, required for bisindole synthesis. 33

5.1. The total synthesis of (±)-pleiocarpamine (**32**). 33

5.2. Biosynthetic relations among the sarpagine/macroline/ajmaline family of alkaloids. 36

5.3. Synthesis of monomeric macroline units employed for the synthesis of bisindole alkaloids. 39

5.3.1. An improved total synthesis of (-)-alstophylline (**28**) 39

5.3.2. Enantiospecific total synthesis of (-)-anhydromacrosalhine-methine (**33**) via the asymmetric Pictet–Spengler reaction. 40

5.3.3. Improved synthesis of (+)-macroline (**5**). 42

5.3.4. Stereospecific access to the macroline core **(5)**. 45

5.3.5. Enantiomeric total synthesis of (+)-N_a-methylsarpagine (**124**). 46

6. The synthesis of bisindole alkaloids. 48

6.1. Biomimetic partial synthesis of (-)-alstonisidine (**3**). 48

6.2. Biomimetic partial synthesis of (+)-dispegatrine (**131**). 49

6.3. Biomimetic total synthesis of (+)-macralstonidine (**23**). 53

6.4. Biomimetic total synthesis of (+)-macralstonine (**24**). 54

6.5. Partial synthesis of (-)-macrocarpamine (**31**). 54

6.6. Partial synthesis of (+)-villalstonine (**43**). 57

6.7. Improved partial synthesis of (+)-villalstonine (**43**). 59

7. Discussion and Conclusion 60

8. References 62

Chapter 2 73

1. Introduction 73

1.1. Scope of unnatural enantiomers or synthetic alkaloids in modern drug discovery. 73

1.2. Methyl-substituted (C-19 position) sarpagine/macroline/ajmaline monomeric indole alkaloids [1]. 76

2. Isolation and biological activity of representative examples of C-19 methyl substituted sarpagine/macroline/ajmaline indole alkaloids [5]. 77

2.1. Enantiospecific total synthesis of natural C-19 methyl-substituted sarpagine/macroline alkaloids via the general strategy developed in Milwaukee [1]. 79

2.2 Retrosynthetic analysis of unnatural indole alkaloid targets in this study. 83

3. Results and discussion. 85

3.1 Synthesis of L-tryptophan methyl ester (**37**) and N_b-benzyl L-tryptophan methyl ester (**33**). 85

3.2. Large scale synthesis of methyl 4, 4-dimethoxybutyrate (**34**). 87

3.3. Synthesis of N_a-methyl trans-diaster (**35**) via the asymmetric Pictet- Spengler reaction (150 g scale) and this was followed by a N_a -methylation reaction (172 g scale). 88

3.4. Large scale synthesis of N_a –Me, N_b –benzyl tetracyclic ketone (**42**) via a Dieckmann cyclization, ester hydrolysis, and decarboxylation reactions. 90

3.5. Synthesis of N_a –Me, N_b –H tetracyclic ketone (**31**) via a modified catalytic (Pd/C) debenzylation reaction. 92

3.6 The large-scale preparation of (*S*) - 4 –tri-isopropylsilyl-3-butyn-2-yl tosylate (**32**). 93

3.7 Synthesis of the (*S, S*)- ruthenium catalyst (**48**) for the asymmetric hydrogenation on gram scale..... 95

3.8. Alkylation of the tetracyclic ketone, followed by removal of the TIPS protecting group..... 95

3.9. The synthesis of the pentacyclic ketone (**28**) via haloboration and protodeboronation followed by a Cu-mediated cross-coupling reaction. 97

3.10. Synthesis of pentacyclic alcohol (**52**) via a Wittig reaction, which was followed by hydrolysis (in-situ) of the enol ether to aldehyde, and the reduction of the aldehyde (**54**). 101

3.11. Conversion of the alcohol into the silyl ether (**27**), followed by hydroboration and Kabalka oxidation. 103

3.12. Mild and modified Corey-Kim oxidation reaction and the epimerization of the mixture of aldehydes (α and β) into the more stable α aldehyde (**25**). 104

3.13. Quaternization of α aldehyde (**25**), *retro*-Michael reaction, followed by hydrolysis in acidic medium. 107

4. Conclusion. 111

5. Experimental 112

References. 150

Chapter 3 158

1. Introduction 158

1.2. Synthetic ligands which target specific $GABA_A$/BZD receptors. 162

1.2.1. Benzodiazepines (BZDs) as non-selective $GABA_A$ potentiators. 162

1.2.3.1. The α2/α3 subtype selective GABAkine: KRM-II-81 (**7**) is licensed to RespireRX and is progressing clinically for the treatment of epilepsy without side effects, Dravet syndrome and status epilepticus. 166

2. Chemistry and results 167

2.1. Design, synthesis, and characterization of novel KRM-II-81 (**7**) analogs: chiral and/or non-chiral oxazoles and oxazolines..... 167

2.2. Synthesis of KPP-III-34 (**9**) on gram scale and purification without column chromatography in any of the steps. 169

2.3. Biology, and molecular docking studies of novel ligands. 183

2.3.1. Rotarod studies of novel compounds in female CFW mice via oral administration at various doses. 183

2.3.2. Cytotoxicity studies of novel analogs (by Michelle Meyer and Anika Tylek in Dr. Arnold's laboratory, UWM). 186

2.4. Docking studies of KPP analogs 187

2.4.1. Molecular docking studies of KPP-III-51 (**10**). 188

2.4.2. Molecular docking of KPP-III-34 (**9**). 189

2.5.3. Molecular docking studies of KPP-III-96B (**11**). 192

2.5.4. Molecular docking studies of KPP-IV-09 (**12**). 193

2.5.5. Summary primary and secondary binding data of novel ligands in the Psychoactive Drug Screening Program (PDSP) of NIMH run by Dr. Bryan Roth (UNC) in the 46 receptor and HERG assay. 193

2.6. Screening of the novel ligands for antiepileptic activity 197

2.6.1. Effects of KPP-III-34 (**9**) and KPP-III-51 (**10**) in the pentylenetetrazol (PTZ) seizure model by Dr. Witkin, and Dr. Ping (Indiana University School of Medicine). 197

2.6.2. Protection against lethality by oral administration of KPP-III-34 (**9**) 198

2.6.3. Effects of KPP-III-96B (**11**), KPP-IV-09 (**12**), and KPP-IV-35 (**16**) in the pentylenetetrazol (PTZ) seizure model in mice via oral administration (Dr. Jeffrey Witkin and coworkers, Indiana University). 199

2.6.4. Effects of KPP-III-34 (**9**) in the 6Hz seizure model, MES seizure model, and on motor effects (rotarod studies) in CF1 mice (i.p.). 203

2.6.5. KPP-III-34 (**9**) in the PTZ (or Metrazol) seizure model in rats (data source: ETSP, NINDS) 205

2.6.6. KPP-III-34 (**9**) an oral dose anticonvulsant agent in the corneal-kindled mice (data source: ETSP, NINDS). 206

3. Discussion and Conclusion. 225

4. Methods 228

4.1. Rotarod studies caried out by Nick Zahn and Michelle Meyer (Dr. Arnold's laboratory, MIDD) 228

4.2. Cytotoxicity studies by Michelle Meyer and coworkers in Dr. Arnold's lab, University of Wisconsin-Milwaukee and MIDD. 229

4.3. Analysis of ligands in the pentylenetetrazol seizure model (PTZ) by Dr. Jeffery Witkin and 230

4.4. The 6 Hz (44 mA) electroshock seizure model in mice and rotarod impairment assay 230

4.5. Maximal (60 Hz and 50 mA) electroshock seizure (MES) models in mice and rotarod impairment assay 231

4.6. Subcutaneous metrazol seizure model in mice and rats..... 232

4.7. Corneal kindled seizure model in mice..... 234

4.8. The Intrahippocampal kainate (IHK) model of mesial temporal lobe (MTLE) epilepsy model in mice (method source: https://panache.ninds.nih.gov/Home/LegacyModels)..... 235

4.9. Time course of untoward signs in a modified rat Irwin test induced by orally administered KPP-III-34 (**9**) in rats (method source: https://panache.ninds.nih.gov/Home/LegacyModels).. 236

4.10. The 3-day tolerability assay for spontaneous recurrent seizing rats (method source: https://panache.ninds.nih.gov/Home/LegacyModels). 237

4.11. Rotarod test in mice (method source: https://panache.ninds.nih.gov/Home/LegacyModels). 237

4.12. Lamotrigine (LTG)-resistant amygdala kindling model in rats (method source: https://panache.ninds.nih.gov/Home/LegacyModels). 238

4.13. Neuropharmacokinetic in vivo evaluation of ligands in plasma and brain (Source: Dr. Savic and coworkers, University of Belgrade, Serbia) [39] [40]..... 239

4.14. Electrophysiological recordings from Dr. Janet Fisher (University of South Caroline, School of Medicine)..... 241

General experimental conditions. 245

References..... 268

Appendix A (Part I) 275

Single-crystal X-ray Diffraction Analysis of KPP-II-50 (**Cook196**) Pentacyclic ketone (**28**)... 275

X-ray Crystal Data for Compound KPP-III-43 (**29**). 286

NMR -data Part-I 296

Appendix B: Part II..... 336

Cognition: Working memory in Y Maze (Data source: Dr. Thomos Prevot). 338

Antidepressant Predictability (Elevated plus Maze-EPM) (Data source: Dr. Thomos Prevot).. 339

NMR data (Part II)..... 342

HRMS data (Part-II) 353

HPLC analysis (Part-II) 359

PDSP binding data (data source: Dr. Bryon Roth, NIMH)..... 364

Patent which includes newly synthesized including KPP-III-34 (**9**) and KPP-III-51 (**10**) oxazole .
Patent number: WO2018/035246A1..... 398

CURRICULUM VITAE..... 546

LIST OF FIGURES

Chapter 1

Figure 1.1. Proposed biogenetic pathway to (+)-angustilongine G (**8**) and (+)-angustilongine H (**9**)..... 26

Figure 1.2. Proposed biogenetic pathway to (−)-angustilongine E (**6**), (−)-angustilongine F (**7**), and (+)-angustilongine J (**10**). 27

Figure 1.3. Putative biogenetic pathway to (-)-lumusidines A–D (**14–17**)..... 29

Figure 1.4. Putative biogenetic pathway to lumutinines A–D (**16–19**). 30

Figure 1.5. Possible alternative mechanism of bisindole formation via a Friedel–Crafts alkylation process for (+)-macralstonine (**24**) and (+)-lumutinine A (**18**), respectively, as representative examples. 32

Figure 1.6. Pyrolysis of (-)-macrocarpamine (**31**) and macrosalhine (**75**) to generate key olefin (33)..... 33

Figure 1.7. Abbreviated chemical and biosynthetic relations among the sarpagine/macroline/ajmaline family of alkaloids. 38

Figure 2.1. The C-19 methyl-substituted sarpagine/macroline-related alkaloids (representative examples) with their biological activity [1, 5, 19, 21]..... 79

Figure 2.2. Examples of C-19 methylated alkaloids synthesized enantiospecifically by the Milwaukee group [1, 42]. 82

Figure 2.3. A reaction set-up for the Dieckman cyclization on 202 g scale (left) and for ester hydrolysis and decarboxylation reaction on 196 g scale (right). 91

Figure 2.4. The structure and ORTEP view of **29** (left), and the reaction set-up of the removal for the TIPS group in the N_b-alkylated (*R, R, R*)-tetracyclic ketone (**51**) on 73.1-gram scale (right). 97

Figure 2.5. A: The ORTEP view of pentacyclic ketone (**28**). B: The crystals were prepared by crystallization, as the off-white colored pentacyclic ketone, using 100% ethyl acetate. 100

Figure 2.6. A: The reaction set-up showing the yellow-colored mixture of Wittig reagent with potassium *tert*-butoxide in anhydrous benzene. B: The ylide formation was confirmed by the presence of the persistent dark red color after 30 minutes of stirring. 103

Figure 2.7. A: Reaction set-up showing the transparent mixture of NCS in CH_2Cl_2 (left), and the white precipitation of NCS and DMS in CH_2Cl_2. B: The indole components [alcohol (26)

and aldehyde (25)] on the TLC dipped in CAN stain (left), and yellow component (**25**) on the TLC after 2, 4-DNP sprayed (right). C: An oily alpha aldehyde (**25**) material collected after flash column chromatography. 107
Figure 2.8. A: The reaction set-up of the quaternary ammonium salt (**56**) preparation. B: the quaternary ammonium salt (**56**) in dry THF (light yellow color before NaHMDS addition). C: quaternary ammonium salt (**56**) in dry THF where the light-yellow color changed to dark green after the addition of 1. 0 M NaHMDS solution in THF. 111
Figure 3.1. Structure and composition of the GABAA receptor with GABA, BZs binding pocket and subtypes (modified from the original source) [6]. [Picture source: *Gomes, F. I. F.; Aragão, M. G. B.; Bezerra, M. M.; Chaves, H. V., GABAergic transmission and modulation of anxiety: a review on molecular aspects. Brazilian Journal of Biological Sciences 2019, 6, (12), 9-16*]. 160
Figure 3.2. Fab-α1 GABAA composition in detail with flumazenil in the binding pocket (modified from the original source [1]. Picture source: Zhu, S.; Noviello, C. M.; Teng, J.; Walsh, R. M., Jr.; Kim, J. J.; Hibbs, R. E., Structure of a human synaptic GABA(A) receptor. *Nature* 2018, 559, (7712), 67-72. 160
Figure 3.3. Examples of the benzodiazepine classes of drugs on the market. 163
Figure 3.4. GABAA receptor α2/α3 subtype selective imidazodiazepines (GABAkines). 164
Figure 3.5. Representation of novel KRM-II-81 (**7**) analog. 169
Figure 3.6. KPP-III-34 (**9**) in CH2Cl2 (left), and KPP-III-34 (**9**).HCl salt (**17**) in CH2Cl2 (right). 181
Figure 3.7. Rotarod studies of KPP-III-34 (**9**) and KPP-III-51 (**10**) at 40, 80, and 120 mg/kg doses. Diazepam is the control. 184
Figure 3.8. Rotarod studies KPP-III-96B (**11**), and KPP-IV-09 (**12**) at 40, 80, and 100 mg/kg dose. Diazepam is the control. Confidential and unpublished data. 185
Figure 3.9. Rotarod studies ZK-III-51 (**13**), ZK-III-56 (**14**) at 120 mg/dose. Diazepam is the control. Confidential and unpublished data. 186
Figure 3.10. Structures of alprazolam (**2**), HZ-166 (**6**), and KPP-III-34 (**9**) with binding affinity. 189
Figure 3.11. Overlay of the docked conformations of HZ-166 (**6**) (gray) and KPP-III-51 (gold) in the complex with α1β3γ2 interface of GABA(A) receptor 6HUO at the α+γ- interface BZ

binding site (α1 represented as chain D, color: aquamariane and γ2 represented as chain C, color: orchid, dashed line: H-bonding. 189
Figure 3.12A. Structures of compound **9** and **2**. 191
Figure 3.12B. Structures of KPP-III-34 (**9**) (A left), and alprazolam (A right). Showing the best pose of compound KPP-III-34 (**9**) (purple) docked in 6HUO (B left). Showing the best pose of compound KPP-III-34 (**9**) (purple) docked in 6HUO, overlaid with bound alprazolam (grey) in 6HUO. α1 (aquamarine) and γ2 (orchid) subunits of α1β3γ2L GABAA receptor 6HUO (B right). Dashed lines indicate π–π, hydrogen bond and halogen bond interactions. 191
Figure 3.13. The structure of KPP-III-96B (**11**) (left). Molecular docking study of KPP-III-96B (**11**) on the right (shown in blue color), and ALP (shown in organ color) in the complex with the α1β3γ2 interface of the $GABA_A$ receptor 6HUO at the $\alpha^+\gamma^-$ interface of the BZ binding site. Binding energy: -9.3 kcal.mol. Dashed lines indicate π–π, hydrogen bond and halogen bond interactions..... 192
Figure 3.14. The structure of KPP-IV-09 (**12**) (left). Overlay of KPP-IV-09 (**12**) and alprazolam in the complex with the α1β3γ2 interface of GABA(A) receptor 6HUO at the α+γ- interface of the BDZ binding site (right). Binding energy: -9.5 kcal/mol. Dashed lines indicate π–π, hydrogen bond and halogen bond interactions. 193
Figure 3.15. Effects of orally administered KPP-III-34 (**9**), and KPP-III-51 (**10**) on the latency to produce clonic (left panels) or tonic (right panels) seizures after 75 mg/kg PTZ, s.c. in male, C57BL/6N mice. *, **, *** P <0.05, 0.01, and 0.001 compared to respective vehicle control value. N=6-9 mice per group. P.O. oral gavage in carboxymethyl cellulose..... 198
Figure 3.16. Effects of orally administered KPP-III-96B (**11**), KPP-IV-09 (**12**), ZK-III-51 (**13**), ZK-III-56 (**14**), and ZK-III-58 (**15**) on the latency to produce clonic (left panels) or tonic (right panels) seizures after 75 mg/kg PTZ, s.c. in male, C57BL/6N mice at 10 mg/kg dose. Confidential data..... 201
Figure 3.17. Effects of orally administered KPP-IV-35 (**16**) on the latency to produce clonic (left panels) and generalized seizures (right panels) after 75 mg/kg PTZ, s.c. in male, C57BL/6N mice. Confidential and unpublished data. 202
Figure 3.18. KPP-III-34 (**9**) camparison with the baseline for the number of hippocampal paroxysmal discharges. ETSP 548002 is KPP-III-34 (**9**). 212

*P = 0.0336 (paired-*t*-test). 212
Figure 3.19. Electrophysical recording of KPP-III-34 (**9**) and KPP-III-51 (**10**) on GABA (A) $\alpha_1\beta_3\gamma_2$ ion channel. $EC_{3\text{-}5}$ GABA. 218
Figure 3.20. Electrophysical recording of KPP-III-34 (**9**) and KPP-III-51 (**10**) α with b and γ2L subunits. $EC_{3\text{-}5}$ GABA. 218
Figure 3.21. The pharmacokinetic data of KPP-III-34 (**9**) in plasma and brain in male Sprague Dawley rats. The time-dependent systemic distribution of KPP-III-34 (**9**) was determined at 2 mg/kg (p.o.) via the cassette method by Dr. Savic and coworkers (Serbia)..... 220
Figure 3.22. The pharmacokinetic data of KPP-III-51 (**10**) in plasma and brain in male Sprague Dawley rats. The time-dependent systemic distribution of KPP-III-51 (**10**) was determined at 2 mg/kg (p.o.) via the cassette method by Dr. Savic and coworkers (Serbia)..... 221
Figure 3.23. The pharmacokinetic data of KPP-III-96B (**11**) in plasma and brain in male Sprague Dawley rats.The time-dependent systemic distribution of KPP-III-96B (**11**) was determined at 2 mg/kg (p.o.) via the cassette method by Dr. Savic and coworkers (Serbia)..... 222
Figure 3.24. The pharmacokinetic data of KPP-IV-09 (**12**) in plasma and brain in male Sprague Dawley rats.The time-dependent systemic distribution of KPP-IV-09 (**12**) was determined at 2 mg/kg (p.o.) via the cassette method by Dr. Savic and coworkers (Serbia)..... 223
Figure 3.25. The pharmacokinetic data of KPP-IV-35 (**16**) in plasma and brain in male Sprague Dawley rats.The time-dependent systemic distribution of KPP-IV-09 (**12**) was determined at 2 mg/kg (p.o.) via the cassette method by Dr. Savic and coworkers (Serbia)..... 224

LIST OF TABLES

Table 1.1. Indole alkaloids (monomeric units) in bisindoles from *Alstonia* species that are discussed herein. 7
Table 1.2. Bisindoles alkaloids from *Alstonia* species that are discussed herein. 9
Table 1.3. Isolation and plant morphology of bisindole alkaloids from *Alstonia* species. 15
Table 1.4. Bioactivity of bisindole alkaloids (including semisynthetic derivatives) from *Alstonia* species. 22
Table 2.1. Preparation of optically active L-tryptophan methyl ester (**37**) using various reagents. 87
Table 2.2. Optimization of the *retro*-Michael reaction. 109
Table 3.1. Optimization of oxazole forming cyclodehydration reaction. 176
Table 3.2. Hygroscopicity studies of KPP-III-34 (**9**)·HCl salt over 3 days. 182
Table 3.3. Cytotoxicity studies of ligands in HEK 293 cell lines. 187
Table 3.4. Binding affinity (docking score) of bioisosteric ligands in kcal/mol. 188
Table 3.5. Summary of primary and secondary binding data of analogs synthesized. 196
Table 3.6. Protection against lethality induced by 75 mg/kg PTZ (s.c.) after oral administration (60 min prior) of test compounds in male, C57BL/6N mice. 199
Table 3.7. Lethality test of KPP-III-96B (**11**), KPP-IV-09 (**12**), ZK-III-51 (**13**), ZK-III-56 (**14**), and ZK-III-58 (**15**) in clonic/tonic PTZ inducted seizure model. 201
Table 3.8. Lethality test of KPP-IV-35 (**16**) in clonic seizure and gereralized seizure model. .. 202
Table 3.9. Effects of KPP-III-34 (**9**) and KPP-III-51 (**10**) in two acute seizure provocation models (6Hz and MES) and on rotarod performance when administered i.p. in CF1 mice. 204
Table 3.10. The time course of the anticonvulsant effects of orally administered KPP-III-34 (**9**) in the PTZ-induced convulsions in rats. 206
Table 3.11. Dose-response of orally administered KPP-III-34 (**9**) in the PTZ-induced convulsions in rats. 206
Table 3.12. Effects of KPP-III-34 (**9**) when orally administered on corneal kindling in male, CF1 mice. 207
Table 3.13. Effects of KPP-III-34 (**9**) when orally administered on corneal kindling in female mice. 208

Table 3.14. Time course of untoward signs of KPP-III-34 (**9**) in a modified rat Irwin test (p.o.) in rats. 209
Table 3.15. Test result of KPP-III-34 [**9**, (p.o.) against Lamotrigine-resistant-amygdala seizure model. 210
Table 3.16. Test results of KPP-III-34 (**9**) in the IHK model of MTLE epilepsy model in mice. 212
Table 3.17. Three-Day Tolerability Assessment for KPP-III-34 (**9**) in male KA-SRS rats three times a day for 3 days. 213
Table 3.18. Functional Observational Battery for test compound KPP-III-34 (**9**) (ETSP code: 548002) in male KA-SRS rats. 215
Table 3.19. Test drug KPP-III-34 (**9**) at 50 mg/kg (T.I.D.) in chronic seizing post-Kainate rats (phase I). 216
Table 3.20. Summary of pharmacokinetics study of novel imidazodiazepines. 219

LIST OF SCHEMES

Scheme 1.1. Synthesis of *rac*-pleiocarpamine (**32**) and 16-epi-pleiocarpamine (**85**) by Sato *et* al. 35
Scheme 1.2. An improved total synthesis of (-)-alstophylline (**28**) using the modified Wacker (Pd II) conditions..... 40
Scheme 1.3. Enantiospecific total synthesis of (-)-anhydromacrosalhine-methine (**33**) via the asymmetric Pictet–Spengler reaction. 42
Scheme 1.4. Improved synthesis of (+)-macroline (**5**). 44
Scheme 1.5. Stereoselective total synthesis of macroline (**5**) and alstomicine (**123**). 46
Scheme 1.6. Enantiomeric total synthesis of (+)-majvinine (**128**) and (+)-N_a-methylsarpagine (**124**)..... 48
Scheme 1.7. Biomimetic partial synthesis of (-)-alstonisidine (**3**)..... 49
Scheme 1.8. Biomimetic partial synthesis of (+)-dispegatrine (**131**) by oxidative phenolic coupling by Yu *et* al. [79]. 50
Scheme 1.9. The biomimetic total synthesis of the natural P(S)-atropodiastereomer of (+)-dispegatrine (**131**). 52
Scheme 1.10. Biomimetic total synthesis of macralstonidine (**23**) by the condensation of macroline (**5**) with N_a-methyl sarpagine (**124**) via two possible mechanisms. 56
Scheme 1.11. The biomimetic total synthesis of macralstonine (**24**), and *O*-acetylmacralstonine (25)..... 57
Scheme 1.12. Partial synthesis of (-)-macrocarpamine (**31**). 57
Scheme 1.13. Biomimetic partial synthesis of (+)-villalstonine (**43**) 59
Scheme 1.14. Intramolecular cyclization of macroline (5) into dihydroalstonerine (**105**). 59
Scheme 1.15. Improved partial synthesis of (+)-villalstonine (**43**). 60
Scheme 2.1. The access to both natural and unnatural enantiomers of C-19 methyl-substituted sarpagine/macroline indole alkaloids from either D or L-tryptophan (**36**) methyl ester [1, 34]. 81
Scheme 2.2. Retrosynthetic analysis for the targeted unnatural indole alkaloids. 84
Scheme 2.3. Large scale synthesis of L-tryptophan methyl ester (**37**) and N_b-benzyl L-tryptophan methyl ester (**33**). 86

Scheme 2.4. A: large scale synthesis of methyl g-nitrobutyrate (**40**). B: large scale synthesis of 4, 4-dimethoxybutyrate (**34**). 88
Scheme 2.5. Large scale synthesis of N_a-methyl *trans*-diester (**41**) via the asymmetric (*trans*-specific) Pictet- Spengler and N_a -methylation reaction. 89
89
Scheme 2.6. Large scale synthesis of N_a-methyl N_b-benzyl tetracyclic ketone (**42**) via the Dieckmann cyclization, ester hydrolysis, and decarboxylation reactions. 91
Scheme 2.7. Synthesis of N_a –Me, N_b –H tetracyclic ketone (**31**) on large scale via modified catalytic debenzylation reaction. 92
Scheme 2.8. Synthesis of (*S*) - 4 –*tri*-isopropylsilyl-3-butyn-2-yl tosylate (**32**) on large scale. .. 94
Scheme 2.9. Synthesis of (*S, S*)- ruthenium catalyst (**49**) on gram scale. 95
Scheme 2.10: The synthesis of (*R, R, R*)- acetylenic tetracyclic ketone (**29**) via alkylation of tetracyclic ketone 31 and the removal of the TIPS functional group. 96
Scheme 2.11: The synthesis of the vinyl iodide (**30**) via iodoboronation and oxidation, and this was followed by the synthesis of pentacyclic ketone (**28**) via a Cu-mediated cross coupling process. 99
Scheme 2.12: The synthesis of the pentacyclic alcohol (**52**) via the Witting reaction, hydrolysis, and the reduction of alpha aldehyde (**54**). 102
Scheme 2.13. The synthesis of silyl ether (**27**), and the synthesis of the desired primary alcohol (**26**)..... 104
Scheme 2.14. The synthesis of alpha aldehyde (**25**) via the modified Corey-Kim oxidation and the epimerization of the mixture of aldehydes into the thermodynamically more stable a aldehyde. 106
Scheme 2.15. The quaternization of an alpha aldehyde (**25**), *retro*-Michael reaction, acidic hydrolysis, and then intramolecular cyclization (*in-situ*) to give **22** and **23** (enantiomers of natural alkaloids). 110
Scheme 3.1. Large scale synthesis of imidazodiazepine ester (**18**). 170
Scheme 3.2. Synthesis of 8-bromo α-acylaminoaldehydes. 172
Scheme 3.3. Improved synthesis of 8-bromo-*N*-(1-hydroxybutan-2-yl)-6-(pyridin-2-yl)-4*H*-benzo[f]imidazo[1,5-a][1,4]diazepine-3-carboxamide over the published procedure [26]. 173
Scheme 3.4. Oxazole forming cyclodehydration reaction. 175

Scheme 3.5. Proposed mechanism for the oxazole forming reaction for KPP-III-34 (**9**)..... 177
Scheme 3.6. Gram scale synthesis of KPP-III-51 (**10**) oxazole..... 178
Scheme 3.7. Synthesis of KPP-III-93B (**11**), KPP-IV-09 (**12**), and KPP-IV-35 (**16**) oxazolines. 180
Scheme 3.8. Preparation of the KPP-III-34·HCl salt **(17**)..... 181

LIST OF ABBREVIATIONS

ACN	Acetonitrile
BBB	Blood Brain Barrier
BZPs	Benzodiazepines
DCM	Dichloromethane
DMP	Dess-Martin Periodinane
ED_{50}	Effective Dose for the 50% of tested population
ETSP	Epilepsy Therapy and Screening Program
FDA	Food and Drug Administration (US)
GABA	g-aminobutyric Acid
HEK	Human Embryonic Kidney Cells
HPDs	Hippocampal Paroxysmal Discharges
HRMS	High Resolution Mass Spectrometry
IBZD	Imidazobenzodiazepine
IC_{50}	Half Maximal Inhibitory Concentration
IP	Intraperitoneal
IV	Intravenous
KOR	Kappa Opioid Receptor

LCMS	Liquid Chromatography-Mass Spectroscopy
LCMS-IT-TOF	Liquid Chromatography-Mass Spectrometry Ion Trap Time-of Flight
LTG	Lamotrigine
MET	Metrazol
NIH	National Institute of Health
NINDS	National Institute of Neurological Disorders and Strokes
NMR	Nuclear Magnetic Resonance Spectroscopy
PDB	Protein Data Bank
PK	Pharmacokinetics
PTZ	Pentylenetetrazole
SEM	Standard Error of Mean
SC	Subcutaneous
THF	Tetrahydrofuran
TD_{50}	Dose required to produce toxicity in 50% of the test population.
TLC	Thin Layer Chromatography
NIMH	National Institute of Mental Health
PAM	Positive Allosteric Modulator
PBR	Peripheral Binding Receptor
PDSP	Psychoactive Drugs Screening Program

ACKNOWLEDGEMENTS

I would like to express my gratitude to my research advisor Professor James M. Cook for his exceptional supervision over the last several years. Many thanks to my advisor for giving me a great opportunity to work on various projects (natural products chemistry and medicinal chemistry). Dr. Cook's countless suggestions, support, expertise, and motivation was crucial in my Ph.D. program much more than I can express here with my limited vocabulary. I am very thankful to my doctoral thesis committee, Professors Alan Schwabacher, Alexander Arnold (Leggy), Xiaohua Peng, Andrew Pacheco, and Guilherme L. Indig for their helpful suggestions during the committee meetings and lectures. I am very grateful to Dr. Toufique Rahman who trained and helped me many times. His expertise and invaluable suggestions helped me execute the alkaloid total synthesis work. Thanks to Dr. Anna Benko, Dr. Villashini Rajaratanam, and Dr. Shama Mirza for LCMS and HPLC training and equipment which was critical to my success. Moreover, it helped me learn to use the LCMS and HPLC instruments independently and expand my knowledge and skills in analytical chemistry. Mr. Neal Korfhage's outstanding (world-class) skills in scientific glassblowing helped me to set up diverse reactions in the desired and suitable glassware. Dr. Holger Föersterling trained me to run high-resolution NMR instruments and taught me how to interpret NMR spectroscopy. In addition, he taught me many 2D COSY techniques which were invaluable. I want to especially thank Dr. Föersterling, Mr. Neal Korfhage, and Dr. Anna Benko who were always there to help. I want to acknowledge Dr. Jeffrey R. Deschamps and Dr. Greg Imler for their help in X-ray crystallography which was crucial to confirm the structure and stereochemistry of the intermediates in the alkaloid total synthesis research. Thanks to my all seniors, lab mates, and coworkers in Dr. Cook's research group: Dr. Toufique Rahman, Dr. Lalit Golani, Dr. Veera Venkata Naga Phani Babu

Tiruveedula, Dr. Zubair Ahmed Khan, Dr. Rajwana Jahan, Dr. Daniel Knutson, Dr. Farjana Rashid, Dr. Gaunguan Li, Dr. Yeunus Mian, Dr. Taukir Ahmed, Dr. Michael Stephan, Prithu Mondal, Sepideh Rezvanian, and Dishary Sharmin for creating a very friendly working environment and their many helpful suggestions. I am very grateful for being a part of this outstanding research group (Dr. Cook's research group). I am very grateful to Elise D. Nicks, Kevin O Blackburn, Shelley A. Harrington Hagen, Katlyn Mary Jianacopoulos, Annette Pirrung, and Wendy Grober for their help during my doctoral program. I am grateful to Dr. Veera Venkata Naga Phani Babu Tiruveedula for his suggestions and expertise in the purchase of chemicals and equipment required in our laboratory. I sincerely thank Dr. Lalit K. Golani for running and teaching molecular docking studies. Since Dr. Lalit and I worked in the same room, I felt motivated and refreshed to talk chemistry with him. Many thanks to Dr. Farjana Rashid for her help and suggestions during my medicinal chemistry research work. At this moment, I would like to remember and thank all our collaborators including Dr. Jeffrey Witkin, Dr. Arnold and coworkers, Dr. Janet Fisher, Dr. Shalini (ETSP, NIH), Dr. Bryan Roth (PDSP, NIMH) in the US and across the globe (Dr. Miroslav Savic and coworkers) for running and teaching me the biology of the compounds I synthesized for CNS disorders. I want to dedicate my doctoral thesis to my late Mother and Father who always supported and struggled a lot for my growing up and education. I truly believe that your tremendous love and blessings will still be continued forever. I am very thankful to my mother and father-in-law, brothers, sisters, brothers and sister's in-laws, niece Prashamsa for their continuous support for my education including encouragement, and motivation during many ups and down during the journey of life. I would like to thank my friends in the USA and Nepal. Last but not the least, I cannot be luckier to have Sapana Paudel,

as my wife who supported, loved, and motivated me tremendously all the time, including during my doctoral program. Again, I am very thankful to you all

Chapter 1.

Bisindole and indole alkaloids from *Alstonia* species.

1. Introduction

Bisindoles are structurally complex dimers and are intriguing targets for partial and total synthesis. They exhibit stronger biological activity than their corresponding monomeric units. Alkaloids, including those containing C-19 methyl-substitution in their monomeric units, their synthetic derivatives, and their mismatched pairs can be attractive targets for synthesis and may unlock better drug targets. We herein discuss the isolation of bisindoles from various *Alstonia* species, their bioactivity, putative biosynthesis, and synthesis. The total synthesis of macralstonidine, macralstonine, *O*-acetylmacralstonine, and dispegatrine, as well as the partial synthesis of alstonisidine, villalstonine, and macrocarpamine are also discussed in this review. The completion of the total synthesis of pleiocarpamine by Sato *et* al. completes the formal synthesis of the latter two bisindoles.

Alstonia, a major genus in the Apocynaceae family of plants, is comprised nearly 155 species and is found all over the world [1]. Robert Brown named it in 1811 in honor of Charles Alston (1685–1760), an eminent botanist at the University of Edinburgh [1]. The *Alstonia* genus' trees and shrubs are prevalent in the tropical and subtropical parts of Africa, Asia, and Australia [2]. They contribute significant pharmacological activity, including anticancer, antileishmanial, antimalarial, antitussive, antiviral, antiarthritic, and antibacterial activities [1-6]. Several parts of the plants including bark, twigs, and leaves have been traditionally used to treat diseases. Their

useful biological activity has aroused profound interest, as indicated by the increasing number of publications and patents each year. To date, more than 300 patents have been filed under the *Alstonia* genus with various formulations [1]. Notably, 157 different monoterpenoid indole alkaloids have been isolated from this genus between 2010 to 2020 [7].

Alkaloids, the most important class of natural products with structural diversity and significant pharmacological effects, are mainly found in higher plants such as the Apocynaceae, Ranunculaceae, Papaveraceae, and Leguminosae families [8]. These natural products, along with flavonoids, fatty acids, etc., are the major classes of secondary metabolites that are believed to be parts of the plants' defense mechanism. To date, many monoterpenoid indole and bisindole alkaloids have been found in the *Alstonia* genus [1]. Modern clinical application of many of these alkaloids are similar to their traditional or folklore applications; for example, cocaine and morphine were originally used as anesthetics while caffeine and nicotine were used as stimulants [9]. Recently, Fielding *et al*. illustrated that several anti-coronavirus alkaloids showed potential therapeutic value against severe acute respiratory syndrome coronavirus-2 (SARS-CoV-2) in their in silico studies [6].

The indole motif is present in many naturally occurring and biologically active compounds. Some of them have been used in the clinic. In addition, there are numerous examples of synthetic compounds with useful medicinal properties that bear the indole moiety. Consequently, the indole scaffold is one of the few "privileged structures" in modern medicinal chemistry and drug discovery [10, 11]. The prevalence of bioactivity of indole-containing molecules may be attributed to their similarity to the essential amino acid tryptophan, as well as important biomolecules such as tryptamine and serotonin. Many plant extracts, which likely include alkaloids, have been used from time immemorial in folk medicines for fever, general weakness, dysentery, pain, liver

diseases, gastrointestinal diseases, and cancer [12]. Currently, there are many indole alkaloid-based marketed drugs such as sumatriptan for the treatment of migraine; vincristine and vinblastine for the treatment of various cancers, including leukemia and lung cancer; as well as reserpine for the treatment of hypertension and to decrease severe agitation in patients with mental disorders [13].

Bisindole alkaloids are naturally occurring alkaloids containing two indole nuclei. These bisindoles are the products of late-stage biosynthetic processes in higher plants by combining two monomeric units. Depending on the monomeric units involved, bisindoles can be a homo- or heterodimer. As a result, bisindole alkaloids comprise much higher structural complexity than both of the monomeric units that comprise them. As mentioned, bioactive bisindoles are usually more potent than the monomeric units that comprise them, although the mechanism of the action is not known [3]. More structural diversity can be achieved via bisindole-based drug discovery by changing both monomeric units to furnish unnatural and pseudo-natural alkaloids. As such, bisindole alkaloids offer a large pool of natural, semi-natural, and chimeric drug candidates that have greater drug-like characteristics. As a result, due to their important biological applications and complex structural features, bisindole alkaloids have engendered the profound interest of synthetic organic and medicinal chemists, computational chemists, and chemical biologists. Compared to the previously published review [3] from this group, the most recent and updated reports on the isolation, important bioactivity, biosynthetic studies, and synthesis of bisindole alkaloids isolated from *Alstonia* containing either sarpagine, macroline, ajmaline, or pleiocarpamine units form the basis of this review. Moreover, the recent total synthesis of rac-pleiocarpamine (a monomeric unit present in several bisindoles) by Sato *et* al. [14], which resulted in the formal total synthesis of villalstonine and macrocarpamine, the bioactive C-19 methyl-

substituted sarpagine/macroline/ajmaline indole alkaloids, their unnatural enantiomers, and mismatched pairs to form potential bisindoles alkaloids, is also discussed in this review.

2. Occurrence and isolation of bisindoles from *Alstonia* species.

A list of representative families to which the monomeric indole-based units belong, which comprise bisindole alkaloids from *Alstonia*, is shown in **Table 1.1.** In some cases, a monomeric unit itself occurs as an alkaloid, i.e., has been isolated separately and is known by its trivial or given name. Bisindole alkaloids that contain the illustrated monomeric bases are listed in **Table 1.2**. Among various species of the *Alstonia* genus, *A. macrophylla* and *A. angustifolia* are the two major sources of bisindole alkaloids discussed herein (*vide infra*, **Table 1.3**). (+)-Alstomacroline **1**, a bisindole alkaloid consisting of a macroline and an ajmaline unit, was isolated from the bark of *A. macrophylla* [15] and the leaves, stem-bark, and root-bark extracts of A. scholaris, A. glaucescens, and *A. macrophylla* [16, 17]. (+)-Alstomacrophylline **2** (macroline–macroline-type) was isolated from the bark of *A. macrophylla* [15] and the leaves, stem-bark, and root-bark extracts of A. scholaris, A. glaucescens, and *A. macrophylla* [17]. (-) Alstonisidine **3**, which contains a quebrachidine **4** and a macroline **5** unit, was isolated from the bark of A. muelleriana [18, 19]. The structure of (-)-alstonisidine **3** was confirmed by X-ray crystallographic data [20]. Yeap *et* al. recently isolated seven novel bisindoles from the methanol extract of the stem-bark of Malayan A. penangiana [2]. This includes (-)-angustilongine E **6**, (-)-angustilongine F **7**, (+)-angustilongine G **8**, (+)-angustilongine H **9**, (+)-angustilongine J **10**, (+)-angustilongine K **11**, and (-)-angustilongine L **12** (macroline–pleiocarpamine type). (+)-Angustilongine K **11** was converted into (+)-di-O-acetylangustilongine K **13** by stirring it with 10 equivalents of pyridine and 15 equivalents of acetic anhydride for 6 h at room temperature in **95%** yield [2]. Among those, angustilongine G **8** and angustilongine H **9** are C-19 methyl substituted [21] bisindoles. The structures of the

angustilongines were confirmed by various spectroscopic data, including ^{1}H NMR, ^{13}C NMR, 2D NMR, IR, and HRMS by Yeap *et* al. [2]. Angustilongine E **6**, angustilongine F **7**, angustilongine G **8**, angustilongine H **9**, angustilongine J **10**, and angustilongine K **11** are macroline–sarpagine coupled bisindoles. Angustilongine G **8** and angustilongine H **9** differ in stereochemistry only at the C-20 position.

Two macroline units are contained in (-)-lumusidine A **14**, (-)-lumusidine B **15**, (-)-lumusidine C **16**, and (-)-lumusidine D **17** bisindoles. They were isolated from the stem-bark of *A. macrophylla* and the structures were confirmed via NMR spectroscopy, mass spectrometry, UV spectroscopy, and X-ray crystallography [15]. After isolation, the group of Kam *et* al. converted oily (-)-lumusidine A **14**, (-)-lumusidine B **15**, and (-)-lumusidine D **17** into the corresponding crystalline dimethyl diiodide salts (structures not shown) by treatment with an excess of iodomethane for 24 h. The crystalline salts were employed to obtain X-ray crystallographic data to elucidate the exact stereochemical confirmation [15]. (-)-Lumusidine D **17** is also known as thungfaine [22]. (+)-Lumutinine A **18**, (-)-lumutinine B **19**, (+)-lumutinine C **20**, and (+)-lumutinine D **21** are linearly fused bisindoles isolated from the stem-bark of *A. macrophylla* as a light yellowish oil [23]. (+)-Lumutinine A **18** and (-)-lumutinine B **19** are macroline–macroline-type bisindoles, while (+)-lumutinine C **20**, (+)-lumutinine D **21**, and (+)-lumutinine E **22** are macroline–sarpagine-type bisindoles. The structures of the lumutinines were elucidated using spectroscopic means including 1D and 2D NMR, IR, as well as mass spectrometric analysis [23]. The structure of (+)-lumutinine D **21** was confirmed by X-ray crystallographic data [24]. (+)-Lumutinine E **22**, a macroline–sarpagine-type bisindole, was isolated from the stem-bark of *A. angustifolia* [25].

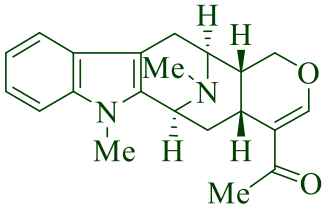
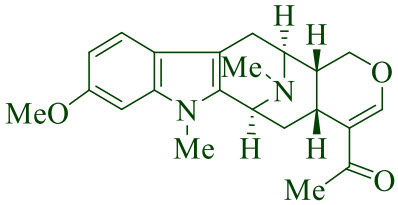
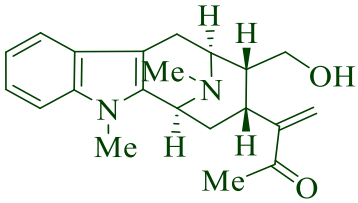
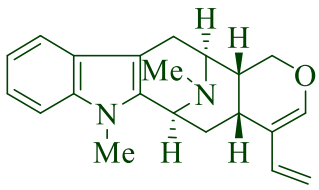
(+)-Macralstonidine **23** (macroline–sarpagine-type) was isolated from the bark of *A. macrophylla* [26, 27], as well as from *A. somersentenis* [26] and *A. spectabilis* [28]. (+)-

Macralstonine **24** was isolated from the leaves, stem-bark, and root-bark extracts of *A. scholaris*, *A. glaucescens,* and *A. macrophylla* extracts [17], *A. macrophylla* [26, 27, 29-31], *A. muelleriana* [32], *A. angustifolia* [33], as well as from *A. glabriflora* [28]. The structure of (+)-macralstonine **24** was confirmed by various NMR spectroscopy, mass spectrometry, and X-ray crystallography [30]. The (+)-macralstonine **24**-related bisindole, (+)-*O*-acetylmacralstonine **25,** was isolated from the leaves, stem-bark, and root-bark extracts of *A. scholaris, A. glaucescens,* and *A. macrophylla* [17]. Also, (+)-*O*-methylmacralstonine **26** was isolated from the leaves, stem-bark, and root-bark of *A. scholaris, A. glaucescens,* and *A. macrophylla* extracts [17]. (-)-Anhydromacralstonine **27** was isolated from the stem-bark of *A. angustiloba* [25] and contains (-)-alstophylline **28** and (+)-macroline **5** as monomeric units. Another (-)-alstophylline **28** and (+)-macroline **5** monomeric bisindole, (+)-des-*N*'a-methylanhydromacralstonine **30,** was isolated from the bark of A. muelleriana [17, 32], the stem-bark of *A. angustifolia* [30], and *A. glabriflora* [28]. (+)-Macrocarpamine **31**, a hetero-dimeric bisindole containing a (+)-pleiocarpamine **32** and (-)-anhydromacrosalhinemethine **33** monomeric unit was isolated from the leaves, stem-bark, and root-bark of *A. scholaris, A. glaucescens*, and *A. macrophylla* [17], as well as the stem-bark of *A. angustifolia* [25]. 10-Methoxymacrocarpamine **34** and 10-methoxymacrocarpamine *N*4′-oxide **35** are structurally related bisindoles. These bisindoles were isolated from *A. angustifolia* leaves [33].

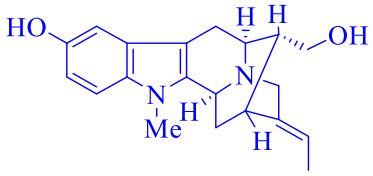
Lim *et* al. [30] reported the isolation of new macroline–macroline-type bisindoles, (-)-perhentidine A **36**, (-)-perhentidine B **37**, and (-)-perhentidine C **38** from the ethanolic extract of the stem-bark of Malayan *A. macrophylla* and *A. angustifolia*. The structurally related bisindole, (-)-perhentinine **39** (macroline–macroline-type), was isolated from the stem-bark and leaves of *A. macrophylla* and the leaves of *A. angustifolia* [15]. The exact structure of (-)-perhentinine **39** was confirmed by X-ray crystallography, converting it into the dimethyl diiodide salt by treating it with

an excess of iodomethane. The X-ray crystallographic data of (-)-perhentinine **39** also helped in the structural characterizations of perhentidines A–C (**36–38**) [30]. Tan *et* al. isolated three macroline–sarpagine-type bisindoles: (+)-perhentisine A **40**, (-)-perhentisine B **41**, and (+)-perhentisine C **42** from the stem-bark of *A. angustifolia* as a light yellow-colored oil together with other bisindoles [25]. The structures of these bisindoles were also elucidated using various NMR and MS techniques [25]. (+)-Villastonine **43**, a macroline–pleiocarpamine-type bisindole, was isolated from the stem-bark, root-bark, and leaves of various *Alstonia* species, including *A. spectabilis* [26] and *A. muelleriana* [34] by LeQuesne *et* al., as well as *A. macrophylla* [30,32,38], and *A. angustifolia* [33, 35]. Schmid et al. elucidated the structure of (+)-villalstonine **43** by spectroscopic means, accompanied by degradation, and Nordman *et* al. confirmed the structure by X-ray crystallography [36, 37].

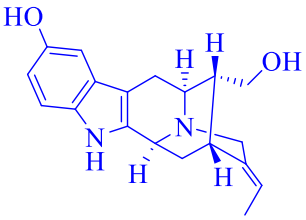
Table 1.1. Indole alkaloids (monomeric units) in bisindoles from *Alstonia* species that are discussed herein.

Types	Indole Alkaloids	
macroline	 (-)-alstonerine **100**	 (-)-alstophylline **28**
	 (+)-macroline **5**	 (-)-anhydromacrosalhine-methine **33**

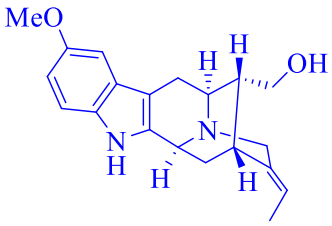
sarpagine



(+)-N_a-methylsarpagine **124**

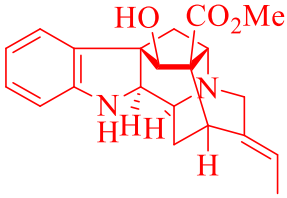


sarpagine **166**



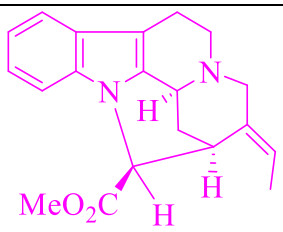
(+)-lochnerine **141**

ajmaline



(+)-quebrachidine **4**

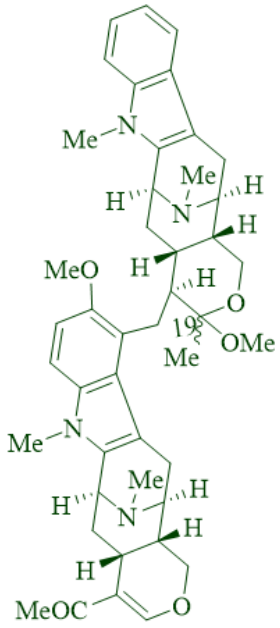
pleiocarpamine



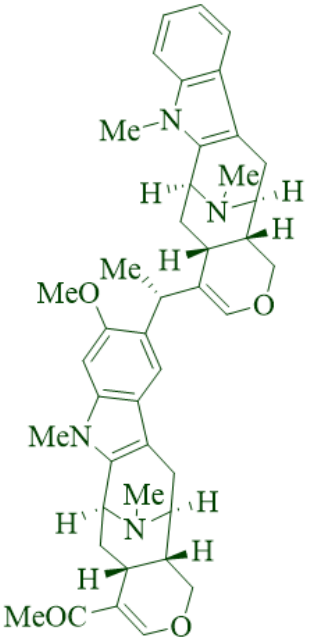
(+)-pleiocarpamine **32**

Table 1.2. Bisindoles alkaloids from *Alstonia* species that are discussed herein.

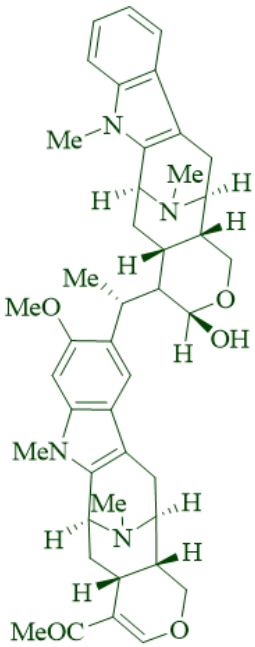
Macroline-macroline



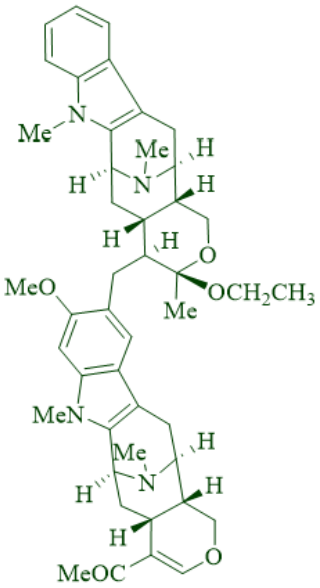
(+)-alstomacrophylline **2**



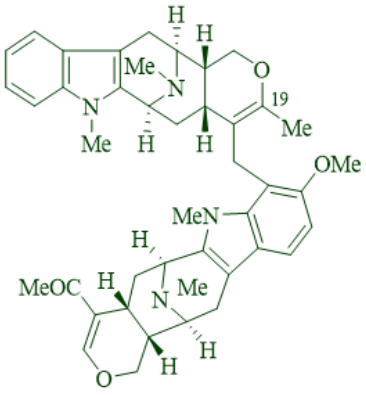
(-)-lumusidine A **14**



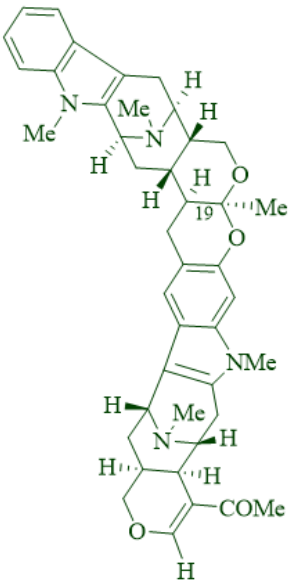
(-)-lumusidine B **15**



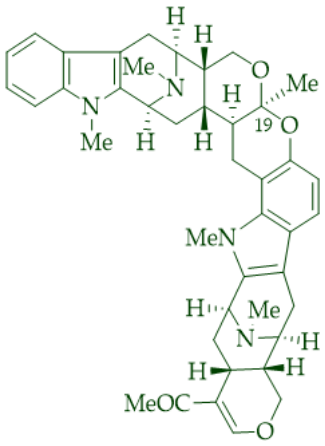
(-)-lumusidine C **16**



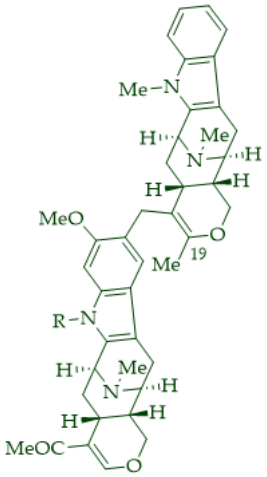
(-)-thungfaine = lumusidine D **17**



(+)- lumutinine A **18**

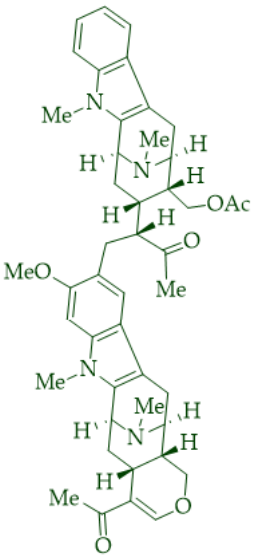


(-)-lumutinine B **19**

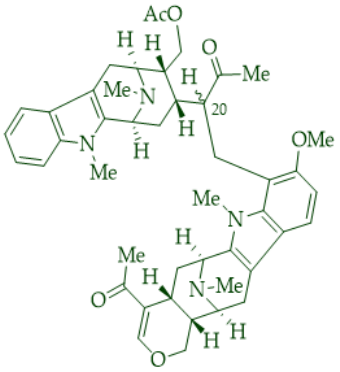


R = H, *Des-N*$_a$-methylanhydro-macralstonine **30**

R = Me, (-)-anhydromacralstonine **27**

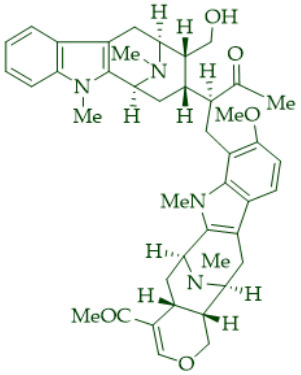


(+)-O-acetyl-*E-seco*-macralstonine **53**

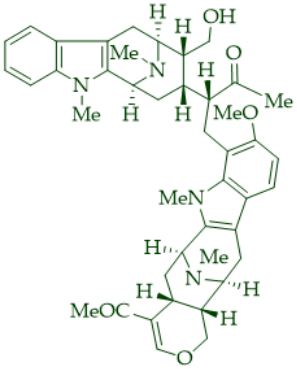


20-H, *S*, *O*-acetylperhentidine A **54**

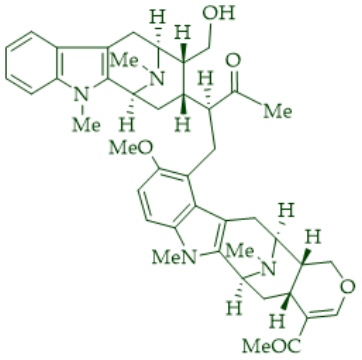
20-H, *R*, *O*-acetylperhentidine B **55**



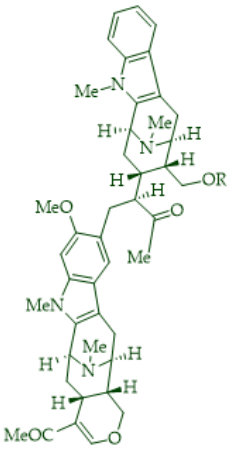
(-)-perhentidine A **36**



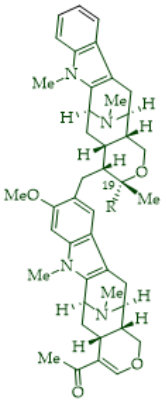
(-)-perhentidine B **37**



(-)-perhentidine C **38**

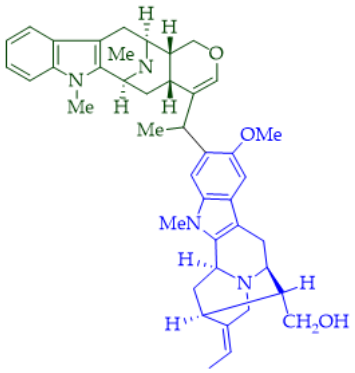


R = H, (-)-perhentinine **39**
R = Ac, *O*-acetylperhentinine **56**

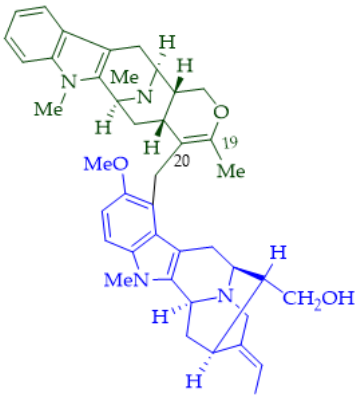


R = OH, (+)-macralstonine **24**
R = $OCOCH_3$, (+)-*O*-acetylmacralstonine **25**
R = OCH_3, (+)-*O*-methylmacralstonine **26**

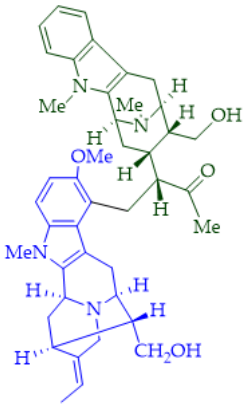
Macroline-ajmaline



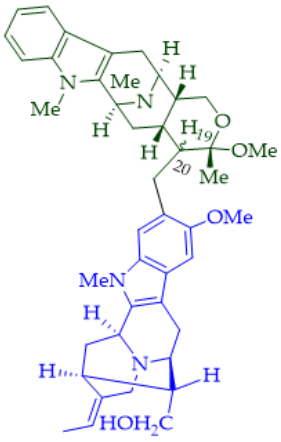
(-)-angustilongine E **6**



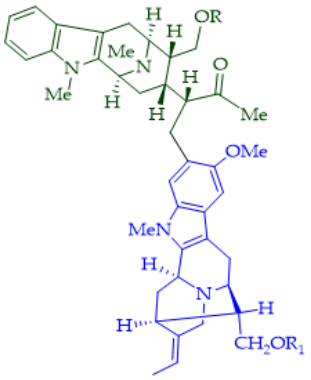
(-)-angustilongine F **7**



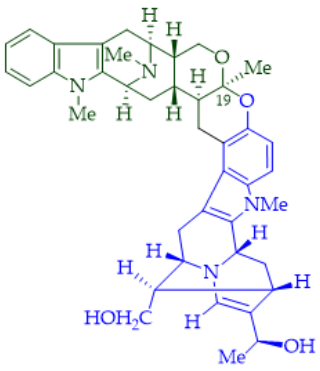
(+)-angustilongine J **10**



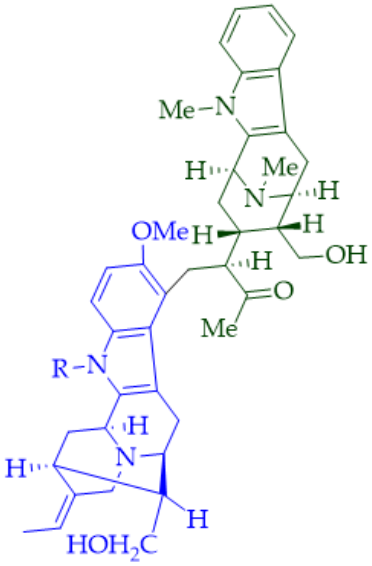
β-20- H: (+)-angustilongine G **8**
α-20- H: (+)-angustilongine H **9**



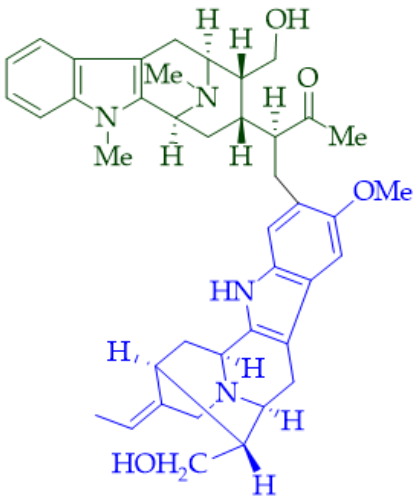
R = H, R_1 = H (+)-angustilongine K **11**
R = Ac, R_1 = Ac,
di-*O*-acetylangustilongine K **13**



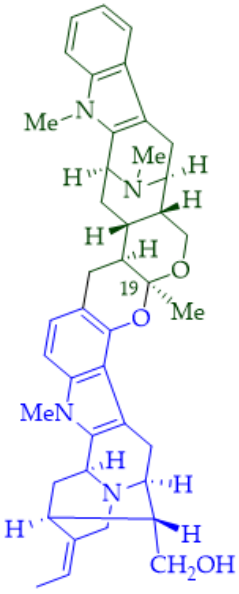
(+)-lumutinine C **20**



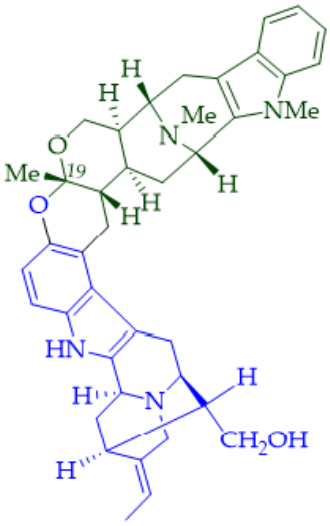
R = Me, (+)-perhentisine A **40**
R = H, (-)-perehentisine B **41**



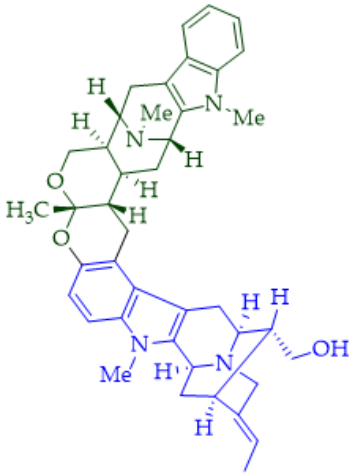
(+)-perhentisine C **42**



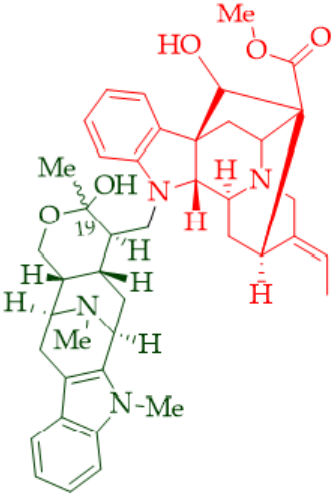
(+)- lumutinine D **21**



(+)-lumutinine E **22**

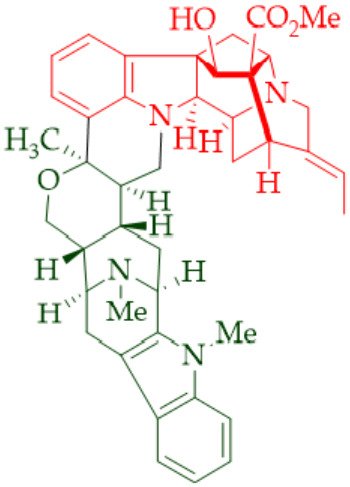


(+)-macralstonidine **23**



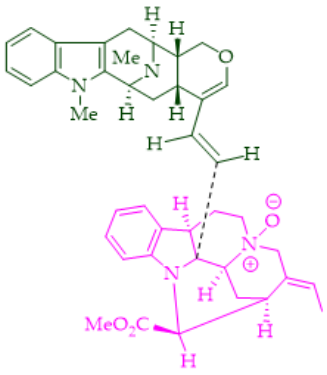
(+)-alstomacroline **1**

Macroline-ajmaline

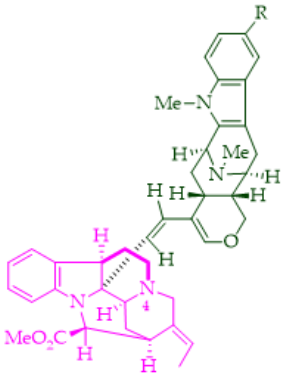


(-)-alstonisidine **3**

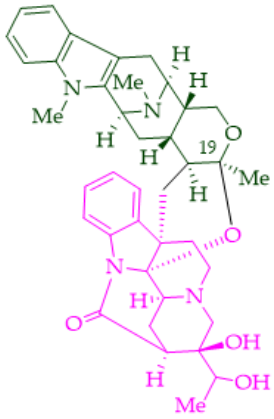
Macroline-pleiocarpamine



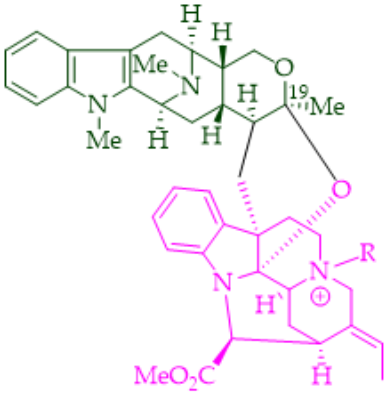
(-) angustilongine L **12**



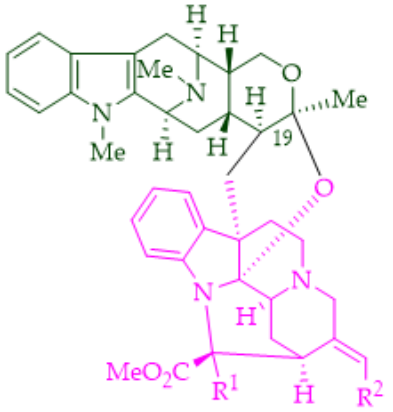
R = H, (-)-macrocarpamine **31**
R = OMe, 10-methoxymacrocarpamine **34**
R = OMe, $N(4) \rightarrow$ oxide (+) charge on $N(4)$, 10-methoxymacrocarpamine $N(4)$-oxide **35**



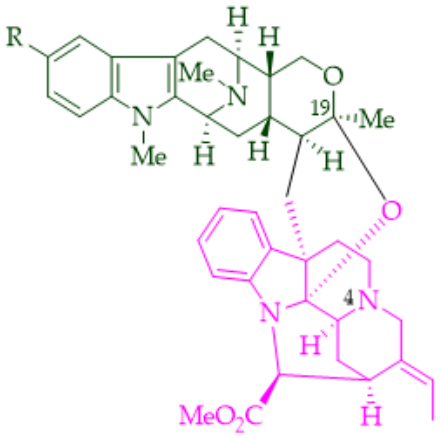
(+)-villalstonidine A **47**



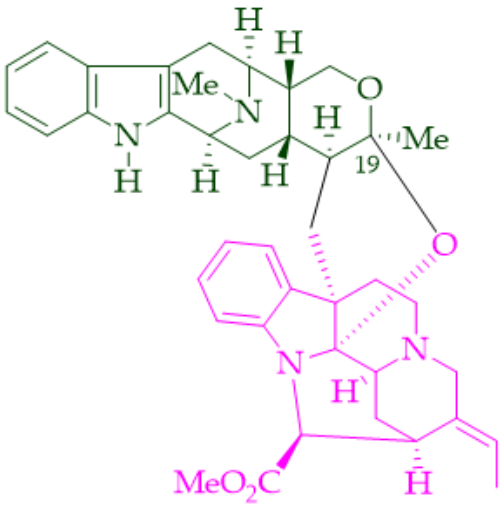
R = $\overset{\ominus}{O}$, villalstoninine $N(4)$-Oxide **44**
R = CH_3, (+)-villalstonidine D **50**
R = CH_2Cl; $\overset{\ominus}{Cl}$ (+)-villalstonidine E **51**



$R^1 = CH_2OH$, R^2 = Me, villalstonidine B **48**
R^1 = H, $R^2 = CH_2OH$, villalstonidine C **49**



R = H, (+)-villalstonine **43**
R = OMe, 10-methoxyvillalstonine **45**
R = OMe,
N(4) → Oxide (+ charge on *N*(4),
10-methoxyvillalstonine-
N(4)-oxide **46**



(+)-villalstonidine F **52**

Table 1.3. Isolation and plant morphology of bisindole alkaloids from *Alstonia* species.

Bisindoles	Types of Monomeric Units Present in Bisindoles	*Alstonia* Species	Morphology and References
(+)-Alstomacroline **1**	Macroline-sarpagine	*A. scholaris*, *A. glaucescens*, and *A. macrophylla* extracts	Leaves, stem-bark, and root-bark [16, 17]
		A. macrophylla	Bark [15]
(+)-Alstomacrophylline **2**	Macroline-macroline	*A. macrophylla*	Bark [16]
		A. scholaris, *A. glaucescens*, and *A. macrophylla* extracts	Leaves, stem-bark, and root-bark [17]
(−) Alstonisidine **3**	Ajmaline-macroline	*A. muelleriana*	Bark [18],[19]
(−)-Angustilongine E **6**	Macroline-sarpagine	*A. penangiana*	Stem-bark [2]
(−)-Angustilongine F **7**	Macroline-sarpagine	*A. penangiana*	Stem-bark [2]

(+)-Angustilongine G **8**	Macroline-sarpagine	*A. penangiana*	Stem-bark [2]
(+)-Angustilongine H **9**	Macroline-sarpagine	*A. penangiana*	Stem-bark [2]
(+)-Angustilongine J **10**	Macroline-sarpagine	*A. penangiana*	Stem-bark [2]
(+)-Angustilongine K **11**	Macroline-sarpagine	*A. penangiana*	Stem-bark [2]
(−)-Angustilongine L **12**	Macroline-pleiocarpamine	*A. penangiana*	Stem-bark [2]
(−)-Anhydromacralstonine **27**	Macroline-macroline	*A. angustifolia*	Stem-bark [25]
(+)-Des-*N*'a-Methylanhydromacralstonine **30**	Macroline-macroline	*A. muelleriana*	Bark [17]
		A. angustifolia	Stem-bark [30]
		A. muelleriana	Leaves, stem-bark and root-bark [17, 32]
(−)-Lumusidine A **14**	Macroline-macroline	*A. macrophylla*	Stem-bark [15]
(−)-Lumusidine B **15**	Macroline-macroline	*A. macrophylla*	Stem-bark [15]
(−)-Lumusidine C **16**	Macroline-macroline	*A. macrophylla*	Stem-bark [15]
(−)-Lumusidine D **17**	Macroline-macroline	*A. macrophylla*	Stem-bark [15]
(+)-Lumutinine A **18**	Macroline-macroline	*A. macrophylla*	Stem-bark [23]
(−)-Lumutinine B **19**	Macroline-macroline	*A. macrophylla*	Stem-bark [23]
(+)-Lumutinine C **20**	Macroline-sarpagine	*A. macrophylla*	Stem-bark [23]
(+)-Lumutinine D **19**	Macroline-sarpagine	*A. macrophylla*	Stem-bark [23]
(+)-Lumutinine E **21**	Macroline-sarpagine	*A. angustifolia*	Stem-bark [25]
(+)-Macralstonidine **23**	Macroline-sarpagine	*A. macrophylla*	Bark [26, 27]
		A. somersentenis	Bark [26]
		A. spectabilis	Bark [28]
(+)-Macralstonine **24**	Macroline-macroline	*A. scholaris*, *A. glaucescens*, and *A. macrophylla* extracts	Leaves, stem-bark and root-bark [19]
		A. macrophylla	[26, 27, 29-31]

		A. angustifolia	[33]
		A. muelleriana	[32]
		A. glabriflora Mgf.	[28]
(+)-*O*-Acetylmacralstonine **25**	Macroline-macroline	*A. scholaris*, *A. glaucescens*, and *A. macrophylla* extracts	[17]
(+)-*O*-Methylmacralstonine **26**	Macroline-macroline	*A. scholaris*, *A. glaucescens*, and *A. macrophylla* extracts	[17]
(+)-Macrocarpamine **31**	Macroline-pleiocarpamine	*A. scholaris*, *A. glaucescens*, and *A. macrophylla* extracts	Leaves, stem-bark, and root-bark [17]
		A. angustifolia	Stem-bark [25]
10-Methoxy macrocarpamine **34**	Macroline-pleiocarpamine	*A. angustifolia*	Leaves [38]
10-Methoxy macrocarpamine 4′-*N*-oxide **35**	Macroline-pleiocarpamine	*A. angustifolia*	Leaves [38]
(−)-Perhentidine A **36**	Macroline-macroline	*A. macrophylla* and *A. angustifolia*	Stem-bark [25, 30]
(−)-Perhentidine B **37**	Macroline-macroline	*A. macrophylla* and *A. angustifolia*	Stem-bark [30]
(−)-Perhentidine C **38**	Macroline-macroline	*A. macrophylla* and *A. angustifolia*	Stem-bark [25, 30]
(−)-Perhentinine **39**	Macroline-macroline	*A. macrophylla*	Stem-bark [15]
		A. angustifolia	Leaves [15]
		A. macrophylla	Leaves [15]
(+)-Perhentisine A **40**	Macroline-sarpagine	*A. angustifolia*	Stem-bark [25]
(−)-Perhentisine B **41**	Macroline-sarpagine	*A. angustifolia*	Stem-bark [25]
(+)-Perhentisine C **42**	Macroline-sarpagine	*A. angustifolia*	Stem-bark [25]
		A. muelleriana	Leaves and stem-bark [34]
(+)-Villalstonidine A **47**	Macroline-pleiocarpamine	*A. angustifolia*	Stem-bark [25]
(+)-Villalstonidine B **48**	Macroline-pleiocarpamine	*A. angustifolia*	Stem-bark [25]
		A. macrophylla	Stem-bark [24]
(+)-Villalstonidine C **49**	Macroline-pleiocarpamine	*A. angustifolia*	Stem-bark [25]

(+)-Villalstonidine D **50**	Macroline-pleiocarpamine	*A. angustifolia*	Stem-bark [25]
(+)-Villalstonidine E **51**	Macroline-pleiocarpamine	*A. angustifolia*	Stem-bark [25]
(+)-Villalstonidine F **52**	Macroline-pleiocarpamine	*A. macrophylla*	Stem-bark [24]
(+)- Villalstonine **43**	Macroline-pleiocarpamine	*A. angustifolia*	Leaves and stem-bark [28,36,39,41]
		A. macrophylla	[38]
		A. villosa	[38]
		A. verticillosa	[38]
		A. somersentensis	[38]
Villalstonine *N*(4)-oxide **44**	Macroline-pleiocarpamine	*A. angustifolia*	Stem-bark [25]
		A. scholaris, *A. glaucescens*, and *A. macrophylla* extracts	Leaves, stem-bark, and root-bark [20,30,32,38]
(+)-10-Methoxy villalstonine **45**	Macroline-pleiocarpamine	*A. angustifolia*	Leaves [38]
10-Methoxy villalstonine 4′-*N*-oxide **46**	Macroline-pleiocarpamine	*A. angustifolia*	Leaves [38]

Villalstonine *N*(4)-oxide **44** was isolated from the stem-bark of *A. angustifolia* [25]. It was also isolated from the leaves, stem-bark, and root-bark of A. scholaris, *A. glaucescens*, and *A. macrophylla* extracts [17]. Moreover, two villalstonine **44**-related bisindoles, (+)-10-methoxy villalstonine **45** and 10-methoxy villalstonine *N*(4)-oxide **46**, were isolated from the leaves of *A. angustifolia* [38]. Villalstonidine A **47**, villalstonidine B **48**, villalstonidine C **49**, villalstonidine D **50**, villalstonidine E **51**, (+)-villalstonidine F **52**, and villalstonine *N*(4)-oxide **44** are macroline–pleiocarpamine-type bisindoles and are close in structure to villalstonine **43**. Villalstonidines A–D (**47–50)** were isolated from the stem-bark of *A. angustifolia* [25]. Additionally, (+)-villalstonidine F **52**, {*N*(1)-demethylderivative of villalstonine **43**}, and (+)-villalstonidine B **48** were isolated from the stem-bark of *A. macrophylla* [24].

3. Bioactivity of bisindole alkaloids from *Alstonia* species.

Studies from various groups have shown that bisindoles have anticancer activity in different cell lines, including HT-29 and vincristine-resistant KB/VJ300 cells. Bisindoles are also reported to have other biological activities, including antiprotozoal activity against Plasmodium falciparum and antileishmanial activity against promastigotes of Entamoeba histolytica. The reported biological activity of bisindoles from various *Alstonia* species including the semi-synthetic derivatives reviewed herein are listed in **Table 1.4**. (+)-Alstomacroline **1** and (+)-alstomacrophylline **2** bisindoles were active against the K1 (multi-drug resistant) strain of *P. falciparum* with an IC_{50} 1.12 ± 0.35 μM and IC_{50} 1.10 ± 0.30 μM, respectively [39]. Newly isolated macroline-sarpagine-type bisindoles, (−)-angustilongine E **6**, (-)-angustilongine F **7**, (+)-angustilongine G **8**, (+)-angustilongine H **9**, (+)-angustilongine J **10**, and (+)-angustilongine K **11** showed *in vitro* growth inhibitory activity against human cancer cell lines, inclusive of KB, vincristine-resistant strains of KB, HCCT 116, PC-3, MDA-MB-231, LNCaP, MCF7, HT-29, and A549 cells with IC_{50} values ranging from 0.02 to 9.0 μM in the study from the group of Kam [2]. Kam *et* al. [15] also reported the anticancer activity of (−)-lumusidine A **14**, (−)-lumusidine B **15**, (−)-lumusidine C **16**, and (−)-lumusidine D **17**. These bisindoles were cytotoxic against KB/VJ300 cells ranging from IC_{50} 0.16 to 5.03 μg/mL (μM) values with 0.12 μM vincristine added [15]. Lumutinine A **18**, lumutinine B **19**, lumutinine C **20**, lumutinine D **21**, and lumutinine E **22** exhibited moderate anticancer activity against KB/VJ300 cells ranging in IC_{50} values from 0.10 to 4.61 μg/mL (μM) again with 0.12 μM vincristine added in the studies from the same group (Kam) [15].

(+)-Macralstonine **24** was active against the K1 strain of *P. falciparum* (IC_{50} 8.92 ± 2.95 μM). Notably, the derivatives of (+)-macralstonine **24** were more active than (+)-macralstonine **24** itself.

(+)-*O*-methyl macralstonine **26** and (+)-*O*-acetyl macralstonine **25** demonstrated more potent activity against the K1 strain of *P. falciparum* with IC_{50} values of 0.85 ± 0.20 μM and IC_{50} 0.53 ± 0.09 μM, respectively [17]. Likely, the functionalization facilitated the transportation of these bisindoles through the cell membranes of parasites and red blood cells, which would have enhanced the activity as lipophilicity rose [17]. (+)-*O*-acetyl macralstonine **25** and (+)-alstomacroline **1** were also somewhat active against the T9-96 strain of *P. falciparum* with IC_{50} values of 12.4 and 10.2 μM, respectively [17]. Heterodimeric alkaloid (−)-anhydromacralstonine **27** showed moderate cytotoxicity (IC_{50} value of 0.44 μg/mL (μM) in KB/VJ300 cells with 0.12 μM of vincristine added [15]. Another semisynthetic analog of macralstonine **24**, the related *O*-acetyl-E-seco-macralstonine **53**, showed strong anticancer activity. It was prepared by the reaction of macralstonine **24** with acetic anhydride/pyridine in DCM [15]. It demonstrated potent activity against vincristine-resistant KB/VJ300 cells with an IC_{50} value of 0.27 μg/mL (μM), with 0.12 μM of vincristine added to the assay [15]. (+)-Macralstonidine **23** was found to exhibit moderately active anticancer activity. It was active against KB/VJ300 cells with an IC_{50} value of 0.13 μg/mL (μM) [15].

(−)-Macrocarpamine **31** exhibited antiprotozoal and anticancer activity in various studies. It showed significant antiprotozoal activity in vitro in studies from Wright *et* al. against E. histolytica and *P. falciparum* with ED_{50} values of 8.12 (95% C.I.) μM and 9.36 (95% C.I.) μM, respectively [40]. Keawpradub *et* al. reported significant activity of (−)-macrocarpamine **31** against the K1 strain of *P. falciparum* with an IC_{50} value of 0.36 μM [17]. Furthermore, (−)-macrocarpamine **31** showed antimalarial activity against the T9-96 strain of *P. falciparum* with an $IC_{50} > 39$ μM. The ancient folklore use of the extracts from *A. angustifolia* in Malaya for treatment of malaria and dysentery is supported by these in vitro studies [41]. (−)-Macrocarpamine **31** was strongly

cytotoxic in KB/VJ300 cells with an IC_{50} value of 0.53 μg/mL (μM) [15]. (−)-Perhentidine A **36** and (−)-perhentidine B **37** showed strong cytotoxicity against KB/VJ300 cells with IC_{50} values of 2.29 and 0.84 μg/mL (μM), respectively [15]. *O*-Acetylperhentidine A **54** and *O*-acetylperhentidine B **55** also exhibited strong cytotoxicity against KB/VJ300 cells with IC_{50} values of 0.36 and 0.28 μg/mL (μM), respectively [15]. (−)-Perhentidine A **36** and (−)-perhentidine B **37** were treated individually by dropwise addition of acetic anhydride in a pyd/DCM solution, followed by stirring at room temperature for 2 h to furnish the semisynthetic (−)-*O*-acetylperhentidine A **54**, and (−)-*O*-acetylperhentidine B **55**, respectively [15]. (−)-Perhentinine **39** and *O*-acetylperhentinine **56** were cytotoxic against KB/VJ300 cells with IC_{50} values of 0.52 and 0.30 μg/mL (μM), respectively, in the studies by Kam *et* al. [15].

(+)-Villalstonine **43** has demonstrated various biological activities including anticancer, antimalarial, and antiamoebic activity. The (+)-Villastonine **43** was 1/15th as potent as chloroquine (antimalarial drug) against malaria [42]. It exhibited potent antiplasmodial activity against the multidrug-resistant K1 strain of *P. falciparum* with an IC_{50} value of 0.27 μM [17]. Wright *et* al. tested this compound for antiamoebic activity against *E. histolytica* [40]. (+)-Villalstonine **43** showed six times less activity (ED_{50} 11.8 μM) than the antiamoebic drug emetine (ED_{50} 2.04 μM). These results also concur with the use of various parts of the *A. angustifolia* plant from ancient times to treat malaria and amoebic dysentery [40]. Moreover, (+)-villalstonine **43** was cytotoxic against KB cells with an ED_{50} value of 11.6 μM [40]. (+)-Villalstonine **43** was also potent against the T9-96 strain of *P. falciparum* with an IC_{50} value of 0.94 μM. It also showed anticancer activity against the HT-29 cell line with an ED_{50} value of 8.0 μM (paclitaxel was the positive control). Also, it was cytotoxic against vincristine-resistant KB/VJ300 cells with an IC_{50} value of 0.42 μg/mL (μM) [15]. On the other hand, the derivative of (+)-villalstonine **43**, villalstonine *N*(4)-

oxide **44** was less potent (IC_{50} 10.7 ± 1.9) than (+)-villalstonine **43** itself. The increase in the ionic charge (decrease in lipophilicity) might have reduced the ability of villalstonine *N*(4)-oxide **44** to cross through the cell membranes of red blood cells or the parasites, which if correct, would explain the weaker activity [17]. Villalstonine *N*(4)-oxide **44** is also an antileishmanial bisindole. It was active against promastigotes of *Leishmania mexicana* with an IC_{50} value of 80.3 μM [35]. (+)-Villalstonine **43**-related alkaloids (+)-villalstonidine B **48** and (+)-villalstonidine F **52** were found to be strongly cytotoxic against KB/VJ300 cells with IC_{50} values of 0.35 and 5.64 μg/mL (μM), respectively [15]. (+)-Villalstonidine D **50** exhibited antileishmanial activity. It was active against promastigotes of *L. mexicana* with an IC_{50} value of 120.4 μM in a study from Pan et al. [35]. Another (+)-villalstonine **43**-related alkaloid, (+)-villalstonidine E **51,** demonstrated anticancer and antimalarial activity. It was cytotoxic against the HT-29 cell lines with an ED_{50} value of 6.5 μM and was active against promastigotes of *L. mexicana* with an IC_{50} value of 78 μM in the study from the same group [35]. Many bisindoles are yet to be screened for their activity because of the paucity of material; however, their significant role in future drug discovery should be considered.

Table 1.4. Bioactivity of bisindole alkaloids (including semisynthetic derivatives) from *Alstonia* species.

Bisindoles	Bioactivity	Refere-nces
(+)-Alstomacroline **1**	Antimalarial, with IC_{50} values of 1.12 ± 0.35 and 10.0 ± 0.4 μM against the K1 strain and T9-96 strain of *P. falciparum*, respectively.	[17]
(+)-Alstomacrophylline **2**	Antimalarial, with an IC_{50} value of 1.10 ± 0.30 μM against the K1 strain of *P. falciparum*.	[17]
Angustilongines E, F, G, H, J, and K (**6**–**11**)	Anticancer, cytotoxic against various human cancer cell lines including KB, vincristine-resistant KB, HCCT 116, PC-3, MDA-MB-231, LNCaP, MCF7, HT-29, and A549 cells with IC_{50} values ranging from 0.02 to 9.0 μM.	[2]

(−)-Lumusidine A, B, and C (**14**–**16**)	Anticancer, moderately cytotoxic in KB/VJ300 cells with IC_{50} values of 0.16, 0.70, and 1.19 μg/mL (μM), respectively. The assay with 0.12 μM added vincristine did not influence KB/VJ300 cell growth.	[15]
(−)-Lumusidine D **17**	Anticancer, cytotoxic in KB/VJ300 cells with an IC_{50} value of 5.03 μg/mL (μM). The assay with 0.12 μM added vincristine did not influence KB/VJ300 cell growth.	[15]
Lumutinine A, B, C, D, and E (**18**–**22**)	Anticancer, moderately cytotoxic in KB/VJ300 cells with IC_{50} 0.21, 0.10, 4.61, 3.93, and 2.74 μg/mL (μM) values, respectively. The assay with 0.12 μM added vincristine did not influence KB/VJ300 cell growth.	[15]
(+)-Macralstonine **24**	Anticancer, strongly cytotoxic in KB/VJ300 cells with an IC_{50} 1.71 μg/mL (μM) value. The assay with 0.12 μM added vincristine did not influence KB/VJ300 cell growth.	[15]
	Antimalarial, active against the K1 strain of *P. falciparum* with an IC_{50} 8.92 ± 2.95 μM value.	[17]
(−)-Anhydromacralstonine **27**	Anticancer, moderately cytotoxic in KB/VJ300 cells with an IC_{50} value of 0.44 μg/mL (μM). The assay with 0.12 μM added vincristine did not influence KB/VJ300 cell growth.	[15]
(+)-*O*-Acetyl macralstonine **25**	Antimalarial, with IC_{50} values 0.53 ± 0.09 and 12.4 ± 1.6 (μM) against the K1 strain and T9-96 strain of *P. falciparum*, respectively.	[17]
(+)-*O*-Methyl macralstonine **26**	Antimalarial, active against the K1 strain of *P. falciparum* with an IC_{50} 0.85 ± 0.20 μM value.	[17]
O-Acetyl-E-*seco*-macralstonine **53**	Anticancer, strongly cytotoxic in KB/VJ300 cells with an IC_{50} value of 0.27 μg/mL (μM). The assay with 0.12 μM added vincristine did not influence KB/VJ300 cell growth.	[15]
(−)-Perhentidine A **36** and (-)-perhentidine B **37**	Anticancer, strongly cytotoxic in KB/VJ300 cells with IC_{50} values of 2.29 and 0.84 μg/mL (μM), respectively. The assay with 0.12 μM added vincristine did not influence KB/VJ300 cell growth.	[15]
(−)-*O*-Acetylperhentidine A **54** and (-)-*O*-Acetylperhentidine B **55**	Anticancer, strongly cytotoxic in KB/VJ300 cells with IC_{50} 0.36 and 0.28 μg/mL (μM) values, respectively. The assay with 0.12 μM added vincristine did not influence KB/VJ300 cell growth.	[15]
(−)-Perhentinine **39** and *O*-Acetylperhentinine **56**	Anticancer, cytotoxic in KB/VJ300 cells with IC_{50} values of 0.52 and 0.30 μg/mL (μM), respectively. The assay with 0.12 μM added vincristine did not influence KB/VJ300 cell growth.	[15]

(+)-Macralstonidine **23**	Anticancer, moderately cytotoxic in KB/VJ300 cells with an IC_{50} value of 0.13 μg/mL (μM). The assay with 0.12 μM added vincristine did not influence KB/VJ300 cell growth.	[15]
(+)-Macrocarpamine **21**	Anticancer, strongly cytotoxic in KB/VJ300 cells with an IC_{50} value of 0.53 μg/mL (μM). The assay with 0.12 μM added vincristine did not influence KB/VJ300 cell growth.	[15]
	Strong antimalarial activity against the K1 strain of *P. falciparum* with an IC_{50} value of 0.36 ± 0.06 μM. Active against the T9-96 strain of *P. falciparum* with an IC_{50} >39 μM value.	[17]
	Strong antiprotozoal activity in vitro against *E. histolytica* and *P. falciparum* with ED_{50} 8.12 (95% C.I.) μM and ED_{50} 9.36 (95% C.I.) μM values, respectively.	[40]
(+)-Villalstonine **43**	Anticancer, cytotoxic in KB/VJ300 cells with an IC_{50} value of 0.42 μg/mL (μM). The assay with 0.12 μM added vincristine did not influence KB/VJ300 cell growth.	[15]
	Anticancer, cytotoxic against the HT-29 cell line with an ED_{50} 8.0 μM value (paclitaxel was used as the positive control).	[35]
	Antimalarial, with IC_{50} values of 0.27 ± 0.06 and 0.94 ± 0.07 μM against the K1 strain and T9-96 strain of *P. falciparum*, respectively.	[17]
	Antiamoebic activity against E. histolytica with an ED_{50} of 2.04 μM.	[40]
Villalstonine *N*(4)-oxide **44**	Antileishmanial activity against promastigotes of *L. mexicana* with an IC_{50} value of 80.3 μM (amphotericin B was used as the positive control).	[35]
	Antimalarial, active against the K1 strain of *P. falciparum* with an IC_{50} 10.7 ± 1.9 (μM) value.	[17]
(+)-Villalstonidine B **48** and (+)-villalstonidine F **52**	Anticancer, strongly cytotoxic in KB/VJ300 cells with IC_{50} values of 0.35 and 5.64 μg/mL (μM), respectively. The assay with 0.12 μM added vincristine did not influence KB/VJ300 cell growth.	[15]
(+)-Villalstodinine D **50**	Antileishmanial, active against promastigotes of *L. mexicana* with an IC_{50} value of 120.4 μM (amphotericin B was used as the positive control).	[35]
(+)-Villalstonidine E **51**	Anticancer, cytotoxic against HT-29 cell lines with an ED_{50} 6.5 μM value (paclitaxel was used as the positive control).	[35]

Antileishmanial against promastigotes of *L. mexicana* with an IC_{50} 78 μM value (amphotericin B was used as the positive control).	[35]

4. Biosynthesis.

4.1. Proposed biogenetic pathway toward angustilongines (6–9).

Yeap *et* al. put forward a plausible biogenetic pathway to the angustilongines [2]. The nucleophilic C-11′ of 10-methoxyaffinisine **57** undergoes conjugate addition onto C-21 of the hypothetical macroline unit **5** to give (+)-angustilongine K **11** and **58** (**Figure 1.1**). The (+)-angustilongine K **11** and **58**, after the E-ring closes to the hemiacetal, would give (+)-angustilongine G **8** and (+)-angustilongine H **9**, respectively. Since methanol was used during the extraction of the alkaloids, there could be the possible formation of bisindoles **8** and **9** as artifacts [2]. Similarly, nucleophilic addition of C-9′ of 10-methoxyaffinisine **57** by conjugate addition (Michael reaction) onto C-21 of the macroline unit **5** would give angustilongine J **10**. The E-ring closure of **10** gives angustilongine F **7** (**Figure 1.2**). The 10-methoxyaffinisine **57** through its nucleophilic C-11′ carbon atom addition to the C-19 of an E-seco-talcarpine derivative **59** results in angustilongine E **6** via hydroxy aldehyde **60** [2]. Another likely mechanism is a Friedel–Crafts alkylation of the oxonium ion of corresponding macroline units (cyclization followed by loss of water) to the respective sarpagine units as suggested by Fukuyama to furnish angustilongines (mechanism not shown for angustilongines **6**–**11** see **Figure 1.5** with representative examples of (+)-macralstonine **24** and (+)-lumutinine A **18** [3].

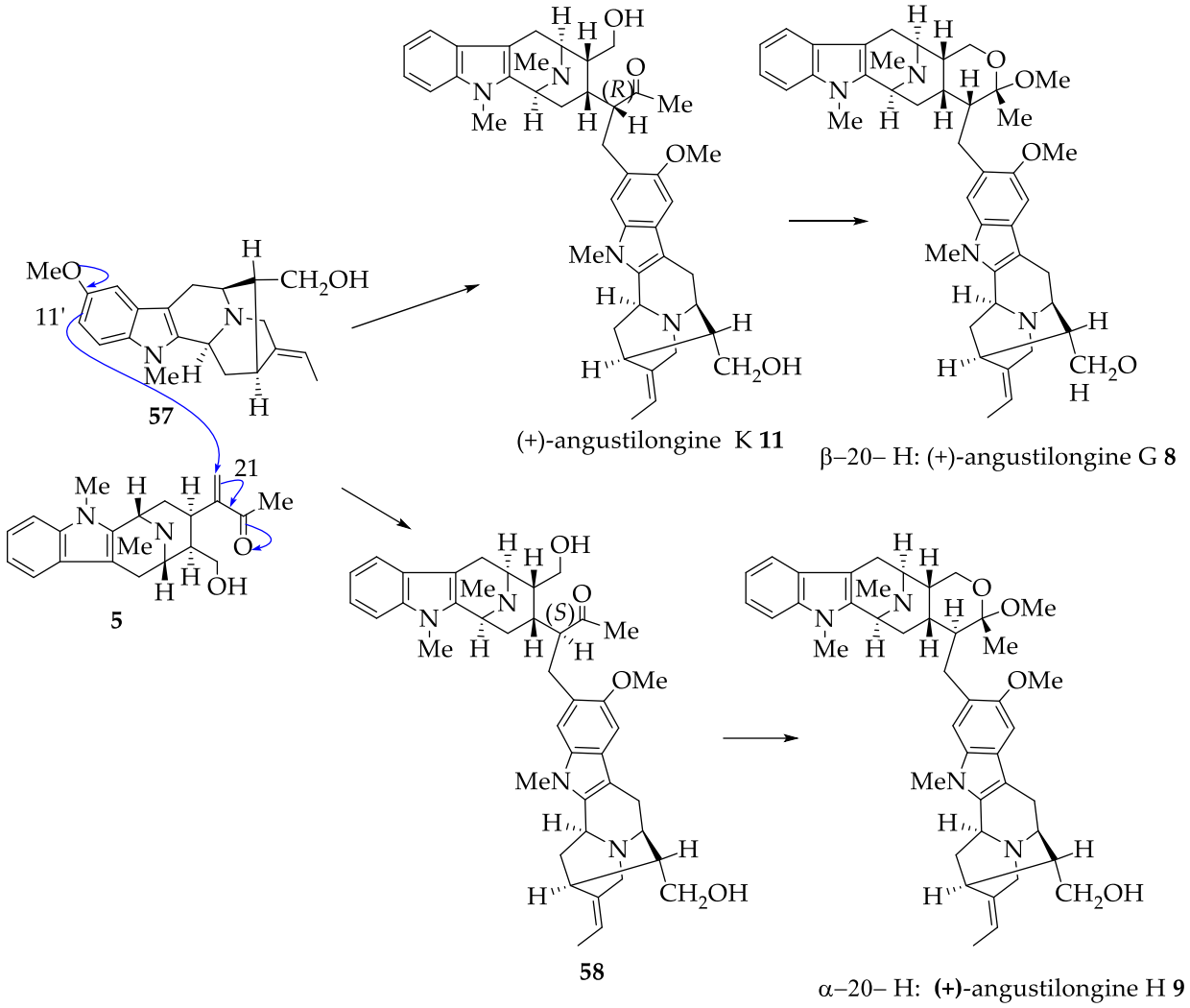


Figure 1.1. Proposed biogenetic pathway to (+)-angustilongine G (8) and (+)-angustilongine H (9).

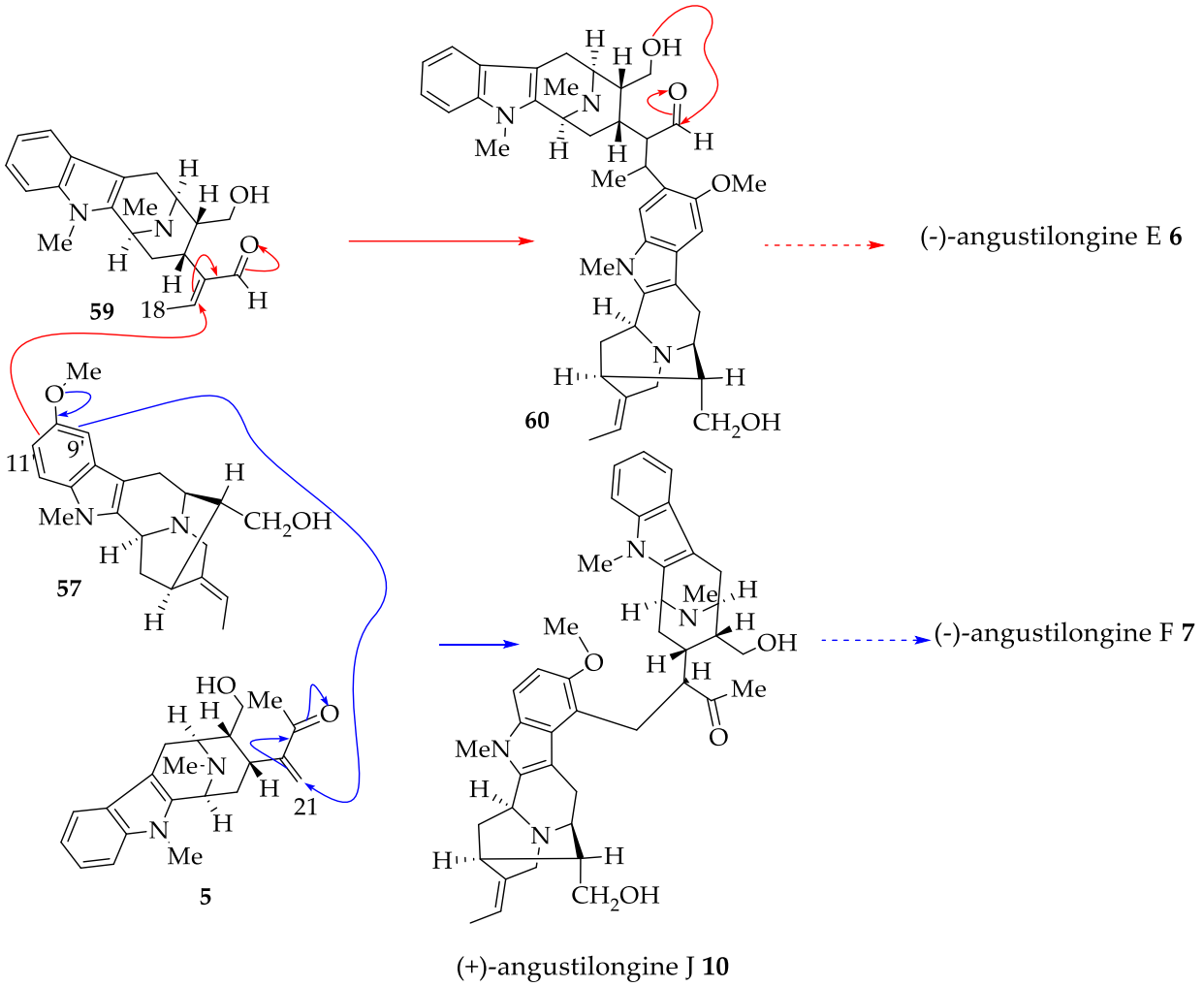
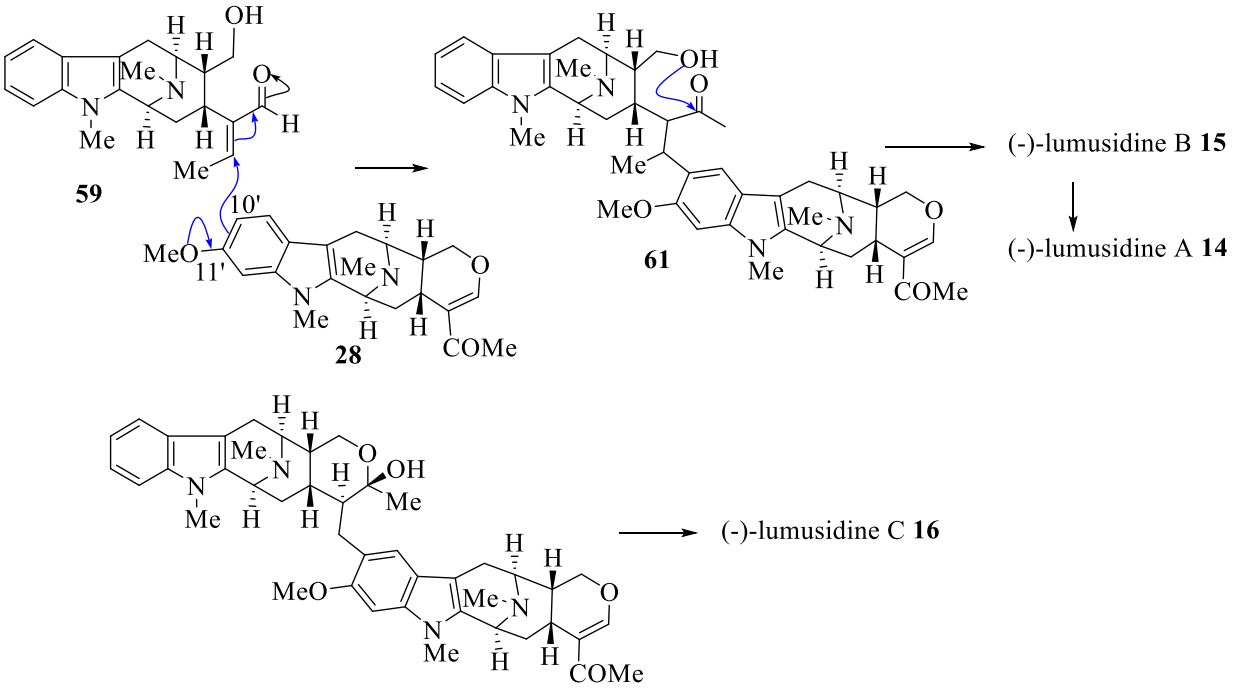


Figure 1.2. Proposed biogenetic pathway to (−)-angustilongine E (6), (−)-angustilongine F (7), and (+)-angustilongine J (10).

4.2. Plausible biogenetic pathway to (-)-lumusidines A-D (14–17).

The conjugate addition of the C-10′ carbon atom of alstophylline **28** by a Michael reaction onto the α, β unsaturated aldehyde **59** (E-ring opened talcarpine derivative) could potentially give hydroxy ketone bisindole alkaloid **61** (**Figure 1.3**). Alcohol **61** on subsequent closing of the E-ring to form a hemiacetal gives (-)-lumusidine B **15**, which after dehydration, gives (-)-lumusidine A **14**. Similarly, the C-12′ carbon atom of alstophylline monomer **28** could add to the α, β

unsaturated macroline counterpart **5** to furnish a hydroxy ketone (not shown). The cyclization of the hydroxy ketone in a similar way to give a hemiacetal **62** would follow. Subsequently, the dehydration of hemiacetal **62** would likely form lumusidine D **17**. The lumusidine C **16** is assumed to be an artifact formed from hemiacetal **63** (a closed form of (-)-perhentinine **39**) as ethanol was used during the extraction [15]. However, again this biosynthetic pathway could occur just as likely via a Friedel–Crafts alkylation of the oxonium ion of **59** (cyclization followed by loss of water) to the olefin of precursor **28** (see **Figure 5** with representative examples for (+)-macralstonine **24** and (+)-lumutinine A **18**) [3].



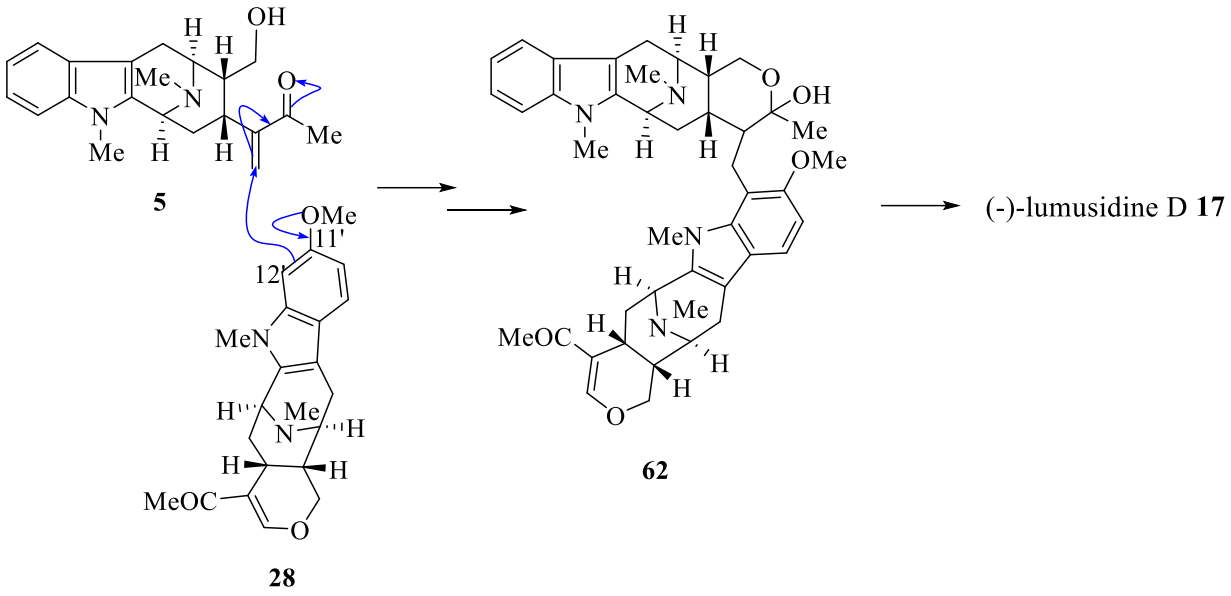
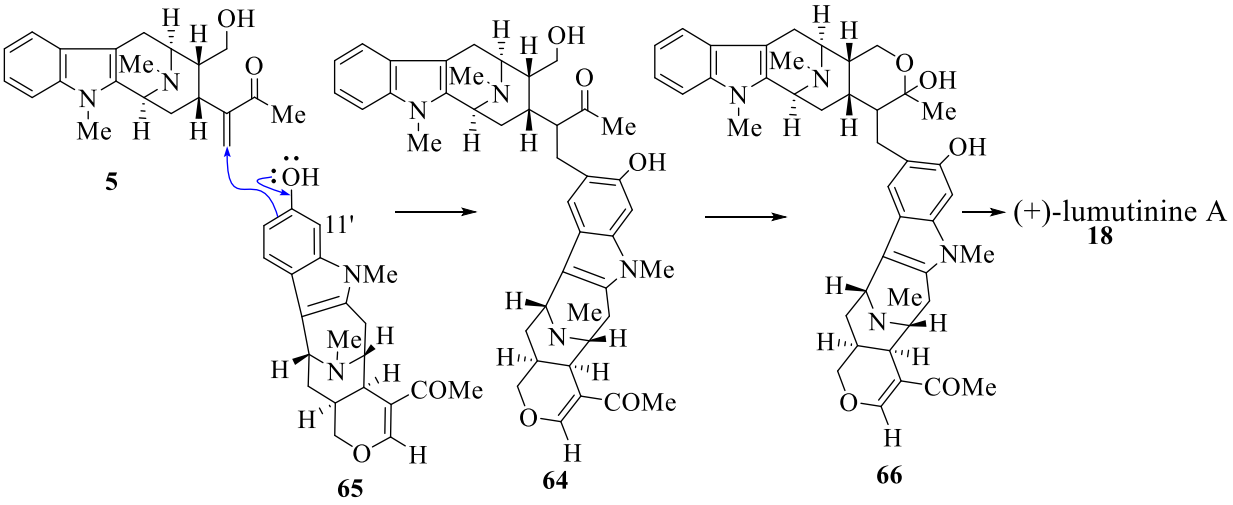


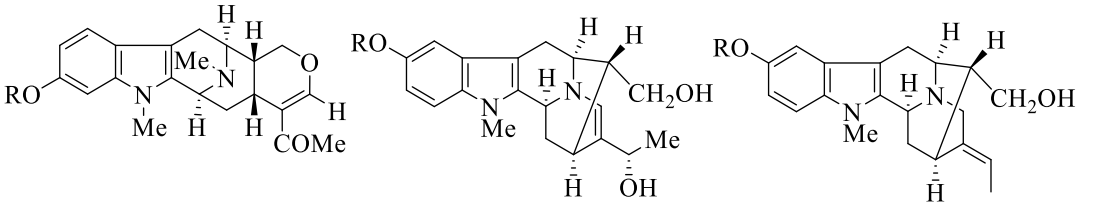
Figure 1.3. Putative biogenetic pathway to (-)-lumusidines A–D (14–17).

4.3. Proposed biogenetic pathway to lumutinines A–D (16–19).

The hydroxy ketone **64** could be formed by Michael addition of the C-10' carbon atom of alstophylline **65** onto the olefinic moiety of macroline **5** (**Figure 1.4**) [23]. The cyclization of the hydroxy ketone would give the hemiketal **66,** which on ketalization furnishes (+)-lumutinine A **18**. Likewise, Michael addition by C-12' of **67**, C-9' of **68,** and C-11' of **69** (**Figure 1.4**) onto macroline **5** yields (-)-lumutinine B **19**, (+)-lumutinine C **20**, and (+)-lumutinine D **21,** respectively [23]. Again, the Friedel–Crafts alkylation of the oxonium ion of **65** (cyclization followed by loss of water) is just as likely (see **Figure 1.5** with representative examples for (+)-macralstonine **24** and (+)-lumutinine A **18**) [3].



Putative biogenetic pathway to (+)-lumutinine A **18**



Precursors (**67-69**) for the putative biogenetic pathway to lumutinines B- D (**19-21**), respectively, via the Michael approach.

Figure 1.4. Putative biogenetic pathway to lumutinines A–D (16–19).

4.4. Possible alternative mechanism of bisindole formation of (+)-lumutinine A (16) and (+)-macralstonine (24) as representative examples via a Friedel–Crafts alkylation process, as suggested by Fukuyama.

In addition to the Michael addition process described above, there is another potential mechanism for the coupling of ring-A oxygenated macroline-type alkaloids with macroline **5** that involves a Friedel–Crafts alkylation process stabilized by an oxonium ion [6]. As shown in **Figure**

1.5, an acid-catalyzed intramolecular cyclization of macroline **5** by nucleophilic attack of the C-19 hydroxyl function onto the carbonyl carbon atom in 1, 2-addition fashion would furnish the cyclic hemiacetal **70**. The loss of a water molecule would generate an oxonium ion species (**71a** or **71b)**. At this stage, an electrophilic attack of the electron-rich aromatic ring of 11-methoxy macroline **67** via the C-10 carbon atom onto the olefin in **71a** would generate a cyclic enol ether **72**. This cyclic hemiacetal could undergo isomerization, generating an oxonium ion intermediate **73** only to be attacked by water to generate the cyclic ether (as in macralstonine **24**). Alternatively, the phenolic hydroxy group at the C-10 carbon atom in 10-hydroxy macroline (see **74**) could attack the oxonium ion to form a cyclic ketal (as in lumutinine A **16**). This type of mechanism was suggested by Fukuyama for some bisindoles isolated from *Alstonia* species [3].

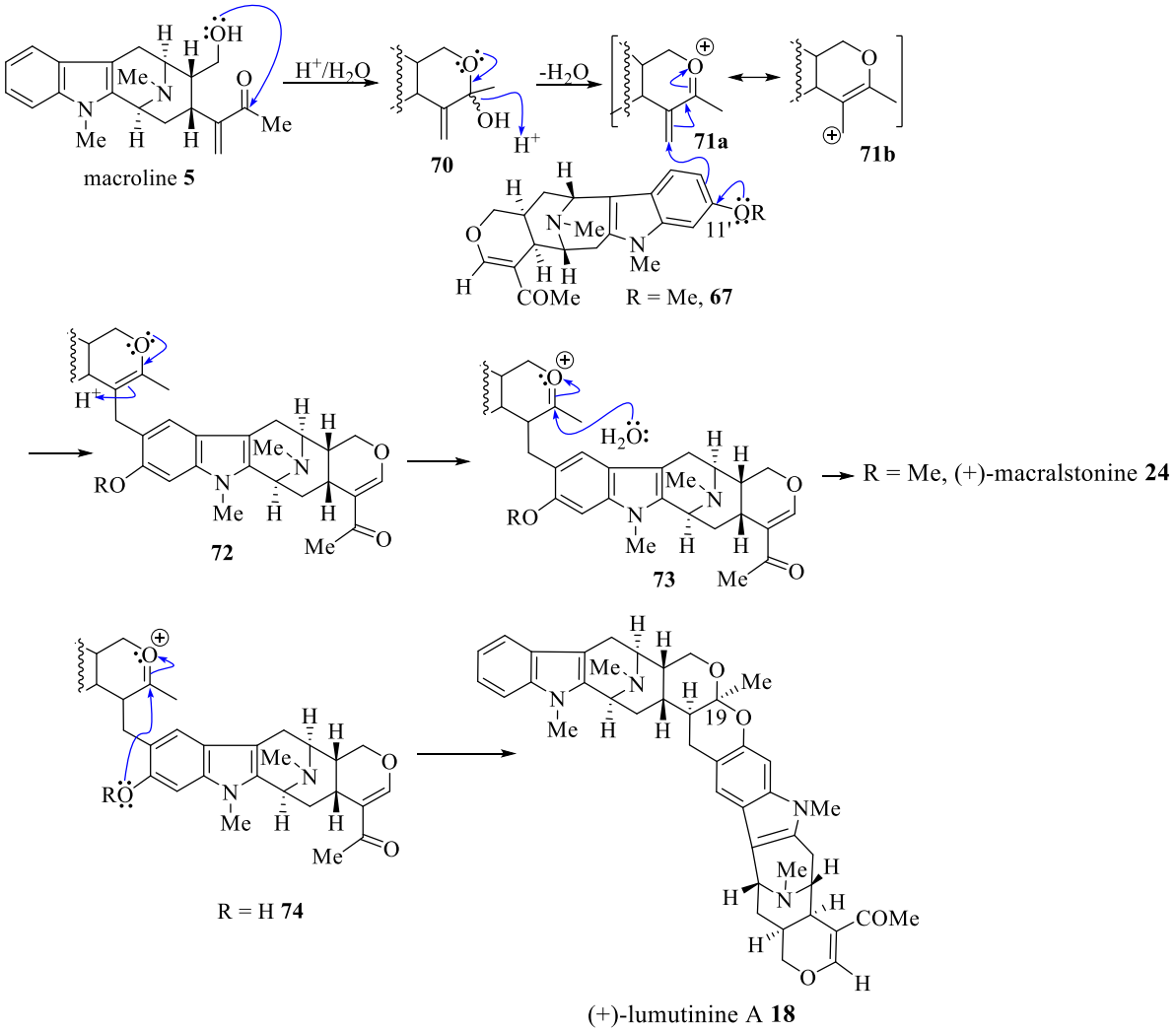


Figure 1.5. Possible alternative mechanism of bisindole formation via a Friedel–Crafts alkylation process for (+)-macralstonine (24) and (+)-lumutinine A (18), respectively, as representative examples.

4.5. Proposed biogenetic pathway to (-)-macrocarpamine (31).

(-)-Macrocarpamine **31**, a bisindole alkaloid comprised of two *Alstonia* monomeric units (+)-pleiocarpamine **32** and (-)-anhydromacrosalhine-methine **33,** was proposed to originate from (-)-anhydromacrosalhine-methine **33** and (+)-pleiocarpamine **32** by Hesse, Schmid *et al.* [43]. (-)-Anhydromacrosalhine-methine **33** and (+)-pleiocarpamine **32** are the degradation products of (-)-

macrocarpamine **31**. (-)-Anhydromacrosalhine-methine **33** was also obtained by dehydration of (+)-macrosalhine **75** in the study by Khan *et al.* (**Figure 1.6**) [3, 44].

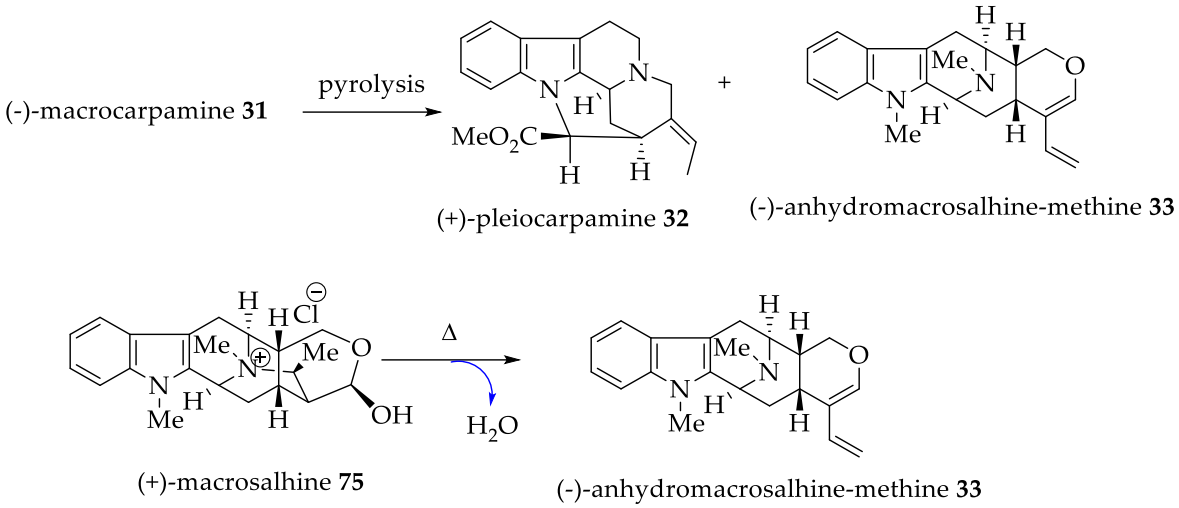


Figure 1.6. Pyrolysis of (-)-macrocarpamine (31) and macrosalhine (75) to generate key olefin (33).

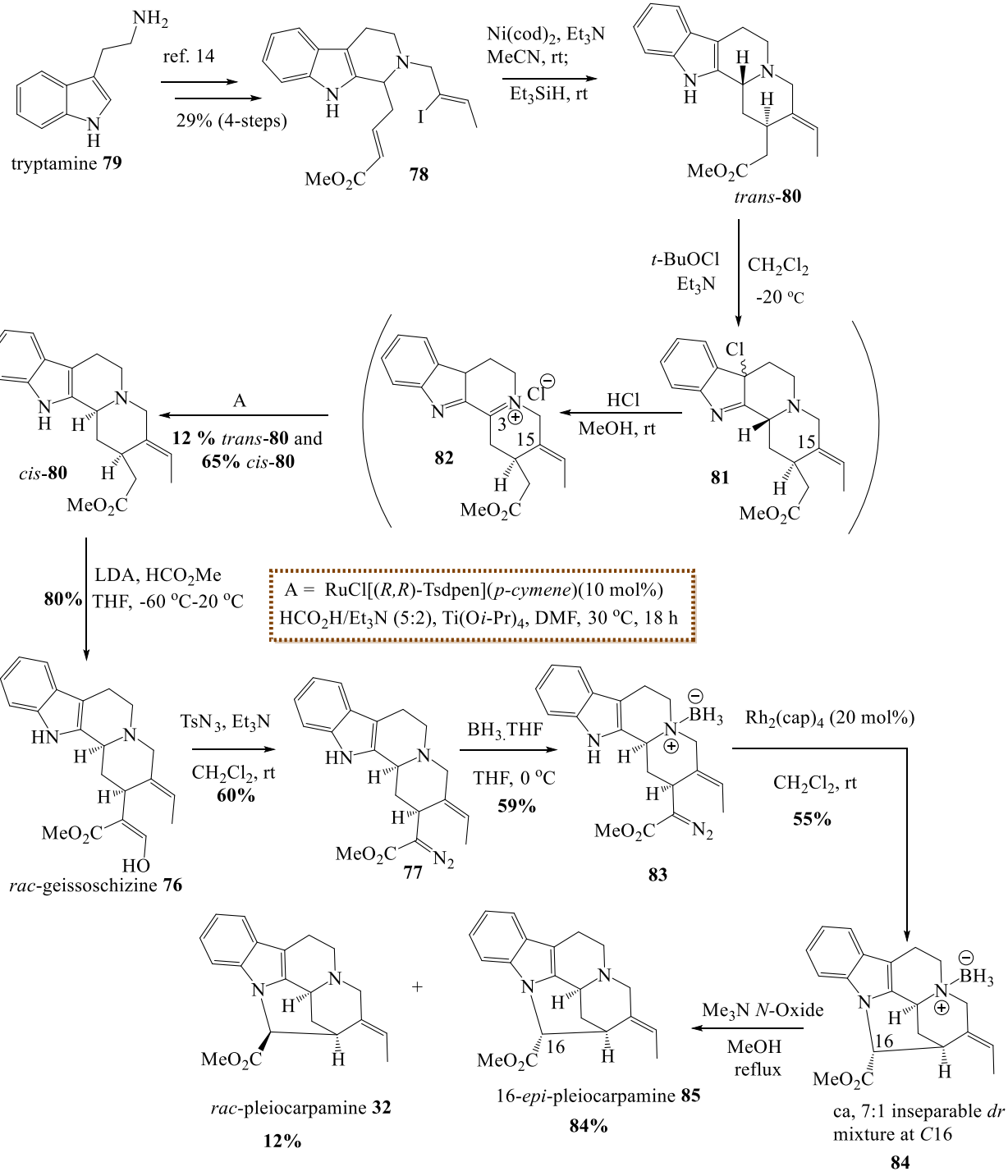
5. Synthesis of representative monomeric units of bisindole alkaloids from *Alstonia* species discussed herein, required for bisindole synthesis.

5.1. The total synthesis of (±)-pleiocarpamine (32).

(+)-Pleiocarpamine **32** has been isolated from various species of *Alstonia* [3, 29, 33, 45-48]. The unprecedented (+)-bipleiophylline (not shown) was found to contain two pleiocarpamine **32** units connected by utilizing an aromatic spacer (pyrocatechuic acid). The homo-dimer (+) bipleiophylline was potentially active against drug-sensitive, vincristine-resistant human KB and Jurkat cells, while its monomeric precursor (+)-pleiocarpamine **32** was not very active [49]. These findings again demonstrate the increased activity of dimeric alkaloids, as compared to their monomeric counterparts. The (+)-pleiocarpamine **32** was thought to be formed biosynthetically by

a ring-closing reaction between N1 and C16 of geissoschizine **76** [14]. Recently Sato *et al.* reported the total synthesis of the C-mavacurine type indole alkaloid, (±)-pleocarpamine **32** via a biomimetic synthesis [14]. A critical step, the direct cyclization between N1 and C16, was thought to be challenging because of the strain generated in the corynanthe pentacyclic framework. This may likely be the reason for the time it took to achieve the total synthesis of pleiocarpamine **32** by many groups since its isolation. In fact, (±)-2,7-dihydropleiocarpamine (not shown) was synthesized in 1993 by Jiménez *et al.* [50]. However, Sato *et al.* successfully cyclized the strained structure of **77** by a carbene N-H insertion reaction between the N1 and C16 bonds (**Scheme 1.1**) [14].

The ester **78**, was prepared in four steps from tryptamine **79** in 29% overall yield [14, 51]. The subsequent reductive cyclization of ester **78** onto *cis*-ester **80** was carried out using $Ni(cod)_2$. However, at this step, the desired cyclized *cis*-ester **80** was formed as a minor product (31%) with the undesired *trans*-ester **80** (55%) predominating [14]. The undesired *trans*-ester **80** was first treated with tert-butyl hypochlorite and triethylamine at –20 ℃ to obtain intermediate **81**, which on further reaction with hydrochloric acid in methanol at room temperature furnished iminium intermediate **82** [14]. Sato *et al.* screened several reducing agents and reaction conditions to reduce the iminium intermediate **82** into the *cis*-ester **80.** The optimized condition for the reduction of the iminium intermediate employed by Sato *et al.* was a Noyori catalyst and formic acid/triethylamine (5:2) mixture with titanium tetra-isopropoxide (at 30 ℃) to yield the desired *cis*-ester **80** as a major product (*cis*/*trans* ratio 5:3.1) [14]. The *cis*-ester **83** was converted into (±)-geissoschizine **76** in 80% yield using an excess of lithium diisopropylamine and methyl formate. The treatment of (±)-geissoschizine **79** with tosyl azide and triethylamine furnished diazo compound **77** in 60% yield [14].



Scheme 1.1. Synthesis of *rac*-pleiocarpamine (32) and 16-epi-pleiocarpamine (85) by Sato *et* al.

While exploring a suitable catalyst for the metal carbenoid cyclization reaction, the $Rh_2(cap)_4$ and $Rh_2(esp)_2$ catalyzed reactions lead to decomposition of substrate **77** [14]. Only $Rh_2(OAc)_4$

furnished the distinguishable but unanticipated product (not shown) via a D-ring expansion reaction [14]. At room temperature, no reaction happened while employing the rhodium complex $(PPh_3)_3RhCl$ or the copper catalyst $Cu(MeCN).BF_4$ [14]. Moreover, the use of the JohnPhosAu(MeCN)SbF_6 catalyst was also unsuccessful because it formed the D-ring expanded product (not shown) with β-hydride elimination (not shown) [14]. Sato *et* al. predicted that a modification of the lone pair on the *N*(4) of the compound **77** would form a *cis*-quinolizidine ring making cyclization more favorable by decreasing the distance between *N*1 and C16. This was the key to the first total synthesis of (±)-pleiocarpamine **32**. Thus, substrate **77** was modified to borane salt **83** by using the BH_3–THF complex to react at the N_b nitrogen atom [14]. Finally, cyclization via a carbene N–H insertion was accomplished by treatment of cyclization precursor **83** with $Rh_2(cap)_4$ (20 mol %) at room temperature, and the products so obtained were an inseparable diastereomeric mixture **84** at C_{16} (ca,7:1) in 55% yield [14]. To remove the borane protecting group, the diastereomeric mixture **84** was refluxed with trimethylamine *N*-oxide in methanol, which furnished (±)-pleiocarpamine **32** and epi-pleiocarpamine **85** [14].

5.2. Biosynthetic relations among the sarpagine/macroline/ajmaline family of alkaloids.

Sarpagine, macroline, and ajmaline indole alkaloids are biosynthetically and structurally related (**Figure 1.7**) [10]. We herein follow the biogenetic numbering system of LeMen and Taylor to discuss their potential formation [52]. The sarpagine series consists of attachment of the C-21 carbon atom to the *N*(4) bond, while the macroline series lack this bond. The stereocenters in the sarpagine alkaloids at C-3 (*S*), C-5 (*R*), C-15 (*R*), and C-16 (*R*) are identical to the macroline series at the respective carbon atoms. The ajmaline series also contain a C-7 and C-17 carbon atom linkage. In comparison with the ajmaline series, the sarpagine family at C-16 is R but antipodal in the ajmaline series. Both the sarpagine and the ajmaline series consist of the characteristic

quinuclidine ring and the C-5 and C-16 carbon atom linkage. Sarpagine and ajmaline alkaloids both contain the characteristic C-21 and N(4) bond [10, 53]. Stöckigt *et al.* reported the conversion of 16-epi-vellosimine **86** (sarpagine) into the vinorine **87** (ajmaline) structure (**Figure 1.7**) by employing the acetyl CoA-dependent vinorine synthase enzyme [54-57]. The macroline and sarpagine alkaloids are biosynthetically related, as shown in **Figure 1.7**. Either of the β-keto quaternary ammonium intermediates **88** or **89** can be furnished by 1, 4 Michael addition of the *N*(4) nitrogen atom of macroline onto the α, β-unsaturated carbonyl system **5** or **90** at C-21. Similarly, α-hydroxy quaternary ammonium compounds **91** and **92** can be formed by direct 1, 2 addition of the *N*(4) nitrogen atom to the C-19 carbonyl carbon of **5** and **90** [10]. In contrast, the retro-Michael reaction of TBS protected intermediate **89,** followed by removal of the silyl protecting group converted sarpagine **89** into the macroline unit **5** in the studies from LeQuesne *et* al. [58] and Cook *et* al. [59]. The sarpagine/macroline/ajmaline group of indole alkaloids have been isolated principally from higher plants, including the Apocynaceae family and the genera *Alstonia* and *Rauwolfia* [10]. The intriguing molecular complexity, interconversions, and their divergent biological activity prompted the successful syntheses of several of these indole alkaloids [4, 60] and bisindole alkaloids [45,64,65] as mentioned earlier.

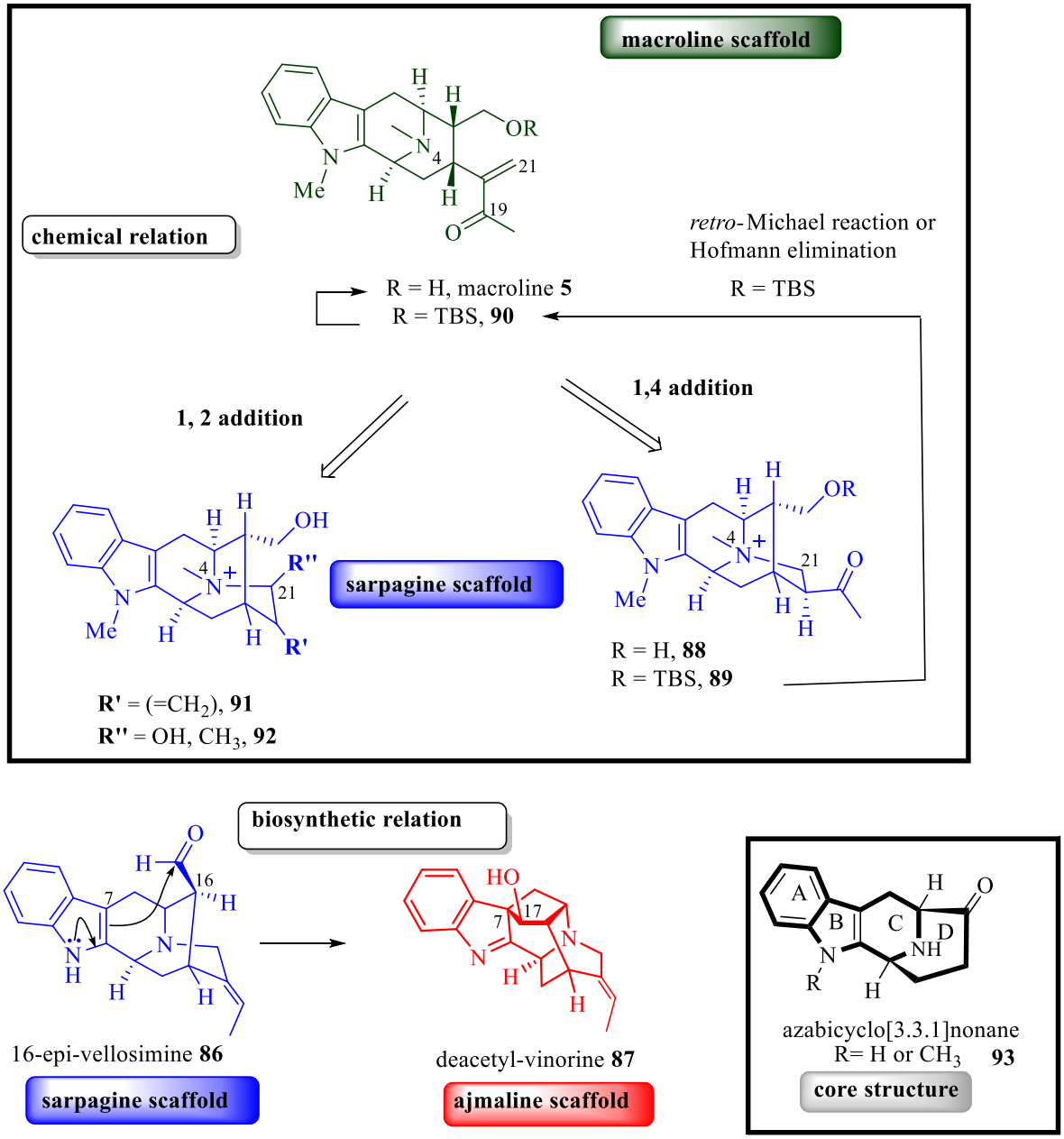
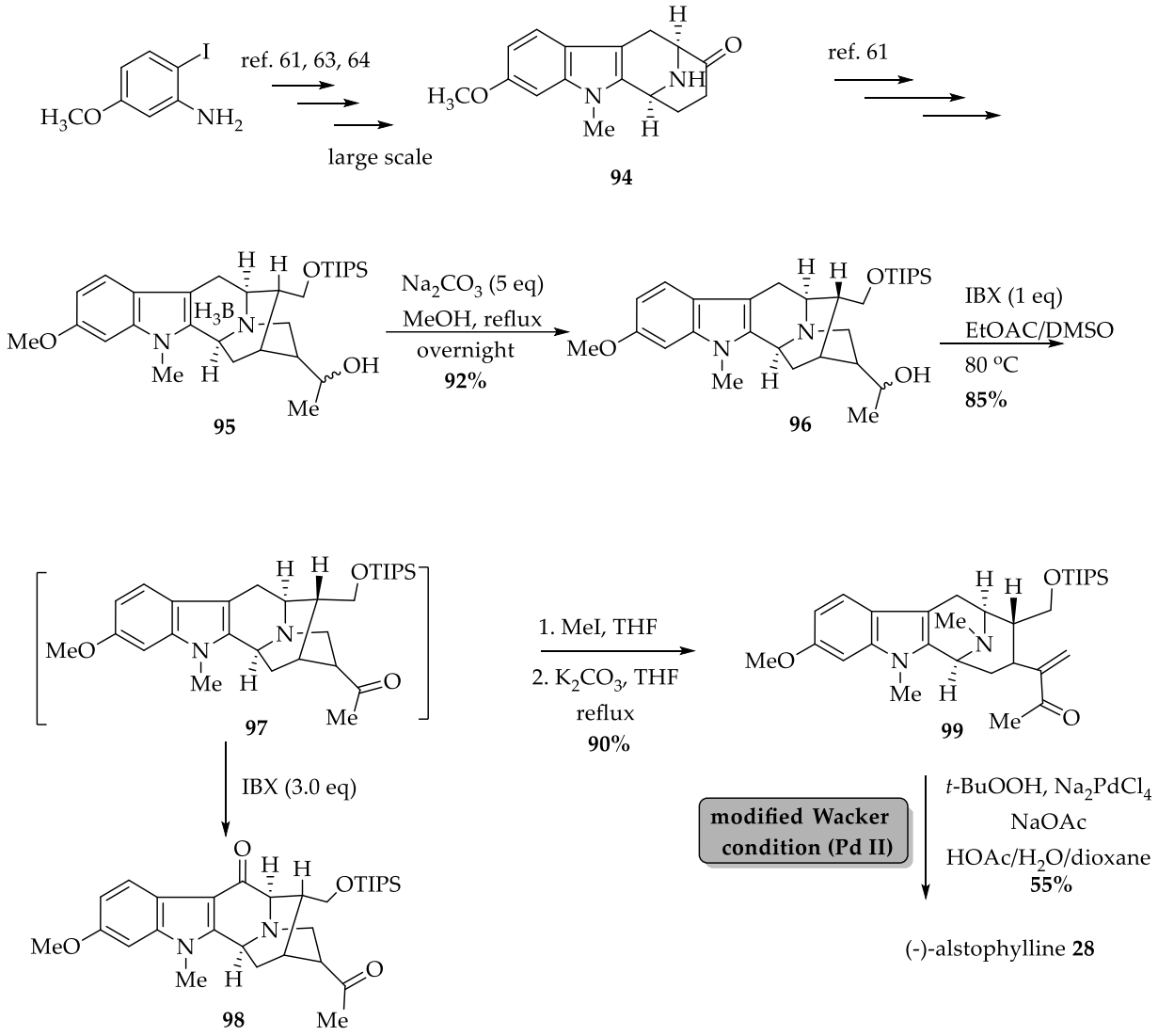


Figure 1.7. Abbreviated chemical and biosynthetic relations among the sarpagine/macroline/ajmaline family of alkaloids.

5.3. Synthesis of monomeric macroline units employed for the synthesis of bisindole alkaloids.

5.3.1. An improved total synthesis of (-)-alstophylline (28).

(-)-Alstophylline **28** has been isolated from various *Alstonia* species including *A. angustifolia* [33], *A. glabriflora* Mgf. [28], and *A. macrophylla* [30,67,68]. Liu *et* al. accomplished a large-scale enantiospecific total synthesis of intermediates, which later resulted in the total synthesis of (-)-alstophylline **28** [61]. Later, Liao *et* al. improved the total synthesis of (-)-alstophylline **28** employing modified Wacker-Tsuji reaction conditions, which provided a faster route for synthesis of macroline-related indole alkaloids (**Scheme 1.2**) [62]. The 6-methoxy tetracyclic ketone **94** was synthesized employing the method using the published procedures [61, 63, 64], which later was converted into the N_b-BH_3 adduct **95** using the method developed by Liu *et* al. earlier [61]. The N_b-BH_3 adduct **95** so formed was refluxed with sodium bicarbonate in methanol overnight to get alcohol **96** in 92% yield. One equivalent of the 2-iodozybenzoic acid (IBX) converted (at high temperature) the alcohol functional group in **96** into the ketone **97** in 85% yield. The addition of three more equivalents of IBX at reflux permitted the formation of the new alkaloid 6-oxoalstophylline **98**. The N_b-quaternization of ketone **97** was carried out using MeI/THF, which was followed by a retro-Michael reaction in the presence of K_2CO_3/THF to furnish α, β-unsaturated ketone **99** in 90% yield. Finally, (-)-alstophylline **28** was obtained using the Wacker-related process (Pd II) modified by Tsuji *et* al. [65] and Liao/Cook *et* al. [62] from ketone **99** in 55% yield. Importantly, the modified Wacker-related process is also an improved route to several indole alkaloids with the enone system including alstonerine **100** [3]. In addition, the key oxidation reaction provides a shorter route from **97** to 6-oxoalstophylline **98**.

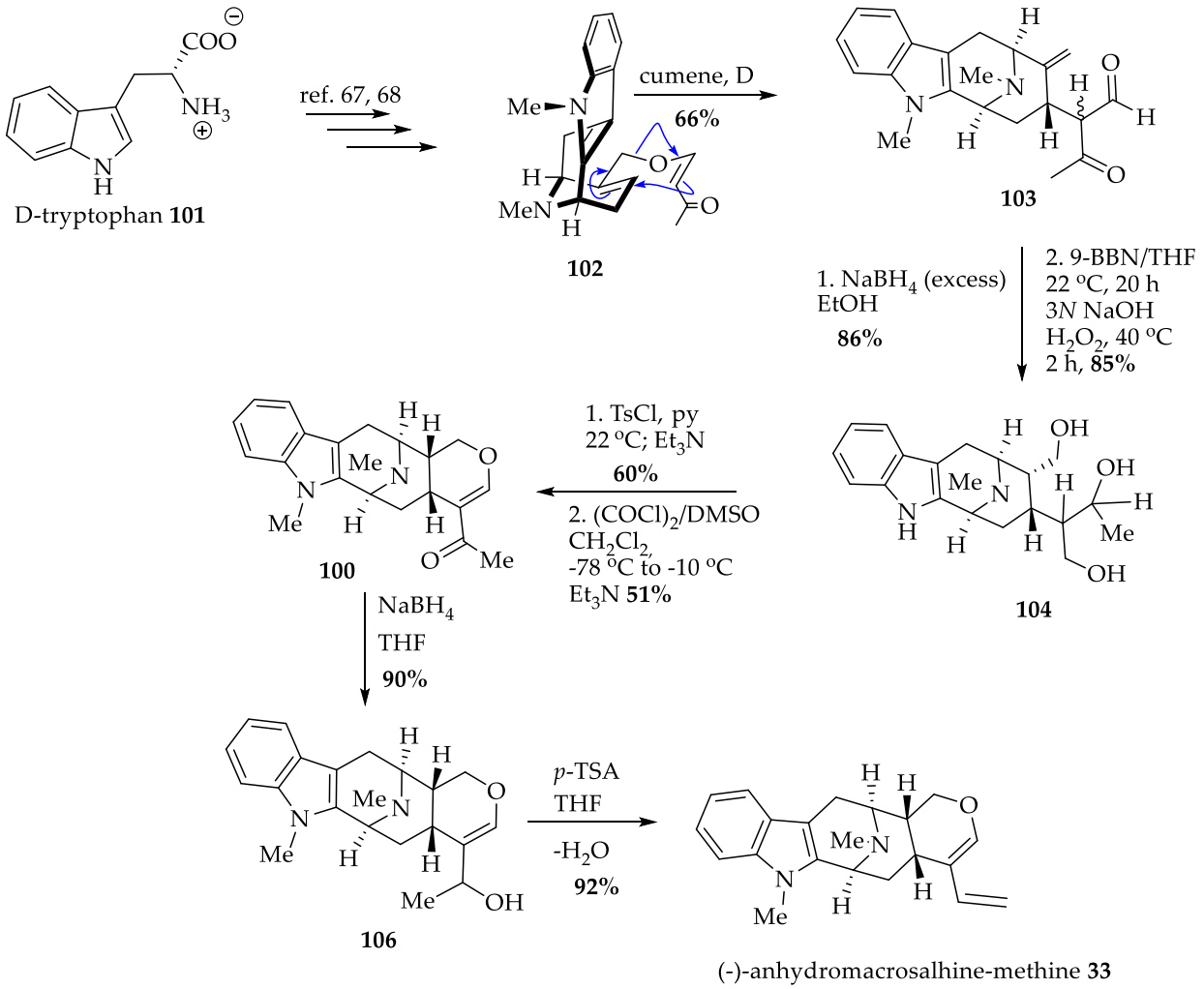


Scheme 1.2. An improved total synthesis of (-)-alstophylline (28) using the modified Wacker (Pd II) conditions.

5.3.2. Enantiospecific total synthesis of (-)-anhydromacrosalhine-methine (33) via the asymmetric Pictet–Spengler reaction.

In a partial synthesis, Gan *et* al. [66] prepared (-)-anhydromacrosalhine-methine **33** via degradation of natural (+)-ajmaline by following the improved procedure of Sakai *et* al. [66]. In addition to the semisynthesis of (-)-anhydromacrosalhine-methine **33** for comparison purposes,

Gan *et al.* also accomplished the total synthesis of **33** starting from D-tryptophan **101** via the asymmetric Pictet–Spengler reaction (>98% ee) (**Scheme 1.3**) [41]. The enone ether **102** was synthesized employing the procedures developed in Milwaukee [67, 68]. The β-dicarbonyl compound **103** was prepared in 66% yield from a stereoselective (α-face) Claisen rearrangement of olefin **102** at high temperature (175 °C) [41]. The reduction of the β-dicarbonyl compound **103** that resulted with $NaBH_4$ provided the diol (not shown), which subsequently underwent a stereospecific hydroboration–oxidation reaction and was converted into triol **104**. (-)-Alstonerine **100** was furnished by the regioselective cyclization reaction of the monotosylate of triol **104**, which was followed by the improved Swern oxidation in 51% yield, accompanied by dihydroalstonerine **105** (not shown in **Scheme 1.3**) in 31% yield [41, 68]. (-)-Alstonerine **100**, upon reduction with $NaBH_4$, furnished allylic alcohol **106** in 90% yield, which later was dehydrated in the presence of p-toluenesulfonic acid to afford (-)-anhydromacrosalhine-methine **33** in 92% yield [41].



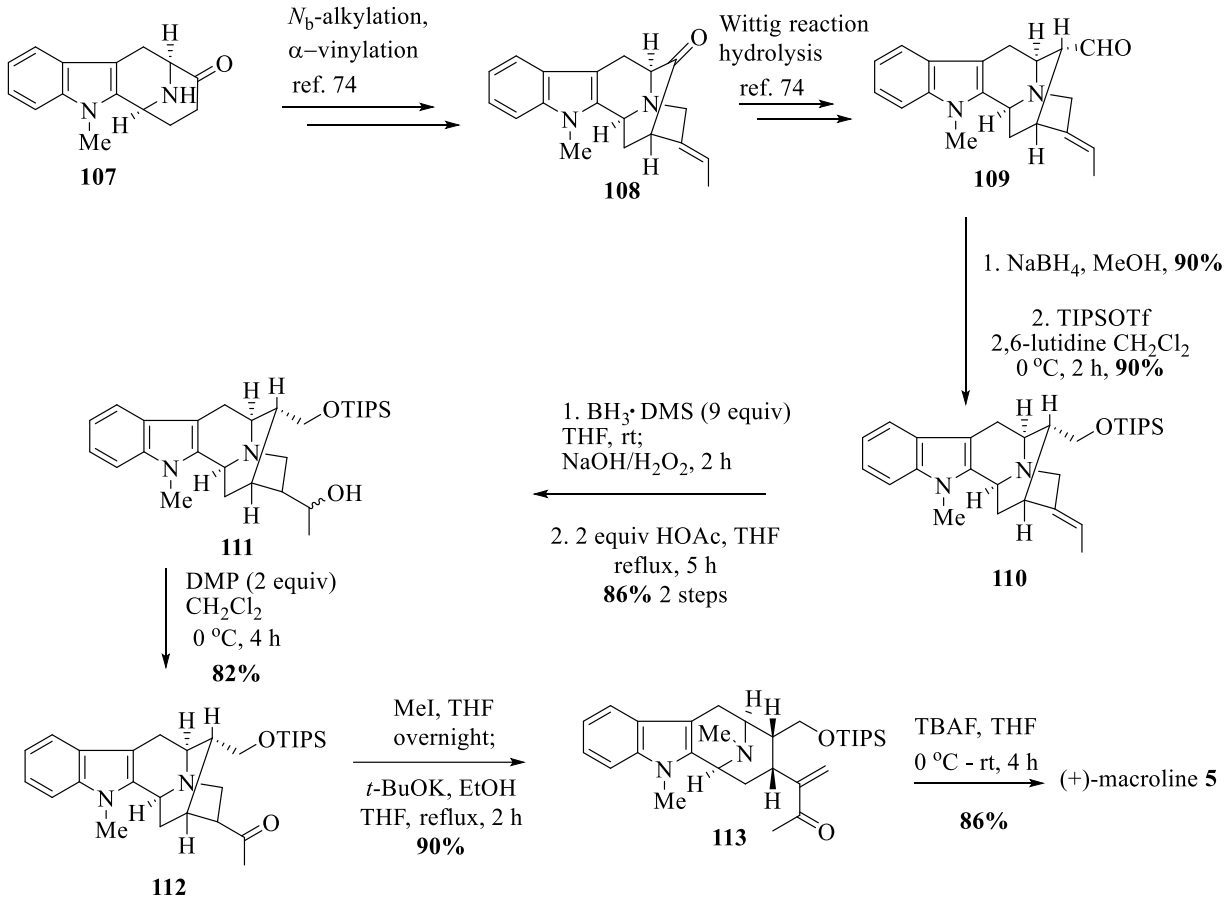
Scheme 1.3. Enantiospecific total synthesis of (-)-anhydromacrosalhine-methine (33) via the asymmetric Pictet–Spengler reaction.

5.3.3. Improved synthesis of (+)-macroline 5.

Alkaloids such as (-)-alstonerine **100**, (+)-alstonisidine **3**, and (-)-alstophylline **28** are believed to originate from (+)-macroline **5** as their biogenetic precursor; however, the isolation of (+)-macroline **5** has not yet been reported [3]. The synthesis of (+)-macroline 5 was improved by Liao *et* al. [76], whereas the first biomimetic synthesis of (+)-macroline **5** was carried out by LeQuesne *et* al. in 1980 [58], following the procedure of Gorman *et al.* [69]. Neukomm *et* al. elucidated the absolute configuration of macroline **5** with X-ray crystallographic data [70]. Bi *et* al. accomplished

the enantiospecific total synthesis of (+)-macroline **5** [71], which was indistinguishable from the spectral data compared to the natural one [72]. The formal synthesis of (+)-macroline **5** was also reported by Kwon utilizing a phosphine-catalyzed annulation process (not shown) [73].

Later, Liao *et al.* improved the total synthesis of (+)-macroline **5** in higher overall yield and fewer steps**.** The tetracyclic ketone **107**, obtained on a large scale by following the procedure developed in Milwaukee, which underwent N_b-alkylation with (*Z*)-1-bromo-2-iodo-2-butene (not shown), was followed by a palladium catalyzed stereospecific α-vinylation to provide pentacyclic ketone **108** (**Scheme 1.4**) [74]. The ketone **108** underwent the usual one-carbon homologation via a Wittig olefination, and this was followed by acidic hydrolysis to obtain the pentacyclic aldehyde **109**. The aldehyde functional group in **109** was reduced using sodium borohydride to provide the first enantiospecific synthesis of (+)-affinisine (not shown) in 90% yield**.** Then triisopropylsilyl (TIPS) triflate and 2,6-lutidine were used to protect the primary alcohol of (+)-affinisine as a TIPS ether **110** in 90% yield. The TIPS ether **110** was employed for the hydroboration–oxidation reaction, which furnished the desired secondary alcohol **111** in 86% yield. The alcohol **111**, so formed, was oxidized to a ketone **112** using the Dess-Martin periodinane reagent in 82% yield. The ketone **112** was quaternized at the N_b-nitrogen atom by treatment with iodomethane in THF at 0 $^{\circ}$C. The stable macroline equivalent **113** was obtained after treatment of N_b-methyl iodide salt with potassium tert-butoxide in ethanol, after which it was treated with tetrabutylammonium fluoride to furnish macroline **5** in **86%** yield (99% *ee*) after removal of the TIPS group [74].

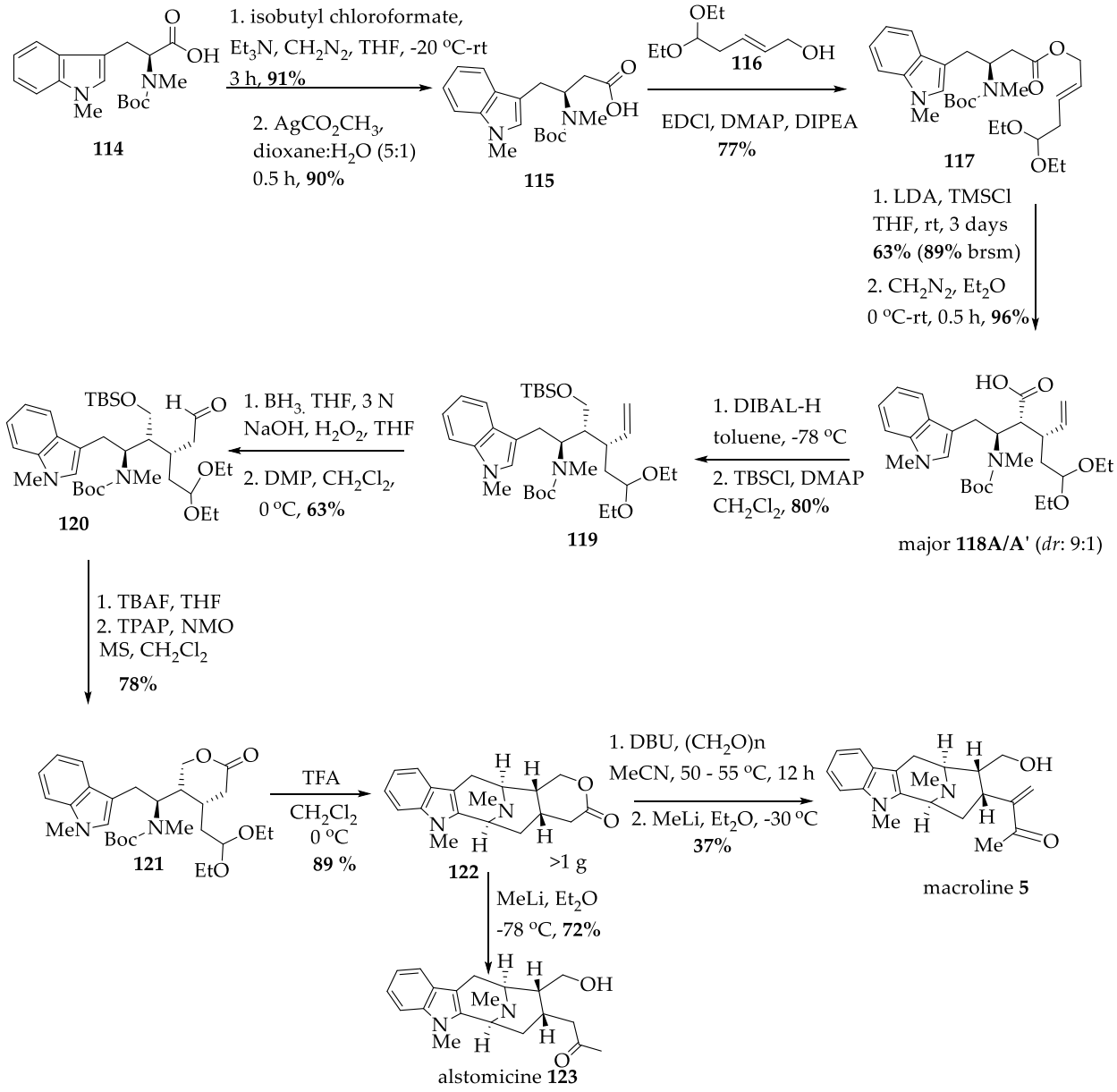


Scheme 1.4. Improved synthesis of (+)-macroline (5).

5.3.4. Stereospecific access to the macroline core (5).

Recently, Kadam *et* al. developed another route to the pentacyclic core of macroline **5**-related alkaloids. Starting from commercially available L-tryptophan (not shown), the core architecture of macroline **5** was accessed via an Ireland–Claisen rearrangement (ICR)/Pictet–Spengler cyclization protocol (**Scheme 1.5**) [75]. The L-tryptophan derivative **114** was subjected to Arndt–Eistert conditions to implement a one-carbon homologation to furnish acid **115**. The acid **115** was subsequently coupled with allylic alcohol **116** under standard amide coupling conditions to furnish the allylic ester **117**, the substrate for the Ireland–Claisen rearrangement. The allylic ester **117** produced the corresponding carboxylic acids (not shown) under ICR as an inseparable mixture that was converted into the corresponding esters **118A/A'** by treating the ICR mixture. The esters were isolated in a 9:1 ratio of diastereomers that was separable. The ester function in **118A** was reduced by DIBAL-H, and the so formed primary alcohol was protected with a TBS group to provide silyl ether **119**. The olefin **119** was subjected to a hydroboration–oxidation sequence and this was followed by oxidation of the so formed alcohol with Dess-Martin periodinane to furnish aldehyde **120**. Upon desilylation with TBAF, the alcohol reacted intramolecularly with the proximate aldehyde function forming the corresponding hemiacetal (not shown). Subsequent tetra-propylammonium perruthenate (TPAP)/N-methylmorpholine N-oxide (NMO) mediated oxidation of the hemiacetal furnished δ-lactone **121**. Deprotection of the Boc protecting group and hydrolysis of the acetal was done under acidic conditions with TFA setting up the conditions for an intramolecular Pictet–Spengler cyclization that furnished the pentacyclic core structure **122** of the macroline alkaloids. The exomethylene was introduced by reacting **122** with the formaldehyde equivalent in the presence of 1,8-di-azabicyclo[5.4.0]undec-7-ene (DBU). This was followed by

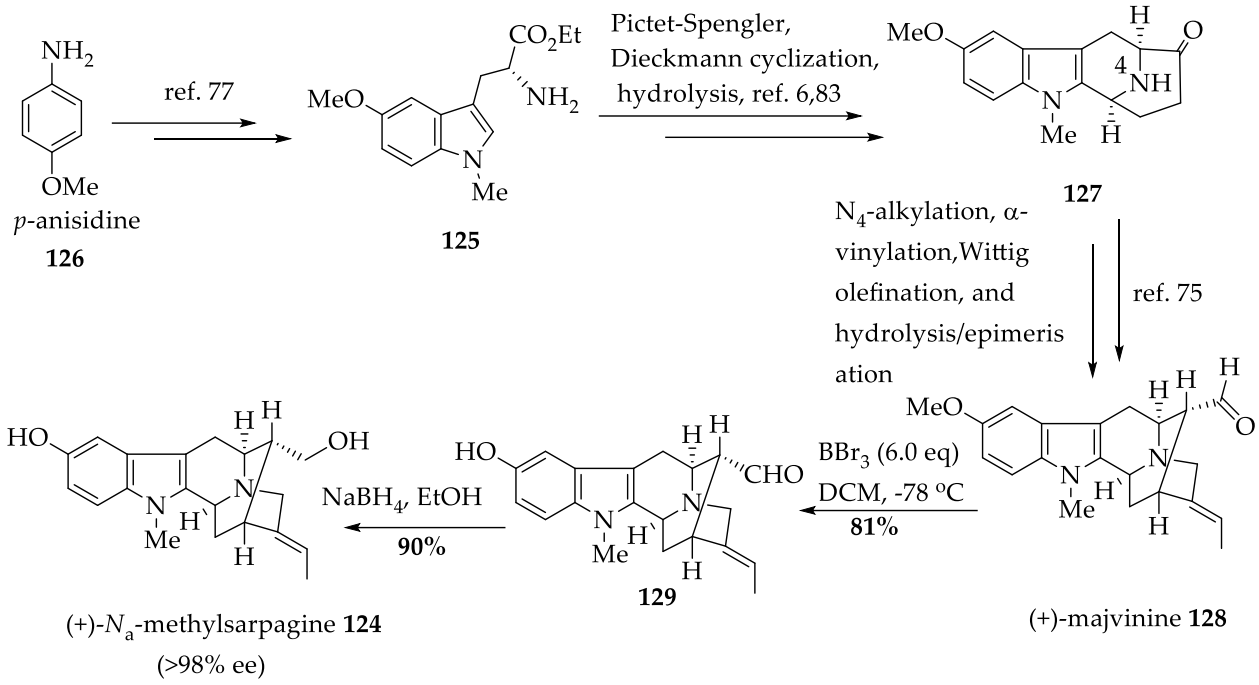
the addition of MeLi to furnish macroline **5**. On the other hand, alstomicine **123** was achieved by treating the lactone **122** with MeLi [75].



Scheme 1.5. Stereoselective total synthesis of macroline (5) and alstomicine (123).

5.3.5. Enantiomeric total synthesis of (+)-*N*a-methylsarpagine (124).

The alkaloid (+)-N_a-methylsarpagine **124** was isolated from the bark of *A. spectabilis* [28, 38], which is present as a monomeric unit in the (+)-macralstonidine **23** bisindole. The first total synthesis of (+)-N_a-methylsarpagine **124** was accomplished by Zhao *et* al. [76, 77]. The 5-methoxy-N_a-methyl D-(+)-tryptophan ethyl ester **125** was prepared on a large scale starting from commercially available p-anisidine **126** (**Scheme 1.6**). The 5-methoxy tetracyclic ketone **127** was furnished in high overall yield from ester **125** employing chemical conversions such as, N_b-benzylation, the asymmetric Pictet–Spengler reaction, diastereospecific Dieckmann cyclization,decarboxylation reaction, and catalytic debenzylation [3, 77]. Furthermore, 5-methoxy tetracyclic ketone **127** upon further usual transformations including N_b-alkylation, the Wittig olefination, hydrolysis/epimerization gave majvinine **128** in 98% *ee* [76, 77]. The 10-hydroxy indole **129** was furnished after the treatment of C-10 methoxy intermediate (+)-majvinine **128** employing six equivalents of BBr_3 in DCM at −78 °C. The subsequent reduction of the aldehyde group in intermediate **129** was effectively carried out using sodium borohydride in ethanol to furnish (+)-N_a-methylsarpagine **124** in 90% yield [77].



Scheme 1.6. Enantiomeric total synthesis of (+)-majvinine (128) and (+)-N_a-methylsarpagine (124).

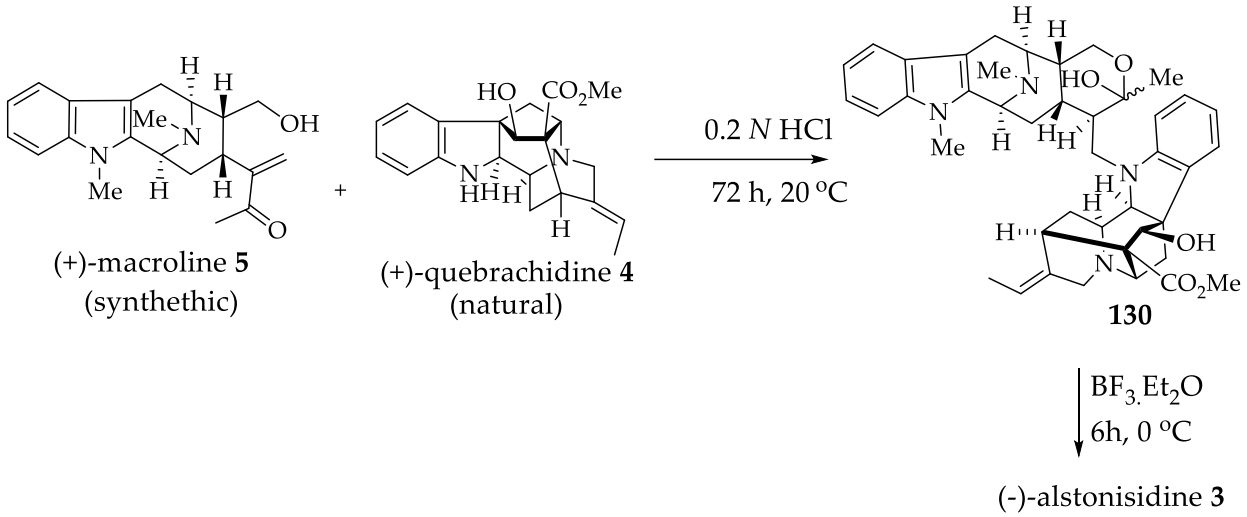
6. The synthesis of bisindole alkaloids.

6.1. Biomimetic partial synthesis of (-)-alstonisidine (3).

(-)-Alstonisidine **3** contains a (+)-quebrachidine **4** (ajmaline-type), and a (+)-macroline **5** piece as monomeric units. Both monomeric alkaloids were employed in the biomimetic partial synthesis of (-)-alstonisidine **3** by LeQuesne, Burke, and Cook [78]. The (+)-macroline **5** used in this partial synthesis was obtained after the degradation of villamine (not shown) by the method of Schmid *et* al. [72].

The hemiketal **130** was formed after the Michael reaction between the N_a-H function of a (+)-quebrachidine **4** and (+)-macroline **5** in the presence of 0.2 *N* HCl at 20 °C for 3 days (**Scheme 1.7**). The hemiketal **130** underwent an electrophilic substitution reaction (ortho to the amino group of (+)-quebrachidine **4**) after the treatment with BF_3 etherate at low temperature (0 °C) to furnish

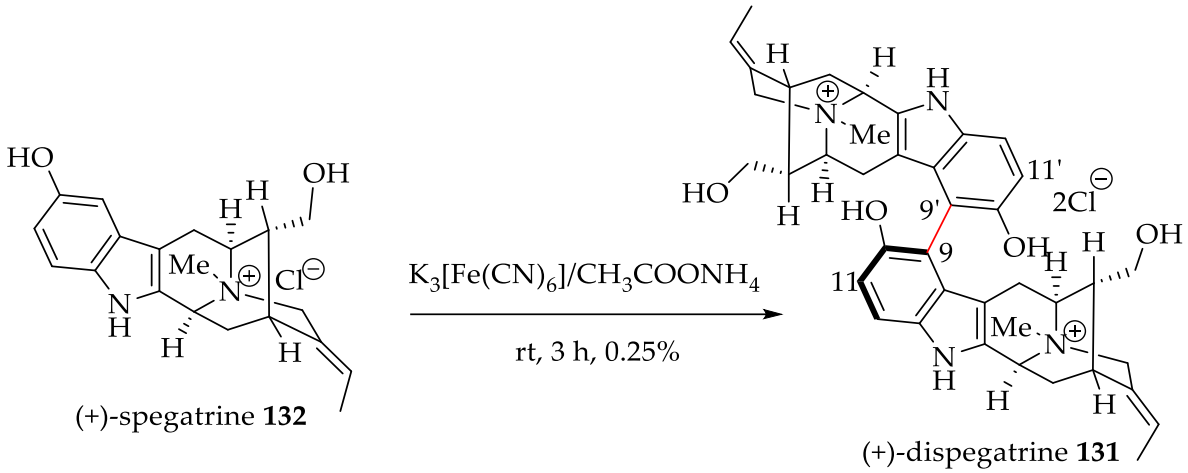
(-)-alstonisidine **3.** The spectral data of (-)-alstonisidine **3** were identical to those of naturally isolated (-)-alstonisidine **3** [34, 48].



Scheme 1.7. Biomimetic partial synthesis of (-)-alstonisidine (3).

6.2. Biomimetic partial synthesis of (+)-dispegatrine (131).

Although the focus of this review is bisindoles from *Alstonia* species, dispegatrine **131**, a hypotensive bisindole, is comprised of two sarpagine units. It is discussed here because some of the monomers such as sarpagine are commonly found in many *Alstonia* species. In the biomimetic partial synthesis of (+)-dispegatrine **131** by Yu *et* al., the monomer spegatrine **132** was subjected to an oxidative phenolic coupling (**Scheme 1.8**). Although the yield of this coupling was very poor, it served as proof of the concept that dispegatrine **131** may actually originate biosynthetically via oxidative phenolic coupling, although the chemical yield was 0.25%. This partial synthesis confirmed the structure of (+)-dispegatrine **131** [79]**.** However, no other diastereomer was observed, and the axial chirality across the C9-C9′ could not be confirmed. In addition, due to the lack of X-ray crystals, the isolation chemists could not assign the important axial chirality at C9-C9′ [79].

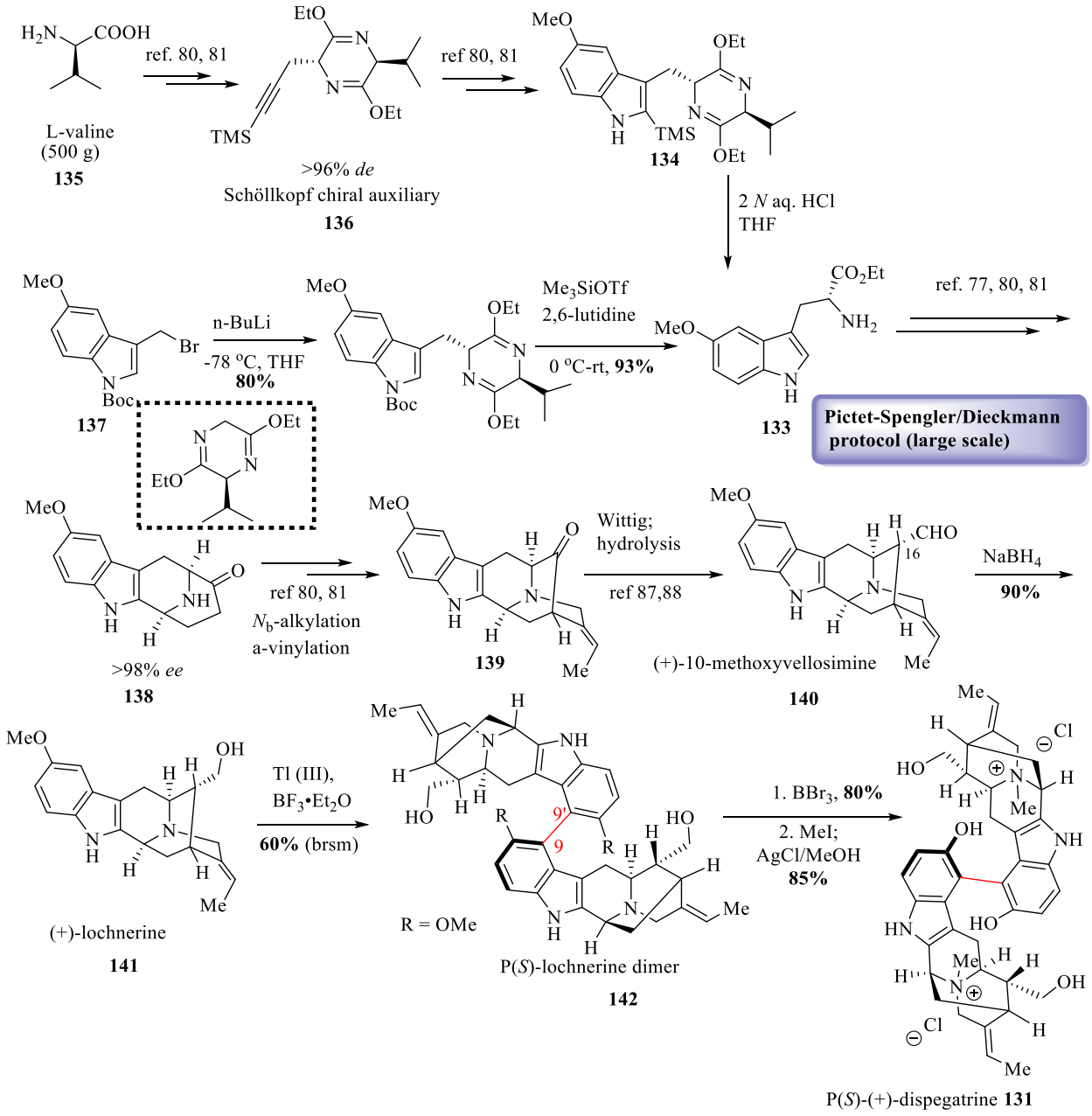


Scheme 1.8. Biomimetic partial synthesis of (+)-dispegatrine (131) by oxidative phenolic coupling by Yu *et* al. [79].

Enantiospecific total synthesis of (+)-dispegatrine (131) in >98% ee.

It was suggested that internal chiral induction was responsible for the atroposelectivity, which was exploited as an advantage in the first enantiospecific and convergent total synthesis of (+)-dispegatrine **131** from spegatrine **132** by Edwankar *et* al. [80, 81]. The total synthesis of (+)-dispegatrine **131** required the 5-methoxy tryptophan unit **133**, which was accessed via the general strategy for the synthesis of ring-A oxygenated D-tryptophan unit **134** previously developed in Milwaukee (**Scheme 1.9**). L-Valine **135** served as the source of chirality in the Schöllkopf chiral auxiliary **136** and was employed in a large-scale reaction (500 g). After obtaining the required chiral starting material, D-tryptophan ethyl ester **133** (which could also be obtained from the Boc protected 5-methoxy indole **137** (**Scheme 1.9**), the large-scale Pictet–Spengler/Dieckmann protocol developed in Milwaukee was employed to gain access to the key tetracyclic ketone **138** in excellent yield and >98% enantiomeric excess. This tetracyclic ketone **138** furnished the sarpagine system **139** after N_b-alkylation and α-vinylation, both of which could also be performed on large scales. The pentacyclic ketone **139** containing the sarpagine architecture was further

functionalized. A one-carbon homologation via a Wittig olefination, followed by hydrolysis under acidic conditions, furnished 10-methoxy vellosimine **140** for the first time (>98% ee). Reduction of the C-16 formyl function with $NaBH_4$ furnished (+)-lochnerine **141** in excellent yield. A thallium (III)-mediated oxidative coupling facilitated by borane trifluoride diethyl etherate as the Lewis acid provided the dimerized lochnerine **142** as the P(S)-atropodiastereomer. The absolute configuration was confirmed by X-ray analysis with a MoKα source at low temperature by Jeffrey Deschamps. At the conclusion of this total synthesis, the final assault, demethylation of the two methoxy groups followed by quaternization of the N_b-nitrogen atoms was performed. Treatment of the lochnerine dimer **142** with boron tribromide etherate furnished the bis-phenolic dimer (not shown) in 80% yield. Quaternization was executed by treating the tertiary amine functions with excess iodomethane, and this was followed by exchange of iodide with chloride as the counter anion with the help of a AgCl additive. This furnished the first and biomimetic total synthesis of the antihypertensive bisindole, the P(S)-atropodiastereomer of (+)-dispegatrine **131** identical to the spectral data of natural product [80, 81].



Scheme 1.9. The biomimetic total synthesis of the natural P(S)-atropodiastereomer of (+)-dispegatrine (131).

6.3. Biomimetic total synthesis of (+)-macralstonidine (23).

(+)-Macralstonidine **23** is composed of a macroline **5** and a N_a-methyl sarpagine **124** unit. (+)-N_a-Methyl sarpagine **124** (sarpagine unit) was isolated from A. spectabilis [28] and its total synthesis was accomplished by Zhao *et* al., as discussed earlier [76, 77]. In a chemical sense, (+)-macralstonidine **23** should arise from the acid-mediated condensation of macroline **5** with (+)-N_a-methyl sarpagine **124**. When macroline **5** was stirred with (+)-N_a-methyl sarpagine **124** under mildly acidic conditions, the so formed cyclic ketal was identical to the authentic sample of macralstonidine **23** [28]. In this case too, the condensation followed by cyclic ketal formation can be explained by two different mechanisms. The straightforward Michael-type cyclization, which was discussed previously, is shown below (**Scheme 1.10**). On the other hand, the Friedel–Crafts alkylation-type mechanism that involved stabilization of the macroline enone with an oxonium anion is somewhat more probable from a chemical sense. As shown in **Scheme 1.10**, after initial intramolecular reaction of the C-17 hydroxyl function with the macroline ketone **5**, followed by acid-catalyzed dehydration, this process produced the oxonium species, which existed in two resonance stabilized forms (**71a** and **71b**). The electron-rich phenolic sarpagine **124** carbon atom could attack this electrophile from the C-9 position, which was *ortho* to the phenolic group. No alkylation at the C-11 position was observed. The so formed enol ether underwent acid-mediated rearrangement forming an oxonium intermediate **143,** which made it susceptible to nucleophilic attack by the phenolic oxygen atom furnishing the cyclic ketal present in macralstonidine **23**. Since macroline **5** and N_a-methyl sarpagine **124** have both been synthesized in Milwaukee, this constitutes an enantiospecific total synthesis of (+)-macralstonidine **23** [71, 74].

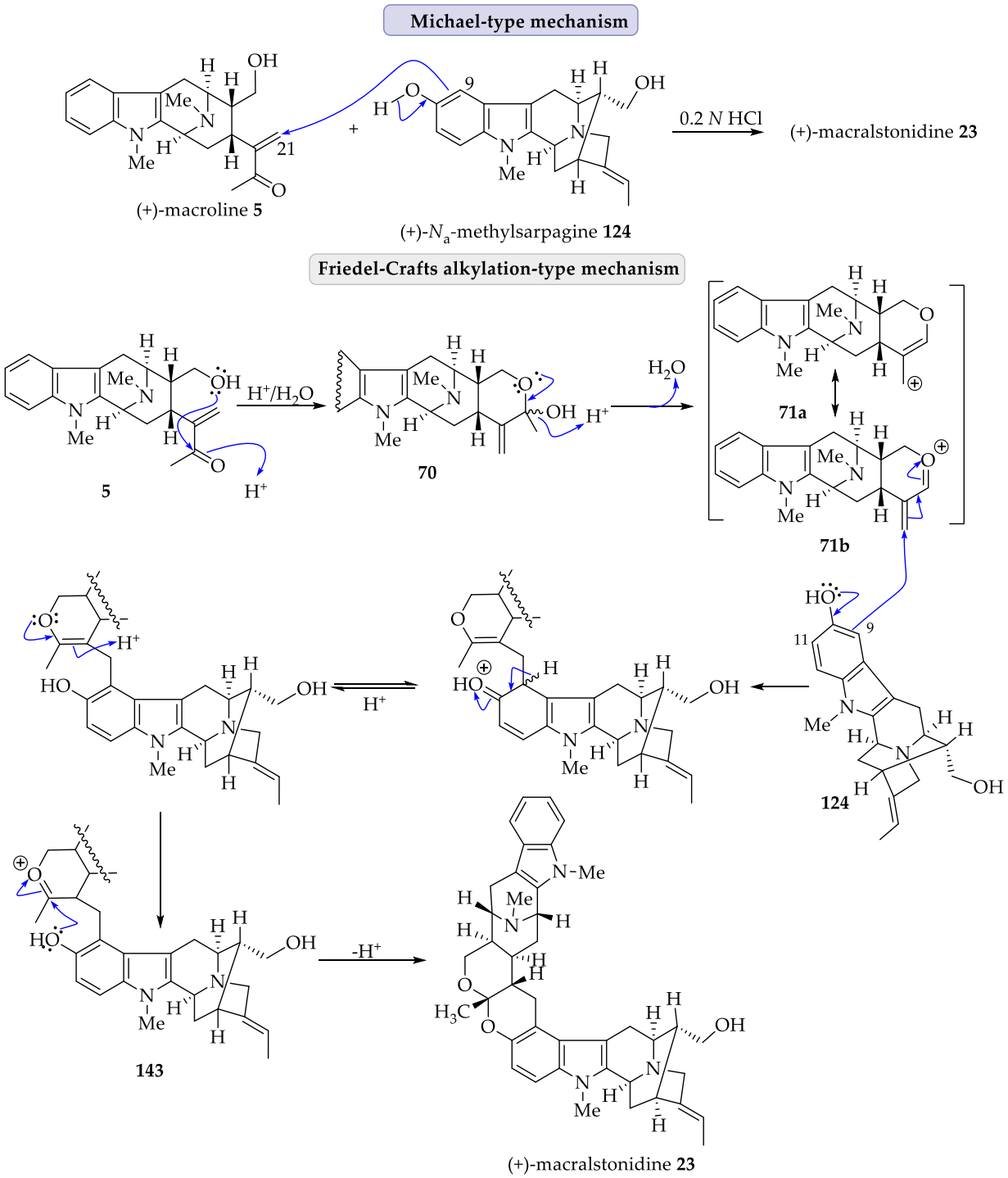
6.4. Biomimetic total synthesis of (+)-macralstonine (24).

LeQuesne *et* al. [89] coupled natural (-)-alstophylline **28** and an excess of (+)-macroline **5** in aqueous 0.2 *N* HCl solution at 20 ℃ for 120 h. The bisindole, (+)-macralstonine **24,** was obtained in 40% yield as a mixture of C-20 epimers, which later was converted into *O*-acetyl macralstonine **25** as the sole product after the treatment with acetic anhydride and pyridine [82]. LeQuesne *et* al. [82] confirmed the biosynthetic route (**Scheme 1**.**11**) of macralstonine **24** proposed by Schmid *et* al.; however the Friedel–Crafts alkylation process**,** as discussed above (**Figure 1.5**) is possible as well. Since the total synthesis of both macroline **5** and alstophylline **28** were accomplished by Liao *et* al., this constitutes the total synthesis of macralstonine **24**, and *O*-acetylmacaralstonine **25** by LeQuesne, Liao, Burke, and Cook *et* al. [74, 82].

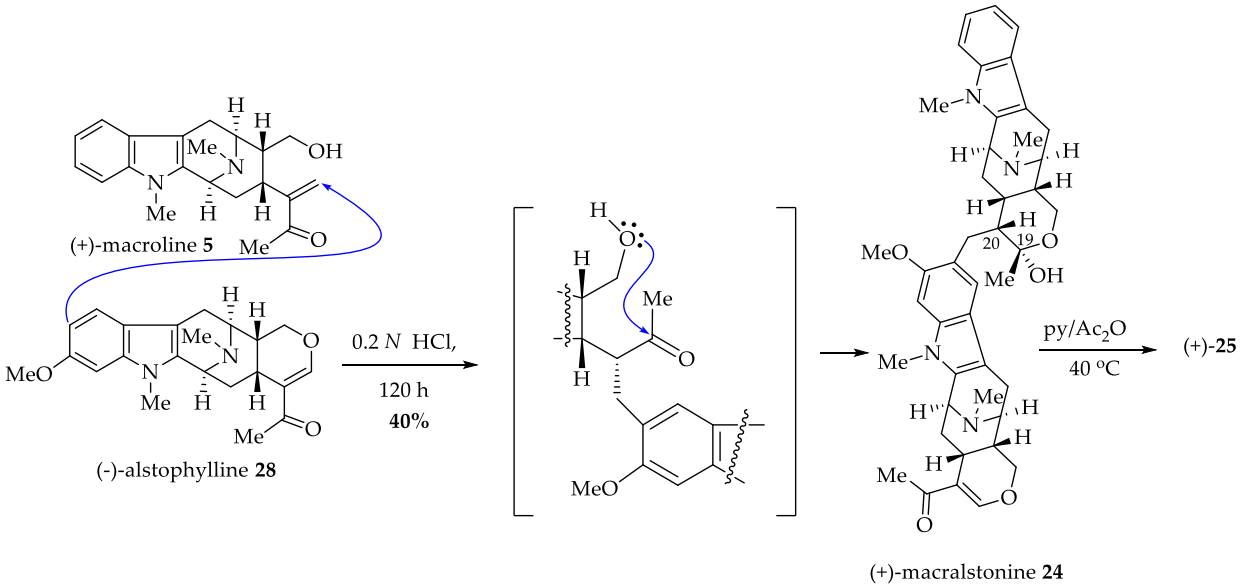
6.5. Partial synthesis of (-)-macrocarpamine (31).

Gan *et al.* accomplished the partial synthesis of (-)-macrocarpamine **31** in stereospecific and enantiospecific fashion via the coupling reaction between the protonated natural (+)-pleiocarpamine **32** and synthetic (-)-anhydromacrosalhine-methine **33** (**Scheme 1.12**) [41]. The portion-wise addition of six equivalents of (-)-anhydromacrosalhine-methine **33** to (+)-pleiocarpamine **32** in 0.2 *N* dry HCl/THF, followed by basic workup (10% NH_4OH), furnished (-)-macrocarpamine **31** in 75% yield [83]. It is important to stir pleiocarpamine **32** in acid to form the iminium ion first and then add (-)-**33** to it. Initial treatment of (-)-anhydromacrosalhine-methine **33** and (+)-pleiocarpamine **32** in aqueous and mild acidic conditions (0.2 *N* HCl) converted enol **33** into its hydrated product, inhibiting the desired product **144** formation. This was reported to be the first coupling reaction between an iminium ion and vinylogous enol ether of such type (**33**) and the first proton-mediated coupling reaction to obtain a bisindole via the coupling of two

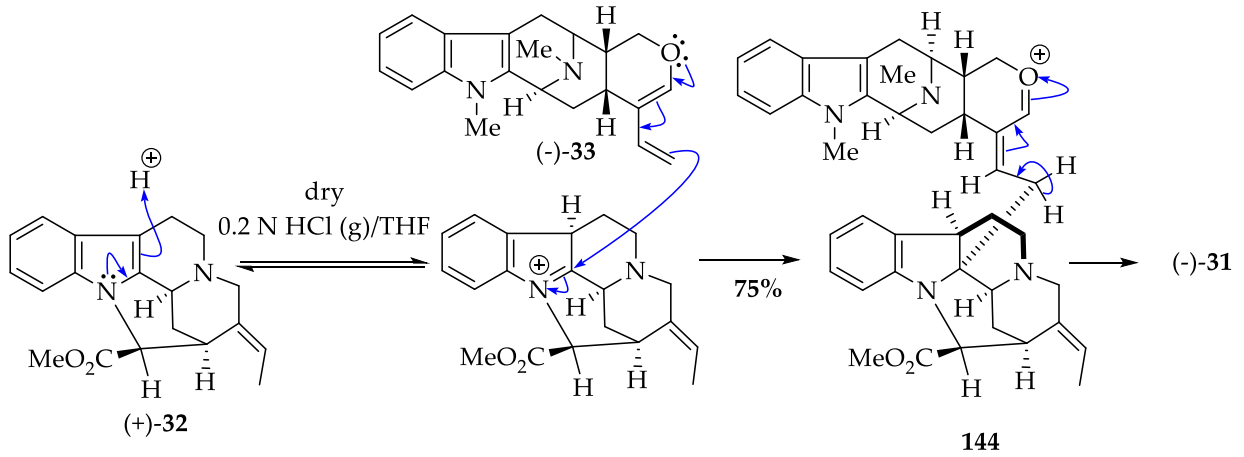
monomeric units from the *Alstonia* genus [83]. The total synthesis of (-)-macrocarpamine **31** has not been reported yet. Since the total synthesis of both of its monomeric units were now successfully completed, the formal total synthesis of (-)-macrocarpamine **31** was completed [14, 41].



Scheme 1.10. Biomimetic total synthesis of macralstonidine (23) by the condensation of macroline (5) with N_a-methyl sarpagine (124) via two possible mechanisms.



Scheme 1.11. The biomimetic total synthesis of macralstonine (24), and *O*-acetylmacralstonine (25).



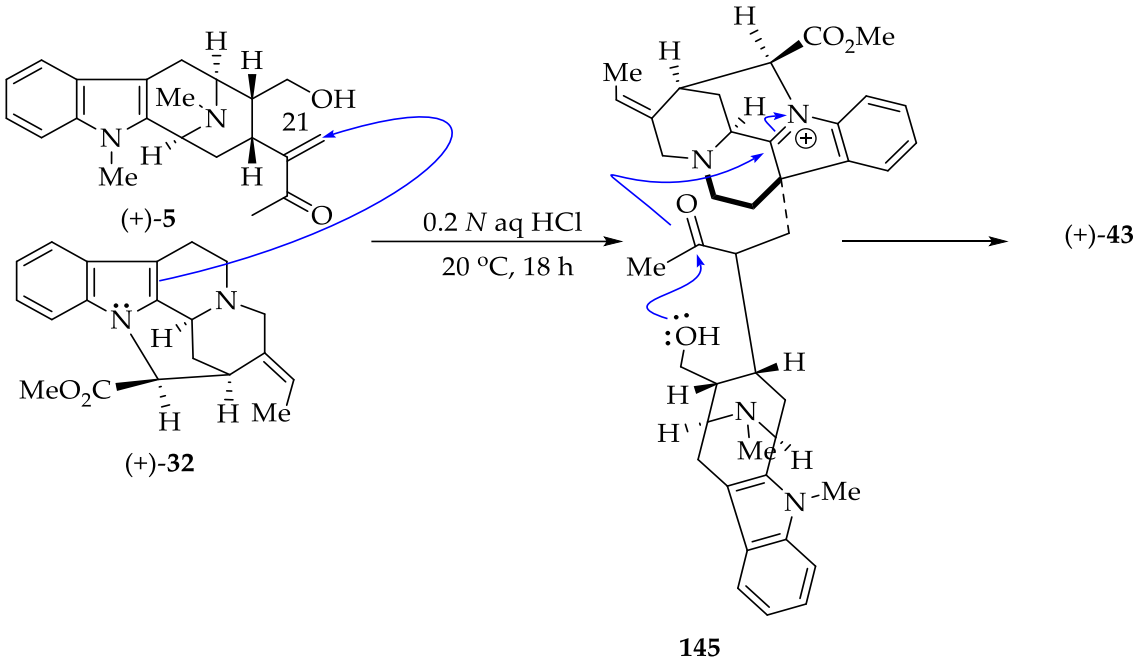
Scheme 1.12. Partial synthesis of (-)-macrocarpamine (31).

6.6. Partial synthesis of (+)-villalstonine (43).

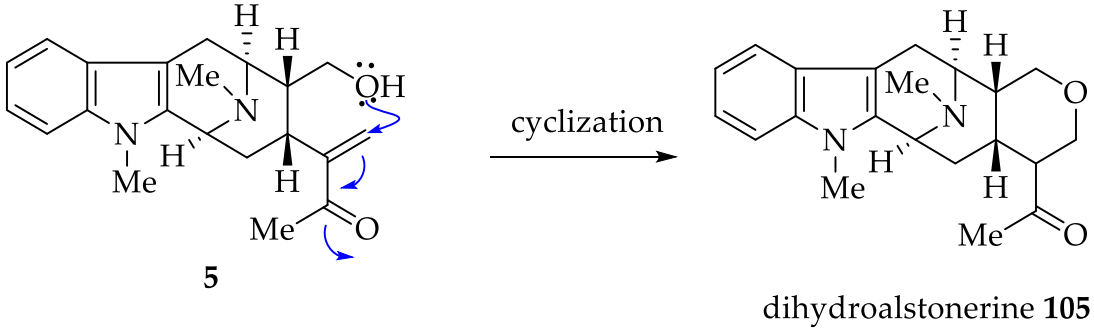
Schmid *et* al. described the degradation of (+)-villalstonine **43** into two monomeric indole alkaloids, (+)-pleiocarpamine **32** and the macroline base **5** [36]. Furthermore, Schmid anticipated forming a new acetal–amino acetal function in (+)-villalstonine **43** by electrophilic addition of the enone function of macroline **5** to the (+)-pleiocarpamine **32**, followed by ring closure. The formal

total synthesis of (+)-villalstonine **43** has recently been accomplished, since Sato *et al.* [14] completed the total synthesis of rac-pleiocarpamine **32** and Liao, Bi, and Zhang prepared macroline **5** [45,90,91]. Initially, LeQuesne, Burke and Cook accomplished the partial synthesis of (+)-villalstonine **43** by a biomimetic-type coupling reaction, which was reported as the first among bisindole alkaloids from the *Alstonia* genus (**Scheme 1.13**) [48]. LeQuesne *et al.* treated (+)-pleiocarpamine **32** with (+)-macroline **5** in the presence of 0.2 N aqueous hydrochloric acid at 20 °C for 18 h to furnish (+)-villalstonine **43** as a single product on TLC [48]. The macroline **5** has a limited shelf life because it cyclizes intramolecularly to give the more stable dihydroalstonerine **105** (**Scheme 1.14**) [3].

The biomimetic synthesis of (+)-villalstonine **43** is thought to begin via electrophilic addition of the macroline enone **5** onto pleiocarpamine **32** from the α-face (less hindered) to give the intermediate **145** (**Scheme 1.13**) [48]. The intermediate **145** then forms a hemiacetal, after which the newly formed acetal sequentially attacks the iminium ion of the indoline from the less hindered side to furnish the acetal–amino acetal function in (+)-villalstonine **43** [48].



Scheme 1.13. Biomimetic partial synthesis of (+)-villalstonine (43)

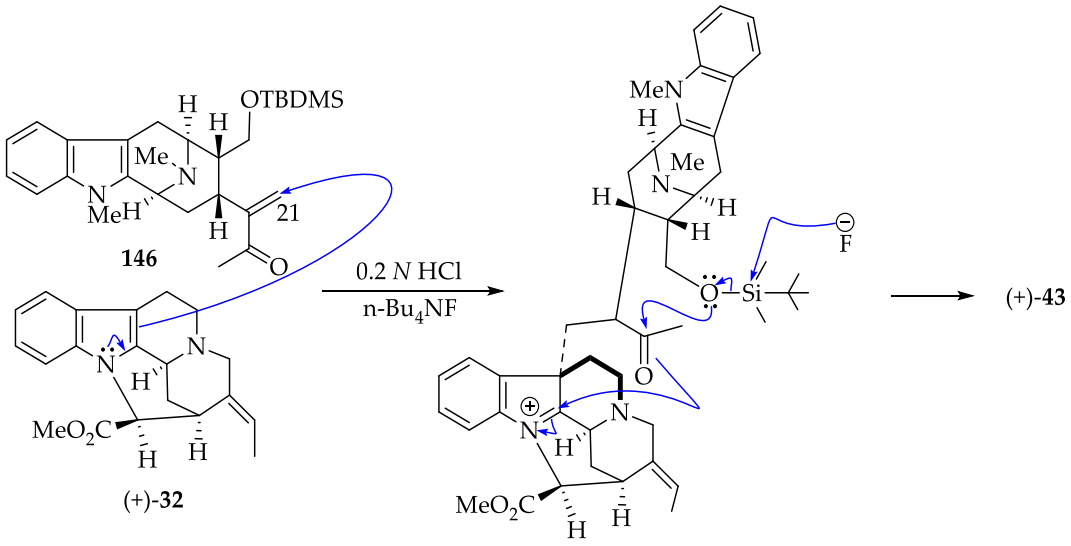


Scheme 1.14. Intramolecular cyclization of macroline (5) into dihydroalstonerine (105).

6.7. Improved partial synthesis of (+)-villalstonine (43).

Because macroline **5** under acidic conditions forms part of the very stable dihydroalstonerine **105** (**Scheme 1.14**), the process was later modified by using the more stable macroline equivalent **146** [42]. The alcohol functional group in the macroline equivalent **5** was protected as its TBDMS ether **146** [71]. The natural (+)-pleiocarpamine **32** was received from Professor LeQuesne and then

treated with the more stable macroline equivalent **146** in the presence of 0.2 *N* aqueous hydrochloric acid and fluoride ion (*tert*-butylammonium fluoride) for 24 h at 22 °C (**Scheme 1.15**). This procedure was followed by a basic workup with aqueous NH_4OH to obtain (+)-villalstonine **43** as an oil in 60% condensation yield. Traces of (+)-pleiocarpamine **32** remained on TLC. The desilylation might occur before condensation to give macroline **146,** or the condensation may take place first as shown in **Scheme 1.15** [3]. The spectroscopic data, including IR and NMR, TLC, and mass spectrometry of synthetic (+)-villalstonine **43,** were identical when compared to the authentic sample separately isolated from A. muelleriana by LeQuesne and Schmid *et* al. [36, 48]. Since the total synthesis of both of its monomeric units are now successfully completed, the formal total synthesis of (+)-villalstonine **43** is completed [47,78, 84].



Scheme 1.15. Improved partial synthesis of (+)-villalstonine (43).

7. Discussion and Conclusion

Natural products and nature-inspired molecules are expected to continue playing an indispensable role in modern drug discovery. Compared to their monomeric units, bisindoles are

more potent in many cases. Bisindole alkaloids including semisynthetic derivatives have been found to possess significant bioactivity, including anticancer, antileishmanial, and antimalarial properties, and thus are promising leads for nature-inspired drug discovery and development. Unnatural medicinal compounds formed by combining bioactive mismatched monomeric units can furnish novel medicinal compounds. Incorporating unnatural enantiomers of monomeric alkaloids into bisindoles can provide access to novel and unnatural bioactive compounds that may have better activity and *in-vivo* stability depending on their metabolism.

8. References

1. Paul, A.T.; George, G.; Yadav, N.; Jeswani, A.; Auti, P.S. Pharmaceutical Application of Bio-actives from Alstonia Genus: Current Findings and Future Directions. In *Bioactive Natural Products for Pharmaceutical Applications*; Pal, D., Nayak, A.K., Eds.; Springer International Publishing: New York, NY, USA, 2021; pp. 463–533.

2. Yeap, J.S.; Saad, H.M.; Tan, C.H.; Sim, K.S.; Lim, S.H.; Low, Y.Y.; Kam, T.S. Macroline-sarpagine bisindole alkaloids with antiproliferative activity from Alstonia penangiana. *J. Nat. Prod.* **2019**, *82*, 3121–3132.

3. Rahman, M.T.; Tiruveedhula, V.V.; Cook, J.M. Synthesis of bisindole alkaloids from the Apocynaceae which contain a macroline or sarpagine unit: A review. *Molecules* **2016**, *21*, 1525.

4. Rahman, M.T.; Deschamps, J.R.; Imler, G.H.; Cook, J.M. Total Synthesis of Sarpagine-Related Bioactive Indole Alkaloids. *Chemistry* **2018**, *24*, 2354–2359.

5. Liao, X.; Zhou, H.; Yu, J.; Cook, J.M. An improved total synthesis of (+)-macroline and alstonerine as well as the formal total synthesis of (−)-talcarpine and (−)-anhydromacrosalhine− methine. *J. Org. Chem.* **2006**, *71*, 8884–8890.

6. Fielding, B.C.; da Silva Maia Bezerra Filho, C.; Ismail, N.S.M.; de Sousa, D.P. Alkaloids: Therapeutic potential against human coronaviruses. *Molecules* **2020**, *25*, 5496.

7. Mohammed, A.E.; Abdul-Hameed, Z.H.; Alotaibi, M.O.; Bawakid, N.O.; Sobahi, T.R.; Abdel-Lateff, A.; Alarif, W.M. Chemical diversity and bioactivities of monoterpene indole alkaloids (MIAs) from six Apocynaceae genera. *Molecules* **2021**, *26*, 488.

8. Lu, J.J.; Bao, J.L.; Chen, X.P.; Huang, M.; Wang, Y.T. Alkaloids isolated from natural herbs as the anticancer agents. *Evid. Based Complement. Altern. Med.* **2012**, *2012*, 485042.

9. Calvert, M.B.; Sperry, J. Bioinspired total synthesis and structural revision of yuremamine, an alkaloid from the entheogenic plant Mimosa tenuiflora. *Chem. Commun.* **2015**, *51*, 6202–6205.

10. Namjoshi, O.A.; Cook, J.M. *The Alkaloids: Chemistry and Biology*; Knölker, H.-J., Ed.; Academic Press: San Diego, CA, USA, 2016; Volume 76, pp. 63–169.

11. Evans, B.E.; Rittle, K.E.; Bock, M.G.; DiPardo, R.M.; Freidinger, R.M.; Whitter, W.L.; Lundell, G.F.; Veber, D.F.; Anderson, P.S.; Chang, R.S.L.; et al. Methods for drug discovery: development of potent, selective, orally effective cholecystokinin antagonists. *J. Med. Chem.* **1988**, *31*, 2235–2246.

12. Zeng, J.; Zhang, D.-B.; Zhou, P.-P.; Zhang, Q.-L.; Zhao, L.; Chen, J.-J.; Gao, K. Rauvomines A and B, two monoterpenoid indole alkaloids from Rauvolfia vomitoria. *Org. Lett.* **2017**, *19*, 3998–4001.

13. Zhang, M.-Z.; Chen, Q.; Yang, G.-F. A review on recent developments of indole-containing antiviral agents. *Eur. Med. Chem.* **2015**, *89*, 421–441.

14. Sato, K.; Kogure, N.; Kitajima, M.; Takayama, H. Total syntheses of pleiocarpamine, normavacurine, and C-mavacurine. *Organic Lett.* **2019**, *21*, 3342–3345.

15. Lim, S.H. Alkaloids from Alstonia Macrophylla. Ph.D. Thesis, University of Malaya, Kuala Lampur, Malaysia, 2013.

16. Keawpradub, N.; Houghton, P.J. Indole alkaloids from Alstonia macrophylla. *Phytochemistry* **1997**, *46*, 757–762.

17. Keawpradub, N.; Kirby, G.C.; Steele, J.C.; Houghton, P.J. Antiplasmodial activity of extracts and alkaloids of three Alstonia species from Thailand. *Planta Med.* **1999**, *65*, 690–694.

18. Elderfield, R.C.; Gilman, R.E. Alkaloids of Alstonia muelleriana. *Phytochemistry* **1972**, *11*, 339–343.

19. Burke, D.E.; Cook, G.A.; Cook, J.M.; Haller, K.G.; Lazar, H.A.; Le Quesne, P.W. Further alkaloids of Alstonia muelleriana. *Phytochemistry* **1973**, *12*, 1467–1474.

20. Hoard, L.G. The Crystal Structures of Altstonisidine, $C_{42}H_{48}N_4O_4$, and Anhydrous Cholesterol, $C_{27}H_{46}O$. Ph.D. Thesis, University of Michigan, Ann Arbor, MI, USA, 1977.

21. Atta-ur-Rahman, F. *Studies in Natural Products Chemistry*; Elsevier: Amsterdam, The Netherlands, 2018.

22. Kitajima, M.; Takayama, H. Chapter Four-Monoterpenoid Bisindole Alkaloids. In *The Alkaloids: Chemistry and Biology*; Knölker, H.-J., Ed.; Academic Press: San Diego, CA, USA, 2016; Volume 76, pp. 259–310.

23. Lim, S.-H.; Tan, S.-J.; Low, Y.-Y.; Kam, T.-S. Lumutinines A–D, linearly fused macroline–macroline and macroline–sarpagine bisindoles from alstonia macrophylla *J. Nat. Prod.* **2011**, *74*, 2556-2562.

24. Lim, S.-H.; Low, Y.-Y.; Subramaniam, G.; Abdullah, Z.; Thomas, N.F.; Kam, T.-S. Lumusidines A− D and villalstonidine F, macroline–macroline and macroline–

pleiocarpamine bisindole alkaloids from Alstonia macrophylla. *Phytochemistry* **2013**, *87*, 148–156.

25. Tan, S.-J.; Lim, K.-H.; Subramaniam, G.; Kam, T.-S. Macroline–sarpagine and macroline–pleiocarpamine bisindole alkaloids from Alstonia angustifolia. *Phytochemistry* **2013**, *85*, 194–202.

26. Sharp, T.M. 265. The alkaloids of Alstonia barks. Part II. A. macrophylla, wall., A. somersetensis, FM Bailey, A. verticillosa, F. Muell., A. villosa, blum. *J. Chem. Soc.* **1934**, 1227–1232.

27. Kishi, T.; Hesse, M.; Vetter, W.; Gemenden, C.; Taylor, W.; Schmid, H. Macralstonin. *Helv. Chim. Acta* **1966**, *49*, 946–964.

28. Hart, N.; Johns, S.; Lamberton, J., Tertiary alkaloids of *Alstonia* spectabilis and *Alstonia* glabriflora (Apocynaceae). *Aust. J. Chem.* **1972,** *25*, 2739-2741.

29. Keawprdub, N.; Houghton, P.; Eno-Amooquaye, E.; Burke, P., Activity of extracts and alkaloids of Thai *Alstonia* species against human lung cancer cell lines. *Planta Med.* **1997,** *63*, 97-101.

30. Lim, S.-H.; Low, Y.-Y.; Tan, S.-J.; Lim, K.-H.; Thomas, N.F.; Kam, T.-S. Perhentidines A–C: Macroline–macroline bisindoles from Alstonia and the absolute configuration of perhentinine and macralstonine. *J. Nat. Prod.* **2012**, *75*, 942–950.

31. Changwichit, K.; Khorana, N.; Suwanborirux, K.; Waranuch, N.; Limpeanchob, N.; Wisuitiprot, W.; Suphrom, N.; Ingkaninan, K. Bisindole alkaloids and secoiridoids from Alstonia macrophylla Wall. ex G. Don. *Fitoterapia* **2011**, *82*, 798–804.

32. Cook, J.; Le Quesne, P. Macralstonine from Alstonia muelleriana. *Phytochemistry* **1971**, *10*, 437–439.

33. Ghedira, K.; Zeches-Hanrot, M.; Richard, B.; Massiot, G.; Le Men-Olivier, L.; Sevenet, T.; Goh, S. Alkaloids of Alstonia angustifolia. *Phytochemistry* **1988**, *27*, 3955–3962.

34. Cook, J.M.; Le Quesne, P.; Elderfield, R. Alstonerine, a new indole alkaloid from Alstonia muelleriana. *J. Chem. Soc. Chem. Commun.* **1969**, 1306–1307.

35. Pan, L.; Terrazas, C.; Muñoz Acuña, U.; Ninh, T.N.; Chai, H.; Carcache de Blanco, E.J.; Soejarto, D.D.; Satoskar, A.R.; Kinghorn, A.D. Bioactive indole alkaloids isolated from Alstonia angustifolia. *Phytochem. Lett.* **2014**, *10*, 54–59.

36. Hesse, M.; Hürzeler, H.; Gemenden, C.; Joshi, B.; Taylor, W.; Schmid, H. Die Struktur des Alstonia-Alkaloides Villalstonin Vorläufige Mitteilung. *Helv. Chim. Acta* **1965**, *48*, 689–704.

37. Nordman, C.; Kumra, S. The structure of villalstonine1. *J. Am. Chem. Soc.* **1965**, *87*, 2059–2060.

38. Buckingham, J.; Baggaley, K.H.; Roberts, A.D.; Szabo, L.F. *Dictionary of Alkaloids with CD-ROM*; CRC Press: Boca Raton, FL, USA, 2010.

39. Keawpradub, N.; Eno-Amooquaye, E.; Burke, P.; Houghton, P. Cytotoxic activity of indole alkaloids from Alstonia macrophylla. *Planta Med.* **1999**, *65*, 311–315.

40. Wright, C.; Allen, D.; Cai, Y.; Phillipson, J.; Said, I.; Kirby, G.; Warhurst, D. In vitro antiamoebic and antiplasmodial activities of alkaloids isolated from Alstonia angustifolia roots. *Phytother. Res.* **1992**, *6*, 121–124.

41. Gan, T.; Cook, J.M. General approach for the synthesis of macroline/sarpagine related indole alkaloids via the asymmetric Pictet-Spengler reaction: The enantiospecific synthesis of (−)-anhydromacrosalhine-methine. *Tetrahedron Lett.* **1996,** *37*, 5033–5036.

42. Bi, Y.; Zhang, L.-H.; Hamaker, L.K.; Cook, J.M. Enantiospecific synthesis of (-)-alstonerine and (+)-macroline as well as a partial synthesis of (+)-villalstonine. *J. Am. Chem. Soc.* **1994**, *116*, 9027–9041.

43. Mayerl, F.; Hesse, M. Macrocarpamin, ein neues Bisindolalkaloid aus Alstonia macrophylla WALL. 167. Mittelung über organische Naturstoffe. *Helv. Chim. Acta* **1978**, *61*, 337–351.

44. Khan, Z.M.; Hesse, M.; Schmid, H. Die Struktur des quartären Alkaloides Macrosalhin. *Helv. Chim. Acta* **1967**, *50*, 1002–1010.

45. Kump, W.; Schmid, H. Über die alkaloide von Pleiocarpa mutica BENTH. *Helv. Chim. Acta* **1961**, *44*, 1503–1516.

46. Kam, T.-S.; Subramaniam, G.; Chen, W. Alkaloids from Kopsia dasyrachis. *Phytochemistry* **1999**, *51*, 159–169.

47. Bartlett, M.; Sklar, R.; Smith, A.; Taylor, W. The alkaloids of Hunteria eburnea Pichon. III. 1 The tertiary bases. *J. Org. Chem.* **1963**, *28*, 2197–2199.

48. Burke, D.E.; Cook, J.M.; Le Quesne, P. Biomimetic synthesis of the bisindole alkaloids villalstonine and alstonisidine. *J. Am. Chem. Soc.* **1973**, *95*, 546–552.

49. Kam, T.-S.; Tan, S.-J.; Ng, S.-W.; Komiyama, K. Bipleiophylline, an unprecedented cytotoxic bisindole alkaloid constituted from the bridging of two indole moieties by an aromatic spacer unit. *Org. Lett.* **2008**, *10*, 3749–3752.

50. Jiménez, J.-M.; Zulaica, E.; Bennasar, M.-L.; Bosch, J. A new synthetic entry to the alkaloids of the mavacurine group. First total synthesis of (±)-2, 7-dihydropleiocarpamine. *J. Chem. Soc. Chem. Commun.* **1993**, 732-733.

51. Jarret, M.; Tap, A.; Kouklovsky, C.; Poupon, E.; Evanno, L.; Vincent, G. Bioinspired oxidative cyclization of the geissoschizine skeleton for the total synthesis of (-)-17-nor-excelsinidine. *Angew. Chem. Int. Ed.* **2018**, *57*, 12294–12298.

52. Le Men, J.; Taylor, W.I. A uniform numbering system for indole alkaloids. *Experientia* **1965**, *21*, 508–510.

53. Rahman, M.T.; Cook, J.M. The C-19 Methyl Substituted Sarpagine-Macroline-Ajmaline Alkaloids: Diversity, Occurrence, Bioactivity, and Synthesis. In *Studies in Natural Products Chemistry*; Atta-ur-Rahman, Ed.; Elsevier: Amsterdam, The Netherlands, 2018.

54. Ruppert, M.; Woll, J.; Giritch, A.; Genady, E.; Ma, X.; Stöckigt, J. Functional expression of an ajmaline pathway-specific esterase from Rauvolfia in a novel plant-virus expression system. *Planta* **2005**, *222*, 888–898.

55. Mattern-Dogru, E.; Ma, X.; Hartmann, J.; Decker, H.; Stöckigt, J. Potential activ-site residues in polyneuridine aldehyde esterase, a central enzyme of indole alkaloid biosynthesis, by modelling and site-directed mutagenesis. *Eur. J. Biochem.* **2002**, *269*, 2889–2896.

56. Pfitzner, A.; Stöckigt, J. Biogenetic link between sarpagine and ajmaline type alkaloids. *Tetrahedron Lett.* **1983**, *24*, 5197–5200.

57. Wu, F.; Kerčmar, P.; Zhang, C.; Stöckigt, J. Sarpagan-Ajmalan-Type Indoles: Biosynthesis, structural biology, and chemo-enzymatic significance. In *The Alkaloids: Chemistry and Biology*; Knölker, H.-J., Ed.; Academic Press: San Diego, CA, USA, 2016; Volume 76, pp. 1–61.

58. Esmond, R.W.; Le Quesne, P.W. Biomimetic synthesis of macroline. *J. Am. Chem. Soc.* **1980**, *102*, 7116–7117.

59. Rahman, M.T.; Deschamps, J.R.; Imler, G.H.; Schwabacher, A.W.; Cook, J.M. Total synthesis of macrocarpines D and E via an enolate-driven copper-mediated cross-coupling process: Replacement of catalytic palladium with copper iodide. *Org. Lett.* **2016**, *18*, 4174–4177.

60. Edwankar, C.R.; Edwankar, R.V.; Namjoshi, O.A.; Rallapalli, S.K.; Yang, J.; Cook, J.M. Recent progress in the total synthesis of indole alkaloids. *Curr. Opin. Drug Discov. Dev.* **2009**, *12*, 752–771.

61. Liu, X.; Deschamp, J.R.; Cook, J.M. Regiospecific, enantiospecific total synthesis of the alkoxy-substituted indole bases, 16-e pi-N a-methylgardneral, 11-methoxyaffinisine, and 11-methoxymacroline as well as the indole alkaloids alstophylline and macralstonine. *Org. Lett.* **2002**, *4*, 3339–3342.

62. Liao, X.; Zhou, H.; Wearing, X.Z.; Ma, J.; Cook, J. M., The first regiospecific, enantiospecific total synthesis of 6-oxoalstophylline and an improved total synthesis of alstonerine and alstophylline as well as the bisindole alkaloid macralstonine. *Org. Lett*. **2005**, *7*, 3501–3504.

63. Allen, M.S.; Hamaker, L.K.; La Loggia, A.J.; Cook, J.M. Entry into 6-methoxy-D (+)-tryptophans. Stereospecific synthesis of 1-benzenesulfonyl-6-methoxy-D (+)-tryptophan ethyl ester. *Synth. Commun.* **1992**, *22*, 2077–2102.

64. Ma, C.; Liu, X.; Li, X.; Flippen-Anderson, J.; Yu, S.; Cook, J.M. Efficient asymmetric synthesis of biologically important tryptophan analogues via a palladium-mediated heteroannulation reaction. *J. Org. Chem.* **2001**, *66*, 4525–4542.

65. Tsuji, J.; Nagashima, H.; Hori, K. A new preparative method for 1, 3-dicarbonyl compounds by the regioselective oxidation of alpha, beta-unsaturated carbonyl compounds, catalyzed by PdCl2 using hydroperoxides as the reoxidant of Pd0. *Chem. Lett.* **1980**, *9*, 257–260.

66. Takayama, H.; Phisalaphong, C.; Kitajima, M.; Aimi, N.; Sakai, S.-I. An efficient synthetic pathway to the macroline-type indole alkaloids, talcarpine and alstonerine from ajmaline. *Tetrahedron* **1991**, *47*, 1383–1392.

67. Zhang, L.-H.; Bi, Y.-Z.; Yu, F.-X.; Menzia, G.; Cook, J.M. Stereospecificity in the Pictet-Spengler reaction. Enantiospecific synthesis of (6S, 10S)-5# 75)-5-methyl-9-oxo-12-benzyl-6, 7, 8, 9, 10, 11-hexahydro-6, 10-imino-5H-cyclooct [b] indole, a template for preparation of macroline/sarpagine alkaloids. *Heterocycles* **1992**, *34*, 517–547.

68. Zhang, L.; Cook, J. General approach to the synthesis of macroline-related alkaloids. Stereospecific total synthesis of (-)-alstonerine. *J. Am. Chem. Soc.* **1990**, *112*, 4088–4090.

69. Gorman, M.; Sweeny, J. Perivine. *Tetrahedron Lett.* **1964**, *5*, 3105–3111.

70. Neukomm, G.; Kletzhäundler, E.; Hesse, M. Die absolute konfiguration von macrolin, einem abbauprodukt des alkaloides villalstonine 179. Mitteilung über organische naturstoffe. *Helv. Chim. Acta* **1981**, *64*, 90–96.

71. Bi, Y.; Cook, J.M. General approach for the synthesis of macroline/sarpagine alkaloids. The total synthesis of (+)-macroline. *Tetrahedron Lett.* **1993**, *34*, 4501–4504.

72. Hesse, M.; Bodmer, F.; Gemenden, C.; Joshi, B.; Taylor, W.; Schmid, H. Die struktur des Alstonia-alkaloides villalstonin. *Helv. Chim. Acta* **1966**, *49*, 1173–1182.

73. Tran, Y.S.; Kwon, O. An application of the phosphine-catalyzed [4+ 2] annulation in indole alkaloid synthesis: Formal syntheses of (±)-alstonerine and (±)-macroline. *Org. Lett.* **2005**, *7*, 4289–4291.

74. Liao, X.; Zhou, H.; Yu, J.; Cook, J.M. An improved total synthesis of (+)-macroline and alstonerine as well as the formal total synthesis of (−)-talcarpine and (−)-anhydromacrosalhine− methine. *J. Org. Chem.* **2006**, *71*, 8884–8890.

75. Kadam, V.D.; Rao, B., S.S.; Mahesh, S.; Chakraborty, M.; Vemulapalli, S.P.B.; Dayaka, S.N.; Sudhakar, G. Stereoselective access to the core structure of macroline-type indole alkaloids: Total synthesis of macroline and alstomicine. *Org. Lett.* **2018**, *20*, 4782–4786.

76. Zhao, S.; Liao, X.; Wang, T.; Flippen-Anderson, J.; Cook, J.M. The enantiospecific, stereospecific total synthesis of the ring-A oxygenated sarpagine indole alkaloids (+)-majvinine,(+)-10-methoxyaffinisine, and (+)-N a-methylsarpagine, as well as the total synthesis of the Alstonia bisindole alkaloid macralstonidine. *J. Org. Chem.* **2003**, *68*, 6279–6295.

77. Zhao, S.; Liao, X.; Cook, J.M. Enantiospecific, stereospecific total synthesis of (+)-majvinine,(+)-10-methoxyaffinisine, and (+)-N a-methylsarpagine as well as the total synthesis of the alstonia bisindole macralstonidine. *Org. Lett.* **2002**, *4*, 687–690.

78. Burke, D.E.; Cook, J.M.; Le Quesne, P. Biomimetic synthesis and structure of the bisindole alkaloid alstonisidine. *J. Chem. Soc. Chem. Commun.* **1972**, 697-697.

79. Lin, M.; Yang, B.-Q.; Yu, D.-Q. Studies on the quaternary alkaloids of Rauvolfia verticillata (lour.) Baill var. Hainanensis Tsiang. *Acta Pharmacol. Sin.* **1986**, *21*, 114–118.

80. Edwankar, C.R.; Edwankar, R.V.; Deschamps, J.R.; Cook, J.M. Nature-inspired stereospecific total synthesis of p-(+)-dispegatrine and four other monomeric sarpagine indole alkaloids. *Angew. Chem. Int. Ed.* **2012**, *51*, 11762–11765.

81. Edwankar, C.R.; Edwankar, R.V.; Namjoshi, O.A.; Liao, X.; Cook, J.M. Stereospecific approach to the synthesis of ring-A oxygenated sarpagine indole alkaloids. Total synthesis of the dimeric indole alkaloid P-(+)-dispegatrine and six other monomeric indole alkaloids. *J. Org. Chem.* **2013**, *78*, 6471–6487.

82. Burke, D.E.; DeMarkey, C.A.; Le Quesne, P.; Cook, J.M. Biomimetic synthesis of the bis-indole alkaloid macralstonine. *J. Chem. Soc. Chem. Commun.* **1972**, 1346–1347.

83. Gan, T.; Cook, J.M. Partial synthesis of the antiamoebic bisindole alkaloid (−)-macrocarpamine. *Tetrahedron Lett.* **1996**, *37*, 5037–5038.

84. Pandey, K. P.; Rahman, M.T.; Cook, J. M. Bisindoles alkaloids from the *Alstonia* species: recent isolation, bioactivity, Biosynthesis, and synthesis. *Molecules*, **2021**, *26*, 3459.

[Note: chapter 1 is based on published review article: Pandey et *al. Molecules, 2021 (*doi.org/10.3390/molecules27051738)].

Chapter 2

Enantiospecific Total Synthesis of Unnatural Enantiomers of C-19 Methylated Sarpagine/Macroline/Ajmaline-Type Biologically Active Indole Alkaloids Via the Pictet-Spengler Reaction/Dieckmann Cyclization Protocol.

1. Introduction

1.1. Scope of unnatural enantiomers or synthetic alkaloids in modern drug discovery.

Nature has been an extensive and sustainable source of biologically active molecules for medications including cancer, malaria, and antiarrhythmic agents since time immemorial [1]. Natural molecules are generally chiral and are the secondary metabolites, and purportedly, used in the defense mechanism of plants or organisms [1]. Many clinical drugs are either directly inspired or derived from natural products [2]. Besides their use from historical times, importantly, natural products bring about new avenues in modern medicinal chemistry as drugs "***beyond Lipinski's rule of five***" [3]. When compared to the synthetic small molecules, natural molecules interact better with biological molecules, proteins, and enzymes. In addition, these molecules contain fewer trace heavy metals and have better molecular rigidity, as compared to the synthetic small molecules [4]. Natural products-based drug discovery also has some

challenges such as isolation, synthesis in bulk amount, complete characterization, structural complexity, and paucity of the isolated compounds. These challenges, to some extent limit the opportunity of natural products in modern drug discovery.

Despite the challenges, as discussed above, the advent of innovative and promising technologies such as automation, quantum computing, cheminformatics and artificial intelligence may propel natural product-based drug discovery into the next stride forward [1, 5]. Recently, Atanasov *et.* al (2021) discussed emerging technologies such as genome mining and engineering, use of analytical tools, and microbial culturing advances, which could be even more significantly useful in natural product-based drug discovery [3]. It is well-known that the plants or organisms usually produce only one enantiomer. As a result, it is possible to isolate and screen the biological activity of the enantiomers, i.e., the natural enantiomer. Rationally, the unnatural enantiomers might actually be as good as the natural enantiomer or even better in activity on occasion. This is not a common phenomenon, but an important one. The unnatural enantiomers metabolize slower or differently, thus their toxicity profile can be better depending on the metabolic pathway. A blockbuster drug discovered by Professor Dennis C. Liotta, Lamivudine (brand name: Epivir) was an unnatural L-nucleoside based drug, discovered by accident, and it is one of the essential drugs in the WHO's list of important drugs [1, 6]. This drug has been very efficient in saving millions of lives of HIV patients. Another drug discovered by Professor Liotta, emtricitabine (brand name: Emtriva) was hundreds of times more potent, as compared to its natural D-nucleoside analog [6]. A recent report from Newman *et* al. mentioned that almost 65 % (120) of new drugs, out of the 185 new small molecules that were approved by the FDA since 1981 (for the treatment of cancer), are either natural product or natural products inspired synthetic drugs [7]. This finding, undoubtedly, highlights the importance of natural products-

based small molecules including the synthetic derivatives for the treatment of various types of cancers.

As discussed here, the natural bioactive alkaloids such as morphine, vincristine and reserpine exhibit biological activity, and contain the particular stereochemistry [8, 9]. Etorphine, an opioid enantiomer is so potent it is used to put elephants so sleep for medical work. It requires one shot. Besides the molecules derived from nature directly, the biological activity of unnatural enantiomers (or their synthetic analogs) is also of keen interest, as stated above. A review of the literature shows the plethora of work related to the synthesis of derivatives of enantiomers and their screening in biology, over many years [8]. Chuang *et* al. reported a promising mild and general Larock-indole formation process for the synthesis of unnatural tryptophan derivatives, as well as the synthesis of (-) aspergelazine A (bisindole: structure not shown here) [10]. Lindsley *et* al. reported the one pot, microwave assisted synthesis of unnatural canthine alkaloids and the their significant activity at Akt inhibition [11]. In another report, when tested against human tumor cell lines, the C'-20 urea enantiomeric derivates of vinblastine (a marketed drug) were found to be 10–200 times higher in anticancer potency, as compared to the natural vinblastine urea analogs tested against various human tumor cell lines [1, 12]. It was reported that the synthetic or unnatural bryotoxin, vincristine, and vinblastine might exhibit excellent biological activity compared to the natural products [1, 13-15]. Moreover, a study from the Boger group reported that the modified Vinca alkaloids (10′-fluorovinblastine and 10′-fluorovincristine, structures not shown) exhibited potent activity against the sensitive and vinblastine-resistant tumor cell lines [1, 9]. Thus, it is crucial to synthesize unnatural enantiomers or synthetic analogs of natural products including the indole alkaloids themselves to evaluate their biological activity.

As pointed earlier, the indole scaffold is considered as one of the few 'privileged structures' in modern drug discovery because of the structural similarity with the molecules of life such as serotonin, tryptamine, and melatonin [1]. Thus, the synthesis of unnatural enantiomers of indole alkaloids are particularly of interest, despite the associated challenges, such as the control of absolute and desired stereochemistry, and the execution of large scale multistep total synthesis (if required).

1.2. Methyl-substituted (C-19 position) sarpagine/macroline/ajmaline monomeric indole alkaloids [1].

The C-19 methyl-substituted sarpagine/macroline/ajmaline-type alkaloids are an important sub-group of structurally and biosynthetically related indole alkaloids [5]. Lounasma first described, in detail, about this subgroup [16, 17]. To date, more than 70 monomeric indole alkaloids that belong to this sub-family have been isolated. These bioactive C-19 methyl-substituted sarpagine/macroline/ajmaline bases were isolated from various medicinal plants mainly from *Alstonia* species. Among those, the reported bioactivity of representative alkaloids is listed herein **(Figure 2.1)**. The alkaloids in this sub-group contain at least one monomeric unit with a C-19 methyl group as their obligate substituent. The chiral methyl function at the C-19 position could, presumably, originate from similar synthetic or related biosynthetic precursors as the desmethyl analogs. As a result, the total synthesis of these alkaloids should be possible from some common intermediates or core architecture [1]. The macroline, sarpagine, and ajmaline alkaloids are essentially biosynthetic relatives, and they contain the azabicyclo[3.3.1]nonane core (as discussed earlier in **Chapter 1, Figure 1.7**) present in their structures. Thus, any effective and divergent synthetic strategy should involve robust access to the common intermediates, preferably containing the azabicyclo[3.3.1]nonane core system **31**. Recently, Hashimoto *et* al. (2022) also

reported an enantioselective construction of an *N*-bridged [3.3.1.] ring system, by amide insertion (via metal-carbene species) and biocatalytic asymmetric desymmetrization [18].

2. Isolation and biological activity of representative examples of C-19 methyl substituted sarpagine/macroline/ajmaline indole alkaloids [5].

The diversity, occurrence, and bioactivity of monomeric sarpagine/macoline/ajmaline alkaloids including C-19 methyl substituted indoles has reported by Rahman *et* al. in 2018 in detail [5]. As discussed, over seventy C-19 methylated sarpagine/macroline/ajmaline type indole alkaloids have been reported, and many of those exert important biological activity, as shown below as representative examples (**Figure 2.1)** [5]. Talpinine **1** (**Figure 2.1**), a sarpagine indole alkaloid, was isolated from the stem bark and root bark of *Pleiocarpa talbotii* (Apocynaceae) [19]. It exhibited cytotoxicity against KB/VJ300 cells with IC_{50} values ranging between 14-22 mg/mL [20]. Another sarpagine indole, *O*-acetyltalpinine **2** was isolated from the stem bark and leaves of *Alstonia angustifolia* [20]. This indole alkaloid also exhibited anticancer activity against the KB/VJ300 cells) [21]. A macroline-type indole alkaloid, (-) N_4 -methyl, N_4 -21 -secotalpinine **3** was isolated from the stem bark of *A. macrophylla* and *A. angustifolia* [22, 23]. It exhibited antileishmanial activity against the promastigotes of *Leishmania mexicana* with an IC_{50} value of 57.8μM. A sarpagine-type indole alkaloid, alstonerinal **4** was isolated the stem bark, and leaves of *A. macrophylla* and *A. angustifolia* plant [21, 24, 25]. It exhibited anticancer activity against the colon cancer cell lines (HT-29 cells with an ED_{50} value of 8.6 μM), as well as antileishmanial activity against the promastigotes of *L. mexicana* (IC_{50} 145.4 μM) [21]. A sarpagine-type monomeric indole alkaloid, alstiyunnanenine **5** was isolated from *A. yunnanensis* Diels [25]. It also exhibited weak cytotoxicity (anticancer activity) against the osteosarcoma cell lines: Saos-2 (IC_{50} values of 26.8± 4.1) and M663 (IC_{50} values of 27.7 ± 4.0 μM) [25]. A macroline type

indole alkaloid, talcarpine **6**, was isolated from the stem bark and leaves of various plant species: *Pleiocarpa talbotii Wernham*, *A. macrophylla*, and *A. angustifolia* [21, 26-29]. This monomeric indole alkaloid exhibited weak antimalarial activity against *Plasmodium falciparum* (the K1 strain, IC_{50} 40.3 ±2.9 μM) [29]. A sarpagine-type indole alkaloid, isolated from the stem bark and leaves of *A. angustifolia*, N_4-methyl secotalpinine **7** exhibited potent anticancer activity against the NF-kB cell lines with an ED_{50} value of 1.2 μM) [23]. It also exhibited moderate antileishmanial activity against the promastigotes of *L. Mexicana* with an IC_{50} value of 57.8 μM) [30]. An alkaloid alstoyunine A **8** is a sarpagine-type monomeric indole alkaloid, and it was isolated from aerial parts of *R. vomitoria* [31]. It exhibited weak anticancer activity against the human colon cancer cell lines HT-29 (IC_{50} 35.2 μM) and SW480 (IC_{50} 45.3 μM). Moreover, the alkaloid **8** exhibited weak anti-inflammatory activity in the RAW 264.7 macrophage cell line (IC_{50}75.3 μM) [31].

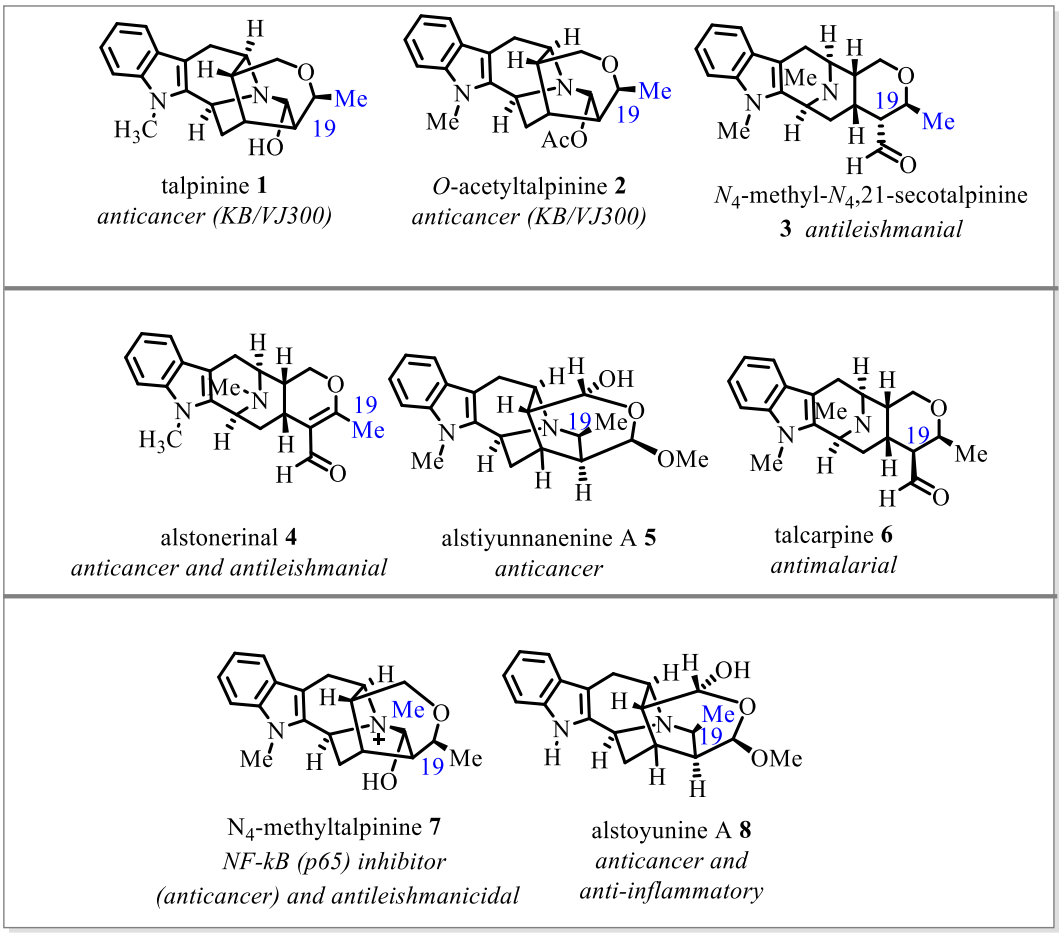


Figure 2.1. The C-19 methyl-substituted sarpagine/macroline-related alkaloids (representative examples) with their biological activity [1, 5, 19, 21].

2.1. Enantiospecific total synthesis of natural C-19 methyl-substituted sarpagine/macroline alkaloids via the general strategy developed in Milwaukee [1].

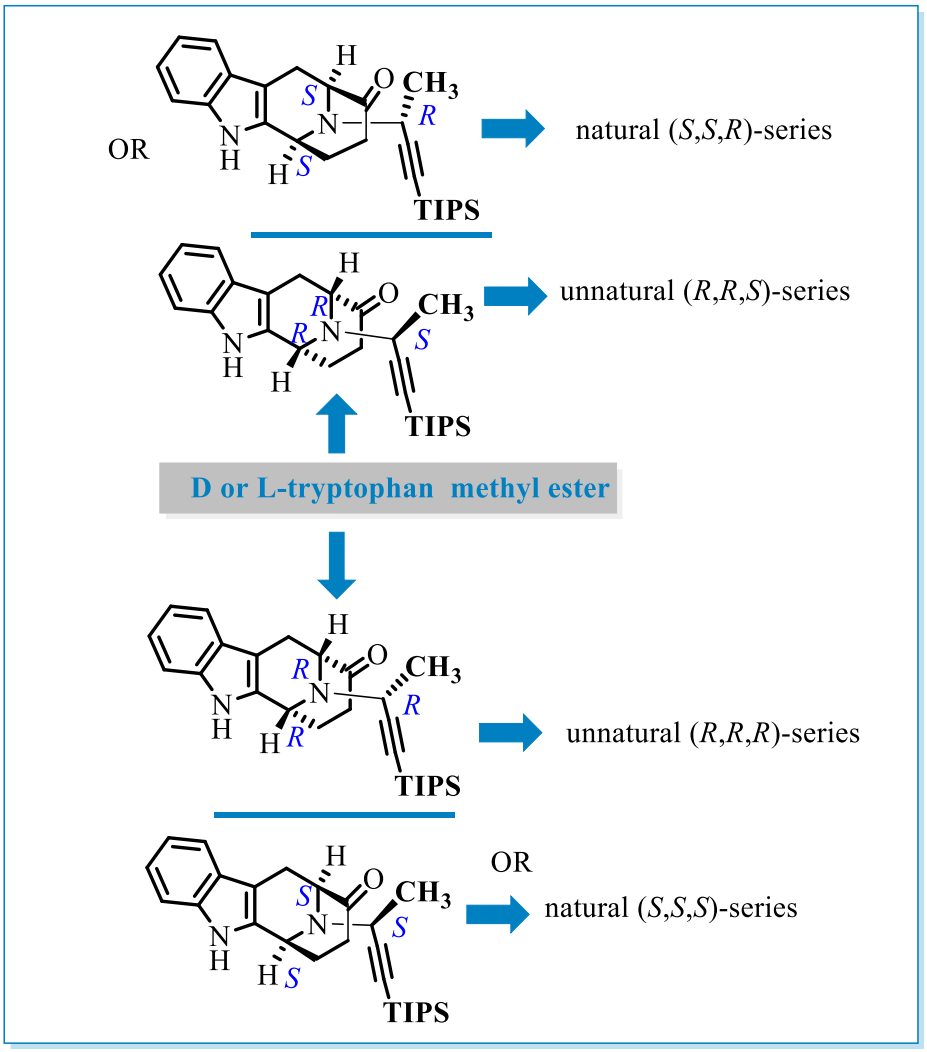
The Milwaukee group has developed an efficient and practical method for the total synthesis of a number of sarpagine/macroline/ajmaline-related bioactive indole alkaloids [5, 32, 33]. Moreover, an ambidextrous Pictet Spengler strategy by accessing both enantiomers (individually) of the azabicyclo[3.3.1]nonane core structures, while starting from the same tryptophan auxiliary was developed by the Milwaukee group [34]. This unified general strategy has been successfully

employed in the total synthesis of more than a dozen indole alkaloids from this sub-family (**Figure 2.2)** [5, 32, 35-38]. This was an important step forward for the synthesis of C-19 methyl substituted indole alkaloids.

By employing a unified general strategy, the enantiospecific total synthesis of the first example of sarpagine-type alkaloids (isolated from the root-culture of *R. serpentina*) that belong to this C-19 methylated group was reported by Edwankar *et* al. [35]. The 19(*S*), 20(*R*)-dihydroperaksine-17-al **9** and 19(*S*), 20(*R*)-dihydroperaksine **10** (**Figure 2.2**), represented the novel subgroup of sarpagine-type indole alkaloids, identified by Stöckigt *et* al. [1, 39]. Moreover, by employing the same unified general strategy, the total synthesis of peraksine **11**, macrosalhine-N_b-oxide **12**, and talcarpine **6** (formal synthesis) from this group were reported. Afterwards, Rahman *et* al. reported a robust and efficient copper-mediated enolate-driven cross-coupling process, adapted from the earlier work by Kabir *et* al. [40], that substituted the previous palladium-catalyzed cross coupling with an improved yield to access the core pentacyclic ketone [36]. This copper catalyzed route is important because it does not require the expensive palladium metal. Moreover, the Milwaukee group also reported the total synthesis of a number of sarpagine and macroline alkaloids, including talcarpine **6**, N_4-methyl-N_4,21-secotalpinine **3**, macrocarpines **15-17**, dihydroperaksine **18**, and deoxyperaksine **19**, by employing a two-step shorter route with an increased overall yield to achieve access to the key tetracyclic ketone intermediates [1, 37].

The ambidextrous Pictet-Spengler/Dieckmann-cyclization protocol, developed by Rahman *et*. al (Milwaukee group) [34] permits an efficient and stereospecific access to the synthesis of natural and unnatural/synthetic enantiomers of a number of alkaloids either from D- or L-tryptophan (**Scheme 2.1**) [1, 34]. By employing the ambidextrous Pictet-Spengler/Dieckmann cyclization protocol, the totally synthesis of several natural indole alkaloids N_4-methyltalpinine **7 (**potent NF-

kB inhibitor), talpinine **1** (anticancer), *O*-acetyl talpinine **2** (anticancer), as well as the macrocarpines F-G (**20**-**21**) were reported (**Figure 2.1**) [41, 42]. Using the ambidextrous Pictet-Spengler reaction/Dieckmann cyclization process, the total synthesis of either enantiomer of the bioactive monomeric C-19 methylated alkaloids would be possible either from L or D tryptophan.



Scheme 2.1. The access to both natural and unnatural enantiomers of C-19 methyl-substituted sarpagine/macroline indole alkaloids from either D or L-tryptophan (36) methyl ester [1, 34].

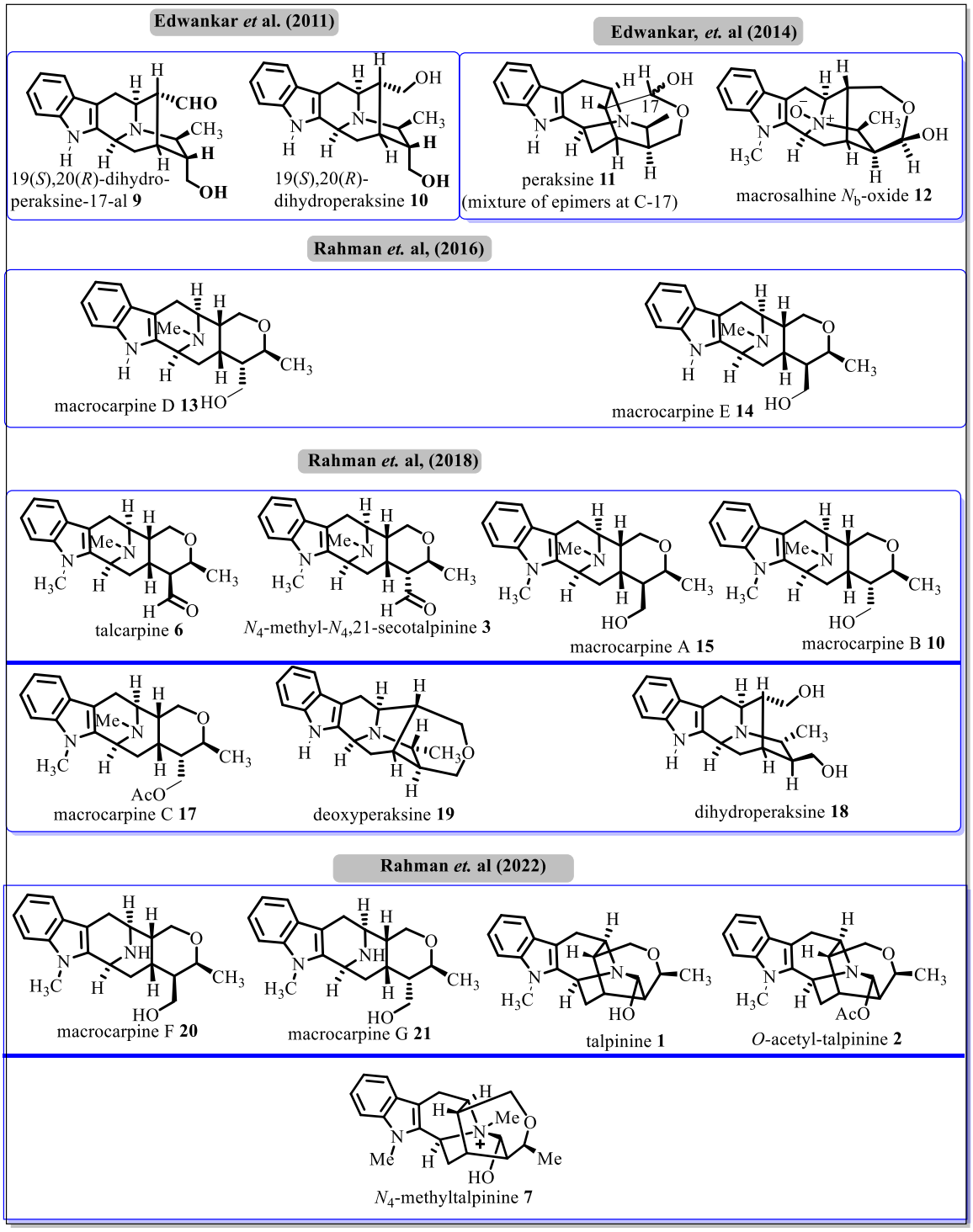
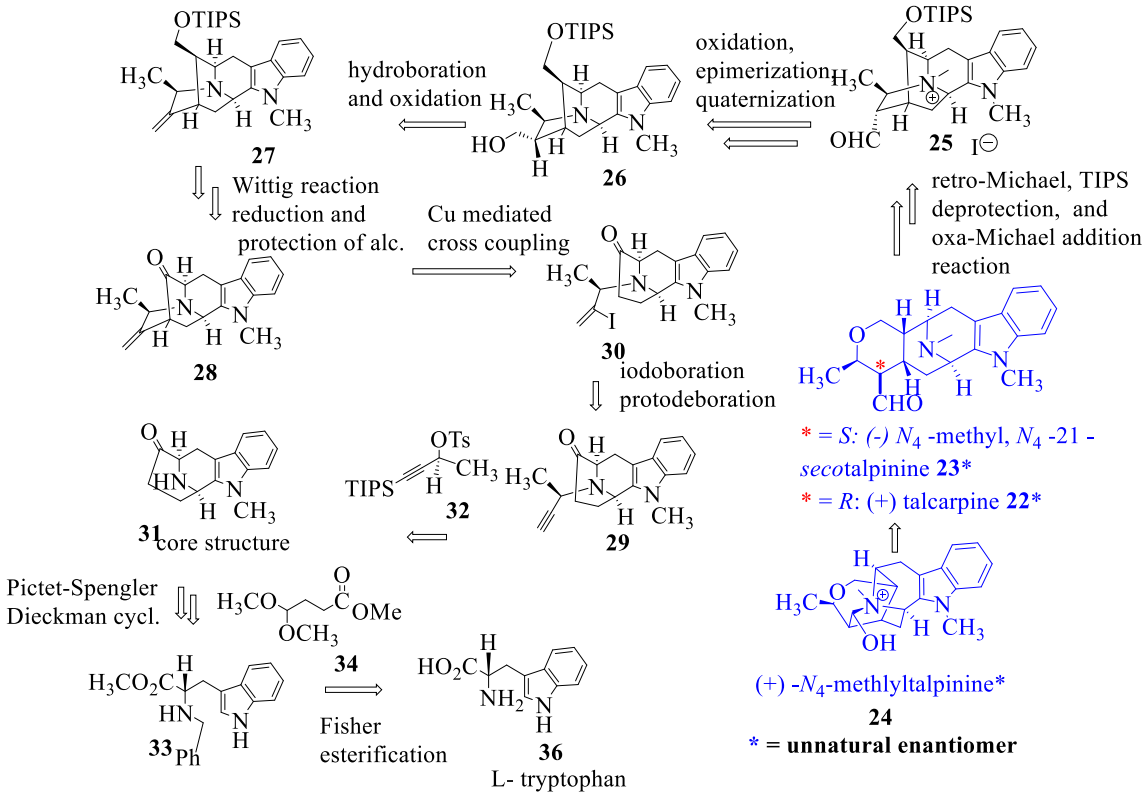


Figure 2.2. Examples of C-19 methylated alkaloids synthesized enantiospecifically by the Milwaukee group [1, 42].

2.2 Retrosynthetic analysis of unnatural indole alkaloid targets in this study.

The retrosynthetic analysis of C-19 methylated sarpagine/macroline-type unnatural alkaloid targets: (+)-talcarpine **22**, (-)-N_4-methyl, N_4-21-secotalpinine **23**, and N_4-methyltalpine **24** was based on the approach for their natural enantiomers [42]. As shown in **Scheme 2.2**, the (+)-N_4-methyltalpine **24** was anticipated to originate from the nucleophilic addition reaction by the *N*(4) nitrogen atom at the carbonyl carbon atom in (-)-N_4-methyl, N_4-21-secotalpinine **23**. The *retro*-Michael reaction, TIPS deprotection, and *Oxa*-Michael reaction of the quaternary salt **25** should result in both the desired (-)-N_4-methyl, N_4-21-secotalpinine **23** (unnatural) and (+)-talcarpine **22** (unnatural) alkaloids. The methiodide salt **25** was expected to result from the sequence; oxidation of primary alcohol **26**, and this would be followed by the methylation of the *N*(4) atom with methyl iodide. The hydroboration and Kabalka oxidation of alkene intermediate **27** would result in the primary alcohol **26**. A key intermediate, the core pentacyclic ketone **28,** after a Wittig reaction (one carbon homologation), reduction of the aldehyde so formed, and the subsequent protection of the alcohol functional group with TIPS triflate should result in the silyl ether intermediate **27**. The iodoboration protodeboronation reaction of the ethynyl tetracyclic ketone **29** would result in the desired vinyl iodide **30**, with the desired chemo and regiospecific structure, after which the Cu-mediated cross coupling reaction would result in the desired pentacyclic ketone **28,** as a sole product [32, 36]. The alkylation at the *N*(4) atom of the core tetracyclic ketone **31** by the chiral (*S*) alkyl moiety **32**, and subsequent deprotection of the TIPS group would result in the ethynyl tetracyclic ketone **29**, as shown in **Scheme 2.2**. The Pictet-Spengler reaction between N_b-benzyl-L-tryptophan methyl ester **33** and the 4,4-dimethoxy butyrate **34** would result in the usual *trans*-diester **35** (not shown in **Scheme 2.2)**, after which after a series of reactions (Dieckmann cyclization, ester hydrolysis, decarboxylation, and

debenzylation) would result in the desired azabicyclo[3.3.1]nonane core **31** with the desired enantiomeric stereochemistry, as required for the unnatural enantiomers [32]. The intermediate **33** can be obtained after the esterification of the cheaper, (compared to D-tryptophan) natural L-tryptophan **36,** followed by the N_b-benzylation reaction. The acetal, 4, 4-dimethoxy butyrate **34**, as well as the ethynyl TIPS **45** (not shown in **Scheme 2.2)** should be accessible in a few steps synthesis, individually [32].



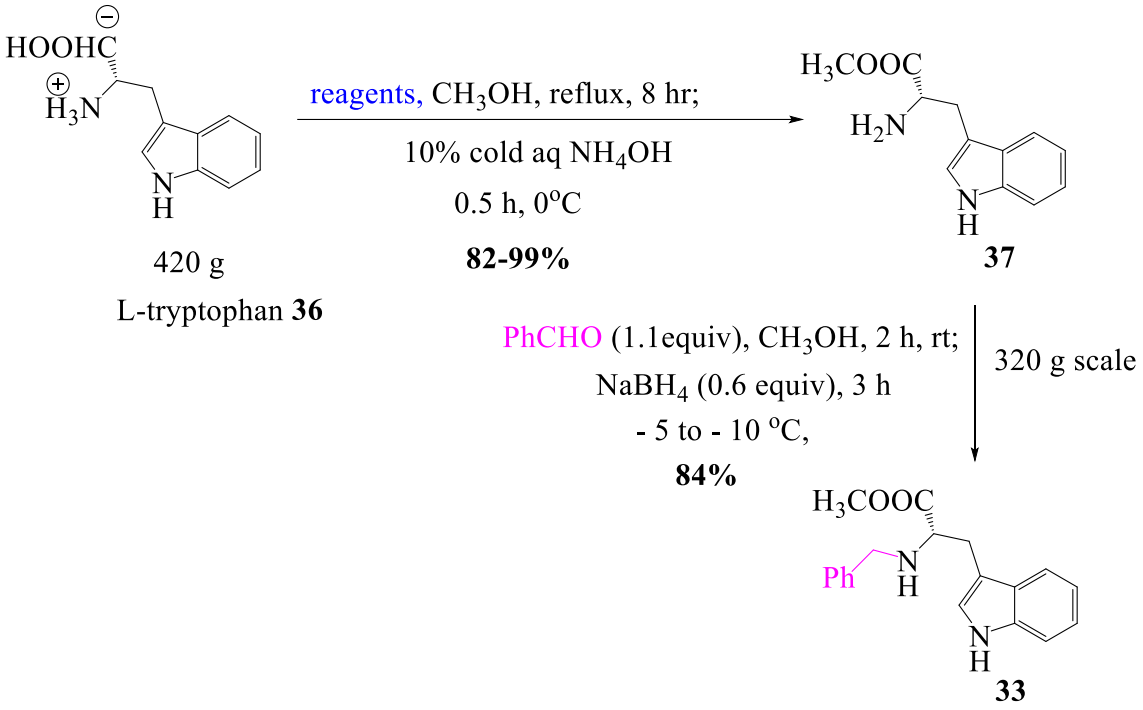
Scheme 2.2. Retrosynthetic analysis for the targeted unnatural indole alkaloids.

3. Results and discussion.

3.1 Synthesis of L-tryptophan methyl ester (37) and *N*ᵇ-benzyl L-tryptophan methyl ester (33).

In the very first step, commercially available L-tryptophan **36** was converted into L-tryptophan methyl ester **37** by the employment of the Fischer-esterification reaction. For this conversion, previously, anhydrous HCl (g) in methanol was used [32, 35, 36]. The reaction provided 97% yield (on 265 g scale, **Table 2.1**) with anhydrous HCl (g) in methanol; however, another source of acid was sought to minimize the cost and the risk associated with the use of HCl (g) from a tank. Also, difficulty was associated to control the addition of the right amount of HCl (g) in the methanol solvent. For this purpose, at the beginning, the 4 M anhydrous HCl in ether was purchased. This reagent when used in excess and provided a very good yield (98%) on a smaller scale (2 g), however, on the larger scale (10 g) reaction, a slight decrease in the reaction yield (82%) was observed (**Table 2.1**). Moreover, the large amount of the reagent (4 M anhydrous HCl) required on the bigger scale would result in a substantial amount of the diethyl ether rather than the desired safer methanol in the reaction mixture. The concentrated acids: HCl (aq), and H_2SO_4 (aq), however, worked for this reaction, but the employment of these acids was omitted because of the unsatisfactory optical rotation (with conc HCl, see **Table 2.1)**. Finally, adding 3 equivalents of acetyl chloride in methanol generated dry HCl gas (*in-situ*) for this conversion (Fisher esterification reaction). The acetyl chloride-methanol method consistently provided excellent yields on various scales with the desired optical rotation (**Table 2.1**). Moreover, the use of this reagent was easier on bigger scale (420 g) and also was found to be safer as compared to the use of an acidic methanolic solution prepared by passing HCl (g) into it from the tank. The

free base **37** was obtained by dropwise addition of 10 % NH_4OH solution (aqueous) at 0 ^oC to free the HCl salt (structure not shown).



Scheme 2.3. Large scale synthesis of L-tryptophan methyl ester (37) and N_b-benzyl L-tryptophan methyl ester (33).

The L-tryptophan methyl ester **37**, which resulted, was converted into the N_b -benzyl L-tryptophan methyl ester **33** on 320 g scale in 84% yield by the employment of benzaldehyde and the reducing agent (sodium borohydride), as shown in **Scheme 2.3**. It is important to add the reducing agent at lower temperature, and portionwise to avoid racemization of the imine intermediate (imine enamine tautomerization), at this step [43].

Table 2.1. Preparation of optically active L-tryptophan methyl ester (37) using various reagents.

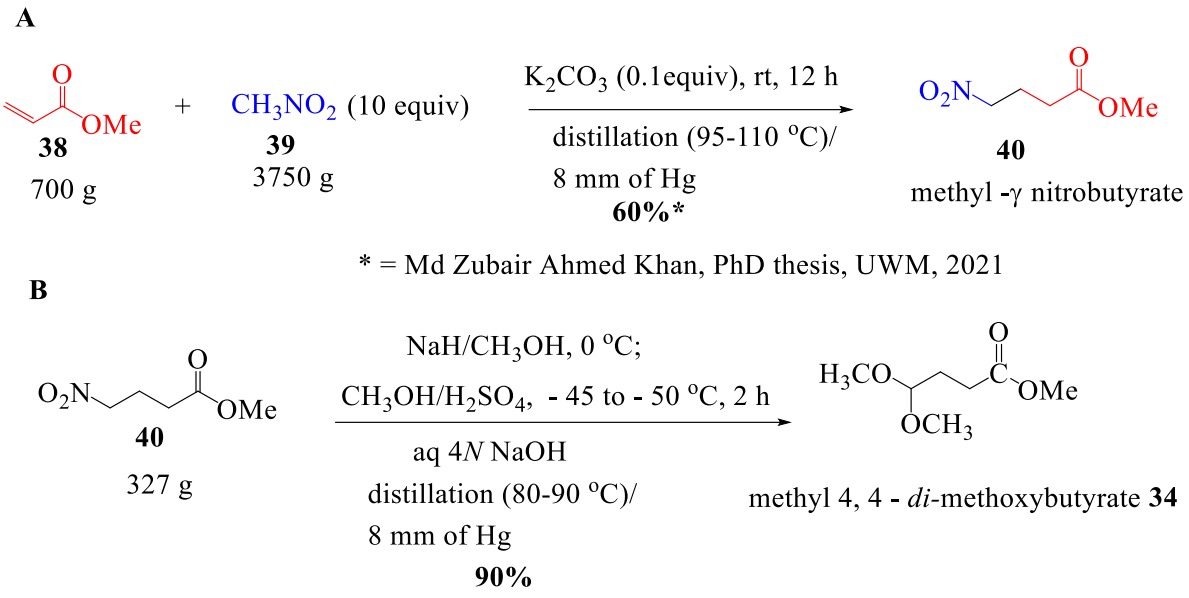
Scales	Reagents	Amount	% Yield	The optical rotation of product (ester)
265 g	HCl (g) from tank	Excess	97%	$[\alpha]_D^{25}$ + 35.4 (c 1.18, MeOH) Ref $[\alpha]_D^{27}$ - 37.2 (c 1.0 in MeOH)[1]
2, 10 g	2 M HCl in ether ($ 125 per 800 ml Oakwood)	8 ml, 200 mL	98, 82%	$[\alpha]_D^{25}$ + 36.1 (c 1.34, MeOH)
1 g	Conc. HCl	3.5 equivalents	97%	$[\alpha]_D^{25}$ + 18.8 (c 0.55, MeOH)
1 g	Conc. H_2SO_4	1.2 equivalents	93%	ND
2, 10, 100, 420 g	Acetyl chloride (AcCl)	3 equivalents	98, 99, >99, 99%	$[\alpha]_D^{25}$ + 35.7 (c 1.0, MeOH)

ND = not determined

3.2. Large scale synthesis of methyl 4, 4-dimethoxybutyrate (34).

The 4, 4-dimthoxybutyrate **34** was prepared on large scale via two synthetic steps: a Michael addition reaction and a Nef reaction (**Scheme 2.4)**. In the first step, the Michael addition reaction was carried out using methylacrylate **38**, nitromethane **39** (Michael donor: nitromethane, Michael acceptor: methyl acrylate), and potassium carbonate (0.1 equivalents, **Scheme 2.4**). The mixture, which resulted, was stirred at rt for 12 hours to provide the methyl -γ-nitro butyrate **40** in 60% yield. The employment of potassium carbonate (0.1 equivalents) to improve the yield (60%), as compared to the yield (30%) reported earlier with the 0.1 *N* NaOH solution, was perfected later by Zubair [43]. The crude product was purified by distillation under reduced pressure at 90-110 ^oC (8 mm/Hg). It is important that any compound be neutral before distillation. In the second step, the methyl -γ-nitro butyrate **40** was converted (in Nef reaction) into the methyl 4, 4-dimthoxybutyrate **34** using sequentially

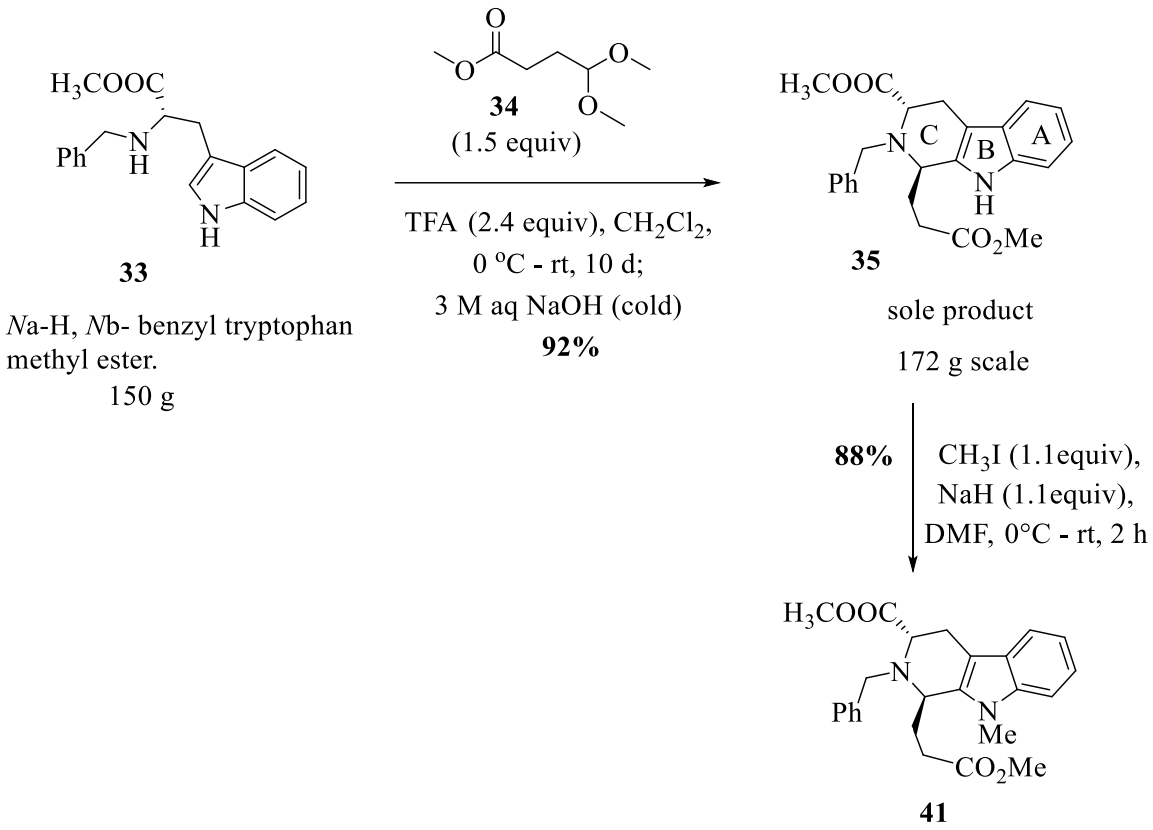
strong base (sodium methoxide), then acidic methanolic solution, which was followed using 4 *N* NaOH solution, as shown in the **Scheme 2.4**.



Scheme 2.4. A: large scale synthesis of methyl γ-nitrobutyrate (40). B: large scale synthesis of 4, 4-dimethoxybutyrate (34).

3.3. Synthesis of N_a-methyl *trans*-diaster (35) via the asymmetric Pictet- Spengler reaction (150 g scale) and this was followed by a N_a -methylation reaction (172 g scale).

The asymmetric Pictet-Spengler reaction has been highly studied and executed on a large scale in Milwaukee for years, which resulted in the successful total synthesis of many natural products [44-47]. Recently, the ambidextrous Pictet-Spengler reaction/Dieckmann cyclization protocol was developed by Rahman *et* al. (as discussed above) [34]. The ambidextrous Pictet-Spengler reaction/Dieckman cyclization protocol permits the synthesis of both natural and unnatural indole alkaloids starting either from L-tryptophan **36** or D-tryptophan [1, 34]. The employment of N_a-H, N_b -benzyl L-tryptophan **33** and the methyl 4, 4- dimethoxy butyrate **34** in the presence strong acid (TFA), herein, provided *trans*-diester **35** as the sole product in 92% yield after stirring for 10 days (**Scheme 2.5**).



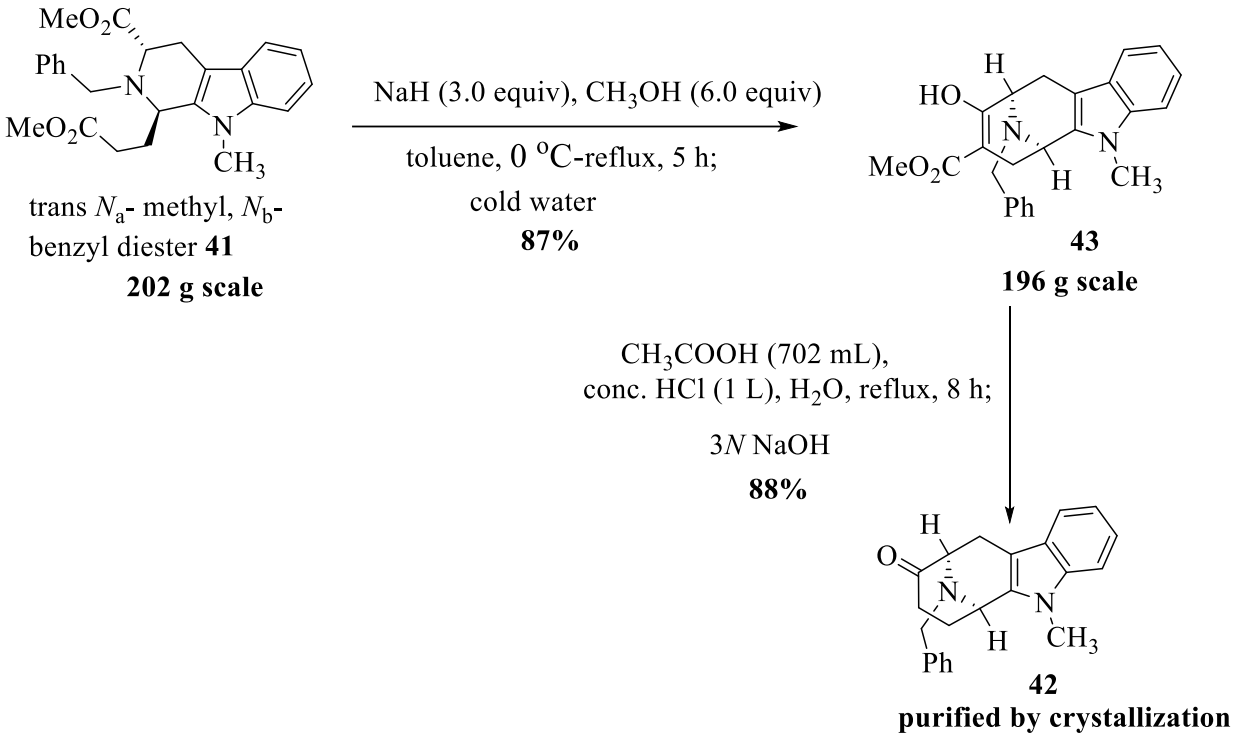
Scheme 2.5. Large scale synthesis of N_a-methyl *trans*-diester (41) via the asymmetric (*trans*-specific) Pictet- Spengler and N_a -methylation reaction.

The employment of the D-tryptophan-based starting material and the use of acetic acid (weaker acid) via a *cis*-specific Pictet-Spengler reaction/Dieckman cyclization protocol also allows the desired intermediate to proceed to the unnatural enantiomers, as discussed [34]. However, the L-tryptophan based starting material with a *trans*-specific Pictet-Spengler reaction was carried out because of the low cost of natural L-tryptophan. The *trans*-diester **35**, which resulted, was immediately converted into the N_a-Me, *trans*-diester **41** (**Scheme 2.5**) in 88% yield. Both N_a-H,

trans-diester **35**, and N_a-Me, *trans*-diester **41** were purified by crystallization (please see **Experimental** section for details).

3.4. Large scale synthesis of N_a –Me, N_b –benzyl tetracyclic ketone (42) via a Dieckmann cyclization, ester hydrolysis, and decarboxylation reactions.

After installing the C-ring (N_a-H, N_b –benzyl, *trans*-diester **35**) attached to the indole via a Pictet-Spengler reaction and the methylation of the subsequent product, the synthesis turned towards the formation of the 4th ring (D-ring) containing the N_a –Me, N_b –benzyl tetracyclic ketone structure **41** (**Scheme 2.6**) on large scale. The N_a-Me, N_b –benzyl, *trans*-diester **41** (202 g) was converted into the b-keto ester **43** via a Dieckmann cyclization reaction at reflux conditions, which resulted in 87% yield. The toluene was pre-dried by azeotropic distillation prior to the use in this reaction and then methanol was added to it. **The top of the sides of the flask was covered with aluminum foil to maintain the temperature at reflux without carbonizing the compound on the sides of the flask, as shown in Figure 2.3** [43]. This would also facilitate the heating process by decreasing the heat loss. The two chiral centers in the b-keto ester **43** formed in this step contained the desired *R*, *R* stereochemistry, which was later confirmed (after the product, which formed, after the debenzylation, N_b-alkylation, and removal of TIPS group see **Figure 2.4**) by X-ray crystallography. The b-keto ester **43**, which resulted, from the Dieckmann cyclization reaction was used directly in the next step without further purification and characterization.



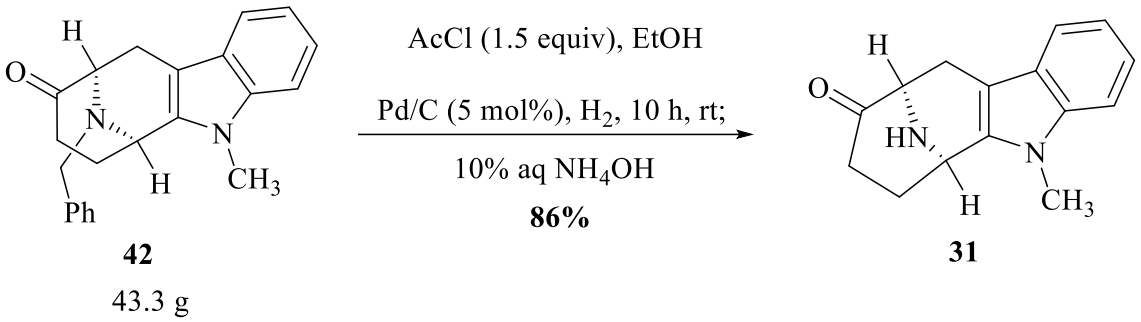
Scheme 2.6. Large scale synthesis of N_a-methyl N_b-benzyl tetracyclic ketone (42) via the Dieckmann cyclization, ester hydrolysis, and decarboxylation reactions.



Figure 2.3. A reaction set-up for the Dieckman cyclization on 202 g scale (left) and for ester hydrolysis and decarboxylation reaction on 196 g scale (right).

The methyl ester of the crude product (β-keto ester **43**) was hydrolyzed (in acidic medium) into the corresponding carboxylic acid (not shown) on 196 g scale. This was followed by the decarboxylation under refluxing conditions in the same reaction vessel. The conditions are shown in **Scheme 2.6** and **Figure 2.3**. The use of excess 3 *N* aq NaOH (to basify the crude product) was minimized by removal of most of the solvents (glacial acetic acid and conc. hydrochloric acid) under reduced pressure (3 L, one neck, round bottom flask with a Keck adaptor worked well) prior to basifying the crude product. These two chemical transformations resulted in the desired N_a –Me, N_b –benzyl, tetracyclic ketone **42** with 88% yield, which was then purified by crystallization.

3.5. Synthesis of N_a –Me, N_b –H tetracyclic ketone (31) via a modified catalytic (Pd/C) debenzylation reaction.



Scheme 2.7. Synthesis of N_a –Me, N_b –H tetracyclic ketone (31) on large scale via modified catalytic debenzylation reaction.

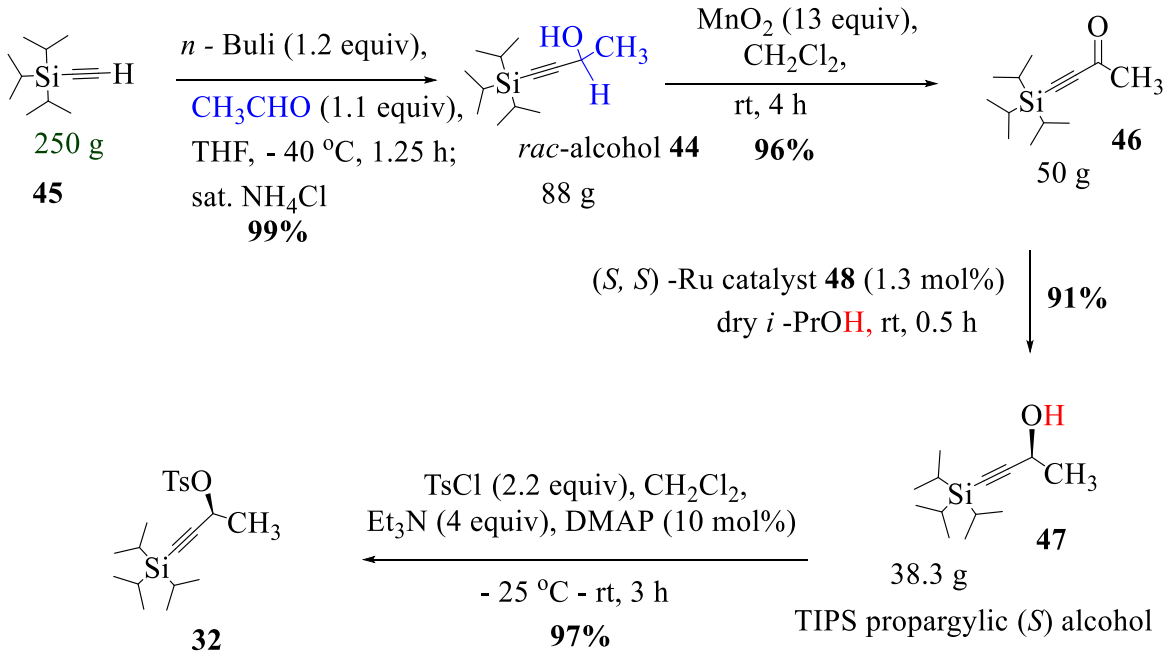
The N_a –Me, N_b –benzyl tetracyclic ketone **42** was then subjected to the catalytic debenzylation process. The starting material **42** (ketone, 43.3-gram scale) was first converted into the hydrochloride salt by *in-situ* generation of dry HCl (gas) using 1.5 equivalents of acetyl chloride (**Scheme 2.7**). The acetyl chloride was added into the mixture (starting material and dry ethanol)

dropwise at room temperature until the starting material was completely dissolved. The salt was then employed in the catalytic debenzylation process in the presence of a catalytic amount of Pd/C (5 mol%) and H_2 gas (filled in a balloon and passed through a needle into the reaction mixture) at room temperature [35]. The product, which resulted (86% yield), after filtration through celite and a and basic workup (with aqueous 10% ammonium hydroxide solution) was pure by spectroscopic analysis (^{1}H NMR and ^{13}C NMR, see **Appendix Part I**). Thus, no further purification of the product such as column chromatography or crystallization was required using this method. The starting material can also be converted into its hydrochloride salt by adding HCl (g) dissolved in ethanol, as reported; however, the purification steps required either crystallization or column chromatography [32, 34, 43]. In conclusion, the desired 4 rings (A, B, C, and D) contained in the tetracyclic ketone **31** was prepared on the large scale by an improved procedure. The tetracyclic core **31** can now be employed in the total synthesis of unnatural enantiomers of C-19 methyl substituted sarpagine/macroline/ajmaline-type indole alkaloids [1]. Also, this tetracyclic ketone **31** was an optically active enantiomer of the core structure prepared from D-tryptophan, as reported in the published articles [32, 37]. Moreover, the synthesis of this core structure **31** can also be executed via the ambidextrous Pictet-Spengler reaction either from D or L tryptophan [34].

3.6 The large-scale preparation of (*S*) - 4 –*tri*-isopropylsilyl-3-butyn-2-yl tosylate (32).

The large-scale (250-gram scale) preparation of the (*S*) - 4 –*tri*-isopropylsilyl-3-butyn-2-yl tosylate **32** was carried out by following the procedure published by Edwanker *et* al. for the synthesis of its enantiomer (*R*) - 4 –*tri*-isopropylsilyl-3-butyn-2-yl tosylate (not shown) [32]. The synthesis of *rac*-propargylic alcohol **44** was executed starting from TIPS acetylene **45** with

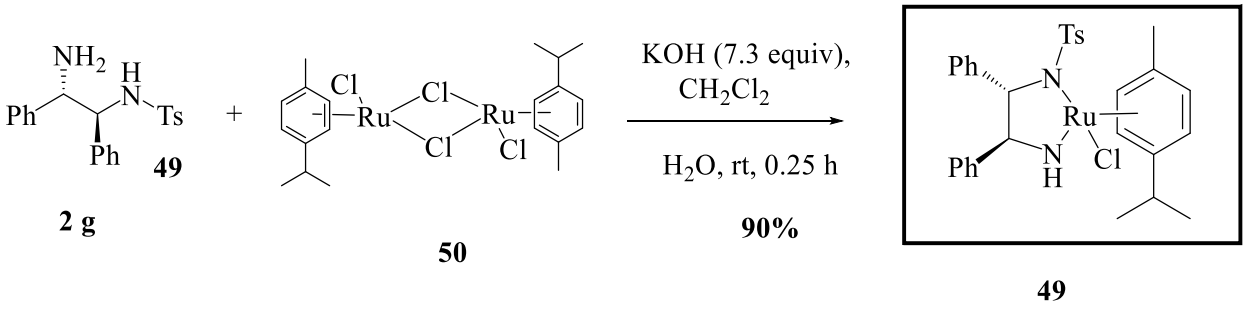
strong base (*n*-Buli), and acetaldehyde in 99% yield (**Scheme 2.8**) at – 40 °c. The *rac*-alcohol **44**, which resulted, was oxidized by using activated manganese dioxide into the corresponding ketone **46** in 86% yield. The ketone **46**, which resulted, was reduced back to the optically active (*S*)-alcohol **47** in 90% yield by a Noyori asymmetric hydrogenation in presence of ruthenium chiral catalyst (*S, S*) **48** and isopropanol (dried by distillation) on 50-gram scale (**Scheme 2.8**). The desired chirality (*S*) of the propargylic alcohol **47** was confirmed on comparison with the optical rotation (see **Experimental** for detail) [32, 43] of the enantiomer.



Scheme 2.8. Synthesis of (*S*) - 4 –*tri*-isopropylsilyl-3-butyn-2-yl tosylate (32) on large scale.

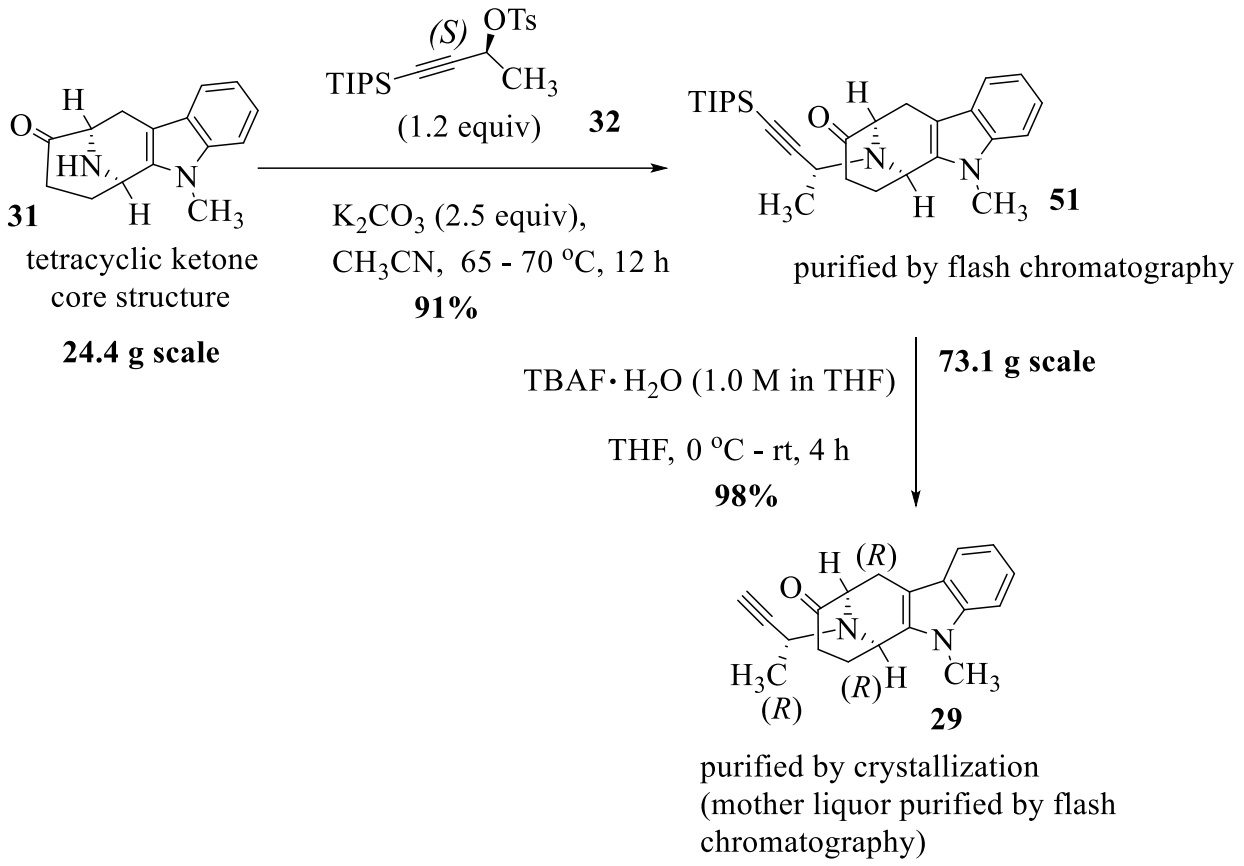
3.7 Synthesis of the (*S, S*)- ruthenium catalyst (48) for the asymmetric hydrogenation on gram scale.

The preparation of the (*R*, *R*)-ruthenium catalyst (enantiomer of **48**, structure not shown) is published in the literature [32, 41, 43]. To reduce the ketone **46** into the desired chiral (*S*) alcohol **47**, the (*S, S*)-ruthenium catalyst **48** was prepared on gram scale (**Scheme 2.9**) by employing (1*S*, 2*S*)-(+)-*N*-*p*-toluenesulfonyl-1, 2-diphenyl ethylene-diamine **49**, dichloro (*p* - cymene) ruthenium (II) dimer **50**, and the base (powdered KOH) in 90% yield. **The value of the optical rotation of the diamine 49, which was purchased (Oakwood Chemicals), was checked against the literature value before using it in the reaction.** A dark-red colored asymmetric catalyst **48**, which resulted, was used directly in the next step (asymmetric hydrogenation of ketone **46** to the (*S*)-alcohol **47** without purification and characterization).



Scheme 2.9. Synthesis of (*S, S*)- ruthenium catalyst (49) on gram scale.

3.8. Alkylation of the tetracyclic ketone, followed by removal of the TIPS protecting group.



Scheme 2.10: The synthesis of (*R, R, R*)- acetylenic tetracyclic ketone (29) via alkylation of tetracyclic ketone 31 and the removal of the TIPS functional group.

After successful synthesis of (*S*)-TIPS tosylate **32**, and (*R, R*)-tetracyclic ketone **31** (core structure with A, B, C and D ring) on large scale, the research direction turned towards the preparation of the E-ring (the 5th ring) which contained the pentacyclic ketone **28**. The (*R, R*)-tetracyclic ketone **31** was alkylated using 1.2 equivalents of (*S*)-TIPS tosylate **32** and 2.5 equivalents of anhydrous potassium carbonate at reflux conditions, with stirring (**Scheme 2.10**) to yield 91% of N_b-alkylated (*R, R*)-tetracyclic ketone **51**, which was purified by flash chromatography. The N_b-alkylated (*R, R*)-tetracyclic ketone **51** underwent deprotection of the *tri*-isopropylsilane (TIPS) group (73.1 gram scale, as shown in **Figure 2.4**) in the presence of fluoride ion (TBAF·H_2O) at 0 °C to afford ketone **29** in 98% yield. The desired (*R, R, R*) stereochemistry in ketone **29** was needed to synthesize the unnatural enantiomers, and this was

confirmed by X-ray crystallography by Dr. Jeffrey Deschamps (US Naval Research Laboratory). Moreover, the value of the optical rotation (see **Figure 2.4** and **Appendix Part I** for X-ray crystallographic data) of the ketone **29** was in complete agreement with that reported value in the literature for its enantiomer (structure not shown) [32, 37, 43].

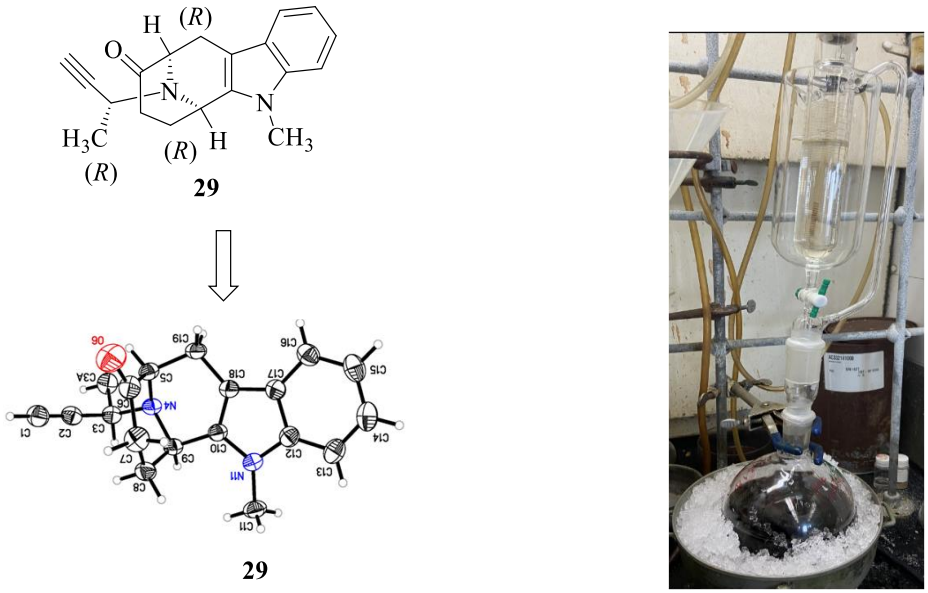
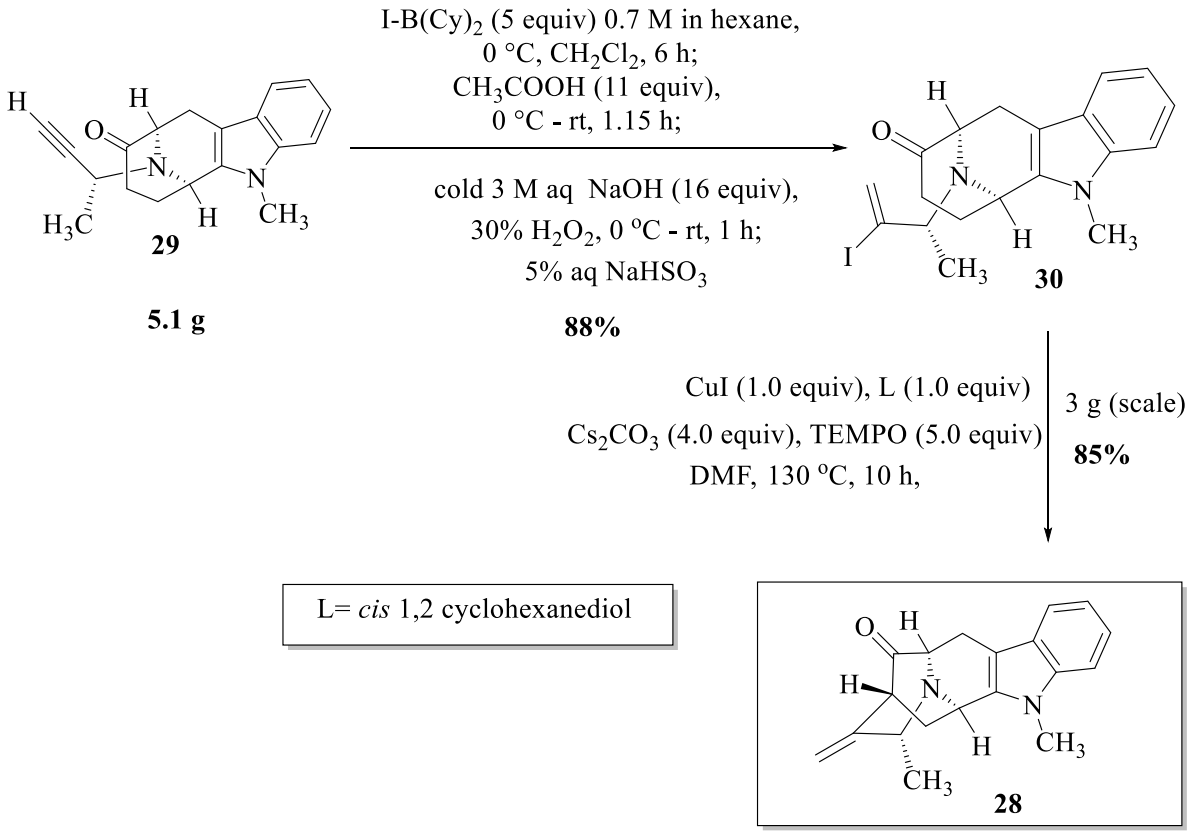


Figure 2.4. The structure and ORTEP view of 29 (left), and the reaction set-up of the removal for the TIPS group in the N_b-alkylated (*R, R, R*)-tetracyclic ketone (51) on 73.1-gram scale (right).

3.9. The synthesis of the pentacyclic ketone (28) via haloboration and protodeboronation followed by a Cu-mediated cross-coupling reaction.

There were several techniques were reported to prepare vinyl iodides including the use of regioselective B-iodo-9-BBN [BBN = borabicyclo (3.3.1) nonane] [48] as well as the Mo-catalyzed hydrostannation or the Pd-catalyzed stannation followed by iodination have been reported [32]. However, none of these techniques worked well for the synthesis of the required vinyl iodide [enantiomer of **30**: acetylenic (*S, S, S*) tetracyclic ketone (not shown here)] as

discussed by Edwankar *et.* al [32]. The bicyclohexyl iodoborane [$IB(Cy)_2$] was reported as a highly efficient regioselective reagent for the enolboration for the acetylenic (*S, S, S*) tetracyclic ketone (not shown)] [32]. Consequently, the desired vinyl iodide **30** was synthesized by following the published work of Edwankar *et.* al using regioselective $IB(Cy)_2$ on 5.1 gram scale [32]. The enolboration of acetylenic ketone **29** was carried out by the employment of 5 equivalents self-prepared solution of of $IB(Cy)_2$ in hexane (0.7 M in anhydrous hexanes), whereas the protodeboronation was carried out by using 11 equivalents of glacial acetic acid, which was added with stirring, at 0 ^oC. This was followed by the addition of 3 M NaOH and hydrogen peroxide to oxidize the boron by products and then followed by the addition of 5 % aqueous sodium bisulfite (to remove the excess iodine), was added as shown in **Scheme 2.11**. The vinyl iodide **30**, which resulted was isolated in 80% yield, after flash chromatography (please see **Experimental** section for details).



Scheme 2.11: The synthesis of the vinyl iodide (30) via iodoboronation and oxidation, and this was followed by the synthesis of pentacyclic ketone (28) via a Cu-mediated cross coupling process.

The vinyl iodide **30**, which resulted, was converted into the pentacyclic ketone **28** via a Cu-mediated cross coupling reaction by following the procedure, reported by Rahman *et.* al [36]. This procedure involves the employment of 1 equivalent each of copper iodide, *cis* 1, 2-cyclcohexane diol (ligand), as well as the 4 equivalents of cesium carbonate, and 5 equivalents of TEMPO (as a free radical scavenger) [36]. The Cu-mediated cross coupling technique to prepare pentacyclic ketone (enantiomer of **28**) reported here in, was an improved method with an increased yield (without the undesired 7-membered by product), when compared to the use of a palladium catalyst [32, 36].The preparation of the pentacyclic ketone **28** was afforded in 85% yield after purification by flash column chromatography on neutral alumina (see **Experimental** section for details). More than 20 grams of off-white colored pentacyclic ketone (in total) was

prepared, of which a small amount of which was crystallized using 100% ethyl acetate for X-ray crystallography, as shown in **Figure 2.5**. The X-ray crystal structure of pentacyclic ketone **28** was determined by Dr. Gregory Imler (US Naval Research Laboratory) at low temperature. The ORTEP view confirmed the desired stereochemistry and the atomic configuration. Moreover, the spectroscopic data (1H NMR, 13C NMR), HRMS, LCMS, R_f value, and the optical rotation of **28** (see below) in complete agreement with that reported for its enantiomer (structure not shown) [36].

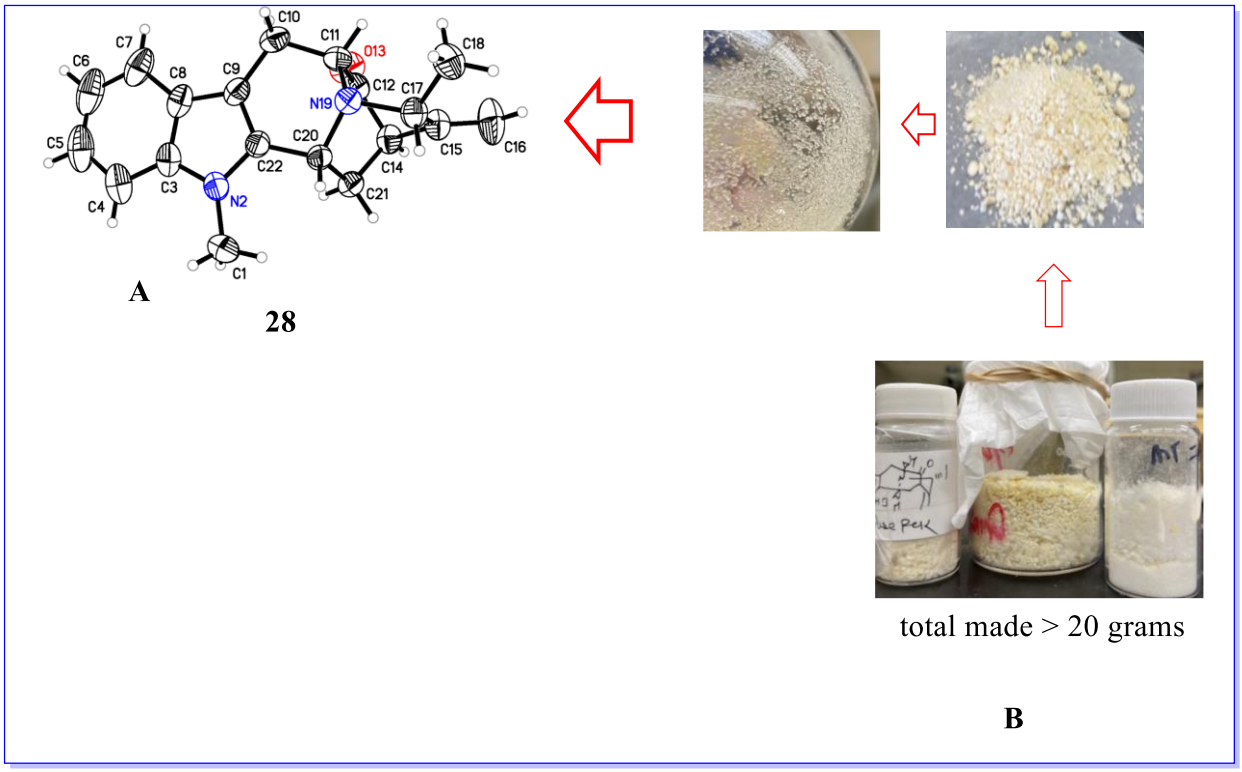
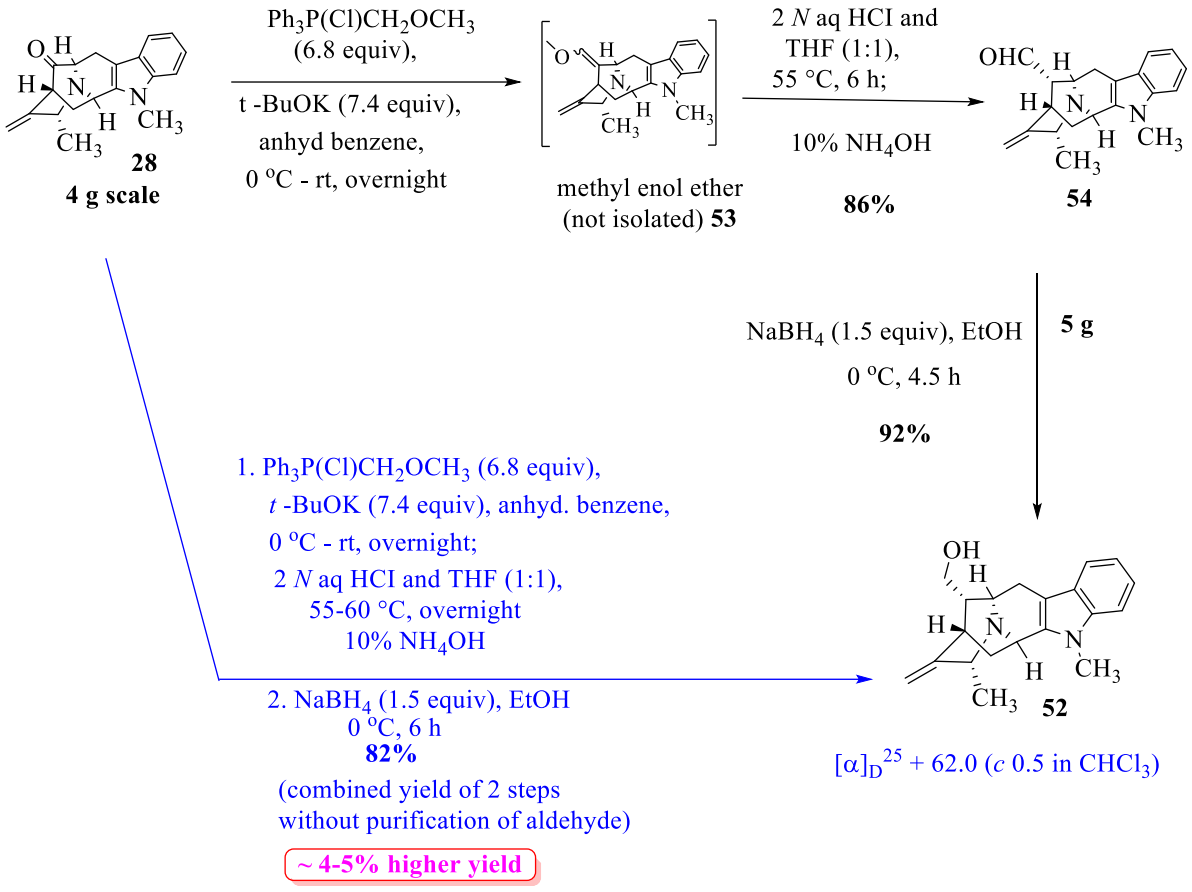


Figure 2.5. A: The ORTEP view of pentacyclic ketone (28). B: The crystals were prepared by crystallization, as the off-white colored pentacyclic ketone, using 100% ethyl acetate.

3.10. Synthesis of pentacyclic alcohol (52) via a Wittig reaction, which was followed by hydrolysis (*in-situ*) of the enol ether to aldehyde, and the reduction of the aldehyde (54).

After synthesis of the pentacyclic ketone **28**, it was then subjected to a one carbon homologation process via a Wittig reaction, according to the published procedure [32, 35, 36, 43]. The ylide (not shown) was prepared by stirring the Wittig reagent [(methoxymethyl)triphenylphosphonium chloride) with potassium *tert*-butoxide in dry benzene at room temperature. The yellow color formed in the reaction mixture changed to a dark red color after the mixture, which resulted, was stirred for 30 minutes. The presence of a persistent dark red color confirmed the formation of the ylide (**Figure 2.6**), after which the starting material was added to the reaction mixture at 0 ^{o}C. The pentacyclic methyl enol ether (intermediate) **53**, which resulted, was not isolated but subjected to acid hydrolysis to afford the pentacyclic aldehyde **54** (86%). The phosphorous byproducts present in the reaction mixture were removed by washing with hexanes 6-7 times, shaking vigorously, and then decanting the upper layer (hexane layer). The pentacyclic aldehyde **54** was found to have an a stereochemistry because the R_f value matched exactly with the authentic sample of its enantiomer (not shown), in which the alpha position had been confirmed by NMR spectroscopy and verified by analysis by 1D NOE [36, 37]. The pentacyclic aldehyde **54** was then reduced to the pentacyclic alcohol **52** (92% yield) with sodium borohydride (1.5 equivalents) as the reducing agent. Without isolating the aldehyde intermediate **54**, if the pentacyclic ketone **28** was converted into the pentacyclic alcohol **52** via the aldehyde **54** (as shown in **Scheme 2.12**) in another batch, the yield was improved by 5%. The slight increase in yield resulted because of the (possible) loss of alpha aldehyde **54** on a silica gel column, which was avoided, by omitting the purification step of the alpha aldehyde **54** by column chromatography. The pentacyclic alcohol **52** (white colored waxy solid), formed after the reduction of aldehyde **54** in the next step, was purified by flash column chromatography.



Scheme 2.12: The synthesis of the pentacyclic alcohol (52) via the Witting reaction, hydrolysis, and the reduction of alpha aldehyde (54).

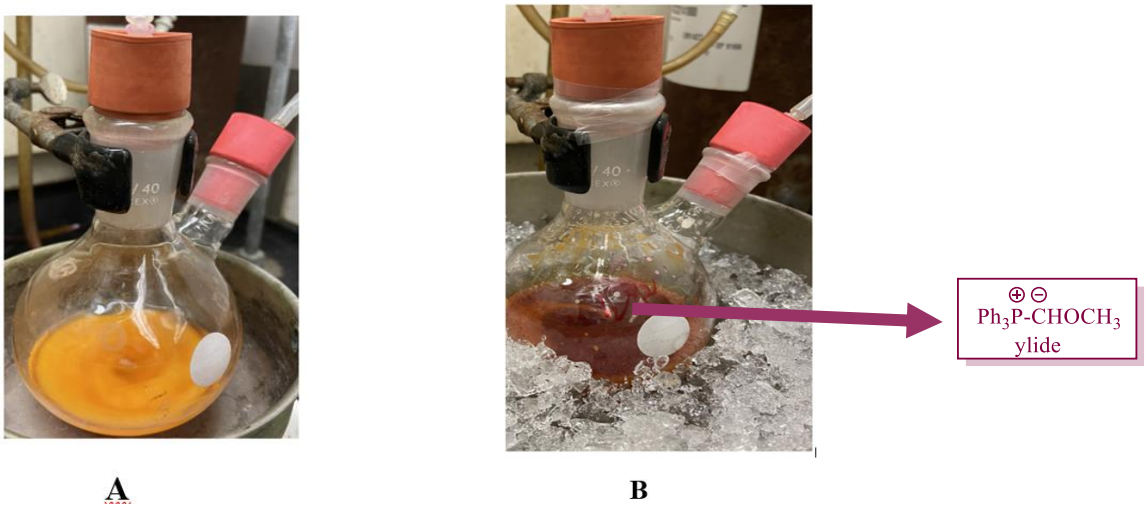
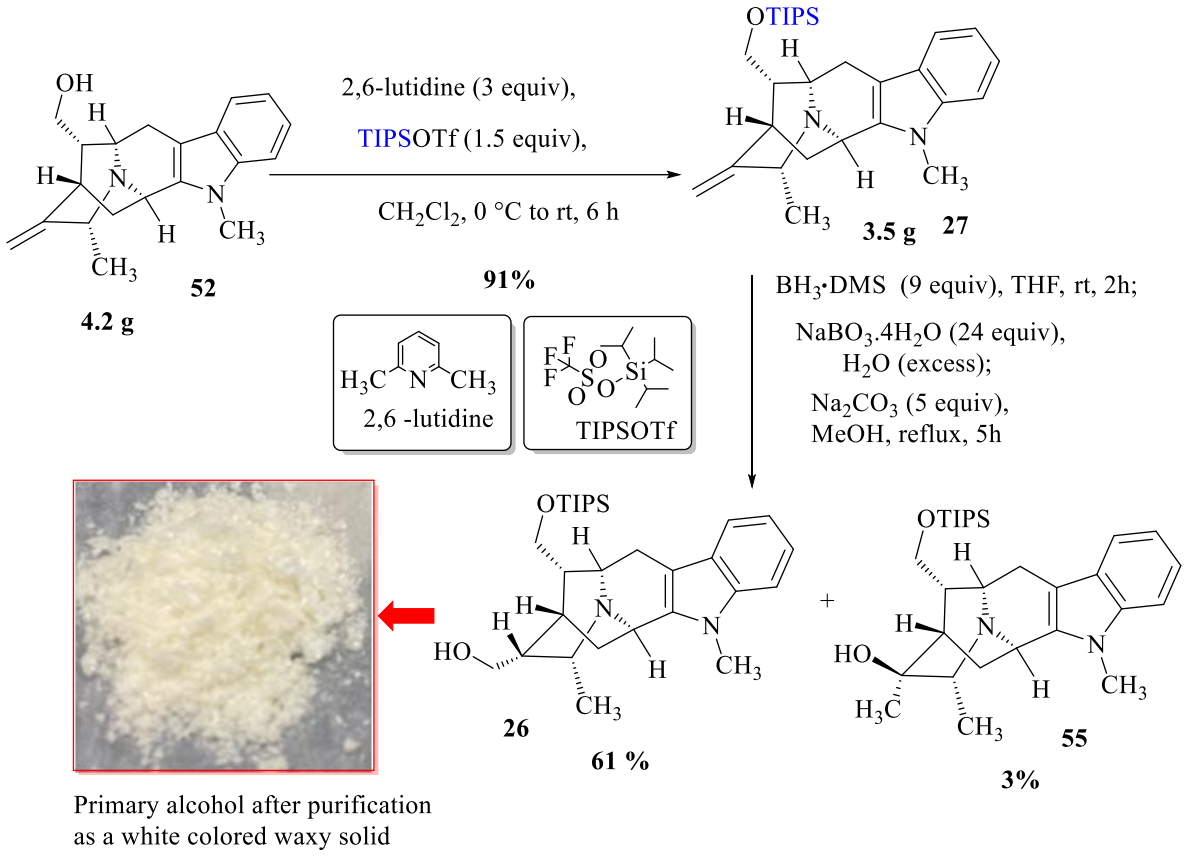


Figure 2.6. A: The reaction set-up showing the yellow-colored mixture of Wittig reagent with potassium *tert*-butoxide in anhydrous benzene. B: The ylide formation was confirmed by the presence of the persistent dark red color after 30 minutes of stirring.

3.11. Conversion of the alcohol into the silyl ether (27), followed by hydroboration and Kabalka oxidation.

The pentacyclic alcohol **52**, was then protected by a TIPS protecting group using the hindered base (2, 6-lutidine) base and TIPS-triflate (**Scheme 2.13**). This step resulted in the silyl ether **27** in excellent yield (91%). The silyl ether **27**, which resulted, was then subjected to hydroboration ($DMS.BH_3$) and a Kabalka oxidation on 3.5-gram scale by following the published procedure by the Milwaukee group [32, 37, 43]. **The use of hydrogen peroxide as an oxidizing agent was avoided because of the susceptibility to the formation of an N_b-oxide, which would be difficult to remove, as discussed by Edwankar *et* al.** [32]. Thus, sodium perborate was employed as an oxidizing reagent. The crude mixture, which resulted, was heated to reflux with 5 equivalents of sodium carbonate in methanol to cleave the N_b - boronate bond [32] . This hydroboration and Kabalka oxidation step resulted in two alcohols (**26** and **55** in an overall yield of 64%), and majority of which was the desired primary

alcohol **52** in 61% yield. The primary alcohol was purified by flash column chromatography and obtained as a white-colored waxy solid.

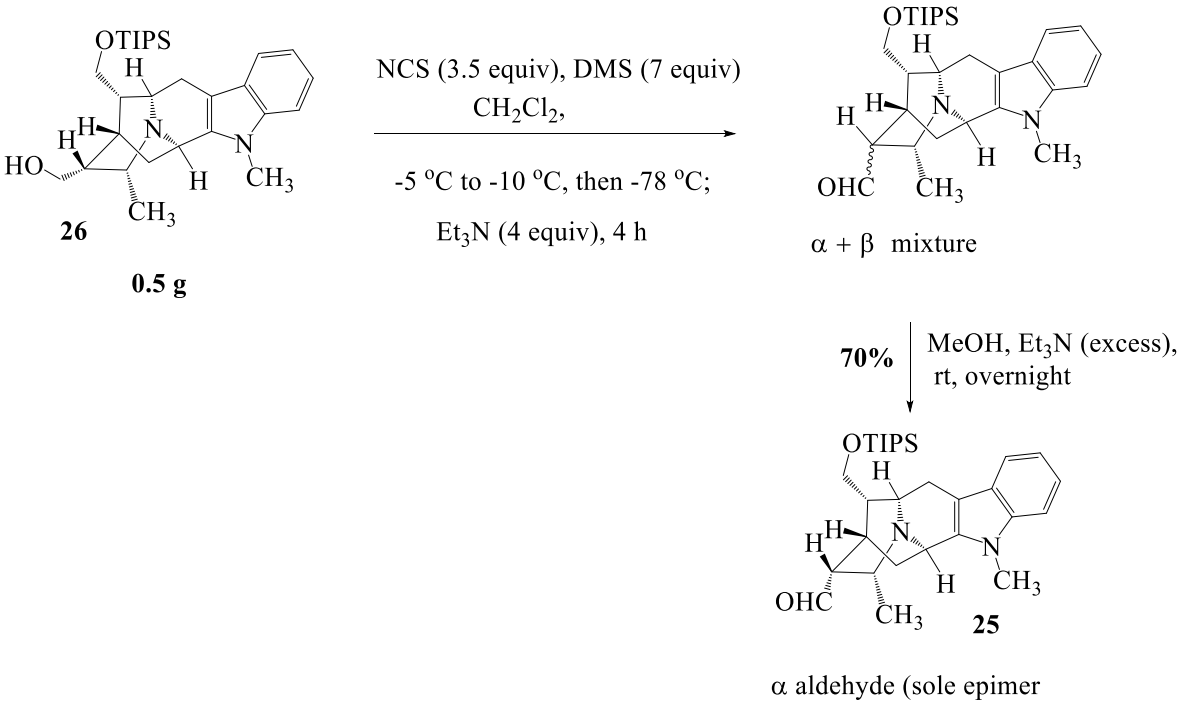


Scheme 2.13. The synthesis of silyl ether (27), and the synthesis of the desired primary alcohol (26).

3.12. Mild and modified Corey-Kim oxidation reaction and the epimerization of the mixture of aldehydes (α and β) into the more stable α aldehyde (25).

An efficient and modified Corey-Kim oxidation was reported by the Milwaukee group earlier [32, 43]. It was reported in this procedure that lowering the temperature to -78 °C and using 3.5 equivalents (instead of 5 equivalents) of *N*-chlorosuccinimide (NCS) and dimethyl sulfide (DMS) in the process was successful. The use of other oxidizing such as Dess-Martin

periodinane or hydrogen peroxide were avoided because of the susceptibility of the N_4 nitrogen atom to form the corresponding *N*-oxide adduct, as discussed [32]. The Initial attempts on small scale (10 mg, 15 mg, 12 mg, 15 mg, 8 mg, and 20 mg) reactions, were not successful and resulted in either the recovery of starting material or mixtures of products (several components on the TLC plate were observed; however, attempts for complete characterization of the products at such scales were not successful). Afterwards, the primary alcohol **26** (starting material) was resynthesized on a large scale. **When the reaction was redone on the higher scale (100 mg - 500 mg), following the same procedure as reported, the primary alcohol 26 was successfully oxidized to the mixture of aldehydes (α and β) as shown in Scheme 2.14, as desired.** In this oxidation reaction the formation of a white precipitate was observed immediately after adding the DMS dropwise to the solution of NCS in dichloromethane, as shown in **Figure 2.7(A).** This indicated the formation of the reactive sulfur cationic species. This was followed by the addition of alcohol (starting material) **26** at -78 ^{o}C. Using this modified Corey-Kim oxidation method, the primary alcohol (starting material **26**) was completely converted into the desired aldehyde without formation of by products, as shown in the **Scheme 2.14** and as indicated by analysis by TLC in **Figure 2.7(B)**. The epimeric mixture of aldehydes (α and β, see **Scheme 2.14**) were then subjected to epimerization in the presence of excess triethylamine in methanol. This resulted in conversion into the more stable α aldehyde **25** (thermodynamic product), as the sole epimer in 70% yield. The desired a aldehyde, which resulted, was purified by flash column chromatography as an oil (**Figure 2.7C)**. The formation of an aldehyde was confirmed by LCMS, HRMS, and spectral analysis (^{1}H NMR, ^{13}C NMR, DEPT ^{13}C spectra, please see **Experimental** section and **Appendix Part I** for details).



Scheme 2.14. The synthesis of alpha aldehyde (25) via the modified Corey-Kim oxidation and the epimerization of the mixture of aldehydes into the thermodynamically more stable a aldehyde.

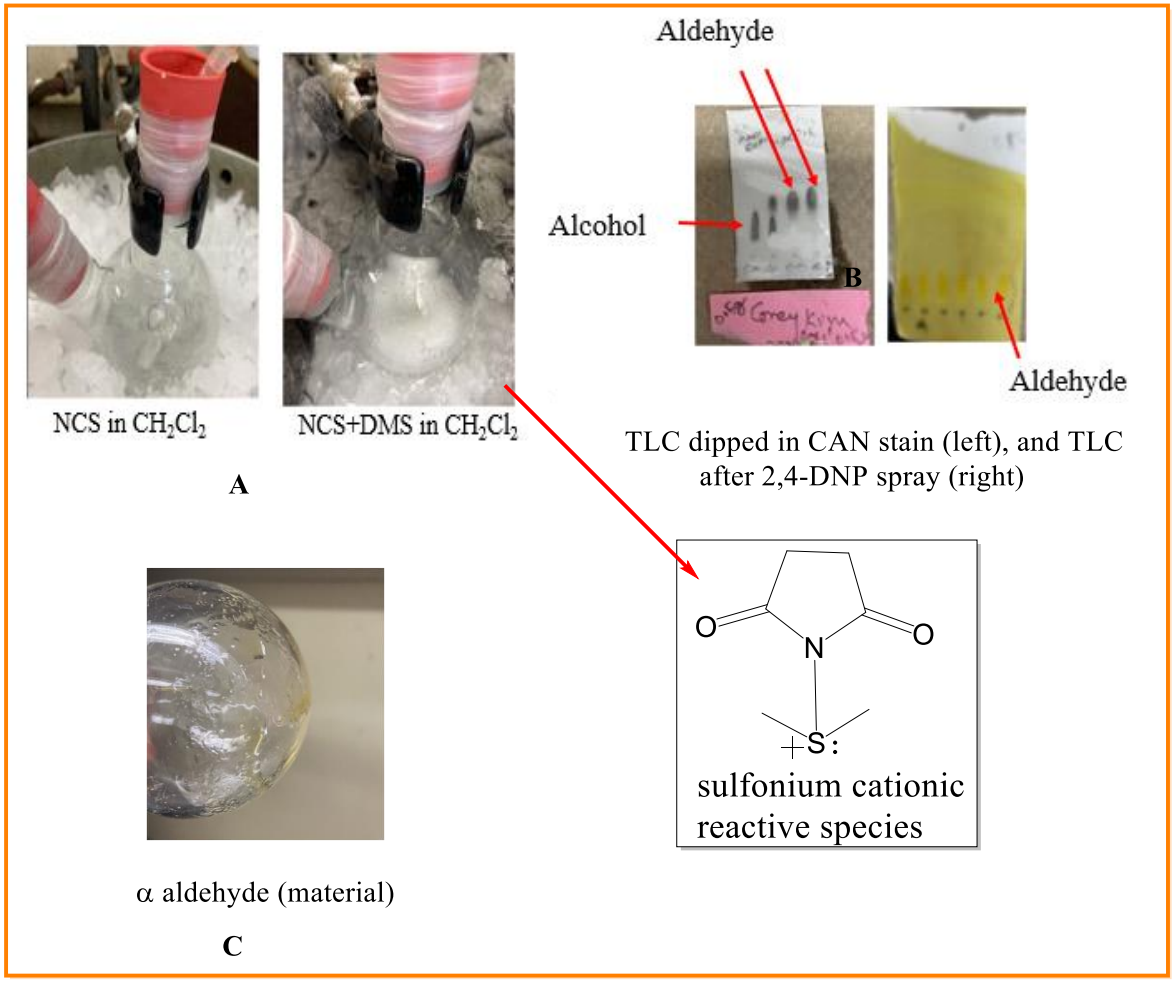


Figure 2.7. A: Reaction set-up showing the transparent mixture of NCS in CH_2Cl_2 (left), and the white precipitation of NCS and DMS in CH_2Cl_2. B: The indole components [alcohol (26) and aldehyde (25)] on the TLC dipped in CAN stain (left), and yellow component (25) on the TLC after 2, 4-DNP sprayed (right). C: An oily alpha aldehyde (25) material was collected after flash column chromatography.

3.13. Quaternization of α aldehyde (25), *retro*-Michael reaction, followed by hydrolysis in acidic medium.

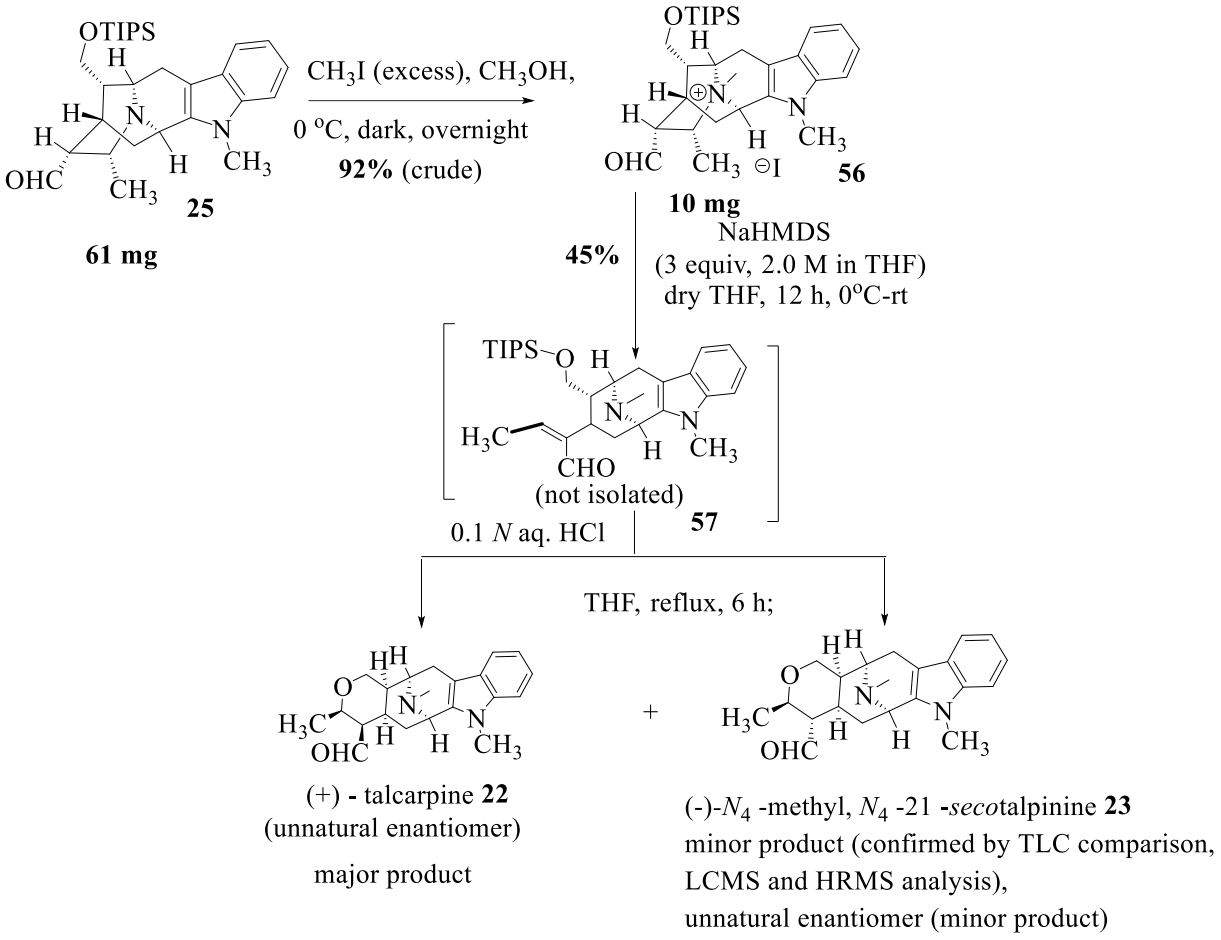
After the synthesis of the α -aldehyde **25**, it was subjected to quaternarization at the N_b Nitrogen position using an excess of iodomethane in methanol (the flask was covered with aluminum foil and argon gas was supplied to the reaction mixture by filling it in balloon, as shown in **Figure 2.8**). The formation of the quaternary salt was easily confirmed by LCMS, HRMS (please find

LCMS and HRMS data in **Appendix, Part I**), R_f (compared with the authentic sample: enantiomer of **56** by Rahman *et.* al [37], and by analysis of HRMS and NMR (crude ^{1}H NMR and ^{13}C NMR) spectroscopic data. The salt quaternary ammonium salt **56**, which resulted, was then employed in the *retro*-Michael reaction. At this step, when the solid NaHMDS base was used, the reaction did not work (**Table 2.2**). However, when NaHMDS (1.0 M) in THF was employed, the reaction worked, albeit in lower yield (35-41%), as compared to that reported in the literature for its enantiomer [37]. During the addition of NaHMDS (2.0 M in THF), the change in color from light yellow to dark green was observed, as shown in the **Figure 8** however, the reaction yield was 45%. The formation of the α, β–unsaturated aldehyde **57** was confirmed by analysis by LCMS, and HRMS. Moreover, the R_f value (0.27, silica gel, 5 % MeOH in DCM) when compared to the authentic sample of its enantiomer also matched in [37]. The crude α, β–unsaturated aldehyde **57** was then used in the final step without isolation and further characterization. The TIPS protecting group in the crude α, β–unsaturated aldehyde **57** was removed by heating the mixture to reflux, and the alcohol which resulted *in-situ*, underwent an *Oxa*-Michael reaction. After 6 hours of heating at reflux, the analysis by TLC indicated the formation of two components. When the TLC (same) plate was dipped into the ceric ammonium nitrate solution in phosphoric acid (CAN stain), the color which appeared (dark blue), which indicated the presence of two indole components: one intense component (higher R_f) and another fainter (lower R_f) component. The R_f values of both components were identical, as expected to those of the authentic samples of the corresponding natural enantiomers {(-)-talcarpine **6** and (+) N_4 -methyl, N_4 -21 -secotalpinine **3**} [37, 41]. The analysis by LCMS of the crude products exhibited the base peak at 339 amu (base peak in H_2O and 0.1% formic acid/acetonitrile mobile phase). The crude material was purified by flash column chromatography (silica gel, 2-3%

MeOH in DCM and a small amount of aqueous NH_4OH in the pasteur pipette). The synthesis of the unnatural enantiomer (+)-talcarpine **22** was confirmed by ^{1}H NMR, ^{13}C NMR, LCMS, HRMS and comparison of the R_f values on silica gel TLC plate with an authentic sample [(enantiomers of **22** and **3**) please see **Appendix, Part I** for spectral data). The lower faint indole component which appeared on the TLC plate, also exhibited a LCMS of 339 amu after isolation by flash chromatography. The analysis on HRMS: (ESI) m/z $(M + H)^+$ calcd for $C_{21}H_{26}N_2O_2$, predicted 339.2067, measured 339.2074 and it had a similar R_f value when compared to the natural (-) N_4 -methyl, N_4 -21 -secotalpinine **3**. Thus, the minor product obtained in this reaction, apparently, was the desired unnatural (-) N_4 -methyl, N_4 -21 -secotalpinine **23** indole alkaloid. Unfortunately, this material was not present in high enough amount for further characterization and structural conformation.

Table 2.2. Optimization of the *retro*-Michael reaction.

Scale	Reagent	Equivalent	Time	% Yield
40 mg	NaHMDS (solid)	1.5	10 h	No reaction
55 mg	NaHMDS (solid)	2	12 h	No reaction
65 mg	NaHMDS (solid)	2.5	20 h	Baseline impurities (in TLC) (No desired product seen in TLC and LCMS analysis)
22 mg	NaHMDS (0.5 M solution in THF)	2.5	16 h	35%
15 mg	NaHMDS (1 M solution in THF)	3	16 h	41%
10 mg	NaHMDS (2 M solution in THF)	3	16 h	45%



Scheme 2.15. The quaternization of an alpha aldehyde (25), *retro*-Michael reaction, acidic hydrolysis, and then intramolecular cyclization (*in-situ*) to give 22 and 23 (enantiomers of natural alkaloids).

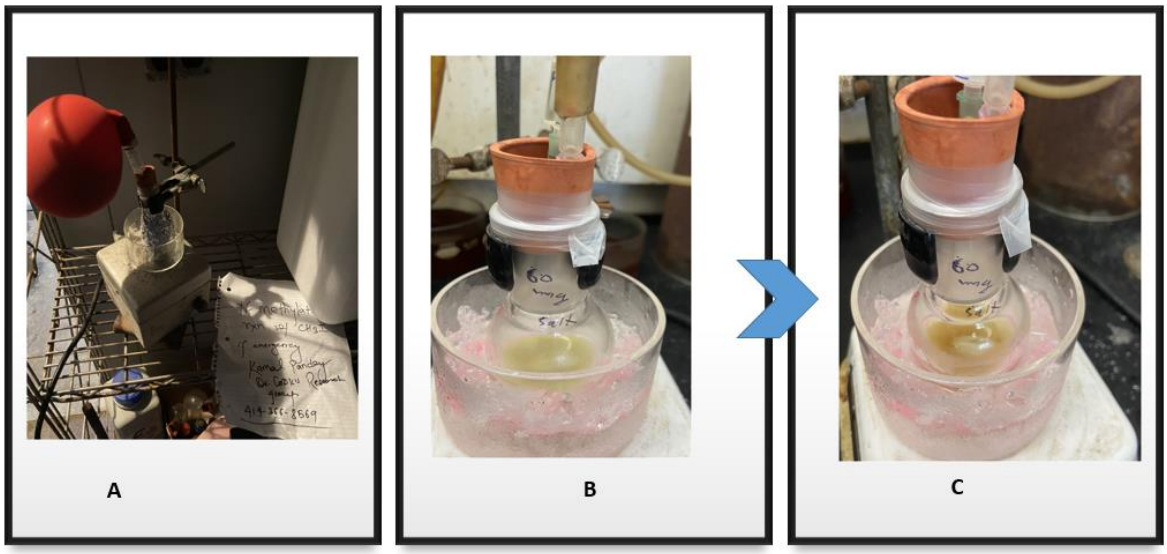


Figure 2.8. A: The reaction set-up of the quaternary ammonium salt (56) preparation. B: the quaternary ammonium salt (56) in dry THF (light yellow color before NaHMDS addition). C: quaternary ammonium salt (56) in dry THF where the light-yellow color changed to dark green after the addition of 1. 0 M NaHMDS solution in THF.

4. Conclusion.

By employing the Pictet-Spengler reaction/Dieckmann protocol or the ambidextrous Pictet-Spengler reaction developed in Milwaukee, the enantiospecific total synthesis of the unnatural enantiomer of biologically active (+)-talcarpine **22** was executed starting from the cheaper, natural, and DNA encoded L-tryptophan **36** for the first time. The desired stereochemical control was successfully carried out and this was confirmed by the X-ray analysis of key intermediates (tetracyclic ketone **29**, and pentacyclic ketone **28**), by determining the optical rotation values, and spectral data (^{1}H NMR and ^{13}C NMR). These were then compared to the natural enantiomers. As discussed above, the large-scale synthesis was executed and the crystallization techniques were employed to purify the products in most of the steps, where possible. The Pictet-

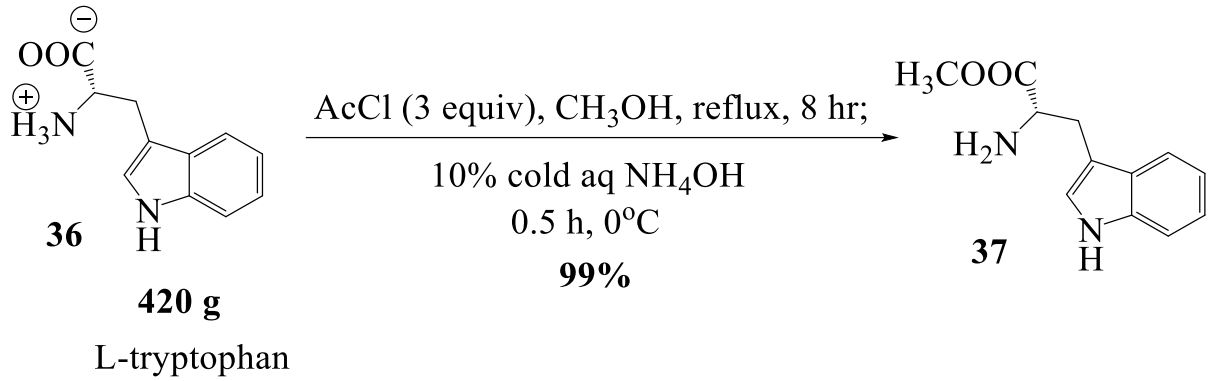
Spengler/Dieckmann protocol afforded the excellent yields in most of the steps, except in the *retro*-Michael ring opening reaction, as compared to that for the natural enantiomers [41].

5. Experimental

General Experimental conditions

Unless otherwise specified, for all reaction, oven-dried round-bottom flasks or screw-cap test tubes were used. Chemicals were purified by standard methods and purchased from commercially available vendors. The flash column chromatography was carried out for the purification of analogs on silica gel (230-400 mesh, Dynamic Adsorbents), neutral alumina, or basic alumina. The melting points were determined on a Stuart melting point SMP3 apparatus manufactured by Barloworld Scientific US Ltd. The ^{1}H and ^{13}C NMR spectra were obtained on a Bruker Spectrospin 500 MHz or 300 MHz instruments in $CDCl_3$ or in methanol-d^4. Isopropyl alcohol was purified by distillation over calcium sulfate and dried [molecular sieves (3 A^o)]. The chemical shifts are reported in δ (ppm). Multiplicities are represented as follows: singlet (s), broad signal (br), doublet (d), triplet (t), quartet (q), dd (doublet of doublets), dt (doublet of triplets), td (triplet of doublets) and multiplet (m). The technique employed for HRMS was carried out on an LCMS-IT-TOF at the Milwaukee Institute for Drug Discovery (MIDD) in the Shimadzu Laboratory for Advanced and Applied Analytical Chemistry. Optical rotations were measured on a JASCO Model DIP-370 digital polarimeter. Benzene was distilled over calcium hydride and dried using molecular sieves (3 A^o). **It was handled in the hood with caution.**

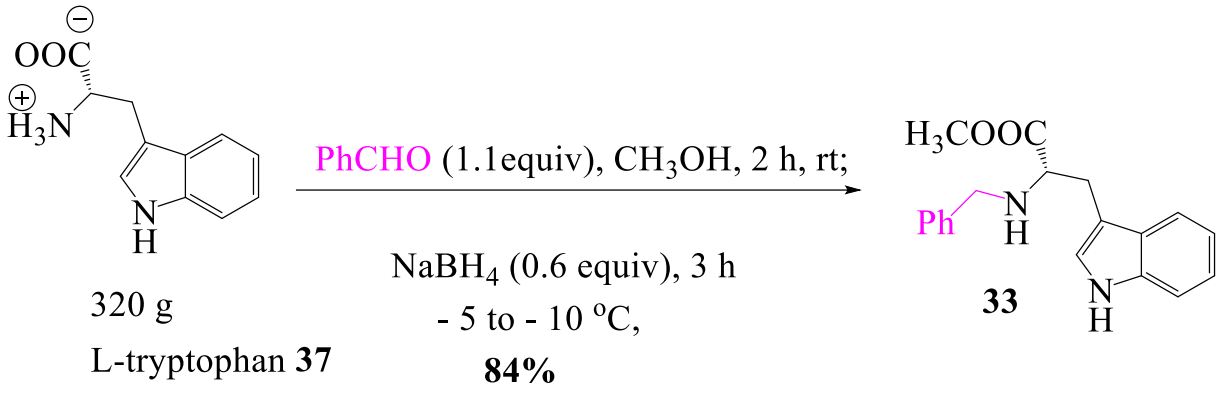
Synthesis of L-tryptophan methyl ester (37)



In a 3 neck round bottom flask (5 L), L-tryptophan **36** (420 g, 2.05 mol) and 2000 mL of anhydrous methanol were added. The temperature of the flask was decreased to 0°C (ice bath). To the reaction mixture 3 equivalents (6.16 mol, 440 mL) of acetyl chloride was added dropwise and the reaction mixture was allowed to warm to rt and then heated to reflux for 8 h. The completion of the reaction was confirmed on analysis by TLC ($\boldsymbol{R_f}$ 0.4 in 5% methanol/dichloromethane + a few drops of 14% ammonium hydroxide solution). The free base **37** was prepared by basifying the reaction mixture (PH=10) by dropwise addition of 10% aq NH_4OH solution at 0°C. The aq layer was extracted with CH_2Cl_2 (3 x 100 mL). The combined organic layer was washed with brine (100 mL) and dried (K_2CO_3). The evaporation of the organic solvents under reduced pressure furnished a pure light brown colored crystalline product: $\boldsymbol{[\alpha]_D^{25}}$ + 35.4 (c 1.18, MeOH); Lit. value for its enantiomer: $[\alpha]_D^{27}$ - 37.2 (c 1.0, MeOH) [43]; **^{1}H NMR** (500 MHz, $CDCl_3$) δ 8.36 (s, 1H), 7.64 (d, *J* = 7.9 Hz, 1H), 7.37 (d, *J* = 8.1 Hz, 1H), 7.22 (t, *J* = 7.4 Hz, 1H), 7.15 (t, *J* = 7.4 Hz, 1H), 7.06 (d, *J* = 1.4 Hz, 1H), 3.86 (dd, *J* = 7.6, 4.8 Hz, 1H), 3.74 (s, 3H), 3.31 (dd, *J* = 14.4, 4.7 Hz, 1H), 3.15 – 3.04 (m, 1H), 1.70 (s, 2H); **^{13}C NMR** (126 MHz, $CDCl_3$) δ 175.77 (s), 136.32 (s), 127.48 (s), 123.02 (s), 122.16 (s), 119.53 (s), 118.76

(s), 111.07 (s), 54.97 (s), 52.06 (s), 30.75 (s). The spectroscopic data (^{1}H and ^{13}C NMR), and optical rotation value for this compound **37** were in complete agreement with that reported in the literature for its enantiomer [32, 35, 43].

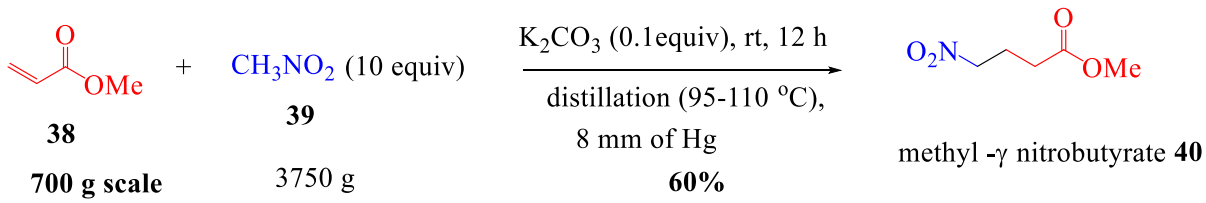
Preparation of methyl benzyl-L-tryptophanate (33).

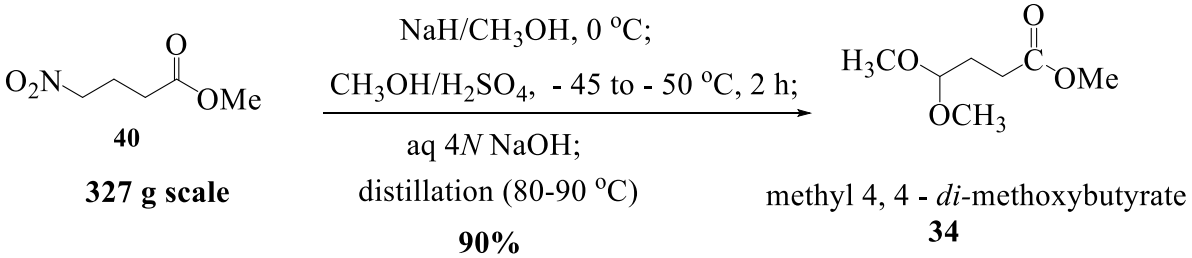


To a solution of L-tryptophan methyl ester **37** (320 g, 1.46 mol) in anhydrous methanol (1200 mL), benzaldehyde (165 mL) was added, and the mixture, which resulted, was stirred at rt for 2 h. After the completion of the reaction, as indicated by analysis by TLC (silica gel, 5% MeOH in CH_2Cl_2 + few drops of NH_4OH), the temperature was decreased to about -10 °C (ice and salt bath), and $NaBH_4$ (33.2 g, 0.87 mmol) was added portionwise every 15 min. After the addition of the last potion of $NaBH_4$, the reaction mixture was stirred for 4 h at 0 °C. To avoid racemization of the imine intermediate (not shown), the reagent $NaBH_4$ was added portionwise and the mixture, which resulted, stirred only for the time (over stirring avoided) until the analysis by TLC (silica gel, EtOAc: hexane, 4:6+ a few drops of 10% aq NH_4OH) indicated completion of process. The reaction was then quenched by cold water (45 mL). The organic solvent was removed under reduced pressure, and the residue was dissolved in CH_2Cl_2 (2000 mL) and washed with brine (2 x 500 mL). The organic layer was dried (K_2CO_3) and the solvent was

removed under reduced pressure to give the N_b-benzyl-L-tryptophan methyl ester **33** (380 g, 84%), which was further purified by crystallization from EtOH. The spectral data and the optical rotation were in complete agreement with the data of N_b-benzyl D-tryptophan methyl ester (enantiomer): **$[\alpha]_D^{25}$** - 9.9 (c 1.01, MeOH) [reference value for its enantiomer: $[\alpha]_D^{27}$ + 9.07 (c 1.0, MeOH) [32, 43, 49]; **^{1}H NMR** (500 MHz, $CDCl_3$) δ 8.18 (s, 1H), 7.59 (d, J = 7.9 Hz, 1H), 7.36 (d, J = 8.1 Hz, 1H), 7.30 – 7.24 (m, 5H), 7.23 – 7.19 (m, 1H), 7.13 (td, J = 7.6, 0.9 Hz, 1H), 7.07 (d, J = 2.3 Hz, 1H), 3.88 (d, J = 13.2 Hz, 1H), 3.78 – 3.70 (m, 2H), 3.66 (s, 3H), 3.24 (qd, J = 14.5, 6.5 Hz, 2H); **^{13}C NMR** (126 MHz, $CDCl_3$) δ 175.27 (s), 139.48 (s), 136.20 (s), 128.39 (s), 128.23 (s), 127.66 (s), 127.50 (s), 127.02 (s), 122.93 (s), 122.08 (s), 119.44 (s), 118.81 (s), 111.19 (s), 61.20 (s), 52.13 (s), 51.80 (s), 29.26 (s). The spectroscopic data (^{1}H and ^{13}C NMR), and optical rotation for this compound **33** were in complete agreement with that reported in the literature for its enantiomer [32, 43, 49].

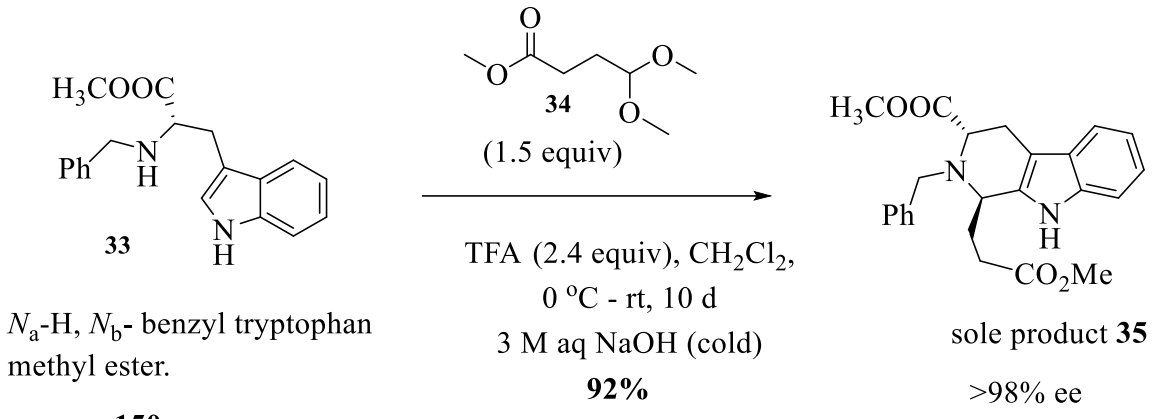
Preparation of 4, 4-dimethoxybutyrate (34)





To a round bottom flask (with overhead stirrer), methyl acrylate **38** (700 g, 7 mol), nitromethane **39** (3750 g, 70 mol), and K_2CO_3 (96.8 g, 0.7 mol) were added at 0 °C. The mixture, which resulted, was stirred at rt for 12 h. The organic layer was separated using a separatory funnel and was washed with a small amount of CH_2Cl_2. The solvents were removed under reduced pressure, which resulted in a crude oil. The crude oil was purified by distillation under reduced pressure (95-100 °C/8 mm of Hg) to afford pure methyl g-nitro butyrate **40** (615.2 g, 60%). The pure methyl g -nitro butyrate **40** was dissolved in methanolic sodium methoxide [6160 mL, 0.8 *N*, which had been freshly prepared from 197 g of NaH (60% dispersion in mineral oil)], and the solution, which resulted, was added dropwise with an overhead stir at a rate of 1 drop per second to a round bottom flask which contained a solution of cone sulfuric acid (1540 mL) in methanol (4050 mL) at -45 to -50 °C. After the addition was completed, the reaction mixture was poured into CH_2C1_2 (8000 mL). The organic layer was separated and washed with ice water (2 x 1000 mL), as well as aq 4 *N* NaOH (2 x 600 mL) and dried (K_2CO_3). The solvent was removed under reduced pressure and the residue was distilled (110- 115 °C/8 mm of Hg) to provide methyl 4,4-*di*-methoxybutyrate **34** as oil (610 g, 90%): **^{1}H NMR** (500 MHz, $CDCl_3$) δ_H 4.22 (t, J = 5.6 Hz, 1H), 3.49 (s, 3H), 3.14 (s, 6H), 2.20 (t, J = 7.5 Hz, 2H), 1.74 (td, J = 7.5, 5.6 Hz, 2 H); **^{13}C NMR** (126 MHz, $CDCl_3$) δ_c 173.30 (s), 103.37 (s), 52.75 (s), 51.20 (s), 28.74 (s), 27.58 (s). The proton and carbon NMR data for this compound **34** were identical in all respects with that reported in the literature [32, 43, 49].

Methyl (1*R*,3*S*)-2-benzyl-1-(3-methoxy-3-oxopropyl)-2,3,4,9-tetrahydro-1*H*-pyrido[3,4-b]indole-3-carboxylate (35).



N_a-H, N_b- benzyl tryptophan methyl ester.

150 g

sole product **35**

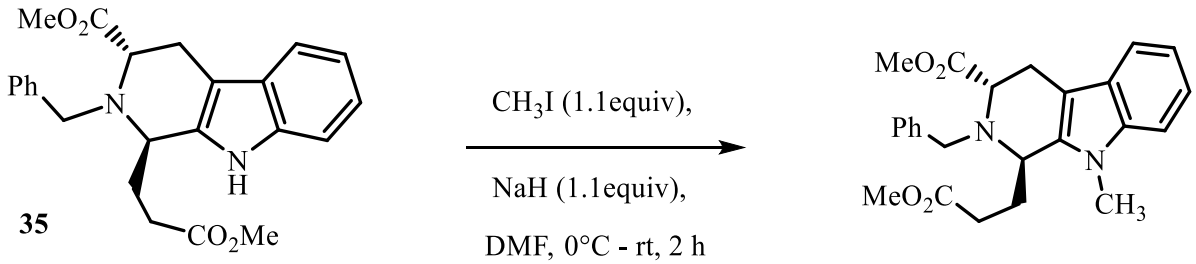
>98% ee

To a 3-neck round bottom flask (5 L), which contained a solution of N_b-benzyl-L-tryptophan methyl ester **33** (150 g, 0.48 mol) in CH_2C1_2 (1400 mL), methyl 4,4-dimethoxybutyrate acetal **34** (112.5 mL, 0.7 mol), and TFA (82.2 mL, 2.4 equiv) was added at 0 °C. The reaction mixture was stirred at rt for 10 d and then cooled to 0 °C (ice bath) and brought to pH = 8 with a dropwise addition of cold aq solution of NaOH (3 *N*). The layers were separated and the aq layer was extracted with CH_2C1_2 (3 x 900 mL). The combined organic layer was washed with brine (2 x 400 mL) and dried (K_2CO_3). The volume of the solution was reduced to 150 mL under reduced pressure after which EtOAc (50 mL) and hexanes (100 mL) were added to the solution. The solution was cooled to -20 °C. The trans diester **35** precipitated out as white crystals and the mother liquor was concentrated. The residue, which resulted, was purified by flash chromatography (silica gel, EtOAc/hexane, 1:4) to provide an additional (5 g) of trans-diester **35**. The combined solids were dried under vacuum overnight (169 g, 76%): $\mathbf{[\alpha]_D^{25}}$ + 36.2 (c 1.02,

CHCl3), Lit. value for its enantiomer: $[\alpha]_D^{27}$ - 35.7 (c 1.4, CHCl3) [43] ; **^{1}H NMR** (500 MHz, $CDCl_3$) δ 7.53 (d, J = 7.7 Hz, 1H), 7.32 (dt, J = 15.0, 7.5 Hz, 5H), 7.19 (dd, J = 22.2, 14.9 Hz, 2H), 7.12 (t, J = 7.4 Hz, 1H), 4.01 (dd, J = 8.9, 5.0 Hz, 1H), 3.93 (d, J = 4.2 Hz, 1H), 3.86 (d, J = 13.5 Hz, 1H), 3.77 (s, 3H), 3.59 (d, J = 13.5 Hz, 1H), 3.51 (s, 3H), 3.14 (dd, J = 15.7, 9.1 Hz, 1H), 3.03 (dd, J = 15.8, 4.8 Hz, 1H), 2.47 – 2.37 (m, 1H), 2.37 – 2.25 (m, 1H), 2.13 – 2.04 (m, 1H), 1.97 (td, J = 14.3, 7.0 Hz, 1H); **^{13}C NMR** (126 MHz, $CDCl_3$) δ 174.28 (s), 173.40 (s), 139.30 (s), 136.24 (s), 134.17 (s), 129.11 (s), 128.26 (s), 127.10 (s), 126.96 (s), 121.81 (s), 119.52 (s), 118.16 (s), 110.92 (s), 107.49 (s), 56.73 (s), 54.64 (s), 53.39 (s), 51.93 (s), 51.48 (s), 29.86 (s), 28.99 (s), 21.23 (s).

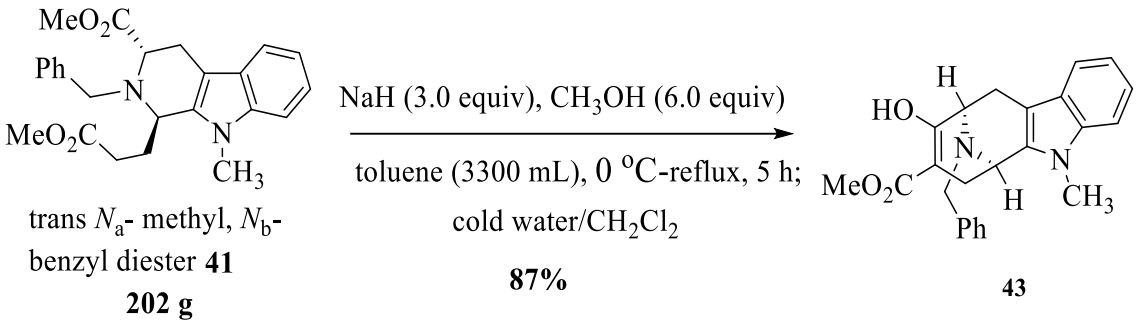
The spectroscopic data (^{1}H and ^{13}C NMR), and optical rotation for this compound **35** were in complete agreement with that reported in the literature for its enantiomer [32, 43, 49].

Methyl (1*R*, 3*S*)-2-benzyl-1-(3-methoxy-3-oxopropyl)-9-methyl-2,3,4,9-tetrahydro-1*H*-pyrido[3,4-b]indole-3-carboxylate (41).



The N_a-H-*trans*-diaster **35** (172 g, 0.42 mol) and dry DMF (1100 mL) were added to a 3-neck round-bottom flask (3000 mL) equipped with a reflux condenser. To the solution, CH_3I (66.1 g, 0.46 mol) was added with stirring, and then the mixture was cooled to 0 °C using an ice bath. Then NaH [60% dispersion in mineral oil (11.1 g, 0.46 mol)] was added portionwise to minimize abrupt hydrogen gas evolution at 0 °C. The slurry, which resulted, was allowed to stir at rt for 2 h until analysis by TLC (silica gel, EtOAc/hexane, 1:4) indicated the disappearance of starting material. The reaction solution was quenched by slow addition of CH_3OH (100 mL) and then neutralized with a saturated aq solution of NH_4CI, and this was followed by extraction with EtOAc (4 x 400 mL). The DMF was removed by washing the organic layer with water (5 x 100 mL). The combined organic layers were washed with brine and dried (K_2CO_3). The solvent was removed under reduced pressure and the residue was purified by crystallization from EtOAc: hexane (50:50) to furnish N_a -methyl *trans*-diester **41** (172.2 gram, 96% yield), which was dried at rt under vacuum for 10 h: **$[\alpha]_D^{25}$** + 51.9 (c 1.02 $CHCl_3$), Lit. value for its enantiomer: $[\alpha]_D^{25}$ - 54.6 (c 1.0, $CHCl_3$) [50]; **^{1}H NMR** (500 MHz, $CDCl_3$) δ 7.60 (d, J = 7.8 Hz, 1H), 7.35 (dt, J = 14.8, 7.3 Hz, 5H), 7.27 (ddd, J = 15.4, 7.6, 2.5 Hz, 2H), 7.17 (dd, J = 11.0, 3.8 Hz, 1H), 4.21 – 4.09 (m, 3H), 3.87 (s, 3H), 3.67 (s, 3H), 3.50 (s, 3H), 3.41 (d, J = 13.3 Hz, 1H), 3.13 (ddd, J = 20.9, 15.9, 8.1 Hz, 2H), 2.62 (ddd, J = 17.3, 9.4, 5.4 Hz, 1H), 2.42 (dt, J = 17.4, 5.5 Hz, 1H), 2.06 – 2.00 (m, 1H), 1.93 – 1.84 (m, 1H); **^{13}C NMR** (126 MHz, $CDCl_3$) δ 173.96 (s), 173.31 (s), 139.09 (s), 137.54 (s), 135.56 (s), 129.43 (s), 128.26 (s), 127.13 (s), 126.54 (s), 121.45 (s), 119.23 (s), 118.22 (s), 109.00 (s), 106.30 (s), 56.20 (s), 53.48 (s), 52.87 (s), 52.15 (s), 51.35 (s), 29.80 (s), 29.69 (s), 27.97 (s), 20.34 (s). The spectroscopic data (^{1}H and ^{13}C NMR), and optical rotation for this compound **41** were in complete agreement with that reported in the literature for its enantiomer [32, 43].

Dieckmann cyclization of N_a -methyl trans diaster (41) to provide methyl (6*R*,10*R*)-12-benzyl-9-hydroxy-5-methyl-6,7,10,11-tetrahydro-5*H*-6,10-epiminocycloocta[b]indole-8-carboxylate (43).



trans N_a- methyl, N_b-benzyl diester **41**
202 g

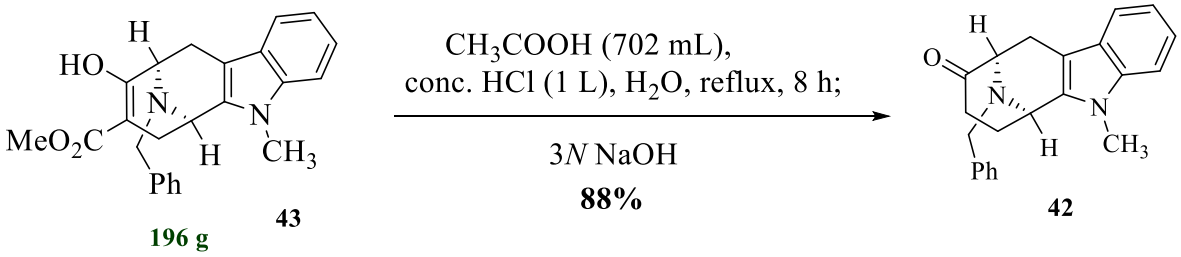
87%

43

In a 3 neck round bottom flask (5 L), which contained 3300 mL of toluene, [(toluene had been pre-dried by azeotropic removal of H_2O by a DST (refluxed 8 h)], the *trans*-diaster **41** (202 g, 0.48 mol) was added. In the same reaction mixture, NaH (59 g: 60% dispersion in mineral oil) at 0 °C was added carefully, which was followed by the slow addition of CH_3OH (105 mL) dropwise under argon. The reaction mixture was allowed to warm to rt and stirred for 0.5 h. After this the solution was heated to reflux for 5 h. While refluxing, the sides of the flask were covered with aluminium foil to maintain the reflux temperature without carbonizing any compound on the sides of the flask. After the disappearance of the starting material (confirmed by analysis by TLC (silica gel, EtOAc/hexane, 1:4), the reaction solution was quenched with cold water (300 mL). The aq layer was extracted with CH_2CI_2 (4 x 1500 mL) and the combined organic layer was washed with brine (2 x 200 mL) and dried (K_2CO_3). The solvent was removed under reduced pressure and the mineral oil was separated by decantation. The residue, which

resulted, was dried under vacuum at 40 °C (10 h) and then used directly in the next step (acidic hydrolysis) without further purification and characterization.

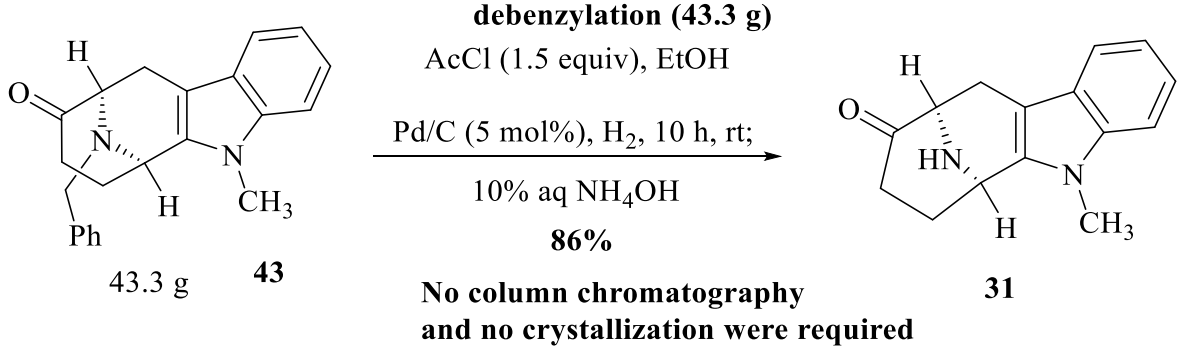
Acid mediated hydrolysis and decarboxylation of methyl (6*R*,10*R*)-12-benzyl-9-hydroxy-5-methyl-6,7,10,11-tetrahydro-5*H*-6,10-epiminocycloocta[b]indole-8-carboxylate (43) to provide (6*R*,10*R*)-12-benzyl-5-methyl-5,6,7,8,10,11-hexahydro-9*H*-6,10-epiminocycloocta[b]indol-9-one (42).



In a 3 neck round bottom flask (5000 mL) containing the b-keto ester **43** (196 g, 0.5 mol), glacial acetic acid (702 mL), aq hydrochloric acid (1000 mL, conc.) and water (280 mL) were added. The solution, which resulted, was stirred and held at reflux for 8 h. The solvent (mostly acid) was removed carefully under reduced pressure (one neck 3000 mL round bottom flask is easier on this scale with a Keck clip). The residue was brought to pH = 9 with the addition of a cold aq solution of NaOH (3 N) at 0 °C dropwise. The mixture, which resulted, was extracted with CH_2Cl_2 (4 x 1500 mL) and the combined organic extracts were washed with a saturated aq solution of NH_4Cl (2 x 400 mL), brine (2 x 300 mL), and dried (K_2CO_3). The product was purified by crystallization from EtOAc/ hexane (1:4, 500 mL). The mothor liquor was

concentrated under reduced pressure and the residue was purified by column chromatography (silica gel with EtOAc/hexane, 1:4) to provide additional tetracyclic ketone **42**. The solid was dried under vacuum at rt for 8h to yield the tetracyclic ketone **42** (145 g, 88%): **$[\alpha]_D^{25}$** + 236.6 (c 1.0, CHCl3), Lit. value for its enantiomer: $[\alpha]_D^{27}$ – 240.2 (c 1.0, $CHCl_3$) [32]; **^{1}H NMR** (300 MHz, $CDCl_3$) δ 7.58 (d, J = 7.7 Hz, 1H), 7.41 – 7.28 (m, 7H), 7.20 (t, J = 7.3 Hz, 1H), 4.13 (s, 1H), 3.87 – 3.76 (m, 3H), 3.66 (s, 3H), 3.32 (dd, J = 16.9, 6.8 Hz, 1H), 2.76 (d, J = 16.9 Hz, 1H), 2.60 – 2.46 (m, 2H), 2.28 – 1.95 (m, 2H); **^{13}C NMR** (75 MHz, $CDCl_3$) δ 210.04 (s), 138.31 (s), 137.27 (s), 133.18 (s), 128.74 (s), 128.53 (s), 127.45 (s), 126.51 (s), 121.63 (s), 119.35 (s), 118.30 (s), 109.00 (s), 105.79 (s), 64.90 (s), 56.27 (s), 48.94 (s), 34.38 (s), 29.80 (s), 29.39 (s), 20.50 (s); **HRMS** (ESI) m/z $(M + H)^+$ calcd for $C_{22}H_{22}N_2O$, 331.1805, found 331.1772. The spectroscopic data (^{1}H and ^{13}C NMR), and optical rotation for this compound **42** were in complete agreement with that reported in the literature for its enantiomer [32, 41, 43].

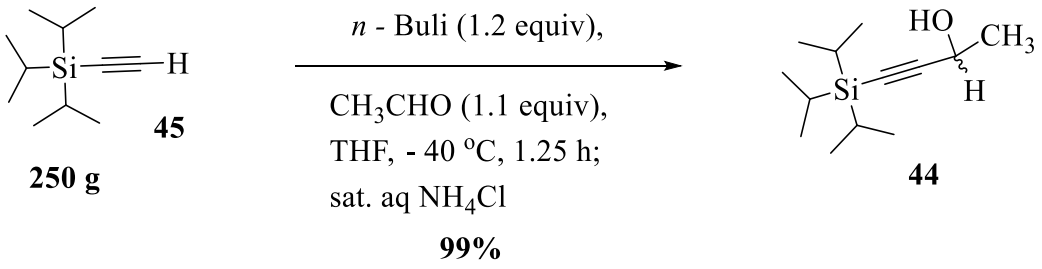
Catalytic debenzylation of (6*R*,10*R*)-12-benzyl-5-methyl-5,6,7,8,10,11-hexahydro-9*H*-6,10-epiminocycloocta[b]indol-9-one (43) to provide (6*R*,10*R*)-5-methyl-5,6,7,8,10,11-hexahydro-9*H*-6,10-epiminocycloocta[b]indol-9-one (31).



In a round bottom flask with a solution of N_b-benzyl tetracyclic ketone **43** (43.3 g, 0.13 mol) in anhydrous (200 proof) EtOH (390 mL), with stirring, was added the acetyl chloride (16.5 g, 0.21 mol) in 150 mL of anhydrous EtOH dropwise at 0 °C. At this point, the solid starting material completely dissolved. The solvent was removed under reduced pressure and moderate temperature (water bath temperature 40 °C). Anhydrous diethyl ether (2 x 100 mL) was poured into the residue and then the diethyl ether was removed under reduced pressure. Finally, the HCl salt was dissolved in anhydrous EtOH (2 x 60 mL) and EtOH was evaporated under reduced pressure to remove excess HCl. The repetition of this step 5-times was crucial to make sure no excess HCl remained in the residue. This was then followed by degassing of the hydrochloride salt at rt under reduced pressure and it was back filled with argon (3 times). The dry EtOH (400 mL), and dry Pd/C (10% by wt, 13 g) were added to the above hydrochloride salt. The mixture, which resulted, was degassed under reduced pressure at rt and back filled with H_2 gas three times (H_2 gas filled in balloon). The mixture, which resulted, was stirred at rt under an atmosphere of H_2 (1 atm) for 10 h or until the disappearance of starting material on analysis by TLC (EtOAc with few drops of MeOH and 10% aq NH_4OH). **The catalyst was filtered off through a short pad of celite, and the solid was washed with EtOH (3 x 90 mL) and discarded safely**. The solvent was removed under reduced pressure. The residue was dissolved in CH_2Cl_2, and the free base was prepared by dropwise addition of 10% aq NH_4OH. The layers were separated and the aq layer was washed with CH_2Cl_2 (2 x 500 mL) and the combined layer was washed with brine (2 x 300 mL) and dried using anhydrous K_2CO_3. The solvent was removed under reduced pressure to yield N_a-Me, N_b-H tetracyclic ketone **31** (27 g, 86%) as a pure solid (no further purification was required), which was dried under vacuum before using it in the next step: **^{1}H NMR** (300 MHz, $CDCl_3$) δ 7.50 (d, J = 7.8 Hz, 1H), 7.38 – 7.21 (m, 2H), 7.15 (t, J = 7.3 Hz,

1H), 4.37 (s, 1H), 3.95 (d, J = 6.7 Hz, 1H), 3.63 (s, 3H), 3.14 (dd, J = 16.5, 6.8 Hz, 1H), 2.84 (d, J = 16.5 Hz, 1H), 2.49 (dt, J = 9.7, 4.2 Hz, 2H), 2.12 (dd, J = 14.9, 7.4 Hz, 2H); **^{13}C NMR** (75 MHz, $CDCl_3$) δ 210.74 (s), 137.00 (s), 135.22 (s), 126.56 (s), 121.63 (s), 119.31 (s), 118.15 (s), 108.93 (s), 106.43 (s), 59.72 (s), 44.90 (s), 34.97 (s), 31.43 (s), 29.30 (s), 25.87 (s); **HRMS** (ESI) m/z $(M + H)^+$ calcd for $C_{19}H_{16}N_2O$, 293.1648, found 293.1614. The spectroscopic data (^{1}H and ^{13}C NMR) of this compound **31** were in complete agreement with that reported in the literature for its enantiomer [32, 43].

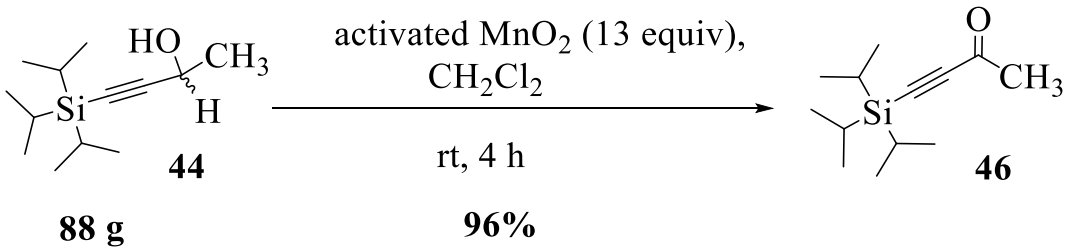
4-(Triisopropylsilyl)but-3-yn-2-ol (44)



In an oven dried 3 neck round bottom flask (5 L) equipped with a stirrer bar and an addition funnel, dry THF (1800 mL) was added. This was then followed by the addition of triisopropylacetylene **45** (250 g, 1.37 mol). The reaction mixture, which resulted, was cooled to - 40 °C (dry ice-ethyl acetate bath), and ***n*-BuLi (685 mL, 1.71 mol, 2.5 M solution in hexane) was added dropwise carefully under argon**. The color of the reaction mixture turned to bright yellow, which was stirred at - 40 °C for 30 min more and dry acetaldehyde (90 mL, 1.5 mol) was added dropwise at - 40 °C. The reaction mixture, which resulted, was stirred for an additional 30 min at -40 °C and then poured onto a saturated aq solution of NH_4CI (5000 mL) at -40 °C and it

was allowed to warm to rt with stirring. After that, the two phases were separated, and the aq layer was extracted with CH_2Cl_2 (3 x 250 mL). The combined organic extracts were washed with brine (2 x 300 mL), and dried ($MgSO_4$). The solvents were removed under reduced pressure and the residue was purified by passing it through a short pad of silica gel. The evaporation of solvents under reduced pressure provided a pale yellow colored racemic alcohol **44** (4 - (triisopropylsilyl)but-3-yn-2-ol) in high yield (307 g, 99%): **^{1}H NMR** (300 MHz, $CDCl_3$) δ 4.72 – 4.22 (m, 1H), 1.87 (d, *J* = 5.3 Hz, 1H), 1.48 (d, *J* = 6.6 Hz, 3H), 1.09 (d, *J* = 1.9 Hz, 21H). The ^{1}H NMR data of this compound **44** was in complete agreement with that reported in the literature [32, 43].

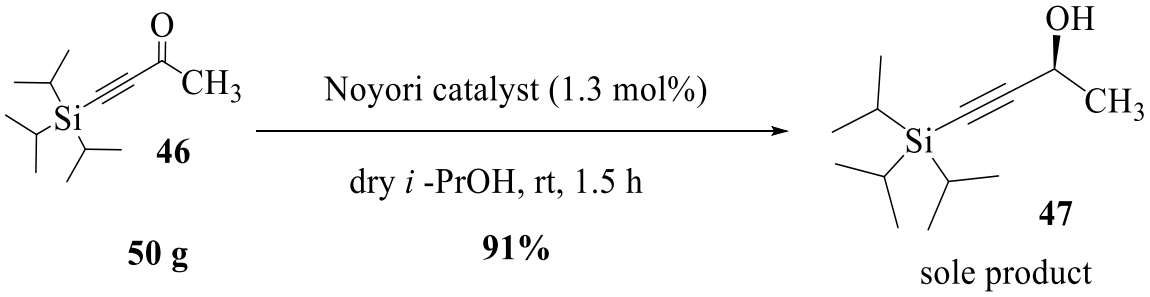
4-(Triisopropylsilyl)but-3-yn-2-one (46)



The racemic alcohol **44** (88 g, 0.39 mol) and CH_2Cl_2 (1700 mL) were added into an oven dried 3 neck round bottom flask (3000 mL). Into the same mixture, activated MnO_2 (488.3 g, 5.05 mol) was added in one portion, and the reaction mixture, which resulted, was stirred for 4 h at rt or until analysis by TLC (silica gel, EtOAc/hexanes, 0.4 mL: 3.6 mL) indicated the disappearance

of starting material. The TLC plate was dipped into $KMnO_4$ solution and dried with a heat gun) and indicated the disappearance of starting material. The reaction mixture was passed through a short pad of celite, and the solvent was removed under reduced pressure. The residue was purified by flash chromatography to yield ketone **46** as a pale-yellow colored oil (83.7 g, 96%): **^{1}H NMR** (300 MHz, CDC13), 2.41 (s, 3H), 1.11 (s, 21H); **^{13}C NMR** (126 MHz, $CDCl_3$) δ 110.08 (d, *J* = 5.9 Hz), 84.02 (s), 58.55 (s), 24.52 (s), 18.48 (s), 11.08 (s). The ^{1}H NMR data of this compound **46** was in complete agreement with that reported in the literature [32, 43].

(*S*)-4-(Triisopropylsilyl)but-3-yn-2-ol (47).

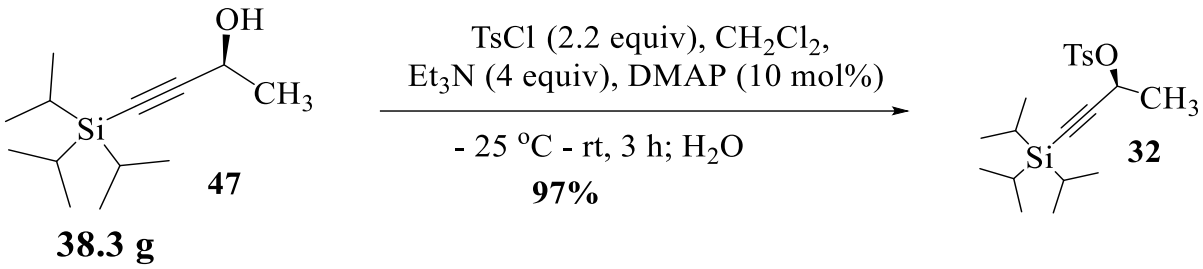


Noyori catalyst: (RuCl[(*S, S*)-NTsCH(C_6H_5)CH(C_6H_5)NH_2(h_6-cymene))
48

In an oven dried 3 neck round bottom flask (2000 mL), which contained ketone **46** (50 g, 0.22 mol) and isopropanol (1300 mL), the Noyori catalyst (1.8 g, mmol), which was dissolved in a minimum amount of CH_2Cl_2 (40 mL), was added into the solution with stirring. The reaction mixture was stirred at rt for 1.5 h, at which time the disappearance of starting material was observed, and the appearance of the alcohol was confirmed by analysis by TLC (silica gel, EtOAc/hexane, 0.4mL/3.6mL). The solvent was removed under reduced pressure and the crude alcohol was purified by flash chromatography (silica gel, EtOAc/hexane, 1:4) to yield optically

active *S*-alcohol **47** (45.9 g, 91%): **$[\alpha]_D^{25}$** -23.13, c 1.2, $CHCl_3$ (Lit. value for its enantiomer: $[a]_D^{25}$ +23.38 (c 3.2, $CHCl_3$) [43]; **^{1}H NMR** (300 MHz, $CDCl_3$) δ 4.56 (m, 1H), 1.98 (br, s, 1H), 1.47 (t, *J* = 20.6, 10.3 Hz, 3H), 1.09 (dd, *J* = 6.2, 1.4 Hz, 21H). The spectroscopic data (^{1}H), and optical rotation for **47** were in complete agreement with that reported in the literature for its enantiomer [32, 43].

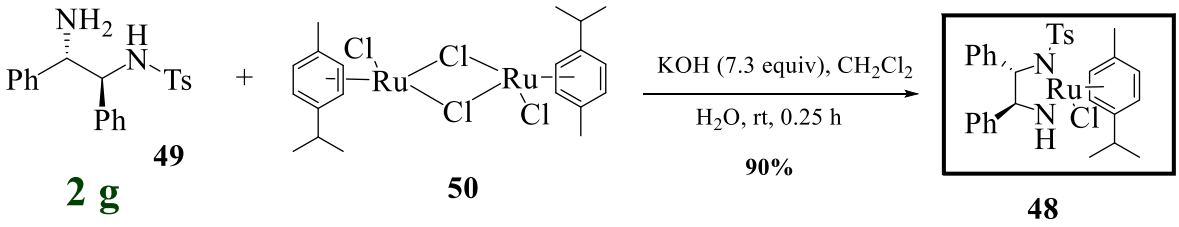
Preparation of (*S*)-4-(triisopropylsilyl)but-3-yn-2-yl 4-methylbenzenesulfonate (46).



In an oven dried 3 L round bottom flask, anhydrous CH_2C1_2 (950 mL) and *S*-alcohol **47** (38.3 g, 0.169 mol) were added, after which the mixture was cooled to -25 °C (outside bath temperature). Triethylamine (68.4 g, 0.67 mol) and a catalytic amount of DMAP (10 mol%) were added. After a few minutes of stirring, tosyl chloride (75 g, 0.39 mol) was added in one portion. The reaction mixture was then allowed to stir at -25 °C for 50 min and the solution was allowed to warm to rt slowly. The reaction mixture was allowed to stir for 3 h at rt, after analysis by TLC indicated the disappearance of the starting material component on analysis by TLC (silica gel, 5% EtOAc in hexane, $\boldsymbol{R_f}$ 0.6). The reaction mixture was quenched with a large excess of water (2000 mL). The biphasic reaction mixture was allowed to stir vigorously for 50 min at rt. After stirring, the two layers were separated (aq layer was not extracted). The CH_2CI_2 layer was dried ($MgSO_4$),

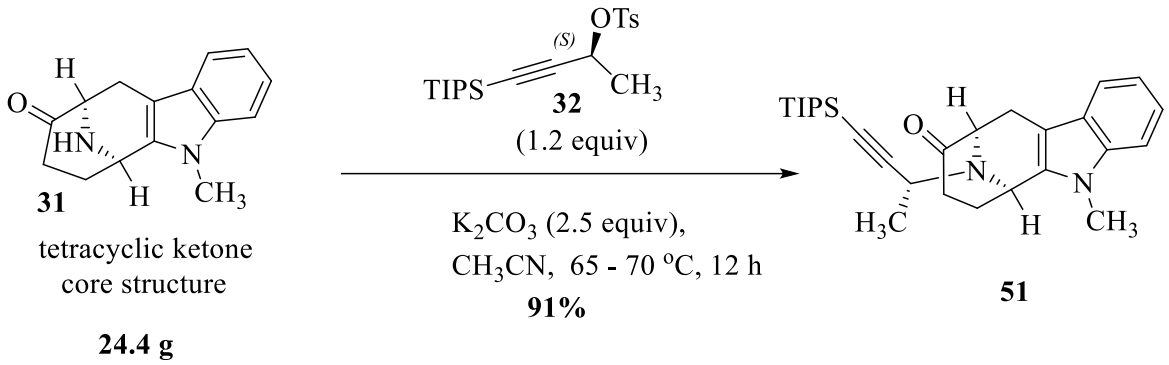
filtered, and concentrated under reduced pressure to yield **32** (62.4 g, 97%) as a light brown colored oil: **^{1}H NMR** (300 MHz, $CDCl_3$) δ 7.82 (d, *J* = 8.3 Hz, 2H), 7.30 (dd, *J* = 6.4, 5.9 Hz, 2H), 5.27 – 5.10 (m, 1H), 2.42 (s, 3H), 1.60 (dd, *J* = 6.7, 0.9 Hz, 3H), 1.01 – 0.93 (m, 21H); **^{13}C NMR** (126 MHz, $CDCl_3$) δ 144.55 (s), 134.13 (s), 129.6 (s), 127.82 (s), 103.08 (s), 89.13 (s), 68.35 (s), 23.20 (s), 18.35 (s), 10.87 (s). The ^{1}H and ^{13}C NMR data of this compound was in complete agreement with that reported in the literature for its enantiomer [32, 43].This material **32** was used to the next step without further characterization and purification.

Preparation of the Noyori catalyst RuCl[(*S, S*)-NTsCH(C_6H_5)CH(C_6H_5)NH_2(h_6-cymene) 48



In an oven dried round bottom flask containing CH_2Cl_2 (100 mL), were added (1*S*, 2*S*)-(+)-*N*-*p*-toluenesulfonyl-1,2-diphenyl ethylene-diamine **49** (2 g, 5.4 mmol), and dichloro (*p* - cymene) ruthenium (II) dimer **50** (1.7 g, 2.6 mmol), and powdered KOH (2.3 g, 41 mmol). **The optical rotation of diamine (49) purchased from Oakwood Chemicals was checked with the literature value before using it in the reaction.** The reaction mixture, which resulted, was stirred at room temperature for 0.5 h. The organic solvent was removed under reduced pressure to yield a dark red colored ruthenium catalyst **48** (3.16 g, 90%) which was used directly in the next step without purification and characterization.

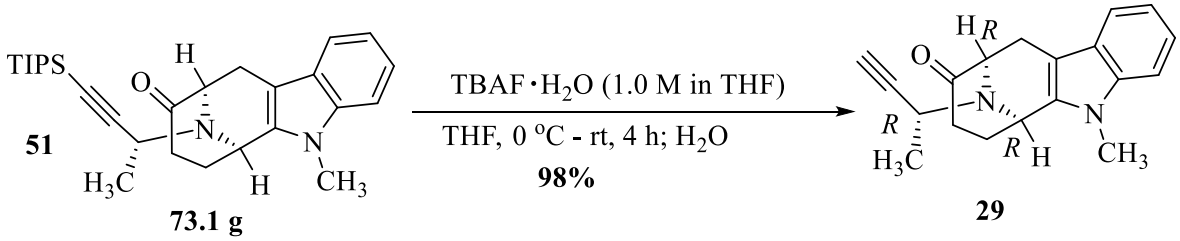
Preparation of (6*R*,10*R*)-5-methyl-12-((*R*)-4-(triisopropylsilyl)but-3-yn-2-yl)-5,6,7,8,10,11-hexahydro-9*H*-6,10-epiminocycloocta[b]indol-9-one (51)



To an oven dried 2 L round bottom flask, N_a-CH_3, N_b-H tetracyclic ketone **31** (24.4 g, 0.1 mol) was added and this was followed by the addition of dry acetonitrile (400 mL). To the solution, (*S*)-4-(triisopropylsilyl)but-3-yn-2-yl 4-methylbenzenesulfonate **32** (50.2 g, 0.116 mol) was added at rt, with stirring. At this point, anhydrous potassium carbonate (17.27 g, 0.132 mol) was added into the reaction mixture. The reaction mixture, which resulted, was stirred at 75 °C (outside oil bath temperature) for 12 h under argon. After 12 h, the analysis by TLC (silica gel, EtOAc/a few drops of 10% aq NH_4OH) indicated the absence of starting material (tetracyclic ketone **31**). The reaction mixture was cooled to rt and the solid (K_2CO_3) was removed by filtration of the solution through a bed of celite using EtOAc as the solvent. The solvent was removed under reduced pressure, after which the crude product was purified by flash chromatography (silica gel, EtOAc/hexanes, 1:10) to provide the (*R*)-N_a-CH_3, N_b-TIPS protected acetylenic tetracyclic ketone **51** as a light yellow colored solid (41.9 g, 91%), which was dried under vacuum at rt overnight. The desired stereochemistry of this product was confirmed after the removal of TIPS group in the next step.

Analysis of **51**; **^{1}H NMR** (500 MHz, $CDCl_3$) δ 7.45 (d, J = 7.8 Hz, 1H), 7.30 (d, J = 8.2 Hz, 1H), 7.21 (ddd, J = 8.2, 7.1, 1.1 Hz, 1H), 7.14 – 7.08 (m, 1H), 4.90 (m, J = 2.5 Hz, 1H), 3.96 (d, J = 6.5 Hz, 1H), 3.67 (s, 3H), 3.64 (q, J = 6.6 Hz, 1H), 3.13 (dd, J = 16.7, 6.6 Hz 1H) 2.69 (d, J = 16.3 Hz, 1H), 2.63 – 2.52 (m, 1H), 2.50 – 2.43 (m, 1H), 2.19 – 1.97 (m, 2H), 1.46 (d, J = 6.6 Hz, 3H), 1.03 (d, J = 5.6 Hz, 21H); **^{13}C NMR** (126 MHz, $CDCl_3$) δ 210.60 (s), 137.42 (s), 133.40 (s), 126.57 (s), 121.71 (s), 119.40 (s), 118.45 (s), 108.99 (s), 107.72 (s), 107.02 (s), 85.60 (s), 63.23 (s), 47.67 (s), 47.45 (s), 34.65 (s), 29.44 (s), 29.34 (s), 22.23 (s), 21.24 (s), 18.76 (s), 11.34 (s). The ^{1}H and ^{13}C NMR data of compound **51** were in complete agreement with that reported in the literature for its enantiomer [32, 43].

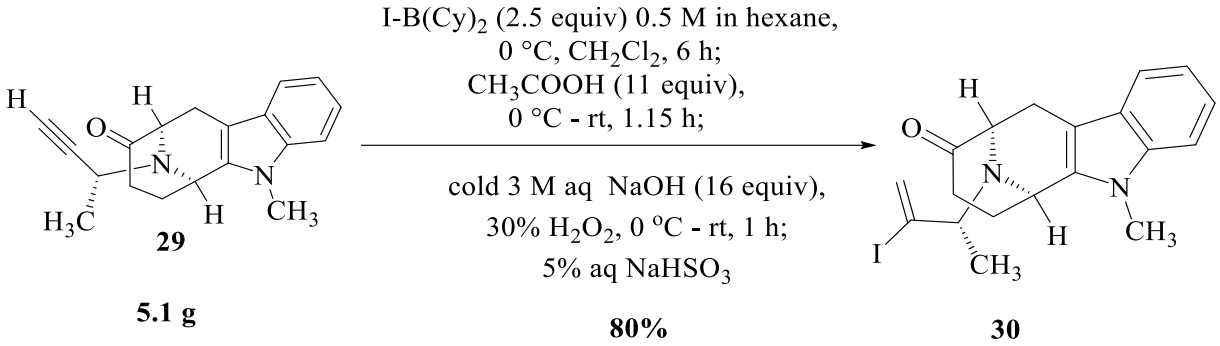
Preparation of (6*R*,10*R*)-12-((*R*)-but-3-yn-2-yl)-5-methyl-5,6,7,8,10,11-hexahydro-9*H*-6,10-epiminocycloocta[b]indol-9-one (29).



To an oven dried 3L round bottom flask equipped with a dropping funnel, TIPS protected acetylenic tetracyclic ketone **51** (73.1 g, 0.16 mol) was added. This was followed by the addition of THF (675 mL) and TBAFxH_2O (245 mL, 1.0 M solution in THF) at 0 °C dropwise via a dropping funnel. During the addition, the wine-red colored solution turned into a black color. After stirring the reaction mixture at 0 °C for 0.5 h, the ice bath was removed, and the mixture was stirred at rt for an additional 4 h or until the analysis by TLC (silica gel, EtOAC/hexane,

1:4)) confirmed the disappearance of the starting material **51**. The reaction solution was then quenched with H_2O (400 mL), and the reaction mixture was diluted with EtOAc (1200 mL). The two layers were separated. The organic layer was washed with water (2 x 200 mL), and then washed with brine (2 x 250 mL, and dried (Na_2SO_4). The organic solvent (EtOAc) was removed under reduced pressure to 1/3rd of its original volume and the slurry was allowed to stay at rt overnight in a beaker for crystallization. The mother liquor, which remained, after crystallization was purified by passing through a short pad of silica gel to yield an additional amount of N_a-Me, acetylenic tetracyclic ketone **29** as a light yellow colored solid (46.6 g, 98% yield), which was dried under vacuum at rt overnight. The optical rotation, proton NMR, carbon NMR and X-ray crystallography indicated the pure compound had the desired stereochemistry (*R, R, R*). Please see **Appendix A** for X-ray crystallography data): **$[\alpha]_D^{25}$** +191.3 (c 1.0, $CHCl_3$), Lit. value for its enantiomer: $[\alpha]_D^{27}$ – 191.0 (c 0.192, $CHCl_3$) [41]; **^{1}H NMR** (500 MHz, $CDCl_3$) δ 7.46 (d, J = 7.8 Hz, 1H), 7.31 (d, J = 8.2 Hz, 1H), 7.22 (t, J = 7.6 Hz, 1H), 7.11 (t, J = 7.4 Hz, 1H), 4.75 (m, J = 2.5 Hz, 1H), 3.95 (d, J = 6.6 Hz, 1H), 3.70 (s, 3H), 3.61 (qd, J = 6.6, 2.1 Hz, 1H), 3.17 – 3.09 (m, 1H), 2.70 (d, J = 16.7 Hz, 1H), 2.61 (m, J = 11.4, 8.7, 5.5 Hz, 1H), 2.48 (m, J = 17.0, 6.2 Hz, 1H), 2.28 (d, J = 2.2 Hz, 1H), 2.18 – 2.03 (m, 2H), 1.45 (d, J = 6.7 Hz, 3H); **^{13}C NMR** (126 MHz, $CDCl_3$) δ 210.28 (s), 137.23 (s), 133.61 (s), 126.33 (s), 121.57 (s), 119.28 (s), 118.18 (s), 108.92 (s), 106.20 (s), 84.75 (s), 72.54 (s), 61.32 (s), 49.30 (s), 47.20 (s), 34.46 (s), 29.37 (s), 29.03 (s), 21.53 (s), 20.45 (s); HRMS (ESI) m/z $(M + H)^+$ calcd for $C_{19}H_{20}N_2O$, 293.1164, found 293.1614. The spectroscopic data (^{1}H and ^{13}C NMR) and optical rotation (compared to the literature value of its enantiomer) of this compound **29** were in complete agreement with that reported in the literature for its enantiomer [32, 43].

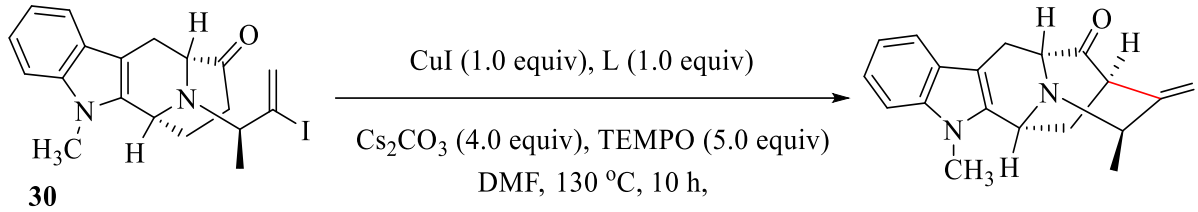
Preparation of (6*R*,10*R*)-12-((*R*)-3-iodobut-3-en-2-yl)-5-methyl-5,6,7,8,10,11-hexahydro-9*H*-6,10-epiminocycloocta[b]indol-9-one (28) via haloboration and protodeboronation of the acetylenic tetracyclic ketone (29).



An oven dried round bottom flask (1000 mL) equipped with an addition funnel was cooled under the continuous flow of argon. The N_a-Me acetylenic tetracyclic ketone **29** (5.1 g, 17.4 mmol) was dissolved in anhydrous CH_2CI_2 (130 mL) and hexanes (17 mL) and then charged into the flask. Using an ice bath (outside) the flask was cooled to 0 °C and I-B(Cy)$_2$ (73.4 mL, 136.4 mmol, 0.5 M solution in hexanes) was added dropwise every 0.5 h in three portions (over a total period of 1.5 h). The mixture, which resulted, after the last addition was stirred at 0 °C for another 0.5 h, after which the ice bath was removed. The mixture was then allowed to warm to rt and stirred for 2.0 h. This was followed by the addition of another 0.5 equiv of I-B(Cy)$_2$ (18.4 mL, 9.2 mmol) dropwise into the mixture at rt. Then the reaction mixture, so formed, was allowed to stir for an additional 2 h at rt. At this point, the glacial acetic acid (4.8 ml, 201.8 mmol) was added into the stirring solution at 0 °C (ice bath) with stirring, and the reaction mixture was allowed to stir at rt for an additional 1.2 h. To this solution, cold aq 3 M NaOH (97.9 mL, 293.8 mmol) and 30% H_2O_2 (6.3 mL, 55.8 mmol) were added with stirring and the temperature was lowered to 0 °C (ice bath), and the mixture, which formed, was stirred for an additional 1.0 h at rt.

The biphasic solution, which resulted, was transferred into a larger flask (3000 mL) and diluted with CH_2CI_2 (1100 mL) and water (170 mL). The two layers were separated. The residual solid, which remained in the original flask (attached to the bottom of the flask) was dissolved in acetone (250 mL) and the solvent was removed under reduced pressure to 1/3rd of the original volume. The mixture, which resulted, was diluted with CH_2Cl_2 (150 mL) and the biphasic layers were separated again. The combined CH_2CI_2 layers were treated with solutions of 5% KF in methanol (390 mL) and 5% aq sodium bisulfite (390 mL) and stirred vigorously for 10 min [32, 43]. [32]. The aq layer was separated and extracted with CH_2CI_2 (2 x 250 mL), after which the combined organic layers were washed with brine (2 x 200 mL), and dried (Na_2SO_4). The organic solvents were removed under reduced pressure and the residue was purified by flash chromatography on silica gel (ethyl acetate/hexanes, 1: 4) to furnish the vinyl iodide **30** as an off-white colored solid (5.8 g, 80%): $\boldsymbol{R_f}$ 0.4 (EtOAc/hexane, 1:4); $\boldsymbol{[\alpha]_D^{25}}$ + 166.36 (c 1.07, $CHCl_3$); **^{1}H NMR** (500 MHz, $CDCl_3$) δ 7.48 (d, J = 7.8 Hz, 1H), 7.31 (d, J = 8.2 Hz, 1H), 7.25 – 7.20 (m, 1H), 7.13 (dd, J = 10.9, 3.9 Hz, 1H), 6.22 (s, 1H), 5.86 (s, 1H), 4.25 (s, 1H), 4.01 (d, J = 6.3 Hz, 1H), 3.64 (s, 3H), 3.12 (dd, J = 16.8, 6.6 Hz, 1H), 2.77 (d, J = 16.7 Hz, 1H), 2.55 (dd, J = 33.7, 19.7 Hz, 3H), 2.18 – 2.07 (m, 1H), 2.03 – 1.96 (m, 1H), 1.19 (d, J = 6.1 Hz, 3H); **^{13}C NMR** (126 MHz, $CDCl_3$) δ 210.36 (s), 137.30 (s), 133.16 (s), 126.55 (s), 125.93 (s), 122.71 (s), 121.75 (s), 119.45 (s), 118.31 (s), 109.08 (s), 106.73 (s), 62.48 (s), 60.90 (s), 47.78 (s), 34.52 (s), 29.84 (s), 29.44 (s), 21.35 (s), 19.89 (s); **HRMS** (ESI) m/z $(M + H)^+$ calcd for $C_{19}H_{21}IN_2O$, 421.0771, found 421.0777. The spectroscopic data (^{1}H and ^{13}C NMR) of compound **30** were in complete agreement with that reported in the literature for its enantiomer [32].

Cu-mediated cross coupling reaction of the vinyl iodide 30 to provide (6*R*,7*R*,8*R*,10*R*,11a*R*)-5,8-dimethyl-9-methylene-5,6,9,10,11a,12-hexahydro-6,10-methanoindolo[3,2-b]quinolizin-11(8H)-one (28).



30 **28**

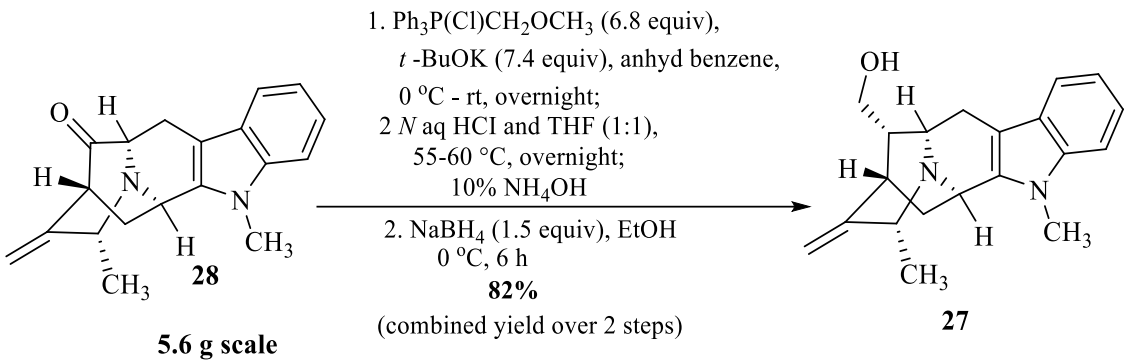
0.5 g **85%**

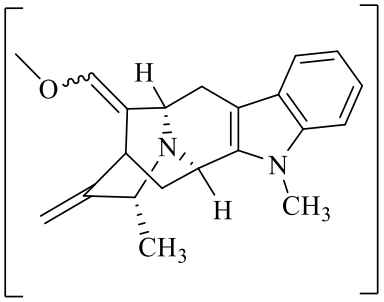
L= *cis* 1,2 cyclohexanediol

The pentacyclic ketone **28** was synthesized by following the published procedure [36]. The vinyl iodide **30** (3 g, 7.13 mmol), CuI (1.36, 7.13 mmol), *cis* 1, 2-cyclohexanediol (0.83 g, 7.13 mmol), and Cs_2CO_3 (9.3 g, 28 mmol) were added into a sealed tube and then dry DMF (40 mL) was added to it. The mixture, which resulted, was degassed at rt under reduced pressure and back filled with argon 4 times. The reaction mixture was then kept on a pre-heated oil bath at 135-140 ^oC temperature and stirred for 10 h. The progress of the reaction was monitored and after 10 h on analysis by TLC (neutral alumina, EtOAC/hexane, 6:4 and few drops of 10% aq NH_4OH); this confirmed no starting material remained. The reaction mixture was allowed to reach rt and diluted with EtOAc (50 mL) and water (25 mL). The biphasic layers were separated and the aq layer was extracted with EtOAc (3 x 40 mL). The combined organic layers were washed with water (2 x 40 mL), brine (3 x 40 mL), and dried (Na_2SO_4). The solvent was removed under reduced pressure and the residue was purified by flash chromatography using neutral alumina (EtOAc/hexane = 1:3) to furnish the pentacyclic ketone **28** as an off-white colored solid, which was crystallized from EtOAc (100%) for X-ray crystallography (please find the X-ray data in

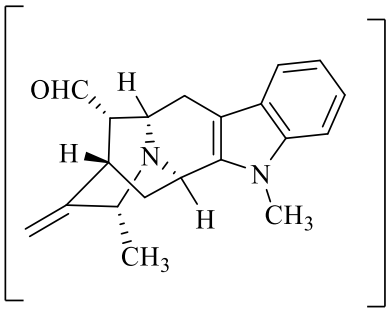
Appendix A): **$[\alpha]_D^{25}$** + 146.7 (c 0.98, $CHCl_3$), reference value for its enantiomer: $[\alpha]_D^{25}$ – 150.0 (c 1.0, $CHCl_3$) [37]; **^{1}H NMR** (500 MHz, $CDCl_3$) δ 7.52 (d, J = 7.8 Hz, 1H), 7.28 (d, J = 8.4 Hz, 1H), 7.21 (dd, J = 11.2, 3.9 Hz, 1H), 7.11 (t, J = 7.4 Hz, 1H), 5.15 (d, J = 2.6 Hz, 1H), 5.03 (d, J = 2.2 Hz, 1H), 4.49 (d, 1H), 3.93 (qd, J = 6.7, 4.4 Hz, 1H), 3.75 (d, J = 5.6 Hz, 1H), 3.62 (s, 3H), 3.37 (d, J = 15.5 Hz, 1H), 3.08 (dd, J = 3.3, 1.8 Hz, 1H), 2.95 (dd, J = 15.5, 6.1 Hz, 1H), 2.69 – 2.57 (m, 1H), 2.21 – 2.10 (m, 1H), 1.52 (d, J = 6.8 Hz, 3H); **^{13}C NMR** (126 MHz, $CDCl_3$) δ 217.66 (s), 148.19 (s), 137.51 (s), 137.30 (s), 126.66 (s), 121.43 (s), 119.14 (s), 118.58 (s), 111.47 (s), 108.76 (s), 105.13 (s), 58.69 (s), 57.95 (s), 51.99 (s), 51.07 (s), 35.79 (s), 29.35 (s), 22.52 (s), 17.51 (s); **HRMS** (ESI) m/z $(M + H)^+$ calcd for $C_{19}H_{20}N_2O$, 293.1648, found 293.1641. The spectroscopic data (^{1}H and ^{13}C NMR) of this compound **28** were in complete agreement with that reported in the literature for its enantiomer [36]. In addition, analysis by X-ray crystallography confirmed the absolute structure and stereochemistry was, as shown here.

Conversion of the pentacyclic ketone (28) into ((6*R*,7*R*,8*R*,10*S*,11*S*,11a*R*)-5,8-dimethyl-9-methylene-5,6,8,9,10,11,11a,12-octahydro-6,10-methanoindolo[3,2-b]quinolizin-11-yl)methanol (27).





methyl enol ether **53**
(not isolated)



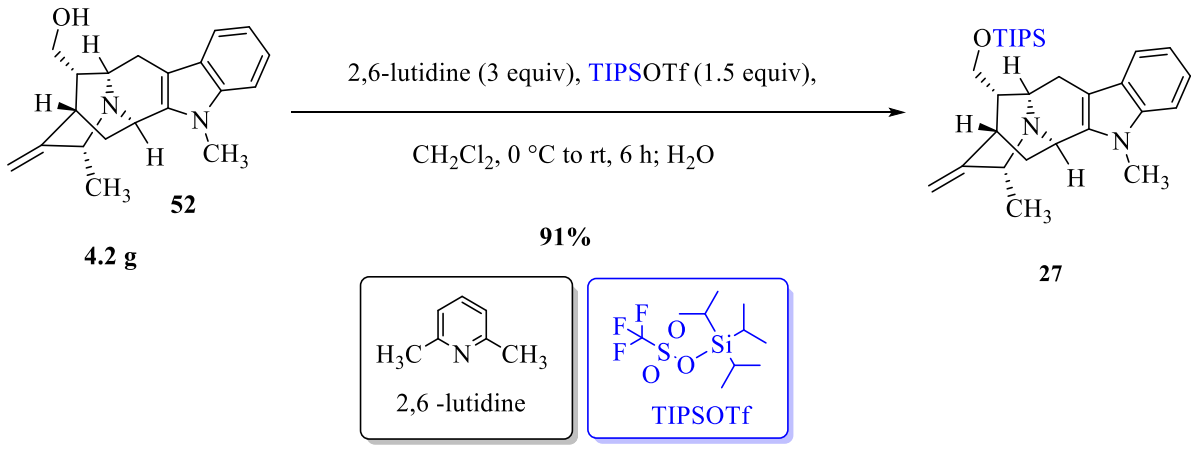
aldehyde intermediate **54**
(not isolated)

In a 2 neck round bottom flask (1000 mL) the mixture of methoxymethyltriphenylphosphonium chloride (44.8 g, 130.2 mmol), anhydrous potassium tert-butoxide (16 g, 141.73 mmol), and dry benzene (350 mL) were stirred for 1 h at rt. Benzene was dried by pre distilling in the presence of CaH_2 (dry benzene from Sigma Aldrich also works). After 1 h of stirring, the yellow-colored mixture then turned to a dark red color, and the temperature of the mixture was lowered to 0 °C. The pentacyclic ketone **28** (5.6 g, 19.15 mmol) was dissolved into a minimum amount of dry THF (50 mL) and added to the above solution dropwise. The reaction mixture, which resulted, was allowed to warm to rt and allowed to stir overnight. After stirring overnight, analysis by TLC (silica gel, 0.3 mL MeOH + 4.7 mL CH_2CI_2) confirmed the disappearance of starting material and the formation of a new component (less polar methyl enol ether intermediate **53**). At this point, the reaction mixture was diluted by adding EtOAc (200 mL) and quenched with water (100 mL). The biphasic layers were separated by extraction and the aq layer was extracted with EtOAc (2 x 200 mL). The combined organic layers were washed with brine (2 x 150 mL) and dried (Na_2SO_4). The evaporation of organic solvents under reduced pressure resulted in a brownish red oil, which was used in the next step (acidic hydrolysis) without further characterization or purification. The aq 12 *N* cone HCl (140 mL) and THF (140 mL) were added to the above mixture of crude oil and the mixture, which resulted, was stirred for 8 h at 55 °C-

60°C (oil bath temperature). The analysis by TLC (silica gel, 0.3 mL MeOH + 4.7 mL CH_2CI_2) indicated the disappearance of the methyl enol ether **53** component and the appearance of an aldehyde component **54** [more polar R_f than starting material (methyl enol ether **53**)]. The reaction mixture was cooled to rt, and the volume of the solvent was reduced to 1/3rd of the original volume by removing the solvents under reduced pressure. At this point, the phosphorus impurities were removed by adding hexane (70 mL), vigorous shaking, and then decanting the upper hexane layer. The process was repeated 6 times. The mixture, which resulted, was then brought to pH 8 by adding 14% aq NH_4OH dropwise at 0 °C. The aq layer was extracted with EtOAc (4 x 100 mL). The organic layer was washed with brine (2 x 60 mL) and dried (Na_2SO_4). The similar R_f value by analysis on TLC comparison with an authentic sample of an enantiomeric aldehyde (the stereochemistry of which was confirmed by X-ray crystallography analysis) indicated the a stereochemistry in aldehyde **54** [32, 49]. The organic solvents were removed under reduced pressure, which resulted in a crude aldehyde **54** (6 g) as a brown colored oil, which was further dried under high vacuum for 7 h. It was used directly in the next step without further purification or characterization. The crude aldehyde (6 g) was placed in a one neck round bottom flask (500 mL) and was dissolved in dry (200 proof) EtOH (95 mL). The temperature of the reaction mixture was lowered to 0 °C using an ice bath (outside the flask). To this solution, the $NaBH_4$ (0.88 g, 0.023 mol) was added in one portion at 0 °C and the mixture, which resulted, was stirred for 6 h at the same temperature (0 °C). Then analysis by TLC (silica gel, 0.3 mL MeOH + 4.7 mL CH_2CI_2) confirmed the formation of the more polar component (***R_f*** 0.3) and by absence of starting material (aldehyde **54**). At this point, the reaction mixture was diluted by adding CH_2Cl_2 (250 mL) and cold water (50 mL). The biphasic layers were separated, and the aq layer was extracted with CH_2Cl_2 (3 x 40 mL). The combined organic layer was

washed with brine (2 x 40 mL), and dried (Na_2SO_4). The organic solvents were removed under reduced pressure and the crude waxy solid, which resulted, was purified on column chromatography (silica gel, 5-7 % CH_3OH in CH_2Cl_2) to provide alcohol **52** as waxy solid (4.48 g, 82%): **[α]D**^{25} + 62.0 (c 0.5, $CHCl_3$); **^{1}H NMR** (500 MHz, $CDCl_3$) δ 7.38 (d, J = 7.8 Hz, 1H), 7.29 (d, J = 5.7 Hz, 1H), 7.22 – 7.17 (t, 1H), 7.12 – 7.05 (t, 1H), 4.89 (d, J = 1.9 Hz, 2H), 4.25 – 4.20 (m, 1H), 3.63 (s, 4H), 3.52 – 3.42 (m, 2H), 3.03 – 2.96 (m, 1H), 2.93 (dd, J = 15.2, 5.2 Hz, 1H), 2.60 (d, J = 15.1 Hz, 1H), 2.34 – 2.29 (br, s, 2H), 2.08 (ddd, J = 12.1, 10.0, 2.0 Hz, 1H), 1.65 – 1.59 (q, 1H), 1.55 – 1.48 (m, 1H), 1.39 (d, J = 6.8 Hz, 3H); **^{13}C NMR** (126 MHz, $CDCl_3$) δ 152.61 (s), 139.43 (s), 137.37 (s), 127.48 (s), 120.86 (s), 118.83 (s), 118.19 (s), 108.71 (s), 107.82 (s), 104.09 (s), 64.91 (s), 58.22 (s), 51.01 (s), 48.23 (s), 44.57 (s), 36.14 (s), 33.24 (s), 29.36 (s), 27.18 (s), 16.87 (s); **HRMS** (ESI) m/z $(M + H)^+$ calcd for $C_{21}H_{24}N_2O$, 309.1961, found 309.1935. The spectroscopic data (^{1}H and ^{13}C NMR) of this compound **52** were in complete agreement with that reported in the literature for its enantiomer [43].

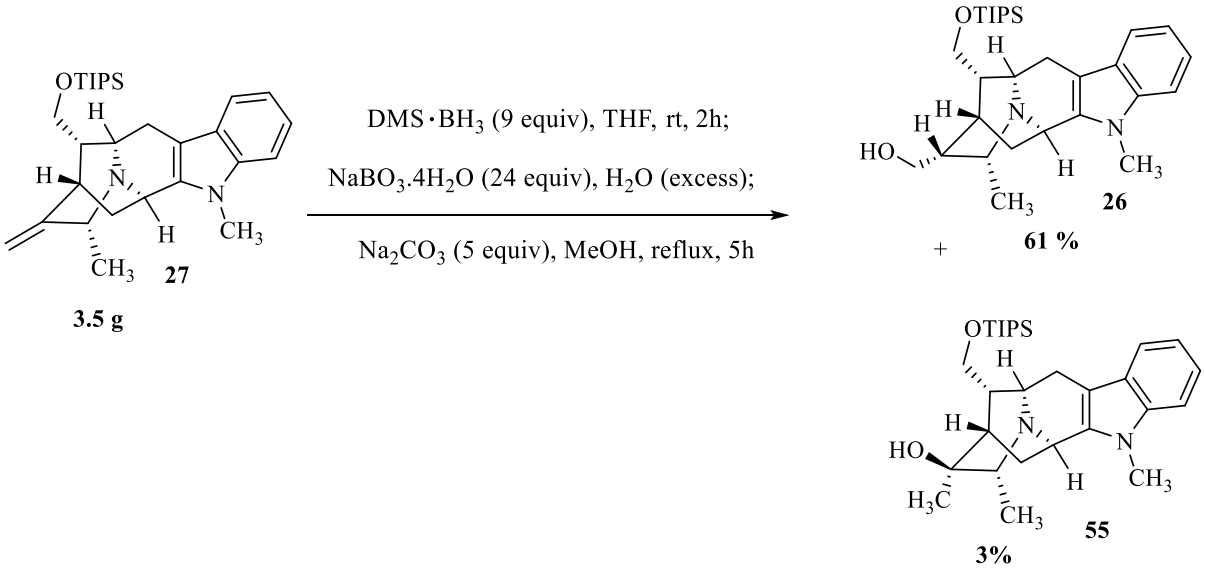
Conversion of the pentacyclic alcohol (52) into (6*R*,7*R*,8*R*,10*S*,11*S*,11a*R*)-5,8-dimethyl-9-methylene-11-(((triisopropylsilyl)oxy) methyl)-5,6,8,9,10,11,11a,12-octahydro-6,10-methanoindolo[3,2-b]quinolizine (27).



To the pentacyclic alcohol **52** (4.2 g, 0.013 mol) in dry CH_2Cl_2 (100 mL), 2, 6-lutidine (4.4 g, 0.04 mol) was added at 0 °C with stirring. To this solution, TIPSOTF (4.3 g, 0.04 mol) was added at 0 °C. The mixture was then allowed to stir for an additional 6 h at 0 °C. At this point, the analysis on TLC indicated the absence of starting material and the presence of a new less polar component (silica gel, 2-4% MeOH in CH_2CI_2), after which the reaction was quenched by adding cold water (10 mL). The reaction mixture was diluted with CH_2CI_2 (300 mL) and cold water (50 mL)**.** The aq layer was extracted with CH_2CI_2 (2 x 50 mL), and the combined organic layer was washed with brine (100 mL), and dried (Na_2SO_4). After removing the solvents under reduced pressure, the crude waxy solid was dried under reduced pressure (at rt for 10 h) to remove the excess 2,6-lutidine and then the solid, which resulted, was purified by flash chromatography (silica gel, CH_2CI_2/CH_3OH, 20:1) to provide the silyl ether **27** as a white colored waxy solid: R_f 0.4 (silica gel, 5% MeOH in CH_2CI_2); **[α]D**^{25} -23.6 (c 1.4, $CHCl_3$); **^{1}H NMR** (500 MHz, $CDCl_3$) δ 7.48 (d, J = 7.7 Hz, 1H), 7.28 (d, J = 8.2 Hz, 1H), 7.18 (ddd, J = 8.2, 7.1, 1.2 Hz, 1H), 7.08 (td, J = 7.5, 1.0 Hz, 1H), 4.94 – 4.87 (m, 2H), 4.27 (dd, J = 9.8, 2.1 Hz, 1H), 3.69 – 3.63 (m, 4H), 3.61 – 3.55 (m, 2H), 2.98 (dt, J = 15.4, 5.3 Hz, 2H), 2.71 (s, 1H), 2.46 – 2.42 (m, 1H), 2.15 (ddd, J = 12.2, 10.0, 2.1 Hz, 1H), 1.80 (dd, J = 14.6, 7.0 Hz, 1H), 1.67 (ddd, J = 12.3, 3.7, 2.8 Hz, 1H), 1.42 (d, J = 6.8 Hz, 3H), 1.04 (dd, J = 5.1, 3.0 Hz, 21H); **^{13}C NMR** (126 MHz, $CDCl_3$) δ 152.50 (s, C), 139.66 (s, C), 137.29 (s, C), 127.60 (s, C), 120.68 (s, CH), 118.68 (s, CH), 118.13 (s, CH), 108.63 (s, CH), 107.60 (s, CH2), 104.29 (s, C), 65.60 (s, CH2), 58.28 (s, CH), 51.18 (s, CH), 48.68 (s, CH), 44.61 (s, CH), 35.75 (s, CH), 33.39 (s, CH2), 29.27 (s, CH3), 27.38 (s, CH2), 18.07 (s, 6 X CH3), 17.01 (s, CH3), 11.95 (s, 3 X CH); **DEPT 135 ^{13}C NMR**, (126 MHz, $CDCl_3$) δ 120.71 (s, CH), 118.71 (s, CH), 118.16 (s, CH), 108.66 (s, CH), 107.63 (s, CH2), 65.63 (s, CH2), 58.31 (s, CH), 51.21 (s, CH), 48.70 (s, CH), 44.64 (s, CH),

35.78 (s, CH), 33.42 (s, CH2), 29.30 (s, CH3), 27.41 (s, CH2), 18.10 (s, 6 X CH3), 17.04 (s, CH3), 11.98 (s, 3 X CH); **HRMS** (ESI) m/z $(M + H)^+$ for $C_{29}H_{44}N_2OSi$, calcd 465.3295, found 465.3299. The spectroscopic data (^1H and ^{13}C NMR) of this compound **27** was in complete agreement with that reported in the literature for its enantiomer [43].

Conversion of the alkene (27) into ((6*R*,7*S*,8*R*,9*R*,10*R*,11*S*,11a*R*)-5,8-dimethyl-11-(((triisopropylsilyl)oxy)methyl)-5,6,8,9,10,11,11a,12-octahydro-6,10-methanoindolo[3,2-b]quinolizin-9-yl)methanol (26) and a trace amount of tertiary alcohol (6*R*,7*S*,8*R*,9*S*,10*S*,11*S*,11a*R*)-5,8,9-trimethyl-11-(((triisopropylsilyl)oxy)methyl)-5,6,8,9,10,11,11a,12-octahydro-6,10-methanoindolo[3,2-b]quinolizin-9-ol (55) via hydroboration, followed by Kabalka oxidation.

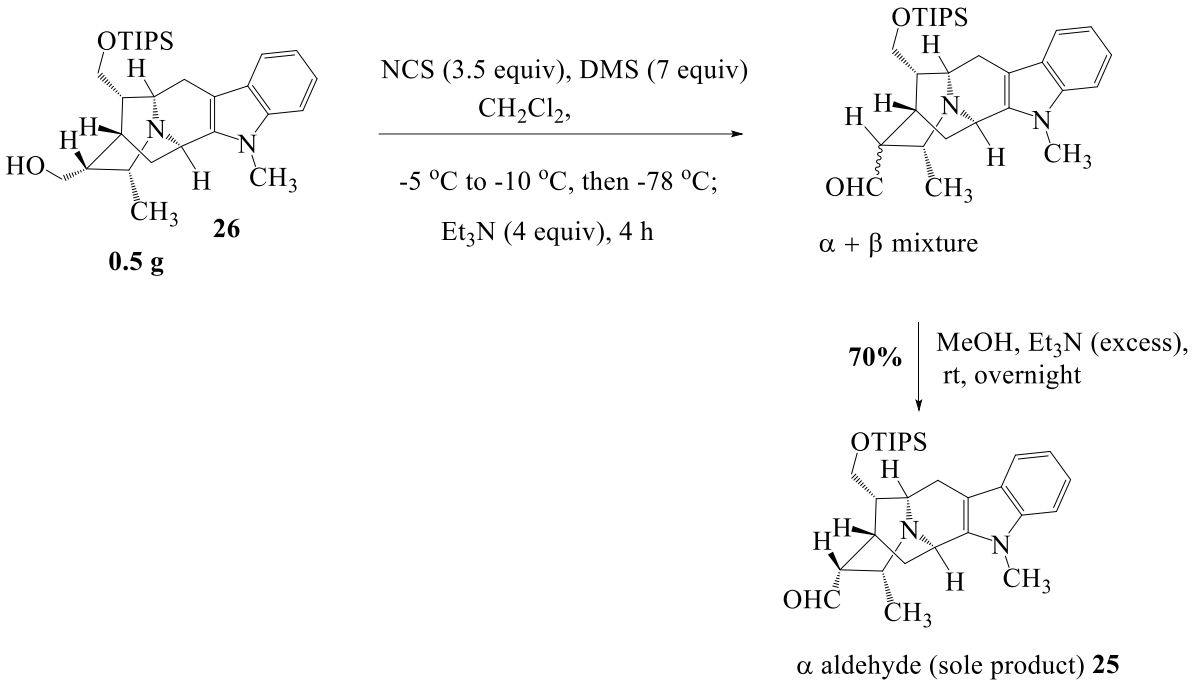


To the solution of alkenyl TIPS ether **27** (3.5 g, 7.53 mmol) in dry THF (50 mL), was added 2.0 M solution of BH_3-DMS in THF (67.7 mmol, 34.3 mL), with stirring, at rt and the mixture was allowed to stir for 2.5 h at rt.

After the reaction mixture, was allowed to stir for 2.5 h, ice cold water (125 mL) was used to quench the reaction at 0 °C (added slowly because the addition of water results in a large amount of effervescence of H_2 gas at the beginning). To the reaction mixture, $NaBO_3 \cdot 4H_2O$ (28 g, 180.7mmol) was added in one portion at 0 °C. The mixture, which resulted, was allowed to warm to rt and stirred at rt for an additional 2 h. At this point, EtOAc (200 mL) and H_2O (90 mL) were added into the reaction mixture. The biphasic layers were separated, and the organic layer was washed with water (2 x 90 mL), brine (2 x 80 mL), and dried (Na_2SO_4). The solvent was then removed under reduced pressure to provide the N_b-BH_3 complex as a mixture of isomers at [C(20)] which was dried under vacuum for 6 h prior to use in the next step. The majority of the mixture was the desired primary alcohol **26**. This crude reaction mixture was used in the next step without any further purification or characterization. To the mixture of isomers, dry MeOH (70 mL) and Na_2CO_3 (4 g, 37.7 mmol) was added, and the mixture was then warmed to 60 °C (oil bath) for 6 h. It was stirred vigorously. At this point, the reaction mixture was allowed to cool to rt, and this was followed by the removal of the solids by filtration through a bed of celite. The filtrate, which resulted, was concentrated under reduced pressure to provide a crude oil, which was then redissolved in CH_2CI_2. The CH_2CI_2 layer was washed with H_2O (50 mL), brine (4x 40 mL) and dried (Na_2SO_4). The solvent was removed under reduced pressure to afford a crude waxy solid, which was purified by flash chromatography [silica gel, CH_2Cl_2/MeOH (v/v 10:1)] to provide the primary alcohol (2.2 g) and the tertiary alcohol **55** (0.1 g, 3%) with a combined yield of 64%. Primary alcohol **26**: $\boldsymbol{R_f}$ 0.3 (basic alumina, EtOAc/hexanes, 1:1 + few

drops of Et_3N) **$[\alpha]_D^{25}$** - 63.6 (c 1.1, $CHCl_3$); **^{1}H NMR** (500 MHz, $CDCl_3$) δ 7.48 (d, J = 7.8 Hz, 1H), 7.31 (d, J = 8.2 Hz, 1H), 7.24 – 7.17 (m, 1H), 7.13 – 7.07 (m, 1H), 4.17 (dt, J = 16.0, 8.0 Hz, 1H), 3.91 (dd, J = 10.5, 8.1 Hz, 1H), 3.81 (dd, J = 8.7, 8.0 Hz, 2H), 3.74 (t, J = 10.0 Hz, 1H), 3.66 (s, 3H), 3.39 (dq, J = 10.7, 7.3 Hz, 1H), 3.20 (dd, J = 8.2, 5.1 Hz, 1H), 3.04 – 2.95 (m, 1H), 2.69 (d, J = 14.9 Hz, 1H), 2.25 (s, 1H), 2.07 – 1.91 (m, 2H), 1.84 (q, J = 8.6 Hz, 1H), 1.62 – 1.52 (m, 1H), 1.33 (d, J = 7.3 Hz, 3H), 1.05 (t, J = 7.0 Hz, 21H); **^{13}C NMR** (126 MHz, $CDCl_3$) δ 139.43 (s), 137.25 (s), 127.58 (s), 120.70 (s), 118.71 (s), 118.14 (s), 108.67 (s), 104.05 (s), 67.06 (s), 63.24 (s), 54.25 (s), 51.42 (s), 48.81 (s), 41.23 (s), 40.11 (s), 36.55 (s), 29.32 (s), 27.74 (s), 24.99 (s), 18.02 (s), 13.32 (s), 11.91 (s); **^{13}C NMR DEPT** 135 (126 MHz, $CDCl_3$) δ 120.70 (s) CH, 118.72 (s) CH, 118.14 (s) CH, 108.67 (s) CH, 67.07 (s) CH2, 63.24 (s) CH2, 54.25 (s) CH, 51.42 (s) CH, 48.81 (s) CH, 41.23 (s) CH, 40.11 (s) CH, 36.55 (s) CH2, 29.32 (s) CH3, 27.74 (s) CH2, 24.99 (s) CH, 18.02 (s) 6XCH3, 13.32 (s) CH3, 11.91 (s) 3X CH; **HRMS** (ESI) m/z $(M + H)^+$ calcd for $C_{29}H_{46}N_2O2Si$, 483.3401, found 483.3410. The NMR spectroscopic data of the desired alcohol **26** were in complete agreement with that reported in the literature for its enantiomer [37, 43].

Corey Kim oxidation of alcohol (26) to provide 6*R*,7*S*,8*R*,9*R*,10*S*,11*S*,11a*R*)-5,8-dimethyl-11-(((triisopropylsilyl)oxy) methyl)-5,6,8,9,10,11,11a,12-octahydro-6,10-methanoindolo[3,2-b]quinolizine-9-carbaldehyde (25).



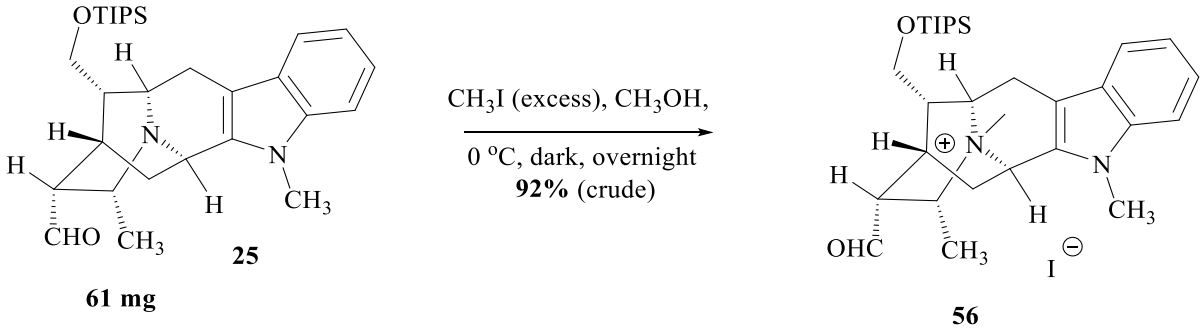
To a solution of *N*-chlorosuccinimide (415 mg, 3.6 mmol) in dry CH_2CI_2 (20 mL), with stirring, was added dimethyl sulfide (0.5 mL, 1.45 mmol) at -5 to -15 °C (outside bath) dropwise under a continuous flow of argon. A white precipitate was observed soon after the addition of the dimethyl sulfide, which was the Corey Kim reagent. At this point, the mixture, which resulted, was stirred for 0.7 h at the temperature range mentioned above. After this, the temperature of the reaction mixture was further lowered (-78 °C, EtOAc-dry ice bath), and the alcohol (500 mg, 0.2 mmol) in dry CH_2C1_2 (10 mL) was added into the reaction mixture under argon. Before the addition of the starting material, the solution of starting material (**26**) in DCM was also cooled to -78 °C. The mixture, which resulted, was stirred for 3 h at -78 °C. At this point, dry triethylamine

(420 mg, 4.1 mmol) was then added to the above mixture dropwise and the stirring was allowed to continue for an additional 1.5 h at the same temperature (-78 °C). The completion of the reaction was confirmed by analysis on TLC (basic alumina, MeOH/DCM, 1:9). The reaction mixture was quenched at -78 °C by addition of CH_2CI_2 (30 mL) and H_2O (10 mL). The reaction mixture, which resulted, was allowed to stir, and warm to rt by removing the cooling bath.

The biphasic layers were separated, and the organic layer was washed with brine (2 x 10 mL) and dried (Na_2SO_4). The solvent was removed under reduced pressure to provide the mixture of crude aldehydes, the majority of which was the b aldehyde epimer (matching R_f and ^{1}H NMR) similar to the enantiomer synthesized earlier [37, 43, 49]. The addition of EtOAc on the sides of flask resulted in precipitation of insoluble solids (sulphur impurities), which were removed by filtration through filter paper. The solvent (EtOAc) was removed under reduced pressure. This process was repeated 4 to 5 times until there was no longer the precipitation of sulfur byproducts. Analysis of the mixture by the ^{1}H NMR indicated the presence of the majority of b aldehyde (peak at 10.01 ppm). The epimerization into the more stable alpha-aldehyde **25** was achieved by following the procedure of Chitra Edwankar *et. al* [41, 43]. To the solution of the crude mixture (aldehyde epimers) in a solution of MeOH (30 mL), triethylamine (8.5 mL) was added with stirring, and the mixture was stirred overnight at rt to permit complete epimerization to the alpha aldehyde **25** (peak at 9.85 ppm in ^{1}H NMR). The methanol was then evaporated under reduced pressure to obtain a crude oil, which was purified by flash column chromatography (basic alumina, 2% MeOH in CH_2Cl_2) to afford the a-aldehyde **25** as a sole product and a colorless oil (348 mg, 70%): **$[\alpha]_D^{25}$** - 125.24 (c 1.03, CHCl3); **^{1}H NMR** (500 MHz, $CDCl_3$) δ 9.85 (s, 1H), 7.50 (d, J = 7.7 Hz, 1H), 7.30 (d, J = 8.2 Hz, 1H), 7.23 – 7.16 (m, 1H), 7.14 – 7.08 (m, 1H), 4.20 (d, J = 7.9 Hz, 1H), 3.87 – 3.77 (m, 2H), 3.63 (s, 3H), 3.46 (dq, J = 13.6, 6.9 Hz, 1H), 3.25 – 3.20

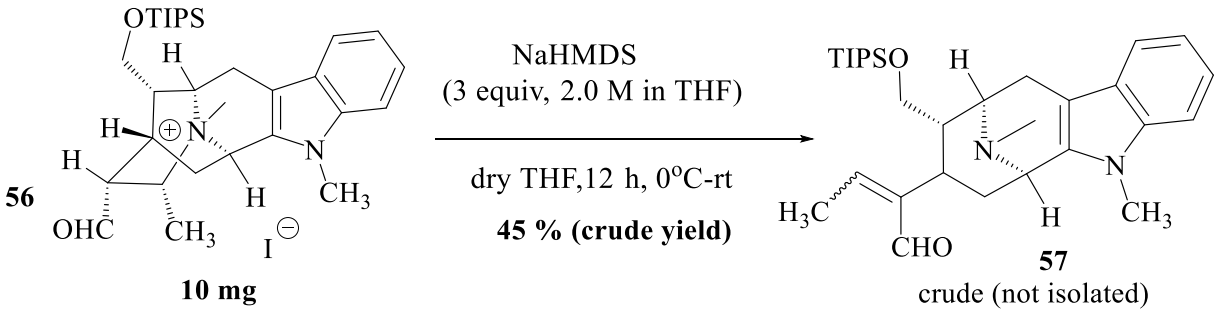
(m, 1H), 3.00 (dd, J = 15.3, 5.1 Hz, 1H), 2.74 (d, J = 14.3 Hz, 1H), 2.53 (d, J = 8.5 Hz, 1H), 2.46 (d, J = 2.0 Hz, 1H), 1.92 (ddd, J = 11.8, 9.8, 1.7 Hz, 1H), 1.81 – 1.74 (m, 1H), 1.45 – 1.39 (m, 1H), 1.36 (d, J = 6.8 Hz, 3H), 1.10 (d, J = 5.9 Hz, 21H); **^{13}C NMR** (126 MHz, $CDCl_3$) δ 203.63 (s CH), 139.21 (s C), 137.29 (s C), 127.44 (s C), 120.87 (s CH), 118.82 (s CH), 118.09 (s CH), 108.73 (s CH), 104.35 (s C), 64.35 (s CH2), 52.05 (s CH), 51.39 (s CH), 51.14 (s CH), 47.66 (s CH), 42.24 (s CH), 29.56 (s CH2), 29.29 (s CH3), 27.00 (s CH2), 26.73 (s CH), 19.37 (s CH3), 18.10 (s 6X CH3), 11.92 (s 6X CH); **DEPT 135 ^{13}C NMR** (126 MHz, $CDCl_3$) δ 120.87 (s CH), 118.82 (s CH), 118.09 (s CH), 108.73 (s CH), 64.35 (s CH2), 52.05 (s CH), 51.39 (s CH), 51.14 (s CH), 47.66 (s CH), 42.24 (s CH), 29.56 (s, CH2), 29.29 5 (s CH3), 27.00 (s CH2), 26.73 (s CH), 19.37 (s CH3), 18.10 (s 6XCH3), 11.93 (s 6 x CH); **HRMS** (ESI) m/z $(M + H)^+$ calcd for $C_{29}H_{44}N_2O_2Si$, 481.3244, found 481.3251. The NMR spectroscopic data of the material **25** was in complete agreement with that reported in the literature for its enantiomer [41, 43].

Quaternization of (25) into (6*R*,7*S*,8*R*,9*R*,10*S*,11*S*,11a*R*)-9-formyl-5,7,8-trimethyl-11-(((triisopropylsilyl)oxy) methyl)-6,7,8,9,10,11,11a,12-octahydro-5*H*-6,10-methanoindolo[3,2-b]quinolizin-7-ium iodide (56).



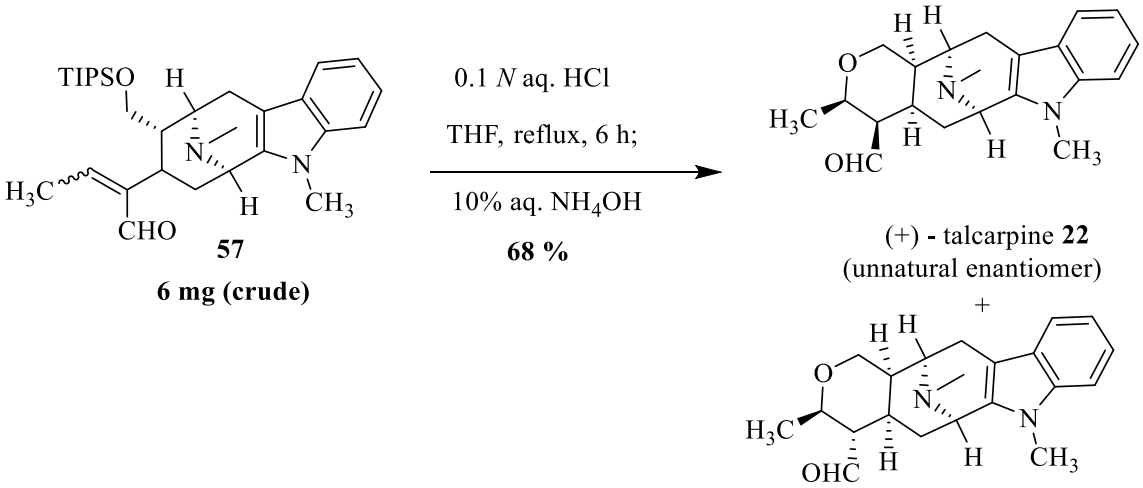
Iodomethane (excess, 0.5 mL) was added to a solution of aldehyde **25** (69 mg, 0.14 mmol) in methanol (3 mL) at 0 °C with stirring, after which the mixture was allowed to stir in the dark

(flask was covered with Al foil) at 0 °C for 16 h. The analysis by TLC (basic alumina, 0.1 mL MeOH in 2.8 mL DCM) indicated the completion of the reaction with a more polar component. At this point. the solvent was removed under high vacuum for 7 h, to provide the N_b-methyl salt **56** (64 mg, 92%): R_f 0.5 (basic alumina, DCM/MeOH, 2.4: 0.1; LCMS 495 (base peak of product desired, water and acetonitrile were used as the mobile phase); HRMS (ESI) m/z $(M)^+$ calcd for $C_{30}H_{46}N_2O_2Si$, 495.3401, found 495.3435. The salt was used in the next step without further purification.



To the solution of N_b-methyl salt **56** (10 mg, 0.12 mmol) in dry THF (>99.9% pure purchased from Sigma Aldrich, 2.5 mL), was added 1.0 M of NaHMDS in THF (44.4 mg, 0.36 mmol), with stirring, at 0 °C. The color (light yellow) of the solution turned into a light green color. The reaction mixture, which resulted, was allowed to warm to rt and then was stirred for 12 h at rt: HRMS (ESI) m/z $(M + H)^+$ calcd for $C_{30}H_{46}N_2O_2Si$ (**57**) 495.3401, found 495.3439. The product was used in the next step without further characterization.

2-((6*R*,9*S*,10*R*)-5,12-Dimethyl-9-(((triisopropylsilyl)oxy) methyl)-6,7,8,9,10,11-hexahydro-5*H*-6,10-epiminocycloocta[b]indol-8-yl)but-2-enal (57) into (+) talcarpine (22) and (-) N_4 -methyl, N_4 -21 -secotalcarpine (23).



To the mixture of crude unsaturated aldehyde **57** (6 mg crude) in THF (5 mL), 0.1 *N* aq HCl (5 mL) was added, and the mixture, which resulted, was heated to reflux and stirred for 6 h. Analysis by TLC (silica gel, 2-3% MeOH in DCM and few drops of 10% aq NH_4OH) indicated the disappearance of starting material **57** and the formation of two new components: upper strong colored component and lower faint component (under UV). When the TLC plate was dipped into ceric ammonium nitrate solution in phosphoric acid (CAN) stain, the color (dark blue) indicated the presence of two indole components (**22** and **23**), the R_f values of which matched with those of the authentic samples (enantiomers of **22** and **23**) [37, 41]. Analysis by LCMS indicated the

base peak of 339 amu for the top (R_f) component (base peak in H_2O and 0.1% formic acid/acetonitrile mobile phase). The reaction mixture was cooled to rt, and the solvents were reduced to 1/3rd of their original volume by removal under reduced pressure. The crude mixture, which resulted, was brought to pH 8 by adding 10% aq NH_4OH dropwise at 0 °C. The biphasic layers were separated, and the aq layer was extracted back with DCM (3 x 10 mL). The combined organic layers, which resulted, were washed with brine (15 mL), and dried (Na_2SO_4). The crude material was purified with flash column chromatography (silica gel, 2-3% MeOH in DCM and aq NH_4OH in a Pasteur pipette) to furnish the (+)-talcarpine **22 (**crude yield: 68%): **$[\alpha]_D^{25}$** + 36.5(c 0.08, $CHCl_3$); reference value for (-)-talcarpine **6**: $[\alpha]_D^{25}$ – 30 (c 0.1, $CHCl_3$) [37]; **^{1}H NMR** ^{1}H NMR (500 MHz, $CDCl_3$) δ 9.95 (s, 1H), 7.48 (d, *J* = 7.8 Hz, 1H), 7.28 (d, *J* = 8.4 Hz, 1H), 7.19 (t, *J* = 7.4 Hz, 1H), 7.10 (t, *J* = 7.0 Hz, 1H), 4.14 (t, *J* = 11.5 Hz, 1H), 3.98 (s, 2H), 3.89 (dd, *J* = 11.3, 4.8 Hz, 1H), 3.62 (s, 3H), 3.27 (dd, *J* = 16.7, 6.7 Hz, 1H), 2.91 (s, 1H), 2.47 (m, *J* = 14.2 Hz, 2H), 2.32 (s, 3H), 2.20 (d, *J* = 13.0 Hz, 1H), 2.05 (s, 1H), 1.79 (s, 1H), 1.45 (d, *J* = 13.2 Hz, 1H), 1.30 (d, *J* = 6.6 Hz, 3H); **^{13}C NMR** (126 MHz, $CDCl_3$) δ 204.76, 137.01 (s), 132.57 (s), 126.37 (s), 121.04 (s), 118.95 (s), 118.18 (s), 108.79 (s), 106.64 (s), 69.48 (s), 68.86 (s), 54.54 (s), 54.43 (s), 53.56 (s), 41.72 (s), 39.41 (s), 28.9 (s), 28.98 (s), 26.95 (s), 22.51 (s), 19.23 (s); **HRMS** (ESI) m/z $(M + H)^+$ calcd for $C_{21}H_{26}N_2O_2$ 339.2067, measured 339.2075. The NMR spectroscopic data (^{1}H and ^{13}C NMR) and the optical rotation (with in experimental error) of this material was in complete agreement with that reported in the literature for its enantiomer [37, 41].

The lower faint indole component which appeared on TLC also exhibited a LCMS of 339 amu. The analysis on HRMS: (ESI) m/z $(M + H)^+$ calcd for $C_{21}H_{26}N_2O_2$, predicted 339.2067,

measured 339.2074 and the similar $\boldsymbol{R_f}$ value, when compared to the natural (+) N_4 -methyl, N_4 -21 -secotalpinine **3**. Thus, the minor product obtained in this reaction is the unnatural (-) N_4 -methyl, N_4 -21 -secotalpinine **23** indole alkaloid (not enough to characterize further).

References.

1. Pandey, K. P.; Rahman, M. T.; Cook, J. M., bisindole alkaloids from the Alstonia species: recent isolation, bioactivity, biosynthesis, and synthesis. *Molecules*, **2021,** *26*, 3459.

2. Newman, D. J.; Cragg, G. M., Natural products as sources of new drugs from 1981 to 2014. *J. Nat. Prod.* **2016,** *79*, 629-661.

3. Atanasov, A. G.; Zotchev, S. B.; Dirsch, V. M.; Orhan, I. E.; Banach, M.; Rollinger, J. M.; Barreca, D.; Weckwerth, W.; Bauer, R.; Bayer, E. A.; Majeed, M.; Bishayee, A.; Bochkov, V.; Bonn, G. K.; Braidy, N.; Bucar, F.; Cifuentes, A.; D'Onofrio, G.; Bodkin, M.; Diederich, M.; Dinkova-Kostova, A. T.; Efferth, T.; El Bairi, K.; Arkells, N.; Fan, T.-P.; Fiebich, B. L.; Freissmuth, M.; Georgiev, M. I.; Gibbons, S.; Godfrey, K. M.; Gruber, C. W.; Heer, J.; Huber, L. A.; Ibanez, E.; Kijjoa, A.; Kiss, A. K.; Lu, A.; Macias, F. A.; Miller, M. J. S.; Mocan, A.; Müller, R.; Nicoletti, F.; Perry, G.; Pittalà, V.; Rastrelli, L.; Ristow, M.; Russo, G. L.; Silva, A. S.; Schuster, D.; Sheridan, H.; Skalicka-Woźniak, K.; Skaltsounis, L.; Sobarzo-Sánchez, E.; Bredt, D. S.; Stuppner, H.; Sureda, A.; Tzvetkov, N. T.; Vacca, R. A.; Aggarwal, B. B.; Battino, M.; Giampieri, F.; Wink, M.; Wolfender, J.-L.; Xiao, J.; Yeung, A. W. K.; Lizard, G.; Popp, M. A.; Heinrich, M.; Berindan-Neagoe, I.; Stadler, M.; Daglia, M.; Verpoorte, R.; Supuran, C. T.; the International Natural Product Sciences, T., Natural products in drug discovery: advances and opportunities. *Nat. Rev. Drug Discov.* **2021**, *20*, 200-216.

4. Mathur, S.; Hoskins, C., Drug development: Lessons from nature (Review). *Biomed Rep* **2017,** 6, 612-614.

5. Rahman, M. T.; Cook, J. M., The C-19 Methyl Substituted Sarpagine-Macroline-Ajmaline Alkaloids: Diversity, Occurrence, Bioactivity, and Synthesis. *Studies in Natural Products Chemistry*, Atta-ur-Rahman, Ed. Elsevier publications: Amsterdam, Netherlands, 2018.

6. Liotta, D. C.; Painter, G. R., Discovery and development of the anti-human immunodeficiency virus drug, emtricitabine (Emtriva, FTC). *Acc. Chem. Res.* **2016,** *49*, 2091-2098.

7. Newman, D. J.; Cragg, G. M., Natural products as sources of new drugs over the nearly four decades from 01/1981 to 09/ 2019. *J. Nat. Prod.* **2020,** 79, 770-803.

8. Brossi, A.; Pei, X.-F., Chapter 3 Biological Activity of Unnatural Alkaloid Enantiomers**This paper is dedicated to Professor Dr. Vladimir Prelog from the Laboratorium for Org. Chemie. ETH-Zentrum, Zürich. Switzerland, on the occasion of his 90th birthday. In *The Alkaloids: Chemistry and Biology*, Cordell, G. A., Ed. Academic Press: 1998; Vol. 50, pp 109-139.

9. Gotoh, H.; Duncan, K. K.; Robertson, W. M.; Boger, D. L., 10′-fluorovinblastine and 10′-fluorovincristine: synthesis of a key series of modified Vinca alkaloids. *ACS Med. Chem. Lett.* **2011,** *2*, 948-952.

10. Chuang, K. V.; Kieffer, M. E.; Reisman, S. E., A mild and general Larock indolization protocol for the preparation of unnatural tryptophans. *Org. Lett.* **2016**, *18*, 4750-4753.

11. Lindsley, C.; Bogusky, M.; Leister, W.; McClain, R.; Robinson, R.; Barnett, S.; Defeo-Jones, D.; Iii, C.; Hartman, G., Synthesis and biological evaluation of unnatural canthine alkaloids. *Tetrahedron Lett.* **2005**, *46*, 2779-2782.

12. Barker, T. J.; Duncan, K. K.; Otrubova, K.; Boger, D. L., Potent Vinblastine C20′ Ureas Displaying Additionally Improved Activity Against a Vinblastine-Resistant Cancer Cell Line. *ACS Med. Chem. Lett.* **2013,** *4*, 985-988.

13. Wender, P. A.; DeChristopher, B. A.; Schrier, A. J., Efficient synthetic access to a new family of highly potent bryostatin analogues via a Prins-driven macrocyclization strategy. *J. Am. Chem. Soc.* **2008,** *130*, 6658-6659.

14. Carney, D. W.; Lukesh, J. C.; Brody, D. M.; Brütsch, M. M.; Boger, D. L., Ultrapotent vinblastines in which added molecular complexity further disrupts the target tubulin dimer–dimer interface. *Proc. Natl. Acad. Sci.* **2016,** *113*, 9691-9698.

15. Ishikawa, H.; Colby, D. A.; Seto, S.; Va, P.; Tam, A.; Kakei, H.; Rayl, T. J.; Hwang, I.; Boger, D. L., Total synthesis of vinblastine, vincristine, related natural products, and key structural analogues. *J. Am. Chem. Soc.* **2009,** *131*, 4904-4916.

16. Lounasmaa, M.; Hanhinen, P.; Westersund, M., In *The Alkaloids: Chemistry and Biology*, Cordell, G. A., Ed. Academic Press: San Diego, CA, 1999; Vol. 52, pp 103-195.

17. Lounasmaa, M.; Hanhinen, P., Interpretation of the formation of nine "artifact indole alkaloids" in the ajmaline/sarpagine series. *J. Nat. Prod.* **2000**, *63*, 1456-1460.

18. Hashimoto, Y.; Harada, S.; Kato, R.; Ikeda, K.; Nonnhoff, J.; Gröger, H.; Nemoto, T., Merging chemo- and biocatalysis to facilitate the syntheses of complex natural products: enantioselective construction of an n-bridged [3.3.1] ring system in indole terpenoids. *ACS Catal.* **2022**, *12*, 14990-14998.

19. Buckingham, J.; Baggaley, K. H.; Roberts, A. D.; Szabo, L. F., *Dictionary of Alkaloids with CD-ROM*. CRC press: 2010.

20. Tan, S. J.; Lim, J. L.; Low, Y. Y.; Sim, K. S.; Lim, S. H.; Kam, T. S., Oxidized derivatives of macroline, sarpagine, and pleiocarpamine alkaloids from Alstonia angustifolia. *J. Nat. Prod.* **2014,** *77*, 2068-2080.

21. Rahman, M.T.; Cook, J.M. The C-19 Methyl Substituted Sarpagine-Macroline-Ajmaline Alkaloids: Diversity, Occurrence, Bioactivity, and Synthesis. In *Studies in Natural Products C Chemistry*; Atta-ur-Rahman, Ed.; Elsevier: Amsterdam, The Netherlands, 2018.

22. Kam, T.-S.; Choo, Y.-M.; Komiyama, K., Unusual spirocyclic macroline alkaloids, nitrogenous derivatives, and a cytotoxic bisindole from Alstonia. *Tetrahedron* **2004,** 60, 3957-3966.

23. Pan, L.; Terrazas, C.; Muñoz Acuña, U.; Ninh, T. N.; Chai, H.; Carcache de Blanco, E. J.; Soejarto, D. D.; Satoskar, A. R.; Kinghorn, A. D., Bioactive indole alkaloids isolated from Alstonia angustifolia. *Phytochem. Lett.* **2014,** *10*, 54-59.

24. Cheenpracha, S.; Ritthiwigrom, T.; Laphookhieo, S., Alstoniaphyllines A–C, unusual nitrogenous derivatives from the bark of Alstonia macrophylla. *J. Nat. Prod.* **2013,** *76*, 723-726.

25. Li, C.-J.; Chen, S.; Sun, C.; Zhang, L.; Shi, X.; Wu, S.-J., Cytotoxic monoterpenoid indole alkaloids from Alstonia yunnanensis Diels. *Fitoterapia* **2017,** *117*, 79-83.

26. Naranjo, J.; Pinar, M.; Hesse, M.; Schmid, H., Über die Indolalkaloide von Pleiocarpa talbotii Wernham. 145. Mitteilung über alkaloide. *Helv. Chim. Acta* **1972,** *55*, 752-771.

27. Wong, W.-H.; Lim, P.-B.; Chuah, C.-H., Oxindole alkaloids from Alstonia macrophylla. *Phytochemistry* **1996,** *41*, 313-315.

28. Ratnayake, C. K.; Arambewela, L. S.; De Silva, K.; Alvi, K., Alkaloids of Alstonia macrophylla. *Phytochemistry* **1987,** *26*, 868-870.

29. Keawpradub, N.; Kirby, G. C.; Steele, J. C.; Houghton, P. J., Antiplasmodial activity of extracts and alkaloids of three Alstonia species from Thailand. *Planta. Med.* **1999,** *65*, 690-694.

30. Pan, L.; Terrazas, C.; Acuña, U. M.; Ninh, T. N.; Chai, H.; De Blanco, E. J. C.; Soejarto, D. D.; Satoskar, A. R.; Kinghorn, A. D., Bioactive indole alkaloids isolated from Alstonia angustifolia. *Phytochem. Lett.* **2014,** *10*, liv-lix.

31. Zeng, J.; Zhang, D.-B.; Zhou, P.-P.; Zhang, Q.-L.; Zhao, L.; Chen, J.-J.; Gao, K., Rauvomines A and B, two monoterpenoid indole alkaloids from Rauvolfia vomitoria. *Org. Lett.* **2017,** *19*, 3998-4001.

32. Edwankar, R. V.; Edwankar, C. R.; Deschamps, J. R.; Cook, J. M., General strategy for synthesis of C-19 methyl-substituted sarpagine/macroline/sjmaline indole alkaloids including total synthesis of 19 (S), 20 (R)-dihydroperaksine, 19 (S), 20 (R)-dihydroperaksine-17-al, and peraksine. *J. Org. Chem.* **2014,** *79*, 10030-10048.

33. Edwankar, C. R.; Edwankar, R. V.; Deschamps, J. R.; Cook, J. M., Nature-inspired stereospecific total synthesis of P-(+)-dispegatrine and four other monomeric sarpagine indole alkaloids. *Angew. Chem. In.t Ed. Engl.* **2012,** *51*, 11762-11765.

34. Rahman, M. T.; Cook, J. M., The ambidextrous Pictet–Spengler reaction: access to the (+)- or (–)-enantiomers of the bioactive C-19 methyl-substituted sarpagine/macroline/ajmaline alkaloids from either d- or l-yryptophan. *Synthesis* **2019,** *51*, 1980-1988.

35. Edwankar, R. V.; Edwankar, C. R.; Deschamps, J.; Cook, J. M., Regiospecific, enantiospecific total synthesis of C-19 methyl substituted sarpagine alkaloids dihydroperaksine-17-al and dihydroperaksine. *Org. Lett.* **2011,** *13*, 5216-5219.

36. Rahman, M. T.; Deschamps, J. R.; Imler, G. H.; Schwabacher, A. W.; Cook, J. M., Total synthesis of macrocarpines D and E via an enolate-driven copper-mediated cross-coupling process: replacement of catalytic palladium with copper iodide. *Org Lett* **2016,** *18*, 4174-4177.

37. Rahman, M. T.; Deschamps, J. R.; Imler, G. H.; Cook, J. M., Total synthesis of sarpagine-related bioactive indole alkaloids. *Chemistry* **2018,** *24*, 2354-2359.

38. Rahman, M. T.; Cook, J. M., Unprecedented stereocontrol in the synthesis of 1, 2, 3-trisubstituted tetrahydro-β-carbolines via a new asymmetric Pictet—Spengler reaction towards sarpagine-type indole alkaloids. *Eur. J. Org. Chem.* **2018**, *32*, 3224-3229.

39. Sheludko, Y.; Gerasimenko, I.; Kolshorn, H.; Stöckigt, J., New alkaloids of the sarpagine group from Rauvolfia serpentina hairy root culture. *J. Nat. Prod.* **2002,** *65*, 1006-1010.

40. Kabir, M. S.; Namjoshi, O. A.; Verma, R.; Lorenz, M.; Tiruveedhula, V. V.; Monte, A.; Bertz, S. H.; Schwabacher, A. W.; Cook, J. M., Base-mediated stereospecific synthesis of aryloxy and amino substituted ethyl acrylates. *J. Org. Chem.* **2012,** *77*, 300-310.

41. Rahman, M.T. Shorter and Improved Access to the Key Tetracyclic Core of Sarpagine-Macroline-Ajmaline Indole Alkaloids: The Total Synthesis of Alkaloids Macrocarpines Ag, Talcarpine, N (4)-methyl-n (4), 21-secotalpinine, Deoxyperaksine, Dihydroperaksine, Talpinine, O-acetyltalpinine, and N (4)-methyltalpinine. Ph.D. Thesis, University of Wisconsin-Milwaukee, Milwaukee, WI, USA, 2018.

42. Rahman, M. T.; Tiruveedhula, V. V.; Stephen, M. R.; Rallapalli, S. K.; Pandey, K. P.; Cook, J. M., Completion of the total synthesis of several bioactive sarpagine/macroline alkaloids including the important NF-κB inhibitor N4-methyltalpinine. *Molecules,* **2022**; *27*.

43. Edwankar, C.R. Part. I: The First Regio-and Atropdiastereoselective Total Synthesis of the Dimeric Indole Alkaloid (+)-Dispegatrine, as Well as The First Total Synthesis of the Sarpagine Alkaloids (+)-Spegatrine, Lochvinerine,(+)-Lochneram and an Improved Total Synthesis of (+)-10-Methoxyvellosimine,(+)-Lochnerine and (+)-Sarpagine. Part. II: Studies Directed toward the Total Synthesis of The Carbon-19 Methyl Substituted Sarpagine-Macroline Alkaloids (+)-Macro-salhine Chloride as Well as Macrocarpine A, B and C. Ph.D. Thesis, The University of Wisconsin-Milwaukee, Milwaukee, WI, USA, 2011.

44. Lorenz, M.; L Van Linn, M.; M Cook, J., The asymmetric Pictet-Spengler reaction. *Curr. Org. Synth.* **2010,** *7*, 189-223.

45. Han, D.; Försterling, F. H.; Deschamps, J. R.; Parrish, D.; Liu, X.; Yin, W.; Huang, S.; Cook, J. M., Conformational analysis of the cis-and trans-adducts of the Pictet− Spengler reaction. evidence for the structural basis for the C (1)− N (2) scission process in the c is-to trans-Isomerization. *J. Nat. Prod.* **2007,** *70*, 75-82.

46. Yu, P.; Wang, T.; Li, J.; Cook, J. M., Enantiospecific total synthesis of the sarpagine related indole alkaloids talpinine and talcarpine as well as the improved total synthesis of alstonerine and anhydromacrosalhine-methine via the asymmetric Pictet− Spengler Reaction. *J. Org. Chem.* **2000,** *65*, 3173-3191.

47. Li, J.; Wang, T.; Yu, P.; Peterson, A.; Weber, R.; Soerens, D.; Grubisha, D.; Bennett, D.; Cook, J., General approach for the synthesis of ajmaline/sarpagine indole alkaloids: enantiospecific total synthesis of (+)-ajmaline, alkaloid G, and norsuaveoline via the asymmetric Pictet− Spengler Reaction. *J. Am. Che. Soc.* **1999,** *121*, 6998-7010.

48. Hara, S.; Dojo, H.; Takinami, S.; Suzuki, A., Organic synthesis using haloboration reaction. I. A simple and selective synthesis of 2-bromo- and 2-iodo-1-alkenes. *Tetrahedron Lett.* **1983,** *24*, 731-734.

49. Edwankar, C. R.; Edwankar, R. V.; Namjoshi, O. A.; Liao, X.; Cook, J. M., Stereospecific approach to the synthesis of ring-A oxygenated sarpagine indole alkaloids. Total synthesis of the dimeric indole alkaloid P-(+)-dispegatrine and six other monomeric indole alkaloids. *J. Org. Chem.* **2013,** *78*, 6471-6487.

50. Wearing, X. Z. Enantiospecific Sereospecific Total Synthesis of the Oxindole Alkaloid (+)-Alstonisine and Stereocontrolled Total Synthesis of (-)-11 -methoxy- 17-epivincamajine as Well as Studies Directed Toward the Total Synthesis of N_b-

demethylalstophylline Oxindole. Ph.D. Thesis, Univeristy of Wisconsin-Milwaukee, WI, 2004.

Chapter 3

Design, Synthesis, and Characterization of Novel Gamma-Aminobutyric Acid Type A ($GABA_A$) Receptor Ligands for the Treatment of Neurological Disorders Including Epilepsy, Depression, Anxiety, Pain, and the Synthesis of Back up Compounds for the Clinically Progressing KRM-II-81 for the Treatment of Pharmaco-Resistant Epilepsy and Dravet Syndrome.

1. Introduction

1.1. Structure, composition, and functions of the $GABA_A$ receptor.

Gamma-aminobutyric acid (GABA) is the major inhibitory neurotransmitter present in the central nervous system (CNS) and is responsible for the control of neuronal excitability and regulation of muscle tone, among other physiological functions [1]. The GABA neurotransmitter was discovered in 1950 by Eugene Roberts and Sam Frankel [2], while the first class of benzodiazepine drugs: chlordiazepoxide was discovered in 1955 by Leo Sternbach for the treatment of neurological disorders such as anxiety, and patented in 1958 [3]. In 1977, Haefley, Squires, and coworkers revealed that the benzodiazepine class of drugs bound to the $GABA_A$ receptor complex protein in the CNS using [^{3}T-diazepam] [4] . Two types of GAB_A receptors are

present in the nervous system: $GABA_A$ and $GABA_B$. $GABA_B$ receptors are G-protein coupled receptors that are widely present in the nervous system and also play a significant role in neuronal excitability. $GABA_B$ receptors, when altered, are known to be related with neurological disorders such as anxiety, epilepsy, depression, and drug addiction. Slow but persistent signals are promoted at $GABA_B$ receptors through G coupled proteins and second messengers [5].

$GABA_A$ receptors, on the other hand, are ionotropic, pentameric, ligand gated chloride ion channels and produce fast inhibitory neurotransmitter action through post synaptic membrane hyperpolarization. When activated, pentameric $GABBA_A$ receptors undergo a confirmational change that opens the chloride channel, which allows more chloride ion influx to take place from the outer to inner part of neuronal membrane. The influx of chloride ion results in inhibition of neuronal excitability because of the hyperpolarization of the neuron. The $GABA_A$ receptors are present in all organisms, which contain a nervous system. Neurological diseases such as epilepsy, anxiety, and insomnia are also related with the alteration of $GABA_A$ receptors [1]. $GABA_A$ receptors, as discussed, are rapid (reacts in milliseconds) acting on binding with the GABA by opening or holding open longer a transmembrane channel, which is selectively permeable to chloride ions [1]. $GABA_A$ receptors are the binding sites for a wide range of drugs including benzodiazepines, flumazenil, alprazolam, and diazepam as well as b-carbolines diindoles (anesthetics and neurosteroids). There are reports that the influence of GABA on the $GABA_A$ receptors is merely to hold open the chloride channel longer which elicits the hyperpolarization of the cell. This has been a controversy, and it is not completely clear if both effects may take place.

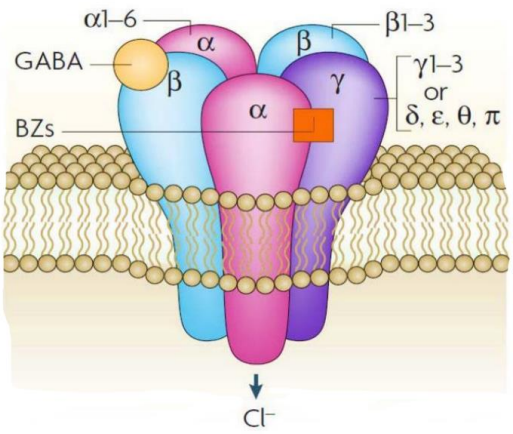


Figure 3.1. Structure and composition of the GABAA receptor with GABA, BZs binding pocket and subtypes (modified from the original source) [6]. [Picture source: *Gomes, F. I. F.; Aragão, M. G. B.; Bezerra, M. M.; Chaves, H. V., GABAergic transmission and modulation of anxiety: a review on molecular aspects. Brazilian Journal of Biological Sciences 2019, 6, (12), 9-16*].

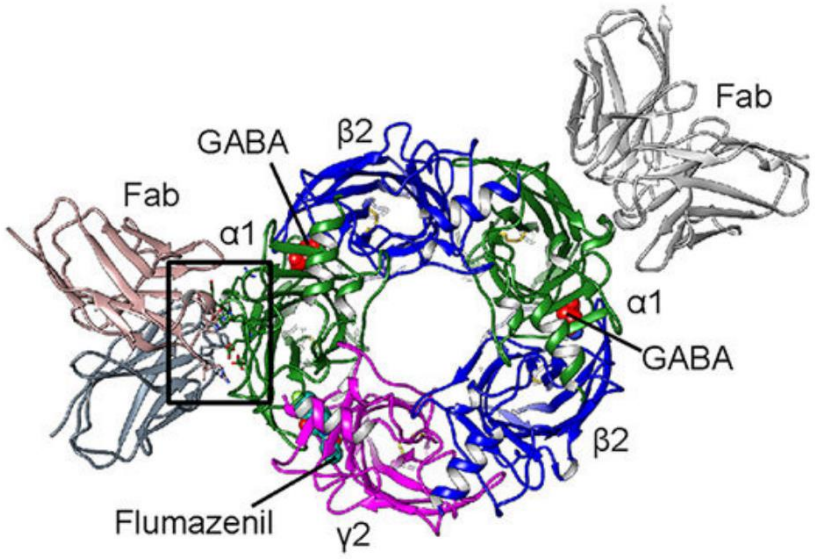


Figure 3.2. Fab-α1 GABAA composition in detail with flumazenil in the binding pocket (modified from the original source [1]. Picture source: Zhu, S.; Noviello, C. M.; Teng, J.; Walsh, R. M., Jr.; Kim, J. J.; Hibbs, R. E., Structure of a human synaptic GABA(A) receptor. *Nature* 2018, 559, (7712), 67-72.

As shown in **Figure 3.1** [6], $GABA_A$ receptors are known to have 19 subtypes which include α (6 types), b (3 types), γ (3 types) , ρ (3 types), p(1 type), ε (1 type), θ (1 type), and δ (1 type) [7].

Among these subtypes, the predominant synaptic isoform consists of two α1, two β2, and one γ2 subunits and the most important subtypes are $\alpha_{1\text{-}6}\beta_{2/3}\gamma_2$ [1]. There are $\alpha_{1\text{-}6}\beta_3\gamma_2$ subtypes that behave identically, to date to the β_2 version. The neurotransmitter GABA binds to the interface between the α and b subunits whereas, benzodiazepine-related ligands bind between the α and γ interface, as shown in **Figure 3.1** [1, 6]. The high resolution cryoEM structure of the human $GABA_A$ $\alpha_1\beta_3\gamma_2$ receptor was recently published in 2019 cryostructure, with flumazenil in the binding pocket [8]. Flumazenil is a benzodiazepine antagonist and is used for depression and BZ overdose. It also binds in the interface between the α1 and γ2 subtypes (**Figure 3.2**) [1]. In the 2019, diazepam, alprazolam and even picrotoxin were placed in the binding sites or ion channel itself [1, 8]. Various subtypes of $GABA_A$ receptors effect different physiological effects when binding with ligands. When a ligand selectively binds with the $\alpha_1\beta_{2/3}\gamma_2$ subtypes, it results in undesired and adverse effects such as ataxia, sedation, anterograde amnesia, tolerance, and addiction, but also some desired anticonvulsant and anxiolytic effects (diazepam or Xanax). On the other hand, when ligands selectively bind with $\alpha_2\beta_{2/3}\gamma_2$ and/or $\alpha_3\beta_{2/3}\gamma_2$ subtypes, it produces the desired therapeutic effects such as anxiolytic, anticonvulsant, and antinociceptive effects. The subtype α4 (binding site) is known to have been associated with lung disorders such as asthma (Arnold and Cook *et* al.) [9]. The subtype α5 is associated with cognition, schizophrenia, and depression but also is important in asthma (Arnold and Cook *et* al.) [9]. It is found in the human lungs [10]. The last key α subtype, α6 is a diazepam-insensitive site but is active in rodent models to decrease the symptoms of migraine, trigeminal orofacial pain, and tourette syndrome. The association of α2 with antihypergesic effects, α4 in lung disorders, α5 in lung disorders but also in schizophrenia and depression, make these ligands important targets. The α6 ligands are involved in with Tic disorders, Tourette's syndrome, migraine, trigeminal orofacial pain, and

schizophrenia (likely) was discovered in Milwaukee in collaboration with pharmacologists (presented at the BBC meeting in San Antonio, March 2018) with Werner Sieghart, Margot Ernst, LC Chiou, and Miroslav Savic as coauthors and UWM students. Thus, it is clear that the design of ligands that selectively bind to a $GABA_A$ subtype (s) is extremely important in order to treat diseases without side effects.

1.2. Synthetic ligands which target specific $GABA_A$/BZD receptors.

1.2.1. Benzodiazepines (BZDs) as non-selective GABA $_A$ potentiators.

Benzodiazepines, as a class of drugs were approved by the FDA (US) for the treatment of various diseases such as insomnia, panic disorder, anxiety, myorelaxation, convulsive seizures and non-convulsive seizure epilepticus [11]. This class of drugs have been in clinical use for more than 50 years and are highly prescribed drugs for a wide range of diseases, as discussed above. In the year 2007, these classes of drugs were prescribed more than 112 million times [11]. Since these drugs are on the market in humans for a long period of time, the physiology, pharmacology, and mechanism of action of most of the BZD are largely understood, to date [11]. The structure of a benzodiazepine is considered a "privileged structure" because they have been used in humans for so long. Besides, the above-mentioned uses, these are also prescribed for bipolar disorders, as sedative agents, and management of alcohol withdrawal etc. The compounds that target metabotropic glutamate receptors are also being studied for the CNS disorders, however only few compounds exhibited potency [12]. Despite the important clinical uses of these minor tranquilizers, the BZD class of drugs, which are positive allosteric modulators of $GABA_A$ receptors, are also known for many unwanted effects such as sedation, addiction, tolerance, dependence, withdrawal symptoms, and amnesia as mentioned above [11].

Diazepam (**1)**, a BZD, (brand name: Valium) is on the list of preferred medicines by the WHO and is highly prescribed drug for epilepsy, anxiety, panic disorders and muscle spasms, as mentioned [13]. In between 1968 to 1982 more than 7 billion tablets of Valium were sold in the US market [13]. Diazepam (**1**) is a positive allosteric modulator (PAM) of $GABA_A$, the mechanism of which is known after decades of its discovery. Since it binds to the α1-3,5βγ2 $GABA_A$ receptors (without selectivity) in the interface of the α an γ subtypes, as discussed earlier, side effects are inevitable [14]. Although, diazepam (**1)** is a blockbuster drug, it is largely devoid of dangerous side effects when used as prescribed except perhaps tolerance and dependence. The major side effects of diazepam (**1)** include sedation, depression, confusion, ataxia, addiction, amnesia, dizziness etc., as described before. In some cases, anxiety and seizures are exacerbated in very rare but significant cases [13].

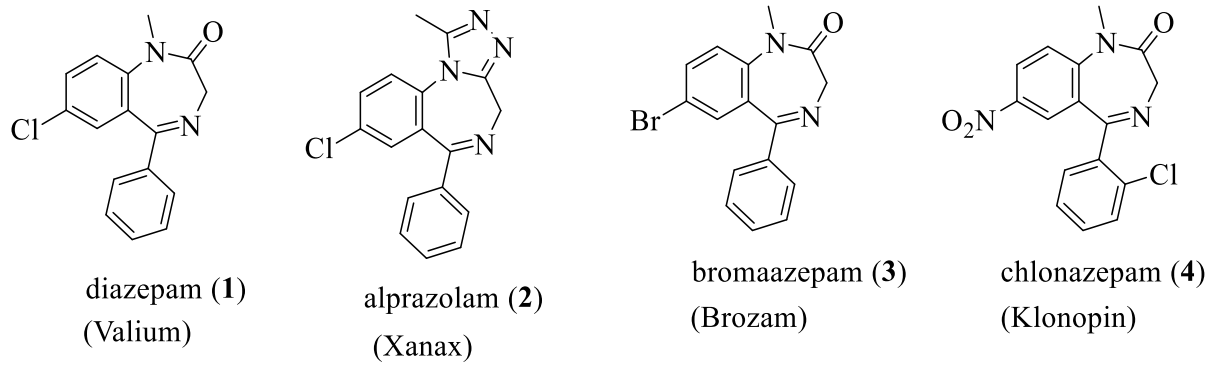


Figure 3.3. Examples of the benzodiazepine classes of drugs on the market.

Alprazolam (**2**) is another highly prescribed BZD class of drug. It is prescribed in the US under the brand name Xanax for the treatment of panic disorders and anxiety. Like diazepam (1), alprazolam (**2**) is also a non-selective GABAA receptor potentiator. It is known to bind (non-selectively) with various α subtypes (α1, α2, α3, and α5) [15]. Non-selective binding with the GABAA receptor subunits again results in unwanted side effects because of its many effects.

Both diazepam (**1**) and alprazolam (**2**) are marketed drugs, but the development of tolerance is one of the adverse effects that leads to dependence. The adverse effects of alprazolam (**2**) in patients are many, some of them are sleep disorders, dizziness, drowsiness, withdrawal symptoms, nausea, and memory problems. Misuse liability is another main concern of alprazolam [16]. Bromazepam (**3**), used for severe anxiety and panic disorders, is also associated with the same side effects with the risk of misuse and addiction, as well. Clonazepam (**4**) is another $GABA_A$ receptor agonist, and is marketed for the treatment of acute anxiety, non-convulsive status epilepticus, and epilepsy. The side effects of clonazepam (**4**) are also similar to other drugs in the BZD class, as discussed above. It also develops tolerance to the anticonvulsive effects in 2 or 3 days. This is a real problem and leads to an unmet need for better anticonvulsants. It is obvious that the selectivity (among the $GABA_A$ subtypes) is lacking in the highly used marketed BZD drug class resulting in unwanted effects in all these drugs.

1.2.2. Background

1.2.3. The key α2/α3 subtype selective imidazodiazepines (GABAkines): XHe-II-053 (5), HZ-166 (6), KRM-II-81 (7), and MP-III-080 (8).

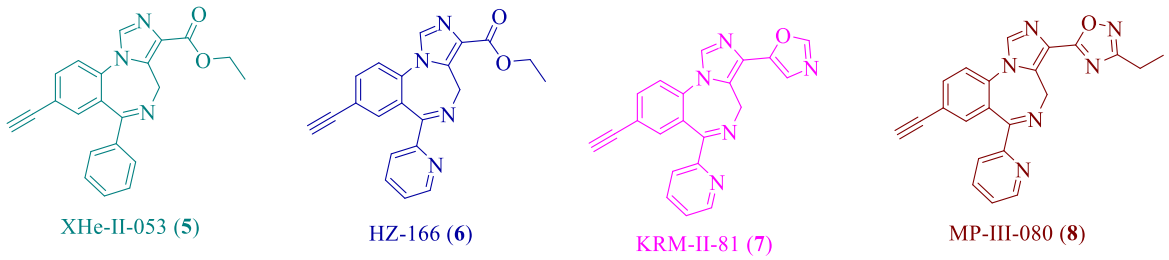


Figure 3.4. GABAA receptor α2/α3 subtype selective imidazodiazepines (GABAkines).

As discussed, the functions of each GABA(A) receptor subtype may exert a selective effect. The focus here is related to those ligands that selectively potentiate the α2/α3 subtypes, which are reported to exert anxiolytic, anticonvulsive, and antihyperalgesic activities, importantly devoid of unwanted and adverse effects [14]. Employing the "privileged scaffold" of BZDs, the design, synthesis, and activity of the α2/α3 subtype selective imidazodiazepines (XHe-II-053 (**5**), HZ-166 (**6**), KRM-II-81 (**7**), and MP-III-080 (**8**) has been widely studied for several years (**Figure 3.4**) [14, 17-19]. For the first time compounds such as XHe-II-053 (**5**) and HZ-166 (**6**) were characterized to have the desired α2/α3 subtype selectivity [14]. These compounds were potent anxiolytic and anticonvulsants and completely devoid of unwanted side effects [20]. Ligand HZ-166 (**6**) demonstrated anxiolytic activity in primates without sedation as did lead compound XHe-II-053 (**5**). The ester functional group was metabolized into the corresponding carboxylic acid (less active) in XHe-II-053 (**5**) in human livers, but not in primate livers. This resulted in poor blood brain barrier (BBB) penetration, low exposure at the target site (brain) and high clearance [14]. The lead XHe-II-053 (**5**) was in Phase-I clinical trials with BMS; however, it was metabolized to rapidly, but only in human livers, as discussed above [14, 20]. In fact, if XHe-II-053 (**5**) had been placed in a slow-release tablet, it would have been clinically useful. When the ester functional group in HZ-166 (**6**), and XHe-II-053 (**5**) was converted into the oxazole (KRM-II-81 (**7**), and the ethyl-substituted 1, 2, 4-oxadiazole [MP-III-080 (**8**)], it improved the metabolic stability of the compounds, as expected, and resulted in high exposure in brain and low clearance as desired. Importantly, the non-sedating anxiolytic activity of HZ-166 (**6**) and XHe-II-053 (**5**) was retained in KRM-II-81 (**7**) and MP-III-080 (**8**) [14]. Further preclinical studies revealed the efficacy of 1,2,4-oxadiazole MP-III-080 (**8**) against convulsions in seizure models and also it was non-sedating [14, 21]. Moreover, Bickerstaff *et* al. showed that KRM-II-81 (**7**) and MP-III-

080 (**8**) were active against neuropathic pain and did not develop tolerance, whereas the control, gabapentin did develop tolerance [22, 23]. In other work, Jun-Xu Li showed both KRM-II-81 (**7**) and MP-III-080 (**8**) were active against neuropathic pain, while KRM-II-81 (**7**) was the most potent of the two agents [22].

1.2.3.1. The α2/α3 subtype selective GABAkine: KRM-II-81 (7) is licensed to RespireRX and is progressing clinically for the treatment of epilepsy without side effects, Dravet syndrome and status epilepticus.

For the treatment of neurological diseases such as epilepsy, anxiety, pain, and depression, as discussed earlier herein, a number of BZD marketed drugs are available. However, as shown, this class of drugs, available on the market, carry a plethora of unwanted side effects. In about 70% of patients, the standard of the care medications are not effective completely for the treatment of epilepsy [24]. Addiction, tolerance, sedation, and other side effects caused the early withdrawal of drugs in some patients. Thus, there is an unmet need for new BZ-selective ligands for the treatment of psychiatric disorders, importantly without side effects. The α2/α3 subtype selective GABAkines with desired efficacy would solve the current problems associated with BZDs. One of the selective α2/α3 GABAkines, KRM-II-81 **(7)** is active against convulsive, non-convulsive, as well as pharmaco-resistant epilepsies without sedation, ataxia, loss of rightening response, tolerance, amnesia, tremors and behavioral effects with exceptional pharmacokinetics and metabolism [17, 18, 22, 24]. Besides this, KRM-II-81 **(7)** is effective against pain and depression [22]. KRM-II-81 **(7)** is one of the lead imidazodiazepines developed in Milwaukee, which at the current stage, is being pushed towards the clinic [22]. It is licensed by RespireRx Biopharmaceuticals Inc. Importantly, KRM-II-81 **(7)** suppressed the development of the seizure sensitivity towards the chemoconvulsants cocaine and petylenetetrazol in seizure kindling

models; whereas diazepam did not block the seizures [24].With the advancement of the this compound towards the clinic, the procedure for synthesizing it in the large scale was disclosed by Knutson *et.* al [24]. Since the lead compound, KRM-II-81 **(7)** is progressing towards the clinic, it is crucial to have back up analogs/bioisosteres of KRM-II-81 **(7)**, if allergies, liver toxicity, or other side effects raise their ugly head. The design, synthesis, and characterization of the novel KRM-II-81 **(7)** bioisosteres for the treatment of neurological disorders such epilepsy, anxiety, and pain, as well as the synthesis of back up compounds for the lead KRM-II-81 **(7)** will be discussed thoroughly herein. Out of the many novel compounds synthesized, KPP-III-34 **(9)** was the most active in several models of epilepsy including therapy-resistant epilepsy and chronic epilepsy, importantly, without any adverse effects up to 500 mg/kg oral dose in the preclinical studies.

2. Chemistry and results

2.1. Design, synthesis, and characterization of novel KRM-II-81 (7) analogs: chiral and/or non-chiral oxazoles and oxazolines.

The conversion of the ester functional group in XHe-II-053 (**5**), and HZ-166 (**6**) into oxazole [KRM-II-81 (**7**)] and oxadiazole [MP-III-080 (**8**)] greatly improved the metabolic stability and pharmacokinetics [25] of these compounds. As the result, the compounds were found to have enhanced efficacy against seizures, pain and depression and better target site exposure (brain) [25]. Encouraged from this result, the ester functional group of earlier lead compound HZ-166 (**6**) was converted into substituted oxazoles and oxazolines as novel analogs, as shown in the **Figure 3.5**. The oxazole-type functional group of 1, 3-oxazole, KRM-II-81 **(7**), was partly retained in novel 1, 4-oxazoles [KPP-III-34 (**9**) and KPP-III-51 (**10**)] with some modifications

such as an alkyl substituent in the oxazole ring and a bromine substituent in the 8-positon. In KPP-III-51 (**10**), the position of nitrogen and oxygen is altered and a hydrogen atom in the oxazole ring [of KRM-II-81 (**7**)] is substituted by an ethyl group to see the effect of alkyl substitution. KPP-III-34 (**9**) is the 8-bromo analog of KPP-III-51 (**10**) (**Figure 3.5**). Chiral alkyl substituted oxazolines KPP-III-96B (**11**), and KPP-IV-09 (**12**), were also designed, synthesized and evaluated [26]. Among these, chiral KPP-III-96B (**11**) and KPP-IV-09 (**12**) are ethyl substituted oxazolines and enantiomeric pairs. The methyl substituted oxazolines ZK-III-51 (**13**) and ZK-III-56 (**14**) (enantiomeric pairs), and non-chiral methyl oxazole ZK-III-58 (**15**) were also synthesized on larger scale for further evaluation including cytotoxicity, sedation, ataxia, seizure models, and pharmacokinetic studies by following the procedures published in 2020 [26]. To evaluate the motor activity, and efficacy in seizures of a bromine replacement at C-8 in KPP-III-96B (**11**), the ethynyl analog KPP-IV-35 (**16**) was designed, synthesized, characterized, and evaluated. The lead, non-sedating, anticonvulsant, and advanced compound KPP-III-34 (**9**) was converted into its hydrochloride salt to make it more bioavailable. The KPP-III-34.HCl (**17**) salt does have much improved water solubility and stability.

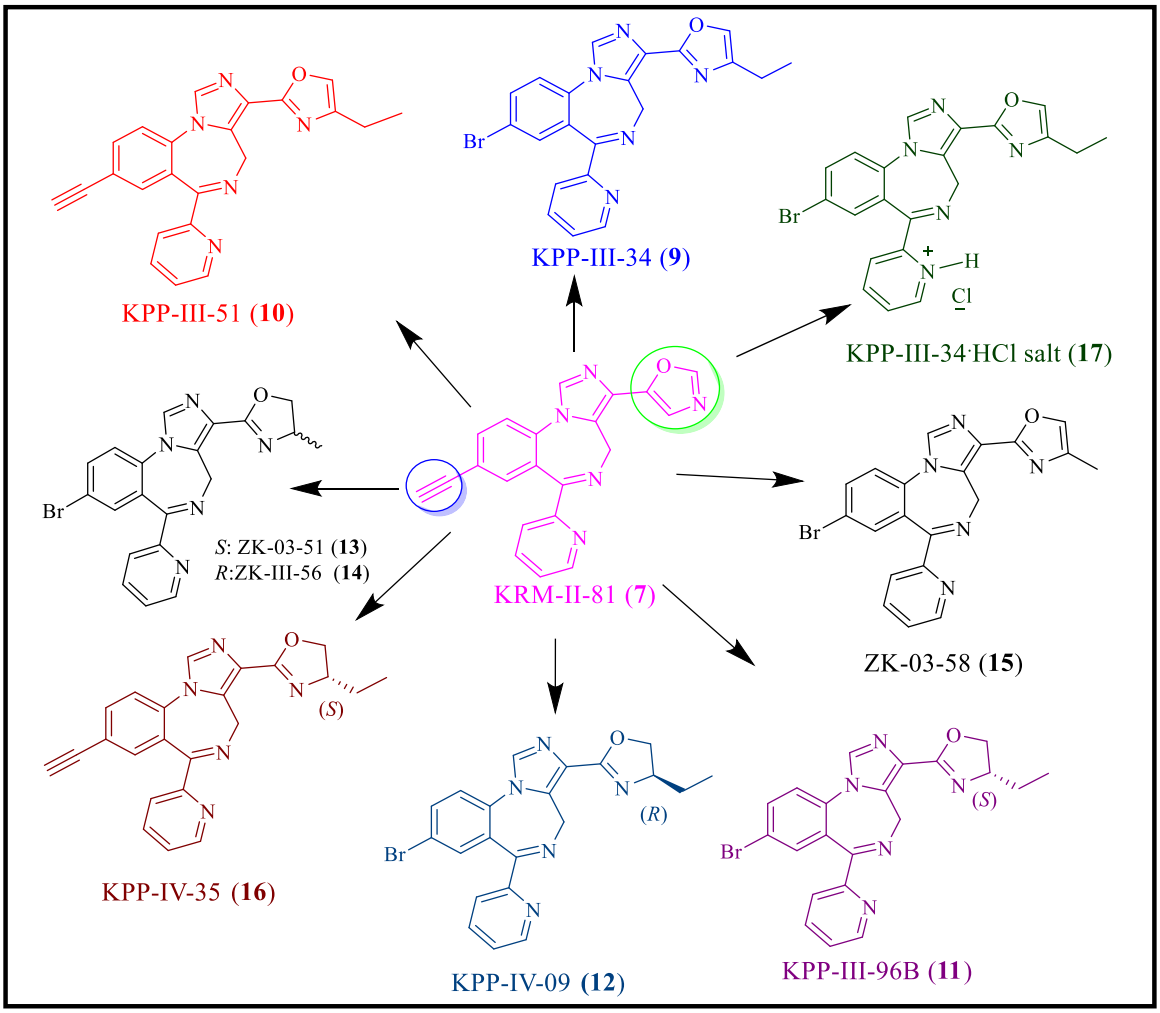


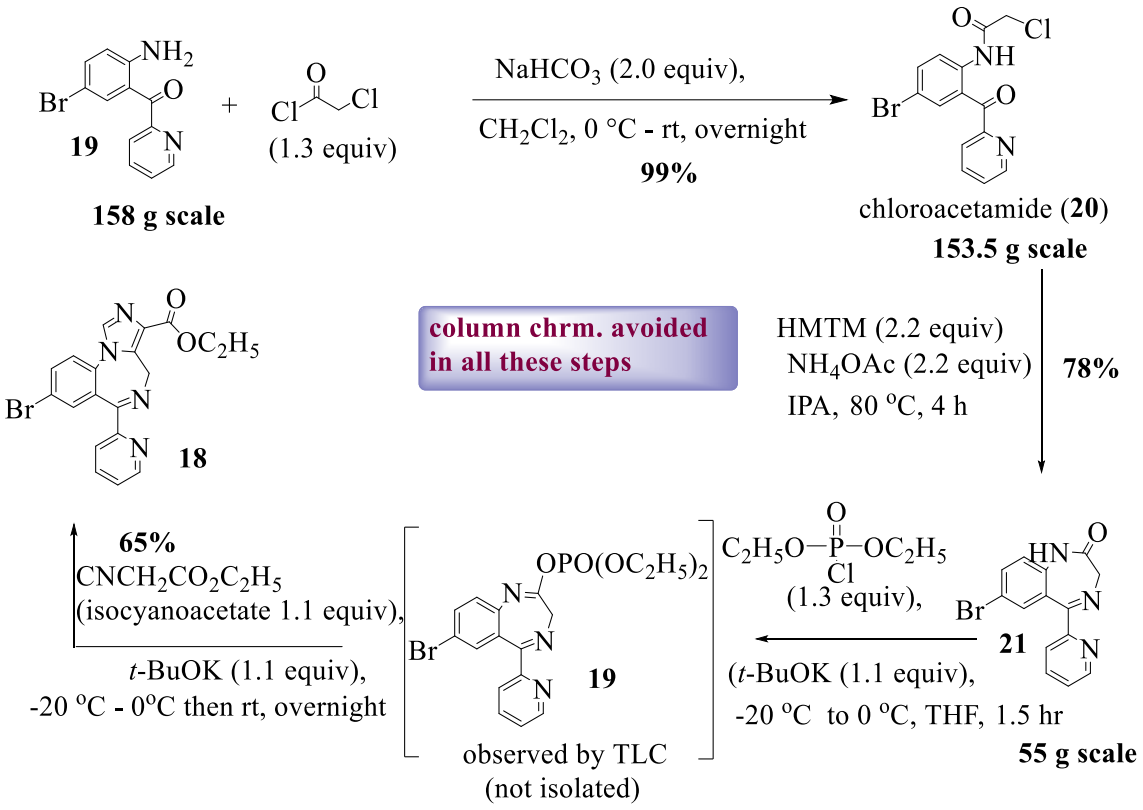
Figure 3.5. Representation of novel KRM-II-81 (7) analog.

2.2. Synthesis of KPP-III-34 (9) on gram scale and purification without column chromatography in any of the steps.

2.2.1. Large scale synthesis of imidazodiazepine (IMDZ) ester (18).

Recently, the synthetic protocol for the clinically progressing lead imidazodiazepine, KRM-II-81 **(7)** on large scale was published [24]. The key imidazodiazepine ester (**18**) intermediate was synthesized on large scale following here, by this published protocol [24]. The key intermediate imidazodiazepine ester (**18**) was synthesized in three steps starting from 2´-pyridyl ketone (**19**). The chloroacetamide intermediate (**20**) was synthesized on 158-gram scale reaction using 2'-

pyridyl ketone (**19**), sodium bicarbonate (2.0 equivalents), and chloroacetyl chloride (1.3 equivalents), with stirring (overnight) at low temperature (0 °C) to room temperature in excellent yield (90%), as shown in **Scheme 3.1**. In this nucleophilic acyl substitution reaction to the carbonyl carbon atom, the replacement of bromoacetyl bromide (not shown) by chloroacetyl chloride was done because the later reagent was found to be much less expensive, albeit slightly less reactive.



Scheme 3.1. Large scale synthesis of imidazodiazepine ester (18).

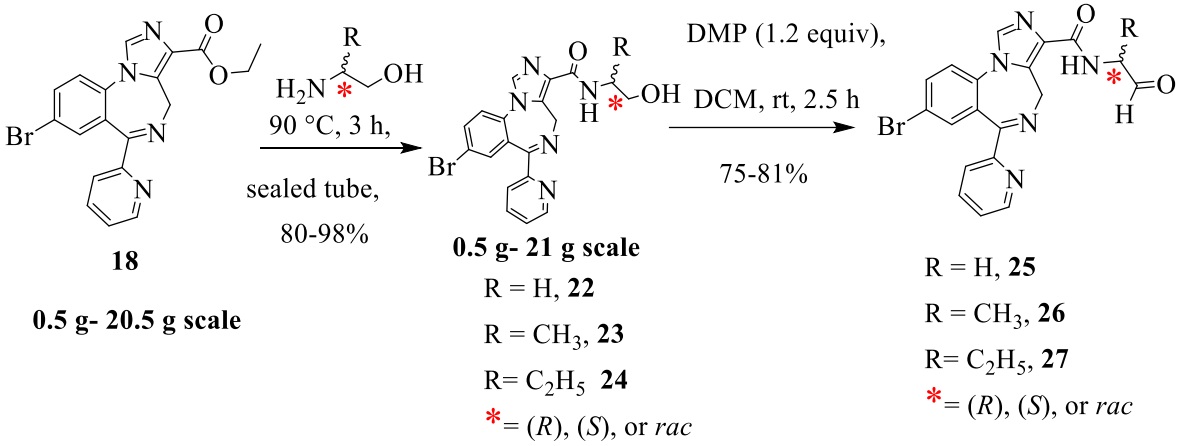
The cyclized intermediate, diazepine core (**21**), was synthesized by employing a Délepine reaction invented by Stephane Marcel Délepine [24]. The reaction mixture of the chloroacetamide (**20**), hexamethylene tetramine (HMTM, 2.2 equivalents), and ammonium

acetate (2.2 equivalents) in IPA was heated to reflux at 80 ^{o}C for 4 hours to yield diazepine core **21** in 78% yield, as shown in **Scheme 3.1**. The next step, installation of the imidazole top was done on 55 g scale. The diazepine intermediate (**21)** was treated with ethylchlorophosphate (1.3 equivalents), potassium *tert*-butoxide (1.1 equivalents) until the intermediate had formed and no more starting material appeared in the silica gel TLC (please see **Experimental** section for details). The imine intermediate (**19)** formed in this reaction was not isolated and characterized. This was followed by the addition of ethyl isocyanoacetate (1.3 equivalents) and another 1.1 equivalents of potassium *tert*-butoxide, with stirring, at -20 ^{o}C to room temperature, (**Scheme 3.1**) to yield imidazodiazepine ester intermediate (**18)**. All the intermediates (**20, 21**, and **18**), discussed herein, were purified by crystallization (please see **Experimental** section for details) and column chromatography was avoided, as mentioned previously.

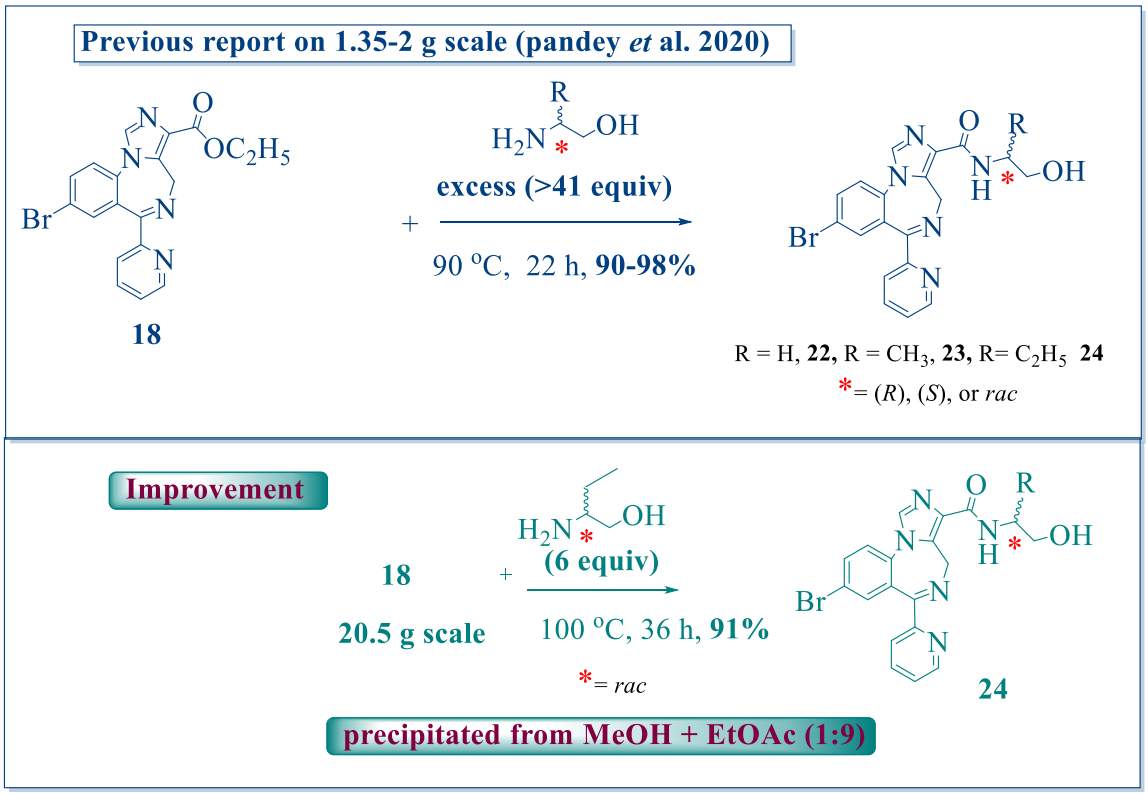
2.2.2. Synthesis of 8-bromo α-acylaminoaldehydes.

Recently, the synthetic procedures for the oxazoles and oxazolines were disclosed [26]. After large-scale synthesis of the ethyl ester intermediate (**18)** was completed, then heated in a sealed tube at 90 °C with a substituted chiral or *rac*-ethanolamines (individually) to yield the corresponding β-hydroxy amides. They were purified by flash column chromatography and obtained in 80-98% yield [26]. This process involved the use of only 6 equivalents of ethanolamines to afford β-hydroxy amides (**22, 23**, and **24**), as shown in **Scheme 3.3**, which was an improvement over synthesis of the β-hydroxy amides reported earlier using the huge excess (>40 equivalents) of the ethanolamine [26]. In addition, these β-hydroxy amides (**22, 23**, and **24**) were purified by precipitation from 10-20 % MeOH in EtOAc. The oxidation of the hydroxy functional group, so formed, in the β-hydroxy amides (**22, 23**, and **24**) were carried out using the

Dess-Martin reagent (1.2 equivalents) to provide the corresponding α-acylaminoaldehydes (**25, 26**, and **27**), which were purified by purified by precipitation in 10-20 % MeOH in EtOAc [26].



Scheme 3.2. Synthesis of 8-bromo α-acylaminoaldehydes.



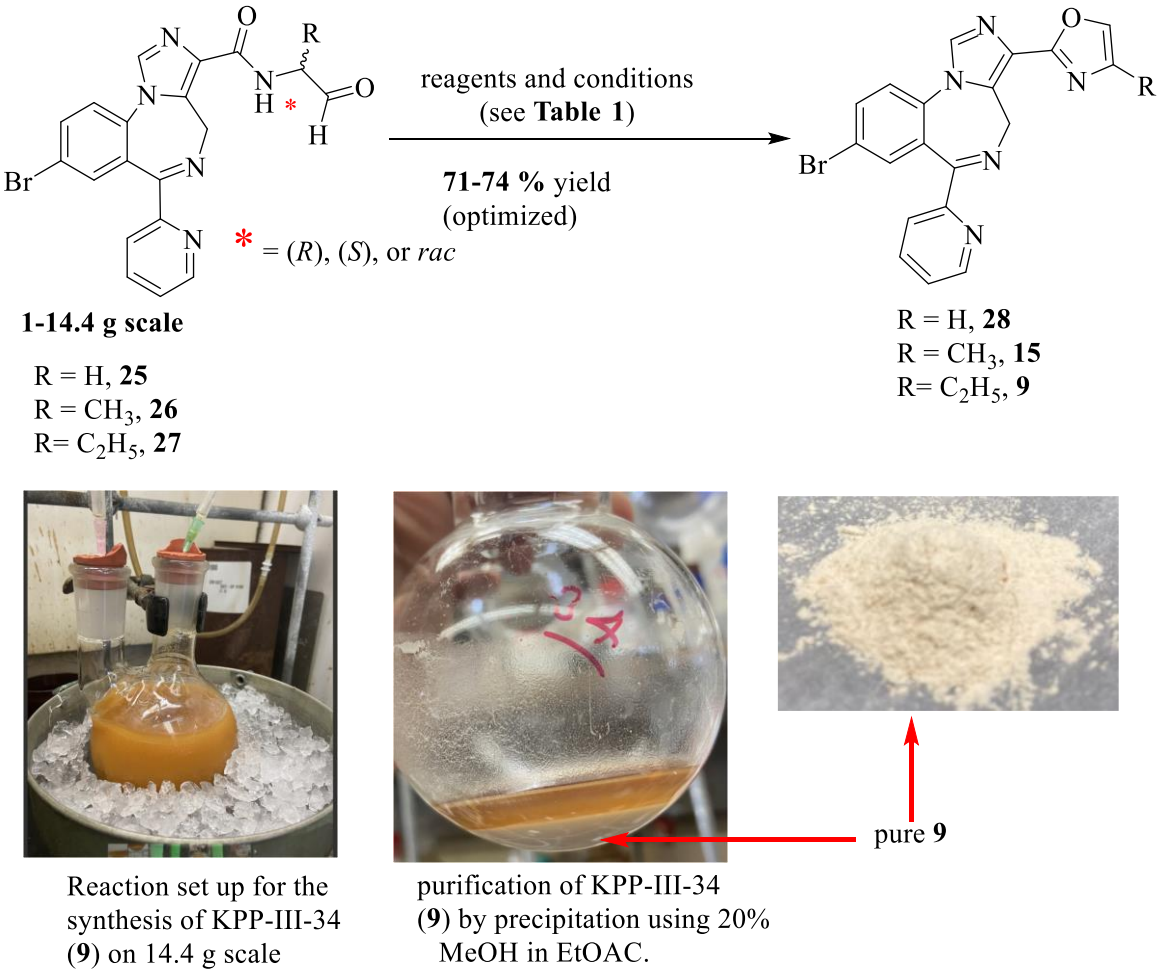
Scheme 3.3. Improved synthesis of 8-bromo-*N*-(1-hydroxybutan-2-yl)-6-(pyridin-2-yl)-4*H*-benzo[f]imidazo[1,5-a][1,4]diazepine-3-carboxamide over the published procedure [26].

2.2.3. large scale synthesis of KPP-III-34 (9) via cyclodehydration.

After the large-scale synthesis of α-acylaminoaldehydes, as shown in **Scheme 3.2** and **Scheme 3.3**, the research was directed toward cyclizing them into their corresponding oxazoles. Recently, the optimization of an oxazole forming cyclodehydration reaction was published [26]. At the beginning, the Robinson-Gabriel synthesis was carried out for cyclodehydration reaction, as shown in **Table 3.1**. The Burgess reagent was employed in the initial attempts to dehydrate the aldehydic analogs. The aldehyde starting material (**Scheme 3.4**) was dissolved in anhydrous THF, which was followed by the addition of the Burgess reagent (2-3 equivalent). Then, the reaction mixture, which resulted, was refluxed for 1.5 hours. Unfortunately, the above reaction resulted in poor yields of 20-24% (entries 1 and 2 in **Table 3.1**). Also, this cyclo-dehydrating agent (Burgess reagent) was

found to have poor shelf-life (moisture sensitive), as discussed by the Wipf group: they also obtained the best yields only with freshly prepared Burgess reagent [27].

The Wipf group also demonstrated that 5-unsubtituted oxazoles (not shown) can be prepared employing α-acylaminoaldehydes, triphenylphosphine, and iodine [28]. Also, the reaction of triphenylphosphine and iodine resulted in poor yields of the oxazoles (entry 3, **Table 3.1**). A review of literature indicated that the reactions conditions of Morwick, T., *et* al. in which triphenylphosphine and hexachloroethane were employed, to synthesize 5-unsubtituted oxazoles from α-acylaminoaldehydes, might be useful [29]. Finally, the triphenylphosphine and hexachloroethane-mediated reaction conditions provided better yields of the oxazole (entries 4 and 5, **Table 3.1**). The best optimized condition, was by using triphenylphosphine (3 equivalent), hexachloroethane (3 equivalents), and triethylamine (6 equivalents), with stirring for 2h at 0 ^{o}C-room temperature, provided the yield of 71-74%. Using this method, the lead compound KPP-III-34 (**9**) was successfully synthesized in the large scale and purified by precipitation in 20% MeOH in EtOAc as an off-white colored solid as shown in the **Scheme 3.4**. It is important to note that KPP-III-34 (**9**) can be synthesized in the large scale without column chromatography (for purification) in any synthetic steps.



Scheme 3.4. Oxazole forming cyclodehydration reaction.

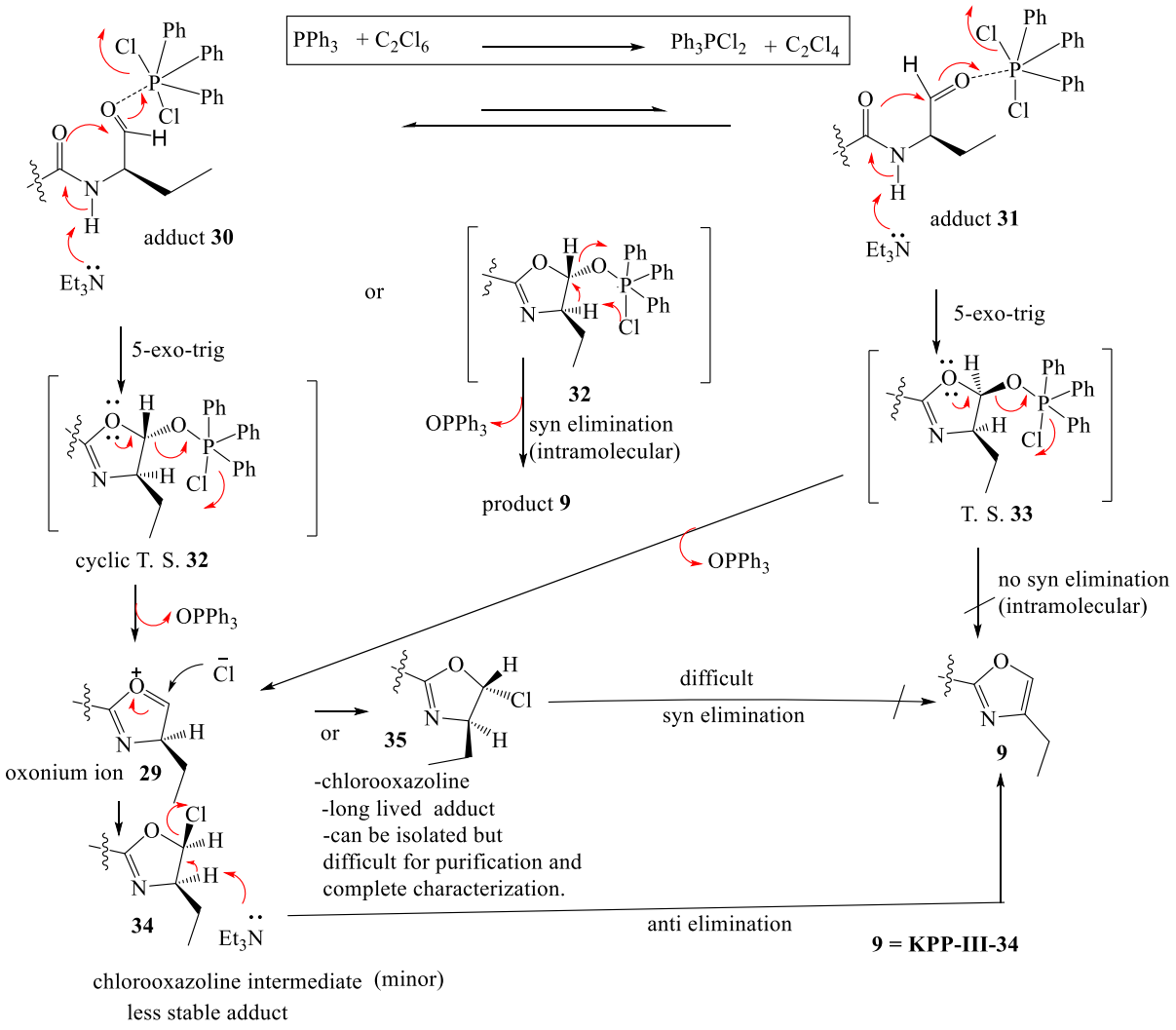
Table 3.1. Optimization of oxazole forming cyclodehydration reaction.

Entry	Reagents and conditions	%Yield of 1,4-oxazole
1	Burgess reagent (2 equiv), THF (anhy), 1.5 h, reflux	20%
2	Burgess reagent (3 equiv), THF (anhy), 1.5 h, reflux	24%
3	PPh_3 (2 equiv), I_2 (2 equiv), ACN (anhy), Et_3N (4.5 equiv), 1.5 h, rt	28%
4	PPh_3 (2 equiv), C_2Cl_6 (2 equiv), ACN (anhy), pyridine (4 equiv), 2 h, 60 ^oC	55%
5	PPh_3 (3 equiv), C_2Cl_6 (3 equiv), Et_3N (6 equiv), ACN (anhy), 2 h, 0 ^oC-rt	71-74%

2.2.4. Proposed mechanism of KPP-III-34 (9) oxazole ring formation.

The mechanism for the formation of the oxazole was suggested by Morwick *et* al., as shown in **Scheme 3.5** [29]. Herein is shown a slight modification via the possible oxonium ion intermediate (**29**). The Ph_3PCl_2 species formed by reacting Ph_3P and C_2Cl_6, which activates the aldehyde forming either adduct **30** or adduct **31 (Scheme 3.5)**. The stereochemistry may favor the adduct **30**. Both adducts in the presence of base (Et_3N) undergo intramolecular 5-*exo-trig* cyclization (allowed) to form the cyclic transition state **32** or **33**. The lone pair on oxygen in the cyclic transition state **32** or **33** favors the formation of oxonium ion intermediate **29** via the loss of triphenyl phosphonium oxide and chloride ion. The intramolecular syn elimination in the transition state **33** is not favorable since hydrogen and Ph_3PCl group are on opposite faces. The chloride ion (Cl^-) can attack on either side of the sp2 hybridized carbon atom in oxonium ion intermediate **29** which results in either the chloroxazoline intermediate **34** or **35**. As discussed by Morkwick *et* al. [29] , the chloroxazoline intermediate **35** (*trans*), presumably is the long lived

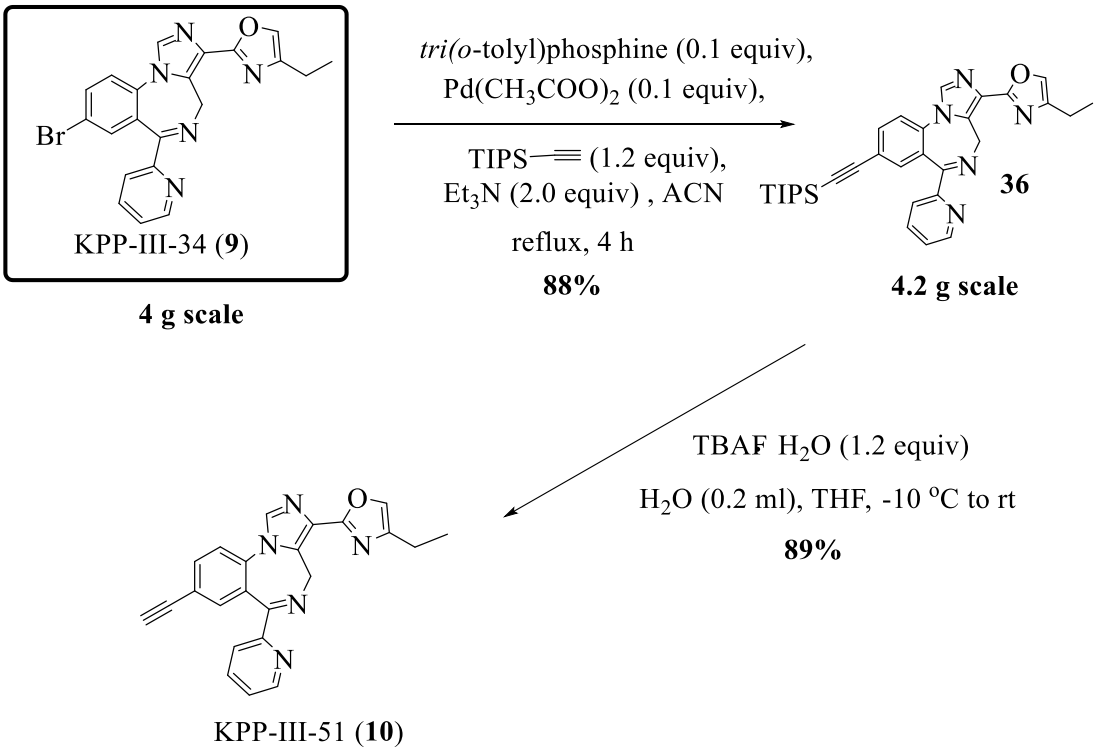
intermediate. It is more likely that the less stable intermediate **34** (*cis*) undergoes an antielimination process, which provides the oxazole product **9** rapidly. The more stable intermediate **35** on syn elimination (less likely) would give the oxazole product **9** or remain unreacted with additional stirring . No intermediates were isolated and characterized.



Scheme 3.5. Proposed mechanism for the oxazole forming reaction for KPP-III-34 (9).

2.2.5. Preparation of KPP-III-51 (10) on gram scale.

Since KPP-III-34 **(9)** was in hand, the Cu-free Sonogashira coupling reaction was executed (**Scheme 3.6**) employing palladium acetate (0.1 equivalent) and *tri*-*O*-tolyl phosphine (0.1 equivalent), TIPS acetylene (1.2 equivalents), and triethylamine (2.0 equivalents). The reaction mixture when refluxed for 4 h, afforded TIPS acetylenic oxazole **36** in 88% yield. Deprotection of the TIPS group in TIPS acetylenic oxazole **36** in the presence of a fluoride ion source (1.2 equivalents) of *tert*-butyl ammonium fluoride) at -10 ^{o}C to rt resulted in KPP-III-51 **(10)** in 89% yield. The oxazole **10** was purified by flash chromatography (see **Experimental** for details).

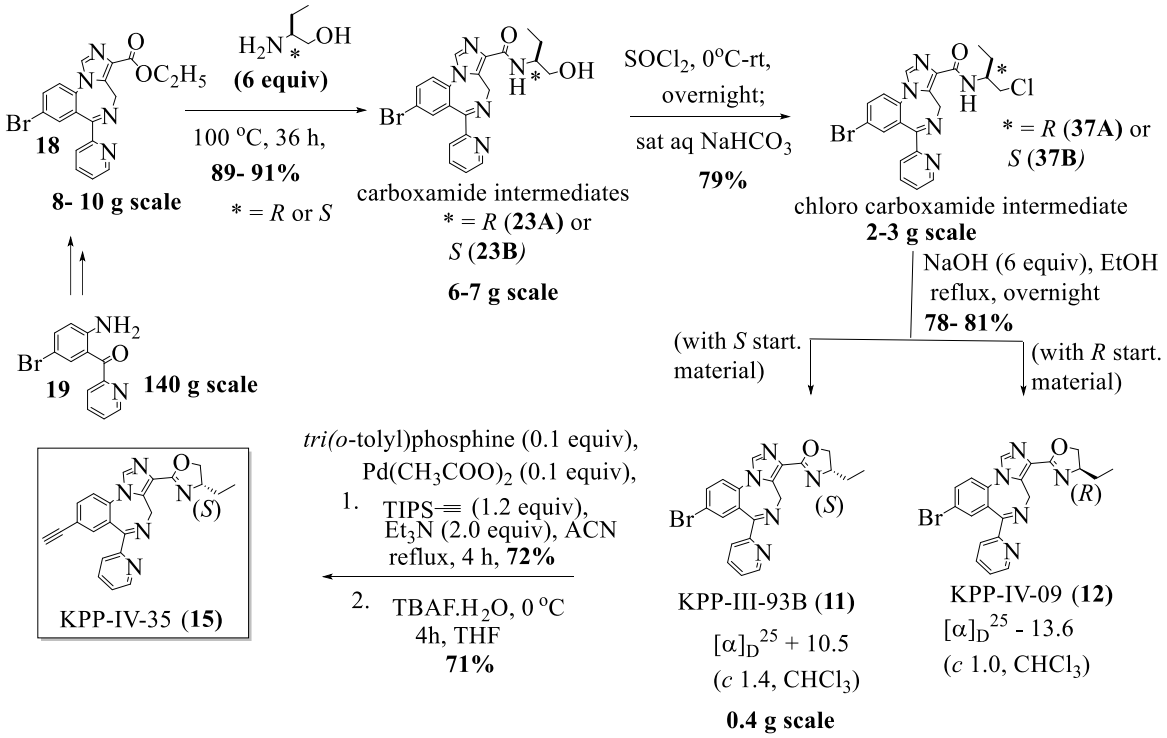


Scheme 3.6. Gram scale synthesis of KPP-III-51 (10) oxazole.

2.2.6. The synthesis of oxazoline ligands.

The imidazodiazepine ester intermediate (**18)** was synthesized on large scale (140 g) following the procedure as discussed earlier for KPP-III-34 **(9)**. The 5-membered heterocyclic oxazolines were also employed as bioisosteric replacements of carboxylic acid esters [30]. As shown in the **Scheme 3.7**, alkyl (methyl or ethyl) substituted chiral enolamines were used to synthesize chiral oxazolines [26]. The synthesis of ligands ZK-III-51 **(13)** and ZK-III-56 **(14)** were executed following the published procedures [26]. The β-hydroxy amides (**24A** or **24B**) reacted first with thionyl chloride (6 equivalents) in dichloromethane to afford β-halo amides (**37A** or **37B**). The compounds **37A** or **37B** were then heated to reflux with 6 equivalents of sodium hydroxide in dry ethanol to afford the cyclized five-membered oxazolines (**11** and **12**, respectively) in 75-85% yield (**Scheme 3.7**) [26, 31, 32]. The chiral oxazolines KPP-III-96B **(11)** and KPP-IV-09 **(12)** (individually and a 50:50 mixture of both), were evaluated by chiral HPLC to detect any racemization. Both enantiomers were found to have more than 99% enantiomeric excess (please see **Appendix part II** for HPLC data), which confirmed no racemization in the sodium hydroxide mediated cyclization. The optical rotation for these enantiomeric pairs were also in agreement within experimental error (**Scheme 3.7**). The 8-bromo chiral oxazoline KPP-III-96B **(11)** was converted into the corresponding 8-ethynyl oxazoline KPP-IV-35 **(16)** to see if the bromine (at the 8^{th} position) replacement by ethynyl would reduce the motor impairing and block the epileptic convulsions in the convulsant models. For this conversion, a Cu-free Sonogashira coupling reaction, as discussed earlier (for oxazole), was carried out to afford the TIPS acetylenic product (**38),** which was purified by flash column chromatography on neutral alumina to afford 72% of the product. The deprotection of the TIPS group from the TIPS acetylenic oxazoline (not shown) resulted in ethynyl oxazoline, KPP-IV-35

(16), which was purified by crystallization (CH_2Cl_2, EtOAc, and hexane (2:7:1) to afford the product in 71% yield.



Scheme 3.7. Synthesis of KPP-III-93B (11), KPP-IV-09 (12), and KPP-IV-35 (16) oxazolines.

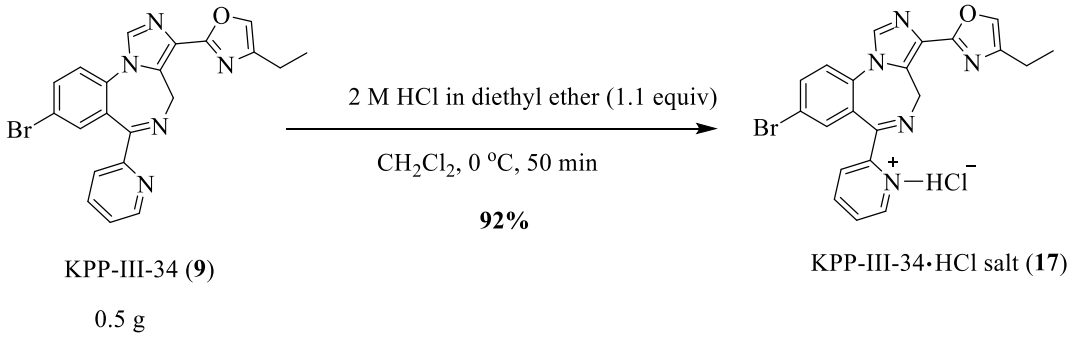
2.2.7. Preparation of KPP-III-34·HCl salt (17).

As discussed, the lead compound KRM-II-81 **(7)** is progressing to clinical trials. When this compound (**7**) was converted into its hydrochloride salt (structure not shown). This resulted in an increase in water solubility by 12 times [18]. It also increased bioavailability, and therapeutic effects [18]. As a result of this work, it was found in several laboratories that KRM-II-81·HCl salt had better solubility, partition coefficient, PH solubility profile, less hygroscopicity, and importantly enhanced pharmacokinetics and oral anticonvulsant activity

in a pentylenetetrazole convulsions seizure model (PTZ), as compared to the free base KRM-II-81 **(7)**, as desired [18]. Encouraged from this result, the advanced antiepileptic compound KPP-III-34 **(9)** was also converted into its HCl salt using 2 M anhydrous HCl in diethyl ether (1.1 equivalents) dropwise at 0 ^{o}C, as shown in **Scheme 3.8** and **Figure 3.6** below (please see **Experimental** section for detail). Before testing the biological activity of the compound **17**, a hygroscopicity study was carried out.



Figure 3.6. KPP-III-34 (9) in CH_2Cl_2 (left), and KPP-III-34 (9).HCl salt (17) in CH_2Cl_2 (right).



Scheme 3.8. Preparation of the KPP-III-34·HCl salt (17).

2.3. Hygroscopicity study of KPP-III-34·HCl salt (17).

After conversion of the non-sedating antiepileptic compound KPP-III-34 **(9)** into its hydrochloride salt, the salt (**17**) was tested for hygroscopicity. Hygroscopicity of the compound is related to its shelf-life stability. The more hygroscopic the compound is, the less stable their shelf-life, when exposed to the environment. The experiment was run at 25±1 ^{0}C with a relative humidity of 71%.

The pure KPP-III-34·HCl salt **(17)** was dried in an oven at 45 ^{0}C under reduced pressure for 12 h to ensure no moisture was present in the salt. The anhydrous salt **(17)** was immediately weighed within an accuracy of 0.1 mg. This was followed by the transfer of 0.2556 gram of sample into the 20 mL vial and it was spread out evenly on the bottom of the vial. The vial was weighed every 20 minutes until 4 h had passed, after which the analysis was continued for 3 days at various time intervals. The maximum weight (0.5%) gained by the salt (due to moisture) was found after 16 hours of exposure to the environment and then it decreased slightly and reached 0.39% after 3 days (**Table 3.2).** From the hygroscopic point of view, KPP-III-34·HCl **(17)** salt demonstrates very weak hygroscopicity (with in experimental error) and is expected to have a very stable shelf life.

Table 3.2. Hygroscopicity studies of KPP-III-34 (9)·HCl salt over 3 days.

Weight of empty vial (20 mL)	13.1372 g
Weight of empty vial + sample	13.3928 g
Weight of sample	0.2556 g
Weight of vial with sample after 20 min	13.3930 g
Weight of vial with sample after 1h	13.3932 g
Weight of vial with sample after 16 h	13.3941 g
Weight of vial with sample after 1 day	13.3940 g
Weight of vial with sample after 2 days	13.3939 g
Weight of vial with sample after 3 days	13.3938 g

Maximum % increase (after 16 h)	0.5%
% Increase in weight after 3 days	**0.39%**

2.3. Biology, and molecular docking studies of novel ligands.

2.3.1. Rotarod studies of novel compounds in female CFW mice via oral administration at various doses.

The rotarod studies of the KPP ligands were carried out in female Charles River Swiss Wester mice at the University of Wisconsin-Milwaukee (by Nick Zahn and Michelle Meyer in Dr. Arnold's laboratory). The objective of this experiment was to evaluate the compounds for potential undesired motor side effects, which is thought to be α1-mediated and can not be tolerated in the proposed antiepileptic drugs. The rotarod experiment was performed, according to the previously published protocol [26]. Prior to the rotarod test, mice were trained on a rotating rod until they can maintain their balance for 3 consecutive times (3 minute sessions). Diazepam (**1**) was used as a control. The test compounds at various doses (40, 80, 100 or 120 mg/kg) were administered to the mice orally via gavage and then the mice were placed on the rotating rod for a maximum of 3 minutes. The 2% hydroxypropyl methylcellulose was used as a vehicle in this experiment. In this experiment, besides sedation, mice were also observed for ataxia, loss of rightening response, and tremors, as an indication of undesired CNS effects. Both oxazoles KPP-III-34 (**9**) and KPP-III-51 (**10**) did not show sedation at 40, 80, and 120 mg/kg doses in contrast to the control diazepam (**1**), 5 mg/kg), as shown in **Figure 3.7**. Importantly, in this test, both KPP-III-34 (9) and KPP-III-51 (**10**) oxazoles also did not show any sign of ataxia, loss of rightening response, or tremors in the rotarod test up to 120 mg/kg. The non-sedating nature of KPP-III-34 (**9**) in mice is consistent with the key toxicity test carried out at ETSP

where KPP-III-34 (**9**) did not show any sedation and side effects up to a dose of 500 mg/kg in rats (**Table 3.14**).

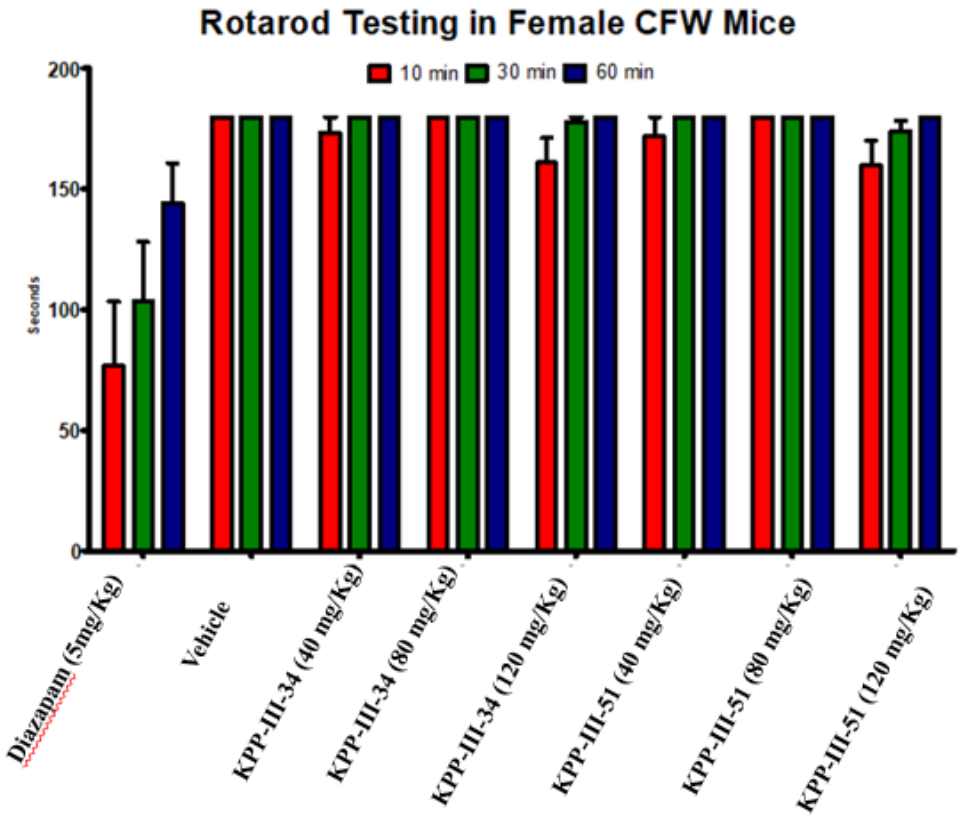


Figure 3.7. Rotarod studies of KPP-III-34 (9) and KPP-III-51 (10) at 40, 80, and 120 mg/kg doses. Diazepam is the control.

The 8-bromosubstituted oxazolines, KPP-III-96B (**11**) and KPP-IV-09 (**12**), also did not show any sedation and undesired CNS effects at lower (40 mg/kg) and moderate (80 mg/kg) doses (**Figure 3.8**). However, these two oxazolines exhibited sensorimotor deficits at the higher dose of 100 mg/kg as shown in **Figure 3.8**. These sedative effects, which resulted at higher doses (100 mg/kg) of KPP-III-96B (**11**) and KPP-IV-09 (**12**) occurred, presumably, because of some α1-

$GABA_AR$ efficacy/binding has occurred and resulted in ataxia and sedation at the higher dose. It is possible this is caused by a different binding position of the chiral oxazolines (non-planner geometry) in the α1-$GABA_AR$ ion channel, as compared to the non-sedating and planner oxazoles [KPP-III-34 (**9**), and KPP-III-51 (**10**)] or some metabolic effect. On the other hand, methylated chiral oxazolines: ZK-III-51 (**13**) and ZK-III-56 (**14**) did not exhibit sensorimotor deficits at higher dose (120 mg/kg) as shown in **Figure 3.9**. Moreover, the oxazolines (**13** and **14**) did not exhibit tremor, ataxia, and loss of rightening response at the dose of 120 mg/kg in mice.

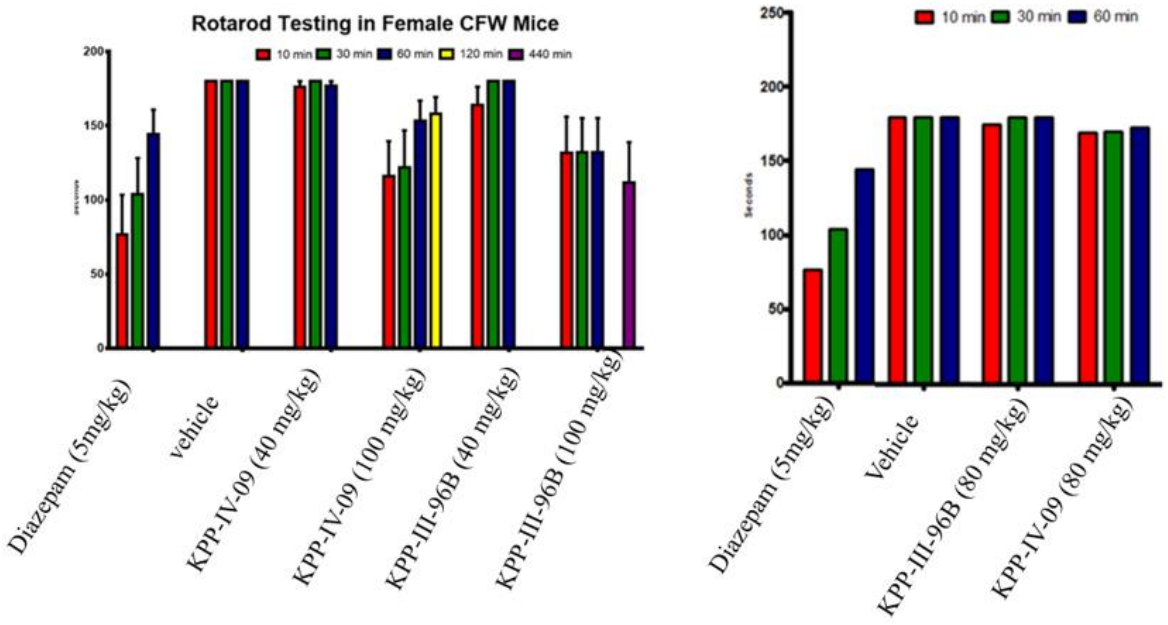


Figure 3.8. Rotarod studies KPP-III-96B (11), and KPP-IV-09 (12) at 40, 80, and 100 mg/kg dose. Diazepam is the control. Confidential and unpublished data.

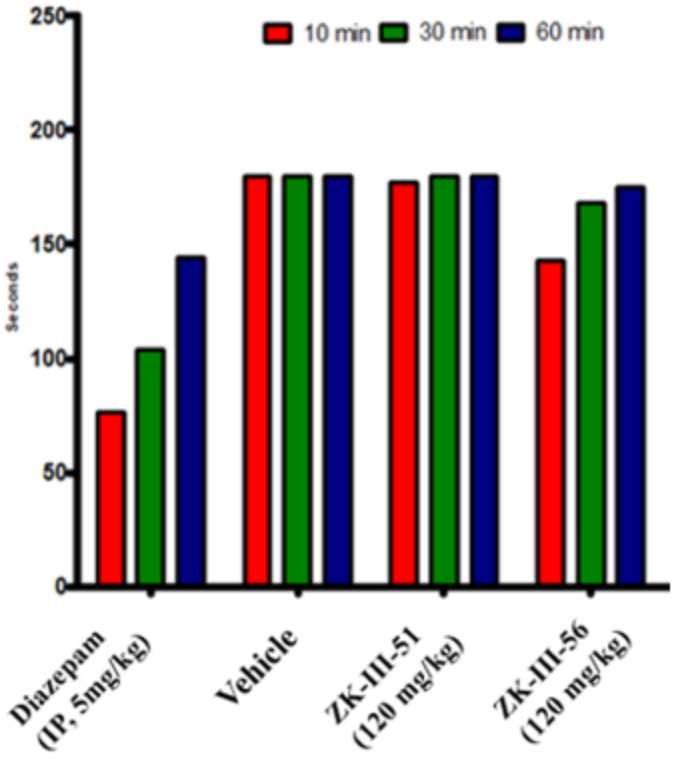


Figure 3.9. Rotarod studies ZK-III-51 (13), ZK-III-56 (14) at 120 mg/dose. Diazepam is the control. Confidential and unpublished data.

2.3.2. Cytotoxicity studies of novel analogs (by Michelle Meyer and Anika Tylek in Dr. Arnold's laboratory, UWM).

The newly synthesized imidazodiazepines were evaluated for cytotoxicity in HEK 293 cell lines (human embryonic kidney cells). The 3-dibutylamino-1-(4- hexyl-phenyl)-propan-1-one was used as a positive control at 150 µM; all cells were killed at this concentration with this reagent. For all the oxazoles and oxazoline analogs of KRM-II-81 **(7)** discussed herein, the IC_{50} was >300 µM for cytotoxicity in HEK 293 cells (**Table 3.3).** It is obvious from **Table 3.3**, the compounds discussed herein: ethyl substituted aromatic (oxazoles), non-aromatic (oxazolines), as well as 8-bromo, or 8-ethynyl analogs all are non-toxic in the HEK 293 cell line.

Table 3.3. Cytotoxicity studies of ligands in HEK 293 cell lines.

Compound number	Compound code	Toxicity in HEK293 [26] (IC50)
9	KPP-III-34	>600
10	KPP-III-51	>600
11	KPP-III-93B	>300
12	KPP-IV-09	>400
16	KPP-IV-35	In progress
13	ZK-III-51	>400
14	ZK-III-56	>400

2.4. Docking studies of KPP analogs

One of the lead imidazodiazepines, HZ-I66 (**6**), is a non-sedating, anxiolytic and anticonvulsant [26]. To determine if the new biosterers might undergo a similar binding pose in the GABA(A) α1-ion channel, the molecular docking of the above ligands was performed in AutoDock Vina 1.5.6. using the published CryoEM structure of the human full-length α1β3γ2L GABA(A) receptor ion complex by Masiulis *et* al. [8] with alprazolam (PDB: 6HUO) [33]. The molecular docking/binding study was carried out with the help of Dr. Lalit Golani (Post-doctoral researcher at UWM). Moreover, the non-sedating results in the rotarod studies of KPP-III-51 (**10**) and KPP-III-34 (**9**) when administered orally (120 mg/kg) to the mice encouraged the execution of the molecular docking studies. Importantly, it was noted that the binding poses (in BZR binding pocket) of all the ligands described herein were similar to the binding pose of HZ-166 (**6**) because the difference in the binding affinities was lower than ±1 kcal/mol (**Table 3.4.**) [26].

Table 3.4. Binding affinity (docking score) of bioisosteric ligands in kcal/mol.

Compound code	Binding affinity (kcal/mol)
Diazepam	-9.9
Alprazolam	-10.9
KPP-III-51 **(10)**	-9.6
KPP-III-34 **(9)**	-9.1
KPP-III-96B **(11)**	-9.3
KPP-IV-09 **(12)**	-9.5
HZ-166 **(6)**	-9.0

The bigger the minus number the tighter the binding affinity.

2.4.1. Molecular docking studies of KPP-III-51 (10).

Molecular docking studies demonstrated that the ethynyl oxazole: KPP-III-51 **(10)** overlapped well with HZ-I66 (**6**), as shown in **Figure 3.11.** From the docking studies in **Figure 3.11**, it can be expected that KPP-III-51 **(10)** would presumably have a little less affinity towards the α1-GABA(A) receptors because of its binding score in the α1β3γ2L $GABA_A$ receptor ion complex similar to HZ-166 **(6)**. But more importantly KPP-III-51 **(10)**, and KPP-III-34 (**9**) bound much less tightly than alprazolam **2** (-10.9), as shown in the **Table 3.4**. This docking studies of KPP-III-51 **(10)** can be related to the non-sedating results (in rotarod studies) of KPP-III-51 **(10)** up to 120 mg/kg (**Figure 3.7)**.

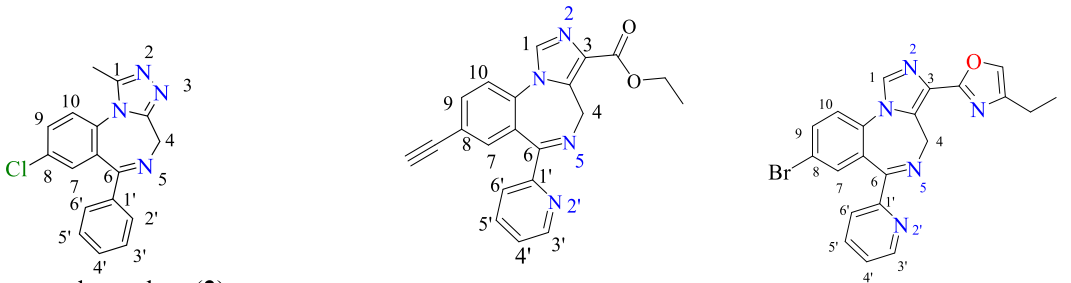


Figure 3.10. Structures of alprazolam (2), HZ-166 (6), and KPP-III-34 (9) with binding affinity.

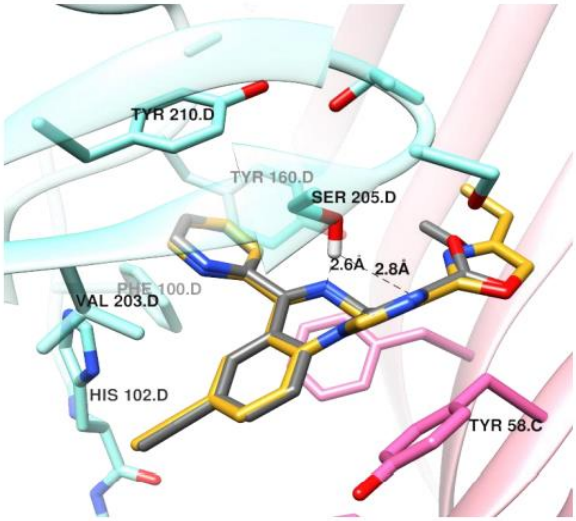
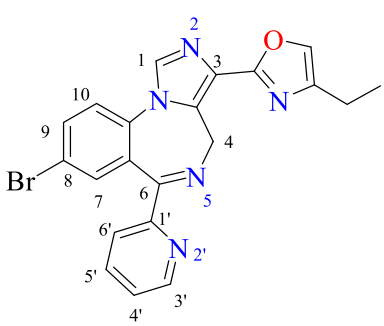


Figure 3.11. Overlay of the docked conformations of HZ-166 [(6, (gray)] and KPP-III-51 (gold) in the complex with α1β3γ2 interface of GABA(A) receptor 6HUO at the α+γ- interface BZ binding site (α1 represented as chain D, color: aquamariane and γ2 represented as chain C, color: orchid, dashed line: H-bonding.

2.4.2. Molecular docking of KPP-III-34 (9).

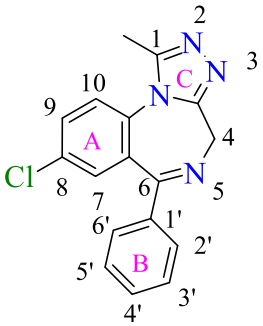
From the docking studies, the bond angle between the oxygen atom of the carbonyl carbon atom (α1His102 amino acid), and the chlorine and carbon atoms of alprazolam was found to be 168 °, which is closer towards the linear bond angle of 180 ° desired for a potent halogen bond with the

C-loop histidine carbonyl. In contrast, the bond angle between the oxygen atom of carbonyl carbon (α1His102 amino acid), bromine and carbon atom of KPP-III-34 (**9**) was found to be 122.5 ^{o}, which clearly is a large deviation from the required linear bond angle. The closer the bond angle towards linearity, the stronger the halogen bond [34], which supports the non-sedating activity of KPP-III-34 (**9**). However, the bond angle is not the sole factor that determines halogen bonding. The halogen bond also depends upon the size of halogen atom. The bigger the size of the halogen atom, the stronger the halogen bond [34]. From the docking studies (**Figure 3.12B**) of KPP-III-34 (**9**) overlapped with alprazolam (**1**), it is obvious that the binding pose of KPP-III-34 (**9**) is different, as compared to that of alprazolam (**1**), with a much large deviation of the position of the 8-bromo analog (bond angle: 122.5 ^{o}) to the chlorine atom of **1** (168 ^{o}). This presumably resulted in less binding potency of KPP-III-34 (**9**) at the α1β3γ2 binding site, which, presumably, led to no sedation in rats up to 500 mg/kg via oral administration (**Table 3.14**) [19]. The disorientation of the diazepine ring, which occurs in the predicted binding pose of KPP-III-34 (**9**), is probably due to compensation for the binding of the ethyl substituted oxazole ring that allows the ligand to fit in the binding pocket slightly differently (**Figure 3.12B**). Also, the Br atom of KPP-III-34 (**9**), in place of the ethynyl moiety of KPP-III-51 (**10**), enables reduced covalent interactions due to length differences of these two substituents. Control sedating anticonvulsant diazepam (**1**) and alprazolam (**2**) clearly show a halogen bond interaction with the carbonyl oxygen atom of α1His102 amino acid in the cryoEM structure [26].



KPP-III-34 (**9**)

bond angle: 122.75 º



alprazolam (**2**)

bond angle: 168 º

Figure 3.12A. Structures of compound 9 and 2.

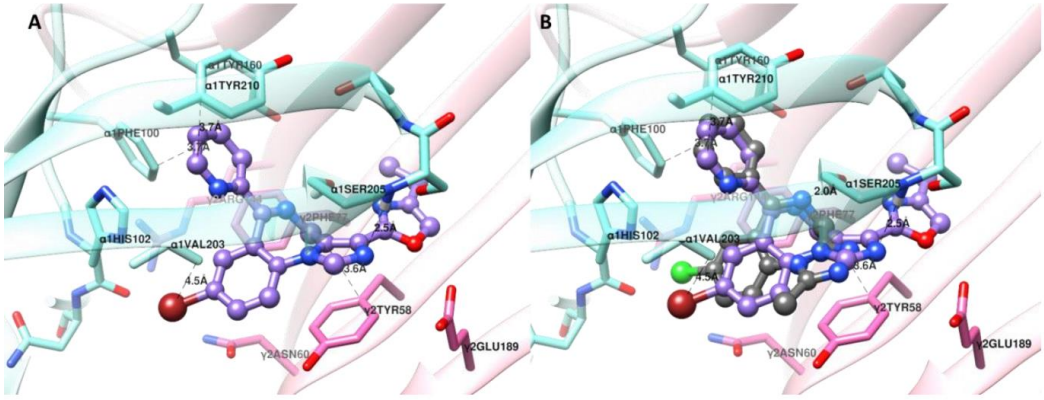
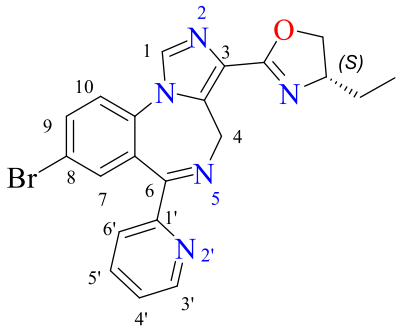


Figure 3.12B. Structures of KPP-III-34 (A left), and alprazolam (A right). Showing the best pose of KPP-III-34 (purple) docked in 6HUO (B left). Showing the best pose of compound KPP-III-34 (9) (purple) docked in 6HUO, overlaid with bound alprazolam (grey) in 6HUO. α1 (aquamarine) and γ2 (orchid) subunits of α1β3γ2L GABAA receptor 6HUO (B right). Dashed lines indicate π–π, hydrogen bond and halogen bond interactions.

2.5.3. Molecular docking studies of KPP-III-96B (11).



KPP-III-96B (**11**)
binding affinity = **-** 9.3 kcal/mol

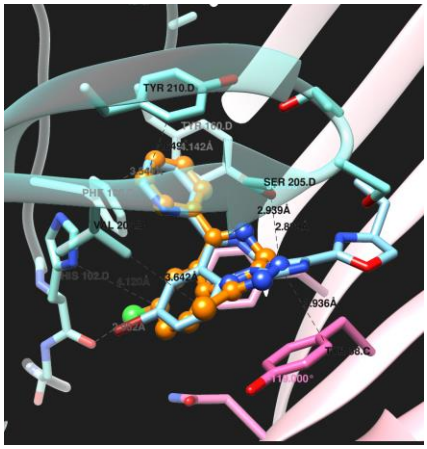


Figure 3.13. The structure of KPP-III-96B [11, (left)]. Molecular docking study of KPP-III-96B (11) on the right (shown in blue color), and ALP (shown in organ color) in the complex with the α1β3γ2 interface of the $GABA_A$ receptor 6HUO at the $\alpha^+\gamma^-$ interface of the BZ binding site. Binding energy: -9.3 kcal.mol. Dashed lines indicate π–π, hydrogen bond and halogen bond interactions.

The docking studies of 8 bromo-substituted oxazolines discussed herein, KPP-III-96B **(11)** and KPP-IV-09 **(12)** also showed halogen bond interactions with the carbonyl carbon atom of α1His102 amino acid similar to the case of diazepam (**1**) and alprazolam (**2**) mentioned earlier. The halogen bonding can be related to the α1 efficacy in $GABA_A$ receptors which could be the reason for the motor effects seen at higher dose (100 mg/kg) in the rotarod studies of KPP-III-96B **(11)** and KPP-IV-09 **(12)**, when administered orally (**Figure 3.8**) in Dr. Arnold's group, UWM. However, the binding energy of **11** (-9.3 kcal/mol) is closer to the binding energy of non-sedating HZ-166 (**6**), so a closer look at the halogen bond of KPP-III-09 (**12**) and KPP-III-96B (**11**) is required here in terms of bond angles. The halogen bond angles of the bromo group of KPP-IV-09 (**12**) and chloro group of the alprazolam (**2**) bear a closer examination since the -9.5 kcal/mol is close to diazepam (-9.9 kcal/mol).

2.5.4. Molecular docking studies of KPP-IV-09 (12).

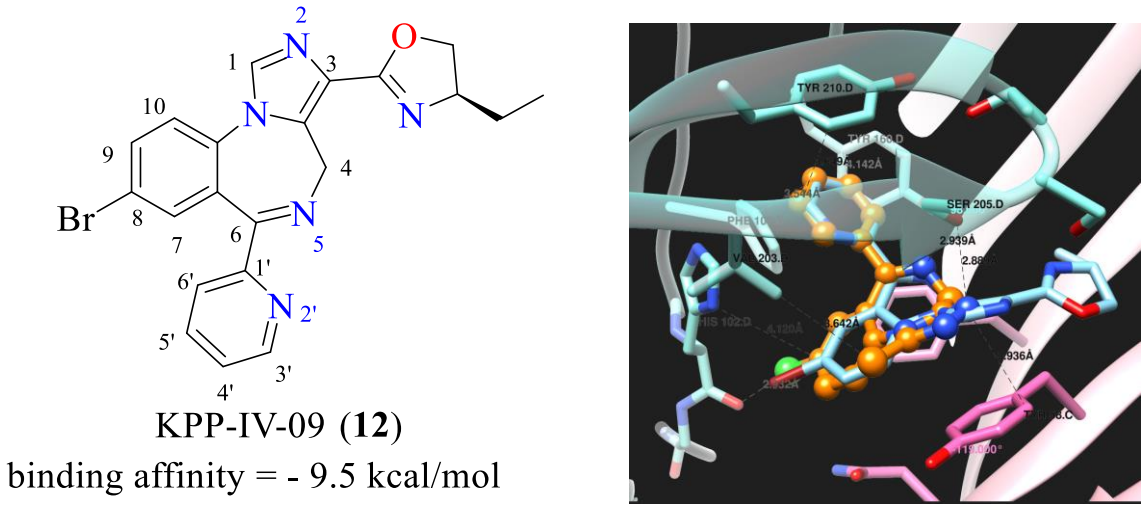


Figure 3.14. The structure of KPP-IV-09 [12, (left)]. Overlay of KPP-IV-09 (12) and alprazolam in the complex with the α1β3γ2 interface of GABA(A) receptor 6HUO at the α+γ- interface of the BDZ binding site (right). Binding energy: -9.5 kcal/mol. Dashed lines indicate π–π, hydrogen bond and halogen bond interactions.

2.5.5. Summary primary and secondary binding data of novel ligands in the Psychoactive Drug Screening Program (PDSP) of NIMH run by Dr. Bryan Roth (UNC) in the 46 receptor and HERG assay.

Primary and secondary binding of all novel ligands and the potential intermediates synthesized were screened in the 46 receptor panal (PDSP, UNC), including the HERG channel, PBR (translocator protein, TPSO), and ion channels by the National Institute of Mental Health Psychoactive Drug Screening Program (NIMH PDSP). All the PDSP data included herein were received generously from NIMH (PDSP), Dr. Bryan Roth and Estela Lopez). Cloned and expressed receptors were executed in HEK-293 cells in this screening. The protocol used in this

screening was, according to the published protocol [see details in (Roth, B.L., 2018. ASSAY PROTOCOL BOOK - Version III [WWW Document]. National Institute of Mental Health Psychoactive Drug Screening Program (NIMH PDSP), URL: University of North Carolina at Chapel Hill (unc.edu)]. Generally, investigational compounds were screened at a single concentration of 10 µM in quadruplicate in 96-well plates. The compounds, which exhibited, at-least 50% inhibition at 10 µM concentration in the primary screening were tagged for secondary radioligand binding assays. The goal of the secondary radioligand binding was to identify the equilibrium binding affinity at specific targets. In the absence or presence of 10 µM of the appropriate reference compound, the total binding (ref compound 3H]-flunitrazepam) and nonspecific binding (reference compound: DZP) affinities were determined, respectively. The summary of primary and secondary binding is listed in **Table 3.5**. The details of PDSP binding results of all analogs and potential intermediates are included in the **Appendix Part II** herein. All ligands exhibited >90% binding (mean%) with the benzodiazepine binding site assessed by inhibition of [3H]-flunitrazepam binding in rat brain homogenates, except KPP-IV-35 (**16**), ZK-III-51 (**13**), ZK-III-56 (**14**), and ZK-III-58 (**15**) ligands which exhibited slightly reduced primary mean % binding (81.5, 87.5, 87.7, 86.3 respectively) compared to other analogs discussed herein [35]. None of the investigational ligands exhibited any affinity at the HERG channel (human ether-a-go-go related gene) receptors, as desired. The advanced compound KPP-III-34 (**9**) also showed weak agonist activity against the KOR receptor (Kappa opioid receptor), with 90.6% primary mean % binding (assessed by inhibition of [3H]-U69593 binding) and a Ki 380 (nM), which was confirmed by a functional group assay. The oxazole, KPP-III-34 (**9**) was 5.9 times more selective for the BZD receptor, as compared to the KOR receptor. The compound **9** also showed weaker affinity towards 5-HT1A receptor (serotonin 1A receptor: assessed by inhibition

of [3H]-WAY100635 binding) with 50.2 % primary mean inhibition and 38.7 times less selectivity in the secondary assay, as compared to the desired receptor BZD binding. Moreover, KPP-III-34 (**9**) showed 12.5 times less selective binding affinity at the peripheral binding receptor, PBR (assessed by inhibition of [3H]-PK11195 in rat brain homogenates) receptor, as compared to the BZD receptor as listed in **Table 3.5**. This is the translocator receptor protein (TPSO), which is involved in numerous functions including steroid biosynthesis and cell proliferation thus, binding at the PBR receptor is not preferred. From the primary and the secondary functional binding assays, it is obvious that KPP-III-34 (**9**) binds strongly with the rat brain benzodiazepine receptor as desired with weaker affinity with some of the other receptors out of the 46 receptors, ion channels and transporters. In secondary functional assay, KPP-III-34 (**9**) exhibited weak agonist activity in the KOR receptor (Ki 380 nM). Ethynyl oxazole KPP-III-51 (**10**) exhibited very similar binding affinity as its bromo analog, KPP-III-34 (**9**) with reduced affinity towards the KOR receptor (**Table 3.5**). Among these analogs, the chiral (*R*) oxazoline KPP-IV-09 (**12**) showed the highest affinity towards the desired benzodiazepine receptor with 97.6% mean primary binding and with a Ki 25 (nM) in the secondary binding assay. The (*S*) enantiomer of KPP-IV-09 (**12**), 8-bromo ethyl oxazoline KPP-III-96B (**11**) was more selective (8.8 times) towards the BZD receptor, as compared to its ethynyl analog KPP-IV-09 (**12**).

Table 3.5. Summary of primary and secondary binding data of analogs synthesized.

Compound	Receptor	Primary (mean % inhibition)	Secondary (K_i in nM)	Fold Selectivity
KPP-III-34 (**9**)	BZD	92.2	47.4	NA
	5-HT_{1A}	50.2	1835	38.7
	KOR	90.6	380	5.9
	PBR	63.9	591	12.5
KPP-III-51 (**10**)	BZD	92.0	182	NA
	5-HT_{1A}	51.5	2108	11.6
	KOR	65.6	1292	7.1
	PBR	74.3	1263	6.9
KPP-III-96B (**11**)	BZD	94.5	221.7	N/A
	5-HT_{1A}	65.0	1365.8	6.2
	KOR	80.9	238.3	1.0
	PBR	64.1	1728.6	7.8
KPP-IV-09 (**12**)	BZD	97.6	25.0	N/A
	KOR	74.0	462.9	18.5
	PBR	52.9	2014.6	80.5
KPP-IV-35 (**16**)	BZD	81.5	807.9	N/A
	NET	59.1	>10,000	>12.4
	PBR	68.1	2506.7	3.1
	KOR	51.2	1994.3	2.5
ZK-III-51 (**13**)	5-HT_{1A}	51.9	3806.2	5.7
	KOR	67 .2	1393.5	2.1
	BZD	87.5	669.3	N/A
ZK-III-56 (**14**)	BZR	87.7	581.0	N/A
	KOR	68.3	1751.5	2.9

ZK-III-58 (**15**)	BZD	86.3	394.6	N/A
	KOR	83.1	2134.1	5.4
	V	60.2	>10,000	>25.3

BZD: Benzodiazepine binding site assessed by inhibition of [^{3}H]-flunitrazepam binding in rat brain homogenates. The remainder of the PDSP data is in Appendix Part II.
5-HT$_{1A}$: Serotonin 1A receptor was assessed by inhibition of [^{3}H]-WAY100635 binding
KOR: Kappa opioid receptor was assessed by inhibition of [^{3}H]-U69593 binding
PBR: Peripheral benzodiazepine receptor site was assessed by inhibition of [^{3}H]-PK11195 in rat brain homogenates; NET: Norepinephrine transporter receptor,
NA: Not applicable.

2.6. Screening of the novel ligands for antiepileptic activity

2.6.1. Effects of KPP-III-34 (9) and KPP-III-51 (10) in the pentylenetetrazol (PTZ) seizure model by Dr. Witkin, and Dr. Ping (Indiana University School of Medicine).

The oxazoles KPP-III-34 (**9**) and KPP-III-51 (**10**) were screened in the pentylenetetrazol seizure model by Dr. Jeffrey Witkin and coworkers (Indiana University School of Medicine, IN). Both oxazoles were found to be active against PTZ seizures. Clonic and tonic seizures were induced in the mice (total number = 6) by subcutaneous injection of PTZ (75 mg/kg). The pentylenetetrazole (PTZ) was dissolved in 0.9% saline. The positive allosteric modulator (PAM) KPP-III-34 (**9**) significantly delayed both clonus seizures ($F_{2,20}$ = 4.68; P = 0.023) and tonus seizures ($F_{2,20}$ = 9.13; P = 0.002) when administered at the dose of 10 mg/kg orally (**Figure 3.15**). Only the 30 mg/kg dose of KPP-III-34 (**9**) significantly increased seizure latencies (**Figure 3.15**). It's 8-ethynyl 3-oxazole, KPP-III-51 (**10**), also delayed both clonic seizures ($F_{2,20}$ = 14.4; P = 0.0002) and tonic seizures ($F_{2,20}$ = 6.54; P = 0.007) induced by PTZ, as shown in **Figure 3.15**, at the doses of 10 mg/kg and 30 mg/kg. Whereas only 10 mg/kg significantly increased the latency to produce clonus seizures. Both 10 and 30 mg/kg of KPP-III-51 (**10**) significantly increased the

latency for PTZ to induce tonus seizures (**Figure 3.15**). The increases in latency to produce tonus by KPP-III-51 (**10**) were less than those increases produced by its 8-bromo analog (KPP-III-34 (**9**). Thus KPP-III-34 (**9**) was clearly more potent than its 8-ethynyl analog **10** in these models.

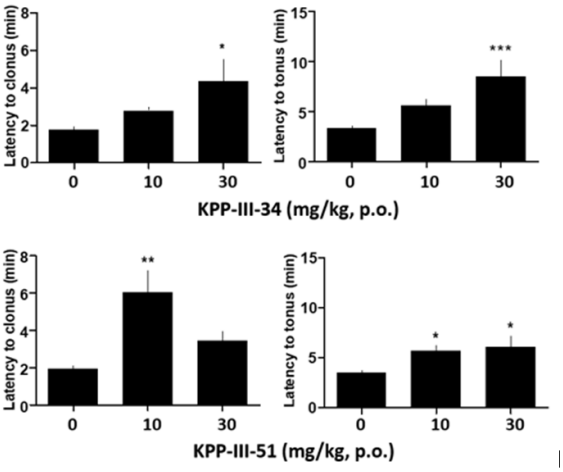


Figure 3.15. Effects of orally administered KPP-III-34 (9), and KPP-III-51 (10) on the latency to produce clonic (left panels) or tonic (right panels) seizures after 75 mg/kg PTZ, s.c. in male, C57BL/6N mice. *, **, *** P <0.05, 0.01, and 0.001 compared to respective vehicle control value. N=6-9 mice per group. P.O. oral gavage in carboxymethyl cellulose.

2.6.2. Protection against lethality by oral administration of KPP-III-34 (9) and KPP-III-51 (10) against PTZ (s.c) (75 mg/kg) induced seizures in mice (data source: Dr. Jeffrey Witkin and coworker, Indiana University School of Medicine).

In the PTZ induced seizure model, all mice were protected against lethality (total 6) by oral administration of KPP-III-34 **(9)** at the lower dose of 10 mg/kg (**Table 3.6**) whereas, 4 mice were protected at the increased dose (30 mg/kg). KPP-III-51 **(10)** protected 5 animals out of 6 at the dose of 10 mg/kg and 2 mice were protected at the elevated dose of 30 mg/kg (with 31 min latency to death), as compared to the vehicle (1% carboxymethylcellulose) where only 3 mice were reported out of 15 (with 32 ± 11.6 min of latency to death). From the PTZ model and lethality observations in mice, it is clear that both compounds were found to have oral antiepileptic activity in mice and KPP-III-34 **(9)** was the more potent oxazole when compared to its ethynyl analog, KPP-III-51 **(10)**.

Table 3.6. Protection against lethality induced by 75 mg/kg PTZ (s.c.) after oral administration (60 min prior) of test compounds in male, C57BL/6N mice.

Compounds	**Lethality/ Number Tested**	**Latency to death (min)**
Vehicle	12/15	32.5 ± 11.6
KPP-III-34 **(9)** (10 mg/kg)	0/6*	NA
KPP-III-34 **(9)** (30 mg/kg)	2/6	30 ± 14.1
KPP-III-51 **(10)** (10 mg/kg)	1/6*	31.1
KPP-III-51 **(10)** (30 mg/kg)	4/6	36.5 ± 10.7

Shown are the number of mice that died/number of mice tested. *P < 0.05.

NA: Not applicable.

2.6.3. Effects of KPP-III-96B (11), KPP-IV-09 (12), and KPP-IV-35 (16) in the pentylenetetrazol (PTZ) seizure model in mice via oral administration (Dr. Jeffrey Witkin and coworkers, Indiana University).

The oxazolines: KPP-III-96B (**11**), KPP-IV-09 (**12**), ZK-III-51 (**13**), ZK-III-56 (**14**), KPP-IV-35 (**16**), and oxazole **15** were also investigated in the pentylenetetrazol (PTZ) seizure model in mice via oral administration at 10 mg/kg doses. Both enantiomers: (*S*) KPP-III-96B (**11**) and (*R*) KPP-IV-09 (**12**) as well as ZK-III-58 oxazole (**15**) significantly delayed the clonic seizures (**Figure 3.16**); however, the effect on latency towards tonic seizures was not very significant. Compounds **11** and **12** delayed the latency to death, whereas no death was reported with compounds **13**, **14**, and **15** (**Table 3.7**). Moreover, oxazolines **13** and **14** significantly delayed the clonic and tonic seizure as shown in **Figure 3.16**. When the 8-bromo oxazoline **11**, was converted into the 8-ethynyl oxazoline **16**, the anti-seizure activity improved. KPP-IV-35 (**16**) significantly increased the latency to produce both clonic seizure incidence and generalized seizure incidence (**Figure 3.17**). The ethyl substituted chiral oxazolines **13** and **14** delayed both clonic and tonic seizures (**Figure 3.16**). For lethality test of this compound, there were 2/4 mice who died with PTZ alone (vehicle group) but 0/11 died in the KPP-IV-35 (**16**) treated group. Thus, this effect showed a trend for significance and using additional historic vehicle controls, the effect of oxazoline KPP-III-35 (**16**) on decreased lethality is highly significant (**Table 3.8**).

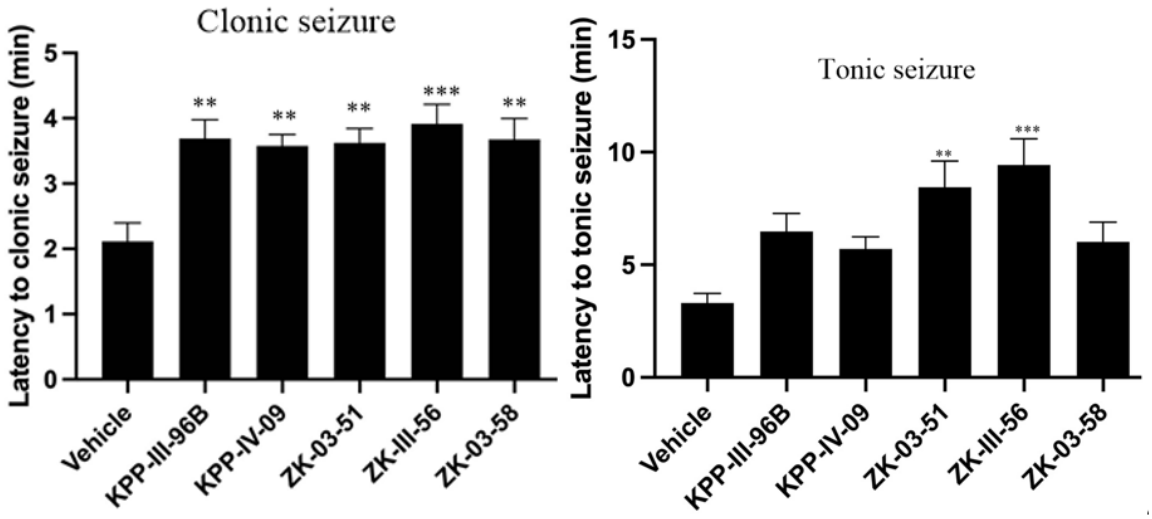
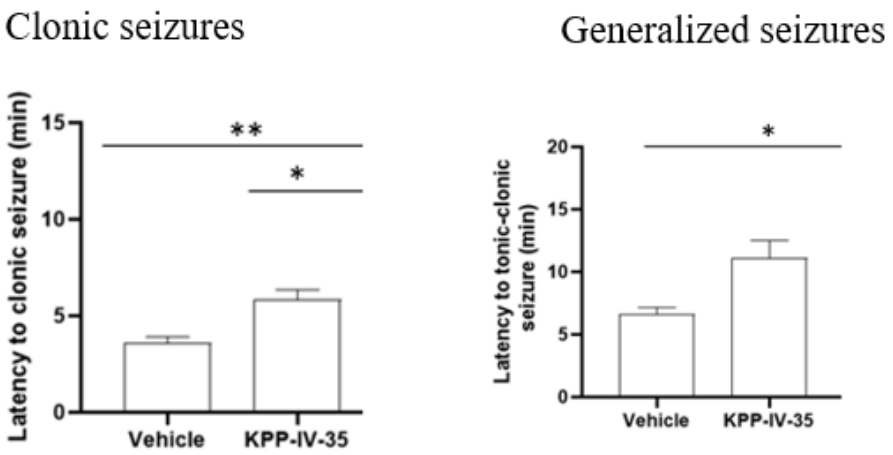


Figure 3.16. Effects of orally administered KPP-III-96B (11), KPP-IV-09 (12), ZK-III-51 (13), ZK-III-56 (14), and ZK-III-58 (15) on the latency to produce clonic (left panels) or tonic (right panels) seizures after 75 mg/kg PTZ, s.c. in male, C57BL/6N mice at 10 mg/kg dose. Confidential data

Table 3.7. Lethality test of KPP-III-96B (11), KPP-IV-09 (12), ZK-III-51 (13), ZK-III-56 (14), and ZK-III-58 (15) in clonic/tonic PTZ inducted seizure model.

Compounds	**Lethality/ Number Tested**	**Latency to death (min)**
Vehicle	1/6 (16.7%)	26
KPP-III-96B **(11)**	4/6 (66.7%)	29.8 ± 10.9
KPP-IV-09 **(12)**	2/6 (33.3%)	36.0 ± 7.1
ZK-III-51 (**13**)	0/6 (0%)	-
ZK-III-56 (**14**)	0/6 (0%)	-
ZK-III-58 (**15**)	0/6 (0%)	-

Administration: P.O. Dose: 10 mg/Kg.



***, **, *p* < 0.05, 0.01, One-way ANOVA**

followed by Tukey's multiple comparisons test

Figure 3.17. Effects of orally administered KPP-IV-35 (16) on the latency to produce clonic (left panels) and generalized seizures (right panels) after 75 mg/kg PTZ, s.c. in male, C57BL/6N mice. Confidential and unpublished data.

Table 3.8. Lethality test of KPP-IV-35 (16) in clonic seizure and gereralized seizure model.

Group	**Generalized seizure (N/F)**	**Latency to death (min)**
Vehicle	0/10	19.5 (2/4, 50%)
KPP-IV-35 **(16)**	6/11	No death reported

***p* < 0.0001, two-sided, statistically significant (*p* < 0.05).**

N= total number of mice protected from seizures. F= total number of mice tested.

Confidential data.

2.6.4. Effects of KPP-III-34 (9) in the 6Hz seizure model, MES seizure model, and on motor effects (rotarod studies) in CF1 mice (i.p.).

Previous test results including the PTZ, rotarod, cytotoxicity and PDSP studies encouraged the further evaluation of KPP-III-34 **(9**) and KPP-III-51 (**10**) against seizures. These compounds were sent to the epilepsy therapy and screening program (ETSP, NINDS). In the identification stage of the NINDS drug development, these test compounds were first investigated against two acute seizure models: the 6 Hz seizure model and the maximal electrode seizure model, which was followed also by the rotarod studies. The objective of the 6 Hz seizure model screening is to test if the investigational compounds can prevent psychomotor seizures caused by a low-frequency (6 Hz) stimulus delivered through corneal electrodes (44 mA current 2 times the CC97) for a 3 sec time duration. If animals do not show seizure symptoms such as initial momentary stun followed by jaw clonus, forelimb clonus, twitching of the vibrissae and Straub tail (last for at least 1 second) then they were deemed to be protected. Effects of KPP-III-34 (**9**) were studied in mice using this 6Hz (44mA) electrical stimulation to induce seizures. A second experiment was conducted with doses of 50-300 mg/kg (N=8, total number of mice) given 1 h prior to 6Hz stimulation. The ED_{50} for blocking seizures for KPP-III-34 (**9**) was 115.5 mg/kg with 95% confidence limits of 62.0 -177 mg/kg. In contrast, the ED_{50} for rotarod impairment was calculated to be > 300 mg/kg with the mice affected only at 300 mg/kg (2 out of 8), as shown in **Table 3.9**. Both compounds were also tested in the maximal electroshock seizure model where seizures were induced by a high frequency (50 mA) electroshock in mice given for 0.2 sec. The MES test identifies if the ligands are able to block the seizure spread in the brain in the stage of maximally active neuronal circuits. Both compounds were screened in 4 male CF-1 mice with the default doses of 30, 100, and 300 mg/kg (IP) at 0.5 and 2 h time points after

administration of the investigational compounds. KPP-III-34 (**9**) was also active in the MES seizure model as it protected 3 (out of 4) animals at the doses of 300 mg/kg at 2 hours. Both in the 6 Hz and MES models dose dependent activity was observed for KPP-III-34 (**9**). The KPP-III-51 (**10**), on the other hand, didn't show activity in both the 6 Hz and MES seizure models. In the rotarod studies, KPP-III-51 (**10**) was safer up to 100 mg/kg dose whereas, only 3 animals (out of 8) were impaired at higher dose (300 mg/kg) after 2 h (**Table 3.9**).

Table 3.9. Effects of KPP-III-34 (9) and KPP-III-51 (10) in two acute seizure provocation models (6Hz and MES) and on rotarod performance when administered i.p. in CF1 mice.

Compounds	**Test**	**Dose**	**N/F at 0.5 h**	**N/F at 2.0 h**
KPP-III-34 (**9**)	6Hz	30	0/4	0/4
		100	3/4*	0/4
		300	3/4*	2/4
	MES	30	0/4	0/4
		100	2/4	0/4*
		300	2/4	3/4*
	Rotorod	30	0/8	0/8
		100	2/8	0/8
		300	8/8*	2/8
KPP-III-51 (**10**)	6Hz	30	0/4	0/4
		100	0/4	0/4
		300	0/4	2/4
	MES	30	0/4	0/4
		100	0/4	0/4&
		300	0/4	0/4
	Rotarod	30	0/8	0/8

		100	2/8	0/8
		300	8/8*#	3/8

Historical controls were employed, where under vehicle conditions there was neither any protection from seizures nor impairment of rotarod performances (C, Metcalf, University of Utah, personal communication).* P < 0.05: &Death associated with tonic seizure; #Unable to grasp rotarod. CF1 mice were used. For the 6 Hz and MES, N/F = number of mice protected/number of mice tested. For rotarod, N/F = number of mice with toxicity/ number of mice tested.

On analysis of the various seizure models including PTZ (discussed earlier), 6 Hz, and MES, KPP-III-34 **(9)** was found to be more active as an anticonvulsant with a better safety profile, therefore, it was chosen for the advancement, whereas KPP-III-51 **(10)** was not as good as KPP-III-34 **(9)** as a drug candidate in several assays.

2.6.5. KPP-III-34 (9) in the PTZ (or Metrazol) seizure model in rats (data source: ETSP, NINDS)

The KPP-III-34 (**9**) was selected for the further study by NINDS based on the previous findings in the anticonvulsant screening program. For the PTZ model in rats (ETSP, NINDS), the investigational compound **9** was administered orally at different doses (5, 10, and 20 mg/kg) 0.5 h prior to PTZ infusions and observations were made at the time points of 0.25, 0.5, 1, 2, and 4 hours (**Table 3.10**). In this study, rats did not show any motor impairment nor deaths effected by KPP-III-34 (**9**) administration. Pentylenetetrazol-induced convulsions were blocked, and the activity was time and dose-dependent (**Table 3.10** and **Table 3.11**) with an ED_{50} of 15.5 mg/kg with 95% confidence limits (8.75-25.0). This is in contrast to the data in mice, where they have a more active metabolism which results in side effects, it is believed.

Table 3.10. The time course of the anticonvulsant effects of orally administered KPP-III-34 (9) in the PTZ-induced convulsions in rats.

Compound	Dose (mg/kg)	0.25 h	0.5 h	1 h	2 h	4 h
KPP-III-34 **(9)**	5	1/4	1/4	0/4	1/4	0/4
	20	3/4*	4/4*	3/4*	3/4*	2/4
	50	6/8*	8/8*	6/8*	7/8*	7/8*

Male, Sprague-Dawley rats were tested for seizure induction by PTZ at different times after dosing of KPP-III-34 (9). ED_{50}=15.5 mg/kg. Route of administration: P.O. Vehicle: carboxy methyl cellulose. Data are shown as number of rats protected/number of rats tested. * p < 0.05 compared to vehicle control.

Table 3.11. Dose-response of orally administered KPP-III-34 (9) in the PTZ-induced convulsions in rats.

Dose (mg/kg)	Number of animals protected /Number of animals tested	Number of animals showing adverse effects/number of animals tested
5	1/4	0/8
10	1/8	0/8
20	5/8	0/8
50	8/8*	0/8

Male, Sprague-Dawley rats were tested at 0.5 h post dosing of KPP-III-34 (9).
Data are shown as number of rats protected/number of rats tested.
*** p < 0.05 compared to vehicle control. Vehicle: carboxy methyl cellulose.**

2.6.6. KPP-III-34 (9) an oral dose anticonvulsant agent in the corneal-kindled mice (data source: ETSP, NINDS).

The corneal seizure model bears a resemblance to the human focal seizures from the pharmacological profile point of view. In this test, the test compound **9** was administered orally to the kindled mice at various doses and time points, as shown in **Table 3.12**. Male mice (C57BL/6 or CF-1) were first kindled electronically using corneal electrodes to the criterion of five consecutive stage 5 seizures (severe seizure). Mice after seizure kindling by daily electrical corneal stimulation, were then tested with compound **9** (**Table 3.12.**) and the seizure severity in animals was measured at the scale of 0-5. Animals exhibiting less than a seizure score of 3 were regarded as protected.

Table 3.12. Effects of KPP-III-34 (9) when orally administered on corneal kindling in male, CF1 mice.

Dose (mg/kg)	Number Protected /Number Tested	Individual Seizure Scores	Mean Seizure Score (S.E.M)
3.5	1/8	0,4,5,4,4,5,5,4	3.88 (0.58)
15	6/8*	0,0,0,4,0,5,0,0	1.12 (0.74)**
30	5/8	0,0,3,0,4,4,0,0	1.38 (0.68)*
60	6/8*	0,0,0,0,0,2,0,3	0.62 (0.42)***
120	8/8*	0,0,0,0,0,0,0,0	0.00 (0.00)***

A mouse was considered protected from seizures when it did not exhibit any seizure signs (see methods for details); such mice were given a score of 0 for their seizure score.
***P < 0.05; **P < 0.01; ***P < 0.001 compared to effects at 3.5 mg/kg.**

Oral doses of KPP-III-34 **(9)** were dose-dependent and reduced the seizure incidences in mice ($F_{4,39} = 7.17$, $p < 0.001$) with an ED_{50} of 12.7 mg/kg (95% confidence limits: 4.35-21.9). It is obvious from **Table 3.12** that KPP-III-34 **(9)** was significantly active against corneal kindled

seizures in mice when given orally. Moreover, KPP-III-34 **(9)** was fully efficacious in corneal kindled seizure (CKM) model in female mice with ED_{50} of 14.3 mg/kg (95% confidence limits: 8.04-21.13) without any adverse effects as shown in **Table 3.13**. It is obvious from **Table 3.12** and **Table 3.13** that oxazole **9** is active in both male and female mice in chronic seizure model (CKM). The ED_{50} values were identical (**Table 3.12** and **Table 3.13**) within experimental error. The oxazole **9** did not exhibited efficacy difference in both sexes. Thus, KPP-III-34 **(9)**, presumably, will be active against human focal seizures (without sex difference) if previous studies hold true.

Table 3.13. Effects of KPP-III-34 (9) when orally administered on corneal kindling in female mice.

ED_{50}					
Test	**Time (hrs)**	**ED_{50}**	**95% confidence interval**	**Slope**	**Std. error**
CKM	1	14.3	8.04-21.13	3.58	1.02
ED_{50} response					
Test	**Time**	**Dose (mg/kg)**	**Deaths**	**N/F**	**Comment**
CKM	1	5		0/8	
CKM	1	15		6/8	
CKM	1	30		6/8	
CKM	1	60		8/8	
CKM	1	120		8/8	

'N' indicates number of animals protected and 'F' indicates total number of animals tested. C indicates comment code; no comment indicates no toxicity or side effects were observed in any mice. Vehicle: 0.5% methylcellulose.

2.6.7. Time course of untoward signs in a modified rat Irwin test induced by orally administered KPP-III-34 (9) in rats. (Data courtesy: ETSP, NINDS)

As discussed above, the compound KPP-III-34 **(9)** was non-sedating, non-toxic, and active against various seizure models up to 300 mg/kg. A modified Irwin test was carried out (ETSP, NINDS) to evaluate further if high doses (up to 500 mg/kg) can cause any adverse effects in rats. In this experiment, KPP-III-34 **(9)** was administered orally at various doses (50, 100, 300, 500 mg/kg) to rats (total rats=8) and they were observed carefully at different time points. Two independent observers evaluated them for the impaired autonomic (e.g., porphyrin, salivation), sensorimotor (e.g., hyperesthesia, loss of righting reflex), neuromuscular (e.g., tremors, ataxia), and behavioral (e.g., grooming, vocalizations) functions. The test results in the modified Irwin test are listed in **Table 3.14**. Importantly, in this test, the advance compound KPP-III-34 **(9)** did not cause any untoward effects at any of the time points evaluated (0.25, 0.5, 1, 2, 4, and 8 h). Also, no adverse events or lethality were observed in the rats in a functional test battery that observed autonomic, neuromuscular, sensorimotor, and behavioral functions. Moreover, no observed behavioral problems or signs were seen at 24 h post dosing of KPP-III-34 **(9)** (data not shown). Thus, from this modified Irwin test, it is clear that KPP-III-34 **(9)** is not only active against many epilepsy models (both in mice and rats administered either via oral gavage or IP) but also has an impressive safety profile up to a very high dose of 500 mg/kg in rats.

Table 3.14. Time course of untoward signs of KPP-III-34 (9) in a modified rat Irwin test (p.o.) in rats.

KPP-III-34 (9)					
Dose (mg/kg)	**N/F at 0.25 h**	**N/F at 0.5 h**	**N/F at 1 h**	**N/F at 2 h**	**N/F at 4 h**
50	0/8	0/8	0/8	0/8	0/8
100	0/8	0/8	0/8	0/8	0/8
300	0/8	0/8	0/8	0/8	0/8
500	0/2	0/2	0/2	0/2	0/2

N/F: Numbers of animals showing adverse effects/numbers of animals tested.

2.6.8. Oral anticonvulsant activity of KPP-III-34 (9) in a therapy resistant- seizure model (Lamotrigine-resistant-amygdala seizure model, data source: ETSP, NINDS)

After completion of screening in the identification stage (ETSP, NINDS) with impressive anticonvulsant activity and a very good safety profile, further advancement of the test compound **9** at ETSP (NINDS) was continued in a differentiation phase. The test drug **9** was tested in a Lamotrigine (LTG)-resistant seizure model where seizures were induced by electrical stimulation of the amygdala. Lamotrigine is a marketed drug to treat seizures and bipolar disorder. To investigate KPP-III-34 **(9)**, if active in the therapy-resistant seizure model and secondarily generalized seizure models, adult male Sprague-Dawley CD rats (275-300 g) were given 5 mg/kg of LTG (IP) once a week after kindling (stage 4-5 seizures) by embedding a bipolar stimulating electrode under stereotaxic guidance and anesthesia in the right amygdala. The test compound KPP-III-34 **(9)** was administered orally, and observation of seizure score was made. Animals were considered to be protected if the seizure score is less than 3 in the Racine scale.

Table 3.15. Test result of 9 (p.o.) against Lamotrigine-resistant-amygdala seizure model.

Dose (mg/kg)	Time (h)	Seizure score +/- SEM	Duration (sec) +/- S.D.	Number of animals protected/number of animals tested
Control	0	4.88 +/- 0.13	140 +/-45.71	0/8
50	0.5	5 +/- 0	144.9 +/- 42.41	0/8
Control	0	4.88 +/- 0.13	135 +/- 45.23	0/8
100	0.5	2.5 +/- 0.8	120.6 +/- 41.39	4/8
Control	0	4.86 +/- 0.14	76.14 +/- 23.9	0/8
200	0.5	2.43 +/- 0.72	75.86+/- 41.52	4/7

***Indicates data is significantly different from control.**

As shown in **Table 3.15**, the test compound KPP-III-34 **(9)** protected 4 animals (out of 8) at the dose of 100 mg/kg and 4 animals (out of 7) at the dose of 200 mg/kg compared to the control (0 protected out of 8). Also, the seizure score decreased (.5 +/- 0.8) compared to the control (4.88 +/- 0.13). It was found that the test drug KPP-III-34 **(9)** was an active anticonvulsant also in the Lamotrigine-resistant amygdala seizure model.

2.6.9. Activity of KPP-III-34 (9) in the intrahippocampal kainate (IHK) model of mesial temporal lobe (MTLE) epilepsy (data source: ETSP, NINDS)

The status epilepticus condition caused by temporal lobe epilepsy (TLE) is related with damages in the brain such as hippocampal sclerosis, and disruption of the vascular component of the blood brain barrier (BBB) [36]. The tissue recovery caused by such damages is pharmaco-resistant epilepsy and in some patients, requires surgery, which is very costly and dangerous [36]. In the differentiation phase of drug testing (ETSP, NINDS workflow), the test compound KPP-III-34 **(9)** was screened to determine if it is active against non-convulsive status epilepticus (SE) which lasts for a longer period of time (several hours). This test (mesial temporal lobe epilepsy model) was carried out at ETSP (NINDS). A total of 7 mice received kainic acid (1 nM kainic acid solution in 0.9% sterile saline**)** into the dorsal hippocampus via injection, which induced non-convulsive status epilepticus (SE). This was followed by epileptogenesis with brusts, discharges, spikes and resulted in electrographic hippocampal paroxysmal discharges (HPDs) associated with behavioral effects as well as impaired mental status (see details of the test protocol in the **Method** section). Bipolar electrodes were implanted in mice to record such discharges. KPP-III-34 **(9)** was administered orally at the dose of 115 mg/kg and mice were evaluated after 60 min. The reference period was compared with the effect of the test compound. The number of

hippocampal paroxysmal discharges (HPDs), as well as any behavioral effects were observed. Importantly, in the mesial temporal lobe epilepsy model, KPP-III-34 **(9)** significantly reduced the number of the baseline level of spontaneous recurrent hippocampal paroxysmal discharges (t_6 = 2.74, p = 0.034) (**Table 3.16** and **Figure 3.18**). HPDs counts were 49.54 % ± 16.01 of baseline levels in mice that were administered the investigational compound. Thus, KPP-III-34 **(9)** was significantly active against non-convulsive status epilepticus (SE).

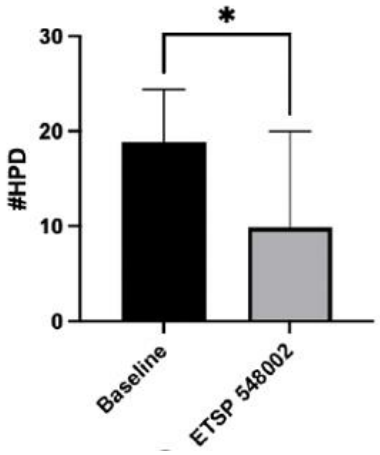


Figure 3.18. KPP-III-34 (9) camparison with the baseline for the number of hippocampal paroxysmal discharges. ETSP 548002 is KPP-III-34 (9).
***P = 0.0336 (paired-*t*-test).**

Table 3.16. Test results of KPP-III-34 (9) in the IHK model of MTLE epilepsy model in mice.

Recording period	**Number of HPDs observed Mouse number**							**Mean HPDs ± SEM**	
	1	2	3	4	5	6	7		
Baseline	16	21	11	15	28	19	22	18.86	2.09
Peak time 60 minutes	6	26	4	9	22	2	0	9.86	3.83
Peak effect %	37.5	123.81	36.36	60.0	78.57	10.53	0.00	49.54	16.01
Behavior at peak time	Quiet	Quiet	Quiet	Quiet	Quiet	Quiet	Quiet		

SEM: standard error of mean. Dose: 115 mg/kg.
TPE: time per effect.

2.6.10. Evaluation of intraperitoneal (IP) administration of KPP-III-34 (9) in a tolerability assay in spontaneous recurrent seizing rats (KA-SRS). Data source: ETSP, NINDS.

Prior to the investigation in the chronic KA-SRS model, the test compound KPP-III-34 **(9)** was first evaluated in a 3-day tolerability assay in rats (male Sprague-Dawley rats). Rats after receiving the test drug KPP-III-34 **(9)**, were evaluated at 5 different timepoints (0.25, 0.5, 1.0, 2.0, and 4.0 h) at 3 times a day for 3 days. Animals were observed and evaluated carefully for any overt signs of impaired neurological or muscular functions, ataxia, abnormal gait/stance, sensorimotor and deaths. In this test, as shown in **Table 3.17**, no animals showed any adverse effects and no deaths reported up to 3 days of the testing period after the administration (IP) of KPP-III-34 **(9)**. Thus, the test drug **9** was found to have impressively clean results in the tolerability assay done at ETSP, NINDS (**Table 3.17**). Besides the 3 day tolerability assay, the compound was also tested in the modified functional observational battery (FOB) assay to assess a compound's effect on autonomic, neuromuscular, sensorimotor and behavioral functions on the 3rd day of the tolerability assessment. Performance of the investigational compound in the FOB assay is detailed in (**Table 3.18**). No adverse effects for autonomic, neuromuscular, sensorimotor and behavioral functions were observed and noted for the advanced compound **9** (**Table 3.18**).

Table 3.17. Three-Day Tolerability Assessment for KPP-III-34 (9) in male KA-SRS rats three times a day for 3 days.

	Time points hour	**7 am**	**12:15 pm**
		Numbers of animals showing adverse	**Numbers of animals showing adverse effects/numbers of animals tested.**

Day 1		**effects/numbers of animals tested.**	
	0.25	0/4	0/4
	0.5	0/4	0/4
	1.0	0/4	0/4
	2.0	0/4	0/4
	4.0	0/4	0/4
Day 2	**Time points hour**	**7 am**	**12:15 pm**
		Numbers of animals showing adverse effects/numbers of animals tested.	**Numbers of animals showing adverse effects/numbers of animals tested.**
	0.25	0/4	0/4
	0.5	0/4	0/4
	1.0	0/4	0/4
	2.0	0/4	0/4
	4.0	0/4	0/4
Day 3	**Time points hour**	**7 am**	**12:15 pm**
		Numbers of animals showing adverse effects/numbers of animals tested.	**Numbers of animals showing adverse effects/numbers of animals tested.**
	0.25	0/4	0/4
	0.5	0/4s	0/4
	1.0	0/4	0/4
	2.0	0/4	0/4
	4.0	0/4	0/4

Dose: 50 mg/kg, three times a day (IP). Vehicle: 0.5% carboxy methylcellulose.

Table 3.18. Functional Observational Battery for test compound KPP-III-34 (9) in male KA-SRS rats.

Rat #	6	34	37	41	35 - Blinded Vehicle	11 - Un-Blinded Control
Observations /Comment Codes						
General Comments						

No comments in this table means no adverse effects. Dose: 50 mg/kg, three times a day. Vehicle: 0.5% carboxy methylcellulose.

From the 3-day tolerability test and functional observational battery assay (FOB), it is obvious that the test drug KPP-III-34 (**9**) was found to have clean safety results (no adverse effects) in the rats while administrating it three times a day for 3 days at the dose of 50 mg/kg (IP).

2.6.11. KPP-III-34 (9) in the post-kainic acid spontaneous recurrent seizure (KA-SRS) rat model of mesial temporal lobe epilepsy (data source: ETSP, NINDS).

The potency of a novel but advanced compound in two acute seizure models (6Hz and MES) is discussed above. The KPP-III-34 (**9**) was also investigated in the post-kainic acid status epilepticus-induced recurrent spontaneous chronic seizures, where the chronic seizure was

induced by kainic acids in rats (250-300 g), Sprague-Dawley rats. After that, the rats were treated by administrating 50 mg/kg of the test drug KPP-III-34 (IP) for three times a day for 5 days. The 0.5% methyl cellulose was used as the vehicle. During this time the rats were observed for the seizures. Wilcoxon rank sum was used to detect significant differences between seizure burdens ($p<0.05$ whereas, the Fisher's exact test was used to identify the differences between the seizure freedom ($p<0.05$). The test drug compound **9** was administered three times a day, as discussed above.

Table 3.19. Test drug KPP-III-34 (9) at 50 mg/kg (T.I.D.) in chronic seizing post-Kainate rats (phase I).

Dose	**Freq[a]**	**Seizure Burden**			**Seizure Freedom**		
50	T.I.D.	Baseline	Drug	Vehicle	Baseline	Drug (KPP-III-34)	Vehicle
		9.1 ± 3.1	0.1±0.1	8.4±3.8	1/12	11/12*£	4/12

Data are reported as mean ± s.e. (*) indicates a significant difference between the vehicle and drug, and (£) indicates a significant difference between drug and baseline. [a]Dose frequency: t.i.d. (three times daily).

As shown in **Table 3.19**, KPP-III-34 (**9**) significantly reduced the seizure burden (0.1±0.1), as compared to both vehicle (8.4±3.8) and baseline (9.1 ± 3.1) with the Wilcoxon rank sum, $p<0.05$. Moreover, there was a significant seizure freedom (11 out of 12 rats), as compared to the vehicle (4 out of 12) and the baseline (1 out of 12). The seizure burden was significantly reduced as

compared to vehicle (Wilcoxon rank sum, $p<0.05$). Only a slight weight gain (higher than 5%) was observed in some rats (3 out of 12). Thus, it is obvious that the test drug KPP-III-34 (**9**) was also found significantly active against the chronic seizure model in the rats as no seizure was observed during the treatment.

2.6.12. Selectivity study (electrophysiological recording) of KPP-III-34 (9) and KPP-III-51 (10).

The selectivity study of oxazoles were carried out by Dr. Janet Fisher, following the published procedure [37]. Transiently transfected HEK-293T cells were used to record whole-cell voltage clamp ion flux. In this assay, α1-α6 subunits as indicated were co-transfected with the β1 and γ2L GABA conc. with an EC_{3-5} GABA.

The selectivity data (**Figure 3.19**) shows both oxazoles (KPP-III-51 **(10)** and KPP-III-34 **(9)**) have poor selectivity (efficacy) over the α1, α2, α3, and α5 at 0.1 mM. However, the efficacy increased for α1, α2 at higher concentration (1 mM) in the case of KPP-III-34 **(9)**. In the subtype selectivity studies, (**Figure 3.20**), related to the much earlier work of Gee *et.* al [38], α with the γ2L subunit, the efficacy of both oxazoles against β1 and β3 substituted ion channels did not differ significantly. The poor selectivity of KPP-III-34 **(9)** in this assay for GABAA subtypes, is not congruent with the many seizure models, rotarod studies, and behavioral studies discussed above. It is possible that the efficacy of KPP-III-34 **(9)** in all 4 subunits is below the efficacy threshold at the α1 subtype; one does not see sedation, nor ataxia with either the β1 or β3 subunit.

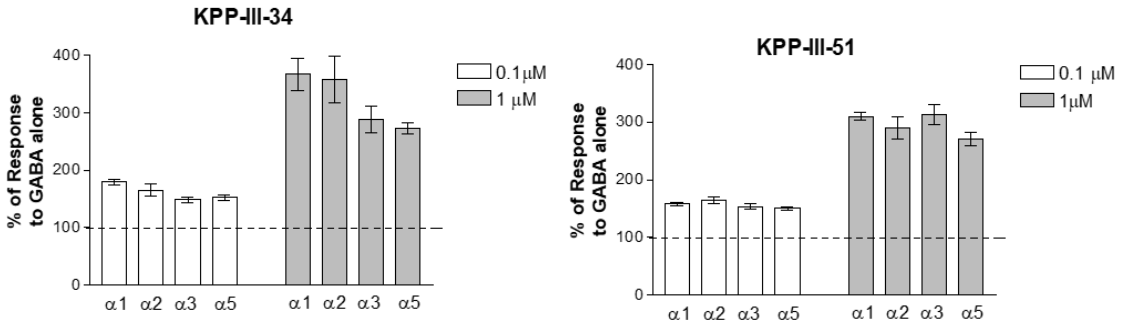


Figure 3.19. Electrophysical recording of KPP-III-34 (9) and KPP-III-51 (10) on GABA (A) $\alpha_1\beta_3\gamma_2$ ion channel. $EC_{3\text{-}5}$ GABA.

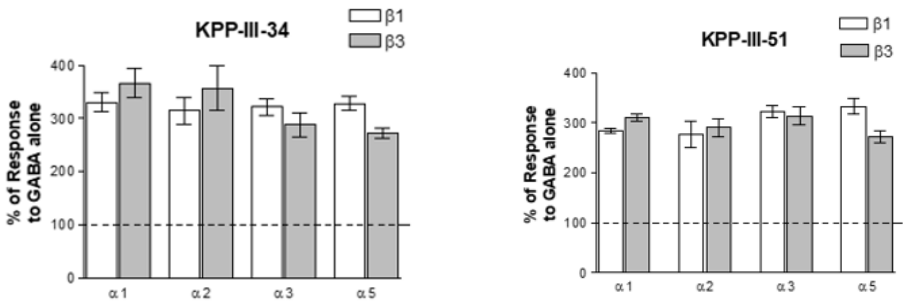


Figure 3.20. Electrophysical recording of KPP-III-34 (9) and KPP-III-51 (10) α with b and γ2L subunits. $EC_{3\text{-}5}$ GABA.

2.6.13 *In-vivo* pharmacokinetic (PK) study of KPP-III-51 (10), KPP-III-34 (9), KPP-III-96B (11), KPP-IV-09 (12), and KPP-IV-35 (16).

The *in-vivo* pharmacokinetic study of the test ligands was conducted by Dr. Savic and coworkers (Serbia) following the published procedure [39] [40]. The neurophamacokinetic studies of the novel investigational compounds was carried out on male Sprague Dawley adult rats (280-330 g) to obtain the pharmacokinetic profiles of the compounds in plasma and brain. Each test

compound was administered orally at the dose of 2.0 mg/kg (concentration of 0.4 mg/mL in 0.25% methyl cellulose solution). This assay was done by the cassette method. The $T_{1/2}$ exhibited the stability of the compounds in plasma. The time-dependent systemic distribution of these ligands is shown in **Figure 3.21, 3.22, 3.23,** and 3.**24**. The pharmakokinetics was also improved, as hypothesized, while designing the compounds by replacing the ester functional group of the earlier lead compound HZ-166 **(6)** with the metabolically more stable oxazoles and oxazolines analogs discussed above. The PK studies of these ligands is summarized in **Table 3.20.**

Table 3.20. Summary of pharmacokinetics study of novel imidazodiazepines.

Compound code	C_{max} (Plasma)	C_{max} (Brain)	C_{max} (Brain/Plasma)	AUC 24h (Plasma)	AUC 24 h (Brain)	AUC 24 h (Brain/Plasma)	T_{max} (Brain, h)	$T_{1/2}$ (Plasma) in h
KPP-III-34 **(9)**	228.2	259.2	1.14	462.18	1014.6	2.20	16.08	4.06
KPP-III-51 **(10)**	39.3	69.6	1.77	96.13	430.25	4.48	10.67	5.71
KPP-III-96B **(11)**	157.64	50.49	0.32	90.94	134.64	1.48	8.75	9.60
KPP-IV-09 **(12)**	553.41	195.18	0.35	365.38	184.93	0.51	0.39	1.22
KPP-IV-35 **(16)**	818.29	305.9	0.37	226.74	1253.45	5.5	0.33	6.65

This work was done by the cassette method by Dr. Savic and coworkers (Serbia).

Among the listed compounds in **Table 3.20**, the most stable compound in plasma was KPP-III-96B **(11)** (*S*-oxazoline) with a half-life of 9.6 h and the least stable compound was its enantiomer (*R*-oxazoline) KPP-IV-09 **(12)**. Compared to other analogs, KPP-III-34 **(9)** took a longer time (T_{max} = 16.08 h) to reach maximum concentration in brain but reached it in plasma quickly (T_{max} =0.39 h). The ligand KPP-IV-35 **(16)** demonstrated the highest brain concentration (C_{max} = 305.9 nM) on comparison to the other ligands. KPP-III-34 **(9)** exhibited the highest exposure (AUC) in plasma (462.18 ng h/mL) and KPP-IV-35 **(16)** exhibited the highest exposure (AUC) in brain

(1253.45 ng h/g). All the compounds were able to cross the BBB with the order of KPP-III-51>KPP-III-34>KPP-IV-35>KPP-IV-09>KPP-III-96B (see **Table 3.20**).

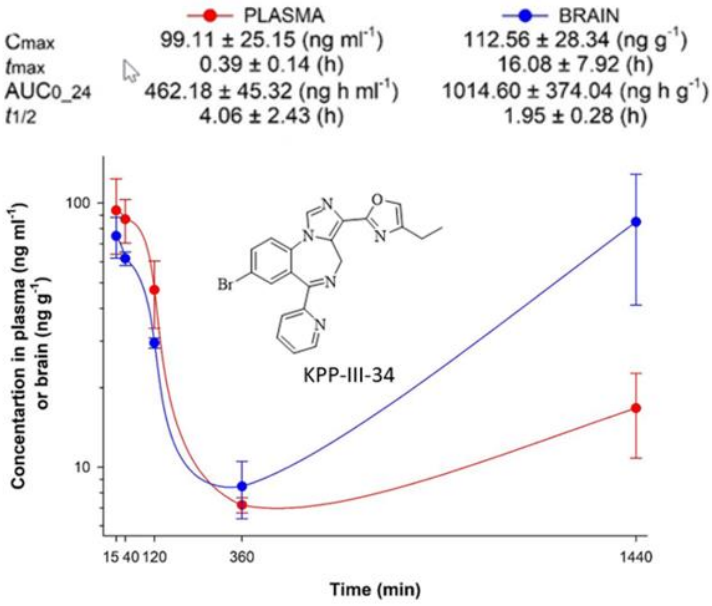


Figure 3.21. The pharmacokinetic data of KPP-III-34 (9) in plasma and brain in male Sprague Dawley rats. The time-dependent systemic distribution of KPP-III-34 (9) was determined at 2 mg/kg (p.o.) via the cassette method by Dr. Savic and coworkers (Serbia).

The pharmakokinetic data of clinically chosen lead imidazepine KRM-II-81 **(7)** was published recently [18]. On comparison of KRM-II-81 **(7)** to the oxazole KPP-III-51 **(10)**, the latter has relatively lower exposure both in terms of AUCs in plasma (systemic exposure) and AUCs in brain (target site exposure). However, KPP-III-34 **(9)** demonstrated brain exposure that is not-inferior (indeed, it is nominally insignificantly higher) to that of KRM-II-81 **(7)**. As the brain tissue is the targeted site of action, KPP-III-34 **(9)** has relatively lower systemic exposure accompanied with an equivalent brain exposure when compared to lead compound KRM-II-81 **(7)**, which makes KPP-III-34 **(9)** a drug candidate with an improved pharmacokinetic profile.

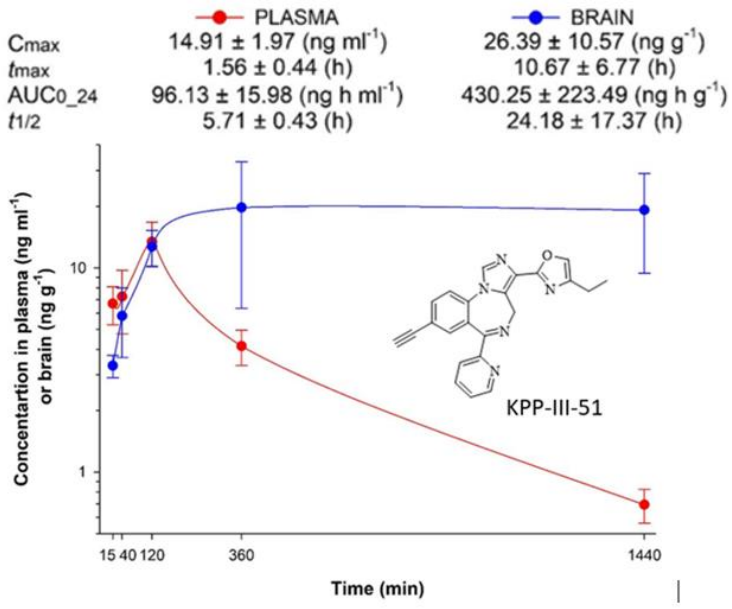


Figure 3.22. The pharmacokinetic data of KPP-III-51 (10) in plasma and brain in male Sprague Dawley rats. The time-dependent systemic distribution of KPP-III-51 (10) was determined at 2 mg/kg (p.o.) via the cassette method by Dr. Savic and coworkers (Serbia).

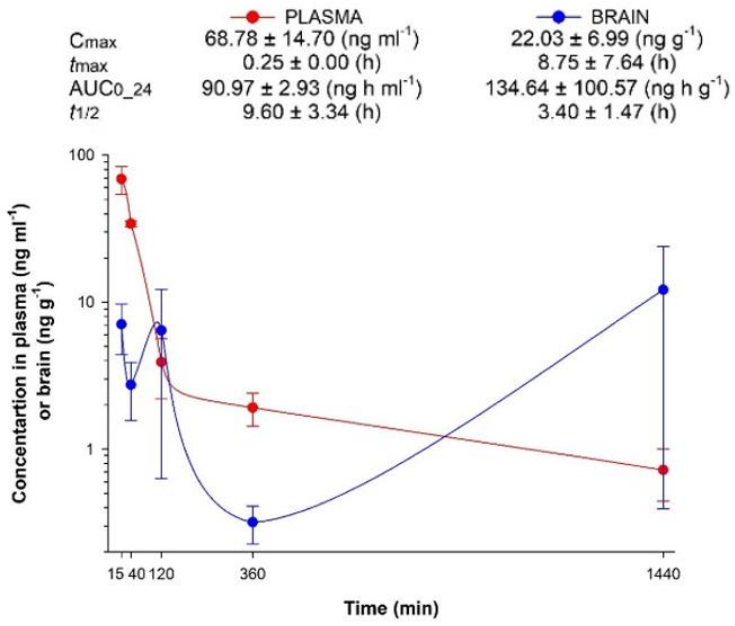


Figure 3.23. The pharmacokinetic data of KPP-III-96B (11) in plasma and brain in male Sprague Dawley rats.The time-dependent systemic distribution of KPP-III-96B (11) was determined at 2 mg/kg (p.o.) via the cassette method by Dr. Savic and coworkers (Serbia).

In the case of KPP-IV-35 **(16)**, the plasma and brain AUCs resulted in higher values of Kp (not shown) as compared to other analogs (oxazoles and oxazolines). It might be possible that the structural changes due to the introduction of the *S*-oriented 4-alkyl oxazoline and the 8-ethynyl substituent into a ring has resulted in their enhanced distribution into the brain (highest AUC among the compounds listed herein), where pharmacodynamic activity is expected (**Figure 3.25** and **Table 3.20**). More studies must be carried out before the reasons for this novel activity of KPP-IV-35 **(16)** is determined.

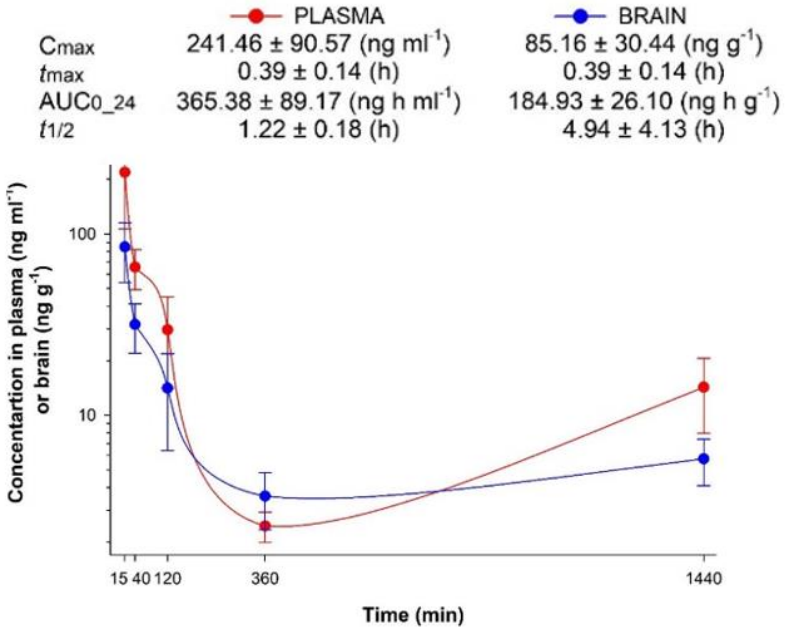


Figure 3.24. The pharmacokinetic data of KPP-IV-09 (12) in plasma and brain in male Sprague Dawley rats.The time-dependent systemic distribution of KPP-IV-09 (12) was determined at 2 mg/kg (p.o.) via the cassette method by Dr. Savic and coworkers (Serbia).

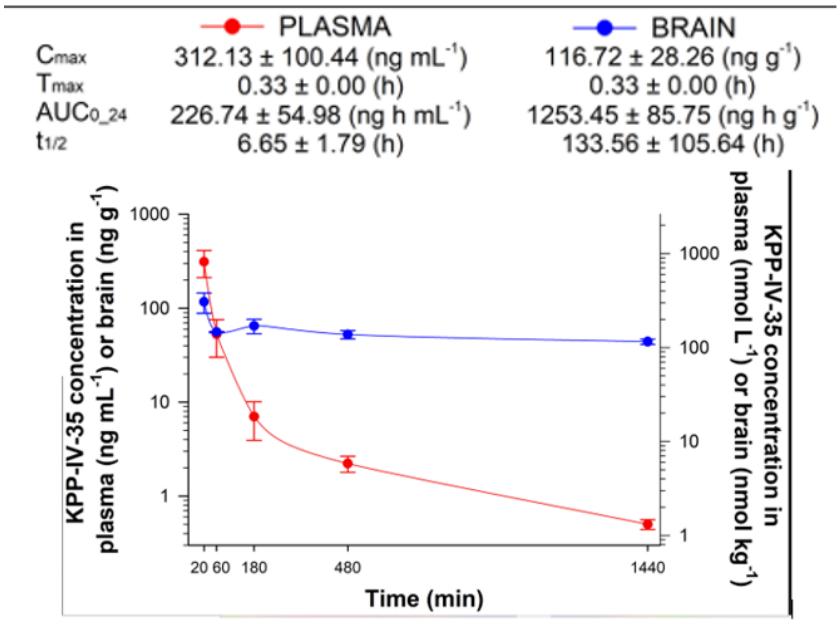


Figure 3.25. The pharmacokinetic data of KPP-IV-35 (16) in plasma and brain in male Sprague Dawley rats.The time-dependent systemic distribution of KPP-IV-09 (12) was determined at 2 mg/kg (p.o.) via the cassette method by Dr. Savic and coworkers (Serbia).

In summary, the enhanced blood brain barrier penetration [C_{max}(Brain/Plasma)] was observed in the case of oxazoles as compared to the oxazoline analogs discussed above. However, the 8-ethynyl (*S*)-oxazoline, KPP-IV-35 **(16)** exhibited impressive target site exposure and the stability both in plasm and brain. The significant activity of KPP-IV-35 **(16)** in pentylenetetrazol induced clonic and generalized seizures is congruent with the pharmacokinetic study discussed herein. **KPP-IV-35 (16) appears to need additional studies.**

3. Discussion and Conclusion.

Studying the protein-ligand docking techniques, as discussed above, the novel oxazoles and oxazoline analogs of KRM-II-81 (**7**) were designed, which followed the execution of their synthesis on the gram scale. The novel analogs were also evaluated in many *in-vitro* and *in-vivo* animal models (via oral or ip in mice and rats) aimed for the treatment of neurological conditions including epilepsy, anxiety, and pain. As mentioned above, the α2/α3 subtype selective lead imidazodiazepine, KRM-II-81 (**7**) is progressing towards the clinic for the treatment of epilepsy, as it exhibited excellent activity in preclinical studies in many seizure models; importantly in the therapy resistant (Lamotrigine) seizures, and Dravet syndrome without adverse effects, tolerance, and addiction. Undoubtedly, it is crucial to synthesize and evaluate novel compounds which could work as back-up compound (s) of the lead [KRM-II-81 (**7**)] if it fails in clinical trials. In order to discover the back-up compound (s) of lead GABAkine KRM-II-81 (**7**), the novel compounds (oxazoles and oxazolines) were designed with subtle modification of the structure of KRM-II-81 (**7**). Besides screening against convulsions, toxicity and motor effects, many behavioral effects of the compounds were also evaluated. These compounds were screened against the panel of 47 receptors (PDSP, NIMH), cytotoxicity against HEK-293 cell lines, rotarod studies in mice/rats at diverse doses (40, 80, 100 or 120 mg/kg doses). In the PDSP assays, most of the compounds, in the primary screen, effectively and selectively bound (>85%) to the targeted rat benzodiazepine receptor site, notably with no HERG receptor binding, as desired. None of the synthesized novel compounds were found to have any cytotoxicity in HEK-291 cell lines. The ethynyl oxazoline KPP-IV-35 (**16**) exhibited significant anticonvulsant activity in PTZ seizure model orally and it was found completely non-toxic in the lethality test done in mice. The ethyl subtituted oxazolines; ZK-III-51 (**13**) and ZK-III-56 (**14**) on further

evaluation exhibited potent anticonvulsant activity on PTZ induced seizure model. These oxazolines **13** and **14** were found to be non-sedating without ataxia, tremor, and loss of rightening response up to 120 mg/kg dose.

Two oxazole bio isosteres of KRM-II-81 (**7**): KPP-III-34 (**9**) and KPP-III-51 (**10**) were found to be non-sedating up to the higher dose [120 mg/kg dose (p.o.)] in mice with no sign of ataxia, tremors, and the loss of righting response. This is significant because in mice KRM-II-81 (**7**) effected significant tremors at 100 mg/kg, whereas KPP-III-24 (**9**) did not even at 120 mg/kg dose. One significant difference is the latter compound bears C-8 bromo substituted while KRM-II-81 bears an ethynyl group. Perhaps the ethynyl group is metabolized to tremorgenic metabolites in mice but not rats in KRM-II-81 (**7**). Moreover, it was non-toxic in rats up to 500 mg/kg. KPP-III-34 (**9**) exhibited excellent oral bioavailability and potent anticonvulsant activity: which delayed both clonus and tonus at 10 mg/kg in the pentylenetetrazol (PTZ) seizure model and protected all animals (6 out of 6) animals. The pharmacokinetic (PK) studies revealed excellent exposure of KPP-III-34 (**9**) at the target site (brain) with C_{max} brain/plasma = 1.14 and AUC brain/plasma = 2.0. In addition, from the PK studies, it is obvious that KPP-III-34 (**9**) was metabolically stable and penetrates the BBB effectively, as desired. KPP-III-34 (**9**) is an active anticonvulsant in both maximal electroshock (MES, 50 mA), and 6Hz (44 mA) psychomotor seizure models (ip) in mice without any adverse effects (including sedation, ataxia, parasympathetic activity, seizures, tremor, and death) up to 300 mg/kg. There was no mortality reported in any animals after 72 h post dosing. Moreover, KPP-III-34 (**9**) was fully efficacious on oral administration in the subcutaneous metrazol (pentylenetetrazole) seizure model (s.c. MET) in mice with an ED_{50} of 31.1 mg. KPP-III-34 (**9**) exhibited excellent anticonvulsant

activity with a desired safety profile, thus it was further evaluated in the differentiation phase of the drug test (ETSP, NINDS).

In the differentiation phase, KPP-III-34 (**9**) was also fully efficacious with an ED_{50} of 12.71 mg/kg for fully kindled (stage 5) seizures in mice, importantly without adverse effects. This confirms the potent activity of KPP-III-34 (**9**) even in the severe seizure model without adverse effects. It was evaluated continuously in the differentiation phase. In another seizure model: intrahippocampal kainate (IHK) model of mesial temporal lobe (MTLE) epilepsy in mice, KPP-III-34 (**9**) significantly decreased the number of hippocampal paroxysmal discharges. Consequently, it was also efficacious against non-convulsive status epilepticus. The non-convulsive status epilepticus is the prolonged stage of seizure in which patients show altered mental status with confusion or abnormal behavior [41].

In the modified Irwin test (rats), at the elevated oral dose up to 500 mg/kg, KPP-III-34 **(9**) impressively exhibited no adverse effects up to 4 h. Moreover, KPP-III-34 (**9**) was found impressively clean; devoid of any adverse effects including autonomic, neuromuscular, sensorimotor, and behavioral functions in the 3 days tolerability test and functional battery test, as discussed above. Molecular docking studies indicate that KPP-III-34 (**9**) has a different pose than the sedating marketed drug alprazolam. As discussed above, as compared to alprazolam, KPP-III-34 (**9**) was found to have weaker halogen bond with the α1His102 amino acid side chain, which presumably is the reason for no sedation or could be. While evaluating the plethora of data in detail, and the molecular docking/binding studies KPP-III-34 **(9**) is likely to be an α2/α3 PAM, as the lead compound KRM-II-81 (**7**). A novel and advanced compound KPP-III-34 (**9**) was also tested against behavioral side effects via a modified Irwin test (up to 500 mg/kg dose in rats), in 3 days tolerability assay and functional battery assay (rats). KPP-III-34 (**9**)

exhibited slightly less activity (in epilepsies) than the lead compound KRM-II-81 (**7**) but KPP-III-34 (**9**) exhibited a much better safety profile.

In conclusion, KPP-III-34 (**9**) is now one of the lead imidazodiazepines designed and synthesized in Milwaukee, which is fully efficacious in many seizure models including pharmaco-resistant epilepsy with an excellent safety profile, as desired. The easier and cheaper synthetic route to prepare this compound (on gram scale) was optimized and developed (as discussed in above). Importantly, for the purification of the final product or any intermediates, column chromatography is not required (in any steps). Moreover, this compound can be synthesized without using any palladium chemistry and using a shorter route than that needed for the synthesis of the lead imidazodiazepine KRM-II-81 (**7**). Importantly, the newly advanced compound KPP-III-34 (**9**) is now a strong back up compound to the clinically progressing KRM-II-81 (**7**) for treatment of epilepsy as it exhibited better safety profile. The further evaluation of this compound including in depth studies in the Dravet syndrome model as well as a treatment for drug abuse is ongoing.

4. Methods

4.1. Rotarod studies caried out by Nick Zahn and Michelle Meyer (Dr. Arnold's laboratory, MIDD).

The rotarod studies employed here were carried out by Nick Zahn, and Michelle Meyer (Professor Alexander Arnold's lab, MIDD, UWM), according to the published protocol [26] [42]. For this research, female Swiss Webster mice were first trained to maintain their balance on a rotating rod (Omnitech Electronics Inc., Nova Scotia, Canada) at a constant speed of 15 rounds per minute until the mice could perform for 3 minutes for three consecutive times without falling. The vehicle used for the oral dosing was 2% hydroxypropyl methylcellulose and 2.5% polyethylene glycol. Different groups of mice were given either vehicle or the test compounds (40, 80, 100, or 120 mg/kg) in a volume of 200 μL orally (gavage) before the test was initiated. Mice were give diazepam (ip) as a control at 5 mg/kg in 10% DMSO, 40% propylene glycol, and 50% PBS [42]. After mice received test compounds via oral gavage, they were tested on the rotarod at three different time points (10, 30, or 60 minutes) and observed for falling, ataxia, tremors, and loss of rightening response. Mice falling two times off the rod before the 3 minutes were up considered 'a fail' and the time period was recorded. It is normal to fall once when mice were given vehicle (i.p.), so one fall was not significant [42].

4.2. Cytotoxicity studies by Michelle Meyer and coworkers in Dr. Arnold's lab, University of Wisconsin-Milwaukee and MIDD.

Cytotoxicity studies were carried out at the University of Wisconsin-Milwaukee (Professor Arnold's lab). In this experiment, the method executed was according to the published procedure, and the cultured human embryonic kidney HEK293T cells were employed [25]. In this study, dimethyl sulfoxide (DMSO) was used as a negative control while 3-dibutylamino-1-

(4- hexyl-phenyl)-propan-1-one (150 µM in DMSO) was used as a positive control. After 18 h of incubation, cell levels were assayed for cell death by standard methods [14].

4.3. Analysis of ligands in the pentylenetetrazol seizure model (PTZ) by Dr. Jeffery Witkin and Dr. Xingjie at Indiana University, School of Medicine.

For the pentylenetetrazol (PTZ) seizure model, Charles River, C57BL/6N male mice (Indianapolis, Indiana) were employed. The solution of PTZ was prepared by dissolving it in 0.9% NaCl solution and the test compounds were suspended in 1% carboxy methylcellulose. The test compounds were administered orally (10 mL/kg) and after that, these mice were placed back into their home cages. These mice were given PTZ subcutaneously (75 mg/kg) after 60 min. At this point, the delayed time to cause clonic or tonic seizures was measured using a stopwatch. During the 60 min time period, after administration of PTZ, the number of mice (if they died) were recorded and latency to clonus and tonus was analyzed by one-way ANOVA separately and Dunnett's T- test. A priori probabilities of 0.05 were set for statistical significance. Statistical evaluation of lethality was done using Fisher's Exact Probability test at 0.05 [24].

4.4. The 6 Hz (44 mA) electroshock seizure model in mice and rotarod impairment assay (method source: https://panache.ninds.nih.gov/Home/LegacyModels).

The test was done in the epilepsy therapy screening program (ETSP, NINDS). The 4 male mice (CF-1) were screened in an initial qualitative screen with the default doses of 30, 100, and 300 mg/kg (i.p.) at 0.5 h and 2 h time points after administration of the test compounds. However, the time points and doses were adjusted if supported by the data. At the time of peak (TPE), the ED_{50} was quantified. Mice were administered the test compounds at 0.25, 0.5, 1.0, 2.0, and 4 hours or the time points based on the previous data and studies. Different doses of test compounds (at least 4 doses) were given to 8 mice (n = 8) until at least 2 points can be clearly recognized between the limits of 100% protection or 0% protection or toxicity. The data for this test are presented as N/F where N stands for number of mice protected and F stands for number of animals investigated. By using Probit analysis techniques, the ED_{50}, confidence interval, the slope of the regression line and the S.E.M. of the slope were calculated.

4.5. Maximal (60 Hz and 50 mA) electroshock seizure (MES) models in mice and rotarod impairment assay (method source: https://panache.ninds.nih.gov/Home/LegacyModels).

The test was done at the epilepsy therapy screening program (ETSP, NINDS) to screen the ability of the test compounds to prevent seizure spread in the brain when all the neuronal circuits are maximally active. These seizure models are consistent with human seizures electro-physiologically and are extremely reproducible. The 60 Hz of alternating current (50 mA in mice and 150 mA in rats) was given for 0.2 sec via corneal electrodes. A drop of anesthetic agent (0.5% tetracaine HCl in 0.9% saline solution) was used in the eyes of animals. Animals were

deemed to be protected from MES-induced seizures if the hindlimb tonic extensor component of the seizure was not observed.

In the MES seizure model, the seizure was induced in the mice by 60 Hz and 50 mA corneal electroshock. [unlike the low frequency 6 Hz seizure (44 mA) seizure model]. Besides the frequency used to induce the seizure, the method employed here is almost similar to that in the 6 Hz seizure model. The 4 male CF-1 mice were screened for the initial qualitative screen with the default doses of 30, 100, and 300 mg/kg (ip) at 0.5 and 2 h time points after administration of the test compounds. However, the time points and doses were adjusted if supported by the data. At the time of peak (TPE), the ED_{50} was quantified. Mice were administered test compounds at 0.25, 0.5, 1.0, 2.0, and 4 hours or the time points were based on the previous data and studies. Different doses of test compounds (at least 4 doses) were given to 8 mice (N=8) until at least 2 points can be clearly recognized between the limits of 100% protection or 0% protection or toxicity. The data for this test are presented as N/F where N stands for the number of mice protected and F stands the number of animals investigated. By employing Probit analysis techniques, the ED_{50}, confidence interval, the slope of the regression line, and the S.E.M. of the slope were calculated. Following the MES test, the test compounds were also investigated for motor impairment in the standard rotarod test.

4.6. Subcutaneous metrazol seizure model in mice and rats (method source: https://panache.ninds.nih.gov/Home/LegacyModels).

This test indicates if the investigational compounds can protect a clonic forebrain seizure, which is induced by the chemo convulsant (metrazol). The chemconvulsant metrazol (pentylenetetrazole) was injected into the loose fold of the skin at the dose of 85 mg/kg for mice and 56.4 mg/kg for rats. Following the administration of test compound KPP-III-34 (**9**) orally, observation was made by keeping the animals in isolation cages (to minimize stress) for 0.5 h for the presence or absence of seizures. Animals were deemed to be protected if they did not exhibit clonic spasms (3-5 sec) of fore and/or hind limb jerks, jaws, or vibrissae twitching, jaw chomping.

As discussed in the 6 Hz (44 mA), and MES (60 Hz and 50 mA) electroshock seizure model, 4 male CF-1 mice were screened for the initial qualitative screen with the default doses of 30, 100, and 300 mg/kg at 0.5 and 2 h time points after administration of the test compound KPP-III-34 (**9**). However, the time points and doses were adjusted if supported by the data. The ED_{50} was quantified at the time of the peak (TPE). Mice were administered test compounds at 0.25, 0.5, 1.0, 2.0, and 4 hours or the time points were based on the previous data and studies (two acute seizure models: 6 Hz and MES). Different doses of test compounds (at least 4 doses) were given to 8 mice (n=8) until at least 2 points can be clearly recognized between the limits of 100% protection or 0% protection or toxicity. The data for this test are presented as N/F, where N stands for number of mice protected and F stands for number of animals investigated. By using Probit analysis techniques, the ED_{50}, confidence interval, the slope of the regression line and the S.E.M. of the slope were calculated.

4.7. Corneal kindled seizure model in mice (method source: https://panache.ninds.nih.gov/Home/LegacyModels).

Human focal seizures are congruent with the corneal kindled mouse seizure model regarding their pharmacological profile. Male C57BL/6 or CF-1 mice (35-42 days old) were kindled electrically using corneal electrodes to the criterion of 5 consecutive stage 5 seizures. Stage 5 seizures were characterized by facial clonus and head nodding progressing to forelimb clonus, and finally rearing and falling with generalized seizures. Male C57BL/6 mice were kindled by a 1.5 mA, 60 Hz, 3 sec stimulations, whereas, CF-1 mice were kindled by a 3 mA, 60 Hz, 3 sec stimulations. Before corneal stimulus, the corneas were treated with 0.5% tetracaine hydrochloride to anesthetize the eyes locally and 0.9% saline solution to enhance electrical conductivity. Mice reached the 5^{th} stage seizures after getting corneal stimulations (2 x a day) in around 10-15 days and continued until all mice achieved the 5 consecutive 5^{th} stage seizures (fully kindled). All animals were confirmed that they were in the 5^{th} stage seizures. On the investigational day, animals were selected randomly and administered as a group of 4 fully kindled (5^{th} stage) animals (per group). The time of peak effect (TPE) and ED_{50} were determined similarly as in the MES and 6 HZ models (acute seizure models). Animals showing a seizure score of less than 3 were deemed to be protected. Investigational compound [KPP-III-34 (**9**)] was given to the animals for identification studies. The quantification was done at 2 time points and 3 different doses. In each group (number of animals=8), 0%-100% protection was evaluated at least at 3 doses. Mice were returned to their home cage when the study was over and allowed to rest at least 3-4 days between tests to 'washout' any test compound after testing and observation was made.

4.8. The Intrahippocampal kainate (IHK) model of mesial temporal lobe (MTLE) epilepsy model in mice (method source: https://panache.ninds.nih.gov/Home/LegacyModels).

In this experiment, kainic acid (KA) was injected into the dorsal hippocampus of mice which induces several hours of lasting non-convulsive status epilepticus (SE). This is followed by a period of 2-3 weeks during which epileptogenesis occurs with the appearance of brusts, discharges, and spikes. Afterwards, the electrographic hippocampal paroxysmal discharges (HPD) were exhibited spontaneously (30-60 minutes per hour and last 15-20 sec) for the whole life of the animals. The HPD are associated with behavioral arrest and/or mild motor automatisms. The record of HPDs were carried out by implanting an intra-hippocampal depth electrode into the brain.

This test was done on male C57BL/6J mice (10 weeks old or more). Animals were anesthetized using 2-3% isoflurane in oxygen and placed in a stereotactic frame in a flat skull position and this was followed by injection of 1 nmol KA solution (Sigma) in 0.9% sterile saline into the right dorsal hippocampus. All mice were implanted with a bipolar electrode into the injected hippocampus when injection of kainic acid took place. Mice were provided buprenorphine (injection, 0.05 mg/kg) before and between 6 and 8 h after the surgery. Mice were kept in individual cages under a 12/12 h light-dark controlled cycle with access to food and water. To allow HPDs, the mice were allowed to recover for 4 weeks before the screening protocol. The electroencephalogram (EEG) was recorded to detect and quantify HPDs in freely moving animals placed in individual plexiglass cages using SystemPlus Evolution (Micromed). HPDs were detected by an expert by using offline analysis. HPDs were defined as rhythmic high-amplitude sharp waves of 5-10 Hz frequency and lasted for at least 5 seconds with an interval of at least 1 second. As per effective dose in previous tests (e.g., 6 Hz or MES), the compounds

were first tested on freely moving animals. EEG recordings were performed for 20 min pre-injection and up to 240 min post-injections based on the compound's TPE. The effects of the injected investigational compounds were evaluated by comparing the data to the reference period. Data were presented as the raw number of HPDs during the analyzed 20 min period of analysis (10 minutes before and 10 minutes after peak time of effect of the compound). For each MTLE mouse; group mean number of HPDs (n = 4-8 MTLE mice), and effect on suppression of epileptic discharges as represented by percent of baseline HPD values was determined. Also, any behavioral effects observed were noted. There were no behavioral effects with KPP-III-34 **(9)**.

4.9. Time course of untoward signs in a modified rat Irwin test induced by orally administered KPP-III-34 (9) in rats (method source: https://panache.ninds.nih.gov/Home/LegacyModels).

In order to know the toxicity and therapeutic effects of KPP-III-34 (**9**) (administered up to 500 mg/kg) by examining their effect on physiologic functions and behavior, the modified Irwin test or Functional Observation Battery (FOB) assay was carried out. Besides vehicle control, mostly 4 animals/dose were used in this experiment. Also, one unblinded control was used to establish baseline activity and to account for environmental variables that may affect the behaviors of healthy animals. After the administration of a single dose of KPP-III-34 **(9)** two independent observers evaluated them for impaired autonomic (e.g., porphyrin, salivation), sensorimotor (e.g., hyperesthesia, loss of righting reflex), neuromuscular (e.g., tremors, ataxia) and behavioral (e.g., grooming, vocalizations) function at different time periods (0.25, 0.5, 1, 2, and 4 h). Prior to testing and drug administrations, all animals were handled to make them familiar with the experiments. After 24 h of post-compound administration, the rats were also evaluated to assess

recovery from any impairment if seen on a previous day [43]. No behavioral effects were observed with KPP-III-34 up to the 500 mg/kg dose **(9)**.

4.10. The 3-day tolerability assay for spontaneous recurrent seizing rats (method source: https://panache.ninds.nih.gov/Home/LegacyModels).

For the 3-day tolerability study of KPP-III-34 **(9)**, in male Sprague-Dawley rats (Charles River Kingston, NY) were used. The status epilepticus (spontaneous recurring seizure) was induced via low-dose kainic acid (KA) paradigm. The test compound was administered at the dose of 50 mg/kg. Both water and food (TEKLAD GLOBAL 2920X-011620M) were freely accessible to the animals. The handling, feeding and housing of the animals were done in a consistent manner with the recommendations in the National Research Council publication, "Guide for the Care and Use of Laboratory Animals" (3). No insecticides that are capable of changing hepatic drug metabolism enzymes were used in the animal facilities. The ethunization of all animals was done accordingly with the Institute of Laboratory Resources policies on the humane care of laboratory animals. All protocols involving the care and use of animals have been approved by the Institutional Animal Care and Use Committee at the University of Utah.

4.11. Rotarod test in mice (method source: https://panache.ninds.nih.gov/Home/LegacyModels).

To investigate the possibility of motor impairment after administration of the test compounds (KPP-III-34 **(9)** and KPP-III-51 **(10)**, each animal (mouse) was kept on a one-inch rotating rod

(knurled steel) at the speed of 6 rounds per minute where an animal can maintain an equilibrium for long periods of time. The animals received the test compounds (i.p.) at various doses (30, 100, and 300 mg/kg) and they were evaluated at three different time points (0.25, 2, 4 h post administration). An animal was deemed to have impaired motor control if it can't maintain equilibrium on the rotating rod for 3 tries for one minute (observation time period) and falls down. The TD_{50} was quantified that indicates the toxicity of 50% of animals treated with the test compounds and conducted at time per effect (TPE) as described.

4.12. Lamotrigine (LTG)-resistant amygdala kindling model in rats (method source: https://panache.ninds.nih.gov/Home/LegacyModels).

The objective of this test model is to test KPP-III-34 **(9)** against Lamotrigine-resistant seizures caused by frequent electrical stimulation of the amygdala. This test model helps to determine if the test compound is effective against convulsions in therapy-resistant patients and against the seizures, which are secondarily generalized. Adult male Sprague-Dawley CD rats (275-300 g) were used in this experiment. Rats were kindled by embedding (via surgery) a bipolar stimulating electrode under stereotaxic guidance and anesthesia in the right amygdala (AP = - 2.2 mm, ML = 4.7 mm, DV = -8.7 mm) of the animals. The rats were administered 5 mg/kg LTG intraperitoneally (i.p.) after one week of kindling. The rats were completely kindled (occurrence of 4 or 5 consecutive Racine scale stage 4-5 seizures) by stimulating with a 200 µAmp, 50 Hz, 2 seconds once daily) for five days a week. Only fully kindled animals were used in this experiment. Rats received a 30 mg/kg dose of LTG (i.p.), two days after the kindling of rats to ensure Lamotrigine resistance. Rats were allowed to washout in 3 days in their home cage and on

the third day of washout animals were pre-stimulated to ensure the recovery from fully kindled seizures. On the 4th day or later, kindled rats received test drug KPP-III-34 **(9)** at different doses (50, 100, and 200 mg/kg) and then underwent the kindling stimulus at the TPE of the drug KPP-III-34 **(9)**. After discharge duration, the median seizure scores were noted, animals were deemed to be protected from seizures if the score was less than 3 seizures on the Racine scale. Based on previous experiments (6 Hz and MES) the doses were chosen accordingly. The capacity of the drug (KPP-III-34 **(9)** to dampen the after-discharge duration and behavioral seizure scores was quantified by changing the dose in between 0% and 100% effect [44].

4.13. Neuropharmacokinetic *in vivo* evaluation of ligands in plasma and brain (Source: Dr. Savic and coworkers, University of Belgrade, Serbia) [39] [40].

The neurophamacokinetic study of ligands in the brain and plasma was conducted on male Sprague Dawley rats (adults), which weighted 280-330 g on the day of experiment. These rats were bred in the vivarium of the Faculty of Pharmacy, Belgrade, Serbia and group-housed (five animals per cage) under standard laboratory conditions (temperature 21±2 °C, relative humidity 40–45% and the illumination 120 lx). Rats were allowed *ad libitum* access to drink tap water as well as to chow pellets. Rats were kept on a 12:12 h light/dark cycle with lights on at 06.00 h and pharmacokinetic testing took place during the light phase of the diurnal cycle. The animals used in this neuropharmacokinetic *in-vivo* evaluation were refined to the minimum number. The experiment was carried out within the project approved by the Ethical Council for the Protection of Experimental Animals of the Ministry of Agriculture, Forestry and Water Management of the Republic of Serbia. A cassette dosing experiment was conducted to determine the

pharmacokinetic parameters characterizing both the amount and rate of transport of the chosen ligands (such as KPP-III-34 **(9)**, KPP-III-51 **(10)**, KPP-IV-35 **(16)**, KPP-III-96B (**11**), and KPP-IV-09 **(12)**) administered via oral gavage. Also, the objective of this experiment was to get the corresponding pharmacokinetic profiles in systemic circulation and brain. The rats were divided into different numbers of cohorts and different numbers of groups of animals depending upon the number of ligands. Each group contained three animals and corresponded to predetermined time intervals (20 min, 60 min, 180 min, 480 min and 1440 min (24 h)). The doses of a given ligand were 2.0 mg/kg (concentration of each ligand 0.4 mg/mL in 0.25% methyl cellulose solution) orally.

At the appropriate time intervals, animals were anesthetized by ketamine hydrochloride (90 mg/kg, intraperitoneal administration, Ketamidor, Richter Pharma AG, Wels, Austria) and samples of blood (collected via cardiac puncture in heparinized syringes) and brains were harvested. After centrifugation for 10 min at 1000 x g (MiniSpin® plus centrifuge, Eppendorf, Germany), a plasma sample was collected. Brain tissue samples were also weighted and homogenized in 1 ml of methanol via an ultrasonic probe (70% amplitude 2 x 20 s). Supernatants were separated after centrifugation for 20 min at 3400 × g (MiniSpin® plus centrifuge, Eppendorf, Germany). The plasma and supernatants obtained were further processed with solid phase extraction using Oasis HLB cartridges (Waters Corporation, Milford, Massachusetts). The concentration of ligands was determined by ultraperformance liquid chromatography–tandem mass spectrometry (UPLC–MS/MS) with ACELLA (Thermo Fisher Scientific Inc., Madison, WI, USA) UHPLC chromatograph, coupled to a triple quadrupole mass spectrometer TSQ Quantum Access MAX (Thermo Fisher Scientific Inc., Madison, WI, USA) with a heated electrospray ionization (HESI) interface. Calibration curves were prepared in the range 0.0005 – 2.5 µmol/L, where the ratios of

the peak, areas of the analyte and the internal standard were used for their construction. A Phoenix WinNonlin Software package (Certara L.P.) was used to analyze non-compartmental pharmacokinetics. Graphs were constructed by commercially available statistical software Sigma Plot 12 (Systat Software Inc., USA) [39] [40].

4.14. Electrophysiological recordings from Dr. Janet Fisher (University of South Caroline, School of Medicine).

The method described by Alexeev *et. al* [37] was used for the electrophysiological recordings of the compounds described in Dr. Fisher's work. The cDNAs for $GABA_AR$ subtypes (full length) were received from Dr. David Weiss, the University of Texas Health Science Center, San Antonio, TX and Dr. Robert Macdonald, Vanderbilt University. These subtypes were transiently transfected into HEK-293T cell lines (GenHunter, Nashville, TN) using calcium phosphate precipitation. Besides α2, all other subtypes were rat clones. The $GABA_AR$ subtype cDNAs (plasmids encoded) were added to the cells in a 1:1:1 ratio (α:β:γ) of 2 μg each and expressed as ion channels. In this experiment, the patch clamping of cells were performed at −50 mV in the entire-cell recording configuration. Either freshly prepared bath solution or frozon stocks (in water) were used to dilute GABA. DMSO was used to prepare the solution of investigational compounds KPP-III-51 **(10)** and KPP-III-34 **(9)**, and the solution of this was diluted with the highest DMSO level applied to cells of 0.01%.

The solutions containing GABA or GABA + compounds were employed to cells for 5 s using a 3-barrelled solution delivery device controlled by a computer-driven stepper motor (SF-77B,

Harvard Apparatus, Holliston, MA, open tip exchange time of < 50 ms). The current was recorded using an Axon 200B (Foster City, CA) patch clamp amplifier and analysis of the whole-cell currents was done using Clampfit (pClamp9 suite, Axon Instruments, Foster City, CA) and Prism (GraphPad, San Diego, CA) programs. In this experiment, the normalization of data was carried out by the response to GABA alone for each cell and then the data were expressed as a % of that response (EC_{3-5} GABA). In a four- parameter logistic equation [Current = minimum current +(maximum current-minimum current)/ (1 + (10(log(EC50) − log(modulator))n)], the concentration-response data was fit, where n represents the Hill number.

4.15. Methods of molecular docking with the help of Dr. Lalit Golani (UWM).

The molecular docking (binding) studies of the compounds were performed, and ligand-protein interactions were analyzed using AutoDock Vina 1.5.6 [26]. The PDB file of the CryoEM structure of the human full-length α1β3γ2L GABAA receptor in the complex with alprazolam (6HUO) was downloaded from the Protein Data Bank. The file was further improved for docking by fixing missing bonds or atoms, adding polar hydrogens, and assigning charges by AM1-BCC, and removing water molecules [26]. The proteins were validated by first removing the bound ligand (alprazolam) and this was followed by docking it in the same binding site. The compounds were drawn, and energy minimized in Chimera.1 A grid size of 17 Å x 17 Å x 17 Å and centered at coordinates 152.80 (x), 163.02 (y), and 161.14 (z) were used. Illustrations of the 3D models were generated using Chimera and Python.1-2. The dockings were performed with standard search parameters and the poses with the best scores were selected for the analysis [26].

4.16. The NIMH psychoactive drug screening program by Dr. Bryan Roth and coworkers (method source: NIMH PDSP).

In order to screen the selectivity of a drug on ion channels, transporters, neurotransmitters etc, and the 46 receptor panel (including the HERG channel), of PDSP was used and the newly synthesized ligands were sent to Dr. Bryan Roth, National Institute of Mental Health Psychoactive Drug Screening Program at UNC (NIMH PDSP). All the PDSP data included herein were obtained generously from NIMH PDSP. The protocol used in this screening was according to the published protocol detailed in [(Roth, B.L., 2018. ASSAY PROTOCOL BOOK - Version III [WWW Document] National Institute of Mental Health Psychoactive Drug Screening Program (NIMH PDSP), URL: University of North Carolina at Chapel Hill (unc.edu)]. In the primary screening most of the investigational compounds were screened at a single concentration of 10 µM in quadruplicate in 96-well plates. HEK-293 cells (American Type Culture Collection ATCCs CRL-1574™) were used in this screening. In the primary binding assay, the compounds exhibiting at-least 50% inhibition at 10 µM concentration were chosen for secondary radioligand binding assays. The goal of the secondary binding assay using a radioligand is to identify the equilibrium binding affinity at specific targets (K_i). For secondary screening, the compounds which were chosen, were tested at 11 different concentrations (0.1, 0.3, 1, 3, 10, 30, 100, 300 nM, 1, 3, 10 µM) and in 3 sets of 96-well plates (triplicate). At the final volume of 125 µl per well, primary, and secondary radioligand binding assays were run. If not mentioned, the hot ligand concentration most of the time is approximated to the Kd value of the ligand on the receptor. In the absence or presence of 10 µM of the appropriate reference compound, the total binding (ref compound 3H]-flunitrazepam) and nonspecific binding [reference compound (3H)-DZP] were determined, respectively. The filters thus recovered were moved to scintillation vials and subjected to

scintillation counting after the addition of 3 mL Rotiszint Eco plus liquid scintillation cocktail. If not specified, the plates were incubated at ambient temperature for 90 minutes (in the dark). Employing 0.3% polyethyleneimine (PEI) soaked 96-well filter mats using a 96-well Filtermate harvester, and this was followed by washing with cold wash buffers thrice, then the reactions were quenched. The equation: log(inhibitor) vs. response-variable slope with top = 100 % and bottom = 0 % Y = 100/(1+10^((logIC50-x)*Hill-slope)) was used for the non-linear regression analysis of the displacement curves. Secondary binding results were analyazed using the equation, Y = Bottom + (top-bottom)/(1+10^x-LogIC50). The GraphPad Prism (LaJolla California USA) was used in both analyses. By using the Cheng-Prusoff relationship (Cheng and Prusoff, 1973) $K_i = IC_{50}/(1+(L/K_D))$, which L indicates the concentration of the radioligand (2 nM). The drug concentrations at half-maximal inhibition of specific [3H]-flunitrazepam binding (IC50) were converted to K_i values and are shown in nM values.

4.16. Rat model of chronic spontaneous seizing post-Kainate (phase I) (method source: https://panache.ninds.nih.gov/Home/LegacyModels).

Before carrying out this test, a sub-chronic tolerability assay was conducted to detect the toxicity of the drug and vehicle for three times a day for three days, as discussed in detail above. KPP-III-34 (**9**) did not exhibit any unwanted signs or adverse effects in any of the mice tested. Then by administration of the low-dose (7.5) kainic acid (KA) frequently (IP), the status epilepticus (SE) was induced in rats (adult male Sprague-Dawley CD rats, 250-300 g). An additional dose (5 mg/kg KA) was injected every 30 minutes up to 3 hours maximum dose until the animal displays

two Racine Stage 4-5 seizures: in the case if rats did not develop a stage 4-5 seizure within an hour. The wet dog shakes, facial/jaw clonus and head nodding indicates the stage 1-2 seizures, according to the Racine scale (Racine, 1972), whereas forelimb clonus as stage 3 and the rearing on hind legs and the loss of balance indicates the stage 4-5 seizures. All animals displayed a minimum of one stage 4-5 seizures every hour for 3.5 hours in experiments by KA and their behaviors were monitored. A TR50B electroencephalographic (EEG) wireless telemetry device (Kaha Telemetry Systems) was planted in all rat's brains under the stereotaxic guidance and anesthesia after 10 weeks post SE. After that, the rats were treated with the test compound (KPP-III-34 (**9**) via intraperitoneal administration three times a day for 5 days at the dose of 50 mg/kg and the EEG data were recorded (24 h/7 d/wk). Seizure burden and seizure freedom are the primary outcome measures. The animals were deemed to have seizure freedom when zero seizures occurred in between the first dose of drug and 12 hours following the last dose.

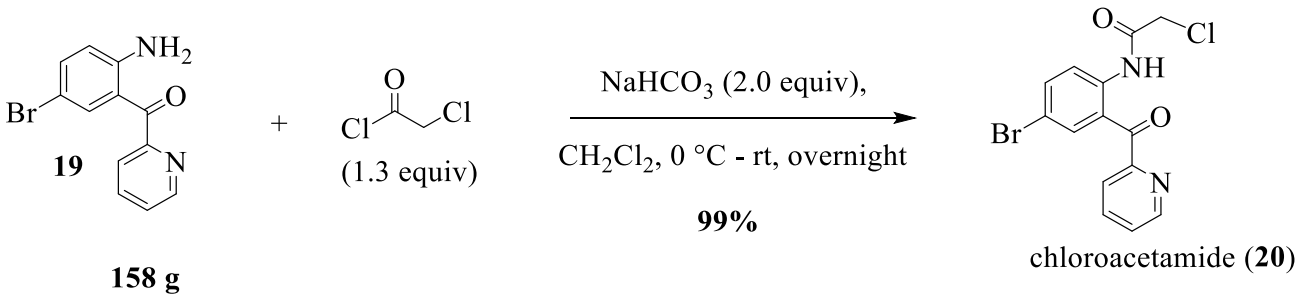
5. Experimental.

General experimental conditions.

Unless otherwise specified, all reactions were carried out in oven-dried round-bottom flasks or screw-cap test tubes were used. Dry solvents were used for all chemical reactions unless otherwise specified and chemicals were purified by standard purification techniques, or the chemicals were purchased from the chemical vendors with the desired purity. The progress of the reactions were monitored using TLC from Dynamic Adsorbents, Inc. (silica gel, neutral alumina, or basic alumina) under ultraviolet (UV) light. For purification of some intermediates or the products, flash column chromatography techniques was used on silica gel (230-400 mesh, Dynamic Adsorbents)

was used or on neutral alumina. A Stuart melting point SMP3 apparatus (Barloworld Scientific US Ltd.) was used to determine the melting point of some of the compounds. The enantiomeric excess (% *ee*) was determined using a CHIRALPAK® IB-N3 HPLC Column from Daicel Corporation. To determine the % purity of the compounds, a C18 1.8 mM column (Shimadzu Nexol company) was used. Optical rotations were measured on a JASCO Model DIP-370 digital polarimeter using a standard. The ^{1}H and ^{13}C NMR spectra were obtained on Bruker Spectrospin 500 MHz or 300 MHz instruments in $CDCl_3$, DMSO or DMSO- d^6. The chemical shifts are reported in δ (ppm). Multiplicities are represented as follows: singlet (s), broad signal (br), doublet (d), triplet (t), quartet (q), dd (doublet of doublets), dt (doublet of triplets), td (triplet of doublets), and multiplet (m). HRMS were determined using LCMS-IT-TOF techniques at the Milwaukee Institute for Drug Discovery (MIDD) in the Shimadzu Laboratory for Advanced and Applied Analytical Chemistry.

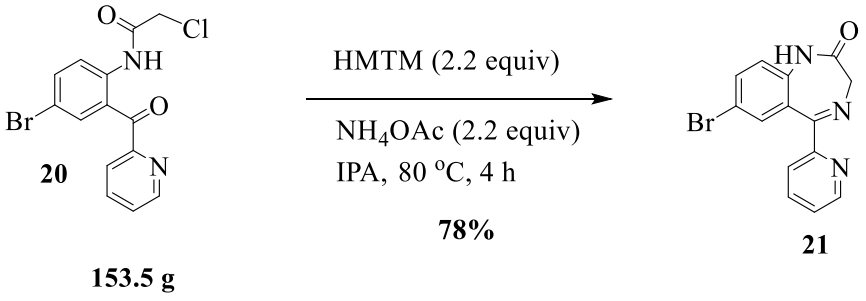
***N*-(4-Bromo-2-picolinoylphenyl)-2-chloroacetamide 20.**



This reaction was carried out following the published procedures of Knutson *et*. al [24]. The (2-amino-5-bromophenyl)(pyridin-2-yl) methanone (**19**) (158 g, 0.57 mol) was dissolved in dry CH_2Cl_2 in a 3-neck round bottom flask (3000 mL) and was allowed to stir stir until the mixture turned into a homogenous solution. Then solid $NaHCO_3$ (95.8 g, 1.14 mol) was added slowly to

the stirring solution and the mixture, which resulted, was cooled to 0 °C using an ice bath. The chloroacetyl chloride (83.7 g, 0.74 mol) was added dropwise to the stirring solution at 0 °C and the reaction mixture allowed to warm to rt. The mixture, which resulted, was stirred overnight at rt or until analysis by TLC (silica gel, EtOAc/hexanes/methanol, 2:1:0.5) indicated completion of the reaction and formation of a new non-polar component by TLC (sole spot with $\boldsymbol{R_f}$ 0.6). After the completion of the reaction progress, the mixture was quenched with cold water (500 mL). The aq layer was washed with CH_2Cl_2 (3 x 500 mL) and the combined organic layers were washed with brine (500 mL) and dried (Na_2SO_4). The solid was dried under vacuum (10 h) at 40 °C to obtain the 2-chloroacetamide (**20**) (199.6 g, 99%), which was used for the next step without further purification and characterization. The spectral data were identical to that reported earlier by Knutson *et*. al [24].

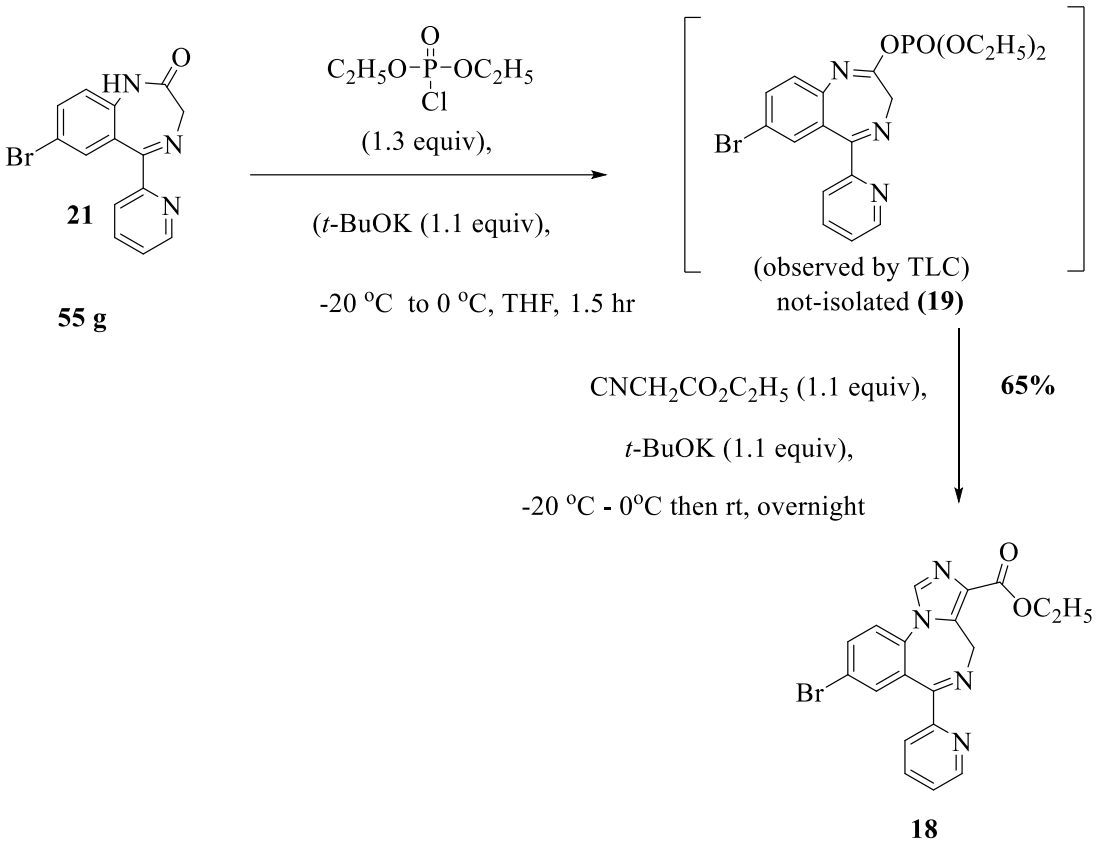
7-Bromo-5-(pyridin-2-yl)-1,3-dihydro-2*H*-benzo[e][1,4]diazepin-2-one (21).



To a round bottom flask (5000 mL), were added *N*-(4-bromo-2-picolinoylphenyl)-2-chloroacetamide (**20**, 153.5 g, 434 mmol), hexamethylenetetramine (133.8 g, 954 mmol),

ammonium acetate (73.3 g, 951 mmol), and isopropanol (2700 mL). The mixture, which resulted, was heated to reflux (80 °C) for 4 h. After the completion of the reaction, as indicated by analysis of TLC (silica gel, EtOAc/hexanes, 1:1), the reaction mixture was then cooled to 0–5 °C (ice bath). The solid, which resulted, was filtered, and washed with cold isopropanol (2 x150 mL) and then water (4 x 150 mL). The solid was dried under vacuum at 40 °C to afford the cyclized product (**21**) as an off-white colored solid (107 g, 78%): $\boldsymbol{R_f}$ 0.4 (EtOAc/hexanes, 1:1 and 2 drops of TEA); **^{1}H NMR** (500 MHz, DMSO) δ 10.65 (s, 1H), 8.57 (d, *J* = 4.1 Hz, 1H), 8.05 (d, *J* = 7.9 Hz, 1H), 7.95 (td, *J* = 7.7, 1.7 Hz, 1H), 7.71 (dd, *J* = 8.7, 2.3 Hz, 1H), 7.50 (ddd, *J* = 7.5, 4.8, 1.0 Hz, 1H), 7.43 (d, *J* = 2.3 Hz, 1H), 7.18 (d, *J* = 8.7 Hz, 1H), 4.23 (s, 2H); **^{13}C NMR** (126 MHz, DMSO) δ 170.35 (s), 168.11 (s), 156.31 (s), 148.87 (s), 139.31 (s), 137.58 (s), 134.47 (s), 134.17 (s), 127.92 (s), 125.40 (s), 123.92 (s), 123.57 (s), 114.50 (s), 57.58 (s). This material was identical with the authentic sample and the spectroscopic data were in complete agreement with the published data [24].

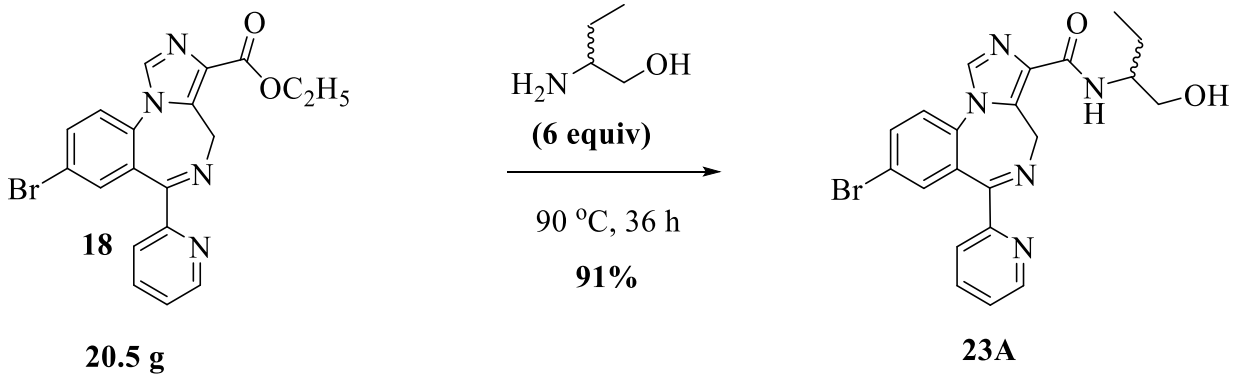
Ethyl 8-bromo-6-(pyridin-2-yl)-4*H*-benzo[f]imidazo[1,5-a][1,4]diazepine-3-carboxylate (18).



The vacuum dried cyclized compound (**21**, 55 g, 174 mmol) was dissolved in very dry THF (1000 mL), and the solution, which resulted, was cooled to – 20 °C. To the stirring solution, potassium *tert*-butoxide (24.5 g, 191 mmol) was added in one portion. The reaction mixture was allowed to stir until it reached 0 °C and then stirred for an additional 0.5 h at 0 °C. The mixture was then cooled to -20 °C after which, diethyl chlorophosphate (39.02 g, 226 mmol) was added and the mixture stirred until it reached 0 °C. At this point, the mixture which resulted, was allowed to stir for 0.5 h, and then the solution was cooled to -78 °C, and ethyl isocyanoacetate (21.6 g,191 mmol)

was added. This was followed by the addition of a second portion of potassium *tert*-butoxide (24.5 g, 191 mmol) at 0 °C. This mixture, which resulted, was allowed to stir overnight, during which time, it was allowed to warm to rt. The competition of the reaction mixture was confirmed by analysis by TLC (silica gel, 1.5 mL EtOAc, 1 mL hexane, 2 drops methanol, and 1 drop of 10% aq NH_4OH), after which the reaction solution was quenched by addition of a cold saturated aq solution of $NaHCO_3$ (40 mL) and extracted with EtOAc (3 x 500 mL). The organic layers were combined and washed with brine (2 x 400 mL), and then dried (Na_2SO_4). The solvent was removed under reduced pressure to $1/4^{th}$ the original volume and then *tert*-butylmethyl ether (400 mL) was added. Addition of the ether resulted in precipitation, after which the *tert*-butylmethyl ether (TBME) was removed by decanting. TBME was added again to the precipitate, and this was stirred for 5 min (this process was repeated 3-5 times). The solid material obtained after final decantation was dried under reduced pressure to afford a light brown to yellow colored solid. The solid material was characterized by analysis by NMR without further purification (not required), and the mother liquor was purified by flash column chromatography (silica gel, EtOAc/hexane, 4:1) to afford more imidazodiazepine ester (**18**) as an off-white colored solid (46.5 g, 65%): **^{1}H NMR** (500 MHz, $CDCl_3$) δ 8.56 (d, *J* = 3.1 Hz, 1H), 8.07 (d, *J* = 7.7 Hz, 1H), 7.91 (s, 1H), 7.87 – 7.72 (m, 2H), 7.58 (s, 1H), 7.47 (d, *J* = 8.6 Hz, 1H), 7.40 – 7.33 (m, 1H), 6.10 (d, *J* = 10.3 Hz, 1H), 4.41 (d, *J* = 5.8 Hz, 2H), 4.14 (d, *J* = 10.7 Hz, 1H), 1.42 (t, *J* = 7.1 Hz, 3H); **^{13}C NMR** (126 MHz, $CDCl_3$) δ 167.08 (s), 162.91 (s), 156.15 (s), 148.70 (s), 138.44 (s), 136.97 (s), 135.29 (s), 135.01 (s), 134.56 (s), 134.44 (s), 129.33 (s), 128.51 (s), 124.92 (s), 124.32 (s), 124.00 (s), 120.58 (s), 60.81 (s), 45.02 (s), 14.44 (s). The proton and carbon NMR data for this compound were identical in all respects with that reported in the literature [24].

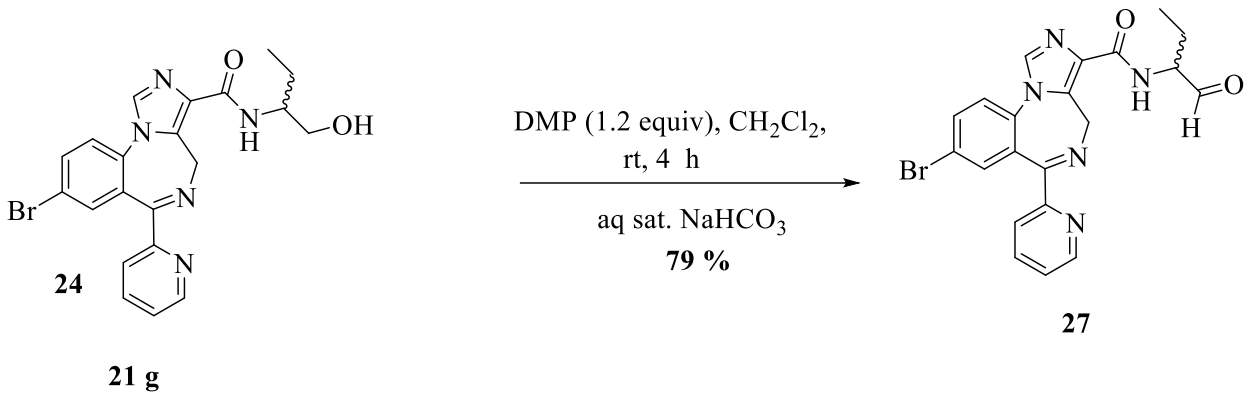
8-Bromo-*N*-(1-hydroxybutan-2-yl)-6-(pyridin-2-yl)-4*H*-benzo[f]imidazo[1,5-a][1,4]diazepine-3-carboxamide (23A).



In a sealed tube, imidazodiazepine ester **18** (20.5 g, 0.04 mol) and *rac*-2-amino-1-butanol (26.6 g, 0.3 mol) were added, and the mixture, which resulted, was heated at 90 °C (preheated oil bath) for 36 h. Analysis by TLC indicated the disappearance of starting material and the appearance of a new component (***R*$_f$** 0.4, silica gel, EtOAc/hexane/methanol, 2:1:0.5 and a few drops of 14% aq NH_4OH). At this point, the reaction mixture was cooled to rt and then diluted by adding EtOAC (350 mL) and water (200 mL). The biphasic layers were separated and the aq layer was extracted with EtOAc (4 x 200 mL). The combined organic layer was washed with brine (200 mL) and dried (Na_2SO_4). The solvent was removed under reduced pressure and the residue was purified by crystallization (15 % MeOH in EtOAc). The solid was dried under vacuum at 40 °C to afford carbxamide **23A** as light-yellow colored solid (20.6 g, 91%): **MP** 255-256 °C; **^{1}H NMR** (500 MHz, $CDCl_3$) δ 8.51 (d, J = 4.4 Hz, 1H), 8.09 (d, J = 8.0 Hz, 1H), 7.78 (td, J = 7.8, 1.7 Hz, 2H), 7.73 (dd, J = 8.6, 2.1 Hz, 1H), 7.54 (d, J = 2.1 Hz, 1H), 7.48 – 7.37 (m, 1H), 7.32 (ddd, J = 7.5, 4.8, 0.9 Hz, 1H), 7.24 (d, J = 8.2 Hz, 1H), 6.21 (t, J = 11.2 Hz, 1H), 4.15 – 4.02 (m, 2H), 4.02 –

3.91 (m, 1H), 3.80 – 3.68 (m, 1H), 3.68 – 3.58 (m, 1H),1.67 (s, 1H), 1.57 (dd, J = 13.6, 6.7 Hz, 1H), 0.98 (d, J = 24.1 Hz, 3H); **^{13}C NMR** (126 MHz, $CDCl_3$): δ_C 166.8 (s),163.3 (s), 156.3 (s), 148.5 (s), 137.0 (s), 135.8 (s), 135.3 (s), 134.9 (s), 134.6 (s), 133.2 (s), 131.2 (s), 128.5 (s), 124.8 (s), 124.2 (s), 124.0 (s), 120.4 (s), 65.4 (s), 53.4 (s), 44.7 (s), 24.3 (s), 10.7 (s); **HRMS** (ESI/IT-TOF) m/z: $[M + H]^+$ calcd for $C_{21}H_{20}BrN_5O_2$ 454.0879; found 454.0866.

8-Bromo-*N*-(1-oxobutan-2-yl)-6-(pyridin-2-yl)-4H-benzo[f]imidazo[1,5-a][1,4]diazepine-3-carboxamide (27).

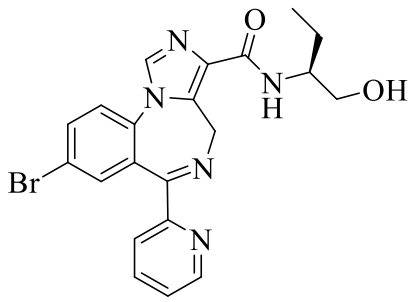


The Dess-Martin periodinane (21.2 g, 0.055 mol) was added in one portion to the stirring solution of racemic carbaxamide (**24,** 19 g, 0.046 mol) in CH_2Cl_2 (300 mL) at rt and the mixture, which resulted, was stirred at rt for 4 h. The progress of the reaction was monitored by analysis by TLC (silica gel, EtOAc/hexane/MeOH 2:1:0.5; less polar product spot turns to yellow with 2, 4 DNP spray reagent). When the reaction was completed, the mixture was diluted with CH_2Cl_2 (350 mL) and quenched by addition of a saturated aq $NaHCO_3$ solution (300 mL), and this was followed by a saturated aq solution of $Na_2S_2O_3$ (300 mL). The mixture, which resulted, was stirred for 20 min

and the biphasic layers were separated. The aq layer was extracted with CH_2Cl_2 (2 x 300 mL) and the combined organic layer was washed with brine (200 mL) and dried (Na_2SO_4). The solvent was removed under reduced pressure and the residue was purified by crystallization (15 % MeOH in EtOAc). The solid was dried under vacuum at 40 ^oC to afford carbaxamide **27** as a light yellow colored solid (16.5 g, 79 %): **^{1}H NMR** (500 MHz, $CDCl_3$) δ 9.66 (d, J = 9.8 Hz, 1H), 8.55 (dd, J = 4.0, 0.7 Hz, 1H), 8.13 (d, J = 7.9 Hz, 1H), 7.86 – 7.79 (m, 2H), 7.77 (dt, J = 6.8, 3.4 Hz, 1H), 7.62 (d, J = 7.3 Hz, 1H), 7.59 (s, 1H), 7.45 (d, J = 8.6 Hz, 1H), 7.36 (ddd, J = 7.5, 4.8, 0.9 Hz, 1H), 6.24 (d, J = 11.6 Hz, 1H), 4.58 (s, 1H), 4.21 – 4.06 (m, 1H), 2.15 – 2.01 (m, 1H), 1.80 (dt, J = 14.5, 7.4 Hz, 1H), 1.02 (s, 3H); **^{13}C NMR** (126 MHz, $CDCl_3$) δ 199.64 (s), 166.81 (s), 162.90 (s), 156.29 (s), 148.57 (s), 136.94 (s), 136.18 (s), 135.38 (s), 134.90 (s), 134.61 (s), 133.38 (s), 130.93 (s), 128.57 (s), 124.84 (s), 124.22 (s), 124.03 (s), 120.49 (s), 59.44 (s), 44.76 (s), 22.25 (s), 9.75 (s); **HRMS** (ESI/IT-TOF) m/z: $[M + H]^+$ calcd for $C_{21}H_{18}BrN_5O_2$ 452.0722; found 452.0705.

(*S*)-8-Bromo-N-(1-hydroxybutan-2-yl)-6-(pyridin-2-yl)-4*H*-benzo[f]imidazo[1,5-a][1,4]diazepine-3-carboxamide (23B)

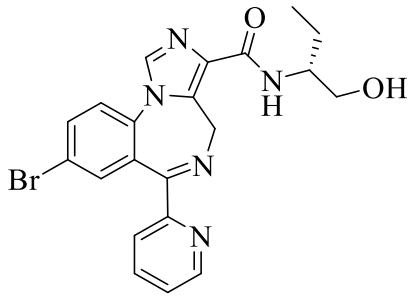
This compound **23B** was synthesized following the procedure analogous to the synthesis of **24** (*rac*) using the optically active *S*- 2-amino-1-butanol instead of *rac*-2-amino-1-butanol.



23B

^{1}H NMR (500 MHz, $CDCl_3$) δ_H 8.54 (d, J 3.6 Hz, 1H), 8.11 (d, J 7.9 Hz, 1H), 7.79 – 7.71 (m, 3H), 7.53 (s, 1H), 7.36 – 7.33 (m, 2H), 7.21 (d, J 7.8 Hz, 1H), 6.21 (t, J 12.5 Hz, 1H), 4.10 – 3.96 (m, 2H), 3.7 (1H), 3.65 – 3.62 (m, 1H), 1.66 (s, 1H), 1.59 – 1.53 (m, 1H), 0.98 (br, 3H). **^{13}C NMR** (126 MHz, $CDCl_3$): δ_C 166.8 (s),163.3 (s), 156.3 (s), 148.5 (s), 137.0 (s), 135.8 (s), 135.3 (s), 134.9 (s), 134.6 (s), 133.2 (s), 131.2 (s), 128.5 (s), 124.8 (s), 124.2 (s), 124.0 (s), 120.4 (s), 65.4 (s), 53.4 (s), 44.7 (s), 24.3 (s), 10.7 (s); **HRMS** (ESI/IT-TOF) m/z: $[M + H]^+$ calcd for $C_{21}H_{18}BrN_5O_2$ 452.0717; found 452.0705 The spectroscopic data for this compound was in complete agreement compared to that for the racemic compound discussed above.

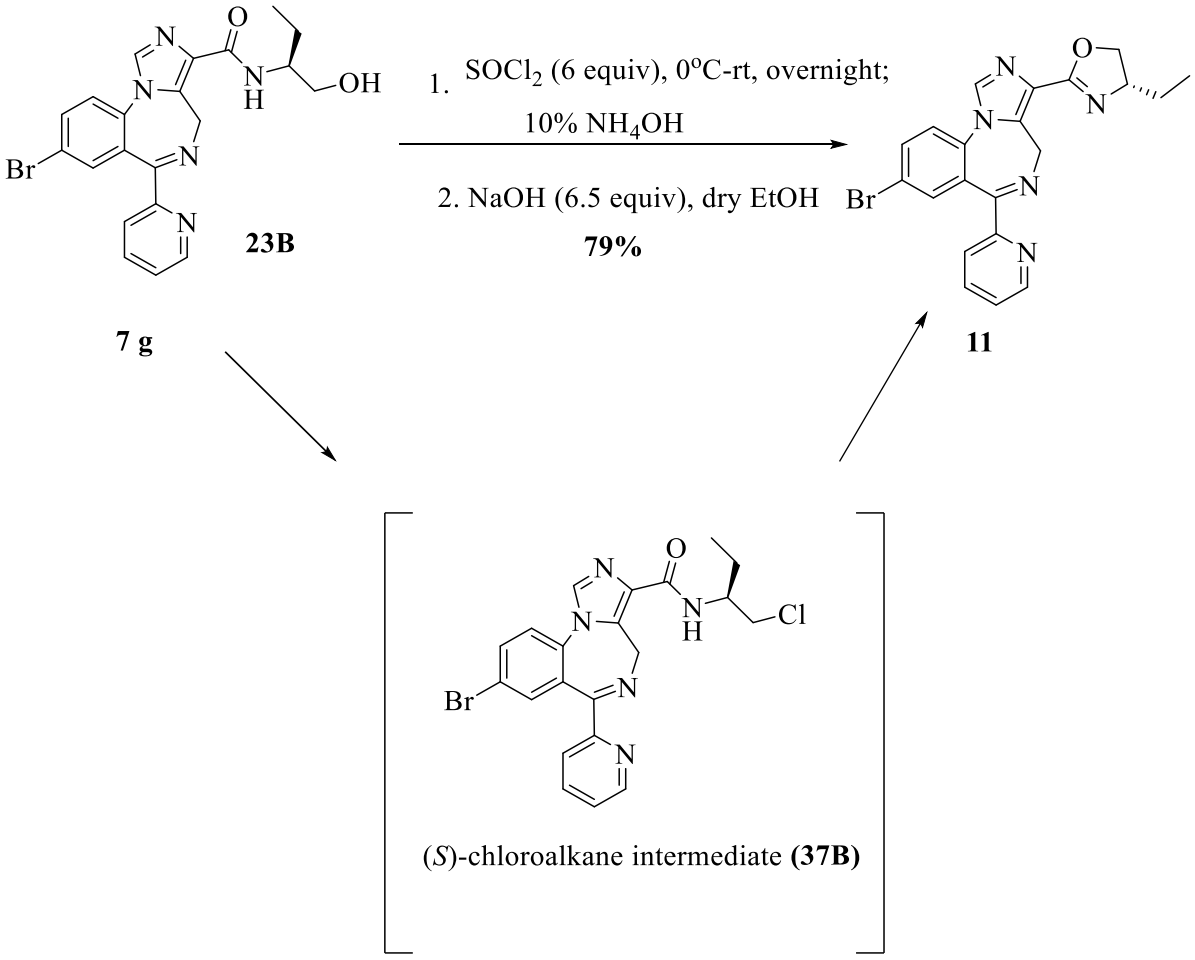
(*R*)-8-Bromo-*N*-(1-hydroxybutan-2-yl)-6-(pyridin-2-yl)-4*H*-benzo[f]imidazo[1,5-a][1,4]diazepine-3-carboxamide (23A)



23A

This enantiomer was also synthesized following the procedure for **23B** but (*R)*-2-amino-1-butanol was used instead of (*S)*-2-amino-1-butanol. The ^{1}H NMR and ^{13}C NMR spectroscopic data were identical to its enantiomer **23B.**

(*S*)-2-(8-Bromo-6-(pyridin-2-yl)-4*H*-benzo[f]imidazo[1,5-a][1,4]diazepin-3-yl)-4-ethyl-4,5-dihydrooxazole (11).



The solution of (*S*)-carboxamide **(23B)** (7 g, 0.015 mol) with stirring in CH_2Cl_2 (120 mL) was cooled to 0 °C (ice bath) and thionyl chloride (837 mg, 7.2 mmol) was added to the solution dropwise. The reaction mixture was allowed to warm to rt and then allowed to stir for 16 h. After completion of the reaction by analysis by TLC (silica gel), the reaction mixture was cooled to 0 °C and a saturated aq solution of $NaHCO_3$ (250 mL) was added slowly. At this point the solution,

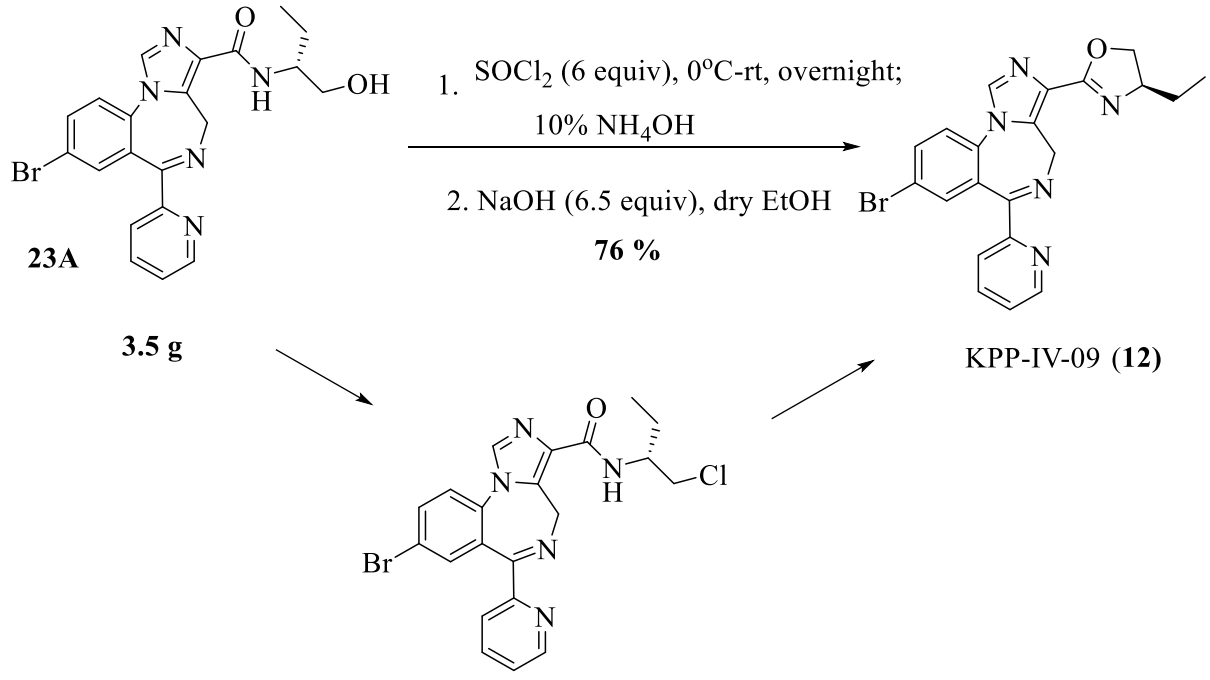
which resulted, was stirred for 30 min at 0 °C. The organic layer was separated, and the aq layer was extracted with CH_2Cl_2 (3 × 150 mL). The combined organic layer was dried (Na_2SO_4). The solvent was removed under reduced pressure, and an off-white-colored solid residue, so formed, was used directly for the next step. The crude material was dissolved in 200 proof ethanol (100 mL) and NaOH (3.9 g, 0.097mol) was added to it. The solution, which was obtained, was heated to reflux for 2 hr. The reaction mixture was cool to rt, and the ethanol was removed under reduced pressure to afford a solid residue. The solid residue, which resulted, was dissolved in CH_2Cl_2 (350 mL) and washed with a saturated aq solution of $NaHCO_3$ (200 mL). The organic layer was separated and the aq layer was extracted with CH_2Cl_2 (3 × 200 mL). The combined organic layer was dried (Na_2SO_4), and this was followed by removal of the organic solvents under reduced pressure. Finally, the crude solid was purified by crystallization (5% MeOH in EtOAc) to afford ethyl (*S)*-oxazoline as a white colored solid [(KPP-III-96B **(11)]** (5.2 g, 78%).

The characterization of the (*S)*-chloroalkane intermediate **37B**: **^{1}H NMR** (500 MHz, $CDCl_3$): δ_H 8.55 (dd, J 4.8, 1.8, 1H), 8.14 (dt, J 8.0, 1.1 Hz, 1H), 7.92 – 7.73 (m, 3H), 7.59 (d, J 2.2 Hz, 1H), 7.37-7.32 (m, 2H), 7.31 – 7.25 (m, 1H), 6.27 (d, J 12.2 Hz, 1H), 4.47 – 3.98 (m, 2H), 3.78 – 3.69 (m, 2H), 1.97 – 1.51 (m, 2H), 1.00 (d, J 9.4 Hz, 3H); **^{13}C NMR** (126 MHz, $CDCl_3$): δ_C 166.8 (s), 162.4 (s), 156.2 (s), 148.5 (s), 137.0 (s), 136.0 (s), 135.4 (s), 134.9 (s), 134.6 (s), 133.2 (s), 131.2 (s), 128.5 (s), 124.9 (s), 124.23 (s) 124.0 (s), 120.5 (s), 50.5, 47.7 (s), 44.8 (s), 24.9 (s), 10.45 (s). HRMS (ESI/IT-TOF) m/z: $[M+H]^+$ calcd for $C_{21}H_{19}N_5OClBr$ 472.0540; found 472.0531.

The characterization of KPP-III-96B **(11)**: **MP** 247-248 °C; **$[\alpha]_D^{25}$** -13.6 (c 1.0, $CHCl_3$); **^{1}H NMR** (500 MHz, $CDCl_3$): δ_H 8.55 (d, J 4.1 Hz, 1H), 8.04 (d, J 6.4 Hz, 1H), 7.89 (s, 1H), 7.79 (td, J 7.7, 1.2 Hz, 1H), 7.74 (dd, J 8.6, 2.0 Hz, 1H), 7.53 (d, J 1.9 Hz, 1H), 7.44 (d, J 8.6 Hz, 1H), 7.34 (dd, J 6.8, 5.1 Hz, 1H), 6.03 (s, 1H), 4.47 (s, 1H), 4.22 (dd, J 15.5, 7.4 Hz, 1H), 4.15 (d, J 11.6 Hz, 1H),

4.03 (t, J 7.9 Hz, 1H), 1.82 – 1.73 (m, 1H), 1.59 (dt, J 13.8, 7.1 Hz, 1H), 1.01 (s, 3H); ^{13}C NMR (126 MHz, $CDCl_3$): δ_C 167.0 (s), 158.9 (s), 156.4 (s), 148.7 (s), 136.9 (s), 135.3 (s), 135.2 (s), 134.9 (s), 134.8 (s), 134.6 (s), 128.5 (s), 127.4 (s), 124.8 (s), 124.2 (s), 124.0 (s), 120.2 (s), 72.0 (s), 68.0 (s), 45.1 (s), 28.7 (s), 10.3 (s); **HRMS** (ESI/IT-TOF) m/z: $[M + H]^+$ calcd for $C_{21}H_{18}BrN_5O$ 436.0773; found 436.0756.

(*R*)-2-(8-Bromo-6-(pyridin-2-yl)-4*H*-benzo[f]imidazo[1,5-a][1,4]diazepin-3-yl)-4-ethyl-4,5-dihydrooxazole [(KPP-IV-09 (12)].



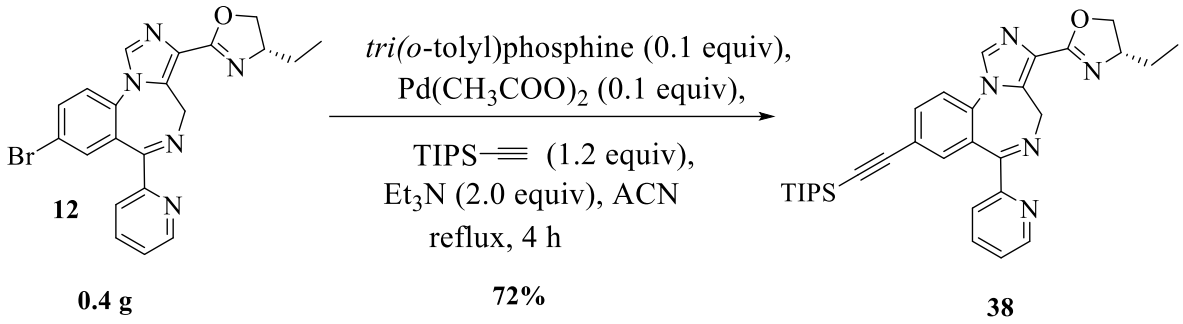
The *(R)*-oxazoline (KPP-IV-09 **(12)**) was prepared following the procedure described for *S*-oxazoline **11**. The chloroalkane intermediate, which resulted, in this process was purified by crystallization (15% DCM and hexane) to afford a yellow colored solid. The ethyl oxazoline

obtained after the cyclization was purified by precipitation (5% MeOH in EtOAc) to afford a white colored solid **12** (2.5 g, 76%).

The characterization of the (*R)*-chloroalkane intermediate **37A**: **^{1}H NMR** (500 MHz, $CDCl_3$) δ_H 8.57 (dd, J 4.9, 1.7 Hz, 1H), 8.16 (d, J 7.9 Hz, 1H), 7.93 – 7.74 (m, 3H), 7.60 (d, J 2.2 Hz, 1H), 7.44 (d, J 8.6 Hz, 1H), 7.37 (dd, J 7.5, 4.8 Hz, 1H), 7.27 (d, J 13.5 Hz, 1H), 6.29 (d, J 12.5 Hz, 1H), 4.32 (m, 1H), 4.16 (d, J 12.1 Hz, 1H), 3.79 – 3.70 (m, 2H), 2.05 – 1.37 (m, 2H), 1.02 (t, J 7.0 Hz, 3H); **^{13}C NMR** (126 MHz, $CDCl_3$) δ_C 166.7 (s), 162.4 (s), 156.2 (s), 148.5 (s), 137.0 (s), 136.0 (s), 135.4 (s), 134.9 (s), 134.6 (s), 133.2 (s), 131.4 (s), 128.8 (s), 124.6 (s), 124.2 (s), 124.0 (s), 120.5 (s), 50.5 (s), 47.7 (s), 44.81(s), 24.1 (s), 10.5 (s); **HRMS** (ESI/IT-TOF) m/z: $[M+H]^+$ calcd for $C_{21}H_{19}N_5OClBr$ 472.0540; found 472.0538.

The characterization of the (*R)*-oxazoline, KPP-IV-09 **(12)**: mp 248-249 °C (crystallized from 5% MeOH in EtOAc); $[\alpha]_D^{25}$ -10.5 (c 1.0, $CHCl_3$); **^{1}H NMR** (500 MHz, $CDCl_3$): δ_H 8.54 (d, J 4.7 Hz, 1H), 8.03 (d, J 7.8 Hz, 1H), 7.89 (s, 1H), 7.78 (td, J 7.8, 1.8 Hz, 1H), 7.73 (dd, J 8.7, 2.3 Hz, 1H), 7.53 (d, J 2.2 Hz, 1H), 7.44 (d, J 8.6 Hz, 1H), 7.33 (dd, J 7.6, 4.8 Hz, 1H), 6.03 (t, J 11.4 Hz, 1H), 4.46 (d, J 10.4 Hz, 1H), 4.25 – 4.12 (m, 2H), 4.01 (t, J 8.0 Hz, 1H), 1.76 (dt, J 14.4, 7.0 Hz, 1H), 1.59 (dt, J 13.9, 7.2 Hz, 1H), 1.00 (t, J 7.4 Hz, 3H); **^{13}C NMR** (126 MHz, $CDCl_3$): δ_C 167.0 (s), 158.9 (s), 156.4 (s), 148.1 (s), 136.9 (s), 135.2 (s), 135.2 (s), 134.9 (s), 134.8 (s), 134.6 (s), 128.5 (s), 127.4 (s), 124.8 (s), 124.3 (s), 124.0 (s), 120.2 (s), 72.0 (s), 68.0 (s), 45.1 (s), 28.5 (s), 10.4 (s). **HRMS** (ESI/IT-TOF) m/z: $[M + H]^+$ calcd for $C_{21}H_{18}BrN_5O$ 436.0773; found 436.0757. The optical rotation values of *R*-oxazoline (**12**) and *S*- oxazoline (**11**) were within the experimental error.

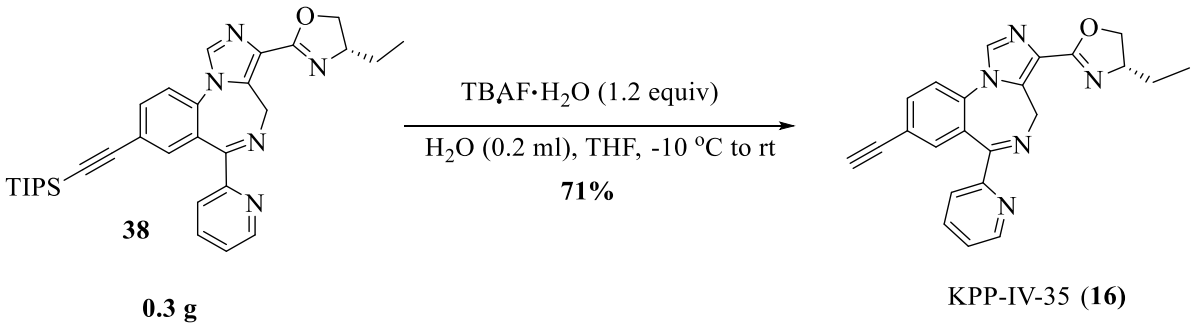
(*S*)-4-Ethyl-2-(6-(pyridin-2-yl)-8-((triisopropylsilyl)ethynyl)-4*H*-benzo[f]imidazo[1,5-a][1,4]diazepin-3-yl)-4,5-dihydrooxazole (38).



A mixture of palladium (II) acetate (26 mg, 0.09 mmol), *tri*-*O*-tolylphosphine (35 mg, 0.09 mmol) and anhydrous acetonitrile (8 mL) was allowed to stir at rt for 15 min. To the mixture, which resulted, the bromo-oxazoline **12** (4 g, 0.9 mmol), *tri*-isopropylsilylacetylene (315 mg, 1.08 mmol), and triethylamine (186 mg, 1.8 mmol) were added to the mixture. At this moment, the reaction mixture, which resulted, was allowed to heat to reflux for 4h. The progress of the reaction was monitored by analysis by TLC (neutral alumnina, EtOAc/hexane/methanol 2:1:0.5 and a few drops of 10% aq NH_4OH). The solvent was removed under reduced pressure and the residue was dissolved in CH_2Cl_2 (100 mL) and filtered through a bed of celite. The filtrate was washed with brine (70 mL) and dried (Na_2SO_4). The solvent was removed under reduced pressure and the residue was purified (to remove Pd by products) by flash column chromatography (neutral alumina, EtOAc/hexanes 2:1) to afford a light yellow colored solid **38** (355 mg, 72%): **^{1}H NMR** (500 MHz, $CDCl_3$) δ 8.59 (d, J = 4.3 Hz, 1H), 8.05 (d, J = 6.1 Hz, 1H), 7.93 (s, 1H), 7.81 (td, J = 7.8, 1.7 Hz, 1H), 7.72 (dd, J = 8.4, 1.7 Hz, 1H), 7.52 (d, J = 8.4 Hz, 1H), 7.48 (d, J = 1.7 Hz, 1H), 7.36 (ddd, J = 7.4, 4.8, 0.8 Hz, 1H), 6.04 (s, 1H), 4.49 (d, J = 4.9

Hz, 1H), 4.29 – 4.20 (m, 1H), 4.15 (dd, J = 13.9, 6.8 Hz, 1H), 4.05 (t, J = 8.0 Hz, 1H), 1.82 – 1.75 (m, 1H), 1.62 (dt, J = 13.8, 7.1 Hz, 1H), 1.11 (d, J = 3.2 Hz, 21H), 1.07 – 1.02 (m, 3H); **^{13}C NMR** (75 MHz, $CDCl_3$) δ 167.74 (s), 159.00 (s), 156.69 (s), 148.72 (s), 136.76 (s), 136.76 (s), 135.72 (s), 135.30 (s), 135.10 (s), 134.66 (s), 127.29 (s), 126.92 (s), 124.68 (s), 124.02 (s), 122.63 (s), 122.35 (s), 104.99 (s), 93.61 (s), 72.03 (s), 67.99 (s), 45.15 (s), 28.75 (s), 18.60 (s), 11.23 (s), 10.33 (s); **HRMS** (ESI/IT-TOF) m/z: $[M + H]^+$ calcd for $C_{32}H_{39}N_5OSi$ 538.2996; found 538.3018.

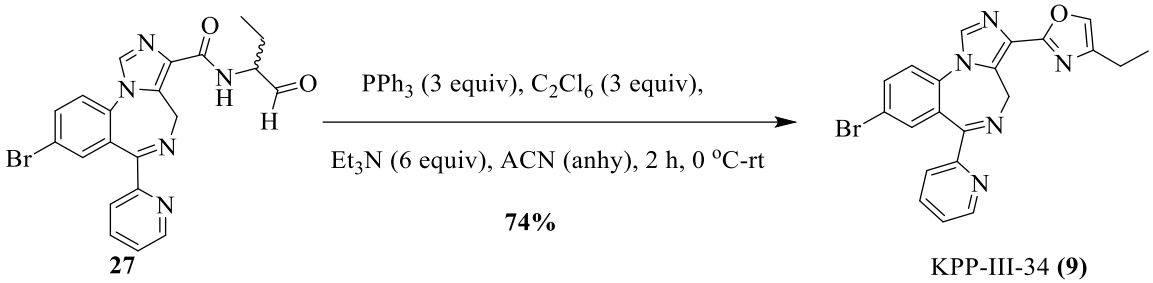
(*S*)-4-Ethyl-2-(8-ethynyl-6-(pyridin-2-yl)-4*H*-benzo[f]imidazo[1,5-a][1,4]diazepin-3-yl)-4,5-dihydrooxazole [KPP-IV-35 (16)].



To the solution of TIPS-oxazoline **38** (0.3 g, 0.55 mmol) in THF (10 mL), water (0.2 mL), and TBAF xH_2O (0.6 mL, 0.66 mmol, 1M in THF) were added dropwise at -10 °C and the mixture, which resulted, was allowed to stir at rt for 1 h. Analysis by TLC (silica gel, EtOAc/hexane/MeOH 2:1:0.5 and a few drops of 14% aq NH_4OH) indicated the disappearance of the starting material and the formation of new non-polar component. At this point, the reaction solution was quenched with water (20 mL) and then diluted with EtOAc (50 mL). The organic layer was separated, as well as washed with brine (50 mL), and dried (Na_2SO_4). The solvents

were removed under reduced pressure and the residue, which resulted, was purified by precipitation (CH_2Cl_2, EtOAc, and hexane (2:7:1) to provide KPP-IV-35 **(16)** as an off-white colored solid (150 mg, 71%): **^{1}H NMR** (500 MHz, $CDCl_3$) δ 8.55 (d, J = 4.3 Hz, 1H), 8.02 (d, J = 7.0 Hz, 1H), 7.90 (s, 1H), 7.78 (td, J = 7.8, 1.4 Hz, 1H), 7.72 (dd, J = 8.3, 1.6 Hz, 1H), 7.52 (dd, J = 8.8, 4.9 Hz, 2H), 7.33 (dd, J = 6.8, 5.1 Hz, 1H), 7.26 (s, 1H), 6.03 (s, 1H), 4.47 (s, 1H), 4.26 – 4.19 (m, 1H), 4.13 (m, J = 17.6, 10.0 Hz, 1H), 4.02 (t, J = 8.0 Hz, 1H), 3.13 (s, 1H), 1.77 (m, J = 13.1, 6.5 Hz, 1H), 1.66 – 1.54 (m, 1H), 1.01 (t, J = 7.1 Hz, 3H); **^{13}C NMR** (126 MHz, $CDCl_3$) δ 167.78 (s), 159.07 (s), 156.78 (s), 148.89 (s), 136.93 (s), 136.35 (s), 135.88 (s), 135.37 (s), 135.33 (s), 134.80 (s), 127.50 (s), 127.13 (s), 124.83 (s), 124.13 (s), 122.91 (s), 121.00 (s), 81.89 (s), 79.42 (s), 72.16 (s), 68.12 (s), 45.27 (s), 28.87 (s), 10.47 (s); **HRMS** (ESI/IT-TOF) m/z: $[M + H]^+$ calcd for $C_{23}H_{19}N_5O$ 382.1662; found 382.1675.

2-(8-Bromo-6-(pyridin-2-yl)-4*H*-benzo[f]imidazo[1,5-a][1,4]diazepin-3-yl)-4-ethyloxazole [(KPP-III-34 (9)].



27

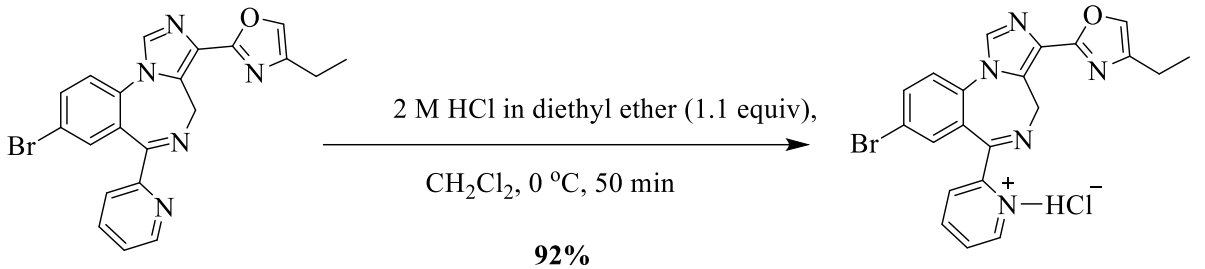
14.4 g

KPP-III-34 **(9)**

The general procedure for the synthesis of KPP-III-34 **(9)** was published by Pandey *et*. al. in 2020 [26]. The hexachloroethane (22.6 g, 0.09 mol) was dissolved in anhydrous acetonitrile (400 mL) and stirred until complete dissolution of the hexachloroethane in the solvent. Then *rac*-

carboxamide **27** (14.4 g, 0.031 mol) was added to the above solution, with stirring, in one portion. The mixture, which resulted, was cooled to 0 °C (ice bath), and triethylamine (19.3 g, 0.5 mol) was added dropwise. At this point, triphenylphosphine (25 g, 0.9 mol) was added into the reaction mixture in three portions over 30 min. After the third addition, the ice bath was removed after 10 min of stirring at 0 °C, and the reaction mixture was allowed to warm to rt and it was stirred for an additional 2 h. It was observed that the light-yellow colored solution gradually changed into a dark brown color. The reaction progress was monitored by analysis by TLC (silica gel, EtOAc/hexane/ methanol 2:1:0.5 and a few drops of 14% aq NH_4OH). After the completion of the reaction, water (200 mL) was added and the aq layer was extracted with ethyl acetate (2 x 300 mL). The combined organic layer was washed with brine (300 mL) and dried (Na_2SO_4). The solvents were reduced to 1/3rd of the original volume and the oxazole was purified by precipitation (15 % MeOH in EtOAc) to afford a light yellow colored solid. The solid was dried under vacuum at 40 °C to provide a light yellow colored solid of KPP-III-34 **(9)** (10.2 g, 74%): **MP** 246-247 °C; **^{1}H NMR** (500 MHz, $CDCl_3$) δ_H 8.59 – 8.52 (m, 1H), 8.06 (d, J 7.9 Hz, 1H), 7.96 (s, 1H), 7.86 – 7.73 (m, 2H), 7.55 (d, J 2.2 Hz, 1H), 7.48 (d, J 8.6 Hz, 1H), 7.40 (s, 1H), 7.37-7.32 (m, 1H), 6.14 (d, J 12.7 Hz, 1H), 4.25 (d, J 13.1 Hz, 1H), 2.62 (q, J 7.5 Hz, 2H), 1.27 (t, J 7.5 Hz, 3H); **^{13}C NMR** (126 MHz, $CDCl_3$) δ_C 167.5 (s), 157.0 (s), 156.7 (s), 149.0 (s), 144.1 (s), 137.3 (s), 135.7 (s), 135.4 (s), 135.3 (s), 135.2 (s), 133.2 (s), 133.1 (s), 128.9 (s), 128.0 (s), 125.3 (s), 124.6 (s), 124.4 (s), 120.7 (s), 45.4 (s), 20.3 (s), 13.0 (s); **HRMS** (ESI/IT-TOF) m/z: $[M + H]^+$ Calcd for $C_{21}H_{16}N_5OBr$ 434.0616; found 434.0596.

Preparation of (2-(8-bromo-3-(4-ethyloxazol-2-yl)-4*H*-benzo[f]imidazo[1,5-a][1,4]diazepin-6-yl)pyridin-1-ium-1-yl)hydridochlorate(I) (KPP-III-34·HCl salt) (17).



KPP-III-34 **(9)**

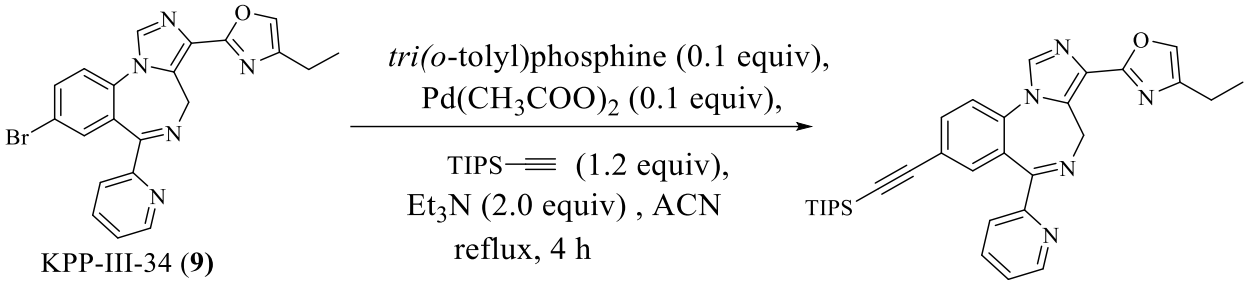
0.5 g

KPP-III-34.HCl salt (**17**)

The cloudy suspension of KPP-III-34 **(9)** (0.5 g, 1.15 mmol) in CH_2Cl_2 (10 mL) was cooled to 0 °C (ice bath) and 2 M HCl in diethyl ether (0.25 mL) was added dropwise into it. It was observed that the cloudy suspension of starting material in CH_2Cl_2 gradually turned into a colorless solution during the addition of 2 M HCl in ether dropwise, with stirring. The solution, which resulted, was stirred for an additional 35 min at 0 °C and then was allowed to warm to rt. At this point, the solution was filtered through filter paper to remove any trace amount of undissolved starting material. The organic solvents (filtrate) were removed under the reduced pressure. The excess of HCl was removed by adding CH_2Cl_2 (15 mL) and removing it under reduced pressure. This process was repeated 4 times to ensure the complete removal of HCl in order to provide an off-white colored solid [(KPP-III-34·HCl salt (**17**)] (498 mg, 92%): **^{1}H NMR** (500 MHz, DMSO-d^6) δ 8.73 (s, 1H), 8.68 (d, J = 4.4 Hz, 1H), 8.20 (t, J = 7.5 Hz, 1H), 8.05 (dd, J = 11.1, 4.5 Hz, 2H), 7.92 (t, J = 4.1 Hz, 2H), 7.75 (t, J = 5.3 Hz, 2H), 5.95 (s, 1H), 4.47 (s, 1H), 2.57 (q, J = 7.4 Hz, 2H), 1.22 (t, J = 7.5 Hz, 3H); **^{13}C NMR** (126 MHz, DMSO) δ 165.52 (s), 155.96 (s), 153.08 (s), 147.10 (s), 143.35 (s), 141.00 (s), 137.10 (s), 135.97 (s), 134.94 (s), 134.37 (s), 132.85 (s),

129.19 (s), 127.64 (s), 126.98 (s), 126.16 (s), 125.90 (s), 125.47 (s), 120.25 (s), 44.66 (s), 19.71 (s), 13.08 (s).

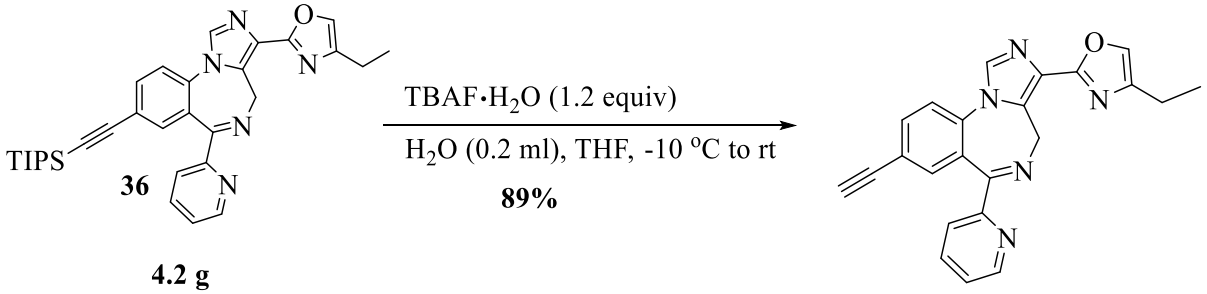
4-Ethyl-2-(6-(pyridin-2-yl)-8-((triisopropylsilyl)ethynyl)-4*H*-benzo[f]imidazo[1,5-a][1,4]diazepin-3-yl)oxazole (36).



A mixture of palladium (II) acetate (206 mg, 0.9 mmol), *tri*-*O*-tolylphosphine (280 mg, 0.9 mmol) and anhydrous acetonitrile (55 mL) was allowed to stir at rt for 15 min. To the mixture, which resulted, the bromide **9** (4 g, 9.2 mmol), triisopropylsilylacetylene (201 mg, 1.1 mmol), and triethylamine (1.8 g, 1.4 mmol) were added to the mixture. The reaction mixture, which resulted, was heated for 4h. The progress of reaction was monitored by analysis of TLC (silica gel, EtOAc/hexane/methanol 2:1:0.5 and a few drops of triethylamine). The solvent was then removed under reduced pressure and the residue, which resulted, was dissolved in CH_2Cl_2 (200 mL) and filtered through a bed of celite. The filtrate was washed with brine (150 mL), and dried (Na_2SO_4). The organic solvent was removed under reduced pressure and the residue was purified by flash column chromatography (silica gel, EtOAc/hexanes 3:1 with 3% triethylamine) to afford a light yellow colored solid **36**: **^{1}H NMR** (500 MHz, $CDCl_3$): δ_H 8.60 – 8.56 (m, 1H), 8.07 – 8.03 (m, 1H), 7.80 (td, J 7.7, 1.8 Hz, 2H), 7.72 (dd, J 8.3, 1.9 Hz, 1H), 7.53 (d, J 8.3 Hz, 1H), 7.47 (d, J 1.8

Hz, 1H), 7.40 (d, J 1.4 Hz, 1H), 7.36 (ddd, J 7.5, 4.8, 1.3 Hz, 1H), 6.21 – 6.04 (m, 1H), 4.25 (s, 1H), 2.62 (dd, J 7.5, 1.3 Hz, 2H), 1.27 (t, J 7.5 Hz, 3H), 1.10 (d, J 3.5 Hz, 21H); **^{13}C NMR** (126 MHz, $CDCl_3$): δ_C 167.8 (s), 156.7 (s), 156.5 (s), 148.7 (s), 143.7 (s), 136.9 (s), 135.8 (s), 135.5 (s), 135 (s), 134.9 (s), 132.9 (s), 132.7 (s), 127.6 (s), 126.9 (s), 124.8 (s), 124.1 (s), 122.7 (s), 122.5 (s), 104.9 (s), 93.7 (s), 45.0 (s), 19.9 (s), 18.6 (s), 12.7 (s), 11.24 (s). **HRMS** (ESI/IT-TOF) m/z: $[M + H]^+$ calcd for $C_{32}H_{37}N_5OSi$ 536.2846; found 536.2855.

4-Ethyl-2-(8-ethynyl-6-(pyridin-2-yl)-4*H*-benzo[f]imidazo[1,5-a][1,4]diazepin-3-yl)oxazole (10).



To the solution of TIPS-oxazole **36** (4.2 g, 7.8 mmol) in THF (50 mL), were added water (0.5 mL) and TBAF xH_2O (8.4 mL, 9.36 mmol, 1M in THF) dropwise at -10 °C. The reaction mixture, which resulted, was allowed to warm to rt and stirred at rt for an additional 1 h. The analysis by TLC (silica gel, EtOAc/hexane/MeOH 2:1:0.5 and a few drops of 14% aq NH_4OH) indicated the disappearance of starting material. At this point, the reaction solution was quenched with water (20 mL) and then diluted with EtOAc (50 mL). The organic layer was separated and washed with

brine (50 mL), and dried (Na_2SO_4). The solvents were removed under reduced pressure and the residue, which resulted, was purified using flash column chromatography (silica gel, EtOAc/hexane 2:1 and 3% triethylamine) to afford a light yellow colored 8-ethynyl, ethyl oxazole [KPP-III-51 (**10**)] solid, which was dried under vacuum at 40 °C (2.6 g, 89%): **MP** 240-241 °C (crystallized from EtOAc); **^{1}H NMR** (500 MHz, $CDCl_3$): δ_H 8.60 (d, J 4.8, 1.3 Hz, 1H), 8.08 (d, 1H), 8.01 (s, 1H), 7.83 (td, J 7.7, 1.8 Hz, 1H), 7.77 (dd, J 8.4, 1.9 Hz, 1H), 7.61 (d, 1H), 7.78 – 7.76 (dd, 1H), 7.43 (s, 1H), 7.4-7.32 (m, 1H), 6.18 (br, 1H), 4.29 (br, 1H), 3.17 (s, 1H), 2.65 (m, J 7.5, 1.2 Hz, 2H), 1.42 – 1.26 (t, 3H); **^{13}C NMR** (126 MHz, $CDCl_3$): δ_C 167.0 (s), 156.0 (s), 156.4 (s), 148.0 (s), 143.1 (s), 137.7 (s), 136.2 (s), 135.7 (s), 135.4 (s), 134.9 (s), 132.8 (s), 132.7 (s), 127.5 (s), 126.9 (s), 124.8 (s), 123.1 (s), 122.8 (s), 121 (s), 81.1 (s), 78.8 (s), 45.0 (s), 19.9 (s), 12.6 (s). **HRMS** (ESI/IT-TOF) m/z: $[M + H]^+$ calcd for $C_{23}H_{17}N_5O$ 380.1506; found 380.1478.

References

1. Zhu, S.; Noviello, C. M.; Teng, J.; Walsh, R. M., Jr.; Kim, J. J.; Hibbs, R. E., Structure of a human synaptic GABA(A) receptor. *Nature* **2018,** *559,* 67-72.

2. Ghit, A.; Assal, D.; Al-Shami, A. S.; Hussein, D. E. E., GABA(A) receptors: structure, function, pharmacology, and related disorders. *J. Genet. Eng. Biotechnol.* **2021,** *19,* 123.

3. López-Muñoz, F.; Alamo, C.; García-García, P., The discovery of chlordiazepoxide and the clinical introduction of benzodiazepines: half a century of anxiolytic drugs. *J. Anxiety Disord.* **2011,** *25*, 554-562.

4. Nutt, D. J.; Malizia, A. L., New insights into the role of the GABAA–benzodiazepine receptor in psychiatric disorder. *Br. J. Psychiatry* **2018,** *179,* 390-396.

5. Terunuma, M., Diversity of structure and function of GABA(B) receptors: a complexity of GABA(B)-mediated signaling. *Proc. Jpn. Acad., Ser. B. Phys.* **2018,** *94*, 390-411.

6. Gomes, F. I. F.; Aragão, M. G. B.; Bezerra, M. M.; Chaves, H. V., GABAergic transmission and modulation of anxiety: a review on molecular aspects. *Braz. J. Bio. Sci.* **2019,** *6,* 9-16.

7. Mortensen, M.; Patel, B.; Smart, T., GABA potency at GABAA receptors found in synaptic and extrasynaptic zones. *Front. Cell. Neurosci.* **2012,** 6.

8. Masiulis, S.; Desai, R.; Uchański, T.; Serna Martin, I.; Laverty, D.; Karia, D.; Malinauskas, T.; Zivanov, J.; Pardon, E.; Kotecha, A.; Steyaert, J.; Miller, K. W.; Aricescu, A. R.,

GABA(A) receptor signalling mechanisms revealed by structural pharmacology. *Nature* **2019,** *565*, 454-459.

9. Zahn, N. M.; Huber, A. T.; Mikulsky, B. N.; Stepanski, M. E.; Kehoe, A. S.; Li, G.; Schussman, M.; Rashid Roni, M. S.; Kodali, R.; Cook, J. M.; Stafford, D. C.; Steeber, D. A.; Arnold, L. A., MIDD0301 - A first-in-class anti-inflammatory asthma drug targets GABA(A) receptors without causing systemic immune suppression. *Basic Clin. Pharmacol. Toxicol.* **2019,** *125*, 75-84.

10. Gallos, G.; Yocum, G. T.; Siviski, M. E.; Yim, P. D.; Fu, X. W.; Poe, M. M.; Cook, J. M.; Harrison, N.; Perez-Zoghbi, J.; Emala, C. W., Sr., Selective targeting of the alpha5-subunit of GABAA receptors relaxes airway smooth muscle and inhibits cellular calcium handling. *Am. J. Physiol. Lung. Cell. Mol. Physiol.* **2015,** *308*, L931-42.

11. Griffin, C. E., 3rd; Kaye, A. M.; Bueno, F. R.; Kaye, A. D., Benzodiazepine pharmacology and central nervous system-mediated effects. *Ochsner J.* **2013,** *13*, 214-23.

12. Witkin, J. M.; Pandey, K. P.; Smith, J. L., Clinical investigations of compounds targeting metabotropic glutamate receptors. *Pharmacol. Bio. Behav.* **2022,** *219*, 173446.

13. Calcaterra, N. E.; Barrow, J. C., Classics in chemical neuroscience: diazepam (valium). *ACS Chem. Neurosci.* **2014,** *5*, 253-260.

14. Poe, M. M.; Methuku, K. R.; Li, G.; Verma, A. R.; Teske, K. A.; Stafford, D. C.; Arnold, L. A.; Cramer, J. W.; Jones, T. M.; Cerne, R., Synthesis and characterization of a novel γ-aminobutyric acid type A (GABAA) receptor ligand that combines outstanding metabolic stability, pharmacokinetics, and anxiolytic efficacy. *J. Med. Chem.* **2016,** *59*, 10800-10806.

15. Tan, K. R.; Rudolph, U.; Lüscher, C., Hooked on benzodiazepines: GABAA receptor subtypes and addiction. *Trends. Neuro.* **2011,** *34*, 188-97.

16. Ait-Daoud, N.; Hamby, A. S.; Sharma, S.; Blevins, D., A review of alprazolam use, misuse, and withdrawal. *J. Addict. Med.* **2018,** *12*, 4-10.

17. Witkin, J. M.; Methuku, K. R.; McDermott, J.; Cerne, R.; Gleason, S.; Cramer, J.; Jones, T. M.; Catlow, J.; Poe, M.; Li, G.; Arnold, L. A.; Ping, X.; Jin, X.; Hobbs, J.; Smith, J. L.; Schkeryantz, J., 5-(8-Ethynyl-6-(Pyridin-2-yl)-4H-benzo[f] imidazo [1,5a] [,4] diazepine-3-yl) oxazole (KRM-II-81) is a novel alpha 2,3- selective potentiator of GABAA receptors: improved bioavailability enhances anticonvulsent effcacy. *Neuropharmacology, (Submitted)* **2018**.

18. Mian, M. Y.; Divović, B.; Sharmin, D.; Pandey, K. P.; Golani, L. K.; Tiruveedhula, V.; Cerne, R.; Smith, J. L.; Ping, X.; Jin, X.; Imler, G. H.; Deschamps, J. R.; Lippa, A.; Cook, J. M.; Savić, M. M.; Rowlett, J.; Witkin, J. M., Hydrochloride salt of the GABAkine KRM-II-81. *ACS omega* **2022,** *7*, 27550-27559.

19. Golani, L. K.; Yeunus Mian, M.; Ahmed, T.; Pandey, K. P.; Mondal, P.; Sharmin, D.; Rezvanian, S.; Witkin, J. M.; Cook, J. M., Rationalizing the binding and α subtype selectivity of synthesized imidazodiazepines and benzodiazepines at GABAA receptors by using molecular docking studies. *Bioorganic Med. Chem.y Lett.* **2022,** *62*, 128637.

20. Fischer, B. D.; Licata, S. C.; Edwankar, R. V.; Wang, Z.-J.; Huang, S.; He, X.; Yu, J.; Zhou, H.; Johnson Jr, E. M.; Cook, J. M., Anxiolytic-like effects of 8-acetylene imidazobenzodiazepines in a rhesus monkey conflict procedure. *Neuropharmacology* **2010,** *59*, 612-618.

21. Knutson, D. E.; Kodali, R.; Divović, B.; Treven, M.; Stephen, M. R.; Zahn, N. M.; Dobričić, V.; Huber, A. T.; Meirelles, M. A.; Verma, R. S., Design and synthesis of novel deuterated ligands functionally selective for the γ-aminobutyric acid type A receptor (GABAAR) α6 subtype with improved metabolic stability and enhanced bioavailability. *J. Med. Chem.* **2018,** 61, 2422-2446.

22. Witkin, J. M.; Lippa, A.; Smith, J. L.; Jin, X.; Ping, X.; Biggerstaff, A.; Kivell, B. M.; Knutson, D. E.; Sharmin, D.; Pandey, K. P.; Mian, M. Y.; Cook, J. M.; Cerne, R., The imidazodiazepine, KRM-II-81: An example of a newly emerging generation of GABAkines for neurological and psychiatric disorders. *Pharmacol. Bio. Behav.* **2022,** *213*, 173321.

23. Biggerstaff, A.; Kivell, B.; Smith, J. L.; Mian, M. Y.; Golani, L. K.; Rashid, F.; Sharmin, D.; Knutson, D. E.; Cerne, R.; Cook, J. M.; Witkin, J. M., The α2,3-selective potentiators of GABAA receptors, KRM-II-81 and MP-III-80, produce anxiolytic-like effects and block chemotherapy-induced hyperalgesia in mice without tolerance development. *Pharmacol. Bio. Behav.* **2020**, *196*, 172996.

24. Knutson, D. E.; Smith, J. L.; Ping, X.; Jin, X.; Golani, L. K.; Li, G.; Tiruveedhula, V. V. N. P. B.; Rashid, F.; Mian, M. Y.; Jahan, R.; Sharmin, D.; Cerne, R.; Cook, J. M.; Witkin, J. M., Imidazodiazepine anticonvulsant, KRM-II-81, produces novel, non-diazepam-like antiseizure effects. *ACS Chem.l Neurosci.***2020,** *11*, 2624-2637.

25. Poe, M. M.; Methuku, K. R.; Li, G.; Verma, A. R.; Teske, K. A.; Stafford, D. C.; Arnold, L. A.; Cramer, J. W.; Jones, T. M.; Cerne, R.; Krambis, M. J.; Witkin, J. M.; Jambrina, E.; Rehman, S.; Ernst, M.; Cook, J. M.; Schkeryantz, J. M., Synthesis and characterization of

a novel γ-aminobutyric Acid Type A (GABAA) receptor ligand that combines outstanding metabolic stability, pharmacokinetics, and anxiolytic efficacy. *J. Med. Chem.* **2016,** *59*, 10800-10806.

26. Pandey, K. P.; Khan, Z. A.; Golani, L. K.; Mondal, P.; Mian, Y.; Rashid, F.; Tiruveedhula, V.; Knutson, D. E.; Sharmin, D.; Ahmed, T.; Rezvanian, S.; Zahn, N. M.; Arnold, L. A.; Witkin, J. M.; Cook, J. M., Design, synthesis and characterization of novel gamma-aminobutyric acid type A receptor ligands. *Arkivoc*, **2020,** (Pt 7), 242-256.

27. Wipf, P.; Venkatraman, S., An improved protocol for azole synthesis with PEG-supported burgess reagent. *Tetrahedron Lett.* **1996,** *37*, 4659-4662.

28. Wipf, P.; Miller, C. P., A New Synthesis of Highly Functionalized Oxazoles. *J. Org. Chem.* **1993,** *58*, 3604-3606.

29. Morwick, T.; Hrapchak, M.; DeTuri, M.; Campbell, S., A practical approach to the synthesis of 2,4-disubstituted oxazoles from amino acids. *Org Lett* **2002,** 4, (16), 2665-8.

30. Zhang, Y.-K.; Plattner, J. J.; Easom, E. E.; Jacobs, R. T.; Guo, D.; Sanders, V.; Freund, Y. R.; Campo, B.; Rosenthal, P. J.; Bu, W.; Gamo, F.-J.; Sanz, L. M.; Ge, M.; Li, L.; Ding, J.; Yang, Y., Benzoxaborole antimalarial Agents. Part 4. discovery of potent 6-(2-(alkoxycarbonyl)pyrazinyl-5-oxy)-1,3-dihydro-1-hydroxy-2,1-benzoxaboroles. *J. Med. Chem.y* **2015,** *58*, 5344-5354.

31. Tosaki, S.-y.; Tsuji, R.; Ohshima, T.; Shibasaki, M., Dynamic ligand exchange of the lanthanide complex leading to structural and functional transformation: one-pot sequential catalytic asymmetric epoxidation-regioselective epoxide-opening process. *J. Am. Chem. Soc.* **2005,** *127*, 2147-2155.

32. Gou, D. M.; Liu, Y. C.; Chen, C. S., A practical chemoenzymic synthesis of the taxol C-13 side chain N-benzoyl-(2R,3S)-3-phenylisoserine. *J. Org. Chem.* **1993,** *58,* 1287-1289.

33. Trott, O.; Olson, A. J., AutoDock Vina: improving the speed and accuracy of docking with a new scoring function, efficient optimization, and multithreading. *J. Comput. Chem.* **2010,** *31*, 455-461.

34. Shinada, N. K.; de Brevern, A. G.; Schmidtke, P., Halogens in Protein-Ligand Binding Mechanism: A Structural Perspective. *J. Med. Chem.* **2019,** *62*, 9341-9356.

35. Khan, Z. A. Approach Toward the Total Synthesis of Some Sarpagine Related Indole Alkaloids: Histrixnine, Gelsempervine A, Gelsempervine B, O-Methylmacusine B & 19,20-Dihydro-O-Methylmacusine B,Design, Synthesis & Biological Study of Some Novel Gamma-Aminobutyric Acid Type (GABAA) Receptor Ligands. PhD thesis. University of Wisconsin-Milwaukee. 2021.

36. Curia, G.; Lucchi, C.; Vinet, J.; Gualtieri, F.; Marinelli, C.; Torsello, A.; Costantino, L.; Biagini, G., Pathophysiogenesis of mesial temporal lobe epilepsy: is prevention of damage antiepileptogenic? *Curr. Med. Chem.* **2014,** *21,* 663-688.

37. Alexeev, M.; Grosenbaugh, D. K.; Mott, D. D.; Fisher, J. L., The natural products magnolol and honokiol are positive allosteric modulators of both synaptic and extra-synaptic GABAA receptors. *Neuropharmacology* **2012,** *62,* 2507-2514.

38. Gee, K. W.; Tran, M. B.; Hogenkamp, D. J.; Johnstone, T. B.; Bagnera, R. E.; Yoshimura, R. F.; Huang, J. C.; Belluzzi, J. D.; Whittemore, E. R., Limiting activity at beta1-subunit-containing GABAA receptor subtypes reduces ataxia. *J. Pharmacol. Exp. Ther.* **2010,** *332*, 1040-53.

39. Watanabe, T.; Schulz, D.; Morisseau, C.; Hammock, B. D., High-throughput pharmacokinetic method: Cassette dosing in mice associated with minuscule serial bleedings and LC/MS/MS analysis. *Analytica. Chimica. Acta.* **2006,** *559*, 37-44.

40. Nagilla, R.; Nord, M.; Mcatee, J. J.; Jolivette, L. J., Cassette dosing for pharmacokinetic screening in drug discovery: comparison of clearance, volume of distribution, half-life, mean residence time, and oral bioavailability obtained by cassette and discrete dosing in rats. *J. Pharma. Sci.* **2011,** *100*, 3862-3874.

41. Chang, A. K.; Shinnar, S., Nonconvulsive status epilepticus. *Emerg. Med. Clin. N.* **2011,** *29*, 65-72.

42. Li, G.; Stephen, M. R.; Kodali, R.; Zahn, N. M.; Poe, M. M.; Babu, V. P.; Cooka, J. M., Synthesis of chiral GABAA receptor subtype selective ligands as potential agents to treat schizophrenia as well as depression. *Arkivoc,* **2018**, (part iv), 158-182.

43. Mathiasen, J. R.; Moser, V. C., The Irwin test and functional observational battery (FOB) for sssessing the effects of compounds on behavior, physiology, and safety pharmacology in rodents. *Curr. Protoc. Pharmacol.* **2018,** *83*, e43.

44. Metcalf, C. S.; Huff, J.; Thomson, K. E.; Johnson, K.; Edwards, S. F.; Wilcox, K. S., Evaluation of antiseizure drug efficacy and tolerability in the rat lamotrigine-resistant amygdala kindling model. *Epilepsia. open.* **2019,** *4*, 452-463.

Appendix A (Part I)

Single-crystal X-ray Diffraction Analysis of KPP-II-50 (Cook196) Pentacyclic ketone (28)

Acknowledge

The X-ray crystallographic work was supported by the Office of Naval Research (Award No. N00014-15-WX-0-0149). A clear colorless plate crystal of dimensions 0.330 x 0.270 x 0.088 mm was mounted on a MiteGen MicroMesh using a small amount of Cargille Immersion Oil. Data were collected on a Bruker three-circle platform diffractometer equipped with a PHOTON II CPAD detector. The crystals were irradiated using a 1μs microfocus CuK_α source ($\lambda = 1.54178$) with Montel optics. Data was collected at room temperature (20°C).

Data collection was performed, and the unit cell was initially refined using APEX3 [v2015.5-2].[1] Data Reduction was performed using SAINT [v8.34A][2] and XPREP [v2014/2][3]. Corrections were applied for Lorentz, polarization, and absorption effects using SADABS [v2014/2].[4] The structure was solved and refined with the aid of the program SHELXL-2014/7.[5] The full-matrix least-squares refinement on F^2 included atomic coordinates and anisotropic thermal parameters for all non-H atoms. Hydrogen atoms were located from the difference electron-density maps and added using a riding model.

1. Bruker (2015). APEX3 v2015.5-2. Bruker AXS Inc., Madison, Wisconsin, USA.
2. Bruker (2013). SAINT v8.34A. Bruker AXS Inc., Madison, Wisconsin, USA.
3. Bruker (2014). XPREP v2014/2. Bruker AXS Inc., Madison, Wisconsin, USA.

4. Bruker (2014). SADABS v2014/5, Bruker AXS Inc., Madison, Wisconsin, USA.
5. Sheldrick, G. M. (2014). SHELXL-2014/7. University of Göttingen, Germany.

$C_{19}H_{20}N_2O$, FW = 292.37, monoclinic of KPP-II-50, $P2_1$, a = 10.3448(2) Å, b = 7.8977(2) Å, c = 10.7674(2) Å, α = 90°, β = 117.6662(4)°, γ = 90°, V = 779.12(3) Å^3, Z = 2, ρ_{calc} (293K) = 1.246 Mg/m^3, μ = 0.609 mm^{-1}, F(000) = 312, R_1 = 0.0300 for 3148 observed ($I > 2\sigma I$) reflections and 0.0301 for all 3160 reflections, Goodness-of-fit = 1.022, 201 parameters.

Single-crystal X-ray Diffraction Analysis of KPP-II-43.

$C_{19}H_{20}N_2O$, FW = 292.37, monoclinic, $P2_1$, a = 8.7184(3) Å, b = 8.4717(3) Å, c = 10.3859(3) Å, α = 90°, β = 92.9370(10)°, γ = 90°, V = 766.09(4) Å^3, Z = 2, ρ_{calc} (298 K) = 1.267 Mg/m^3, μ = 0.079 mm^{-1}, *F*(000) = 312, R_1 = 0.0340 for XXXX observed ($I > 2\sigma I$) reflections and 0.0368 for all XXXX reflections, Goodness-of-fit = 0.916, 201 parameters.

An irregular colorless crystal of dimensions 0.452 x 0.355 x 0.272 mm^2 was mounted on a MiteGen MicroMesh using a small amount of Cargille Immersion Oil. Data were collected on a Bruker three-circle platform diffractometer equipped with a SMART APEX II CCD detector. The crystals were irradiated using graphite monochromated MoK_α radiation (λ= 0.71073)].

Data collection was performed, and the unit cell was initially refined using *APEX3* [v2015.5-2].[1] Data Reduction was performed using *SAINT* [v8.34A][2] and *XPREP* [v2014/2][3]. Corrections were applied for Lorentz, polarization, and absorption effects using *SADABS* [v2014/2].[4] The structure was solved and refined with the aid of the programs SHELXL-2014/7 within WingX.[5,6] The full-matrix least-squares refinement on F^2 included atomic coordinates and

anisotropic thermal parameters for all non-H atoms. The H atoms were included using a riding model.

6. Bruker (2015). APEX3 v2015.5-2. Bruker AXS Inc., Madison, Wisconsin, USA.
7. Bruker (2013). SAINT v8.34A. Bruker AXS Inc., Madison, Wisconsin, USA.
8. Bruker (2014). XPREP v2014/2. Bruker AXS Inc., Madison, Wisconsin, USA.
9. Bruker (2014). SADABS v2014/5, Bruker AXS Inc., Madison, Wisconsin, USA.
10. Sheldrick, G. M. (2014). SHELXL-2014/7. University of Göttingen, Germany.
11. Farrugia, L. J. (2012). J. Appl. Cryst. 45, 849-854.

Table A1. Crystal data and structure refinement for KPP-II-50 (**28**)

Identification code	cook196	
Empirical formula	$C_{19}H_{20}N_2O$	
Formula weight	292.37	
Temperature	293(2) K	
Wavelength	1.54178 Å	
Crystal system	Monoclinic	
Space group	$P2_1$	
Unit cell dimensions	a = 10.3448(2) Å	α= 90°.
	b = 7.8977(2) Å	β= 117.6662(4)°.
	c = 10.7674(2) Å	γ = 90°.

Volume	779.12(3) $Å^3$
Z	2
Density (calculated)	1.246 Mg/m^3
Absorption coefficient	0.609 mm^{-1}
F(000)	312
Crystal size	0.330 x 0.270 x 0.088 mm^3
Theta range for data collection	4.637 to 74.631°.
Index ranges	-12<=h<=12, -9<=k<=9, -13<=l<=13
Reflections collected	17046
Independent reflections	3160 [R_{int} = 0.0234]
Completeness to theta = 67.679°	99.1 %
Refinement method	Full-matrix least-squares on F^2
Data / restraints / parameters	3160 / 1 / 201
Goodness-of-fit on F^2	1.022
Final R indices [I>2sigma(I)]	R_1 = 0.0300, wR_2 = 0.0830
R indices (all data)	R_1 = 0.0301, wR_2 = 0.0831
Absolute structure parameter	0.07(4)
Largest diff. peak and hole	0.156 and -0.117 $e.Å^{-3}$

Table A2. Atomic coordinates (x 10^4) and equivalent isotropic displacement parameters ($Å^2$x 10^3) for KPP-II-50. U(eq) is defined as one third of the trace of the orthogonalized U^{ij} tensor.

	x	y	z	U(eq)

N(1)	8010(2)	4675(2)	6899(2)	46(1)
C(2)	6675(2)	4951(2)	6856(2)	38(1)
C(3)	5442(2)	3716(2)	6239(2)	36(1)
N(4)	4096(1)	4609(2)	6031(1)	36(1)
C(5)	4368(2)	5411(2)	7377(2)	39(1)
C(6)	5403(2)	6925(2)	7721(2)	45(1)
C(7)	6699(2)	6404(2)	7547(2)	41(1)
C(8)	8136(2)	7099(2)	8059(2)	47(1)
C(9)	8856(3)	8533(3)	8854(2)	63(1)
C(10)	10314(3)	8773(3)	9193(2)	79(1)
C(11)	11068(3)	7634(4)	8782(2)	76(1)
C(12)	10398(2)	6224(4)	8008(2)	63(1)
C(13)	8926(2)	5984(2)	7644(2)	48(1)
C(14)	5754(2)	2151(2)	7222(2)	42(1)
C(15)	4780(2)	2294(2)	7951(2)	42(1)
C(16)	4941(2)	4066(2)	8539(2)	41(1)
O(17)	5422(2)	4384(2)	9769(1)	62(1)
C(18)	1411(2)	4133(3)	4927(2)	55(1)
C(19)	2915(2)	3322(2)	5599(2)	41(1)
C(20)	3203(2)	2173(2)	6833(2)	45(1)
C(21)	2243(3)	1208(4)	6970(3)	77(1)
C(22)	8422(3)	3212(3)	6351(3)	70(1)

—

Table A3. Bond lengths [Å] and angles [°] for KPP-II-50 (**28**)

N(1)-C(2)	1.378(2)	N(1)-C(13)	1.380(2)
N(1)-C(22)	1.449(3)	C(2)-C(7)	1.361(2)
C(2)-C(3)	1.494(2)	C(3)-N(4)	1.482(2)
C(3)-C(14)	1.561(2)	C(3)-H(3)	0.9800
N(4)-C(5)	1.4842(19)	N(4)-C(19)	1.488(2)
C(5)-C(6)	1.531(2)	C(5)-C(16)	1.535(2)
C(5)-H(5)	0.9800	C(6)-C(7)	1.496(2)
C(6)-H(6A)	0.9700	C(6)-H(6B)	0.9700
C(7)-C(8)	1.433(2)	C(8)-C(9)	1.406(3)
C(8)-C(13)	1.407(3)	C(9)-C(10)	1.389(4)
C(9)-H(9)	0.9300	C(10)-C(11)	1.391(4)
C(10)-H(10)	0.9300	C(11)-C(12)	1.371(4)
C(11)-H(11)	0.9300	C(12)-C(13)	1.398(3)
C(12)-H(12)	0.9300	C(14)-C(15)	1.541(2)
C(14)-H(14A)	0.9700	C(14)-H(14B)	0.9700
C(15)-C(16)	1.513(2)	C(15)-C(20)	1.515(2)
C(15)-H(15)	0.9800	C(16)-O(17)	1.205(2)
C(18)-C(19)	1.519(2)	C(18)-H(18A)	0.9600
C(18)-H(18B)	0.9600	C(18)-H(18C)	0.9600
C(19)-C(20)	1.520(2)	C(19)-H(19)	0.9800
C(20)-C(21)	1.314(3)	C(21)-H(21A)	0.9300
C(21)-H(21B)	0.9300	C(22)-H(22A)	0.9600
C(22)-H(22B)	0.9600	C(22)-H(22C)	0.9600
C(2)-N(1)-C(13)	107.93(15)	C(2)-N(1)-C(22)	126.33(15)
C(13)-N(1)-C(22)	125.61(16)	C(7)-C(2)-N(1)	110.57(14)

C(7)-C(2)-C(3)	126.05(14)	N(1)-C(2)-C(3)	123.16(14)
N(4)-C(3)-C(2)	107.74(12)	N(4)-C(3)-C(14)	111.29(12)
C(2)-C(3)-C(14)	110.50(13)	N(4)-C(3)-H(3)	109.1
C(2)-C(3)-H(3)	109.1	C(14)-C(3)-H(3)	109.1
C(3)-N(4)-C(5)	108.47(11)	C(3)-N(4)-C(19)	107.44(12)
C(5)-N(4)-C(19)	110.63(12)	N(4)-C(5)-C(6)	111.31(13)
N(4)-C(5)-C(16)	109.10(13)	C(6)-C(5)-C(16)	112.43(13)
N(4)-C(5)-H(5)	107.9	C(6)-C(5)-H(5)	107.9
C(16)-C(5)-H(5)	107.9	C(7)-C(6)-C(5)	108.77(13)
C(7)-C(6)-H(6A)	109.9	C(5)-C(6)-H(6A)	109.9
C(7)-C(6)-H(6B)	109.9	C(5)-C(6)-H(6B)	109.9
H(6A)-C(6)-H(6B)	108.3	C(2)-C(7)-C(8)	106.59(15)
C(2)-C(7)-C(6)	120.68(15)	C(8)-C(7)-C(6)	132.61(16)
C(9)-C(8)-C(13)	118.40(19)	C(9)-C(8)-C(7)	134.8(2)
C(13)-C(8)-C(7)	106.83(15)	C(10)-C(9)-C(8)	118.2(2)
C(10)-C(9)-H(9)	120.9	C(8)-C(9)-H(9)	120.9
C(9)-C(10)-C(11)	121.9(2)	C(9)-C(10)-H(10)	119.0
C(11)-C(10)-H(10)	119.0	C(12)-C(11)-C(10)	121.2(2)

Table A4. (continued).

C(12)-C(11)-H(11)	119.4	C(10)-C(11)-H(11)	119.4
C(11)-C(12)-C(13)	117.3(3)	C(11)-C(12)-H(12)	121.4
C(13)-C(12)-H(12)	121.4	N(1)-C(13)-C(12)	129.0(2)
N(1)-C(13)-C(8)	108.08(15)	C(12)-C(13)-C(8)	122.92(19)
C(15)-C(14)-C(3)	108.00(12)	C(15)-C(14)-H(14A)	110.1
C(3)-C(14)-H(14A)	110.1	C(15)-C(14)-H(14B)	110.1
C(3)-C(14)-H(14B)	110.1	H(14A)-C(14)-H(14B)	108.4

C(16)-C(15)-C(20)	105.03(14)	C(16)-C(15)-C(14)	108.07(13)
C(20)-C(15)-C(14)	107.95(14)	C(16)-C(15)-H(15)	111.8
C(20)-C(15)-H(15)	111.8	C(14)-C(15)-H(15)	111.8
O(17)-C(16)-C(15)	124.21(16)	O(17)-C(16)-C(5)	123.86(16)
C(15)-C(16)-C(5)	111.90(13)	C(19)-C(18)-H(18A)	109.5
C(19)-C(18)-H(18B)	109.5	H(18A)-C(18)-H(18B)	109.5
C(19)-C(18)-H(18C)	109.5	H(18A)-C(18)-H(18C)	109.5
H(18B)-C(18)-H(18C)	109.5	N(4)-C(19)-C(18)	111.82(15)
N(4)-C(19)-C(20)	109.59(12)	C(18)-C(19)-C(20)	114.20(15)
N(4)-C(19)-H(19)	106.9	C(18)-C(19)-H(19)	106.9
C(20)-C(19)-H(19)	106.9	C(21)-C(20)-C(15)	122.61(18
C(21)-C(20)-C(19)	126.37(18)	C(15)-C(20)-C(19)	111.01(13)
C(20)-C(21)-H(21A)	120.0	C(20)-C(21)-H(21B)	120.0
H(21A)-C(21)-H(21B)	120.0	N(1)-C(22)-H(22A)	109.5
N(1)-C(22)-H(22B)	109.5	H(22A)-C(22)-H(22B)	109.5
N(1)-C(22)-H(22C)	109.5	H(22A)-C(22)-H(22C)	109.5
H(22B)-C(22)-H(22C)	109.5		

Table A5. Anisotropic displacement parameters ($Å^2 x\ 10^3$) for KPP-II-50 (**28**) The anisotropic displacement factor exponent takes the form: $-2\pi^2[h^2 a^{*2} U^{11} + ... + 2\ h\ k\ a^*\ b^*\ U^{12}]$

	U^{11}	U^{22}	U^{33}	U^{23}	U^{13}	U^{12}
N(1)	43(1)	48(1)	54(1)	-9(1)	29(1)	-9(1)
C(2)	43(1)	36(1)	41(1)	-4(1)	23(1)	-6(1)
C(3)	40(1)	36(1)	36(1)	-7(1)	21(1)	-5(1)
N(4)	38(1)	38(1)	32(1)	0(1)	16(1)	0(1)
C(5)	42(1)	40(1)	37(1)	-2(1)	21(1)	4(1)
C(6)	57(1)	36(1)	44(1)	-6(1)	26(1)	1(1)
C(7)	50(1)	35(1)	38(1)	-4(1)	21(1)	-7(1)
C(8)	57(1)	44(1)	36(1)	0(1)	18(1)	-15(1)
C(9)	83(1)	52(1)	45(1)	-9(1)	22(1)	-26(1)
C(10)	85(2)	80(2)	49(1)	-9(1)	12(1)	-48(1)
C(11)	60(1)	103(2)	51(1)	3(1)	14(1)	-39(1)
C(12)	49(1)	85(2)	53(1)	6(1)	21(1)	-17(1)
C(13)	47(1)	54(1)	41(1)	1(1)	19(1)	-13(1)
C(14)	41(1)	33(1)	52(1)	-1(1)	21(1)	0(1)
C(15)	42(1)	41(1)	39(1)	8(1)	16(1)	-1(1)
C(16)	39(1)	51(1)	34(1)	1(1)	18(1)	-1(1)
O(17)	78(1)	70(1)	35(1)	-3(1)	24(1)	2(1)
C(18)	39(1)	67(1)	49(1)	6(1)	12(1)	3(1)
C(19)	38(1)	45(1)	36(1)	0(1)	14(1)	-4(1)
C(20)	41(1)	47(1)	46(1)	4(1)	19(1)	-4(1)
C(21)	54(1)	87(2)	78(1)	27(1)	22(1)	-20(1)
C(22)	60(1)	66(1)	101(2)	-24(1)	52(1)	-7(1)

Table A6. Hydrogen coordinates (x 10^4) and isotropic displacement parameters ($Å^2$x 10^3) for KPP-II-50 (**28**).

	x	y	z	U(eq)
H(3)	5328	3335	5327	43
H(5)	3433	5827	7280	47
H(6A)	4906	7860	7097	54
H(6B)	5714	7293	8677	54
H(9)	8370	9300	9144	76
H(10)	10799	9722	9710	94
H(11)	12045	7833	9037	91
H(12)	10902	5458	7736	76
H(14A)	5536	1113	6680	51
H(14B)	6775	2131	7917	51
H(15)	5022	1429	8678	50
H(18A)	1275	4754	4109	82
H(18B)	1329	4890	5585	82
H(18C)	679	3267	4664	82
H(19)	2976	2615	4880	49
H(21A)	2522	564	7778	92
H(21B)	1285	1168	6260	92
H(22A)	8768	3577	5707	105
H(22B)	7589	2489	5872	105
H(22C)	9181	2600	7109	105

Table A7. Torsion angles [°] for KPP-II-50 (**28**).

C(13)-N(1)-C(2)-C(7)	0.2(2)	C(22)-N(1)-C(2)-C(7)	176.1(2)
C(13)-N(1)-C(2)-C(3)	-174.71(14)	C(22)-N(1)-C(2)-C(3)	1.2(3)
C(7)-C(2)-C(3)-N(4)	20.7(2)	N(1)-C(2)-C(3)-N(4)	-165.14(14)
C(7)-C(2)-C(3)-C(14)	-101.03(18)	N(1)-C(2)-C(3)-C(14)	73.09(18)
C(2)-C(3)-N(4)-C(5)	-52.90(16)	C(14)-C(3)-N(4)-C(5)	68.39(16)
C(2)-C(3)-N(4)-C(19)	-172.52(11)	C(14)-C(3)-N(4)-C(19)	-51.24(15)
C(3)-N(4)-C(5)-C(6)	71.37(16)	C(19)-N(4)-C(5)-C(6)	-171.02(13)
C(3)-N(4)-C(5)-C(16)	-53.27(16)	C(19)-N(4)-C(5)-C(16)	64.34(16)
N(4)-C(5)-C(6)-C(7)	-48.69(18)	C(16)-C(5)-C(6)-C(7)	74.05(17)
N(1)-C(2)-C(7)-C(8)	0.18(19)	C(3)-C(2)-C(7)-C(8)	174.92(15)
N(1)-C(2)-C(7)-C(6)	-176.31(15)	C(3)-C(2)-C(7)-C(6)	-1.6(2)
C(5)-C(6)-C(7)-C(2)	14.6(2)	C(5)-C(6)-C(7)-C(8)	-160.79(17)
C(2)-C(7)-C(8)-C(9)	-178.8(2)	C(6)-C(7)-C(8)-C(9)	-2.9(3)
C(2)-C(7)-C(8)-C(13)	-0.49(18)	C(6)-C(7)-C(8)-C(13)	175.40(18)
C(13)-C(8)-C(9)-C(10)	-0.2(3)	C(7)-C(8)-C(9)-C(10)	178.0(2)
C(8)-C(9)-C(10)-C(11)	-0.6(3)	C(9)-C(10)-C(11)-C(12)	0.6(4)
C(10)-C(11)-C(12)-C(13)	0.3(3)	C(2)-N(1)-C(13)-C(12)	177.44(18)
C(22)-N(1)-C(13)-C(12)	1.5(3)	C(2)-N(1)-C(13)-C(8)	-0.5(2)
C(22)-N(1)-C(13)-C(8)	-176.5(2)	C(11)-C(12)-C(13)-N(1)	-178.88(19)
C(11)-C(12)-C(13)-C(8)	-1.2(3)	C(9)-C(8)-C(13)-N(1)	179.26(16)
C(7)-C(8)-C(13)-N(1)	0.63(19)	C(9)-C(8)-C(13)-C(12)	1.1(3)
C(7)-C(8)-C(13)-C(12)	-177.49(17)	N(4)-C(3)-C(14)-C(15)	-13.88(17)
C(2)-C(3)-C(14)-C(15)	105.77(15)	C(3)-C(14)-C(15)-C(16)	-48.74(17)
C(3)-C(14)-C(15)-C(20)	64.37(16)	C(20)-C(15)-C(16)-O(17)	127.24(18)
C(14)-C(15)-C(16)-O(17)	-117.71(18)	C(20)-C(15)-C(16)-C(5)	-50.81(16)
C(14)-C(15)-C(16)-C(5)	64.23(17)	N(4)-C(5)-C(16)-O(17)	170.62(16)

C(6)-C(5)-C(16)-O(17)	46.6(2)	N(4)-C(5)-C(16)-C(15)	-11.32(17)
C(6)-C(5)-C(16)-C(15)	-135.30(14)	C(3)-N(4)-C(19)-C(18)	-162.24(14)
C(5)-N(4)-C(19)-C(18)	79.53(17)	C(3)-N(4)-C(19)-C(20)	70.08(16)
C(5)-N(4)-C(19)-C(20)	-48.15(18)	C(16)-C(15)-C(20)-C(21)	-111.0(2)
C(14)-C(15)-C(20)-C(21)	133.9(2)	C(16)-C(15)-C(20)-C(19)	67.80(17)
C(14)-C(15)-C(20)-C(19)	-47.33(19)	N(4)-C(19)-C(20)-C(21)	160.8(2)
C(18)-C(19)-C(20)-C(21)	34.4(3)	N(4)-C(19)-C(20)-C(15)	-18.0(2)
C(18)-C(19)-C(20)-C(15)	-144.29(16)		

X-ray Crystal Data for Compound KPP-III-43 (29).

Table A8. Crystal data and structure refinement for KPP-II-43 (**29**).

Identification code	cook185	
Empirical formula	$C_{19}H_{20}N_2O$	
Formula weight	292.37	
Temperature	296(2) K	
Wavelength	0.71073 Å	
Crystal system	Monoclinic	
Space group	$P2_1$	
Unit cell dimensions	a = 8.7184(3) Å	α= 90°.
	b = 8.4717(3) Å	β= 92.9370(10)°.
	c = 10.3859(3) Å	γ = 90°.
Volume	766.09(4) $Å^3$	
Z	2	
Density (20°C)	1.267 Mg/m^3	

Absorption coefficient	0.079 mm^{-1}
F(000)	312
Crystal size	0.452 x 0.355 x 0.272 mm^3
Theta range for data collection	1.963 to 29.151°.
Index ranges	-10<=h<=11, -11<=k<=11, -14<=l<=14
Reflections collected	8923
Independent reflections	4066 [R_{int} = 0.0142]
Completeness to theta = 25.242°	99.2 %
Refinement method	Full-matrix least-squares on F^2
Data / restraints / parameters	4066 / 1 / 201
Goodness-of-fit on F^2	0.916
Final R indices [I>2sigma(I)]	R_1 = 0.0340, wR_2 = 0.0954
R indices (all data)	R_1 = 0.0368, wR_2 = 0.0992
Absolute structure parameter	0.4(3)
Largest diff. peak and hole	0.212 and -0.162 $e.Å^{-3}$

Table A9. Atomic coordinates (x 10^4) and equivalent isotropic displacement parameters ($Å^2$x 10^3)

for KPP-II-43 (**29**). U(eq) is defined as one third of the trace of the orthogonalized U^{ij} tensor.

	x	y	z	U(eq)
C(1)	634(2)	6863(2)	11114(2)	45(1)
C(2)	-20(2)	6638(2)	10100(2)	36(1)
C(3)	-826(2)	6373(2)	8827(2)	34(1)
C(3A)	-2332(2)	7291(2)	8738(2)	43(1)
N(4)	98(1)	6754(1)	7712(1)	32(1)
C(5)	1029(2)	8200(2)	7870(2)	34(1)
C(6)	2561(2)	7972(2)	8644(2)	39(1)
O(6)	3189(2)	9094(2)	9167(2)	61(1)
C(7)	3334(2)	6369(2)	8639(2)	46(1)
C(8)	2288(2)	4963(2)	8314(2)	38(1)
C(9)	1044(2)	5427(2)	7284(1)	33(1)
C(10)	1755(2)	5974(2)	6074(2)	33(1)
N(11)	2494(2)	4992(2)	5236(1)	36(1)
C(11)	2513(2)	3280(2)	5231(2)	44(1)
C(12)	3106(2)	5934(2)	4301(1)	36(1)
C(13)	3982(2)	5519(2)	3263(2)	43(1)
C(14)	4420(2)	6713(3)	2454(2)	48(1)
C(15)	4007(2)	8286(3)	2664(2)	48(1)
C(16)	3180(2)	8712(2)	3716(2)	42(1)
C(17)	2728(2)	7526(2)	4559(2)	35(1)
C(18)	1890(2)	7520(2)	5714(2)	34(1)

C(19)	1345(2)	8851(2)	6523(2)	38(1)

Table A10. Bond lengths [Å] and angles [°] for KPP-II-43 (**29**).

C(1)-C(2)	1.187(3)	C(1)-H(1)	0.9300
C(2)-C(3)	1.482(2)	C(3)-N(4)	1.4804(19)
C(3)-C(3A)	1.524(2)	C(3)-H(3A)	0.9800
C(3A)-H(3D)	0.9600	C(3A)-H(3E)	0.9600
C(3A)-H(3F)	0.9600	N(4)-C(5)	1.4739(18)
N(4)-C(9)	1.4767(19)	C(5)-C(6)	1.535(2)
C(5)-C(19)	1.543(2)	C(5)-H(5A)	0.9800
C(6)-O(6)	1.211(2)	C(6)-C(7)	1.516(3)
C(7)-C(8)	1.527(3)	C(7)-H(7A)	0.9700
C(7)-H(7B)	0.9700	C(8)-C(9)	1.535(2)
C(8)-H(8A)	0.9700	C(8)-H(8B)	0.9700
C(9)-C(10)	1.503(2)	C(9)-H(9A)	0.9800
C(10)-C(18)	1.369(2)	C(10)-N(11)	1.386(2)
N(11)-C(12)	1.385(2)	N(11)-C(11)	1.451(2)
C(11)-H(11A)	0.9600	C(11)-H(11B)	0.9600
C(11)-H(11C)	0.9600	C(12)-C(13)	1.398(2)
C(12)-C(17)	1.417(2)	C(13)-C(14)	1.381(3)
C(13)-H(13A)	0.9300	C(14)-C(15)	1.400(3)
C(14)-H(14A)	0.9300	C(15)-C(16)	1.387(3)
C(15)-H(15A)	0.9300	C(16)-C(17)	1.403(2)
C(16)-H(16A)	0.9300	C(17)-C(18)	1.435(2)
C(18)-C(19)	1.498(2)	C(19)-H(19C)	0.9700
C(19)-H(19A)	0.9700		
C(2)-C(1)-H(1)	180.0	C(1)-C(2)-C(3)	179.33(19)

N(4)-C(3)-C(2)	114.36(12)	N(4)-C(3)-C(3A)	110.00(12)
C(2)-C(3)-C(3A)	110.18(13)	N(4)-C(3)-H(3A)	107.3
C(2)-C(3)-H(3A)	107.3	C(3A)-C(3)-H(3A)	107.3
C(3)-C(3A)-H(3D)	109.5	C(3)-C(3A)-H(3E)	109.5
H(3D)-C(3A)-H(3E)	109.5	C(3)-C(3A)-H(3F)	109.5
H(3D)-C(3A)-H(3F)	109.5	H(3E)-C(3A)-H(3F)	109.5
C(5)-N(4)-C(9)	110.68(11)	C(5)-N(4)-C(3)	114.38(12)
C(9)-N(4)-C(3)	113.83(11)	N(4)-C(5)-C(6)	114.46(12)
N(4)-C(5)-C(19)	108.61(12)	C(6)-C(5)-C(19)	109.20(13)
N(4)-C(5)-H(5A)	108.1	C(6)-C(5)-H(5A)	108.1
C(19)-C(5)-H(5A)	108.1	O(6)-C(6)-C(7)	120.92(17)
O(6)-C(6)-C(5)	119.84(18)	C(7)-C(6)-C(5)	119.01(13)
C(6)-C(7)-C(8)	116.06(14)	C(6)-C(7)-H(7A)	108.3
C(8)-C(7)-H(7A)	108.3	C(6)-C(7)-H(7B)	108.3
C(8)-C(7)-H(7B)	108.3	H(7A)-C(7)-H(7B)	107.4
C(7)-C(8)-C(9)	110.29(13)	C(7)-C(8)-H(8A)	109.6
C(9)-C(8)-H(8A)	109.6	C(7)-C(8)-H(8B)	109.6
C(9)-C(8)-H(8B)	109.6	H(8A)-C(8)-H(8B)	108.1
N(4)-C(9)-C(10)	106.09(12)	N(4)-C(9)-C(8)	111.79(12)

Table A11. (continued).

C(10)-C(9)-C(8)	110.78(13)	N(4)-C(9)-H(9A)	109.4
C(10)-C(9)-H(9A)	109.4	C(8)-C(9)-H(9A)	109.4
C(18)-C(10)-N(11)	110.66(14)	C(18)-C(10)-C(9)	124.69(13)
N(11)-C(10)-C(9)	124.39(13)	C(12)-N(11)-C(10)	107.63(13)
C(12)-N(11)-C(11)	124.67(15)	C(10)-N(11)-C(11)	127.44(15)
N(11)-C(11)-H(11A)	109.5	N(11)-C(11)-H(11B)	109.5

H(11A)-C(11)-H(11B)	109.5	N(11)-C(11)-H(11C)	109.5
H(11A)-C(11)-H(11C)	109.5	H(11B)-C(11)-H(11C)	109.5
N(11)-C(12)-C(13)	129.90(16)	N(11)-C(12)-C(17)	108.30(14)
C(13)-C(12)-C(17)	121.79(15)	C(14)-C(13)-C(12)	117.65(18)
C(14)-C(13)-H(13A)	121.2	C(12)-C(13)-H(13A)	121.2
C(13)-C(14)-C(15)	121.40(17)	C(13)-C(14)-H(14A)	119.3
C(15)-C(14)-H(14A)	119.3	C(16)-C(15)-C(14)	121.21(17)
C(16)-C(15)-H(15A)	119.4	C(14)-C(15)-H(15A)	119.4
C(15)-C(16)-C(17)	118.65(17)	C(15)-C(16)-H(16A)	120.7
C(17)-C(16)-H(16A)	120.7	C(16)-C(17)-C(12)	119.21(15)
C(16)-C(17)-C(18)	134.04(15)	C(12)-C(17)-C(18)	106.75(13)
C(10)-C(18)-C(17)	106.63(13)	C(10)-C(18)-C(19)	122.17(14)
C(17)-C(18)-C(19)	130.96(14)	C(18)-C(19)-C(5)	108.42(12)
C(18)-C(19)-H(19C)	110.0	C(5)-C(19)-H(19C)	110.0
C(18)-C(19)-H(19A)	110.0	C(5)-C(19)-H(19A)	110.0
H(19C)-C(19)-H(19A)	108.4		

Table A12. Anisotropic displacement parameters ($Å^2 x\ 10^3$) for KPP-II-43 (**29**). The anisotropic displacement factor exponent takes the form: $-2\pi^2[h^2 a^{*2} U^{11} + ... + 2\ h\ k\ a^*\ b^*\ U^{12}]$.

	U^{11}	U^{22}	U^{33}	U^{23}	U^{13}	U^{12}
C(1)	45(1)	42(1)	46(1)	1(1)	-5(1)	-2(1)
C(2)	32(1)	34(1)	42(1)	5(1)	4(1)	0(1)
C(3)	30(1)	32(1)	40(1)	2(1)	2(1)	-2(1)
C(3A)	31(1)	51(1)	47(1)	-1(1)	1(1)	4(1)
N(4)	31(1)	25(1)	39(1)	0(1)	3(1)	-1(1)
C(5)	36(1)	26(1)	40(1)	-3(1)	5(1)	-2(1)
C(6)	36(1)	41(1)	41(1)	-3(1)	3(1)	-9(1)
O(6)	59(1)	54(1)	70(1)	-12(1)	-7(1)	-20(1)
C(7)	34(1)	52(1)	51(1)	-3(1)	-6(1)	2(1)
C(8)	39(1)	35(1)	41(1)	4(1)	3(1)	8(1)
C(9)	36(1)	24(1)	38(1)	0(1)	2(1)	-1(1)
C(10)	37(1)	27(1)	35(1)	-2(1)	1(1)	1(1)
N(11)	44(1)	27(1)	37(1)	-3(1)	3(1)	2(1)
C(11)	56(1)	27(1)	49(1)	-6(1)	-3(1)	5(1)
C(12)	36(1)	36(1)	34(1)	-3(1)	-1(1)	-2(1)
C(13)	39(1)	50(1)	40(1)	-11(1)	0(1)	0(1)
C(14)	38(1)	67(1)	37(1)	-5(1)	3(1)	-7(1)
C(15)	41(1)	60(1)	41(1)	7(1)	3(1)	-12(1)
C(16)	43(1)	40(1)	43(1)	5(1)	1(1)	-7(1)
C(17)	35(1)	35(1)	35(1)	-1(1)	-1(1)	-2(1)
C(18)	39(1)	27(1)	37(1)	1(1)	4(1)	0(1)
C(19)	45(1)	24(1)	45(1)	1(1)	7(1)	1(1)

Table A13. Hydrogen coordinates (x 10^4) and isotropic displacement parameters ($Å^2$x 10^3) for KPP-II-43 (**29**).

	x	y	z	U(eq)
H(1)	1146	7040	11909	53
H(3A)	-1085	5248	8771	41
H(3D)	-2895	7025	7949	64
H(3E)	-2117	8402	8751	64
H(3F)	-2931	7024	9456	64
H(5A)	426	8986	8317	40
H(7A)	3832	6192	9483	55
H(7B)	4131	6398	8021	55
H(8A)	1808	4610	9085	46
H(8B)	2893	4097	7998	46
H(9A)	382	4514	7086	39
H(11A)	3555	2915	5329	66
H(11B)	2055	2901	4430	66
H(11C)	1942	2892	5931	66
H(13A)	4260	4476	3122	52
H(14A)	5003	6467	1756	57
H(15A)	4291	9059	2087	57
H(16A)	2931	9763	3859	51
H(19C)	414	9304	6126	45
H(19A)	2122	9671	6595	45

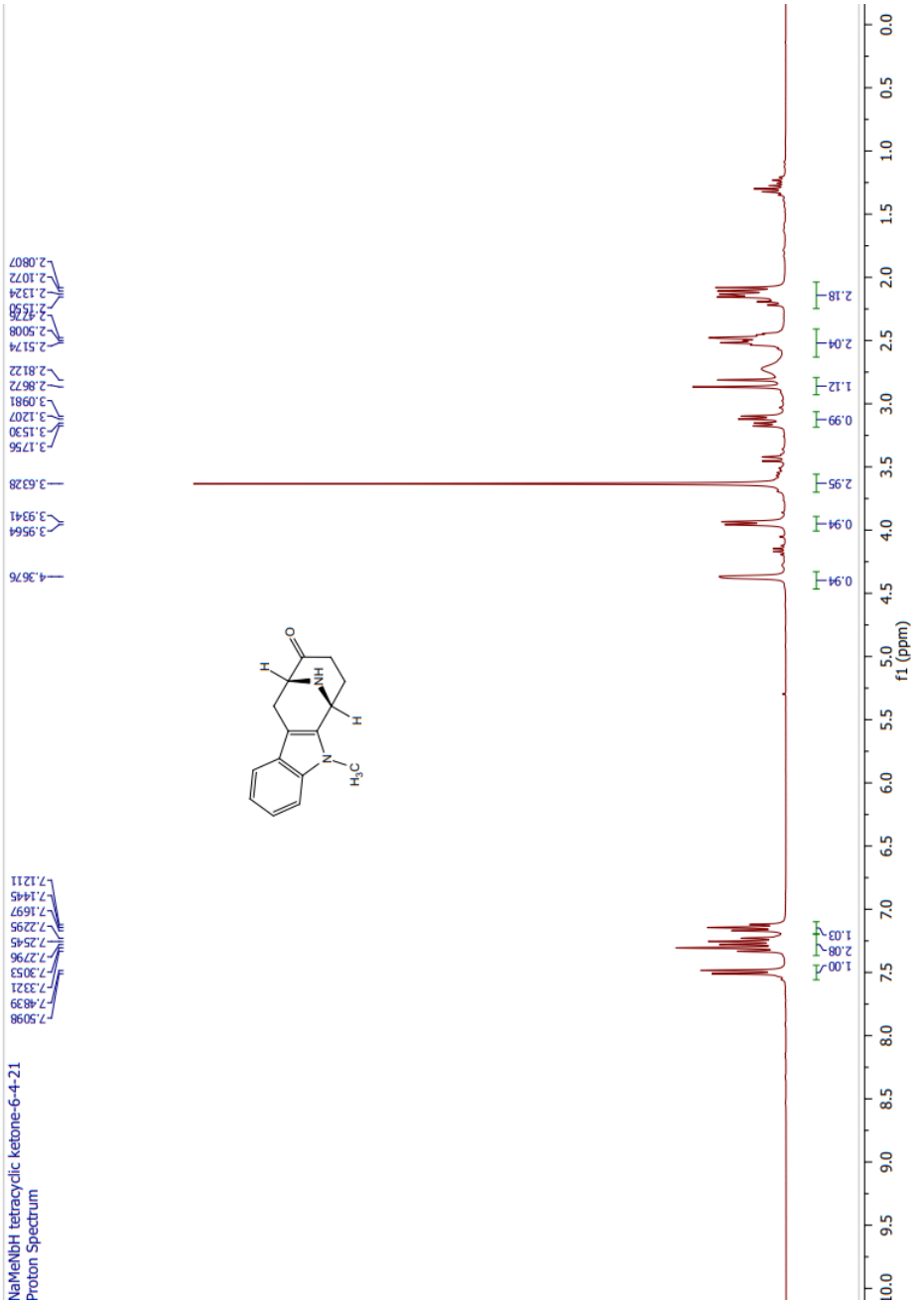
__Table A14. Torsion angles [°] for KPP-II-43 (**29**).

C(2)-C(3)-N(4)-C(5)	-40.66(18)	C(3A)-C(3)-N(4)-C(5)	83.94(16)
C(2)-C(3)-N(4)-C(9)	87.94(16)	C(3A)-C(3)-N(4)-C(9)	-147.46(14)
C(9)-N(4)-C(5)-C(6)	-48.11(17)	C(3)-N(4)-C(5)-C(6)	82.07(16)
C(9)-N(4)-C(5)-C(19)	74.20(15)	C(3)-N(4)-C(5)-C(19)	-155.63(12)
N(4)-C(5)-C(6)-O(6)	-157.51(16)	C(19)-C(5)-C(6)-O(6)	80.51(19)
N(4)-C(5)-C(6)-C(7)	28.0(2)	C(19)-C(5)-C(6)-C(7)	-94.00(17)
O(6)-C(6)-C(7)-C(8)	162.78(17)	C(5)-C(6)-C(7)-C(8)	-22.8(2)
C(6)-C(7)-C(8)-C(9)	36.5(2)	C(5)-N(4)-C(9)-C(10)	-55.49(16)
C(3)-N(4)-C(9)-C(10)	174.05(12)	C(5)-N(4)-C(9)-C(8)	65.37(16)
C(3)-N(4)-C(9)-C(8)	-65.09(16)	C(7)-C(8)-C(9)-N(4)	-58.67(17)
C(7)-C(8)-C(9)-C(10)	59.43(17)	N(4)-C(9)-C(10)-C(18)	19.1(2)
C(8)-C(9)-C(10)-C(18)	-102.44(19)	N(4)-C(9)-C(10)-N(11)	-167.46(14)
C(8)-C(9)-C(10)-N(11)	71.02(19)	C(18)-C(10)-N(11)-C(12)	-0.70(19)
C(9)-C(10)-N(11)-C(12)	-174.96(14)	C(18)-C(10)-N(11)-C(11)	-174.96(16)
C(9)-C(10)-N(11)-C(11)	10.8(3)	C(10)-N(11)-C(12)-C(13)	178.33(16)
C(11)-N(11)-C(12)-C(13)	-7.2(3)	C(10)-N(11)-C(12)-C(17)	-0.54(18)
C(11)-N(11)-C(12)-C(17)	173.91(16)	N(11)-C(12)-C(13)-C(14)	178.63(17)
C(17)-C(12)-C(13)-C(14)	-2.6(2)	C(12)-C(13)-C(14)-C(15)	0.1(3)
C(13)-C(14)-C(15)-C(16)	2.0(3)	C(14)-C(15)-C(16)-C(17)	-1.6(3)
C(15)-C(16)-C(17)-C(12)	-0.9(2)	C(15)-C(16)-C(17)-C(18)	179.82(18)
N(11)-C(12)-C(17)-C(16)	-177.92(14)	C(13)-C(12)-C(17)-C(16)	3.1(2)
N(11)-C(12)-C(17)-C(18)	1.50(18)	C(13)-C(12)-C(17)-C(18)	-177.47(15)
N(11)-C(10)-C(18)-C(17)	1.63(19)	C(9)-C(10)-C(18)-C(17)	175.86(14)
N(11)-C(10)-C(18)-C(19)	-173.45(15)	C(9)-C(10)-C(18)-C(19)	0.8(3)
C(16)-C(17)-C(18)-C(10)	177.41(18)	C(12)-C(17)-C(18)-C(10)	-1.90(18)
C(16)-C(17)-C(18)-C(19)	-8.1(3)	C(12)-C(17)-C(18)-C(19)	172.58(17)

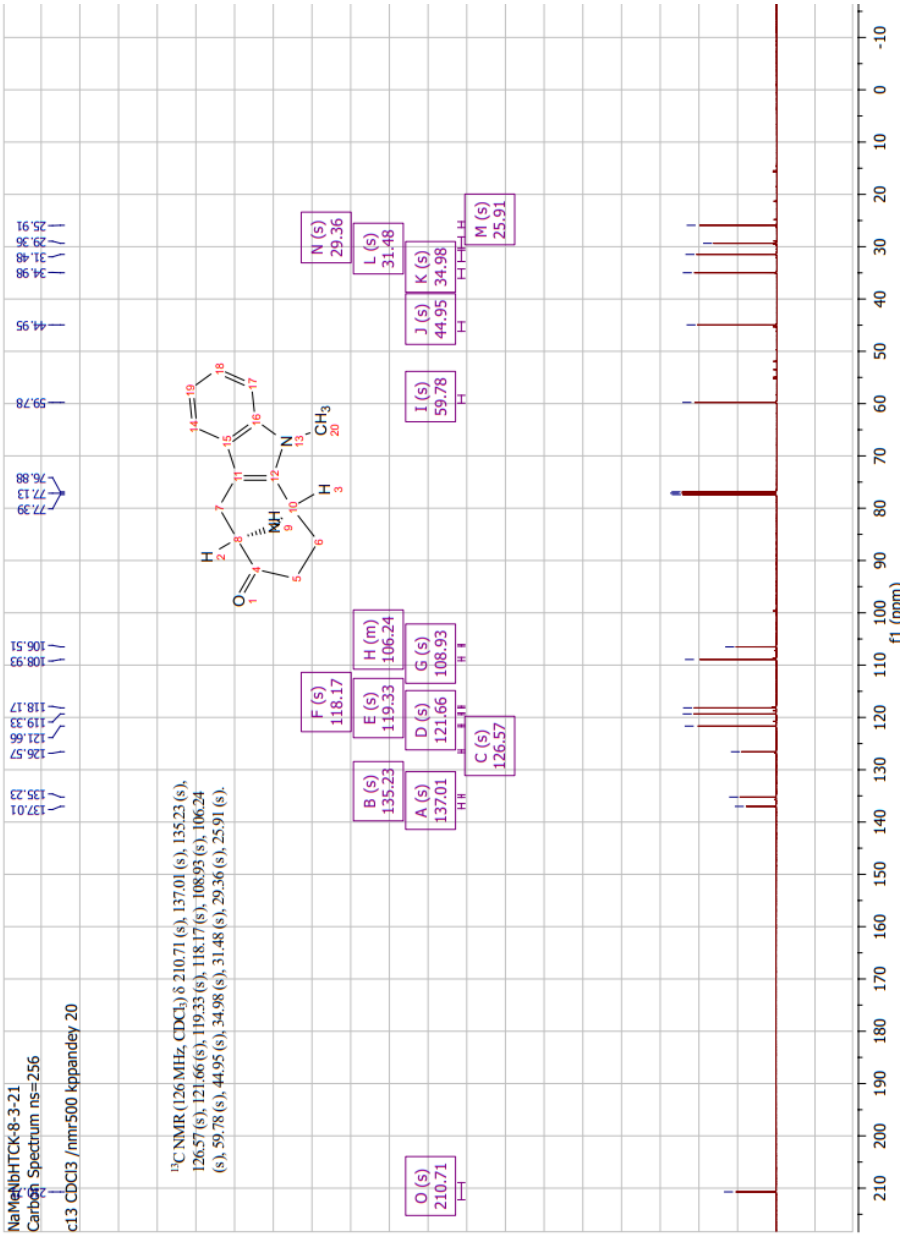
C(10)-C(18)-C(19)-C(5)	13.5(2)	C(17)-C(18)-C(19)-C(5)	-160.21(16)
N(4)-C(5)-C(19)-C(18)	-48.15(17)	C(6)-C(5)-C(19)-C(18)	77.29(16

NMR -data Part-I

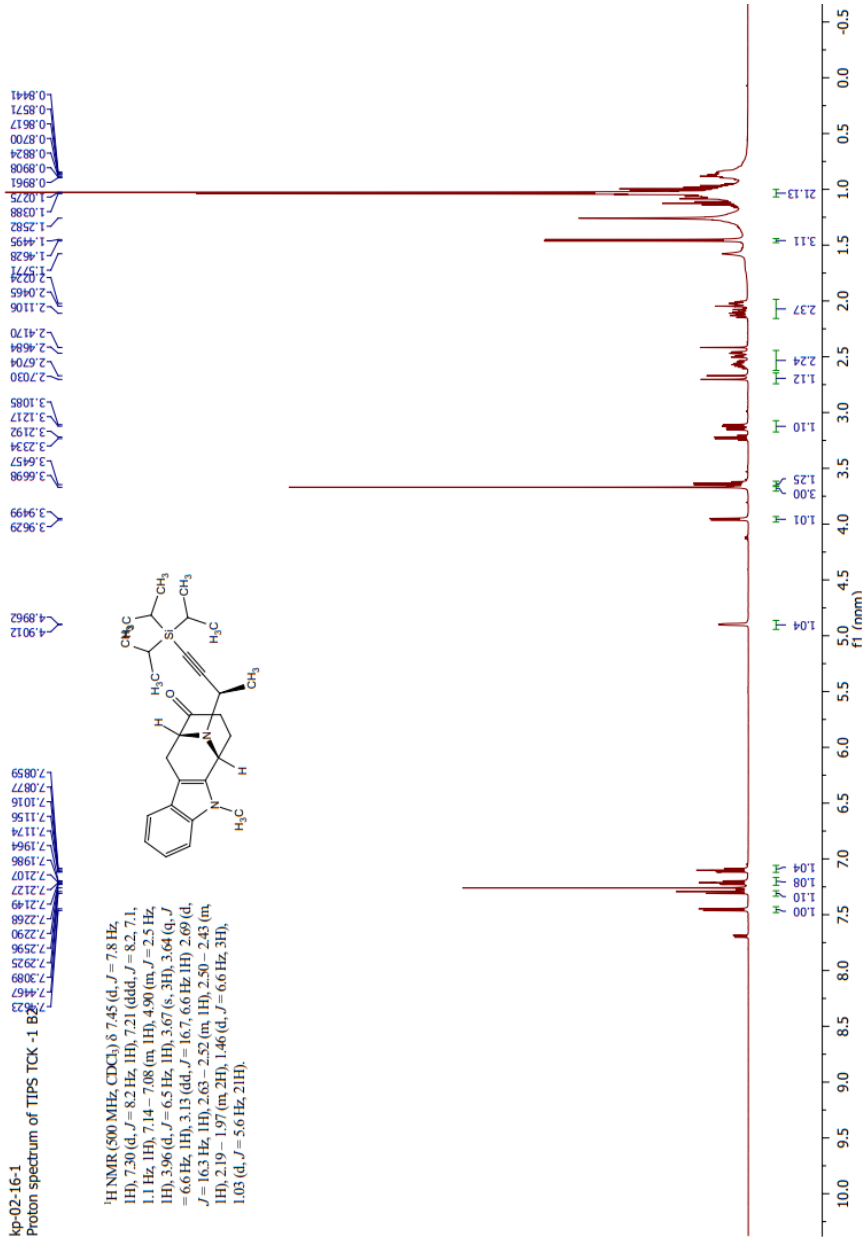
1. **^{1}H NMR of (6*R*,10*R*)-5-methyl-5,6,7,8,10,11-hexahydro-9*H*-6,10-epiminocycloocta[b]indol-9-one** (**31**).



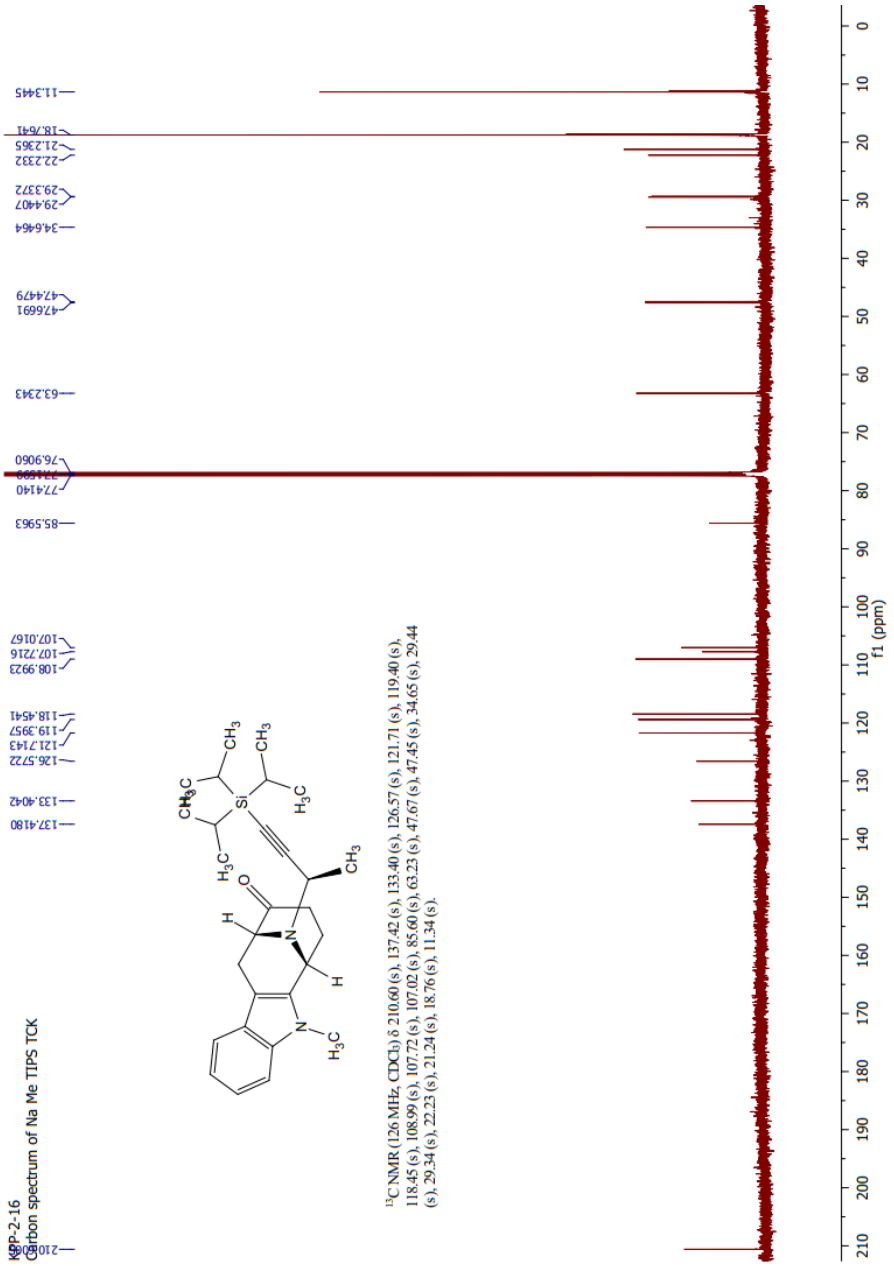
2. **^{13}C NMR of (6*R*,10*R*)-5-methyl-5,6,7,8,10,11-hexahydro-9*H*-6,10-epiminocycloocta[b]indol-9-one (31).**



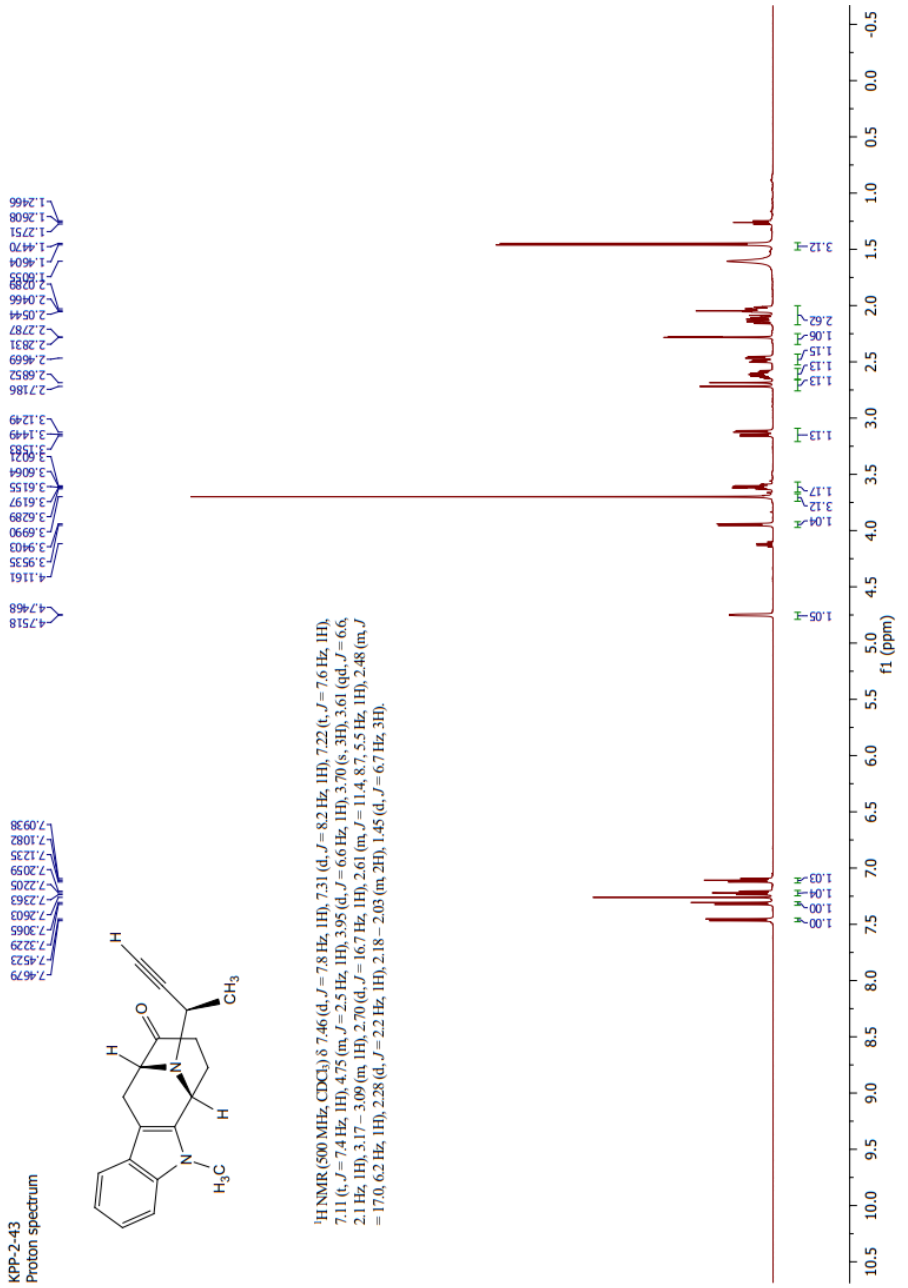
3. **^{1}H NMR of (6*R*,10*R*)-5-methyl-12-((*R*)-4-(triisopropylsilyl)but-3-yn-2-yl)-5,6,7,8,10,11-hexahydro-9*H*-6,10-epiminocycloocta[b]indol-9-one (51).**



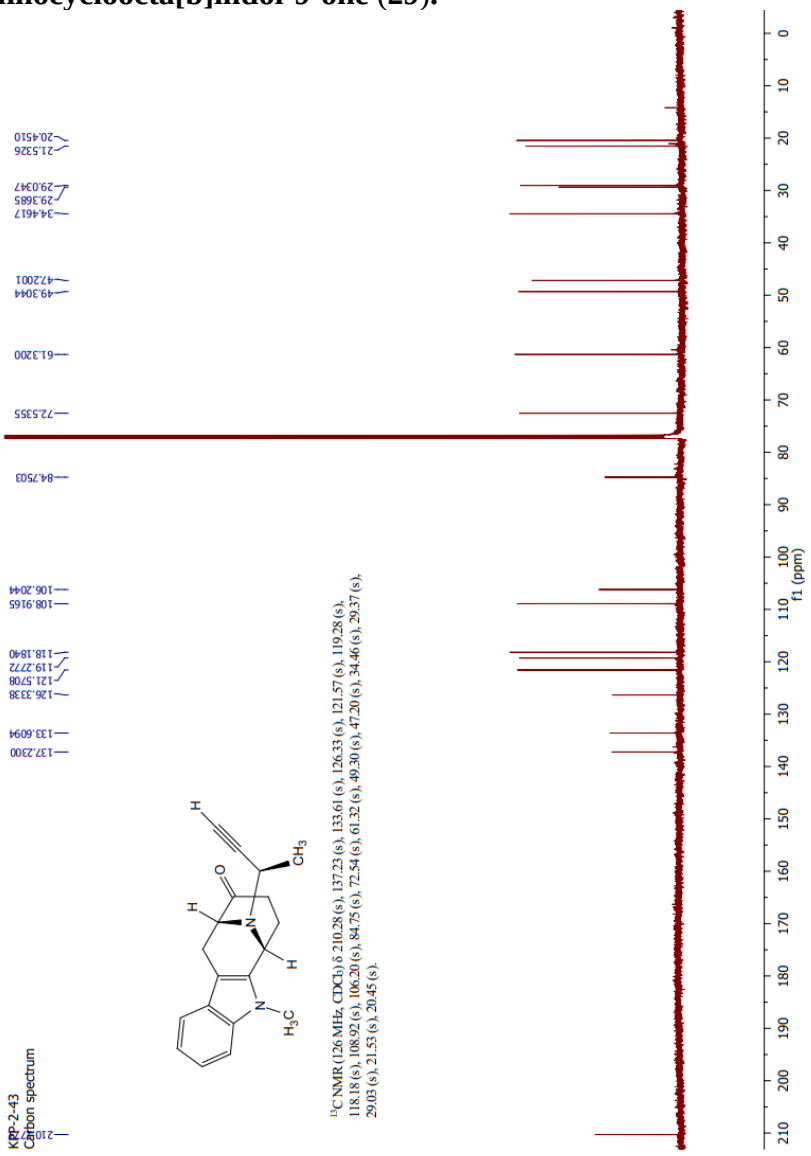
4. **^{13}C NMR of (6*R*,10*R*)-5-methyl-12-((*R*)-4-(triisopropylsilyl)but-3-yn-2-yl)-5,6,7,8,10,11-hexahydro-9*H*-6,10-epiminocycloocta[b]indol-9-one (51).**



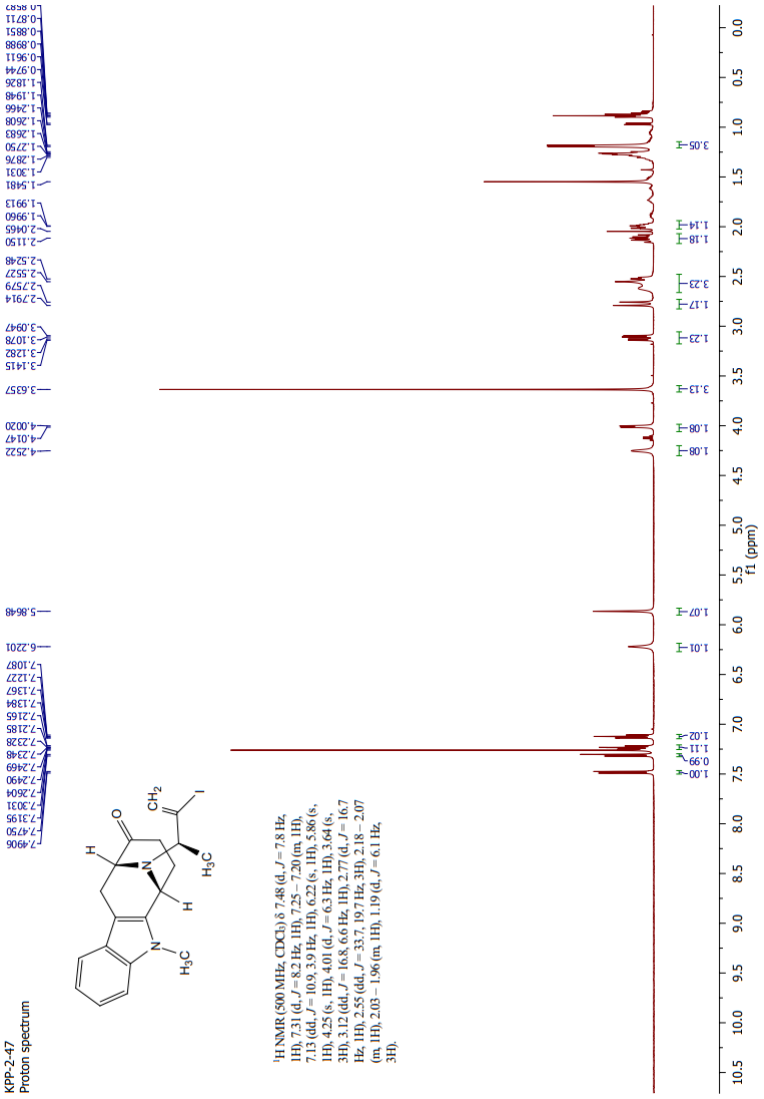
5. **^{1}H NMR of (6*R*,10*R*)-12-((*R*)-but-3-yn-2-yl)-5-methyl-5,6,7,8,10,11-hexahydro-9*H*-6,10-epiminocycloocta[b]indol-9-one (29).**



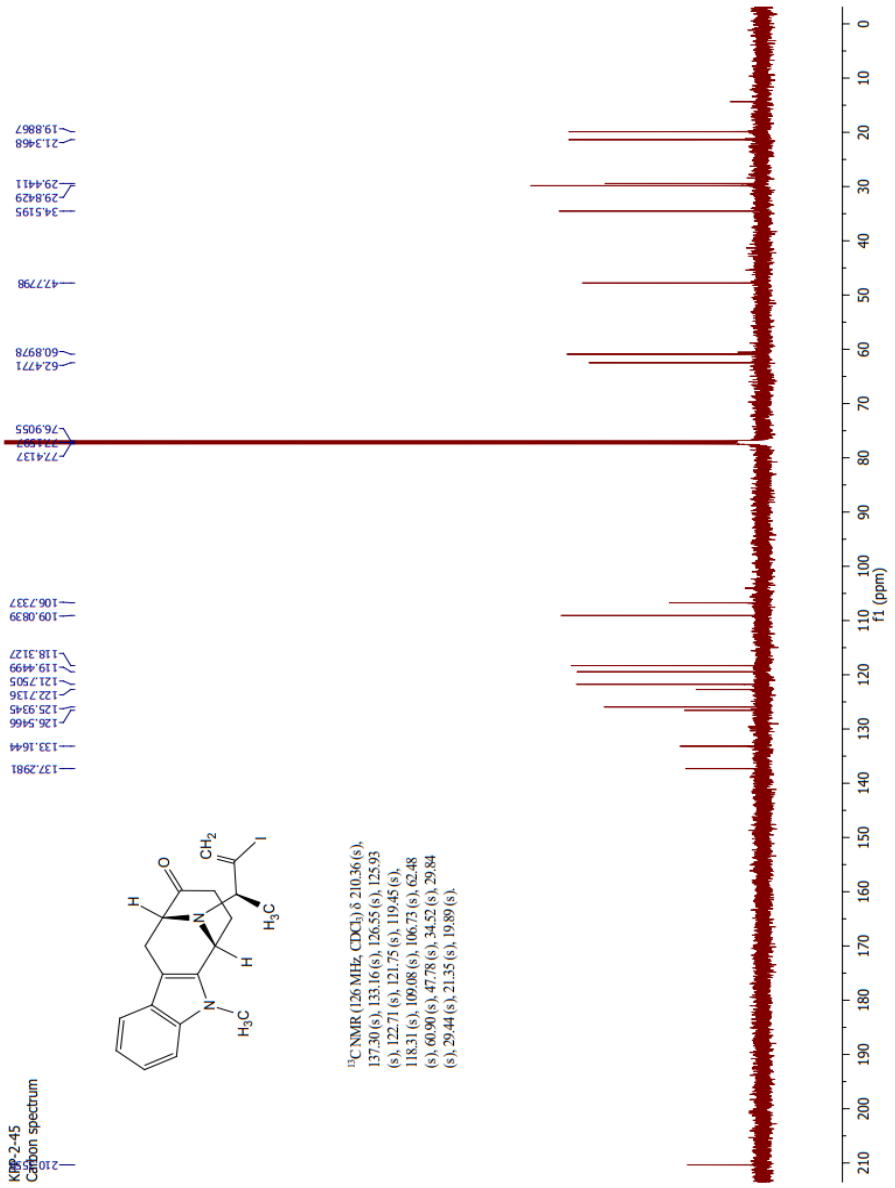
6. **^{13}C NMR of (6*R*,10*R*)-12-((*R*)-but-3-yn-2-yl)-5-methyl-5,6,7,8,10,11-hexahydro-9*H*-6,10-epiminocycloocta[b]indol-9-one (29).**



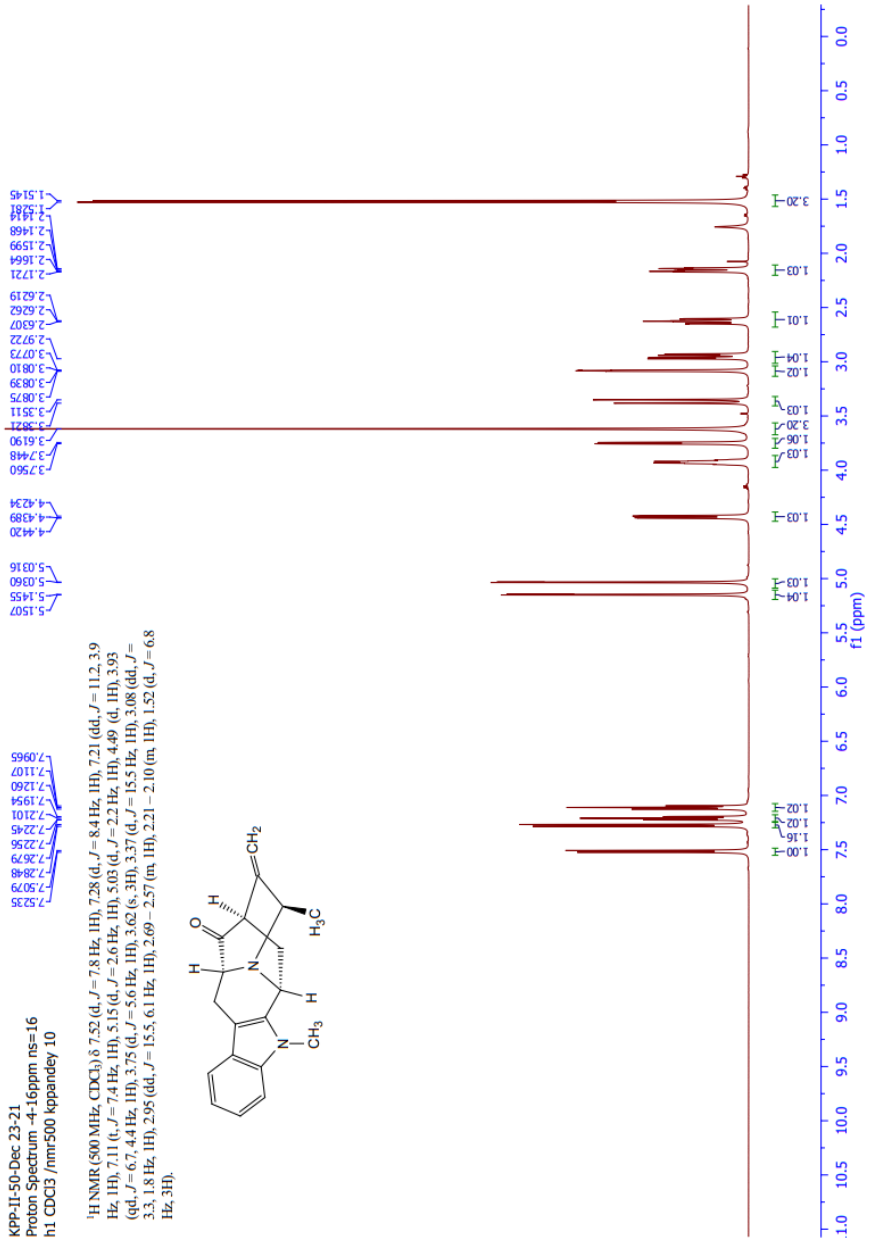
7. **^{1}H NMR of (6*R*,10*R*)-12-((*R*)-3-iodobut-3-en-2-yl)-5-methyl-5,6,7,8,10,11-hexahydro-9*H*-6,10-epiminocycloocta[b]indol-9-one (30).**



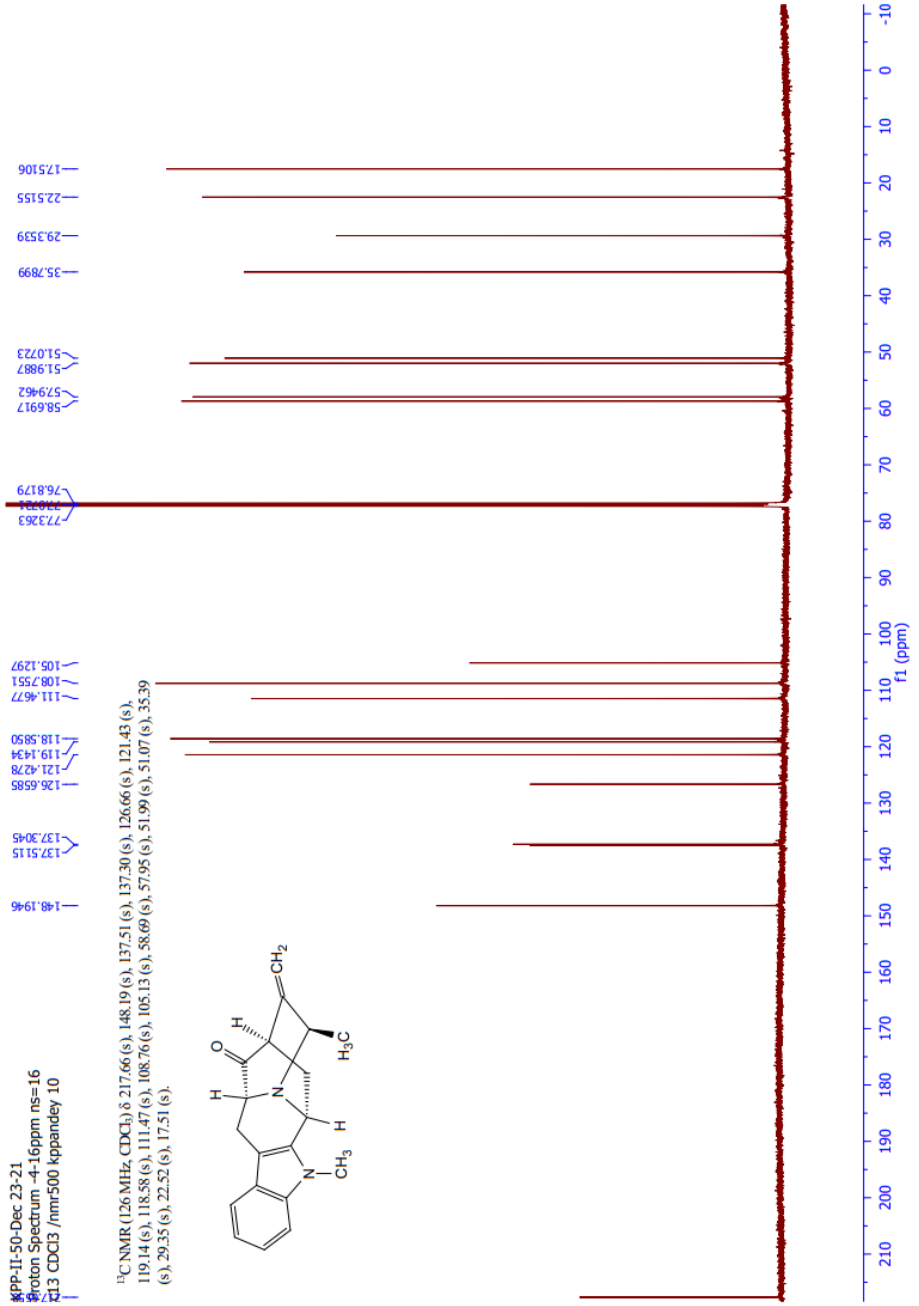
8. **^{13}C NMR of 6*R*,10*R*)-12-((*R*)-3-iodobut-3-en-2-yl)-5-methyl-5,6,7,8,10,11-hexahydro-9*H*-6,10-epiminocycloocta[b]indol-9-one (30).**



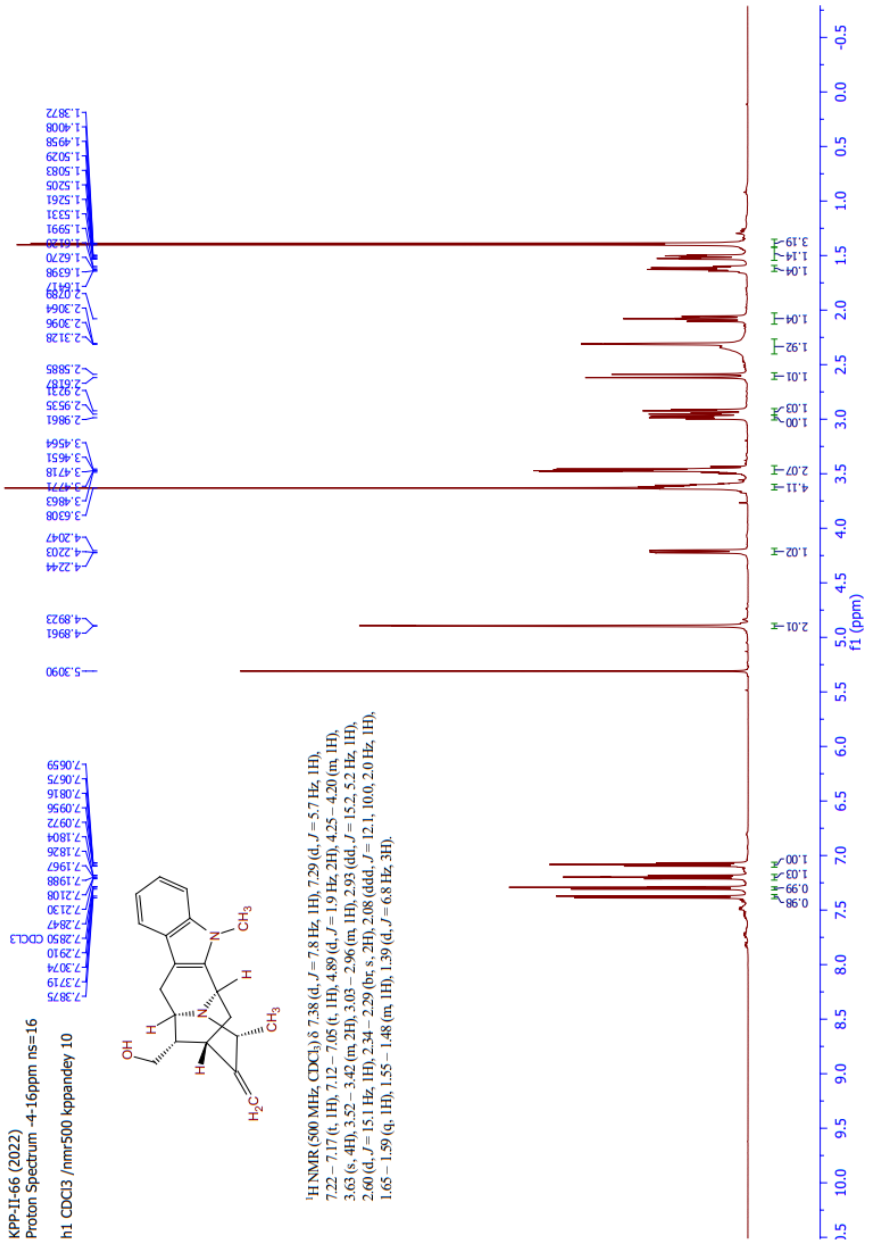
9. **^{1}H NMR of (6*R*,7*R*,8*R*,10*R*,11a*R*)-5,8-dimethyl-9-methylene-5,6,9,10,11a,12-hexahydro-6,10-methanoindolo[3,2-b]quinolizin-11(8H)-one (28).**



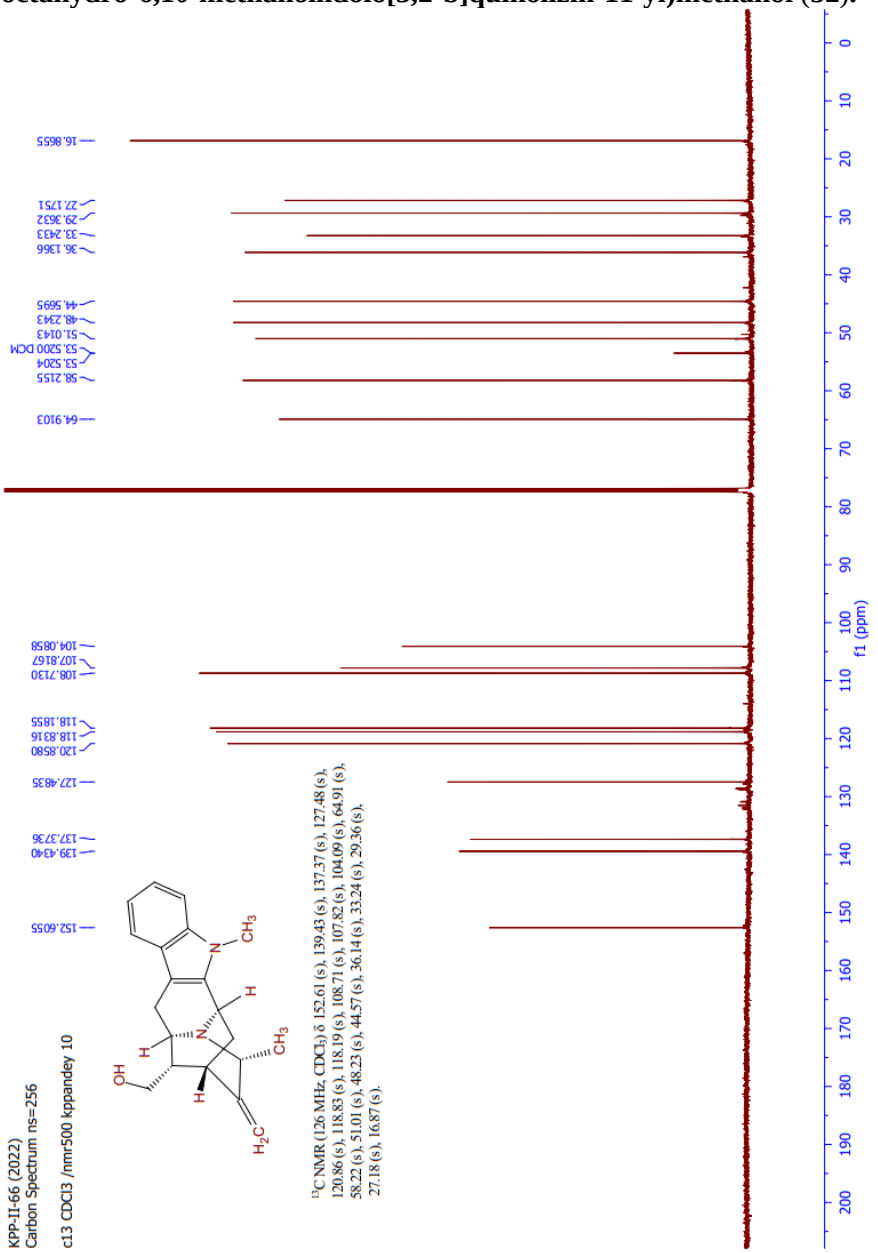
10. **^{13}C NMR of provide (6*R*,7*R*,8*R*,10*R*,11a*R*)-5,8-dimethyl-9-methylene-5,6,9,10,11a,12-hexahydro-6,10-methanoindolo[3,2-b]quinolizin-11(8H)-one (28).**



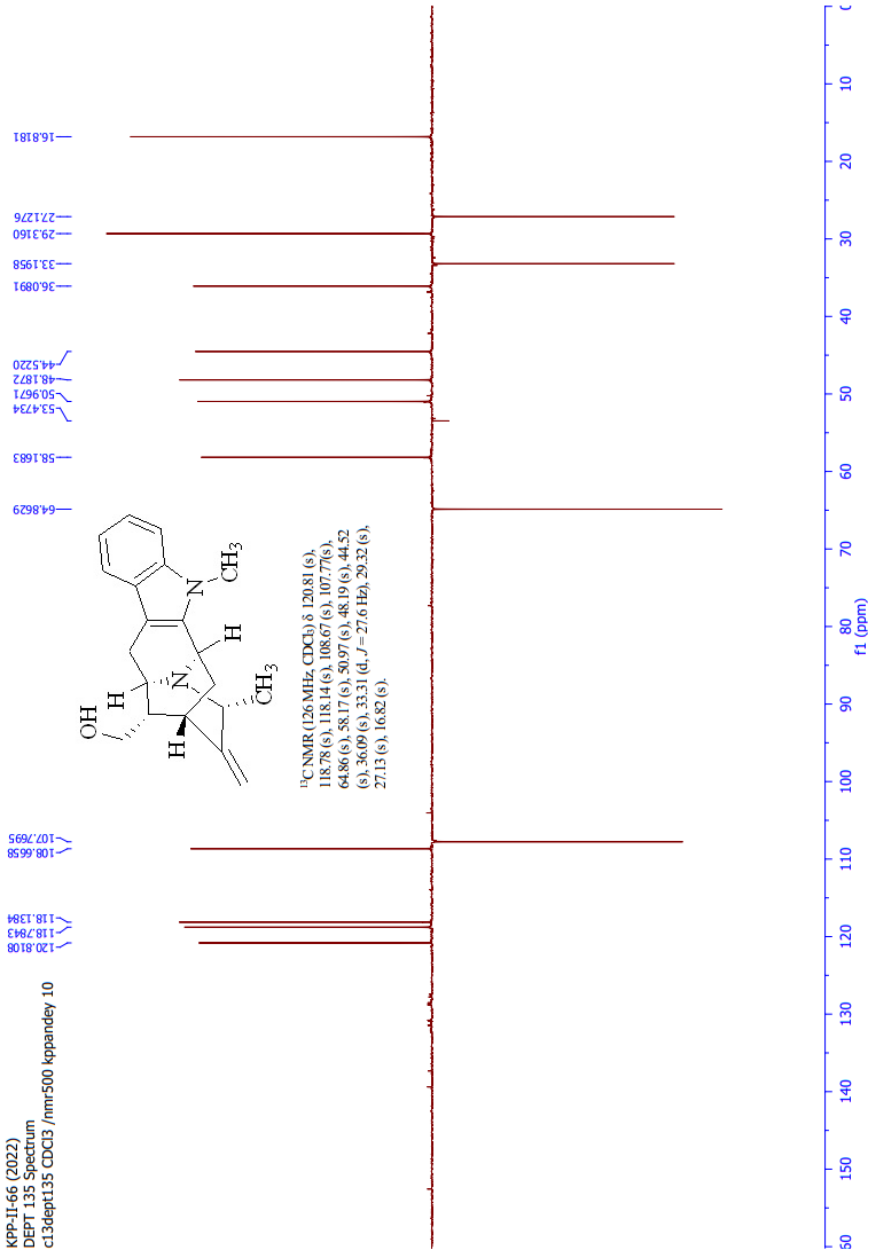
11. **^{1}H NMR of ((6*R*,7*R*,8*R*,10*S*,11*S*,11a*R*)-5,8-dimethyl-9-methylene-5,6,8,9,10,11,11a,12-octahydro-6,10-methanoindolo[3,2-b]quinolizin-11-yl)methanol (52).**



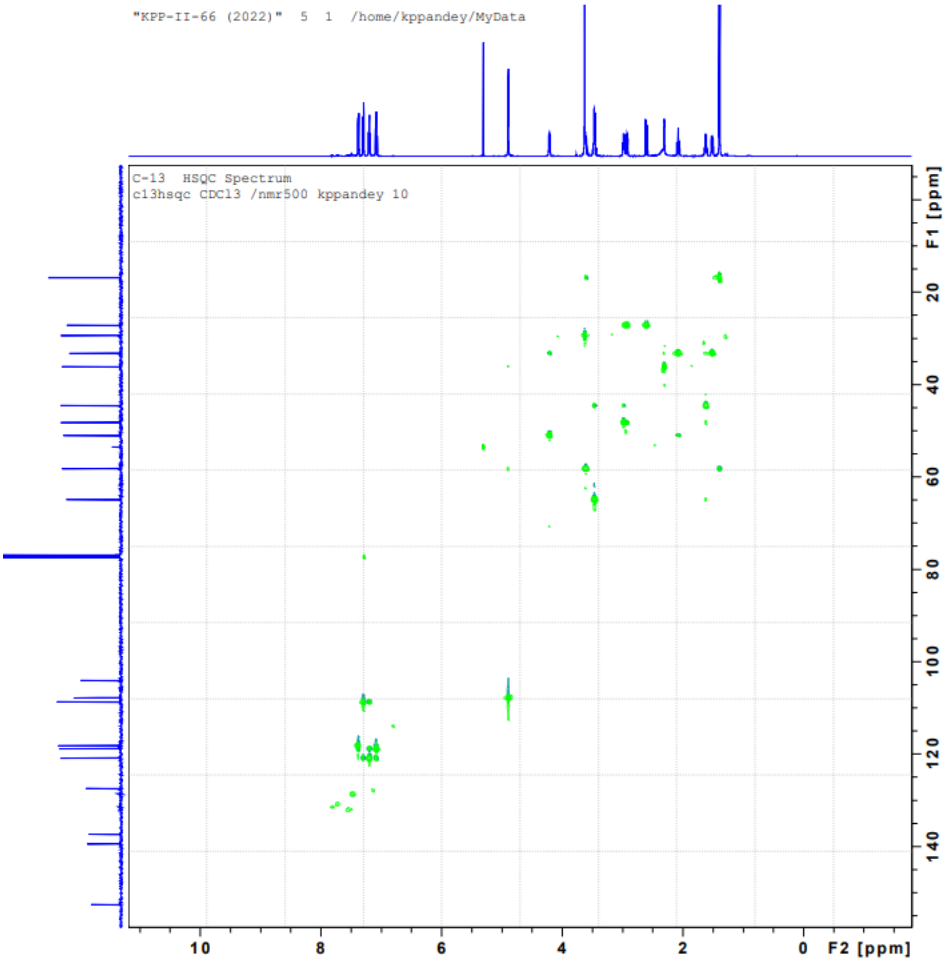
12. **^{13}C NMR of ((6*R*,7*R*,8*R*,10*S*,11*S*,11a*R*)-5,8-dimethyl-9-methylene-5,6,8,9,10,11,11a,12-octahydro-6,10-methanoindolo[3,2-b]quinolizin-11-yl)methanol (52).**



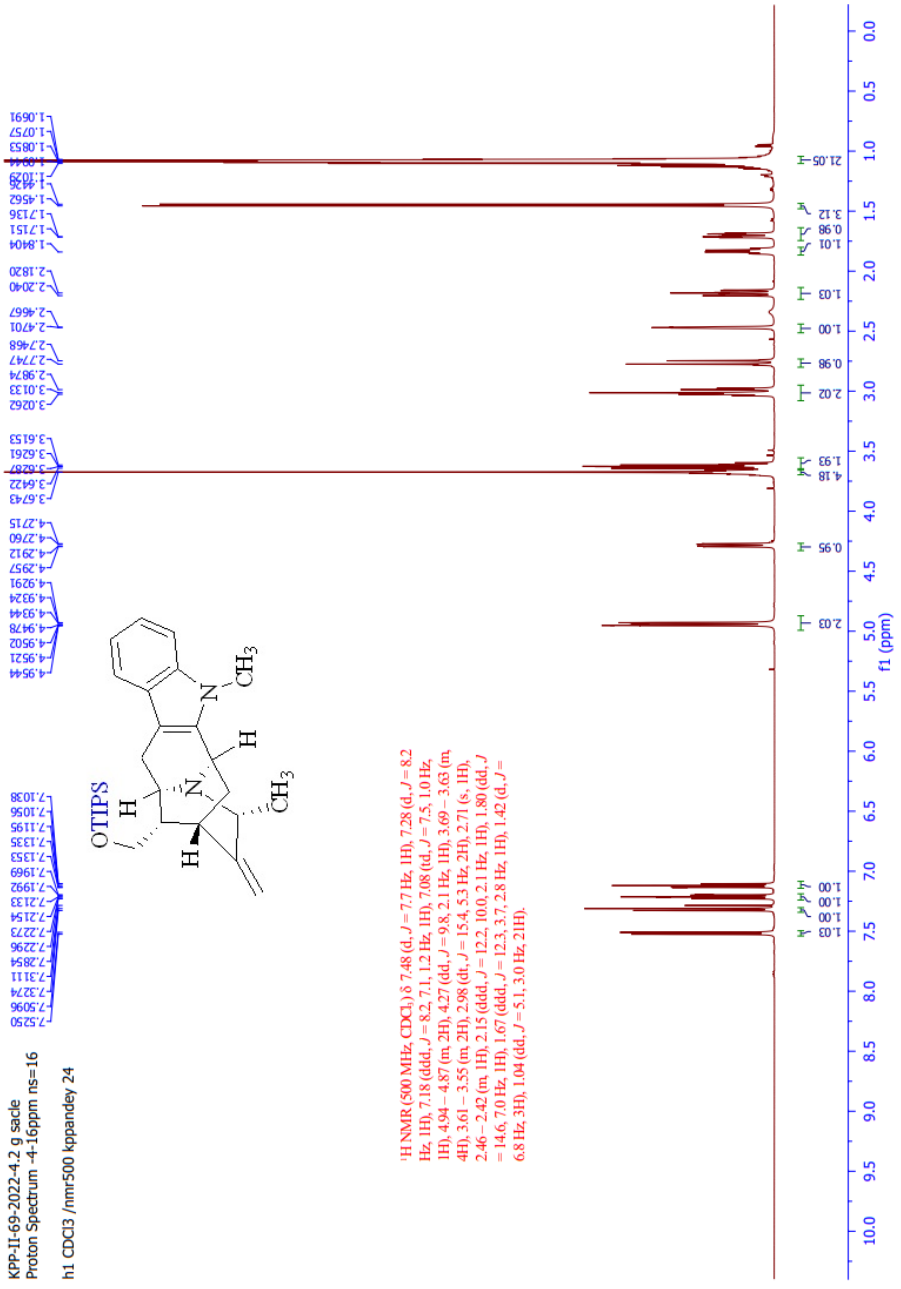
13. **DEPT-135 ^{13}C NMR of ((6*R*,7*R*,8*R*,10*S*,11*S*,11a*R*)-5,8-dimethyl-9-methylene-5,6,8,9,10,11,11a,12-octahydro-6,10-methanoindolo[3,2-b]quinolizin-11-yl)methanol (52).**



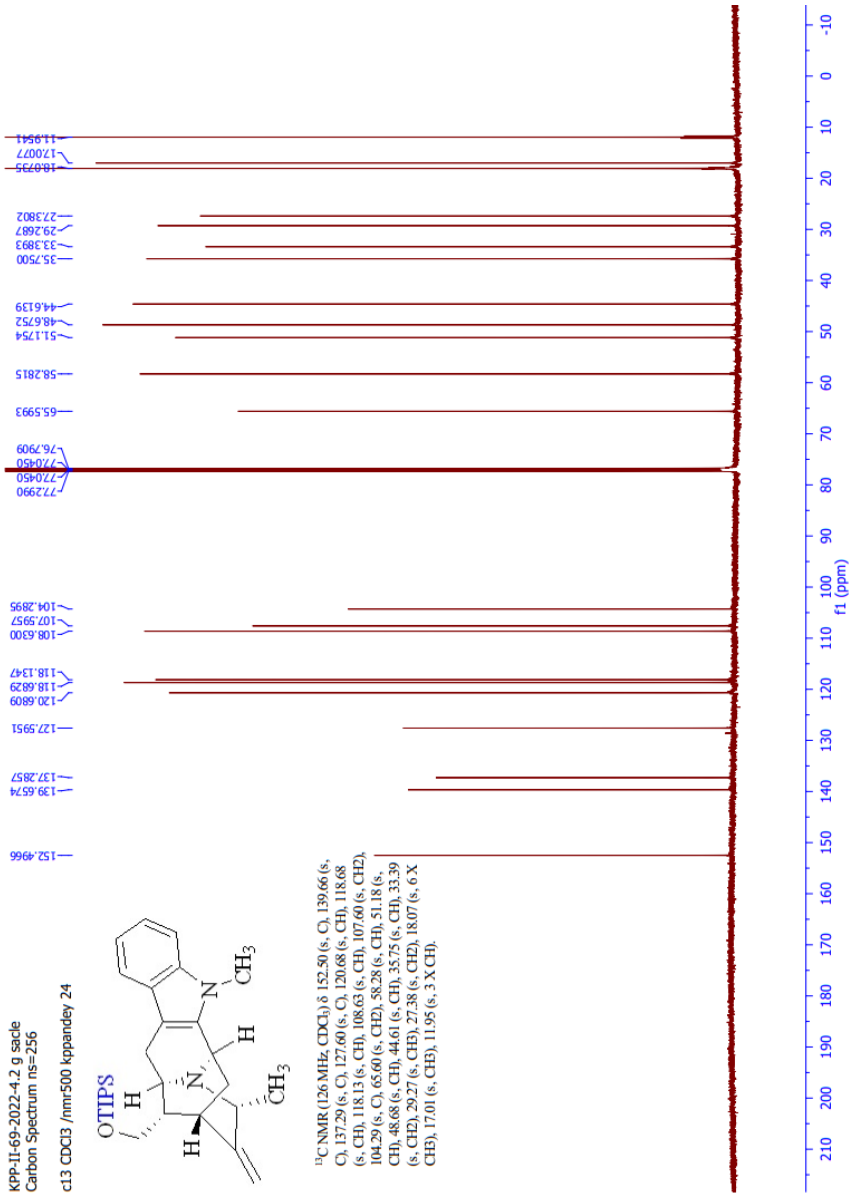
14. **^{13}C HSQC spectrum of ((6*R*,7*R*,8*R*,10*S*,11*S*,11a*R*)-5,8-dimethyl-9-methylene-5,6,8,9,10,11,11a,12-octahydro-6,10-methanoindolo[3,2-b]quinolizin-11-yl)methanol (52).**



15. **^{1}H NMR of (6*R*,7*R*,8*R*,10*S*,11*S*,11a*R*)-5,8-dimethyl-9-methylene-11-(((triisopropylsilyl)oxy) methyl)-5,6,8,9,10,11,11a,12-octahydro-6,10-methanoindolo[3,2-b]quinolizine (27).**

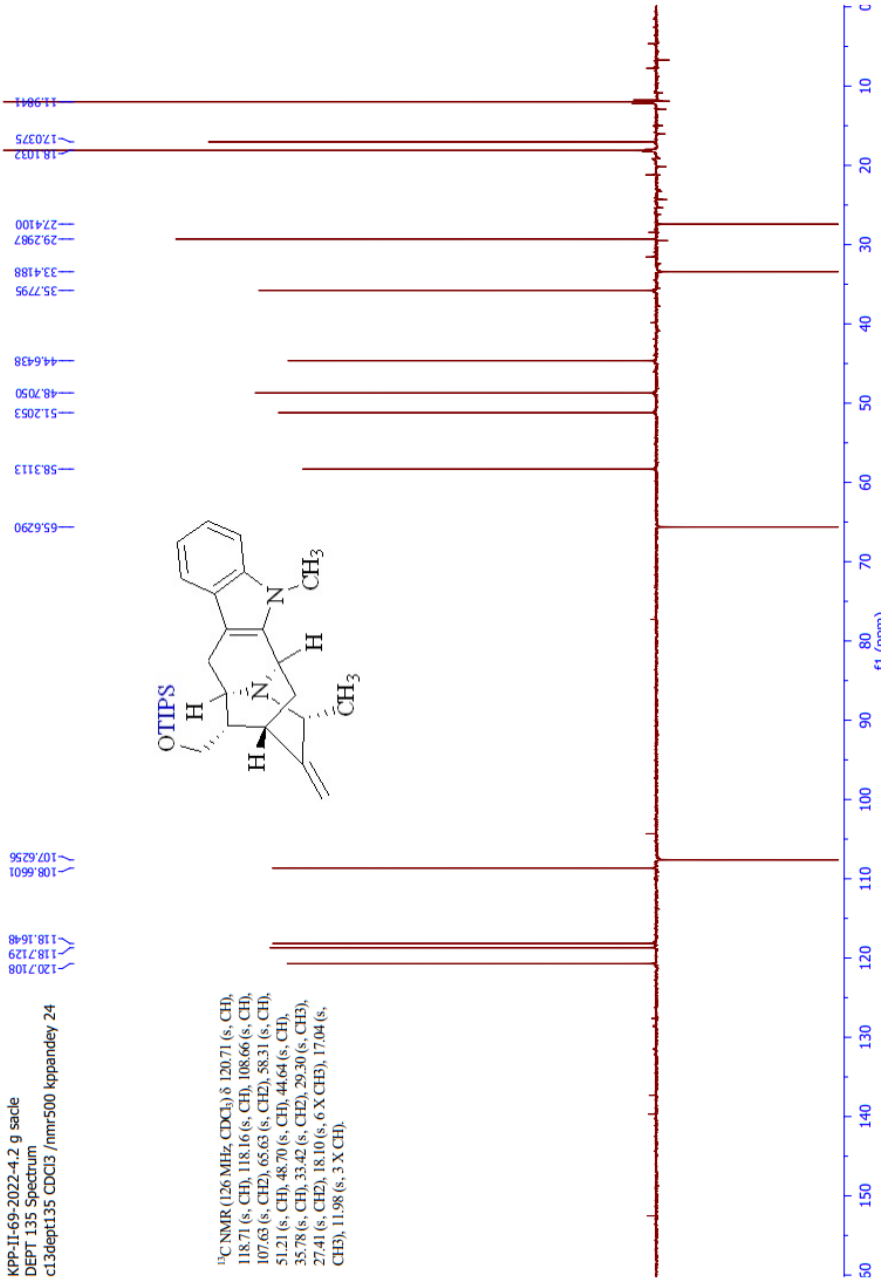


16. **^{13}C NMR of (6*R*,7*R*,8*R*,10*S*,11*S*,11a*R*)-5,8-dimethyl-9-methylene-11-(((triisopropylsilyl)oxy) methyl)-5,6,8,9,10,11,11a,12-octahydro-6,10-methanoindolo[3,2-b]quinolizine (27).**

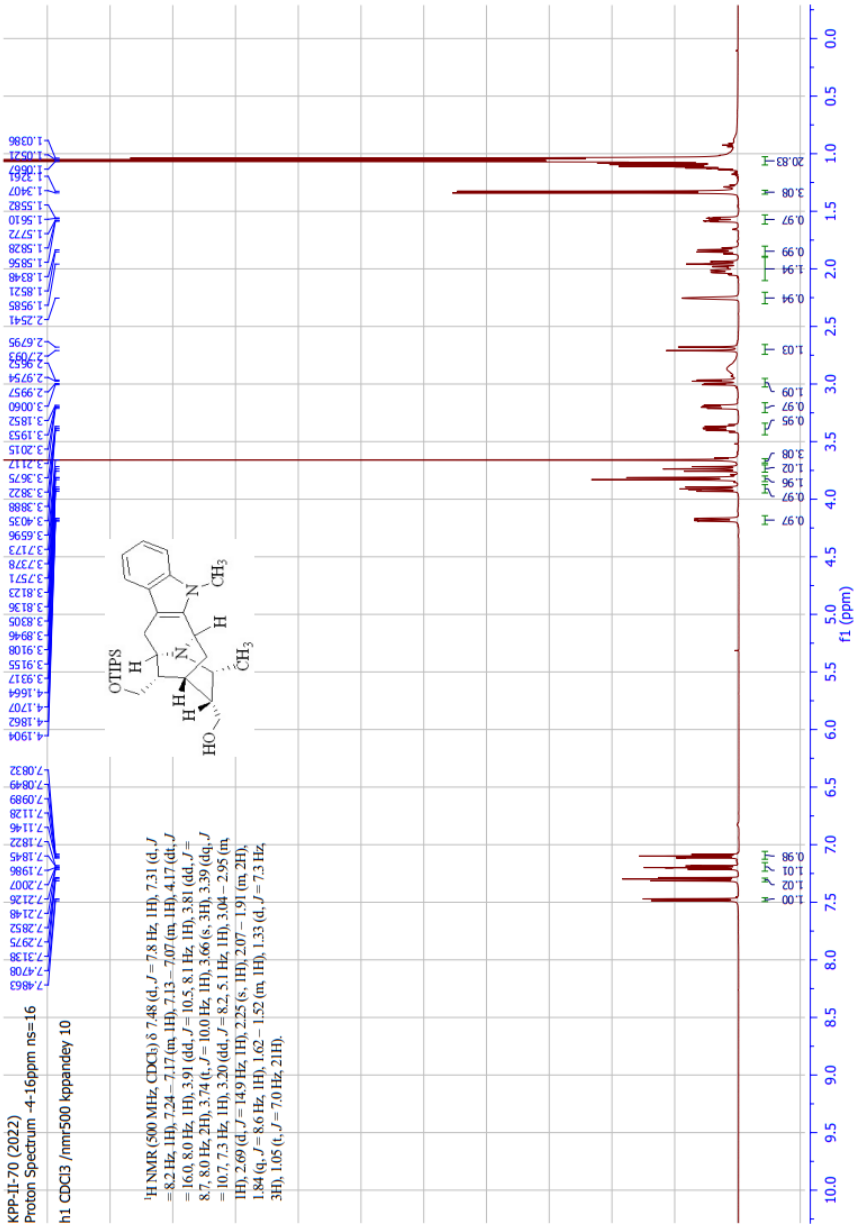


^{13}C NMR (126 MHz, $CDCl_3$) δ 152.50 (s, C), 139.66 (s, C), 137.29 (s, C), 127.60 (s, C), 120.68 (s, CH), 118.68 (s, CH), 118.13 (s, CH), 108.63 (s, CH), 107.60 (s, CH2), 104.29 (s, C), 65.60 (s, CH2), 58.28 (s, CH), 51.18 (s, CH), 48.68 (s, CH), 44.61 (s, CH), 35.75 (s, CH), 33.39 (s, CH2), 29.27 (s, CH3), 27.38 (s, CH2), 18.07 (s, 6 X CH3), 17.01 (s, CH3), 11.95 (s, 3 X CH).

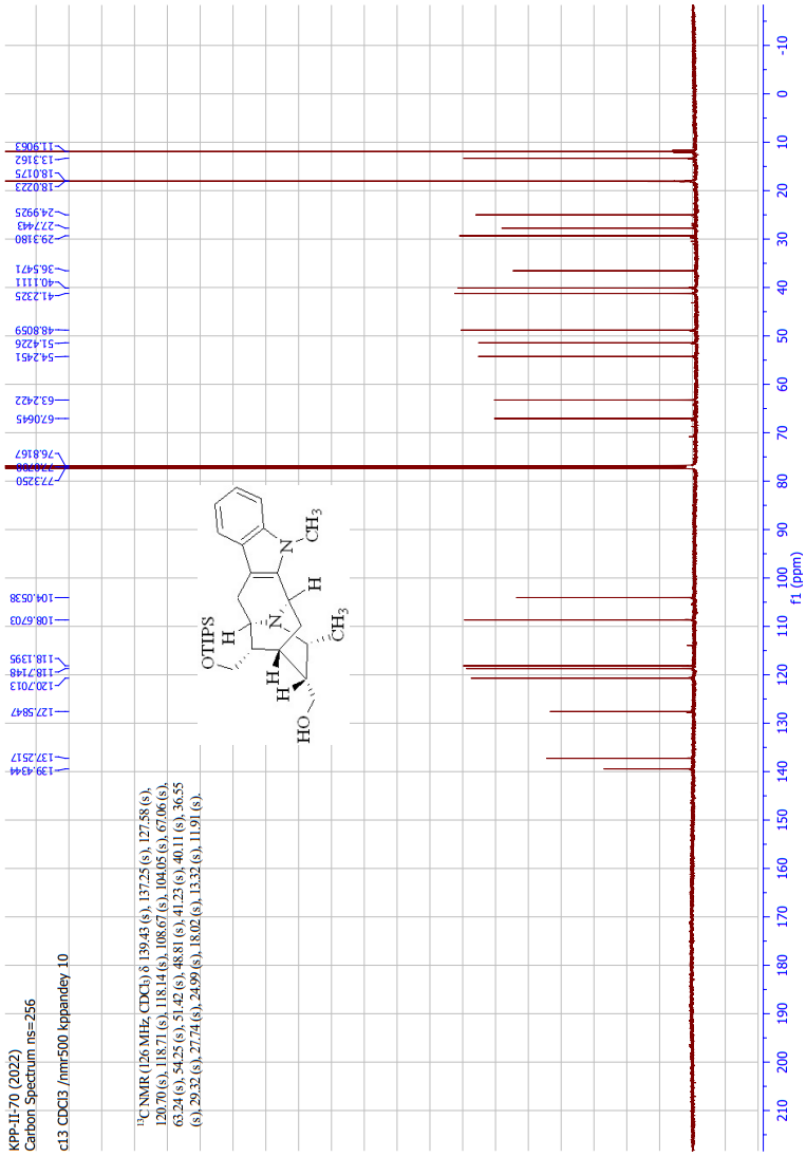
17. **DEPT-135 ^{13}C NMR of (6*R*,7*R*,8*R*,10*S*,11*S*,11a*R*)-5,8-dimethyl-9-methylene-11-(((triisopropylsilyl)oxy) methyl)-5,6,8,9,10,11,11a,12-octahydro-6,10-methanoindolo[3,2-b]quinolizine** (27)**.**



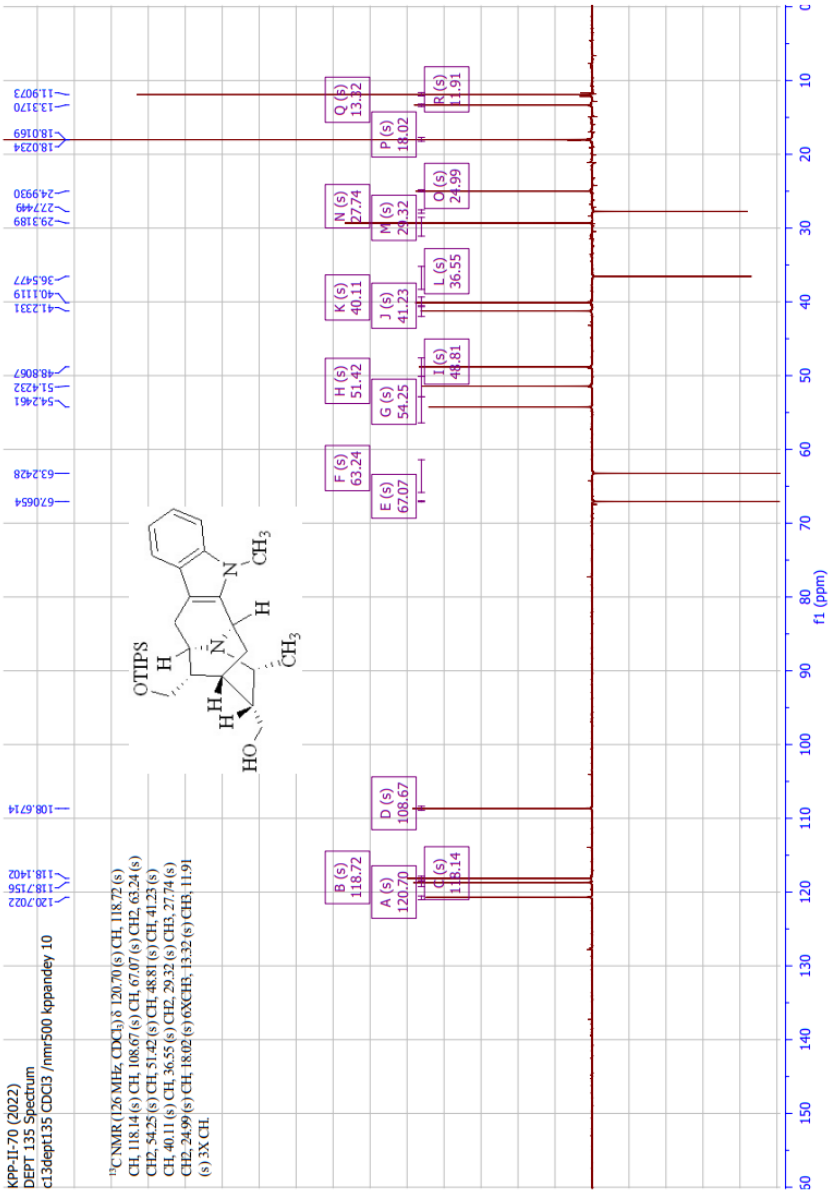
18. **^{1}H NMR of ((6*R*,7*S*,8*R*,9*R*,10*R*,11*S*,11a*R*)-5,8-dimethyl-11-(((triisopropylsilyl)oxy)methyl)-5,6,8,9,10,11,11a,12-octahydro-6,10-methanoindolo[3,2-b]quinolizin-9-yl)methanol** (**26**).



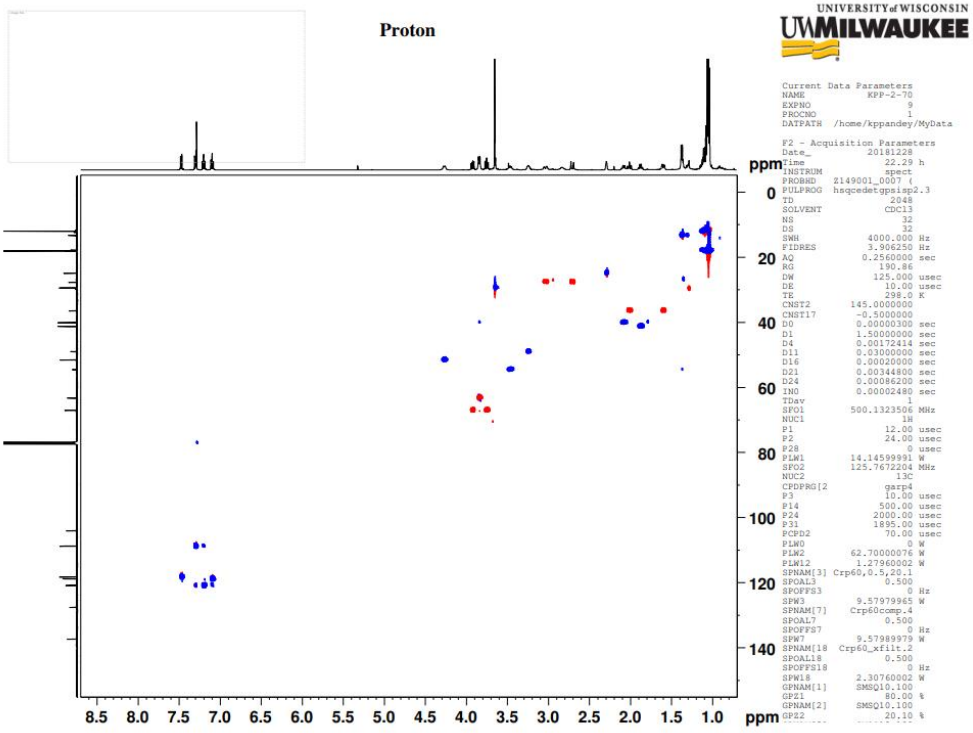
19. **^{13}C NMR of ((6*R*,7*S*,8*R*,9*R*,10*R*,11*S*,11a*R*)-5,8-dimethyl-11-(((triisopropylsilyl)oxy)methyl)-5,6,8,9,10,11,11a,12-octahydro-6,10-methanoindolo[3,2-b]quinolizin-9-yl)methanol (26).**



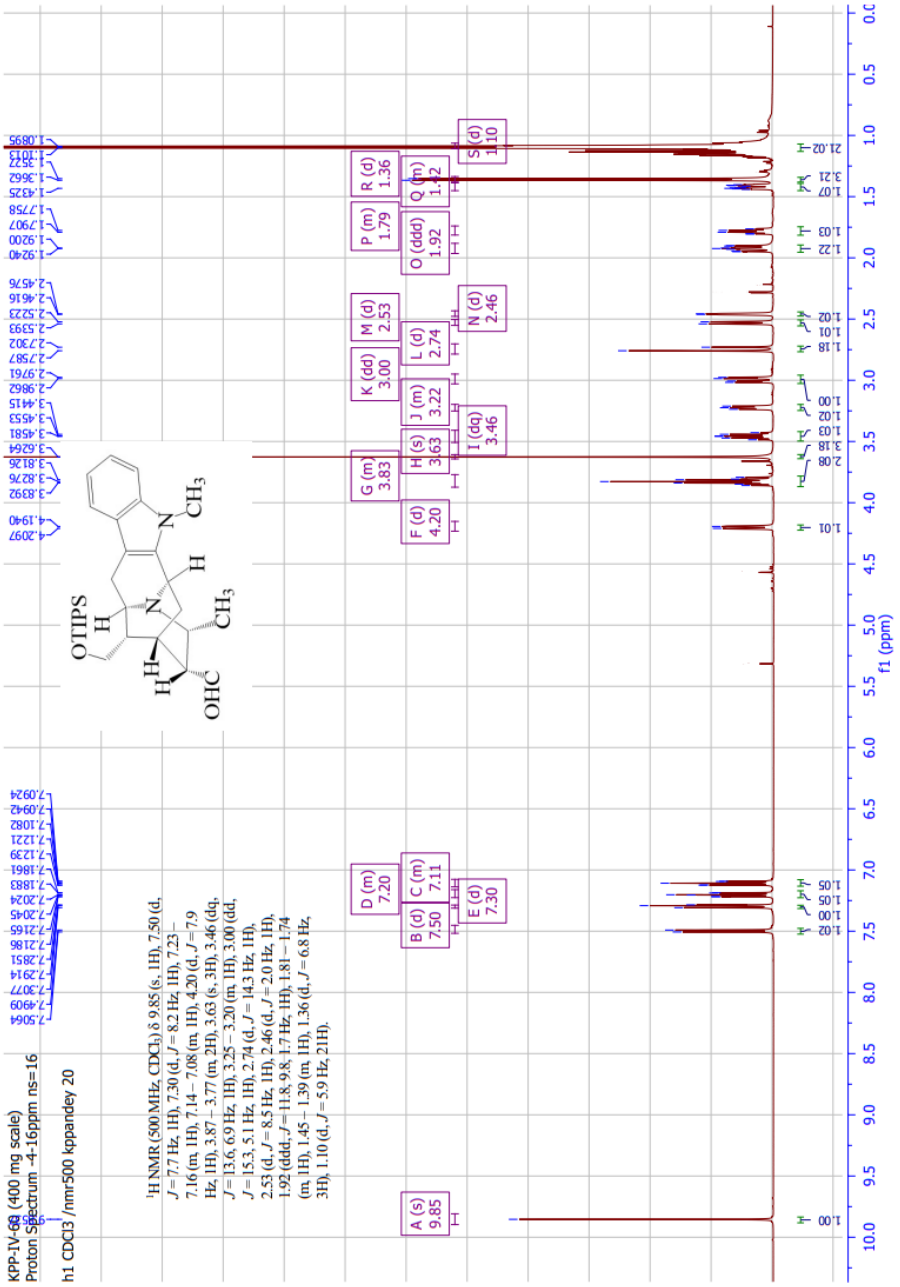
20. **DEPT-135 ^{13}C NMR of ((6*R*,7*S*,8*R*,9*R*,10*R*,11*S*,11a*R*)-5,8-dimethyl-11-(((triisopropylsilyl)oxy)methyl)-5,6,8,9,10,11,11a,12-octahydro-6,10-methanoindolo[3,2-b]quinolizin-9-yl)methanol** (**26**)**.**



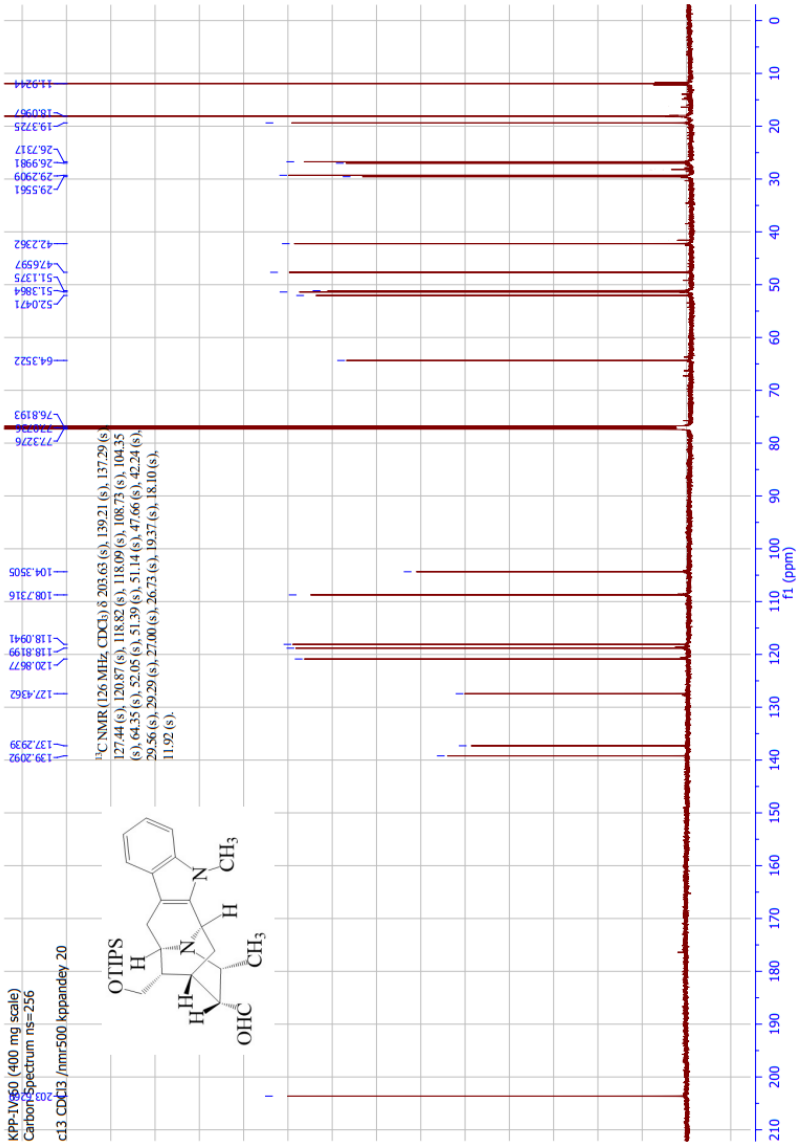
21. **HSQC NMR of ((6*R*,7*S*,8*R*,9*R*,10*R*,11*S*,11a*R*)-5,8-dimethyl-11-(((triisopropylsilyl)oxy)methyl)-5,6,8,9,10,11,11a,12-octahydro-6,10-methanoindolo[3,2-b]quinolizin-9-yl)methanol (26).**



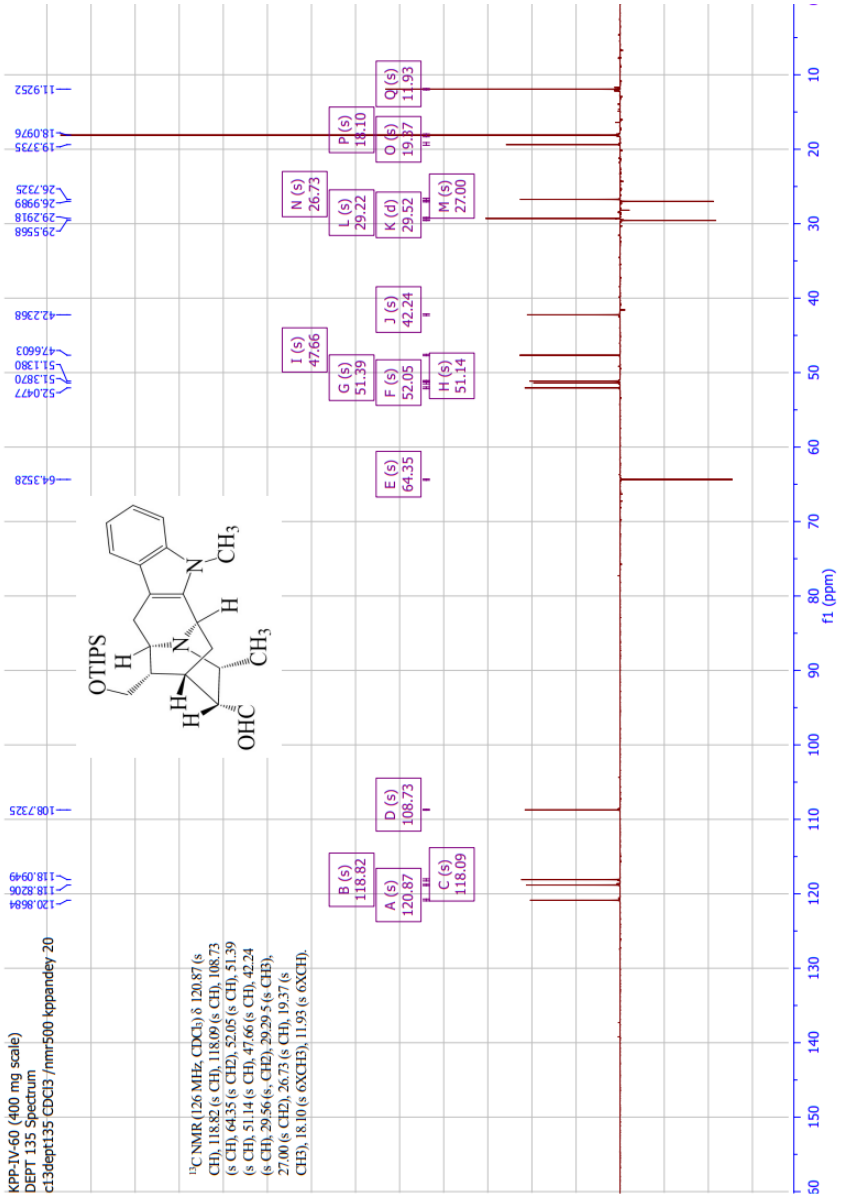
22. **^{1}H NMR of 6*R*,7*S*,8*R*,9*R*,10*S*,11*S*,11a*R*)-5,8-dimethyl-11-(((triisopropylsilyl)oxy) methyl)-5,6,8,9,10,11,11a,12-octahydro-6,10-methanoindolo[3,2-b]quinolizine-9-carbaldehyde (25).**



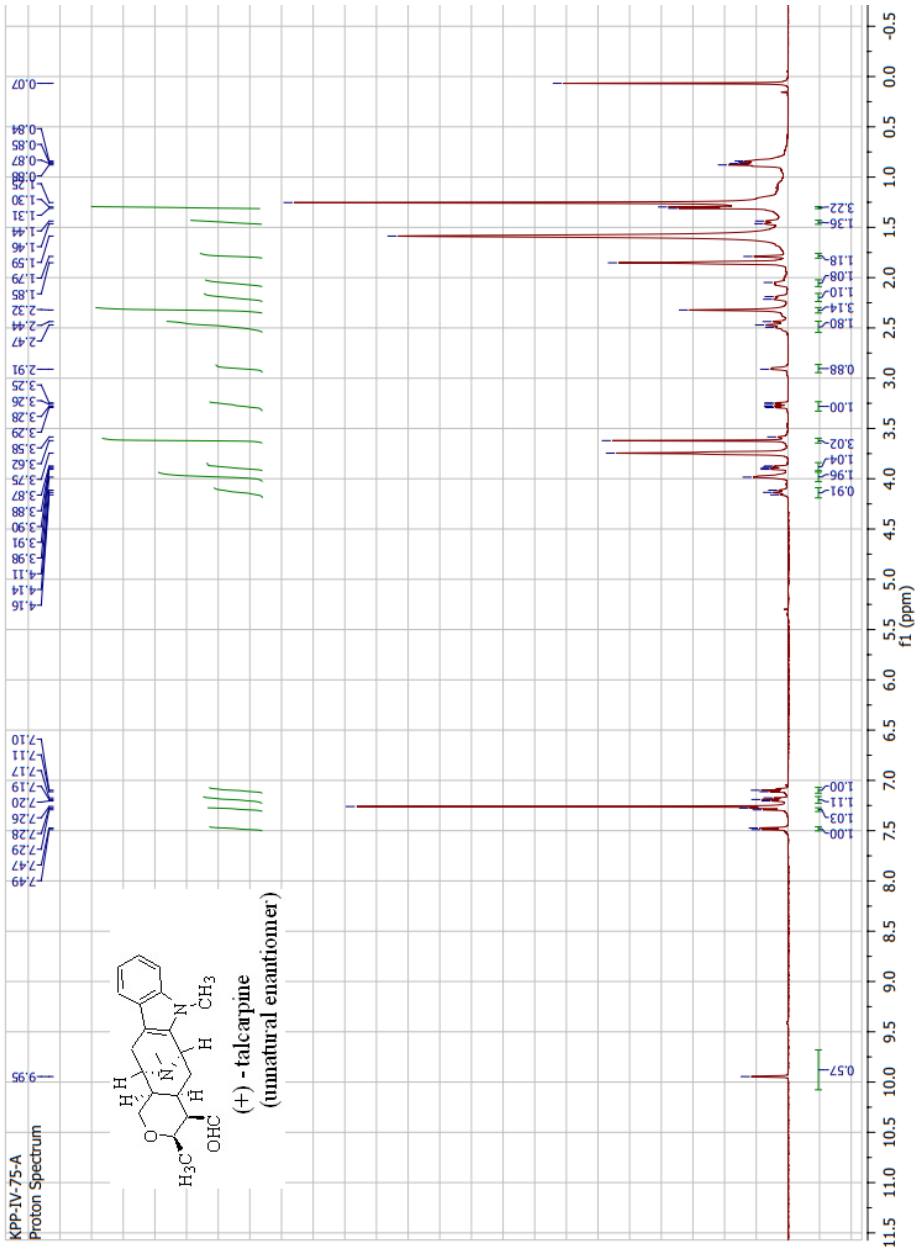
23. **^{13}C NMR of 6*R*,7*S*,8*R*,9*R*,10*S*,11*S*,11a*R*)-5,8-dimethyl-11-(((triisopropylsilyl)oxy) methyl)-5,6,8,9,10,11,11a,12-octahydro-6,10-methanoindolo[3,2-b]quinolizine-9-carbaldehyde (25).**



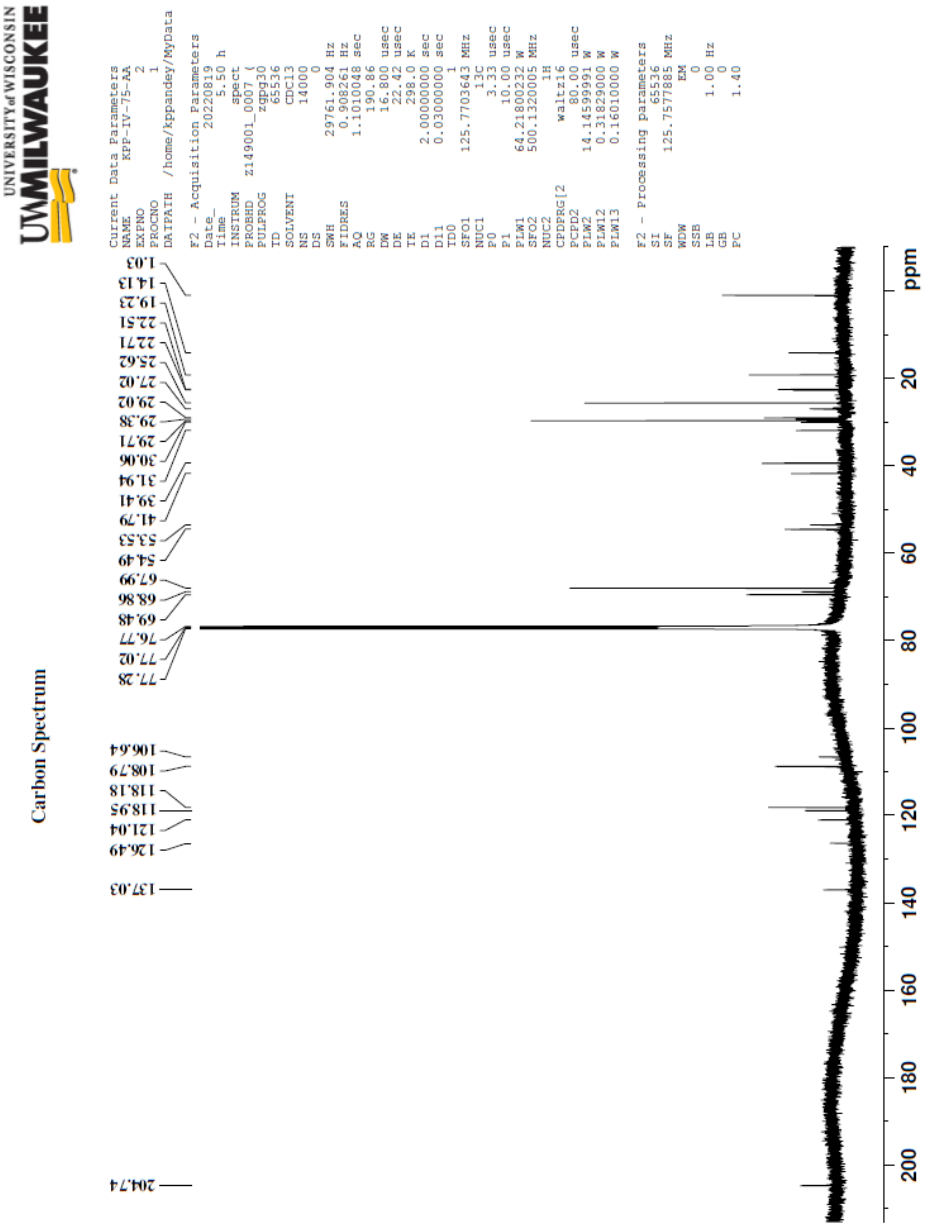
24. **DEPT-135 ^{13}C NMR of 6*R*,7*S*,8*R*,9*R*,10*S*,11*S*,11a*R*)-5,8-dimethyl-11-(((triisopropylsilyl)oxy) methyl)-5,6,8,9,10,11,11a,12-octahydro-6,10-methanoindolo[3,2-b]quinolizine-9-carbaldehyde (25).**



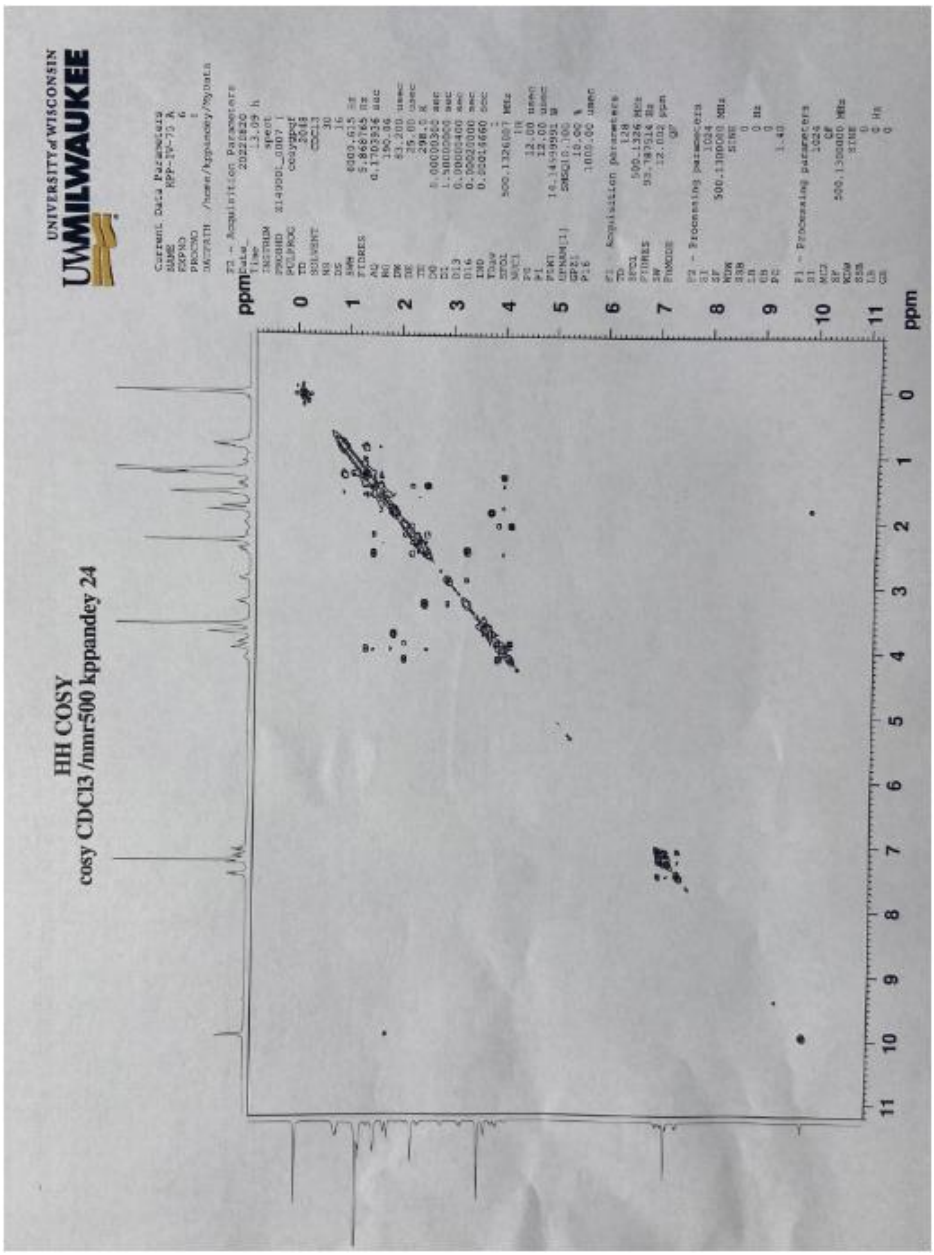
25. **1H NMR spectra of (+) -talcarpine (22).**



26. **^{13} C NMR spectra of (+) -talcarpine (22).**



27. **1H-1H COSY spectra of (+) -talcarpine** (**22**)



HRMS and LCMS spectra (data) Part-I

1. **HRMS analysis of (6*R*,10*R*)-12-((*R*)-but-3-yn-2-yl)-5-methyl-5,6,7,8,10,11-hexahydro-9*H*-6,10-epiminocycloocta[b]indol-9-one (31).**

Formula Predictor Report - kpp-ii-43_Flowscan 700_6.lcd Page 1 of 1

Data File: C:\LabSolutions\Data\AB\MU\02-19-2019\kpp-ii-43_Flowscan 700_6.lcd

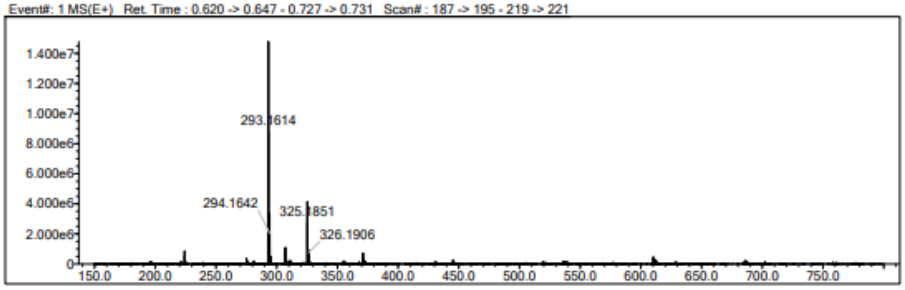
Elmt	Val.	Min	Max	Elmt	Val.	Min	Max	Elmt	Val.	Min	Max	Elmt	Val.	Min	Max	Use Adduct
H	1	15	25	13C	4	0	0	Si	4	0	0	Pb	2	0	0	H
2H	1	0	0	N	3	0	3	S	2	0	2					Na
B	3	0	0	O	2	0	6	Cl	1	0	2					NH4
C	4	18	22	F	1	0	1	Br	1	0	0					

Error Margin (ppm): 1000
HC Ratio: unlimited
Max Isotopes: all
MSn Iso RI (%): 75.00

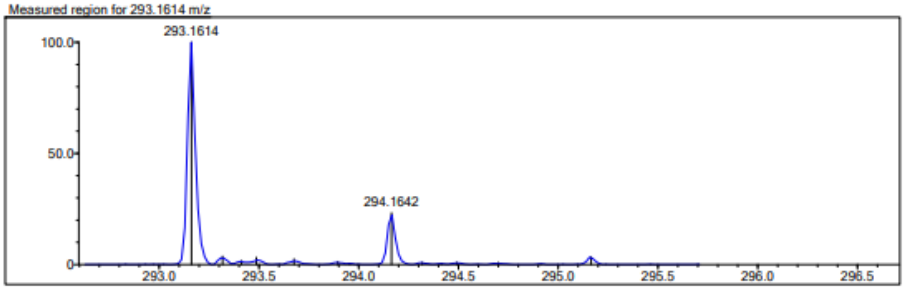
DBE Range: -2.0 - 1000.0
Apply N Rule: yes
Isotope RI (%): 1.00
MSn Logic Mode: AND

Electron Ions: both
Use MSn Info: no
Isotope Res: 10000
Max Results: 10

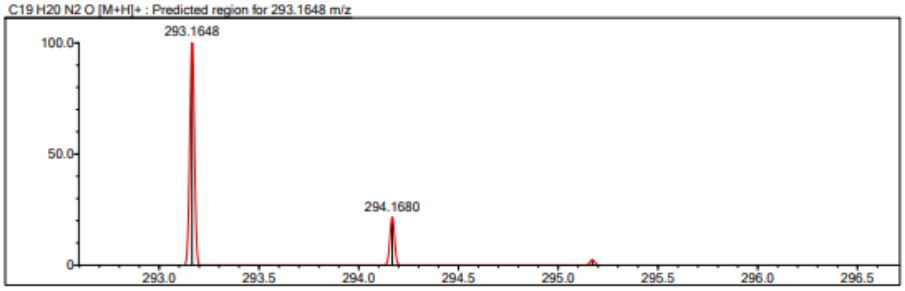
Event#: 1 MS(E+) Ret. Time : 0.620 -> 0.647 - 0.727 -> 0.731 Scan# : 187 -> 195 - 219 -> 221



Measured region for 293.1614 m/z



C19 H20 N2 O [M+H]+ : Predicted region for 293.1648 m/z



Rank	Score	Formula (M)	Ion	Meas. m/z	Pred. m/z	Df. (mDa)	Df. (ppm)	Iso	DBE
1	22.81	C19 H20 N2 O	[M+H]+	293.1614	293.1648	-3.4	-11.60	63.83	11.0

2. HRMS analysis of (6*R*,10*R*)-12-benzyl-5-methyl-5,6,7,8,10,11-hexahydro-9*H*-6,10-epiminocycloocta[b]indol-9-one (42).

Formula Predictor Report - kpp-10100_Flowscan 700_2.lcd

Data File: C:\LabSolutions\Data\AB\MU\02-19-2019\kpp-10100_Flowscan 700_2.lcd

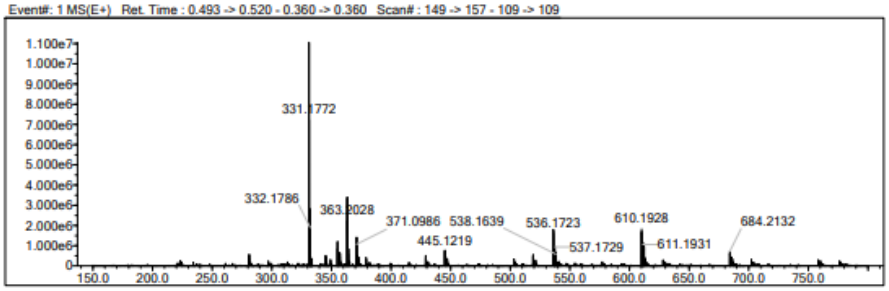
Elmt	Val.	Min	Max	Elmt	Val.	Min	Max	Elmt	Val.	Min	Max	Elmt	Val.	Min	Max	Use Adduct
H	1	15	25	C	4	15	25	O	2	0	3	Cl	1	0	0	H
2H	1	0	0	13C	4	0	0	Si	4	0	2	Br	1	0	0	Na
B	3	0	0	N	3	0	3	S	2	0	0	Pb	2	0	0	NH4

Error Margin (ppm): 1000
HC Ratio: unlimited
Max Isotopes: all
MSn Iso RI (%): 75.00

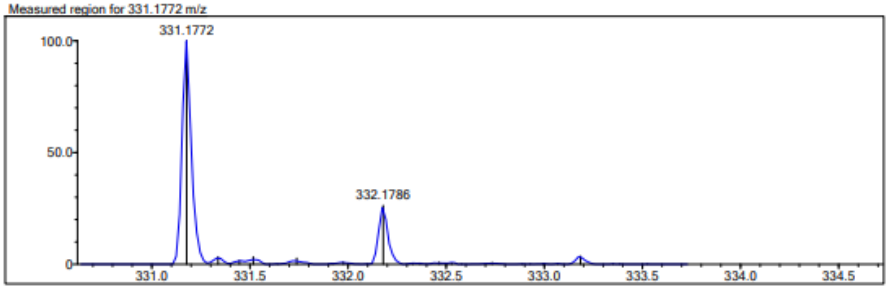
DBE Range: -2.0 - 1000.0
Apply N Rule: yes
Isotope RI (%): 1.00
MSn Logic Mode: AND

Electron Ions: both
Use MSn Info: no
Isotope Res: 10000
Max Results: 10

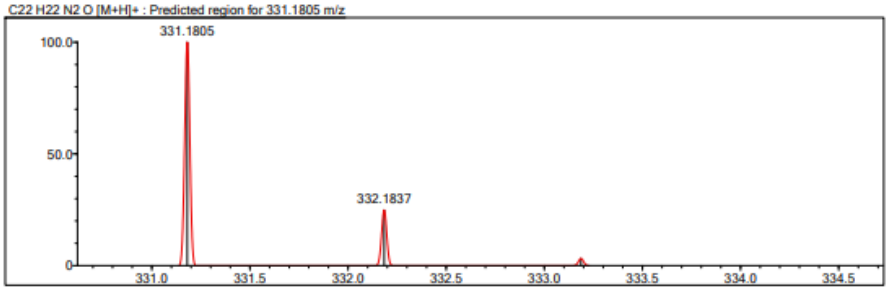
Event#: 1 MS(E+) Ret. Time : 0.493 -> 0.520 - 0.360 -> 0.360 Scan# : 149 -> 157 - 109 -> 109



Measured region for 331.1772 m/z

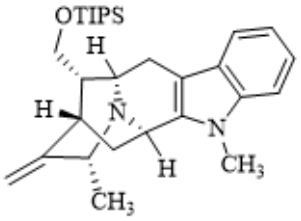


C22 H22 N2 O [M+H]+ : Predicted region for 331.1805 m/z



Rank	Score	Formula (M)	Ion	Meas. m/z	Pred. m/z	Df. (mDa)	Df. (ppm)	Iso	DBE
5	28.30	C22 H22 N2 O	[M+H]+	331.1772	331.1805	-3.3	-9.96	70.05	13.0

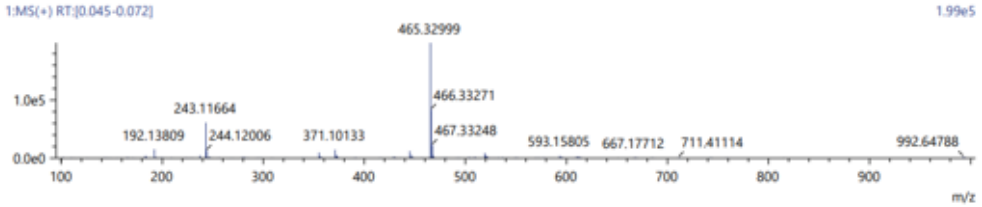
3. **(6*R*,7*R*,8*R*,10*S*,11*S*,11a*R*)-5,8-dimethyl-9-methylene-11-(((triisopropylsilyl)oxy) methyl)-5,6,8,9,10,11,11a,12-octahydro-6,10-methanoindolo[3,2-b]quinolizine** (**27**).

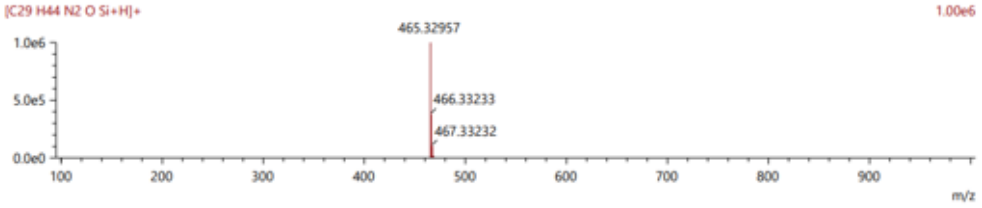


Scan positive no column.lcm

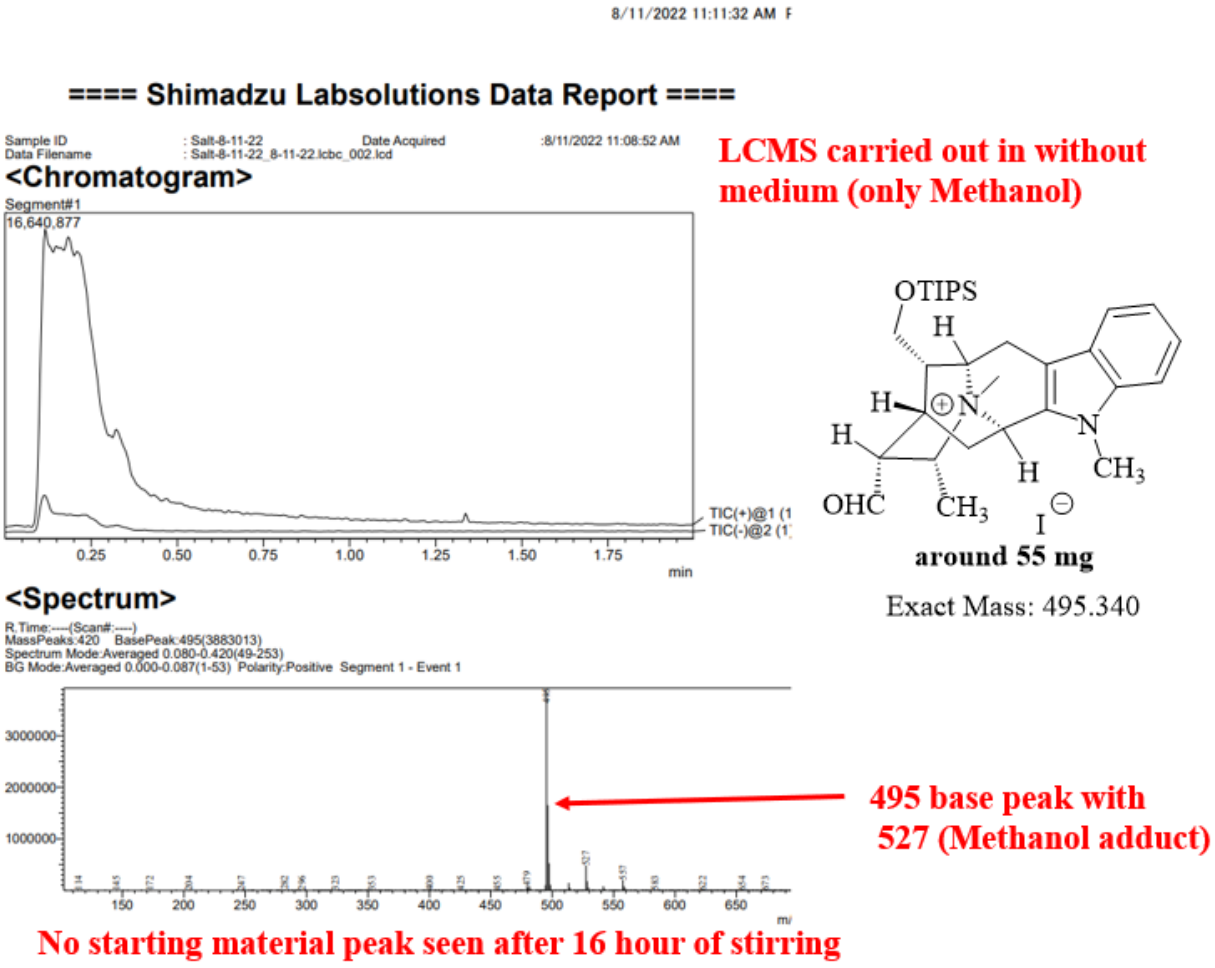
Formula Predictor Result	**C29 H44 N2 O Si**
Mass	465.32999
Error Margin	10 ppm
DBE Range	0 - 1000
Electron Ions	Both configurations
HC Ratio	Not Used
Nitrogen Rule	Used

Score	Pred. (M)	Pred. m/z	Meas. m/z	Diff. (mDa)	Formulae (M)	Ion	Diff. (ppm)	Iso Score	DBE
91.46	464.32229	465.32957	465.32999	0.42	C29 H44 N2 O Si	[M+H]+	0.903	90.96	9.0

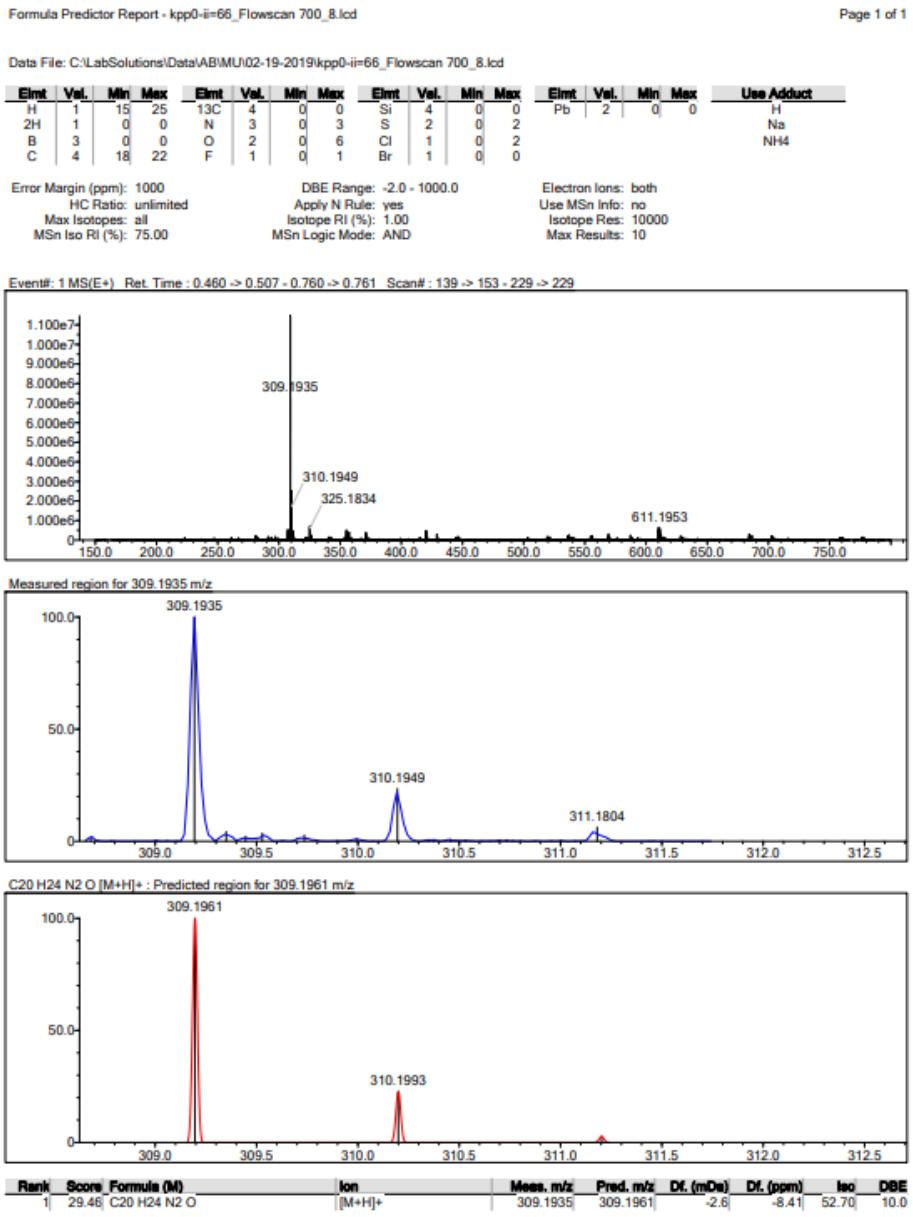




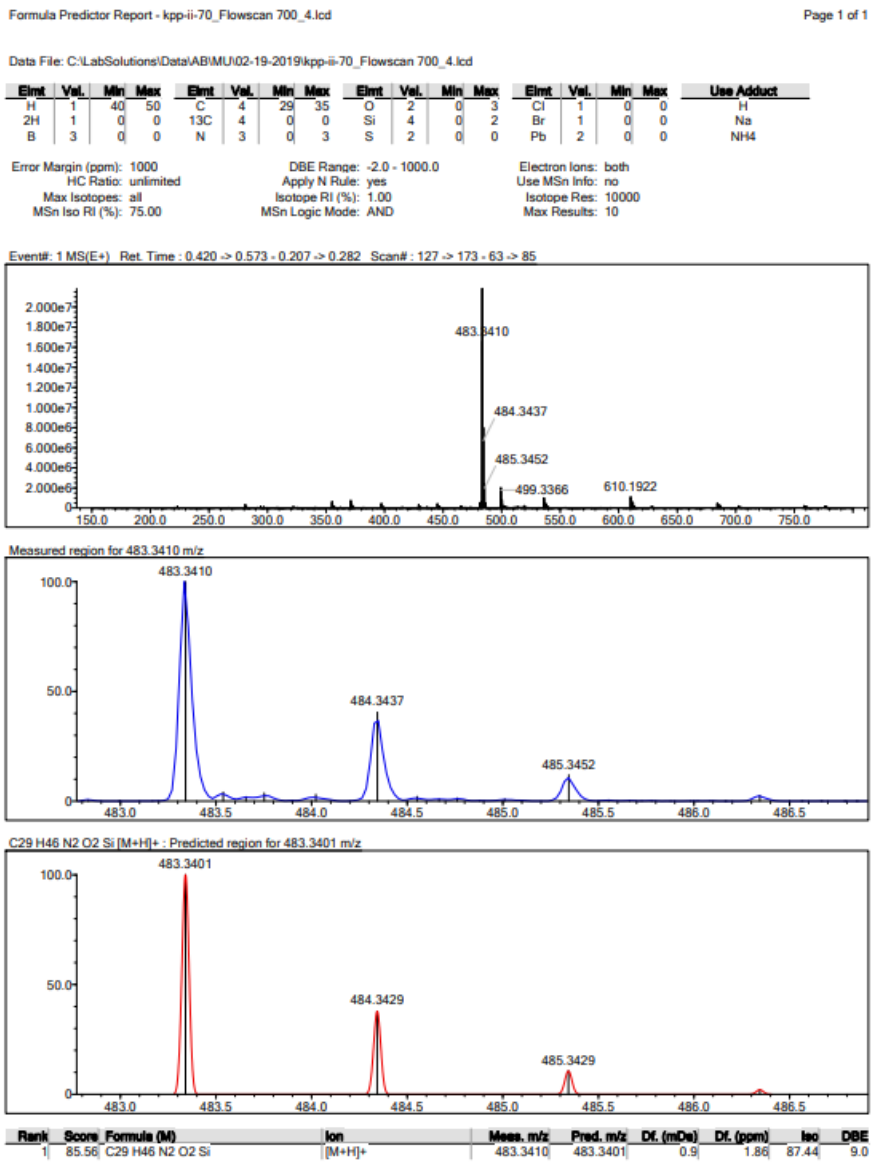
4. **LCMS analysis of ((6*R*,7*R*,8*R*,10*S*,11*S*,11a*R*)-5,8-dimethyl-9-methylene-5,6,8,9,10,11,11a,12-octahydro-6,10-methanoindolo[3,2-b]quinolizin-11-yl)methanol (56).**



5. HRMS analysis of ((6*R*,7*R*,8*R*,10*S*,11*S*,11a*R*)-5,8-dimethyl-9-methylene-5,6,8,9,10,11,11a,12-octahydro-6,10-methanoindolo[3,2-b]quinolizin-11-yl)methanol (27).



6. HRMS analysis of ((6*R*,7*S*,8*R*,9*R*,10*R*,11*S*,11a*R*)-5,8-dimethyl-11-(((triisopropylsilyl)oxy)methyl)-5,6,8,9,10,11,11a,12-octahydro-6,10-methanoindolo[3,2-b]quinolizin-9-yl)methanol (26).



Formula Predictor Report - kpp-ii-70_Flowscan 700_4.lcd Page 1 of 1

Data File: C:\LabSolutions\Data\AB\MU\02-19-2019\kpp-ii-70_Flowscan 700_4.lcd

Elmt	Val.	Min	Max	Elmt	Val.	Min	Max	Elmt	Val.	Min	Max	Elmt	Val.	Min	Max	Use Adduct
H	1	40	50	C	4	29	35	O	2	0	3	Cl	1	0	0	H
2H	1	0	0	13C	4	0	0	Si	4	0	2	Br	1	0	0	Na
B	3	0	0	N	3	0	3	S	2	0	0	Pb	2	0	0	NH4

Error Margin (ppm): 1000
HC Ratio: unlimited
Max Isotopes: all
MSn Iso RI (%): 75.00

DBE Range: -2.0 - 1000.0
Apply N Rule: yes
Isotope RI (%): 1.00
MSn Logic Mode: AND

Electron Ions: both
Use MSn Info: no
Isotope Res: 10000
Max Results: 10

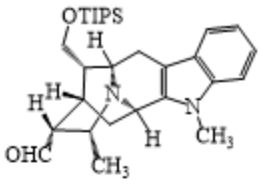
Event#: 1 MS(E+) Ret. Time : 0.420 -> 0.573 - 0.207 -> 0.282 Scan# : 127 -> 173 - 63 -> 85

Measured region for 483.3410 m/z

C29 H46 N2 O2 Si [M+H]+ : Predicted region for 483.3401 m/z

Rank	Score	Formula (M)	Ion	Meas. m/z	Pred. m/z	Df. (mDa)	Df. (ppm)	Iso	DBE
1	85.56	C29 H46 N2 O2 Si	[M+H]+	483.3410	483.3401	0.9	1.86	87.44	9.0

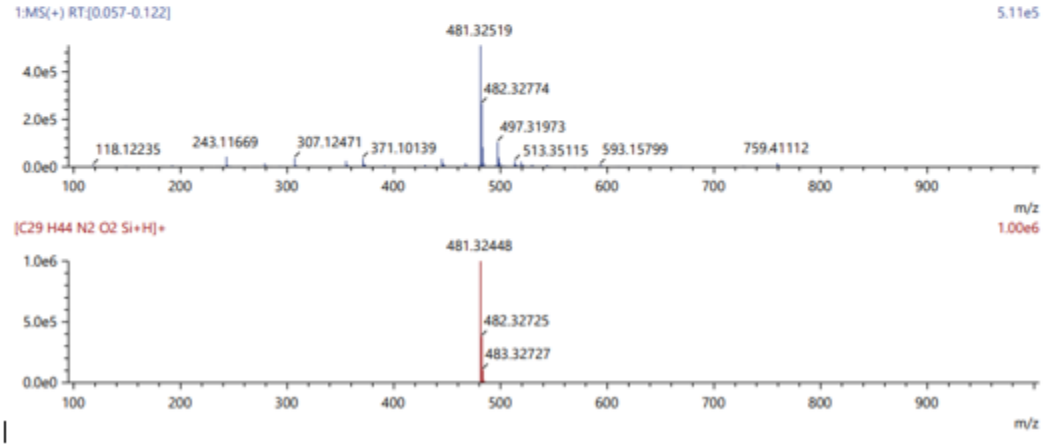
7. **6*R*,7*S*,8*R*,9*R*,10*S*,11*S*,11a*R*)-5,8-dimethyl-11-(((triisopropylsilyl)oxy) methyl)-5,6,8,9,10,11,11a,12-octahydro-6,10-methanoindolo[3,2-b]quinolizine-9-carbaldehyde (25).**



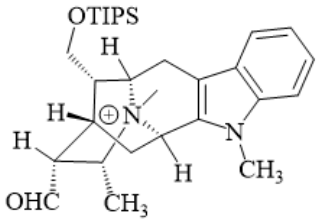
Scan positive no column.lcm

Formula Predictor Result	**C29 H44 N2 O2 Si**
Mass	481.32519
Error Margin	10 ppm
DBE Range	0 - 1000
Electron Ions	Both configurations
HC Ratio	Not Used
Nitrogen Rule	Used

Score	Pred. (M)	Pred. m/z	Meas. m/z	Diff. (mDa)	Formulae (M)	Ion	Diff. (ppm)	Iso Score	DBE
52.29	480.31721	481.32448	481.32519	0.71	C29 H44 N2 O2 Si	[M+H]+	1.475	47.80	9.0



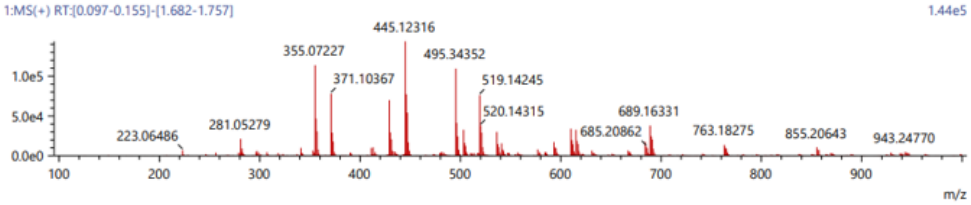
8. HRMS analysis of (6*R*,7*S*,8*R*,9*R*,10*S*,11*S*,11a*R*)-9-formyl-5,7,8-trimethyl-11-(((triisopropylsilyl)oxy) methyl)-6,7,8,9,10,11,11a,12-octahydro-5*H*-6,10-methanoindolo[3,2-b]quinolizin-7-ium (56).

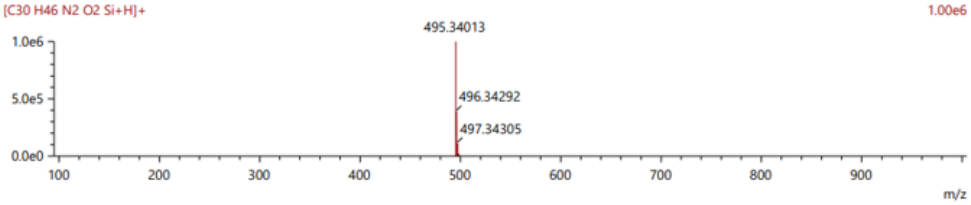


7-29-2022.lcb

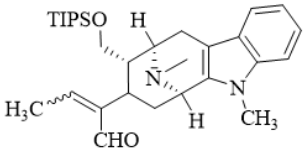
Formula Predictor Result	**C30 H46 N2 O2 Si**
Mass	495.34352
Error Margin	100 ppm
DBE Range	0 - 1000
Electron Ions	Both configurations
HC Ratio	0 - 3
Nitrogen Rule	Used

Score	Pred. (M)	Pred. m/z	Meas. m/z	Diff. (mDa)	Formulae (M)	Ion	Diff. (ppm)	Iso Score	DBE
12.76	494.33286	495.34013	495.34352	3.39	C30 H46 N2 O2 Si	[M+H]+	6.844	14.17	9.0





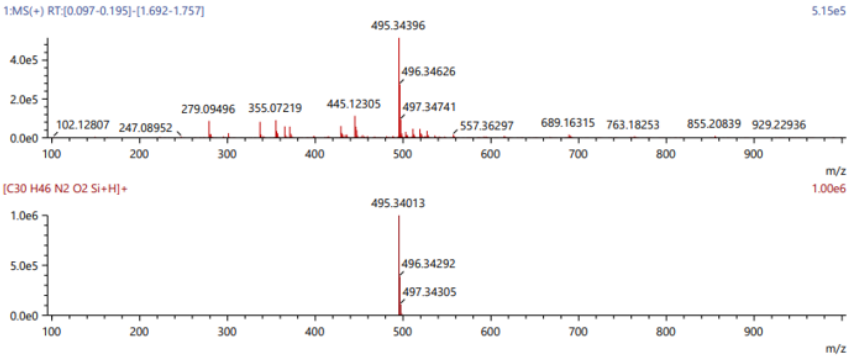
9. HRMS analysis of KPP-IV-68 (57).



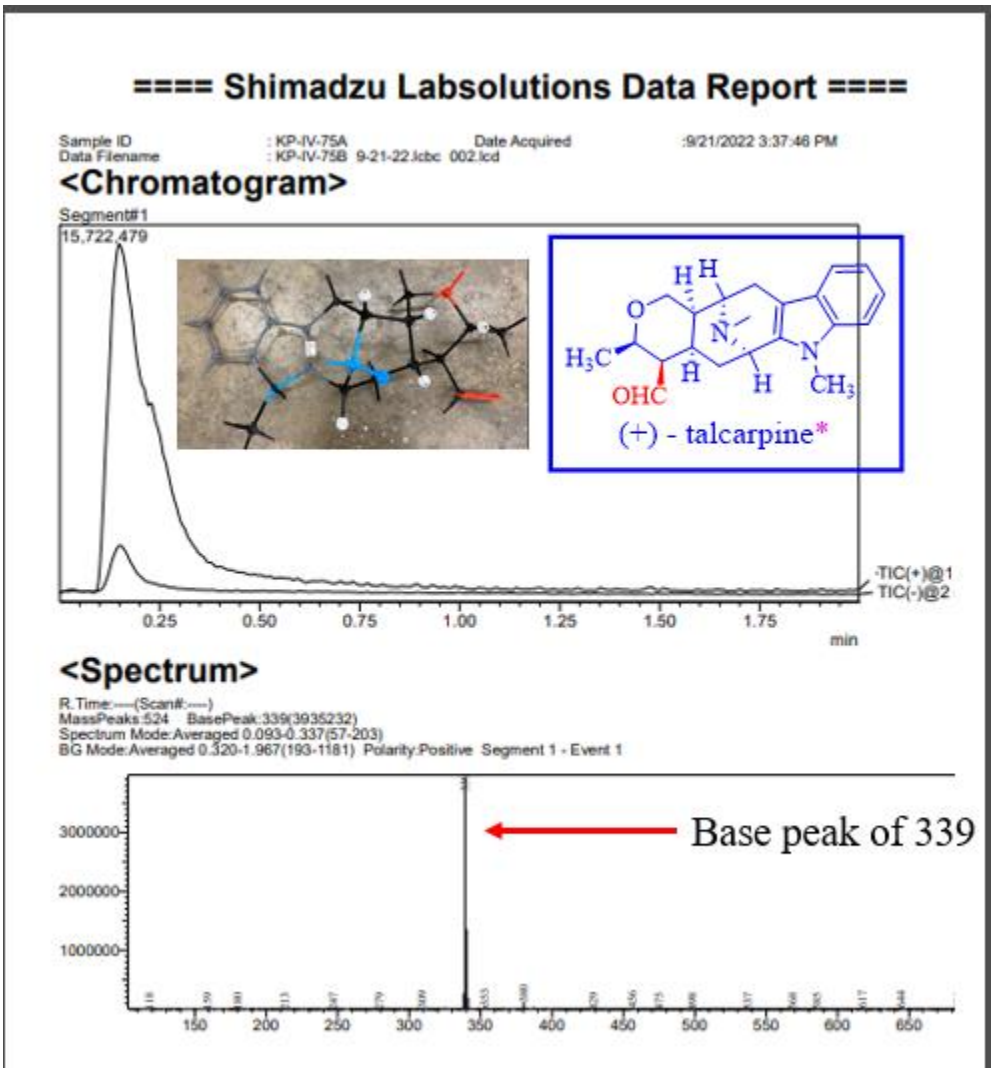
7-29-2022.lcb

Formula Predictor Result	**C30 H46 N2 O2 Si**
Mass	495.34396
Error Margin	100 ppm
DBE Range	0 - 1000
Electron Ions	Both configurations
HC Ratio	0 - 3
Nitrogen Rule	Used

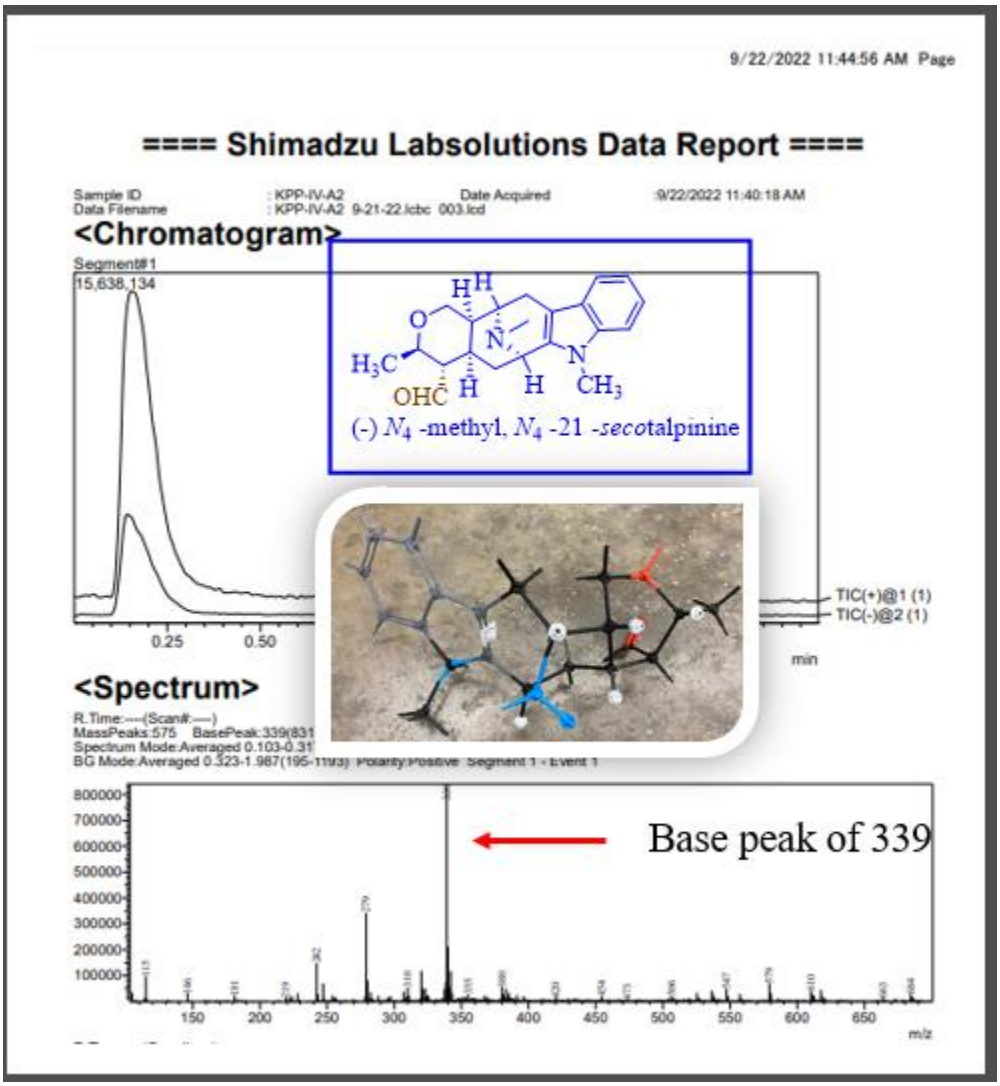
Score	Pred. (M)	Pred. m/z	Meas. m/z	Diff. (mDa)	Formulae (M)	Ion	Diff. (ppm)	Iso Score	DBE
2.82	494.33286	495.34013	495.34396	3.83	C30 H46 N2 O2 Si	[M+H]+	7.732	3.13	9.0



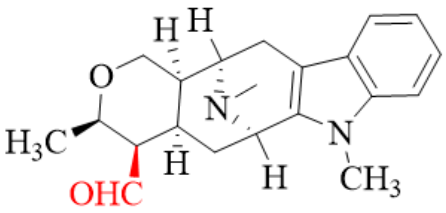
10. LCMS anaysis of (+)-talcarpine (22).



11. LCMS anaysis of (-) N_4 -methyl, N_4 -21 -secotalpinine (23).



12. HRMS analysis of (+)-talcarpine (22).

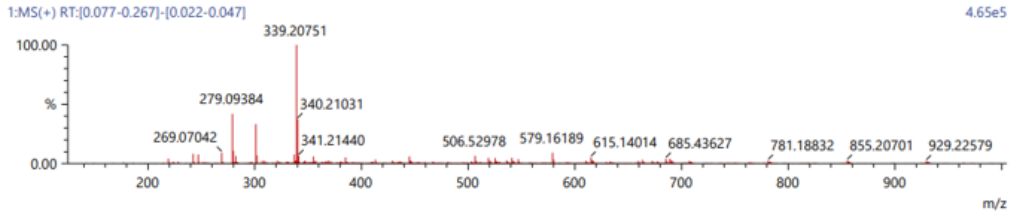


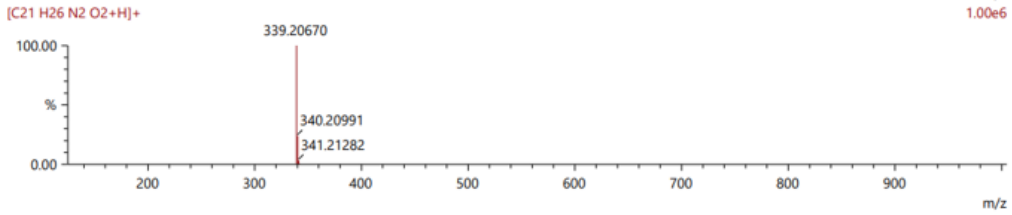
(+) - talcarpine
(unnatural enantiomer)

10-3-2022.lcb

Formula Predictor Result	**C21 H26 N2 O2**
Mass	339.20751
Error Margin	5 ppm
DBE Range	0 - 1000
Electron Ions	Both configurations
HC Ratio	0 - 3
Nitrogen Rule	Used

Score	Pred. (M)	Pred. m/z	Meas. m/z	Diff. (mDa)	Formulae (M)	Ion	Diff. (ppm)	Iso Score	DBE
54.62	338.19943	339.20670	339.20751	0.81	C21 H26 N2 O2	[M+H]+	2.388	51.10	10.0



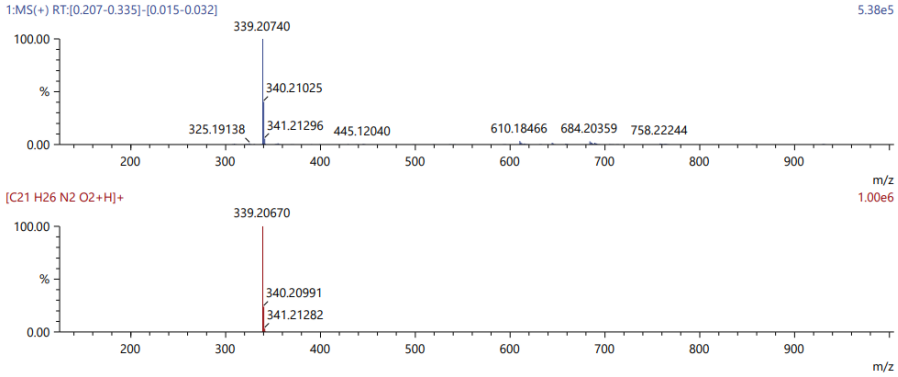


13. HRMS analysis of (-) N_4 -methyl, N_4 -21 -secotalcarpine 23 (presumably based on TLC, LCMS, and HRMS: not confirmed by NMR).

10-3-2022.lcb

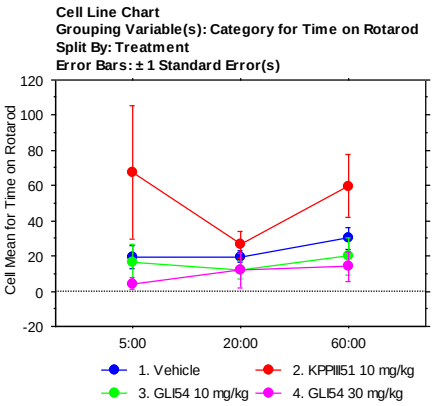
Formula Predictor Result	**C21 H26 N2 O2**
Mass	339.2074
Error Margin	5 ppm
DBE Range	0 - 1000
Electron Ions	Both configurations
HC Ratio	0 - 3
Nitrogen Rule	Used

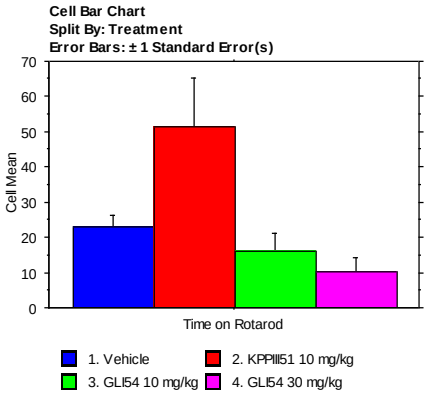
Score	Pred. (M)	Pred. m/z	Meas. m/z	Diff. (mDa)	Formulae (M)	Ion	Diff. (ppm)	Iso Score	DBE
55.19	338.19943	339.20670	339.20740	0.70	C21 H26 N2 O2	[M+H]+	2.064	51.45	10.0



Appendix B: Part II

Effect of KPP-III-51 (10) and GL-I-65 (structure not shown here) on locomotor activity on the Rotarod (Data source: Dr. Thomos Prevot).





ANOVA Table for Time on Rotarod

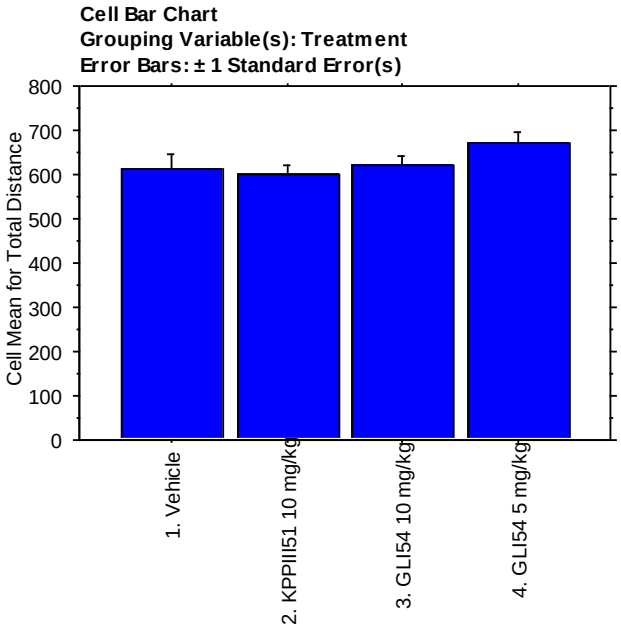
	Treatment	Residual
DF	3	68
Sum of Squares	17965.056	77052.444
Mean Square	5988.352	1133.124
F-Value	5.285	
P-Value	.0025	
Lambda	15.854	
Power	.926	

Scheffe for Time on Rotarod
Effect: Treatment
Significance Level: 5 %

	Mean Diff.	Crit. Diff.	P-Value	
1. Vehicle, 2. KPPIII51 10 mg/kg	-28.333	32.167	.1050	
1. Vehicle, 3. GLI54 10 mg/kg	6.889	32.167	.9446	
1. Vehicle, 4. GLI54 30 mg/kg	12.889	32.167	.7253	
2. KPPIII51 10 mg/kg, 3. GLI54 10 mg/kg	35.222	32.167	.0259	S
2. KPPIII51 10 mg/kg, 4. GLI54 30 mg/kg	41.222	32.167	.0061	S
3. GLI54 10 mg/kg, 4. GLI54 30 mg/kg	6.000	32.167	.9624	

Mice were acclimated to the rotarod over 3 practice trials then administered KPP-III-51 (**10**) (10mg/kg), GL-I-54 (10 mg/kg, 30 mg/kg) or vehicle control via intraperitoneal injection and tested on the rotarod 5, 20 and 60 mintues post injection (n=6 per group). The graph shows aggregate data for all time points. There was a significant difference between KPP-III-51(**10**) at 10 mg/kg and GL-I-54 at either dose, though there was no significant difference between KPP-III-51 (**10**) and vehicle controls.

Locomotor activity in the elevated plus maze (Data source: Dr. Thomos Prevot).



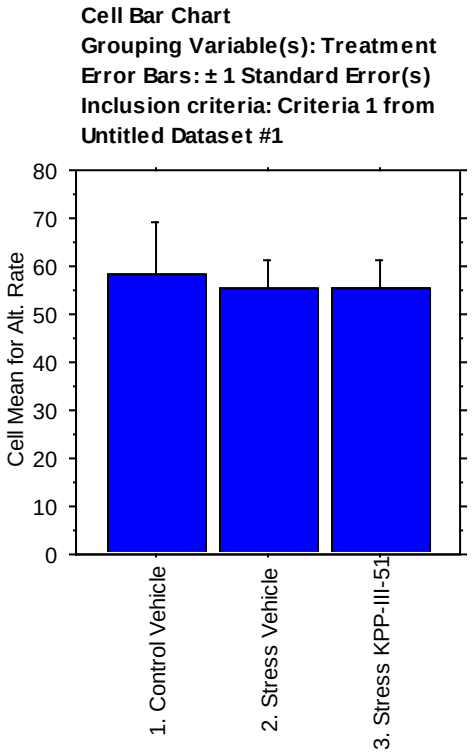
ANOVA Table for Total Distance

	Treatment	Residual
DF	3	246
Sum of Squares	188171.461	10072743.447
Mean Square	62723.820	40946.112
F-Value	1.532	
P-Value	.2068	
Lambda	4.596	
Power	.391	

FIGURE 1. EFFECT OF KPPIII51 AND GLI54 ON LOCOMOTOR ACTIVITY IN THE ELEVATED PLUS MAZE

Mice were administered **10** (KPP-III-51, 10mg/kg), GL-I-54 (10 mg/kg, 5 mg/kg) or vehicle control via intraperitoneal injection and tested in the elevated plus maze 30 minutes post injection (n=6 per group). There were no significant effects of either GL-I-54 at 5mg/kg or 10mg/kg or of KPP-III-51 (**10)** at 10 mg/kg.

Cognition: Working memory in Y Maze (Data source: Dr. Thomos Prevot).



ANOVA Table for Alt. Rate
Inclusion criteria: Criteria 1 from Untitled Dataset #1

	Treatment	Residual
DF	3	11
Sum of Squares	55.556	2092.593
Mean Square	18.519	190.236
F-Value	.097	
P-Value	.9599	
Lambda	.292	
Power	.063	

	Veh	Veh +CRS	KPP-III-51 (**10**) + CRS
Number of Animals	4	4	3

Conducted on Dec 19th, 2019 By MM

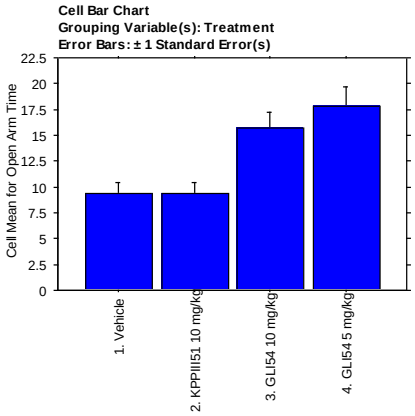
Figure 2. Effect of KPP-III-51 on percent alternation rate in the Y-maze spatial alternation task assessing working memory in mice.

Mice subjected to CRS were injected with (**10**) (KPP-III-51, 10 mg/kg) i.p., 30 min before testing). ANOVA found no significant overall effect of manipulation. CRS mouse group injected with KPP-III-51 (**10**) were not statically different from Control-vehicle group or CRS-Vehicle group. The low alternation rate in the Control vehicle group suggests this data is inconclusive.

Summary of Data

Data is inconclusive due to poor performance of non-stressed controls.

Antidepressant Predictability in elevated plus maze-EPM (Data source: Dr. Thomos Prevot).



ANOVA Table for Open Arm Time

	Treatment	Residual
DF	3	221
Sum of Squares	3283.731	27617.217
Mean Square	1094.577	124.965
F-Value	8.759	
P-Value	<.0001	
Lambda	26.277	
Pow er	.998	

Scheffe for Open Arm Time
Effect: Treatment
Significance Level: 5 %

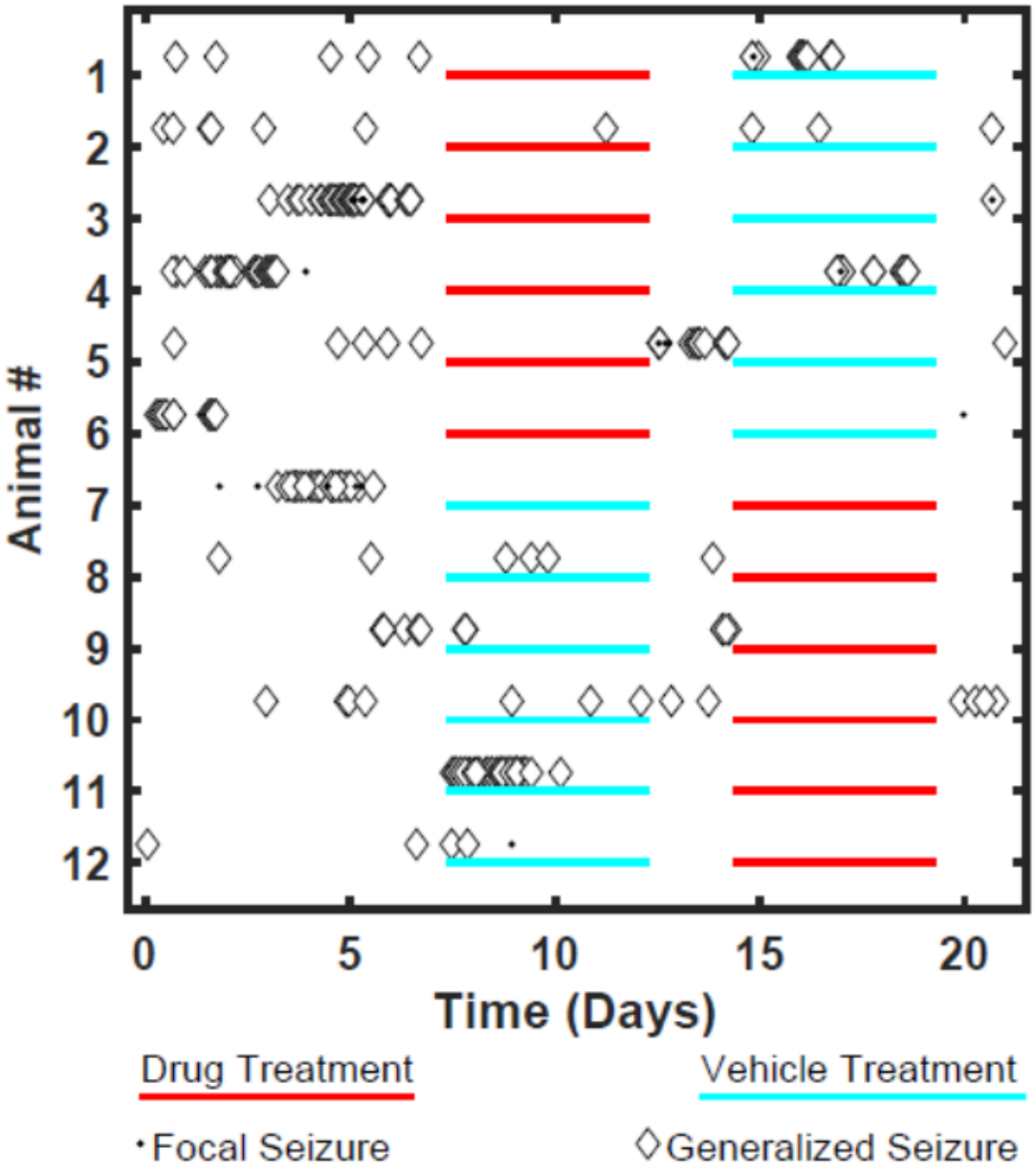
	Mean Diff.	Crit. Diff.	P-Value	
1. Vehicle, 2. KPPIII51 10 mg/kg	-.024	6.061	>.9999	
1. Vehicle, 3. GLI54 10 mg/kg	-6.420	6.061	.0328	S
1. Vehicle, 4. GLI54 5 mg/kg	-8.457	5.840	.0011	S
2. KPPIII51 10 mg/kg, 3. GLI54 10 mg/kg	-6.396	6.061	.0338	S
2. KPPIII51 10 mg/kg, 4. GLI54 5 mg/kg	-8.433	5.840	.0011	S
3. GLI54 10 mg/kg, 4. GLI54 5 mg/kg	-2.037	5.840	.8096	

Conducted on Feb 19th 2020 By MM

FIGURE 3. EFFECT OF KPPIII51 AND GLI54 ON TIME IN THE OPEN ARM OF THE ELEVATED PLUS MAZE

Mice were administered KPP-III-51 (**10**, 10mg/kg), GL-I-54 (10 mg/kg, 5 mg/kg) or vehicle control via intraperitoneal injection and tested in the elevated plus maze 30 minutes post injection (n=6 per group). KPP-III-51 (**10**) had no effect on time spent in the open arm of the elevated plus maze.

Raw data of Test drug KPP-III-34 (9) in 50 mg/kg (T.I.D.) in chronic seizing post-Kainate rats (phase I) (method and data source: ETSP, NINDS).



Dose (50mg/kg, three times a day). Black circles represent stage 0-2 seizures (focal), and black diamonds represent stage 3-5 seizures (generalized). Red lines indicate drug treatment periods, and blue lines indicate vehicle treatments. All seizures were verified using video-EEG analysis by a trained scientist blinded to treatment conditions.

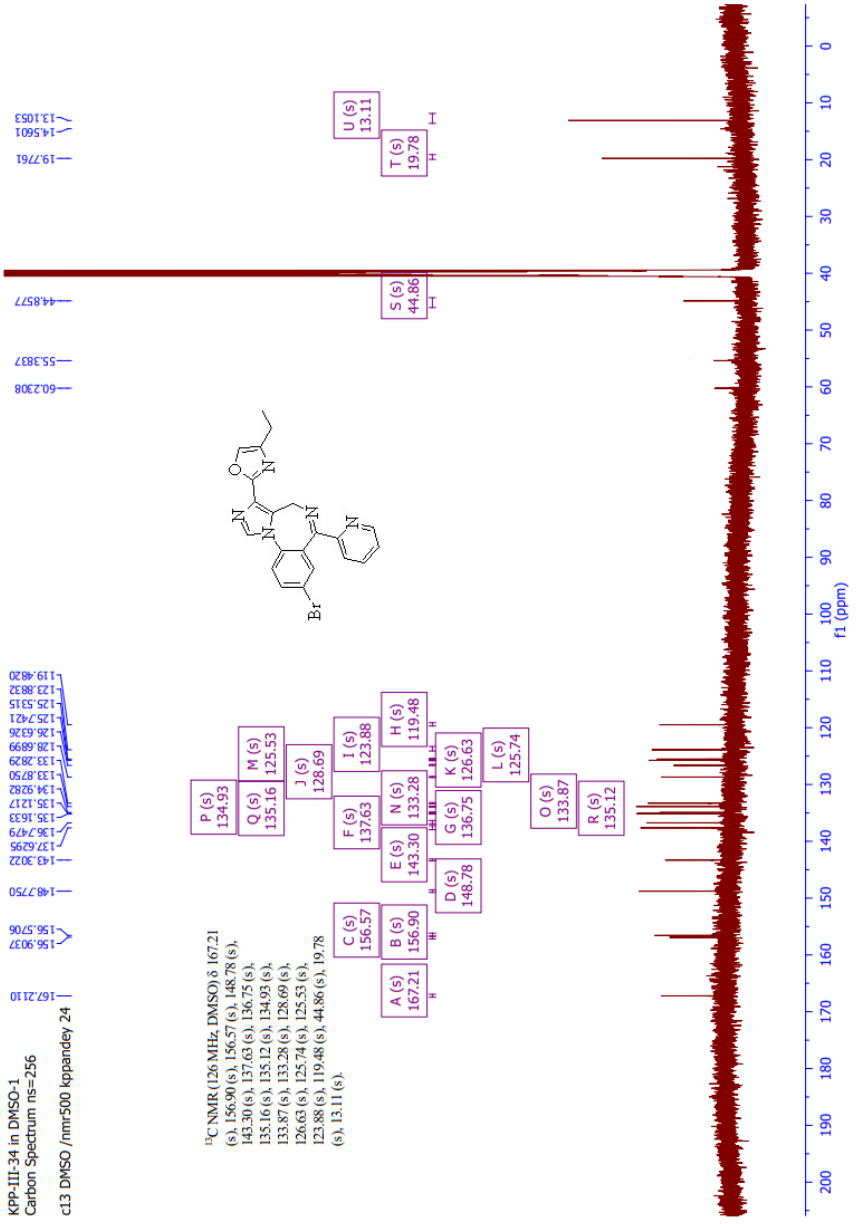
The TPE profile for anticonvulsant activity of 9 (ETSP# 548002, KPP-III-34) in male mice (p.o.) in the 6 Hz 44 mA Test.

Subcontract Site			
Test: 6 Hz 44 mA		Formulation: 0.5% methylcellulose	
Dose: 100 mg/kg		Batch: B	
Time (hr):	Tolerability (N/F)	Protected (N/F)	Comments
0.25 0.5 1.0 2.0 4.0	0/4 0/4 0/4 1/4 0/4	0/4 0/4 2/4 2/4 2/4	
Contract Site (Test 7 Screen 1)			
Test: 6 Hz 44 mA		Formulation: 0.5% methylcellulose	
Dose: 100 mg/kg		Batch: A	
Time (hr):	Tolerability (N/F)	Protected (N/F)	Comments
0.25 0.5 1.0 2.0 4.0	0/4 0/4 0/4 0/4 0/4	2/4 0/4 3/4 0/4 0/4	

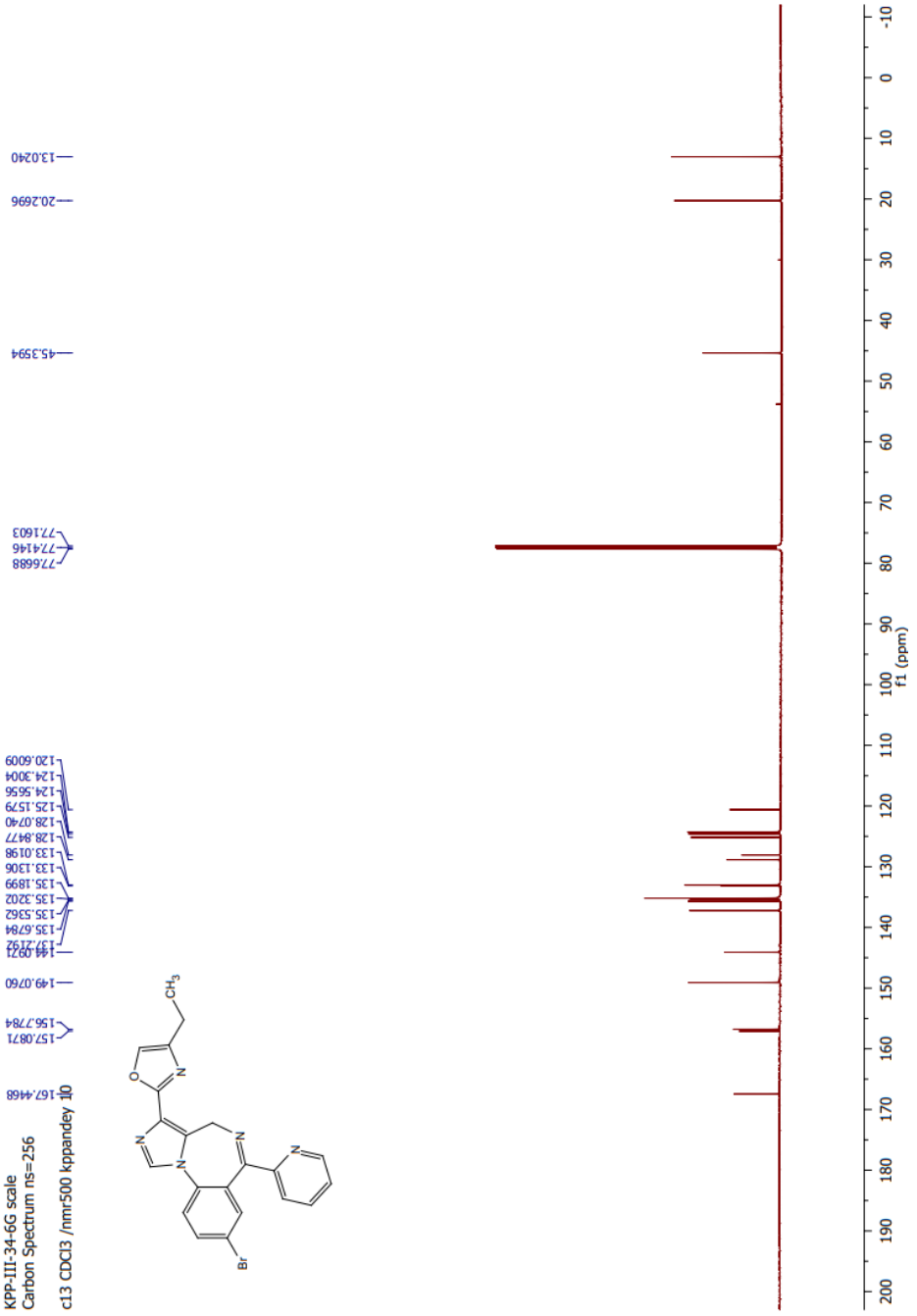
N indicates the number of animals protected, whereas F indicates the number of animals tested. For tolerability, N = number of animals displaying adverse motor effects and F = number of animals tested. Any adverse effects, including deaths, are noted. An observer blinded to treatment confirms behavioral observations.

NMR data (Part II)

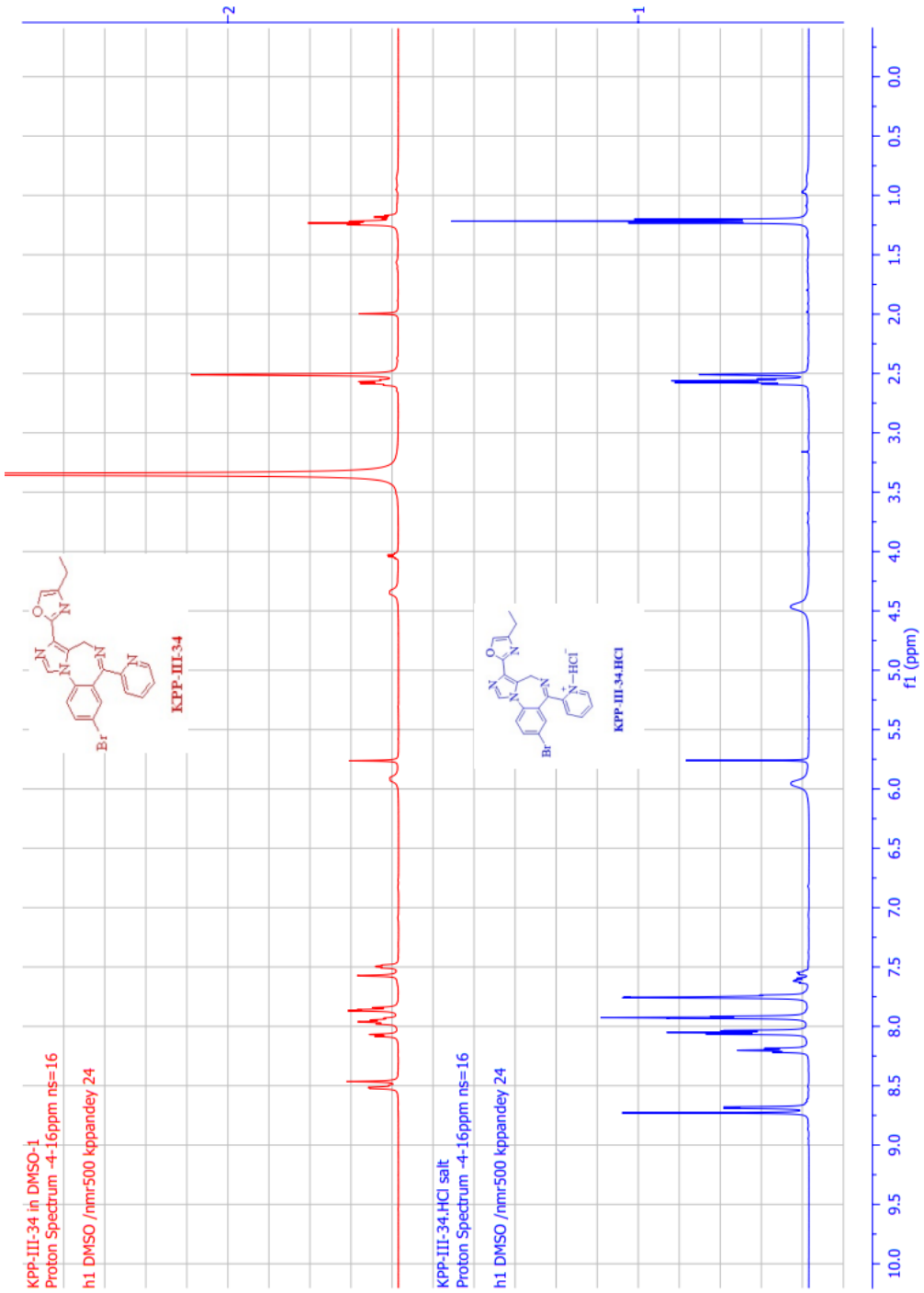
1. **^{13}C NMR (2-(8-bromo-3-(4-ethyloxazol-2-yl)-4*H*-benzo[f]imidazo[1,5-a][1,4]diazepin-6-yl)pyridin-1-ium-1-yl)hydridochlorate(I) [(KPP-III-34·HCl salt) (17)] in DMSO-d^6.**



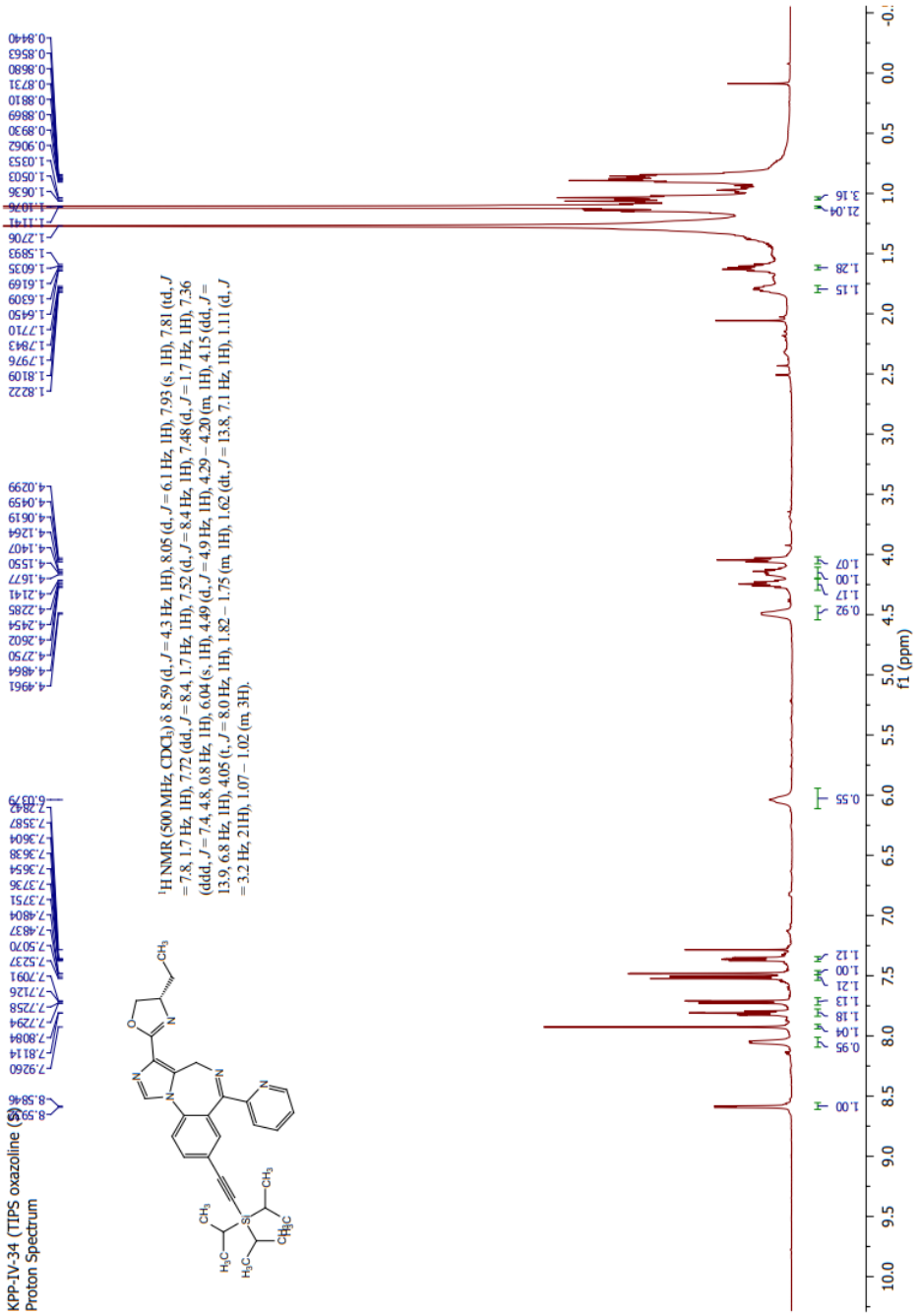
2. ^{13}C NMR (2-(8-bromo-3-(4-ethyloxazol-2-yl)-4*H*-benzo[f]imidazo[1,5-a][1,4]diazepin-6-yl)pyridin-1-ium-1-yl)hydridochlorate(I) [(KPP-III-34·HCl salt) (17)] in CDCl3.



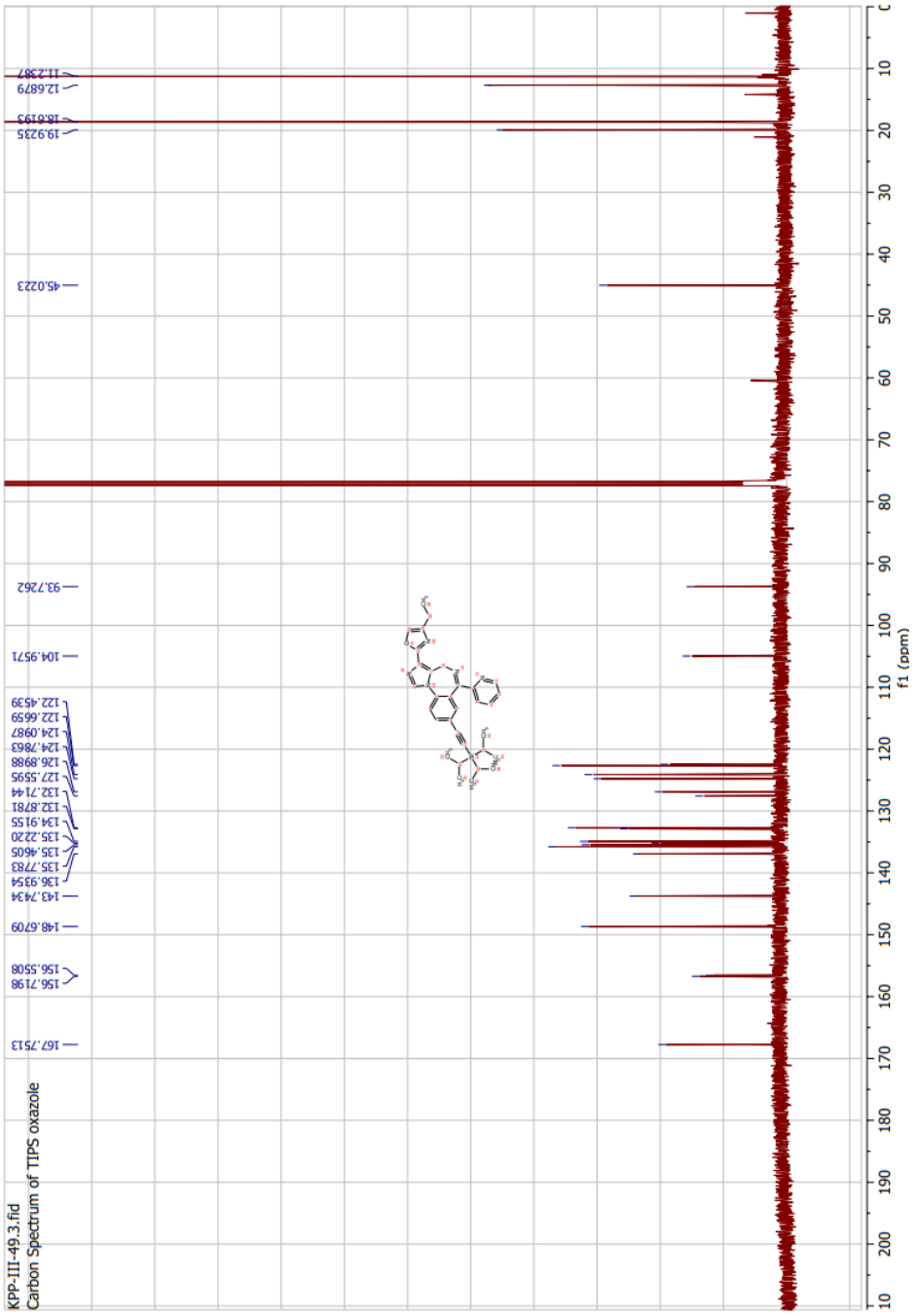
3. Overlay of ^{1}H NMR of (2-(8-bromo-3-(4-ethyloxazol-2-yl)-4*H*-benzo[f]imidazo[1,5-a][1,4]diazepin-6-yl)pyridin-1-ium-1-yl)hydridochlorate(I) [(KPP-III-34·HCl salt) (17)] in CDCl3 VS DMSO-d^{6}.



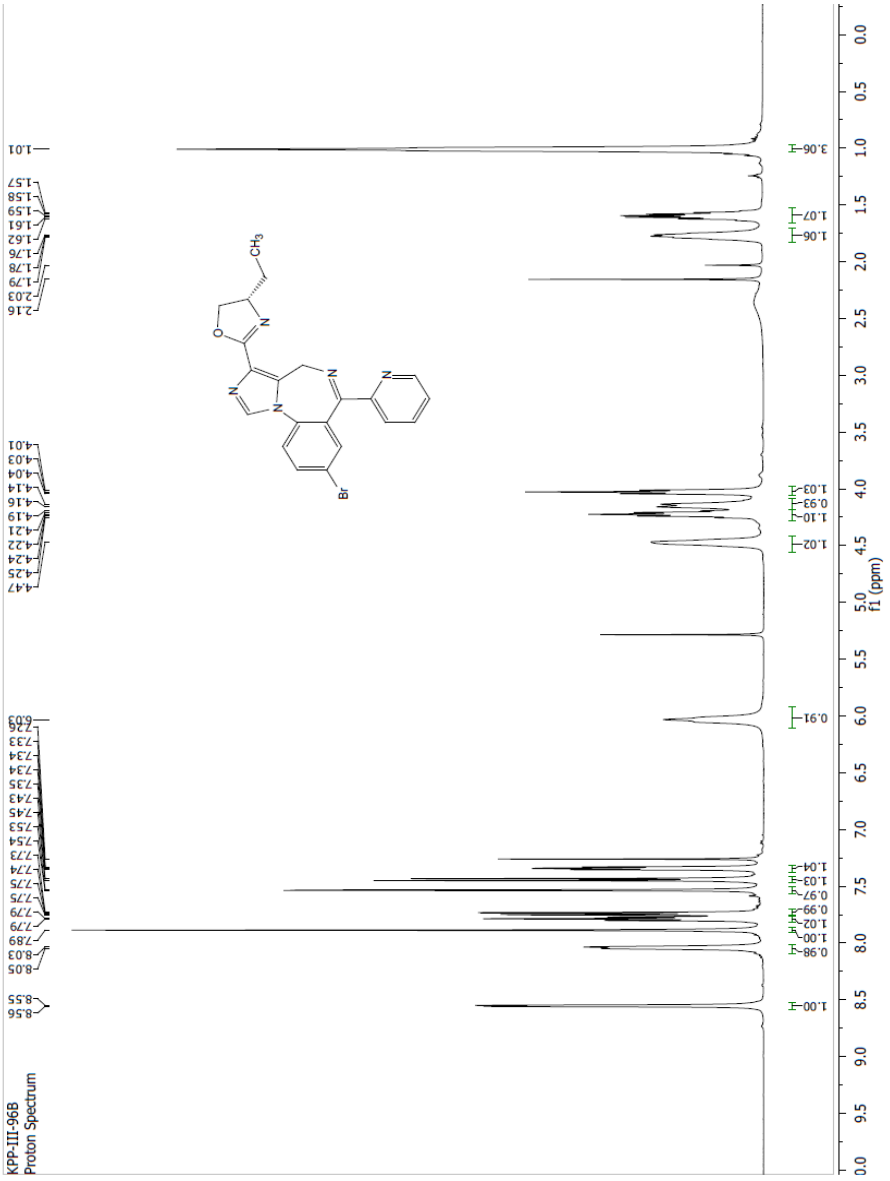
4. [1]HNMR of 4-Ethyl-2-(6-(pyridin-2-yl)-8-((triisopropylsilyl)ethynyl)-4*H*-benzo[f]imidazo[1,5-a][1,4]diazepin-3-yl)oxazole (36).



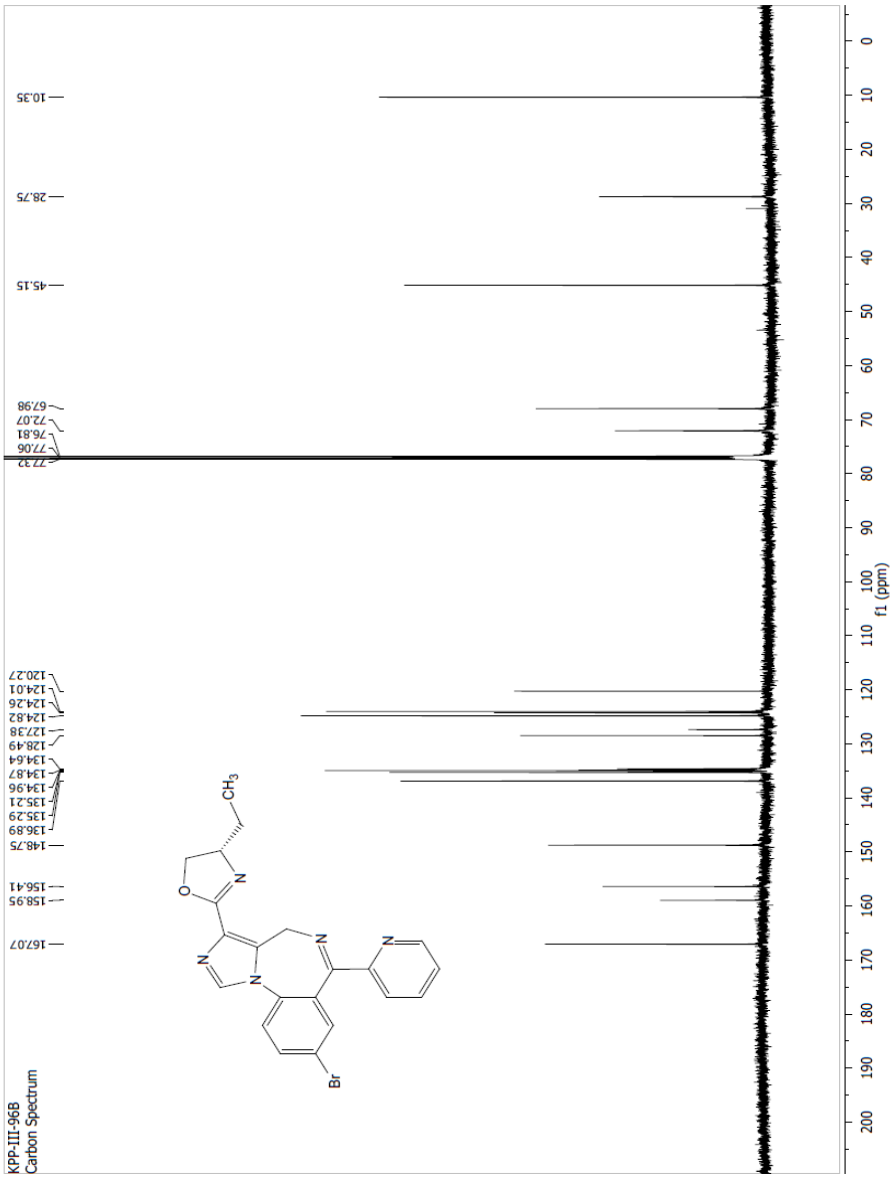
5. **^{13}CNMR of 4-Ethyl-2-(6-(pyridin-2-yl)-8-((triisopropylsilyl)ethynyl)-4*H*-benzo[f]imidazo[1,5-a][1,4]diazepin-3-yl)oxazole (36)**.



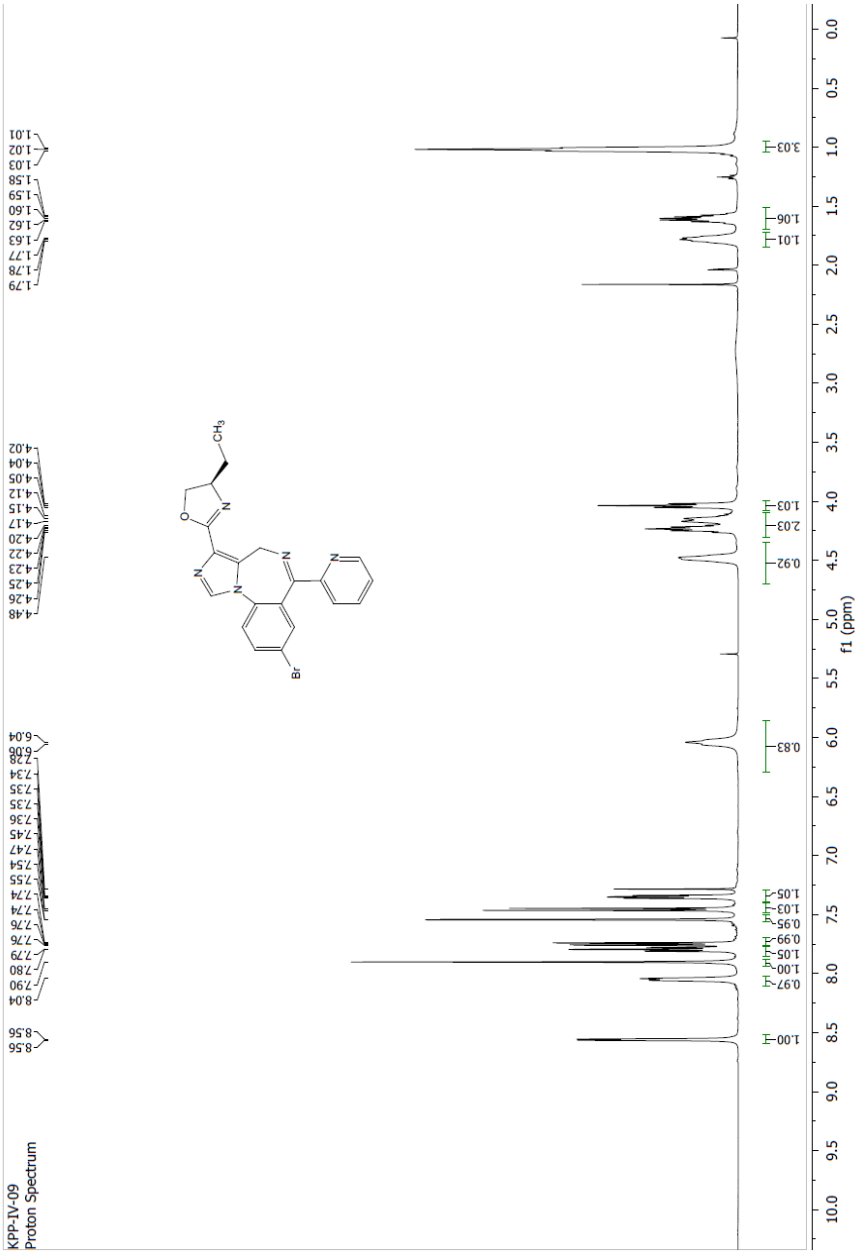
6. **^{1}H NMR of (*S*)-2-(8-Bromo-6-(pyridin-2-yl)-4*H*-benzo[f]imidazo[1,5-a][1,4]diazepin-3-yl)-4-ethyl-4,5-dihydrooxazole [(KPP-III-96B (11)].**



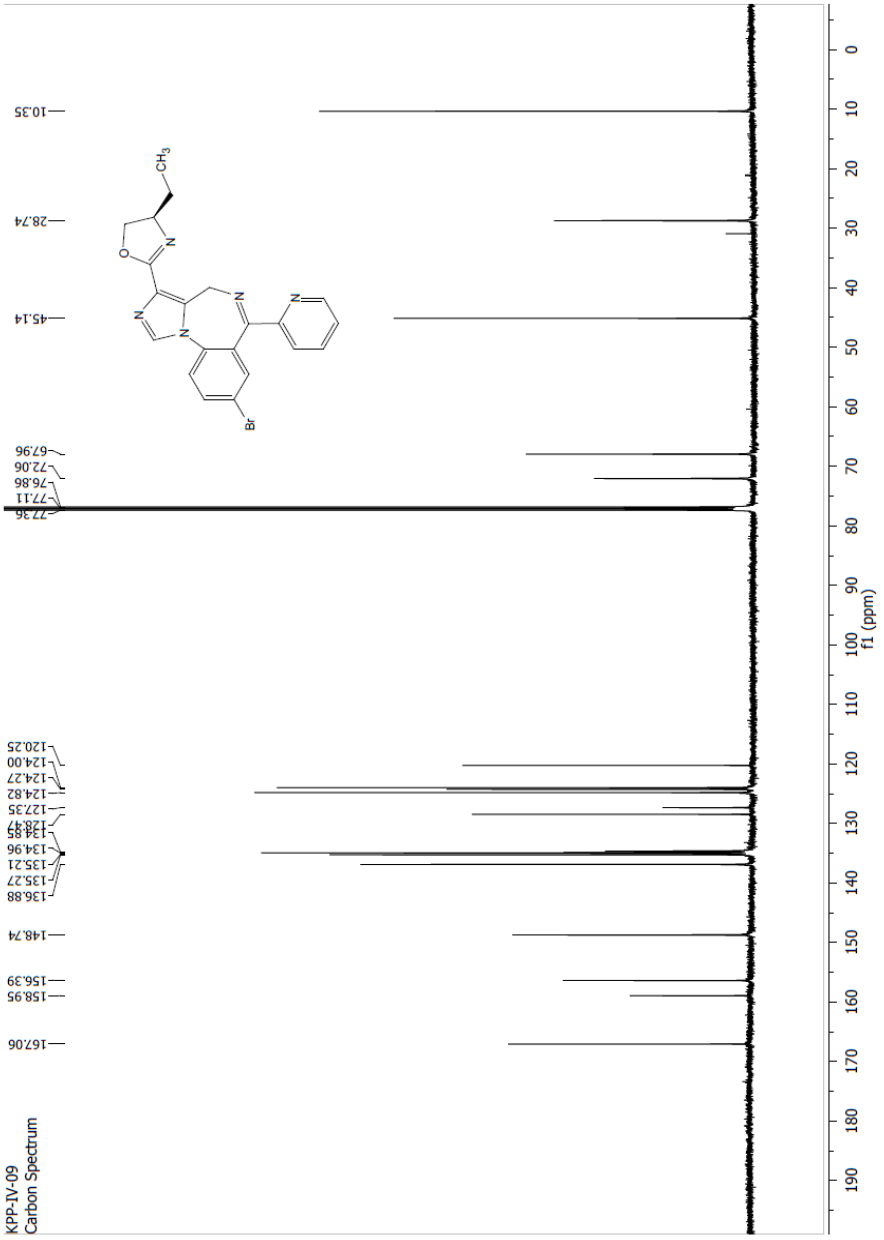
7. **^{13}C NMR of *S*)-2-(8-Bromo-6-(pyridin-2-yl)-4*H*-benzo[f]imidazo[1,5-a][1,4]diazepin-3-yl)-4-ethyl-4,5-dihydrooxazole [(KPP-III-96B (11)].**



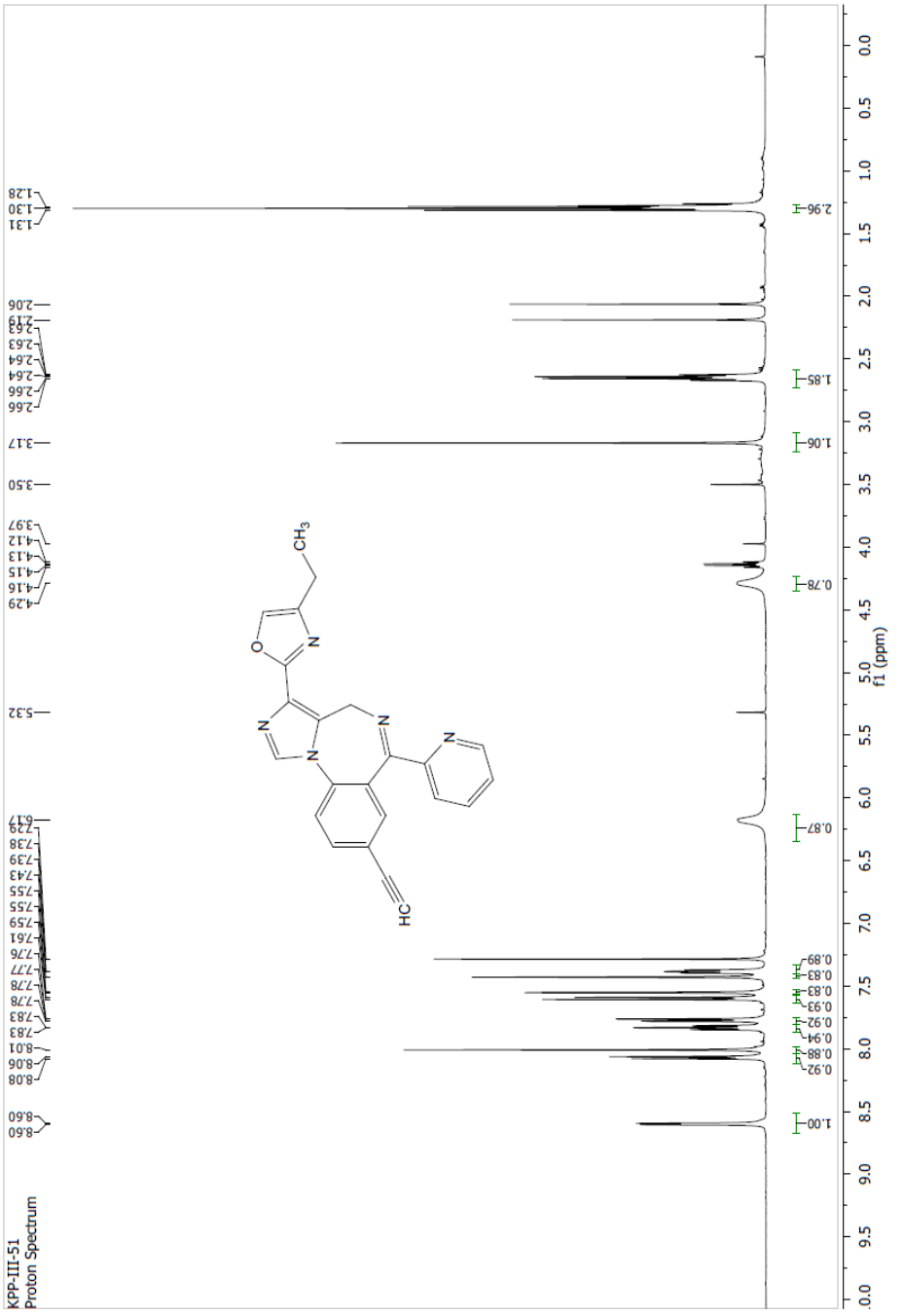
8. **^{1}H NMR of (*R*)-2-(8-Bromo-6-(pyridin-2-yl)-4*H*-benzo[f]imidazo[1,5-a][1,4]diazepin-3-yl)-4-ethyl-4,5-dihydrooxazole [(KPP-IV-09 (12)].**



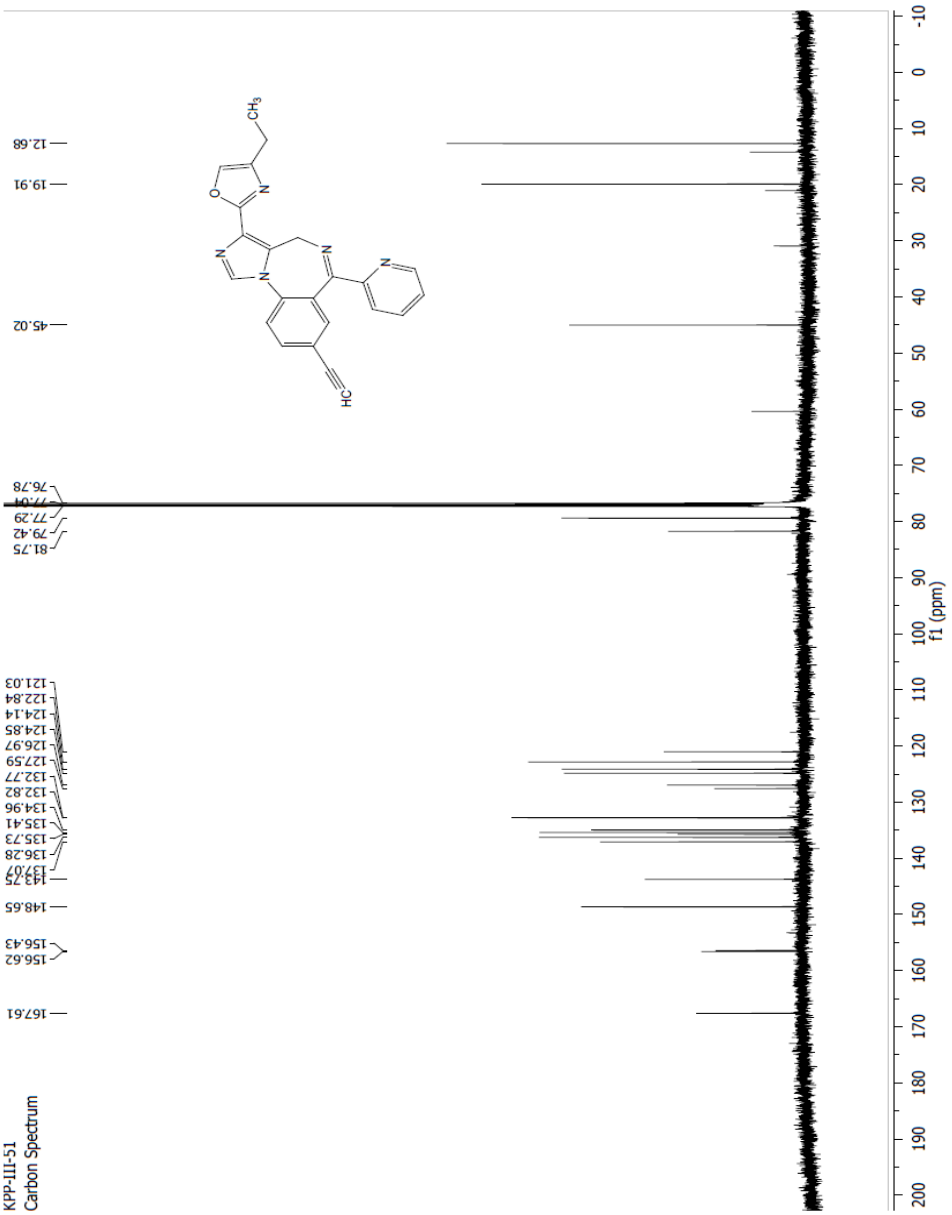
9. **^{1}H NMR of (*R*)-2-(8-Bromo-6-(pyridin-2-yl)-4*H*-benzo[f]imidazo[1,5-a][1,4]diazepin-3-yl)-4-ethyl-4,5-dihydrooxazole [(KPP-IV-09 (12)].**



10. **^{1}H NMR of 4-Ethyl-2-(8-ethynyl-6-(pyridin-2-yl)-4*H*-benzo[f]imidazo[1,5-a][1,4]diazepin-3-yl)oxazole (10).**



11. **^{13}C NMR of 4-Ethyl-2-(8-ethynyl-6-(pyridin-2-yl)-4*H*-benzo[f]imidazo[1,5-a][1,4]diazepin-3-yl)oxazole (10).**



HRMS data (Part-II)

1. **HRMS data of (*S*)-8-Bromo-*N*-(1-hydroxybutan-2-yl)-6-(pyridin-2-yl)-4*H*-benzo[f]imidazo[1,5-a][1,4]diazepine-3-carboxamide (23B).**

Formula Predictor Report - CHO 2_Kamal_08052020 HRMS Analysis_2_6.lcd Page 1 of 1

Data File: C:\LabSolutions\Data\Vilashini Rajaratnam\08052020 Analysis\CHO 2_Kamal_08052020 HRMS Analysis_2_6.lcd

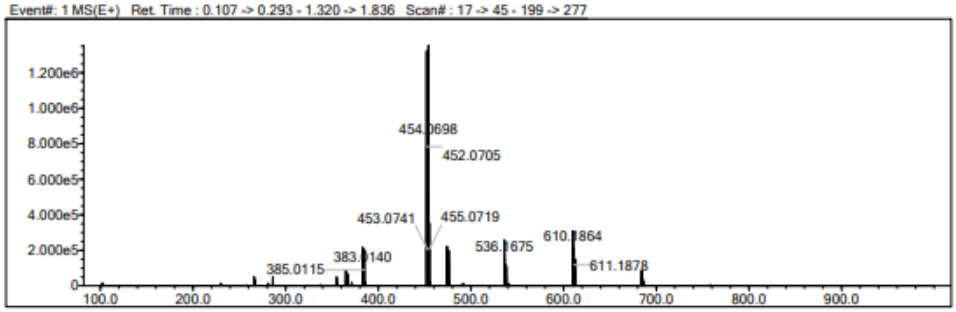
Elmt	Val.	Min	Max	Elmt	Val.	Min	Max	Elmt	Val.	Min	Max	Elmt	Val.	Min	Max	Use Adduct
H	1	15	20	N	3	3	6	Si	4	0	0	Br	1	1	2	H
2H	1	0	0	O	2	0	3	S	2	0	0	I	3	0	0	NH4
C	4	18	22	F	1	0	0	Cl	1	0	0					

Error Margin (ppm): 100
HC Ratio: 0.0 - 10.0
Max Isotopes: all
MSn Iso RI (%): 75.00

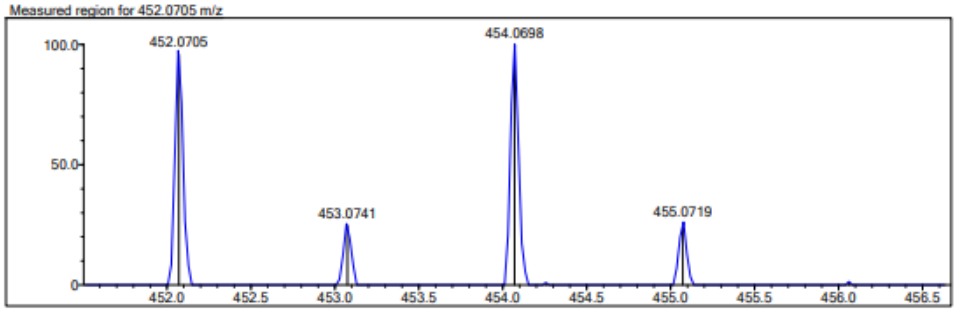
DBE Range: -100.0 - 1000.0
Apply N Rule: yes
Isotope RI (%): 1.00
MSn Logic Mode: AND

Electron Ions: both
Use MSn Info: yes
Isotope Res: 10000
Max Results: 10

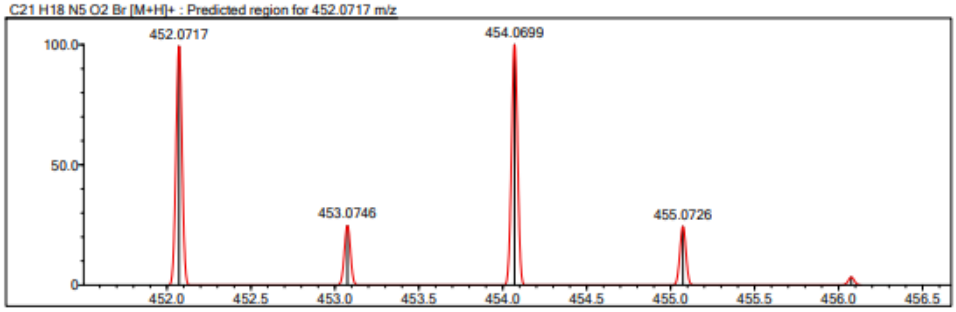
Event#: 1 MS(E+) Ret. Time : 0.107 -> 0.293 - 1.320 -> 1.836 Scan# : 17 -> 45 - 199 -> 277



Measured region for 452.0705 m/z



C21 H18 N5 O2 Br [M+H]+ : Predicted region for 452.0717 m/z



Rank	Score	Formula (M)	Ion	Meas. m/z	Pred. m/z	Df. (mDa)	Df. (ppm)	Iso	DBE
1	56.22	C21 H18 N5 O2 Br	[M+H]+	452.0705	452.0717	-1.2	-2.65	58.64	15.0

1. **HRMS data of 2-(8-Bromo-6-(pyridin-2-yl)-4*H*-benzo[f]imidazo[1,5-a][1,4]diazepin-3-yl)-4-ethyloxazole [KPP-III-34 (9)].**

Formula Predictor Report - 34 2_Kamal_08052020 HRMS Analysis_2_10.lcd

Data File: C:\LabSolutions\Data\Vilashini Rajaratnam\08052020 Analysis\34 2_Kamal_08052020 HRMS Analysis_2_10.lcd

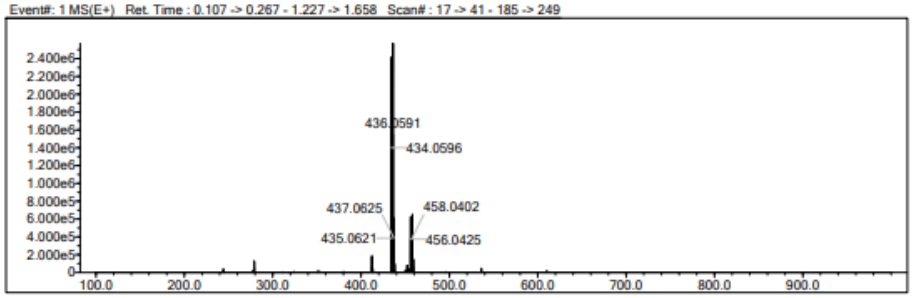
Elmt	Val.	Min	Max	Elmt	Val.	Min	Max	Elmt	Val.	Min	Max	Elmt	Val.	Min	Max	Use Adduct
H	1	10	20	N	3	3	6	Si	4	0	0	Br	1	1	2	H
2H	1	0	0	O	2	0	2	S	2	0	0	I	3	0	0	Na
C	4	18	25	F	1	0	0	Cl	1	0	0					NH4

Error Margin (ppm): 100
HC Ratio: 0.0 - 10.0
Max Isotopes: all
MSn Iso RI (%): 75.00

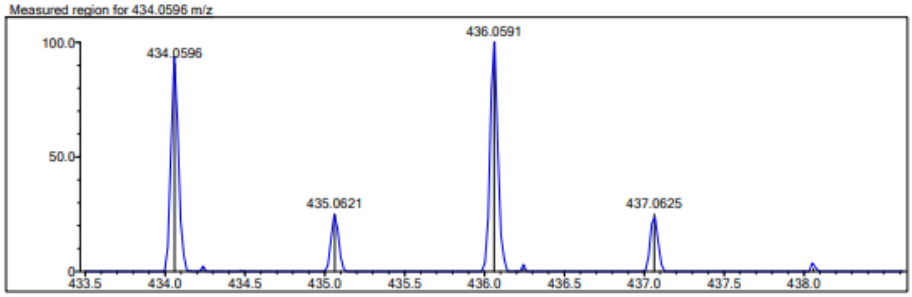
DBE Range: -100.0 - 1000.0
Apply N Rule: yes
Isotope RI (%): 1.00
MSn Logic Mode: AND

Electron Ions: both
Use MSn Info: yes
Isotope Res: 10000
Max Results: 10

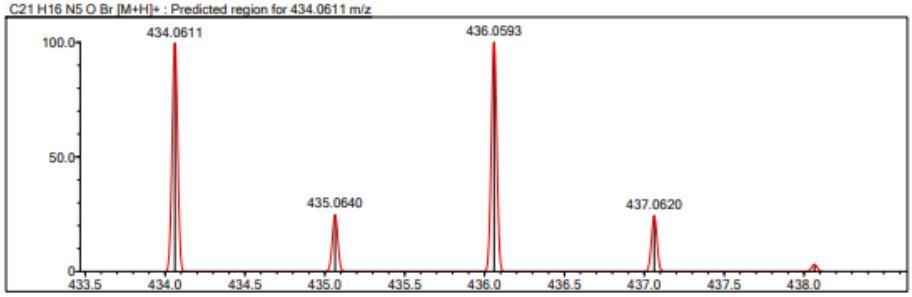
Event#: 1 MS(E+) Ret. Time : 0.107 -> 0.267 - 1.227 -> 1.658 Scan# : 17 -> 41 - 185 -> 249



Measured region for 434.0596 m/z



C21 H16 N5 O Br [M+H]+ : Predicted region for 434.0611 m/z



Rank	Score	Formula (M)	Ion	Meas. m/z	Pred. m/z	Df. (mDa)	Df. (ppm)	Iso	DBE
2	59.86	C21 H16 N5 O Br	[M+H]+	434.0596	434.0611	-1.5	-3.46	63.79	16.0

2. 4-Ethyl-2-(6-(pyridin-2-yl)-8-((triisopropylsilyl)ethynyl)-4*H*-benzo[f]imidazo[1,5-a][1,4]diazepin-3-yl)oxazole (36).

Formula Predictor Report - TIPS 2_Kamal_08052020 HRMS Analysis_2_4.lcd Page 1 of 1

Data File: C:\LabSolutions\Data\Vilashini Rajaratnam\08052020 Analysis\TIPS 2_Kamal_08052020 HRMS Analysis_2_4.lcd

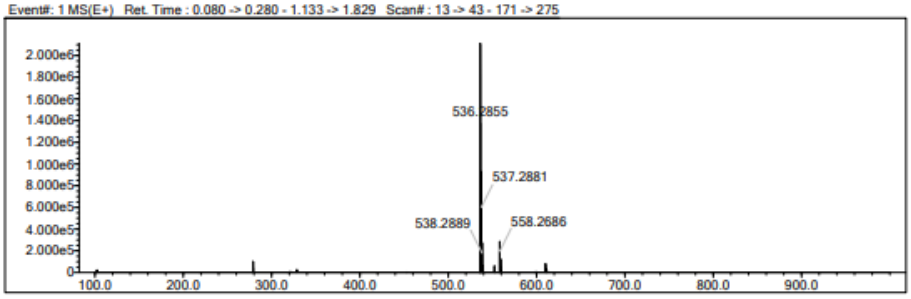
Elmt	Val.	Min	Max	Elmt	Val.	Min	Max	Elmt	Val.	Min	Max	Elmt	Val.	Min	Max	Use Adduct
H	1	30	40	N	3	2	6	Si	4	0	2	Br	1	0	0	H
2H	1	0	0	O	2	0	3	S	2	0	0	I	3	0	0	Na
C	4	30	35	F	1	0	0	Cl	1	0	0					NH4

Error Margin (ppm): 100
HC Ratio: 0.0 - 10.0
Max Isotopes: all
MSn Iso RI (%): 75.00

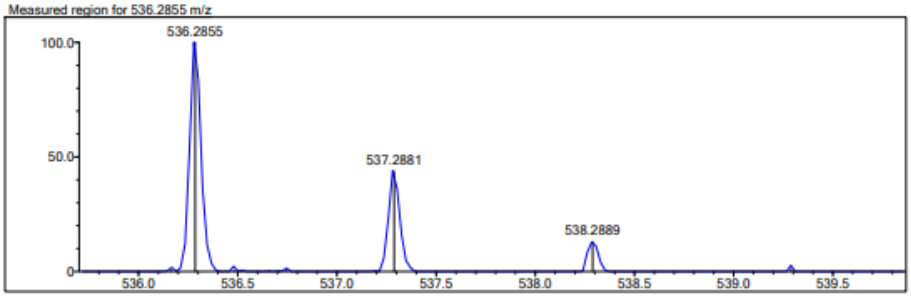
DBE Range: -100.0 - 1000.0
Apply N Rule: yes
Isotope RI (%): 1.00
MSn Logic Mode: AND

Electron Ions: both
Use MSn Info: yes
Isotope Res: 10000
Max Results: 10

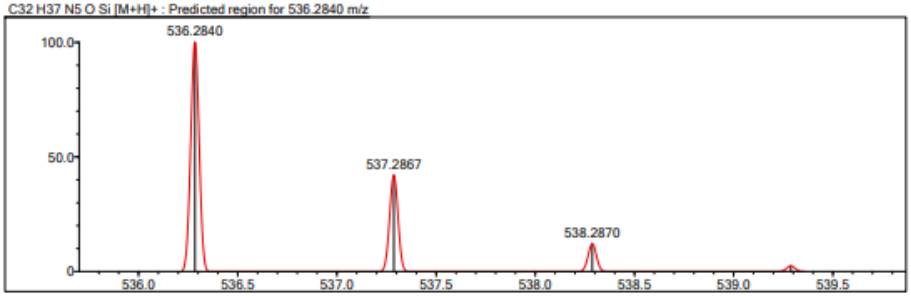
Event#: 1 MS(E+) Ret. Time : 0.080 -> 0.280 - 1.133 -> 1.829 Scan# : 13 -> 43 - 171 -> 275



Measured region for 536.2855 m/z



C32 H37 N5 O Si [M+H]+ : Predicted region for 536.2840 m/z



Rank	Score	Formula (M)	Ion	Meas. m/z	Pred. m/z	Df. (mDa)	Df. (ppm)	Iso	DBE
1	95.10	C32 H37 N5 O Si	[M+H]+	536.2855	536.2840	1.5	2.80	99.58	18.0

3. HRMS data of 4-Ethyl-2-(8-ethynyl-6-(pyridin-2-yl)-4*H*-benzo[f]imidazo[1,5-a][1,4]diazepin-3-yl)oxazole (10).

Formula Predictor Report - 51 2_Kamal_08052020 HRMS Analysis_2_8.lcd

Data File: C:\LabSolutions\Data\Vilashini Rajaratnam\08052020 Analysis\51 2_Kamal_08052020 HRMS Analysis_2_8.lcd

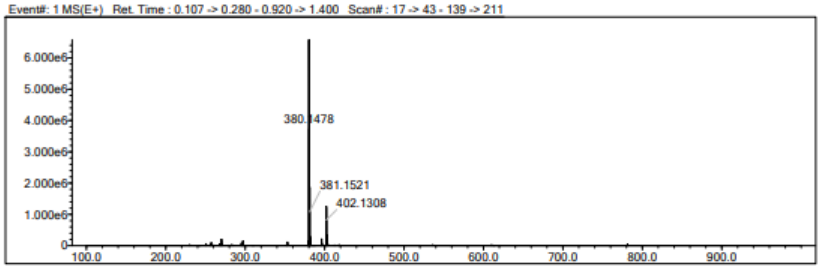
Elmt	Val.	Min	Max	Elmt	Val.	Min	Max	Elmt	Val.	Min	Max	Elmt	Val.	Min	Max	Use Adduct
H	1	15	20	N	3	3	6	Si	4	0	0	Br	1	0	0	H
2H	1	0	0	O	2	0	3	S	2	0	0	I	3	0	0	NH4
C	4	20	25	F	1	0	0	Cl	1	0	0					

Error Margin (ppm): 100
HC Ratio: 0.0 - 10.0
Max Isotopes: all
MSn Iso RI (%): 75.00

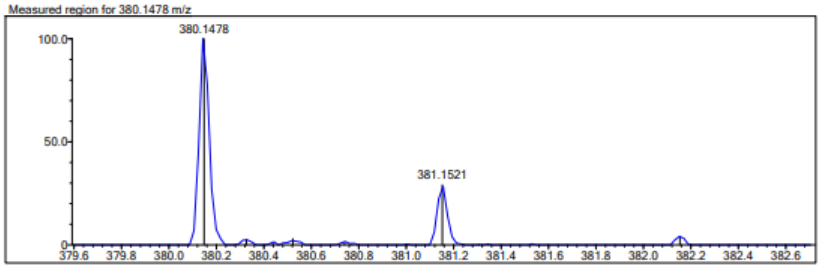
DBE Range: -100.0 - 1000.0
Apply N Rule: yes
Isotope RI (%): 1.00
MSn Logic Mode: AND

Electron Ions: both
Use MSn Info: yes
Isotope Res: 10000
Max Results: 10

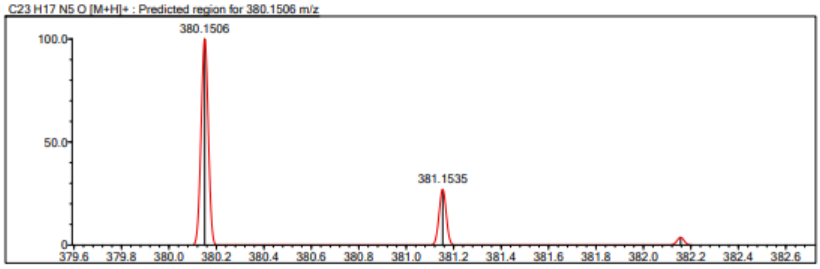
Event#: 1 MS(E+) Ret. Time : 0.107 -> 0.280 - 0.920 -> 1.400 Scan# : 17 -> 43 - 139 -> 211



Measured region for 380.1478 m/z



C23 H17 N5 O [M+H]+ : Predicted region for 380.1506 m/z



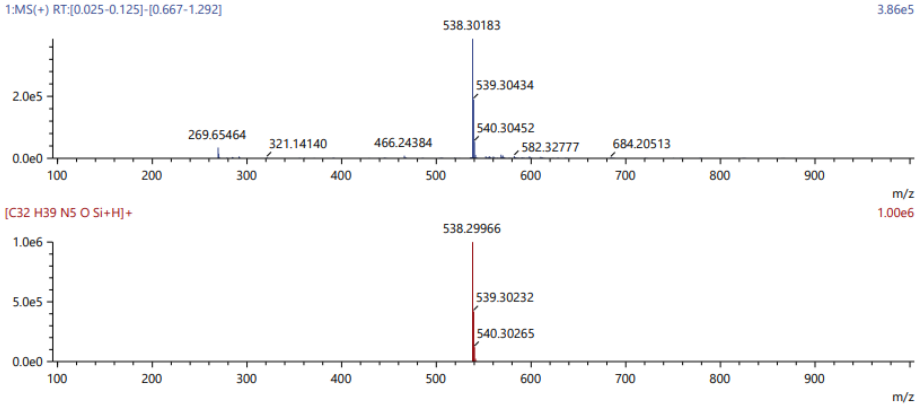
Rank	Score	Formula (M)	Ion	Meas. m/z	Pred. m/z	Df. (mDa)	Df. (ppm)	Iso	DBE
1	50.27	C23 H17 N5 O	[M+H]+	380.1478	380.1506	-2.8	-7.37	75.83	18.0

4. HRMS data of (*S*)-4-Ethyl-2-(6-(pyridin-2-yl)-8-((triisopropylsilyl)ethynyl)-4*H*-benzo[f]imidazo[1,5-a][1,4]diazepin-3-yl)-4,5-dihydrooxazole (38).

kamal_09282021.lcb

Formula Predictor Result	**C32 H39 N5 O Si**
Mass	538.30183
Error Margin	10 mDa
DBE Range	0 - 1000
Electron Ions	Both configurations
HC Ratio	0 - 3
Nitrogen Rule	Used

#	Score	Pred. (M)	Pred. m/z	Meas. m/z	Diff. (mDa)	Formulae (M)	Ion	Diff. (ppm)	Iso Score	DBE
15	38.52	537.29239	538.29966	538.30183	2.17	C32 H39 N5 O Si	[M+H]+	4.031	35.53	16.0

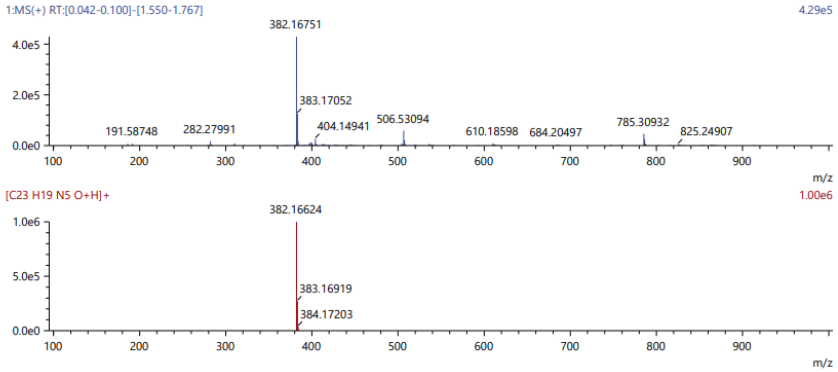


5. (*S*)-4-Ethyl-2-(8-ethynyl-6-(pyridin-2-yl)-4*H*-benzo[f]imidazo[1,5-a][1,4]diazepin-3-yl)-4,5-dihydrooxazole [KPP-IV-35 (16)].

kamal_09282021.lcb

Formula Predictor Result	**C23 H19 N5 O**
Mass	382.16751
Error Margin	10 mDa
DBE Range	0 - 1000
Electron Ions	Both configurations
HC Ratio	0 - 3
Nitrogen Rule	Used

#	Score	Pred. (M)	Pred. m/z	Meas. m/z	Diff. (mDa)	Formulae (M)	Ion	Diff. (ppm)	Iso Score	DBE
3	64.37	381.15896	382.16624	382.16751	1.27	C23 H19 N5 O	[M+H]+	3.323	62.98	17.0



HPLC analysis (Part-II)

1. **HPLC % purity of 2-(8-Bromo-6-(pyridin-2-yl)-4*H*-benzo[f]imidazo[1,5-a][1,4]diazepin-3-yl)-4-ethyloxazole [KPP-III-34 (9)].**

Status:Manual Integration/Temporary

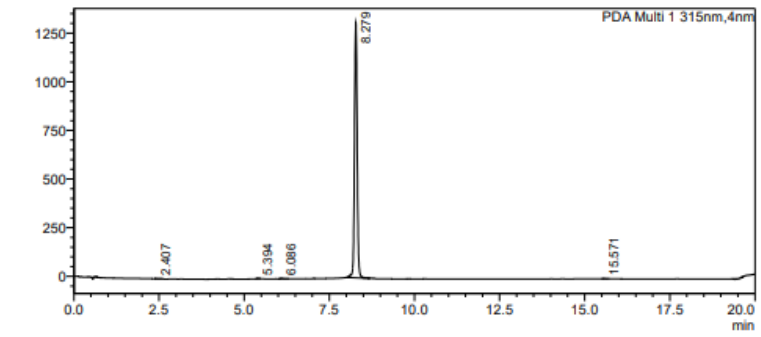
7/13/2022 11:13:17 AM Page 1 / 1

SHIMADZU LabSolutions **Analysis Report**

<Sample Information>

Sample Name	: KPP-III-34		
Sample ID	: KPP-III-34		
Data Filename	: KPP-III-34_7-12-22.lcbc_005.lcd		
Method Filename	: Purity Assay 08052021.lcm2.lcm		
Batch Filename	: 7-12-22.lcbc.lcb		
Vial #	: 3-2	Sample Type	: Unknown
Injection Volume	: 3 uL		
Date Acquired	: 7/12/2022 7:38:31 PM	Acquired by	: Kamal Pandey
Date Processed	: 7/12/2022 7:58:33 PM	Processed by	: Kamal Pandey

<Chromatogram>



<Peak Table>

KPP-III-34_7-12-22.lcbc_005.lcd

PDA Ch1 315nm

Peak#	Ret. Time	Area	Conc.	Area%
1	2.407	4333	0.000	0.060
2	5.394	10813	0.000	0.150
3	6.086	9817	0.000	0.136
4	8.279	7165026	0.000	99.595
5	15.571	4208	0.000	0.058
Total		7194197		100.000

Kamal2020 - 3-232/3-1476-1 - KPP-III-34_7-12-22.lcbc_005.lcd

2. HPLC % purity of 4-Ethyl-2-(8-ethynyl-6-(pyridin-2-yl)-4*H*-benzo[f]imidazo[1,5-a][1,4]diazepin-3-yl)oxazole [KPP-III-51 (10)].

Status:Manual Integration/Temporary

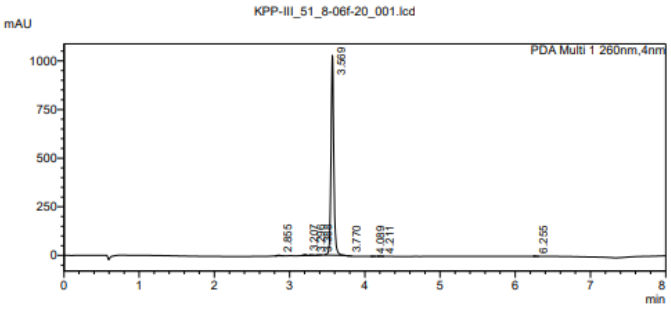
8/6/2020 6:32:26 PM Page 1 / 1

SHIMADZU LabSolutions **Analysis Report**

<Sample Information>

Sample Name	: KPP-III_51		
Sample ID	: KPP-III_51		
Data Filename	: KPP-III_51_8-06f-20_001.lcd		
Method Filename	: scan pos neg purity hplc-ms.lcm		
Batch Filename	: 8-06f-20.lcb		
Vial #	: 3-1	Sample Type	: Unknown
Injection Volume	: 10 uL		
Date Acquired	: 8/6/2020 5:15:46 PM	Acquired by	: Kamal Pandey
Date Processed	: 8/6/2020 5:23:48 PM	Processed by	: Kamal Pandey

<Chromatogram>



<Peak Table>

KPP-III_51_8-06f-20_001.lcd

PDA Ch1 260nm

Peak#	Ret. Time	Area	Height	Area%
1	2.855	7988	2943	0.302
2	3.207	13879	5186	0.524
3	3.296	4418	2100	0.167
4	3.388	1553	552	0.059
5	3.569	2617869	992252	98.811
6	3.770	301	46	0.011
7	4.089	69	74	0.003
8	4.211	2222	803	0.084
9	6.255	1082	666	0.041
Total		2649380	1004621	100.000

Kamal2020 - 3-115/3-684-1 - KPP-III_51_8-06f-20_001.lcd

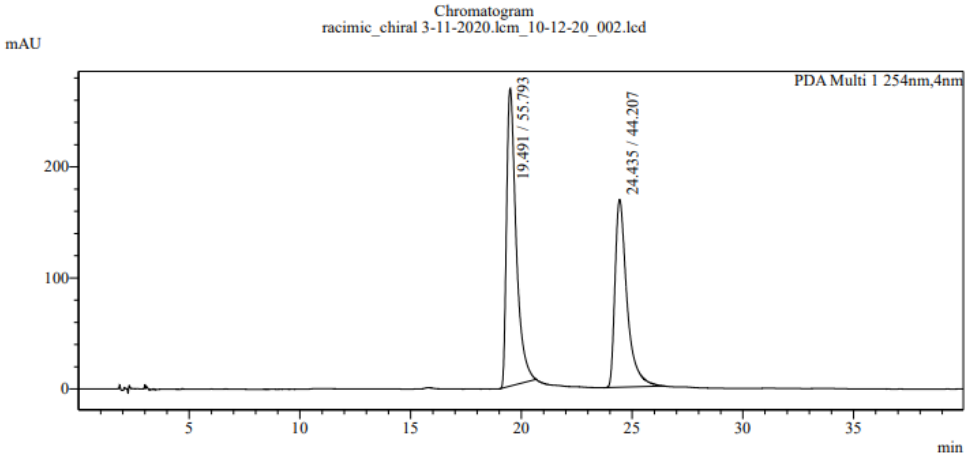
3. HPLC analysis of enantiomers of KPP-III-96B (11) and KPP-IV-09 (12)
Method: 10% EtOH in Hexane.

SHIMADZU LabSolutions **Analysis Report**

<Sample Information>

Sample Name	: racimic		
Sample ID	:		
Data Filename	: racimic_chiral 3-11-2020.lcm_10-12-20_002.lcd		
Method Filename	: chiral 3-11-2020.lcm		
Batch Filename	: 10-12-20.lcb		
Vial #	: Vial 2	Sample Type	: Unknown
Injection Volume	: 5 uL	Level	: 1
Date Acquired	: 10/12/2020 3:26:34 PM	Acquired by	: Kamal Pandey
Date Processed	: 10/12/2020 7:42:38 PM	Processed by	: Kamal Pandey

<Chromatogram>



<Peak Table>

racimic_chiral 3-11-2020.lcm_10-12-20_002.lcd

(3D)DAD Ch1 254nm

Peak#	Ret. Time	Area%
1	19.491	55.793
2	24.435	44.207
Total		100.000

4. HPLC analysis (% ee) of KPP-III-96B (11)

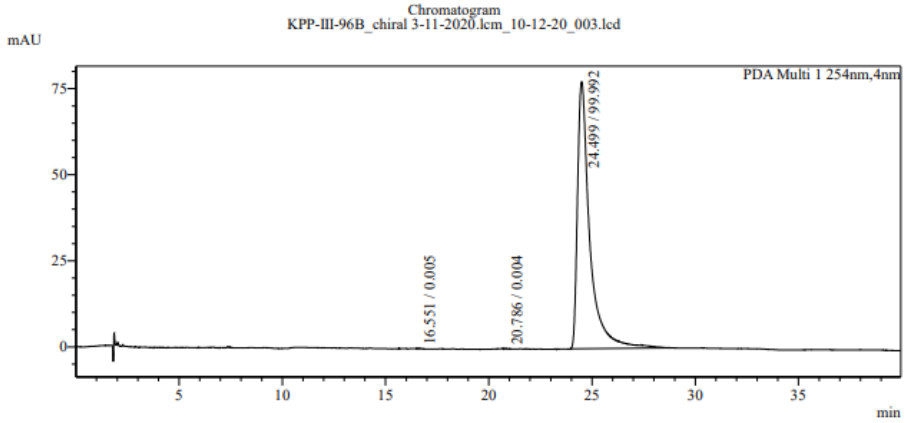
Method: 10% EtOH in Hexane

SHIMADZU LabSolutions **Analysis Report**

<Sample Information>

Sample Name	: KPP-III-96B		
Sample ID	:		
Data Filename	: KPP-III-96B_chiral 3-11-2020.lcm_10-12-20_003.lcd		
Method Filename	: chiral 3-11-2020.lcm		
Batch Filename	: 10-12-20.lcb		
Vial #	: Vial 3	Sample Type	: Unknown
Injection Volume	: 5 uL	Level	: 1
Date Acquired	: 10/12/2020 4:07:34 PM	Acquired by	: Kamal Pandey
Date Processed	: 10/13/2020 11:34:52 AM	Processed by	: Kamal Pandey

<Chromatogram>



<Peak Table>

KPP-III-96B_chiral 3-11-2020.lcm_10-12-20_003.lcd

(3D)DAD Ch1 254nm

Peak#	Ret. Time	Area%
1	16.551	0.005
2	20.786	0.004
3	24.499	99.992
Total		100.000

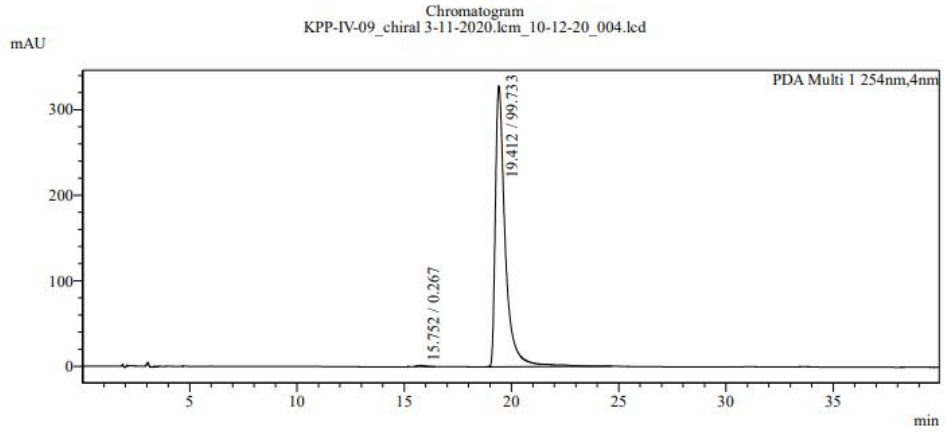
5. HPLC analysis (% ee) of KPP-IV-09 (12) [Method: 10% EtOH in Hexane].

SHIMADZU LabSolutions **Analysis Report**

<Sample Information>

Sample Name	: KPP-IV-09		
Sample ID	:		
Data Filename	: KPP-IV-09_chiral 3-11-2020.lcm_10-12-20_004.lcd		
Method Filename	: chiral 3-11-2020.lcm		
Batch Filename	: 10-12-20.lcb		
Vial #	: Vial 4	Sample Type	: Unknown
Injection Volume	: 5 uL	Level	: 1
Date Acquired	: 10/12/2020 4:48:37 PM	Acquired by	: Kamal Pandey
Date Processed	: 10/12/2020 7:09:47 PM	Processed by	: Kamal Pandey

<Chromatogram>



<Peak Table>

KPP-IV-09_chiral 3-11-2020.lcm_10-12-20_004.lcd

(3D)DAD Ch1 254nm

Peak#	Ret. Time	Area%
1	15.752	0.267
2	19.412	99.733
Total		100.000

PDSP binding data (data source: Dr. Bryon Roth, NIMH).

1. **Primary binding data of KPP-IV-35 (16) in PDSP studies (data source: Dr. Bryon Roth, NIMH).**

Compound #	Receptor	Inhibition 1	Inhibition 2	Inhibition 3	Inhibition 4	Mean %
KPP-IV-35(61381)	Alpha2Beta2	-5.93	0.97	7.32	3.2	1.39
61381	Alpha2Beta4	3.32	5.23	5.75	1.48	3.95
61381	Alpha3Beta2	4.76	-11.41	-8.78	-8.7	-6.03
61381	Alpha3Beta4	-5.26	-2.35	-6.23	-3.62	-4.37
61381	Alpha4Beta2	9.46	9.06	1.36	8.37	7.06
61381	Alpha4Beta2 (Rat Brain)	2.91	5.13	0.26	6.84	3.79
61381	Alpha4Beta4	-0.06	-11.39	-6.83	0.02	-4.57
61381	Alpha7	32.57	10.32	8.51	0.1	12.88
61381	5-HT1A	38.11	16.11	22.78	25.9	25.73
61381	5-HT1B	-26.9	-27.59	-34.28	5.62	-20.79
61381	5-HT1D	-43.79	-49.33	-25.98	-13.33	-33.11
61381	5-HT1E	-3.67	11.87	-8.67	-3.94	-1.1
61381	5-HT2A	15.03	-4.24	-15.22	-4.44	-2.22
61381	5-HT2B	13.56	5.03	-5.07	-0.76	3.19
61381	5-HT2C	14.32	23.95	-0.9	-70.06	-8.17
61381	5-HT3	-0.83	-10.4	-14.95	-6.42	-8.15
61381	5-HT4	15.31	-3.93	-9.5	43.44	11.33
61381	5-HT5A	10.96	24.78	32.67	48.95	29.34
61381	5-HT6	1.86	-3.47	-14.22	-7.36	-5.8
61381	5-HT7A	26.32	24.89	1.07	9.91	15.55
61381	A1	21.05	0	-1.53	12.25	7.94
61381	Alpha1A	-28.57	-18.02	-20.15	-3.35	-17.52
61381	Alpha1B	-31.17	-26.62	-14.72	2.02	-17.62
61381	Alpha1D	4.64	2.43	-5.12	-5.64	-0.92
61381	Alpha2A	11.01	23.74	17.12	33.15	21.26
61381	Alpha2B	49.91	26.44	23.96	46.02	36.58
61381	Alpha2C	27.09	21.33	18.99	21.02	22.11
61381	Beta1	7	-7.86	25.47	30.07	13.67
61381	Beta2	-6.27	2.28	-8.43	-13.7	-6.53
61381	Beta3	20.3	10.96	33.53	77.84	35.66
61381	AT2	1.81	3.16	5.29	9.54	4.95
61381	BZP Rat Brain Site	83.57	77.58	79.12	85.89	81.54
61381	D1	0.4	6.43	-12.61	-13.01	-4.7
61381	D2	50.55	-13.32	10.82	30.83	19.72
61381	D3	18.96	-5.6	-2.73	-7.35	0.82
61381	D4	23.51	7.89	6.68	21.4	14.87
61381	D5	2.11	4.89	-18.82	3.36	-2.12
61381	DOR	-3.71	-20.4	-22.19	-10.69	-14.25
61381	GABAA	11.98	8.65	4.48	2.81	6.98
61381	H1	-2.59	-5.72	-10.42	-12.57	-7.83
61381	H2	20.24	10.89	-0.56	-1.28	7.32
61381	H3	-7.28	-7.85	-20.38	-24.65	-15.04
61381	H4	-5.7	-66.11	1.01	-3.46	-18.57
61381	KOR	48.79	65.18	56.48	34.46	51.23
61381	M1	18.95	19.46	29.95	60.07	32.11

2. Primary binding data of KPP-IV-35 (16) in PDSP studies (data source: Dr. Bryon Roth, NIMH) continued.

61381	M2	-2.64	-18.64	-11.51	-10.16	-10.74
61381	M3	21.2	26.43	6.53	4.06	14.56
61381	M4	-0.38	-4.48	21.04	6.22	5.6
61381	M5	-13.52	-4.65	8.12	3.22	-1.71
61381	MOR	-9.15	-11.22	-15.34	-7.41	-10.78
61381	NET	60.45	55.87	64.33	55.52	59.04
61381	PBR	54.16	64	78.17	76.38	68.18
61381	SERT	15.32	15.2	0.05	3.23	8.45
61381	Sigma 1	49.73	26.83	31.16	36.49	36.05
61381	Sigma 2	60.37	54.66	48.08	11.55	43.67
61381	AMPA	-7.68	-4.49	-5.51	20.49	0.7
61381	Kainate (Rat Brain)	-9.52	-0.1	3.99	-7.47	-3.28
61381	NMDA	14.37	-27.43	-8.04	-11.96	-8.27
61381	NR2B	-13.86	-52.05	-12.17	-13.18	-22.82
61381	HCA2	-11.09	-7.18	14.75	3	-0.13
61381	Ca channel human	8.67	-18.25	-5.18	-3.17	-4.48
61381	HERG	10.07	-15.37	6.83	7.7	2.31
61381	M1 D	9.17	5.47	12.74	-6.33	5.26
61381	M2 D	31.64	21.71	5.47	-6.71	13.03
61381	M3D	16.75	4.02	15.31	-0.82	8.82
61381	M4 D	54.33	50.9	47.89	46.6	49.93
61381	M5 D	16.28	17.77	5.74	10.94	12.68
61381	NTS1	-18.44	-1.71	-9.13	-4.32	-8.4
61381	NOP	23.47	6.81	-28.31	-10.75	-2.2
61381	OT	21.96	20.42	15.67	12.6	17.66
61381	V1A	-8.11	4.61	28.54	0.51	6.39
61381	V1B	-13.4	-14.5	-6.75	-3.13	-9.45
61381	5-HT6	5.48	33.48	15.12	24.53	19.65

3. Secondary binding data of KPP-IV-35 (16) in PDSP studies (data source: Dr. Bryon Roth, NIMH) continued.

Compound #	Tier	Receptor	LogKi	Ki (nM)
61381	1	PBR	-5.48	3311.31
61381	1	PBR	-5.6	2506.69
61381	1	5-HT1D	> -5	> 10,000
61381	1	KOR	-5.78	1664.56
61381	1	KOR	-5.7	1994.34
61381	1	BZP Rat Brain Site	-6.27	536.66
61381	1	BZP Rat Brain Site	-6.09	807.98
61381	1	NET	> -5	> 10,000
61381	1	NET	> -5	> 10,000

4. **Primary binding data of KPP-III-51 (10) in PDSP studies (data source: Dr. Bryon Roth, NIMH).**

Compound #	Receptor	Inhibition 1	Inhibition 2	Inhibition 3	Inhibition 4	Mean %
56645	5-HT1A	57.64	50.31	50.69	47.41	51.51
56645	5-HT1B	0.77	7.51	7.08	10.46	6.46
56645	5-HT1D	-2.4	0.03	-2.06	-0.37	-1.2
56645	5-HT1E	34.94	10.99	-3.37	-2.07	10.12
56645	5-HT2A	-11.2	-1.38	-5.46	5.55	-3.12
56645	5-HT2B	8.47	5.52	15.39	-0.38	7.25
56645	5-HT2C	-4.95	12.31	-4.85	4.46	1.74
56645	5-HT3	20.76	31.24	20.95	-9.65	15.83
56645	5-HT4	-12.45	5.23	-2.76	2.5	-1.87
56645	5-HT5A	-7.15	2.94	6.05	5.53	1.84
56645	5-HT6	-0.26	-7.05	-11.96	10.03	-2.31
56645	5-HT7A	-2.35	-1.88	-1.25	4.08	-0.35
56645	A1	34.54	10.73	43.91	41.03	32.55
56645	A2A	26.38	10.88	10.22	2.14	12.41
56645	Alpha1A	-2.25	-13.84	18.64	-1.63	0.23
56645	Alpha1B	-11.13	8.14	-9.47	2.93	-2.38
56645	Alpha1D	-7.64	4.32	-14.18	13.1	-1.1
56645	Alpha2A	4.8	6.76	6.11	10.03	6.93
56645	Alpha2B	8.57	17.04	11.15	1.69	9.61
56645	Alpha2C	10.98	14.68	9.16	16.04	12.72
56645	Beta1	14	0	-77.23	20.61	-10.66
56645	Beta2	-1.07	3.21	-8.5	6.81	0.11
56645	Beta3	25.13	-23.38	-75.77	14.43	-14.9
56645	BZP Rat Brain Site	91.58	90.15	90.39	95.86	92
56645	D1	30.99	-7.12	-1.32	-18.13	1.11
56645	D2	-3.98	-9.1	-7.47	-4.35	-6.23
56645	D3	-0.33	7.59	0.83	-4.41	0.92
56645	D4	-22.13	-23.77	-11.35	3.91	-13.34
56645	D5	-6.59	5.78	-8.47	-21.71	-7.75
56645	DAT	-25.54	-39.77	-30.52	-7.47	-25.83
56645	DOR	22.95	17.05	10.95	23.15	18.53

5. Primary binding data of KPP-III-51 (10) in PDSP studies (data source: Dr. Bryon Roth, NIMH).

56645	GABAA	14.6	0	-10.21	-1.05	0.84
56645	H1	-17.37	-3.49	-14.68	0.42	-8.78
56645	H2	4.66	-5.65	12.33	11.55	5.72
56645	H3	-12.96	28.43	11.34	-3.84	5.74
56645	H4	-8.67	1.83	18.5	5.53	4.3
56645	KOR	63.01	67.94	59.78	65.63	64.09
56645	M1	-1.74	5.21	-11.67	-0.38	-2.15
56645	M2	-14.29	-14.1	-14.48	-2.89	-11.44
56645	M3	-6.45	2.12	-6.78	2.62	-2.12
56645	M4	-10.53	-6.16	-4.02	13.4	-1.83
56645	M5	-17.31	-5.88	-17.31	14.25	-6.56
56645	MOR	4.79	11.69	17.56	-13.48	5.14

56645	NET	-10.51	-9.24	-20.81	18.55	-5.5
56645	PBR	46.38	81.59	73.56	74.27	68.95
56645	SERT	-19.73	-6.21	-9.68	-2.75	-9.59
56645	Sigma 1	41.93	43.33	36.35	33.55	38.79
56645	Sigma 2	12.25	12.4	10.4	20.6	13.91
56645	AMPA	4.53	-30.95	-3.7	-7.54	-9.42
56645	Kainate (Rat Brain)	23.21	0.16	1.44	4.86	7.42
56645	NMDA	76.89	50.86	25.27	8.26	40.32
56645	NR2B	11.04	-12.05	-11.44	-10.7	-5.79
56645	HCA2	-81.19	-42.98	-29.09	36.9	-29.09
56645	Ca channel human	49.55	40.43	48.57	51.51	47.52
56645	HERG	-16.61	14.2	-2.81	13.24	2.01
56645	M3D	23.59	23.59	-5.44	-0.6	10.29
56645	M4 D	25	-12.99	11.59	-21.93	0.42
56645	NTS1	-14.59	-25.24	-24.79	-15.27	-19.97
56645	Alpha2Beta2	-8.06	-3.71	-0.44	5.41	-1.7
56645	Alpha2Beta4	0.19	16.48	3.17	9.56	7.35
56645	Alpha3Beta2	11.41	15.59	0.41	7.24	8.66
56645	Alpha3Beta4	-5.66	6.7	-2.86	-0.34	-0.54
56645	Alpha4Beta2	2.45	-10.96	-5.24	-1.24	-3.75
56645	Alpha4Beta2 (Rat Brain)	-4.74	2.26	7.1	-1.69	0.73
56645	Alpha4Beta4	2.8	0.81	-1.68	-5.67	-0.94
56645	Alpha7	-1.2	-10.9	-12.11	-15.57	-9.95
56645	OT	17.31	8.48	17.52	37.34	20.16
56645	V1A	-18.54	-1.78	-4.99	-2.47	-6.95
56645	V1B	40.83	36.16	24.78	41.76	35.88
56645	V2	40.75	45.91	36.71	62.51	46.47
56645	OT	20.96	1.82	49.56	19.02	22.84

6. **Secondary binding data of KPP-III-51 (10) in PDSP studies (data source: Dr. Bryon Roth, NIMH).**

Compound #	Tier	Receptor	LogKi	Ki (nM)
56645	1	5-HT1A	-5.68	2108.14
56645	1	KOR	-5.81	1534.26
56645	1	KOR	-5.98	1049.06
56645	1	PBR	-5.9	1263.28

7. **Primary binding data of KPP-III-34 (9) in PDSP studies (data source: Dr. Bryon Roth, NIMH).**

	Primary binding result of KPP-III-34						
2	Compound #	Receptor	Inhibition 1	Inhibition 2	Inhibition 3	Inhibition 4	Mean %
3	56646	5-HT1A	53.1	47.51	48.76	51.37	50.19
4	56646	5-HT1B	7.76	-0.83	5.67	7.21	4.95
5	56646	5-HT1D	-5.73	-6.52	2.23	3.07	-1.74
6	56646	5-HT1E	9.25	-21.23	-21.66	9.25	-6.1
7	56646	5-HT2A	-6.01	-8.86	1.98	9.58	-0.83
8	56646	5-HT2B	-7.42	-3.22	-2.54	1.77	-2.85
9	56646	5-HT2C	3.87	-3.48	7.21	5.54	3.29
10	56646	5-HT3	-4.45	-8.68	-1.56	10.37	-1.08
11	56646	5-HT4	7.59	15.11	3.82	-0.41	6.53
12	56646	5-HT5A	-20.34	16.91	-7.15	0.61	-2.49
13	56646	5-HT6	-12.19	3.71	-6.11	-4.47	-4.77
14	56646	5-HT7A	-5.8	-14.9	-9.41	-5.49	-8.9
15	56646	Alpha1A	-9.7	-12.18	14.71	4.58	-0.65
16	56646	Alpha1B	-14.88	-10.09	-10.51	14.08	-5.35
17	56646	Alpha1D	-43.88	-24.26	-21.46	5.07	-21.13
18	56646	Alpha2A	-14.16	-13.67	8.56	11.34	-1.98
19	56646	Alpha2B	5.7	22.92	9.29	6.13	11.01
20	56646	Alpha2C	-10.58	-0.97	10.75	12.56	2.94
21	56646	Beta2	-12.55	-1.97	14.35	-4.22	-1.1
22	56646	BZP Rat Brain Site	93.01	88.96	94.43	92.29	92.17
23	56646	D1	40.26	7.95	27.22	-2.63	18.2
24	56646	D2	-9.47	-3.85	-2.23	7.13	-2.11

8. Primary binding data of KPP-III-34 (9) in PDSP studies (data source: Dr. Bryon Roth, NIMH).

Primary binding result of KPP-III-34 Part II						
Compound #	Receptor	Inhibition 1	Inhibition 2	Inhibition 3	Inhibition 4	Mean %
56646	D3	2.11	-4.76	-5.46	-5.58	-3.42
56646	D4	-19.63	-14.63	-3.5	-1.61	-9.84
56646	D5	-4.84	3.91	-1.84	-31.96	-8.68
56646	DAT	-41.19	-41.76	-19.28	4.91	-24.33
56646	DOR	28.44	24.57	18.07	25.39	24.12
56646	H1	-10.63	-14.68	-5.78	0.42	-7.67
56646	H3	0.71	10.96	14.76	9.07	8.88
56646	H4	-1.47	6.36	8	11.91	6.2
56646	KOR	93.06	88.75	89.83	90.6	90.56
56646	M1	8.28	7.38	-0.38	7.65	5.73
56646	M2	-21.61	-8.68	-3.36	-0.23	-8.47
56646	M3	-2.16	-12.88	1.46	6.57	-1.75
56646	M4	6.13	-17.33	-12.02	-9.79	-8.25
56646	M5	-24.17	-25.2	-15.71	19.29	-11.45
56646	MOR	7.98	23.44	18.07	-4.53	11.24
56646	NET	-14.04	-18.83	-5.57	20.95	-4.37
56646	PBR	61.45	53.42	71.17	69.48	63.88
56646	SERT	-27.84	-6.55	51.08	-5.54	2.79
56646	Sigma 1	36.7	41.24	39.66	37.39	38.75
56646	Sigma 2	11.05	12.99	21.95	-2.23	10.94
56646	HERG	-29.13	-26.66	-28.38	-8.59	-23.19
56646	NMDA	79.4	58.99	38.55	26.46	50.6

9. Secondary binding data of KPP-III-34 (9) (PDSP # 56646) in PDSP studies (data source: Dr. Bryon Roth, NIMH).

Compound #	Tier	Receptor	LogKi	Ki (nM)
56646	2	5-HT1A	-5.74	1834.85
56646	2	5-HT1A	-5.65	2218.71
56646	2	KOR	-6.42	380.36
56646	2	KOR	-6.74	183.06
56646	2	PBR	-6.23	591.43
56646	2	PBR	-6.13	732.99
56646	2	BZP Rat Brain Site	-7.32	47.46
56646	2	BZP Rat Brain Site	-7.29	51.81
56646	2	NMDA	-8.71	1.96
56646	2	NMDA	-9.28	0.53
56646	2	NMDA	-8.74	1.8
56646	2	NMDA	> -5	> 10,000
56646	2	NMDA	-5.55	2795.76

10. Primary binding data of compound 56647 (ETSP number) in PDSP studies (data source: Dr. Bryon Roth, NIMH).

Compound #	Receptor	Inhibition 1	Inhibition 2	Inhibition 3	Inhibition 4	Mean %
56647	5-HT1A	1.7	-7.17	-2.45	-0.81	-2.18
56647	5-HT1B	-1.13	5.24	0.15	0.28	1.14
56647	5-HT1D	-3.64	-10.01	-12.67	-3.81	-7.53
56647	5-HT1E	5.33	4.9	8.82	9.69	7.19
56647	5-HT2A	9.5	16.3	2.87	9.03	9.43
56647	5-HT2B	4.5	4.27	-8.78	-1.63	-0.41
56647	5-HT2C	14.86	12.11	9.37	5.54	10.47
56647	5-HT3	1.32	-12.63	-7.14	-10.7	-7.29
56647	5-HT4	-6.43	3.63	8.06	-0.32	1.24
56647	5-HT5A	14.84	11.48	-3.53	18.47	10.32
56647	5-HT6	-2.13	-20.14	-0.26	7.45	-3.77
56647	5-HT7A	-3.76	-11.14	-12.55	-5.02	-8.12
56647	A1	-26.06	-12.35	0.63	12.17	-6.4
56647	A2A	30.27	27.04	27.14	-2.8	20.41
56647	Alpha1A	15.75	-10.11	17.2	-7.63	3.8
56647	Alpha1B	-10.72	-3.53	-18.32	-10.3	-10.72
56647	Alpha1D	-15.48	-28.37	-36.41	-6.14	-21.6
56647	Alpha2A	60.72	40.45	44.7	44.21	47.52
56647	Alpha2B	48.03	43.01	42.86	32.39	41.57
56647	Alpha2C	32.61	23.15	7.88	10.67	18.58
56647	Beta1	-0.16	-4.88	19.98	10.22	6.29
56647	Beta2	2.53	0.28	4	-7.93	-0.28
56647	Beta3	17.02	-1.06	-20.61	-1.06	-1.43
56647	BZP Rat Brain Site	92.53	99.2	99.43	96.82	97
56647	D1	28.24	29.11	46.35	17.23	30.23
56647	D2	6.26	-9.1	-6.23	-3.11	-3.05
56647	D3	3.51	13.65	20.99	17.96	14.03
56647	D4	-17.65	-7.21	-9.11	-2.56	-9.13
56647	D5	22.4	19.78	26.52	20.52	22.31
56647	DAT	-12.17	-13.02	-13.02	13.73	-6.12
56647	DOR	19.49	5.46	20.91	24.37	17.56
56647	GABAA	20.71	10.02	0.1	19.18	12.5
56647	H1	-7.4	-8.75	-3.89	9.72	-2.58
56647	H2	5.3	5.84	5.94	0.12	4.3
56647	H3	-9.16	-36.88	10.96	30.33	-1.19
56647	H4	-10.11	5.12	-4.76	-1.47	-2.81
56647	KOR	43.75	39.9	18.94	51.61	38.55
56647	M1	14.78	5.94	-23.32	-2.19	-1.2
56647	M2	-19.23	-6.88	-13.81	-8.97	-12.22
56647	M3	-4.47	4.1	-13.38	3.11	-2.66
56647	M4	-10.25	-16.03	14.89	-0.94	-3.08
56647	M5	0.3	-6.68	-8.62	34.15	4.79
56647	MOR	27.27	10.67	11.18	-7.6	10.38

11. **Primary binding data of compound 27 (*S*) (ETSP # 56647) in PDSP studies (data source: Dr. Bryon Roth, NIMH).**

56647	NET	-6.14	-17	-3.6	12.06	-3.67
56647	PBR	63.42	68.77	61.73	80.32	68.56
56647	SERT	-0.21	-2.24	2.83	7.65	2.01
56647	Sigma 1	34.6	42.81	34.08	36	36.87
56647	Sigma 2	34.98	40.51	38.37	33.69	36.89
56647	AMPA	15.68	-15.22	-15.22	-12.85	-6.9
56647	Kainate (Rat Brain)	45.41	-19.05	6.56	-10.94	5.5
56647	NMDA	48.35	45.09	27.64	48.64	42.43
56647	NR2B	12.48	-37.46	8.86	0.25	-3.97
56647	HCA2	-21.45	-27	-15.2	28.57	-8.77
56647	Ca channel human	31.31	28.71	20.24	34.57	28.71
56647	HERG	-25.7	-28.27	-36.72	-30.2	-30.22
56647	M3D	35.69	-19.96	-4.64	-16.73	-1.41
56647	M4 D	-2.93	-7.4	-7.4	-0.7	-4.61
56647	NTS1	-35.67	-30.91	-19.8	1.27	-21.28
56647	Alpha2Beta2	0.37	-1.67	4.59	-1.94	0.34
56647	Alpha2Beta4	-3.22	5.83	0.61	6.25	2.37
56647	Alpha3Beta2	3.16	1.02	3.06	11.72	4.74
56647	Alpha3Beta4	0.02	-10.81	-2.23	-8.28	-5.33
56647	Alpha4Beta2	5.62	-1.11	1.37	3.84	2.43
56647	Alpha4Beta2 (Rat Brain)	4.68	8.5	2.77	-0.03	3.98
56647	Alpha4Beta4	-2.68	11.52	-4.92	12.02	3.99
56647	Alpha7	18.57	-6.39	-3.61	0.3	2.22
56647	OT	10.63	2.02	-3.15	6.76	4.07
56647	V1A	-9.12	-6.37	2.35	26.69	3.39
56647	V1B	13.77	7.98	-0.05	12.09	8.45
56647	V2	-20.5	-15.79	25.72	-0.53	-2.78
56647	OT	-10.06	-3.27	-8.6	11.75	-2.55

12. **Secondary binding data of compound 27(*S*) (ETSP # 56647)in PDSP studies (data source: Dr. Bryon Roth, NIMH).**

Compound #	Tier	Receptor	LogKi	Ki (nM)
56647	1	PBR	-5.33	4675.20
56647	1	PBR	-5.34	4526.89
56647	1	BZP Rat Brain Site	-7.24	57.81
56647	1	BZP Rat Brain Site	-7.13	74.82

13. Primary binding data of compound 24 (*S*) (ETSP # 56648) in PDSP studies (data source: Dr. Bryon Roth, NIMH).

Compound #	Receptor	Inhibition 1	Inhibition 2	Inhibition 3	Inhibition 4	Mean %
56648	5-HT1A	-1	-7.08	-10.55	-8.43	-6.77
56648	5-HT1B	-4.45	-1.69	-0.21	2.3	-1.01
56648	5-HT1D	-9	-11.59	-13.96	-9.17	-10.93
56648	5-HT1E	-9.03	1.42	12.3	10.56	3.81
56648	5-HT2A	-3.93	-1.17	-8.78	-7.67	-5.39
56648	5-HT2B	5.06	-1.52	-6.4	0.3	-0.64
56648	5-HT2C	10.25	1.23	0.25	12.41	6.04
56648	5-HT3	-19.17	-6.18	-32.93	-3.97	-15.56
56648	5-HT4	-4.46	10.5	10.22	4.1	5.09
56648	5-HT5A	-1.97	0.87	-0.68	-6.89	-2.17
56648	5-HT6	-18.04	-15.23	-23.42	-7.75	-16.11
56648	5-HT7A	-7.69	-6.27	-13.8	-2.04	-7.45
56648	A1	6.4	44.63	4.96	25.88	20.47
56648	A2A	-20.74	-34.34	-8.21	10	-13.32
56648	Alpha1A	20.51	-14.25	27.75	4.78	9.7
56648	Alpha1B	0.64	-18.64	-25.62	15.12	-7.13
56648	Alpha1D	-25.39	-13.24	-39.4	-8.2	-21.56
56648	Alpha2A	-2.23	1.86	-13.02	12.98	-0.1
56648	Alpha2B	34.25	19.62	8.57	18.62	20.27
56648	Alpha2C	-2.56	6.67	30.11	29.73	15.99
56648	Beta1	-0.79	7.39	2.04	35.08	10.93
56648	Beta2	2.19	-2.31	9.74	3.1	3.18
56648	Beta3	3.55	15.54	2.81	-16.19	1.43
56648	BZP Rat Brain Site	93.01	89.91	95.39	94.2	93.13
56648	D1	-24.22	-24.8	-21.32	-46.68	-29.26
56648	D2	1.01	-1.36	-3.23	7.75	1.04
56648	D3	-0.68	-1.27	0.83	0.71	-0.1

14. Primary binding data of compound 24 (*S*) (ETSP # 56648) in PDSP studies (data source: Dr. Bryon Roth, NIMH).

56648	D4	-6.44	-14.2	-15.84	-0.31	-9.2
56648	D5	-15.84	-16.21	-4.22	-22.46	-14.68
56648	DAT	26.25	9.03	11.6	33.79	20.17
56648	DOR	15.63	23.96	23.56	17.26	20.1
56648	GABAA	30.63	15.74	1.62	19.56	16.89
56648	H1	-3.76	-17.24	-14.68	-7.67	-10.84
56648	H2	5.77	-6.58	-10.48	3.99	-1.83
56648	H3	1.85	36.4	18.94	35.64	23.21
56648	H4	-12.38	-3.11	5.94	0.8	-2.19
56648	KOR	53	45.6	37.43	43.13	44.79
56648	M1	-4.81	-12.75	-19.34	14.15	-5.69
56648	M2	-14	-25.79	-6.21	-19.42	-16.36
56648	M3	-8.76	2.78	6.08	12.51	3.15
56648	M4	-14.26	-5.88	-8.11	-3.83	-8.02
56648	M5	-38.47	-21.54	38.73	7.39	-3.47
56648	MOR	-54.35	25.1	-2.87	-1.85	-8.49

15. Primary binding data of compound 24 (*S*) (ETSP # 56648) in PDSP studies (data source: Dr. Bryon Roth, NIMH).

56648	NET	-2.19	1.9	4.3	8.25	3.07
56648	PBR	48.91	54.69	53.84	42.58	50.01
56648	SERT	-1.99	11.2	1.14	-17.45	-1.78
56648	Sigma 1	36.52	42.81	40.89	33.2	38.36
56648	Sigma 2	6.97	10.65	18.76	12.49	12.22
56648	AMPA	5.62	-44.3	-14.13	5.44	-11.84
56648	Kainate (Rat Brain)	31.75	-7.52	10.83	-33.14	0.48
56648	NMDA	62.84	36.22	51.6	41.69	48.09
56648	NR2B	10.09	-41.16	-0.49	-3.95	-8.88
56648	HCA2	-17.28	32.04	34.12	72.33	30.3
56648	Ca channel human	15.35	3.62	18.93	32.94	17.71
56648	HERG	-25.27	-13.83	-15.22	-12.86	-16.8
56648	M3D	51.81	-34.48	-1.41	-19.15	-0.81
56648	M4 D	-2.93	-19.69	2.65	7.12	-3.21
56648	NTS1	-14.82	-8.02	2.86	-8.92	-7.23
56648	Alpha2Beta2	0.1	-10.65	1.19	5.95	-0.85
56648	Alpha2Beta4	0.61	0.72	-0.03	8.28	2.4
56648	Alpha3Beta2	2.75	12.33	4.99	6.93	6.75
56648	Alpha3Beta4	5.62	-3.95	2.64	-4.22	0.02
56648	Alpha4Beta2	-1.75	10.07	-3.78	-3.14	0.35
56648	Alpha4Beta2 (Rat Brain)	2.77	5.06	1.75	0.86	2.61
56648	Alpha4Beta4	6.54	3.8	-5.67	9.28	3.49
56648	Alpha7	-37.6	-27.52	-5.11	-17.22	-21.86
56648	OT	18.38	10.63	1.37	24.63	13.75
56648	V1A	18.65	-14.86	9.7	30.59	11.02
56648	V1B	-0.42	-11.99	18.62	-6.02	0.05
56648	V2	-3	-18.7	8.22	14.5	0.26
56648	OT	-6.18	2.54	11.27	28.23	8.97

16. **Secondary binding data of compound 27 (*S*) (ETSP # 56648) in PDSP studies (data source: Dr. Bryon Roth, NIMH).**

Compound #	Tier	Receptor	LogKi	Ki (nM)
56648	1	PBR	-5.29	5126.25
56648	1	PBR	-5.34	4568.78
56648	1	BZP Rat Brain Site	-6.78	167.38
56648	1	BZP Rat Brain Site	-6.82	152.93

17. Primary binding data of compound KPP-III-96B (11) (ETSP number 58478) in PDSP studies (data source: Dr. Bryon Roth, NIMH).

Compound #	Receptor	Inhibition 1	Inhibition 2	Inhibition 3	Inhibition 4	Mean %
58478 (KPP-III-96B	5-HT1A	66.86	74.57	62.33	56.3	65.02
58478	5-HT1B	14.09	-14.09	-11.83	-4.18	-4
58478	5-HT1D	11.4	-3.53	3.94	-4.77	1.76
58478	5-HT1E	13.17	15.25	8.29	16.34	13.26
58478	5-HT2A	37.16	7.95	-7.57	15.64	13.3
58478	5-HT2B	28.8	2.92	-1.75	18.37	12.09
58478	5-HT2C	32.63	4.74	-14.54	-2.38	5.11
58478	5-HT3	25.95	21.91	21.37	31.16	25.1
58478	5-HT4	2.74	32.91	-34.74	12.8	3.43
58478	5-HT5A	42.22	-4.85	1.51	2.36	10.31
58478	5-HT6	18.24	5.74	-10.29	-10.88	0.7
58478	5-HT7A	16.21	0.58	3.76	0.29	5.21
58478	A1	37.41	42.75	-5.88	56.65	32.73
58478	A2A	2.91	20.8	4.06	47.05	18.71
58478	Alpha1A	11.21	3.36	5.49	6.76	6.71
58478	Alpha1B	8.12	22.7	20.3	16.71	16.96
58478	Alpha1D	0	4.98	4.72	20.03	7.43
58478	Alpha2A	26.32	0.36	5.73	-0.08	8.08
58478	Alpha2B	52.66	28.73	33.47	28.04	35.73
58478	Alpha2C	20.54	-5.06	-22.7	-0.17	-1.85
58478	Beta1	13.66	25.09	20.79	29.73	22.32
58478	Beta2	-30.9	-9.55	0.11	2.04	-9.58
58478	Beta3	30.4	24.5	43.67	77.57	44.04
58478	AT2	-11.41	0.03	-7.92	-2.45	-5.44
58478	BZP Rat Brain Site	91.82	97.23	94.52	94.41	94.5

18. Primary binding data of compound KPP-III-96B (11) (ETSP number 58478) in PDSP studies (data source: Dr. Bryon Roth, NIMH).

58478	D1	20.61	5.23	20.26	9.69	13.95
58478	D2	5.4	3.25	-1.61	24.27	7.83
58478	D3	-0.72	2.23	-4.23	5.74	0.76
58478	D4	-5.22	-10.7	-0.38	-11.33	-6.91
58478	D5	15.7	5.05	14.1	20.66	13.88
58478	DAT	-4.37	-23.49	-27.7	-29.15	-21.18
58478	DOR	10.92	1.12	-1.86	-10.6	-0.11
58478	GABAA	12.56	-22.24	0	-6.82	-4.13
58478	H1	-1.47	8.73	-23.61	10.29	-1.52
58478	H2	-10.76	12.07	18.95	9.35	7.4
58478	H3	-22.62	-12.79	-15.25	-10.34	-15.25
58478	H4	8.55	-4.19	7.18	1.69	3.31
58478	KOR	75.75	76.41	87.34	84.39	80.97
58478	M1	4.29	7.5	8.42	10.02	7.56
58478	M2	-2.89	-6.91	2.99	1.03	-1.45
58478	M3	-3.39	1.62	-3.27	8.53	0.87
58478	M4	17.09	2.56	14.84	15.05	12.39
58478	M5	-21.8	-31.8	-33.94	-4.8	-23.09
58478	MOR	26.23	6.1	3.88	-2.23	8.5
58478	NET	-22.4	-6.9	-14.49	10.75	-8.26
58478	PBR	68.57	59.59	70.77	57.68	64.15
58478	SERT	-3.52	-2.51	-12.17	-18.86	-9.27
58478	Sigma 1	13.18	5.34	9.5	2.72	7.69
58478	Sigma 2	11.58	11.01	-0.72	13.07	8.74
58478	AMPA	-8.68	-7.17	-8.03	-17.98	-10.47
58478	Kainate (Rat Brain)	-16.09	61.42	37.89	36.51	29.93
58478	NMDA	-33.98	-15.57	43.14	30.35	5.99
58478	NR2B	-23.87	13.97	32.6	22.8	11.38
58478	Ca channel v1.2 human	13.41	36.4	10.34	60.92	30.27
58478	HERG	18.44	21.63	5.03	13.33	14.61
58478	M4 D	25.11	38.76	39.72	44.55	37.04
58478	Alpha2Beta2	3.87	7.05	-5.99	9.63	3.64
58478	Alpha2Beta4	2.39	-0.84	-0.14	5.06	1.62
58478	Alpha3Beta2	4.17	1.26	-0.6	-1.52	0.83
58478	Alpha3Beta4	3.2	1.18	2.02	3.2	2.4
58478	Alpha4Beta2	9.16	4.83	10.48	12.52	9.25
58478	Alpha4Beta2 (Rat Brain)	-7.63	0.15	-8.95	5.9	-2.63
58478	Alpha4Beta4	-3.58	5.01	7.65	-2.04	1.76
58478	Alpha7	2.4	2.71	0.23	10.14	3.87
58478	NOP	-22.29	-32.21	-33.08	0.86	-21.68
58478	OT	35.61	31.74	40.33	36.25	35.98
58478	V1A	49.45	39.15	35.32	45.33	42.31
58478	V1B	8.75	24.35	6.35	30.15	17.4
58478	V2	62.03	-19.32	-30.17	1.47	3.5

19. Secondary binding data of compound KPP-III-96B (11) (ETSP number 58478) in PDSP studies (data source: Dr. Bryon Roth, NIMH).

Compound #	Tier	Receptor	LogKi	Ki (nM)
58478	1	KOR	-6.25	561.31
58478	1	KOR	-6.62	238.34
58478	1	5-HT1A	-5.66	2206.99
58478	1	5-HT1A	-5.86	1365.84
58478	1	PBR	-5.76	1728.62
58478	1	PBR	-5.63	2365.37
58478	1	BZP Rat Brain Site	-6.74	184.08
58478	1	BZP Rat Brain Site	-6.65	221.67

20. Primary binding data of compound (ETSP number 58487) in PDSP studies (data source: Dr. Bryon Roth, NIMH).

Compound #	Receptor	Inhibition 1	Inhibition 2	Inhibition 3	Inhibition 4	Mean %
58487	5-HT1A	35.01	-2.37	8.69	13.56	13.72
58487	5-HT1B	-11.14	-1.04	1.04	-0.35	-2.87
58487	5-HT1D	2.7	-18.46	7.26	0.62	-1.97
58487	5-HT1E	9.64	7.68	13.9	15.49	11.68
58487	5-HT2A	-10.03	-18.94	-2.04	19.94	-2.77
58487	5-HT2B	25.56	32.39	19.09	-7.5	17.39
58487	5-HT2C	-13.29	-20.83	-11.4	0.97	-11.14
58487	5-HT3	21.39	7.35	17.17	1.98	11.97
58487	5-HT4	11.46	-25.55	8.1	-17.98	-5.99
58487	5-HT5A	16.57	-13.12	3.21	16.35	5.75
58487	5-HT6	-3.24	-5.74	-3.68	-1.62	-3.57
58487	5-HT7A	18.24	16.5	20.85	24.32	19.98
58487	A1	-15.5	-12.83	10.15	18.7	0.13
58487	Alpha1A	-1.3	2.3	4.85	6.76	3.15
58487	Alpha1B	14.86	7.36	25.31	9.21	14.19
58487	Alpha1D	9.82	23.09	20.54	28.96	20.6
58487	Alpha2A	0.92	-12.95	19.72	5.73	3.36
58487	Alpha2B	20.34	15.82	17.94	25.25	19.84
58487	Alpha2C	-6.45	-20.19	-6.66	-3.24	-9.14
58487	Beta1	-1.65	6.68	12.86	-5.68	3.05
58487	Beta2	-27.18	-6.82	-13.61	-15.55	-15.79
58487	Beta3	49.19	33.35	30.03	-7.19	26.35
58487	AT2	12.13	9.2	14.04	40.13	18.88
58487	BZP Rat Brain Site	97.98	96.84	98.32	97.41	97.64
58487	D1	20.37	41.86	26.71	29.06	29.5
58487	D2	-2.29	-39.59	8.9	-9.64	-10.66
58487	D3	-14.91	3.77	-6.9	-1	-4.76

21. Primary binding data of compound 12 (ETSP # 58487) in PDSP studies (data source: Dr. Bryon Roth, NIMH).

58487	D4	-3.75	-14.59	-30.7	-3.01	-13.01
58487	D5	22.26	-3.7	13.07	33.94	16.39
58487	DAT	-24.07	-32.28	-10.33	6.9	-14.95
58487	DOR	-10.17	-10.38	-7.83	-2.08	-7.62
58487	GABAA	-8.01	-1.29	10.58	27.58	7.22
58487	H1	-4.76	18.94	-7.35	-12.71	-1.47
58487	H2	-5.67	-12.16	-1.5	-19.3	-9.66
58487	H3	8.5	10.54	1.33	12.79	8.29
58487	H4	2.83	17.54	101.53	22.52	36.11
58487	KOR	88.57	71.33	77.26	58.91	74.02
58487	M1	-0.48	-12.27	-5.8	-7.71	-6.57
58487	M2	-9.99	1.12	-6.35	-0.75	-3.99
58487	M3	-12.54	7.65	-9.22	-1.55	-3.92
58487	M4	15.05	23.44	31.83	53.94	31.07
58487	M5	-2.17	-21.51	-19.66	3.56	-9.95
58487	MOR	5.22	16.62	16.46	17.9	14.05
58487	NET	-5.3	-13.05	-11.53	16.59	-3.32
58487	PBR	52.9	51.75	46.88	60.35	52.97
58487	SERT	-22.71	0.4	-27.87	-6.29	-14.12

22. **Primary binding data of compounds 12 (ETSP number 58487) and compound 58488 in PDSP studies (data source: Dr. Bryon Roth, NIMH).**

58487	Sigma 1	0.43	4.23	-18.49	22.36	2.13
58487	Sigma 2	18.96	67.95	6.63	4.48	24.51
58487	AMPA	43.24	22.9	40.64	26.8	33.4
58487	NMDA	33.6	3.06	6.53	-25.53	4.42
58487	NR2B	32.85	21.15	26.97	13.5	23.62
58487	HCA2	27.93	18.5	16.62	31.7	23.69
58487	Ca channel v1.2 human	34.16	-7.06	11.26	18.89	14.31
58487	HERG	35.67	34.4	37.59	57.38	41.26
58487	M4 D	0.82	18.9	19.65	-6	8.34
58487	Alpha2Beta2	7.96	4.63	4.93	-0.99	4.13
58487	Alpha2Beta4	13.07	2.81	14.48	9.84	10.05
58487	Alpha3Beta2	9.59	4.43	6.15	8.26	7.11
58487	Alpha3Beta4	4.21	11.97	5.39	12.14	8.43
58487	Alpha4Beta2	2.67	13.48	15.65	2.79	8.65
58487	Alpha4Beta2 (Rat Brain)	2.9	-9.48	-1.53	13.33	1.31
58487	Alpha4Beta4	-2.7	-13.26	-2.92	-1.6	-5.12
58487	Alpha7	17.11	23.3	16.49	26.86	20.94
58487	NOP	-16.83	-11.94	-13.52	12.37	-7.48
58487	OT	-7.87	2.94	-1.39	6.45	0.03
58487	V2	3.28	56.61	13.22	8.7	20.45
58487	Oxytocin	-7.87	2.94	-1.39	6.45	0.03
58488	5-HT1A	-2.03	9.2	-2.54	3.16	1.95
58488	5-HT1B	14.62	-32.36	-16.01	10.61	-5.79
58488	5-HT1D	-18.46	-17.63	-9.75	-9.75	-13.9
58488	5-HT1E	2.2	18.54	13.54	16.71	12.75
58488	5-HT2A	1.65	5.03	6.72	21.63	8.76
58488	5-HT2B	48.2	16.22	14.42	8.31	21.79
58488	5-HT2C	8.52	7.68	2.65	-5.32	3.38

23. Primary binding data of compounds (ETSP number 58488) in PDSP studies (data source: Dr. Bryon Roth, NIMH).

58488	5-HT3	0.29	5.89	12.72	24.38	10.82
58488	5-HT4	-19.66	7.26	38.38	-15.46	2.63
58488	5-HT5A	5.12	-4.64	-4.43	1.3	-0.66
58488	5-HT6	13.82	-8.38	-3.24	0.15	0.59
58488	5-HT7A	-3.18	19.98	27.51	27.22	17.88
58488	Alpha1A	0.82	15.46	-1.3	4	4.75
58488	Alpha1B	-5.62	-15.85	-2.91	-6.02	-7.6
58488	Alpha1D	13.91	20.29	23.35	17.74	18.82
58488	Alpha2A	-7.91	-7.24	1.15	-7.13	-5.28
58488	Alpha2B	39.12	6	13.88	20.96	19.99
58488	Alpha2C	16.42	3.17	8.54	5.82	8.49
58488	Beta1	46.2	16.31	14.87	1.8	19.8
58488	Beta2	-21.14	-13.9	-11.52	-28.08	-18.66
58488	Beta3	70.57	31.87	-5.34	-0.92	24.05
58488	BZP Rat Brain Site	100.26	97.06	97.41	93.76	97.12
58488	D1	39.28	25.89	29.65	23.9	29.68
58488	D2	-21.16	24.72	-1.05	3.36	1.47
58488	D3	1.25	30.74	22.88	-7.18	11.92
58488	D4	-7.75	-14.59	5.83	16.46	-0.01

24. Primary binding data of compounds 23 A (ETSP number 58488) in PDSP studies (data source: Dr. Bryon Roth, NIMH).

58488	D5	-11.14	7.82	57.57	48.96	25.8
58488	DAT	-25.96	-26.25	-12.44	5.37	-14.82
58488	DOR	1.97	-5.48	-0.59	-6.55	-2.66
58488	GABAA	1.09	5.83	22.05	16.91	11.47
58488	H1	-13.58	11.33	4.06	-9.94	-2.03
58488	H2	-4.46	-7.43	-1.33	-11.28	-6.13
58488	H3	21.6	3.58	-1.74	-10.54	3.23
58488	H4	-2.83	9.39	85.23	16.41	27.05
58488	KOR	65.62	52.08	64.17	75.81	64.42
58488	M1	-1.24	9.42	-2.38	-0.29	1.38
58488	M2	-1.12	-5.04	-0.47	-11.2	-4.46
58488	M3	12.94	2.64	-5.51	-10.56	-0.12
58488	M4	-3.79	43.71	10.95	33.88	21.19
58488	M5	26.99	5.63	-14.78	2.27	5.03
58488	MOR	2.58	7.23	7.95	7.79	6.39
58488	NET	-12.01	-1.55	-3.46	12.43	-1.15
58488	PBR	66.75	68.28	75.74	80.99	72.94
58488	SERT	-26.93	-37.17	-18.5	-20.31	-25.73
58488	Sigma 1	8.81	-20.44	-30.19	-8.25	-12.52
58488	Sigma 2	-1.73	20.2	0.92	5.72	6.28
58488	AMPA	-4.35	4.3	-9.33	14.68	1.33
58488	NMDA	13.72	0.88	8.66	14.3	9.39
58488	NR2B	3.03	3.8	25.81	16.22	12.22
58488	HCA2	13.32	26.52	-4.6	15.67	12.73
58488	Ca channel v1.2 human	11.26	12.79	17.37	5.15	11.64
58488	HERG	37.59	14.6	-24.98	43.97	17.8

25. **Secondary binding data of compound 12 (ETSP number 58487) in PDSP studies (data. source: Dr. Bryon Roth, NIMH).**

Compound #	Tier	Receptor	LogKi	Ki (nM)
58487	1	KOR	-5.88	1315.53
58487	1	KOR	-6.33	462.91
58487	1	PBR	-5.70	2014.65
58487	1	PBR	-5.49	3207.75
58487	1	BZP Rat Brain Site	-7.46	34.87
58487	1	BZP Rat Brain Site	-7.60	25.03

26. Secondary binding data of compound 23 A (ETSP number 58488) in PDSP studies (data source: Dr. Bryon Roth, NIMH).

Compound #	Tier	Receptor	LogKi	Ki (nM)
58488	1	KOR	-5.90	1264.74
58488	1	KOR	-5.90	1272.33
58488	1	PBR	-5.91	1224.90
58488	1	PBR	-5.85	1403.46
58488	1	BZP Rat Brain Site	-6.90	125.03
58488	1	BZP Rat Brain Site	-6.91	123.88
58488	1	A1	-6.13	743.53
58488	1	A1	-5.97	1073.00
58488	1	Kainate (Rat Brain)	-5.70	1978.79

27. Primary binding data of compounds 23A (ETSP number 58488) and 37A (ETSP #58489) in PDSP studies (data source: Dr. Bryon Roth, NIMH).

58488	M4 D	-4.95	6.38	25.78	9.56	9.19
58488	Alpha2Beta2	5.38	8.27	-1.14	-0.38	3.03
58488	Alpha2Beta4	3.09	0.28	-0.28	-4.78	-0.42
58488	Alpha3Beta2	1.26	6.28	-5.22	-3.37	-0.26
58488	Alpha3Beta4	17.02	6.07	6.41	2.36	7.97
58488	Alpha4Beta2	6.88	5.8	3.39	11.92	7
58488	Alpha4Beta2 (Rat Brain)	-2.85	4.22	-0.55	-2.5	-0.42
58488	Alpha4Beta4	0.83	2.81	14.25	8.09	6.5
58488	Alpha7	13.08	14.47	8.75	-9.83	6.62
58488	NOP	-14.67	-15.67	5.9	-6.47	-7.73
58488	OT	4.02	-5.44	-1.66	-0.3	-0.85
58488	V2	-21.13	50.28	-7.57	46.67	17.06
58488	Oxytocin	4.02	-5.44	-1.66	-0.3	-0.85
58489	5-HT1A	-9.41	22.61	-5.05	0.82	2.24
58489	5-HT1B	-16.01	-20.18	-15.14	10.09	-10.31
58489	5-HT1D	-1.87	4.77	-17.63	-5.18	-4.98
58489	5-HT1E	13.54	8.05	14.64	20.73	14.24
58489	5-HT2A	9.03	9.18	15.02	39.92	18.29
58489	5-HT2B	23.41	29.87	14.42	6.51	18.55
58489	5-HT2C	-17.9	-3.01	-3.64	10.61	-3.49
58489	5-HT3	22	9.96	-8.31	-1.78	5.47

28. Primary binding data of compound 37A (ETSP number 58489) in PDSP studies (data source: Dr. Bryon Roth, NIMH).

58489	5-HT4	12.3	9.78	43.43	8.94	18.61
58489	5-HT5A	0.66	5.12	11.69	6.81	6.07
58489	5-HT6	-5.15	-22.35	-18.38	-0.88	-11.69
58489	5-HT7A	4.63	20.27	26.35	28.66	19.98
58489	Alpha1A	4.64	-5.12	-9.37	-9.37	-4.81
58489	Alpha1B	-9.13	-9.93	3.71	2.71	-3.16
58489	Alpha1D	12.22	-8.17	-37.86	-18.73	-13.14
58489	Alpha2A	-2.43	-23.58	12.78	-1.2	-3.61
58489	Alpha2B	11.43	19.82	3.89	-3.93	7.8
58489	Alpha2C	-13.7	-8.33	-0.17	4.92	-4.32
58489	Beta1	45.19	24.79	4.81	-2.08	18.18
58489	Beta2	-25.39	6.31	-4.58	-17.78	-10.36
58489	Beta3	80.52	62.83	-14.92	-6.82	30.4
58489	BZP Rat Brain Site	100.48	96.61	98.66	95.7	97.86
58489	D1	35.17	32	34.23	35.17	34.14
58489	D2	4.94	-1.38	-3.87	-1.38	-0.42
58489	D3	-13.64	20.49	10.8	-7.32	2.58
58489	D4	-7.54	-7.12	-0.59	31.83	4.15
58489	D5	-1.51	31.31	-10.56	35.1	13.59
58489	DAT	-27.19	-28.57	-23.99	18.02	-15.43
58489	DOR	-7.83	-5.7	17.73	-2.08	0.53
58489	GABAA	4.25	24.81	14.14	36.28	19.87
58489	H1	1.82	18.59	8.39	-3.55	6.31
58489	H2	0.81	-4.03	-14.41	-16.83	-8.62
58489	H3	13.41	-0.72	-0.72	-4.61	1.84
58489	H4	-5.55	13.47	69.84	24.56	25.58
58489	KOR	30.7	37.3	51.41	47.82	41.81
58489	M1	9.42	7.9	0.1	17.03	8.61

29. Secondary binding data of compound 37A (ETSP number 58489) in PDSP studies (data source: Dr. Bryon Roth, NIMH).

Compound #	Tier	Receptor	LogKi	Ki (nM)
58489	1	PBR	-5.77	1681.12
58489	1	PBR	-5.67	2125.69
58489	1	M5	-5.29	5075.75
58489	1	M5	-5.07	8519.22
58489	1	BZP Rat Brain Site	-6.88	133.08
58489	1	BZP Rat Brain Site	-7.02	95.41

30. Primary binding data of compound 23B (ETSP number 58490) in PDSP studies (data source: Dr. Bryon Roth, NIMH).

Compound #	Receptor	Inhibition 1	Inhibition 2	Inhibition 3	Inhibition 4	Mean %
58490	5-HT1A	15.57	3.33	-4.04	13.56	7.11
58490	5-HT1B	8.35	12.7	-37.06	-6.09	-5.53
58490	5-HT1D	-19.28	27.99	-37.53	-10.16	-9.75
58490	5-HT1E	9.03	-2.93	-0.73	7.68	3.26
58490	5-HT2A	5.96	28.09	17.02	17.94	17.25
58490	5-HT2B	35.62	23.05	15.5	19.81	23.5
58490	5-HT2C	-4.06	5.37	-12.66	12.29	0.24
58490	5-HT3	26.76	7.35	43.95	11.8	22.47
58490	5-HT4	-15.46	-26.39	-1.16	-8.73	-12.94
58490	5-HT5A	3.42	-4.85	-1.67	8.08	1.25
58490	5-HT6	5.74	2.79	-5	-2.79	0.19
58490	5-HT7A	21.72	29.82	18.24	19.4	22.3
58490	A1	28.29	-45.04	48.39	62.49	23.53
58490	A2A	24.24	34.19	40.45	40.88	34.94
58490	Alpha1A	-8.09	-6.61	-8.52	2.94	-5.07
58490	Alpha1B	5.22	-3.71	-11.54	-6.12	-4.04
58490	Alpha1D	26.79	-15.09	-7.08	-12	-1.85
58490	Alpha2A	-1.65	-10.49	-16.19	10.54	-4.45
58490	Alpha2B	1.26	5.03	7.03	20.56	8.47
58490	Alpha2C	-22.28	10.15	-17.96	-2.41	-8.13
58490	Beta1	56.4	13.87	25.79	23.35	29.85
58490	Beta2	-6.29	-3.76	0.2	0.57	-2.32
58490	Beta3	50.67	53.25	29.3	2.03	33.81
58490	AT2	-18.44	-34.29	-57.78	-16.56	-31.77
58490	BZP Rat Brain Site	99	96.72	96.49	95.47	96.92
58490	D1	24.13	46.56	32.35	34.7	34.44
58490	D2	65.3	-11.33	7.88	-1.38	15.12
58490	D3	-15.47	-12.66	-0.44	-6.48	-8.76
58490	D4	-12.59	-12.8	-1.43	9.94	-4.22
58490	D5	10.45	-0.64	-14.2	22.26	4.47
58490	DAT	-26.1	-33.95	-15.05	10.89	-16.05
58490	DOR	-16.35	0.48	-2.29	10.28	-1.97
58490	GABAA	10.18	-1.68	9	17.3	8.7
58490	H1	-10.46	-3.89	14.44	27.58	6.92
58490	H2	8.45	-21.06	-13.64	16.09	-2.54
58490	H3	-7.88	-7.27	-16.27	-5.22	-9.16
58490	H4	21.27	13.66	-0.03	7.58	10.62
58490	KOR	89.58	103.9	73.91	43.57	77.74
58490	M1	8.09	12.84	4.85	0.29	6.52
58490	M2	7.1	0.19	-12.14	4.2	-0.16
58490	M3	6.93	-0.12	-6	-5.17	-1.09
58490	M4	-1.33	32.04	16.68	20.98	17.09
58490	M5	27.95	62.76	75	85.21	62.73

31. Primary binding data of compound 23B (ETSP number 58490) in PDSP studies (data source: Dr. Bryon Roth, NIMH).

58490	MOR	4.34	1.77	-0.23	9.64	3.88
58490	NET	-7.78	-13.53	-4.42	42.95	4.31
58490	PBR	52.04	60.54	48.41	66.18	56.79
58490	SERT	-19	-15.01	0.11	-20.75	-13.66
58490	Sigma 1	-32.72	0.43	1.01	-10.01	-10.32
58490	Sigma 2	-6.2	-25.64	5.8	1.25	-6.2
58490	AMPA	-2.19	3.87	1.7	16.63	5
58490	Kainate (Rat Brain)	52.23	98.58	46.53	45.39	60.68
58490	NMDA	37.84	38.81	42.7	42.32	40.42
58490	NR2B	17.22	15.06	16.72	5.63	13.66
58490	HCA2	26.99	22.75	15.67	48.2	28.4
58490	Ca channel human	43.32	-11.64	-23.85	29.58	9.35
58490	HERG	32.48	51	19.71	70.79	43.5
58490	M3D	12.74	32.43	10.53	10.45	16.54
58490	M4 D	-19.05	-0.97	16.44	35.91	8.08
58490	Alpha2Beta2	-2.96	4.02	0.83	0.99	0.72
58490	Alpha2Beta4	6.89	12.51	-1.83	8.43	6.5
58490	Alpha3Beta2	4.17	-2.58	2.31	-6.15	-0.56
58490	Alpha3Beta4	-1.52	5.23	12.47	13.32	7.38
58490	Alpha4Beta2	5.56	8.8	3.99	4.95	5.83
58490	Alpha4Beta2 (Rat Brain)	-4.53	-0.82	-4.8	-7.36	-4.38
58490	Alpha4Beta4	5.89	11.39	3.03	9.19	7.38
58490	Alpha7	23.14	25.15	19.12	26.55	23.49
58490	NOP	-4.8	-55.21	0.19	4.18	-13.91
58490	OT	-7.13	-8.22	-6.72	-0.6	-5.67
58490	V1A	11.01	11.98	10.05	19.86	13.23
58490	V1B	-1.16	11.6	20.19	15.78	11.6
58490	V2	0.4	-4.18	20.38	1.32	4.48

32. Secondary binding data of compound 23B (ETSP number 58490) in PDSP studies (data source: Dr. Bryon Roth, NIMH).

Compound #	Tier	Receptor	LogKi	Ki (nM)
58490	1	KOR	-6.35	442.59
58490	1	KOR	-6.31	485.85
58490	1	PBR	-5.67	2145.36
58490	1	PBR	-5.68	2082.57
58490	1	M5	-5.19	6401.77
58490	1	M5	-5.02	9527.96
58490	1	BZP Rat Brain Site	-6.77	171.47
58490	1	BZP Rat Brain Site	-7.09	81.40
58490	1	Kainate (Rat Brain)	-5.43	3727.35

33. Primary binding data of 8-bromo-*N*-(2-hydroxypropyl)-6-(pyridin-2-yl)-4*H*-benzo[f]imidazo[1,5-a][1,4]diazepine-3-carboxamide (ETSP number 58491) in PDSP studies (data source: Dr. Bryon Roth, NIMH).

Compound #	Receptor	Inhibition 1	Inhibition 2	Inhibition 3	Inhibition 4	Mean %
58491	5-HT1A	-14.1	4	1.66	-17.28	-6.43
58491	5-HT1B	-23.14	-11.83	0	-3.65	-9.66
58491	5-HT1D	-19.7	-6.43	13.89	-33.39	-11.41
58491	5-HT1E	12.08	5.37	0.85	-0.37	4.48
58491	5-HT2A	3.8	1.5	3.34	8.26	4.23
58491	5-HT2B	4	30.95	28.08	17.3	20.08
58491	5-HT2C	15.64	7.89	13.55	1.6	9.67
58491	5-HT3	27.22	11.87	27.91	10.65	19.41
58491	5-HT4	-27.23	0.53	-3.68	8.1	-5.57
58491	5-HT5A	-3.37	-12.06	4.48	3.84	-1.78
58491	5-HT6	0.88	-2.94	-7.65	6.32	-0.85
58491	5-HT7A	1.16	23.74	10.42	44.01	19.83
58491	A1	45.92	41.34	55.44	55.44	49.54
58491	A2A	10.86	47.14	56.95	56.1	42.76
58491	Alpha1A	-3.42	-0.45	-19.55	-9.15	-8.14
58491	Alpha1B	4.51	-3.21	-2.91	-11.34	-3.24
58491	Alpha1D	23.15	-17.82	-2.34	-12.91	-2.48
58491	Alpha2A	-10.71	-18.77	0.48	1.26	-6.94
58491	Alpha2B	-2.16	-3.7	17.37	7.54	4.76
58491	Alpha2C	5.33	4.22	-3.1	4.15	2.65
58491	Beta1	11.28	10.99	-63.16	1.08	-9.95
58491	Beta2	-6	-9.58	-8.01	-12.19	-8.95
58491	Beta3	51.04	55.09	49.93	40.72	49.2
58491	AT2	5.83	-70.06	-34.29	-11.41	-27.48
58491	BZP Rat Brain Site	99.46	94.9	96.04	93.87	96.07
58491	D1	18.02	53.25	25.07	41.39	34.43
58491	D2	-2.18	8.22	9.69	-8.73	1.75
58491	D4	-14.07	-8.8	-1.22	26.57	0.62
58491	D5	-4.14	-12.45	1.7	10.74	-1.04
58491	DAT	-28.5	-22.47	-1.97	15.62	-9.33
58491	DOR	-11.02	-12.73	-11.66	-11.45	-11.72
58491	GABAA	7.02	21.65	15.72	31.54	18.98
58491	H1	3.89	3.55	0.61	28.45	9.13
58491	H2	14.27	-3.48	-37.99	-3.15	-7.59
58491	H3	7.06	3.79	-14.02	2.35	-0.21
58491	H4	27.35	8.08	-4.6	5.55	9.1
58491	KOR	78.16	86.44	82.19	59.35	76.54
58491	M1	5.99	8.28	15.51	-4.85	6.23
58491	M2	-11.67	1.21	-1.31	1.77	-2.5
58491	M3	0.85	1.26	-7.93	5.69	-0.03
58491	M4	34.49	13	2.56	40.84	22.72
58491	M5	51.96	69.96	85.09	69.36	69.09

34. Primary binding data of 8-bromo-*N*-(2-hydroxypropyl)-6-(pyridin-2-yl)-4*H*-benzo[f]imidazo[1,5-a][1,4]diazepine-3-carboxamide (ETSP number 58491) in PDSP studies (data source: Dr. Bryon Roth, NIMH).

58491	MOR	4.18	4.74	3.46	3.7	4.02
58491	NET	-8.1	4.68	11.31	54.85	15.69
58491	PBR	54.04	55.67	50.22	70.77	57.68
58491	SERT	-23.8	-22.06	-34.7	-15.08	-23.91
58491	Sigma 1	-20.34	-33.8	-20.63	-7.37	-20.54
58491	Sigma 2	-16.13	-18.69	-24.57	-5.7	-16.27
58491	AMPA	22.47	14.47	-0.46	19.88	14.09
58491	Kainate (Rat Brain)	26.02	78.06	57.93	18.8	45.2
58491	NMDA	40.18	27.72	26.75	33.17	31.96
58491	NR2B	-4.23	-2.57	0.15	-11.66	-4.58
58491	HCA2	29.35	10.02	33.12	28.4	25.22
58491	Ca channel human	67.75	-19.27	32.63	-0.95	20.04
58491	HERG	18.65	-13.11	-7.94	31.21	7.2
58491	M3D	9.18	66.52	9.9	36.55	30.54
58491	M4 D	6.88	-11.34	1.25	33.92	7.68
58491	Alpha2Beta2	-8.27	1.29	-4.32	0.68	-2.66
58491	Alpha2Beta4	-1.26	8.57	4.5	-9.28	0.63
58491	Alpha3Beta2	8	3.37	-1.52	0.33	2.55
58491	Alpha3Beta4	13.99	14.16	6.74	1.52	9.1
58491	Alpha4Beta2	3.39	14.56	-3.33	10.48	6.28
58491	Alpha4Beta2 (Rat Brain)	1.66	5.37	13.15	-2.32	4.47
58491	Alpha4Beta4	-2.7	-1.38	5.23	-11.94	-2.7
58491	Alpha7	5.96	-4.1	2.4	-0.08	1.05
58491	NOP	-7.8	-40.24	8.17	49.1	2.31
58491	OT	-2.64	5.26	6.62	2.54	2.95
58491	V1A	0.24	25.16	20.82	17.93	16.04
58491	V1B	-0.23	16.71	4.41	15.09	9
58491	V2	-16.71	-4.72	-5.88	-7.19	-8.63

35. **Primary binding data of compound 8-bromo-*N*-(2-hydroxypropyl)-6-(pyridin-2-yl)-4*H*-benzo[f]imidazo[1,5-a][1,4]diazepine-3-carboxamide (ETSP number 58491) in PDSP studies (data source: Dr. Bryon Roth, NIMH).**

Compound #	Tier	Receptor	LogKi	Ki (nM)
58491	1	KOR	-6.19	647.59
58491	1	KOR	-6.21	622.30
58491	1	PBR	-5.62	2388.91
58491	1	PBR	-5.56	2737.79
58491	1	M5	> -5	> 10,000
58491	1	M5	-5.30	4992.29
58491	1	BZP Rat Brain Site	-6.75	178.48
58491	1	BZP Rat Brain Site	-6.21	614.04

Raw data of electrophysiological studies of KPP-III-34 (9) and KPP-III-51 (10) at (100 nM and 1 μM)

KPP-III-34, 100 nM					
α1	190.2	173.20	174.20		
α2	186.7	149.50	160.80		
α3	135.7	152.40	140.40	158.80	157.20
α5	150.2	160.30	156.90	142.30	

KPP-III-34, 1 μM					
α1	342.7	366.00	310.2	344.20	469.20
α2	375.5	417.70	279.7		
α3	339.7	249.30	249.0	314.30	
α5	252.1	281.00	285.1		

KPP-III-51, 100 nM				
α1	152.6	161.60	153.60	164.90
α2	154.0	166.20	172.00	
α3	155.5	160.80	144.10	
α5	149.5	145.80	156.40	148.30

KPP-III-51, 1 μM			
α1	295.7	317.20	316.90
α2	326.4	277.90	265.70
α3	277.9	332.60	329.80
α5	255.0	294.10	263.50

% of response to GABA alone (100% = no effect)

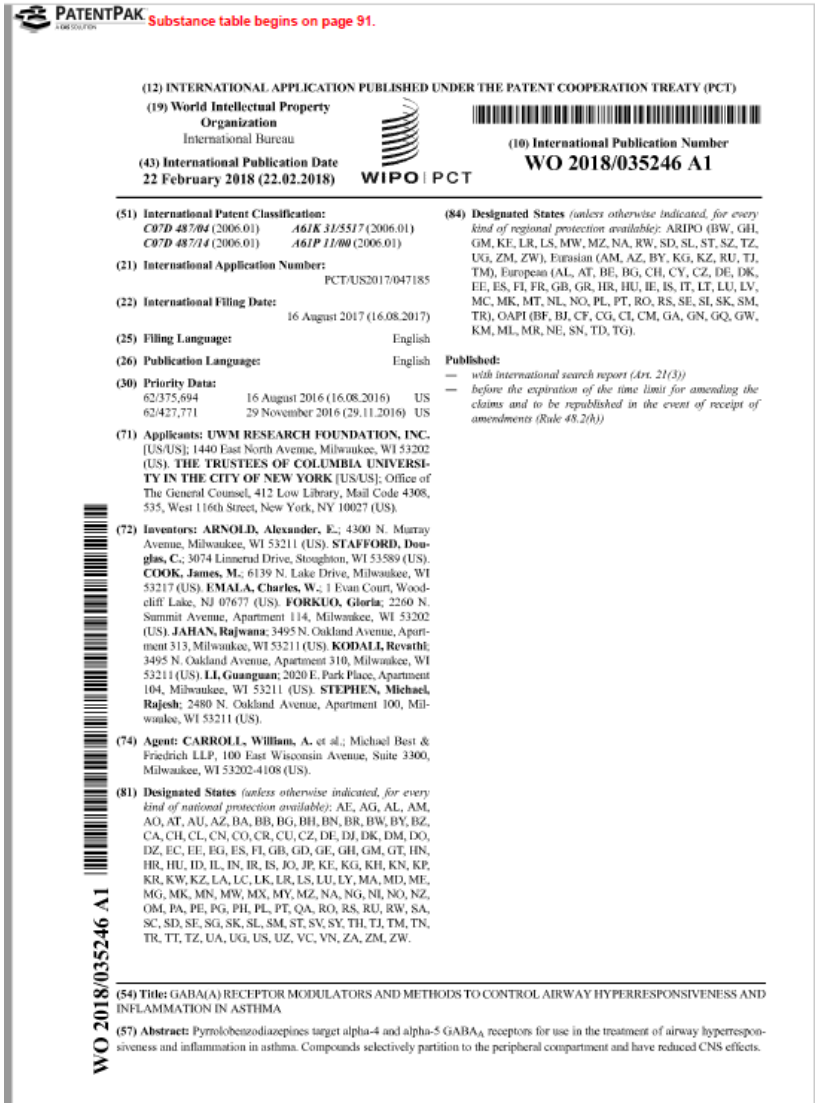
Whole-cell voltage clamp recordings from transiently transfected HEK-293T cells.

GABA concentration is EC_{3-5}

Patent which includes newly synthesized analogs including KPP-III-34 (9) and KPP-III-51 (10) oxazole. Patent number: WO2018/035246A1. Below is the complete patent (as it is).

Patent title: GABA (A) receptor modulators and methods to control airway hyperresponsiveness and inflammation in asthma.

Patent source: https://data.epo.org/publication-server/document?iDocId=5968341&iFormat=2



PATENTPAK Substance table begins on page 91.

(12) INTERNATIONAL APPLICATION PUBLISHED UNDER THE PATENT COOPERATION TREATY (PCT)

(19) World Intellectual Property Organization
International Bureau

(43) International Publication Date
22 February 2018 (22.02.2018)

WIPO | PCT

(10) International Publication Number
WO 2018/035246 A1

(51) International Patent Classification:
C07D 487/04 (2006.01) *A61K 31/5517* (2006.01)
C07D 487/14 (2006.01) *A61P 11/00* (2006.01)

(21) International Application Number:
PCT/US2017/047185

(22) International Filing Date:
16 August 2017 (16.08.2017)

(25) Filing Language: English

(26) Publication Language: English

(30) Priority Data:
62/375,694 16 August 2016 (16.08.2016) US
62/427,771 29 November 2016 (29.11.2016) US

(71) Applicants: **UWM RESEARCH FOUNDATION, INC.** [US/US]; 1440 East North Avenue, Milwaukee, WI 53202 (US). **THE TRUSTEES OF COLUMBIA UNIVERSITY IN THE CITY OF NEW YORK** [US/US]; Office of The General Counsel, 412 Low Library, Mail Code 4308, 535, West 116th Street, New York, NY 10027 (US).

(72) Inventors: **ARNOLD, Alexander, E.**; 4300 N. Murray Avenue, Milwaukee, WI 53211 (US). **STAFFORD, Douglas, C.**; 3074 Linnerud Drive, Stoughton, WI 53589 (US). **COOK, James, M.**; 6139 N. Lake Drive, Milwaukee, WI 53217 (US). **EMALA, Charles, W.**; 1 Evan Court, Woodcliff Lake, NJ 07677 (US). **FORKUO, Gloria**; 2260 N. Summit Avenue, Apartment 114, Milwaukee, WI 53202 (US). **JAHAN, Rajwana**; 3495 N. Oakland Avenue, Apartment 313, Milwaukee, WI 53211 (US). **KODALI, Revathi**; 3495 N. Oakland Avenue, Apartment 310, Milwaukee, WI 53211 (US). **LI, Guanguan**; 2020 E. Park Place, Apartment 104, Milwaukee, WI 53211 (US). **STEPHEN, Michael, Rajesh**; 2480 N. Oakland Avenue, Apartment 100, Milwaukee, WI 53211 (US).

(74) Agent: **CARROLL, William, A.** et al.; Michael Best & Friedrich LLP, 100 East Wisconsin Avenue, Suite 3300, Milwaukee, WI 53202-4108 (US).

(81) Designated States *(unless otherwise indicated, for every kind of national protection available)*: AE, AG, AL, AM, AO, AT, AU, AZ, BA, BB, BG, BH, BN, BR, BW, BY, BZ, CA, CH, CL, CN, CO, CR, CU, CZ, DE, DJ, DK, DM, DO, DZ, EC, EE, EG, ES, FI, GB, GD, GE, GH, GM, GT, HN, HR, HU, ID, IL, IN, IR, IS, JO, JP, KE, KG, KH, KN, KP, KR, KW, KZ, LA, LC, LK, LR, LS, LU, LY, MA, MD, ME, MG, MK, MN, MW, MX, MY, MZ, NA, NG, NI, NO, NZ, OM, PA, PE, PG, PH, PL, PT, QA, RO, RS, RU, RW, SA, SC, SD, SE, SG, SK, SL, SM, ST, SV, SY, TH, TJ, TM, TN, TR, TT, TZ, UA, UG, US, UZ, VC, VN, ZA, ZM, ZW.

(84) Designated States *(unless otherwise indicated, for every kind of regional protection available)*: ARIPO (BW, GH, GM, KE, LR, LS, MW, MZ, NA, RW, SD, SL, ST, SZ, TZ, UG, ZM, ZW), Eurasian (AM, AZ, BY, KG, KZ, RU, TJ, TM), European (AL, AT, BE, BG, CH, CY, CZ, DE, DK, EE, ES, FI, FR, GB, GR, HR, HU, IE, IS, IT, LT, LU, LV, MC, MK, MT, NL, NO, PL, PT, RO, RS, SE, SI, SK, SM, TR), OAPI (BF, BJ, CF, CG, CI, CM, GA, GN, GQ, GW, KM, ML, MR, NE, SN, TD, TG).

Published:
— *with international search report (Art. 21(3))*
— *before the expiration of the time limit for amending the claims and to be republished in the event of receipt of amendments (Rule 48.2(h))*

WO 2018/035246 A1

(54) Title: GABA(A) RECEPTOR MODULATORS AND METHODS TO CONTROL AIRWAY HYPERRESPONSIVENESS AND INFLAMMATION IN ASTHMA

(57) Abstract: Pyrrolobenzodiazepines target alpha-4 and alpha-5 $GABA_A$ receptors for use in the treatment of airway hyperresponsiveness and inflammation in asthma. Compounds selectively partition to the peripheral compartment and have reduced CNS effects.

GABA(A) RECEPTOR MODULATORS AND METHODS TO CONTROL AIRWAY HYPERRESPONSIVENESS AND INFLAMMATION IN ASTHMA

RELATED APPLICATIONS

[0001] This application claims the benefit of U.S. provisional application serial no. 62/375,694, filed August 16, 2016, and U.S. provisional application serial no. 62/427,771, filed November 29, 2016, the entire contents of which are hereby incorporated by reference.

STATEMENT REGARDING FEDERALLY SPONSORED RESEARCH OR DEVELOPMENT

[0002] This invention was made with United States government support under NIH grant numbers R01HL118561, R01MH096463, R01GM065281 and R01HL122340. The United States government has certain rights to this invention.

BACKGROUND

[0003] Bronchoconstrictive diseases are major health concerns worldwide. These include asthma, chronic obstructive pulmonary disease (COPD), and bronchopulmonary dysplasia (BPD), and despite existing treatments such as β-adrenergic agonists, inhaled corticosteroids, and inhaled anti-cholinergics, bronchoconstrictive diseases remain highly prevalent. Asthma by itself affects 300 million people worldwide. Since asthma predisposes patients to severe acute airway constriction, novel therapeutic mechanisms capable of promoting airway smooth muscle relaxation would be clinically valuable.

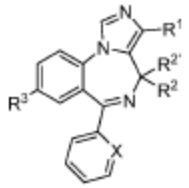
[0004] Thus, there continues to be demand for treatment and preventive agents effective against bronchoconstrictive diseases. New pharmacologic approaches to treat these diseases are limited. Therapeutic limitations are especially apparent in medications that promote acute airway smooth muscle relaxation, as β-adrenoceptor agonists and anti-cholinergics remain the only drug classes currently utilized to treat acute airway constriction.

[0005] The $GABA_A$ receptors ($GABA_AR$) are ligand-gated chloride ion channels well-known for their suppressive effects in the central nervous system (CNS). $GABA_ARs$ are heteropentamers assembled from 19 different subunits (α_{1-6}, β_{1-3}, γ_{1-3}, δ, ε, π, θ, ρ_{1-3}). Classical

$GABA_AR$s consist of two α, two β, and one γ, δ, ε, θ, or π subunit. Compounds that alter the efficacy of function of $GABA_AR$s have been used extensively as medicaments for disorders of the central nervous system. In addition to neurons, $GABA_AR$ subunits have been identified in airway smooth muscle, airway epithelium, and immune/inflammatory cells. Compounds that selectively react to discrete $GABA_AR$ subtypes on airway smooth muscle cells, epithelia cells and immune cells is important is a heretofore novel approach for treating bronchoconstrictive diseases. Compounds with a preference for the $\alpha_4\beta_3\gamma_2$ $GABA_AR$ or $\alpha_5\beta_3\gamma_2$ $GABA_AR$ have been identified as pharmacologically active in the described models of asthma.

SUMMARY

[0006] In one aspect, the invention provides compounds of formula (I), or a pharmaceutically acceptable salt thereof,



(I)

wherein:

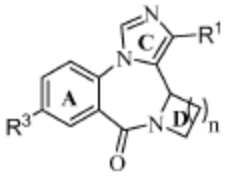
R^1 is COOH, a carboxylic ester, a carboxylic acid isostere, or a carboxylic ester isostere;

X is C–H, C–F, C–Cl, C–Br, C–I, C–CF_3, or N;

R^2 and $R^{2'}$ are each independently H, D, $C_{1\text{-}4}$ alkyl, CD_3, F, Cl, CF_3, CCl_3, or cyclopropyl; or R^2 and $R^{2'}$ together form an optionally substituted ring; and

R^3 is H, F, Cl, Br, CF_3, CHF_2, –OCF_3, –$OCHF_2$, CN, OH, –$OC_{1\text{-}4}$alkyl, –C≡CH, or cyclopropyl.

[0007] Another aspect of the invention provides compounds of formula (II), or a pharmaceutically acceptable salt thereof,



(II)

wherein:

R^1 is COOH, a carboxylic ester, a carboxylic acid isostere, or a carboxylic ester isostere;

n is 1 or 2; and

R^3 is H, F, Cl, Br, CF_3, CHF_2, $-OCF_3$, $-OCHF_2$, CN, OH, $-OC_{1-4}$alkyl, $-C{\equiv}CH$, or cyclopropyl.

[0008] In another aspect, the present invention provides a pharmaceutical composition including a compound of formula (I) or (II), or a pharmaceutically acceptable salt thereof, and a pharmaceutically acceptable carrier. In some embodiments, the composition may be an oral or an aerosol formulation.

[0009] In another aspect, the invention provides a method of reducing airway constriction comprising administering an effective amount of a compound or composition of formula (I) or (II), or a pharmaceutically acceptable salt thereof to a subject in need thereof. In some embodiments, compounds of formula (I) or (II) have reduced benzodiazepine-type CNS effects in a subject compared to diazepam at therapeutic doses.

[0010] In another aspect, the invention provides a method of reducing lung inflammation comprising administering an effective amount of a compound or composition of formula (I) or (II), or a pharmaceutically acceptable salt thereof to a subject in need thereof. In some embodiments, compounds of formula (I) or (II) have reduced benzodiazepine-type CNS effects in a subject compared to diazepam at therapeutic doses.

[0011] In another aspect, the invention provides a method of reducing development of disease in a subject having risk factors associated with lung inflammation comprising administering an effective amount of a compound or composition of formula (I) or (II), or a pharmaceutically acceptable salt thereof to a subject in need thereof. In some embodiments, compounds of formula (I) or (II) have reduced benzodiazepine-type CNS effects in a subject compared to diazepam at therapeutic doses.

[0012] In another aspect, the invention provides a method of treating lung disease comprising administering an effective amount of a compound or composition of formula (I) or (II), or a pharmaceutically acceptable salt thereof to a subject in need thereof. In some embodiments, compounds of formula (I) or (II) have reduced benzodiazepine-type CNS effects in a subject compared to diazepam at therapeutic doses.

[0013] In some aspects, the compounds of the present invention selectively target the α_4 and α_5 subunits of $GABA_ARs$. In some aspects, the compounds of the present invention are allosteric modulators of the $GABA_ARs$ that are selective for the α_4 and α_5 benzodiazepine allosteric modulatory sites on $GABA_ARs$. In some aspects, the compounds of the present invention may have limited inability to cross the blood-brain barrier.

BRIEF DESCRIPTION OF THE DRAWINGS

[0014] FIG. 1A shows dose dependent modulation of GABA elicited currents by SH-053-2'F-R-CH_3-Acid on Xenopus oocytes expressing $GABA_A$ receptor subtypes $\alpha1\beta3\gamma2$, $\alpha2\beta3\gamma2$, $\alpha3\beta3\gamma2$, $\alpha4\beta3\gamma2$ and $\alpha5\beta3\gamma2$.

[0015] FIG. 1B shows automated patch clamp with RJ-02-50 using $\alpha1\beta3\gamma2$ or $\alpha4\beta3\gamma2$ $GABA_A$ receptor expressing HEK293T cells.

[0016] FIG. 2 shows the effect of compounds on sensorimotor coordination in a rotarod test.

[0017] FIG. 3A shows effects on airway smooth muscle contractile force in guinea pig tracheal rings for RJ-02-50 and RJ-03-30.

[0018] FIG. 3B shows effects on airway smooth muscle contractile force in guinea pig tracheal rings for RJ-03-57.

[0019] FIG. 3C shows effects on airway smooth muscle contractile force in guinea pig tracheal rings for SH-053-2'F-R-CH3 Acid and GL-II-93.

[0020] FIG. 4 shows effects of SH-053-2'F-R-CH3 Acid on human airway smooth muscle contractile force.

[0021] FIGs. 5A-5F show compound effects on airway hyperresponsiveness.

[0022] FIGs 6A-6D show pharmacokinetic profiles of compounds in mice blood, lungs, and brain.

[0023] FIGs 7A-7C show effects of compounds on inflammatory cells.

[0024] FIG. 8 shows current recordings in the presence of 600 nM GABA and increasing concentrations of compounds applied together for 3 seconds using CD4+ T-cells isolated from ova s/c BALB/c mice spleen.

[0025] FIG. 9 shows anti-inflammatory properties of compounds in respect to cytokine production.

[0026] FIGs 10A-10B show compound effects on mucin production.

[0027] FIG. 11 shows proliferation of lung cells, either non-treated or treated with GL-II-93.

DETAILED DESCRIPTION

[0028] Recent studies have shown the presence of functional gamma-amino butyric acid type A receptors ($GABA_AR$) on the surface of cell types involved in asthmatic lung pathophysiology. Importantly, $GABA_AR$ signaling can influence the contractile state of airway smooth muscle (ASM), inflammatory processes, and proliferation of airway epithelial cells (AEC). Despite the growing appreciation of $GABA_AR$ signaling acting locally in the lung, a strategy that unifies and targets $GABA_AR$ responses has not been developed or exploited therapeutically for asthma treatment. Accordingly, the inventors contemplate the identification of a novel asthma therapy by systematically probing human lung cell types to identify ligands that are suppressive for ASM and immune/inflammatory cells without stimulating AEC hypertrophy.

[0029] Activation of endogenous airway smooth muscle $GABA_A$ receptors relaxes cholinergic contraction of airway smooth muscle, and molecular analysis of airway smooth muscle reveals that the α-subunit component of these $GABA_A$ receptors is limited to the α4 and α5.

[0030] The present invention provides novel compounds, which may bind to specific ionotropic (ligand-gated) ion channels expressed in immune/inflammatory cells and airway smooth muscle, and consequently relax contraction. This novel finding details a new signaling pathway and protein target for relaxing airway smooth muscle contraction and can potentially be developed into a novel therapeutic against airway constriction, lung inflammation, and inflammation associated with allergic and autoimmune diseases. Thus, among other things, the present invention provides novel compounds that provide a novel therapeutic option against airway constriction, lung inflammation, and inflammation associated with allergic and autoimmune diseases and methods of using these compounds to treat various diseases.

Definitions

[0031] Definitions of specific functional groups and chemical terms are described in more detail below. For purposes of this invention, the chemical elements are identified in accordance with the Periodic Table of the Elements, CAS version, Handbook of Chemistry and Physics, 75th Ed., inside cover, and specific functional groups are generally defined as described therein. Additionally, general principles of organic chemistry, as well as specific functional

moieties and reactivity, are described in Organic Chemistry, Thomas Sorrell, University Science Books, Sausalito, 1999; Smith and March March's Advanced Organic Chemistry, 5th Edition, John Wiley & Sons, Inc., New York, 2001; Larock, Comprehensive Organic Transformations, VCH Publishers, Inc., New York, 1989; Carruthers, Some Modern Methods of Organic Synthesis, 3rd Edition, Cambridge University Press, Cambridge, 1987; the entire contents of each of which are incorporated herein by reference.

[0032] The term "acyl" refers to an alkylcarbonyl, cycloalkylcarbonyl, heterocyclylcarbonyl, arylcarbonyl, or heteroarylcarbonyl substituent. In some embodiments, an acyl may be further substituted (e.g., with one or more substituents). Unless otherwise stated, an acyl is unsubstituted.

[0033] The term "alkyl" refers to a straight or branched hydrocarbon chain, containing the indicated number of carbon atoms. For example, C_1-C_{12} alkyl indicates that the alkyl group may have from 1 to 12 (inclusive) carbon atoms, and C_1-C_4 alkyl indicates that the alkyl group may have from 1 to 4 (inclusive) carbon atoms. In some embodiments, an alkyl group may be optionally substituted. Examples of C_{1-4}alkyl groups include methyl, ethyl, n-propyl, isopropyl, n-butyl, sec-butyl and tert-butyl. Unless otherwise stated, an alkyl is unsubstituted.

[0034] The term "alkenyl" refers to a straight or branched hydrocarbon chain having one or more double bonds. Examples of alkenyl groups include, but are not limited to, allyl, propenyl, 2-butenyl, 3-hexenyl and 3-octenyl groups. One of the double bond carbons may optionally be the point of attachment of the alkenyl substituent. In some embodiments, an alkenyl group may be optionally substituted. Unless otherwise stated, an alkenyl is unsubstituted.

[0035] The term "alkynyl" refers to a straight or branched hydrocarbon chain having one or more triple bonds. Examples of alkynyl groups include, but are not limited to, ethynyl, propargyl, and 3-hexynyl. One of the triple bond carbons may optionally be the point of attachment of the alkynyl substituent. In some embodiments, an alkynyl group may be optionally substituted. Unless otherwise stated, an alkynyl is unsubstituted.

[0036] The term "aryl" refers to an aromatic carbocyclic monocyclic, bicyclic, or tricyclic hydrocarbon ring system, wherein any ring atom capable of substitution can be substituted (e.g., with one or more substituents). Examples of aryl moieties include, but are not limited to, phenyl, naphthyl, and anthracenyl. Unless otherwise stated, an aryl is unsubstituted.

[0037] The term "arylalkyl" refers to an alkyl moiety in which an alkyl hydrogen atom is replaced with an aryl group. Arylalkyl includes groups in which more than one hydrogen atom has been replaced with an aryl group. Examples of arylalkyl groups include benzyl, 2-phenylethyl, 3-phenylpropyl, 9-fluorenyl, benzhydryl, and trityl groups.

[0038] The term "cycloalkyl" as used herein refers to a saturated cyclic, bicyclic, tricyclic or polycyclic hydrocarbon groups having 3 to 12 carbons (e.g., 3, 4, 5, 6 or 7 carbon atoms). Any ring atom can be substituted (e.g., with one or more substituents). Cycloalkyl groups can contain fused rings. Fused rings are rings that share one or more common carbon atoms. Examples of monocyclic cycloalkyl groups include, but are not limited to, cyclopropyl, cyclobutyl, cyclopentyl, and cyclohexyl. Examples of bridged cycloalkyl include adamantyl and norbornyl.

[0039] The term "halo" or "halogen" as used herein refers to any radical of fluorine, chlorine, bromine or iodine.

[0040] The term "haloalkyl" as used herein refers to an alkyl in which one or more hydrogen atoms are replaced with a halogen, and includes alkyl moieties in which all hydrogens have been replaced with halogens (e.g., perfluoroalkyl such as CF_3).

[0041] The term "heteroaryl" as used herein refers to an aromatic 5-8 membered monocyclic, 8-12 membered bicyclic, or 11-14 membered tricyclic ring system having 1-3 heteroatoms if monocyclic, 1-6 heteroatoms if bicyclic, or 1-9 heteroatoms if tricyclic, said heteroatoms independently selected from O, N, S, P and Si (e.g., carbon atoms and 1-3, 1-6, or 1-9 heteroatoms independently selected from O, N, S, P and Si if monocyclic, bicyclic, or tricyclic, respectively). Any ring atom can be substituted (e.g., with one or more substituents). Heteroaryl groups can contain fused rings, which are rings that share one or more common atoms. Examples of heteroaryl groups include, but are not limited to, radicals of pyridine, pyrimidine, pyrazine, pyridazine, pyrrole, imidazole, pyrazole, oxazole, isoxazole, furan, thiazole, isothiazole, thiophene, quinoline, isoquinoline, quinoxaline, quinazoline, cinnoline, indole, isoindole, indolizine, indazole, benzimidazole, phthalazine, pteridine, carbazole, carboline, phenanthridine, acridine, phenanthroline, phenazine, naphthyridines and purines.

[0042] The term "heterocycle" as used herein refers to a nonaromatic, saturated or partially unsaturated 3-10 membered monocyclic, 8-12 membered bicyclic, or 11-14 membered tricyclic ring system having 1-3 heteroatoms if monocyclic, 1-6 heteroatoms if bicyclic, or 1-9 heteroatoms if tricyclic, said heteroatoms selected from O, N, S, Si and P (e.g., carbon atoms and

1-3, 1-6, or 1-9 heteroatoms of O, N, S, Si and P if monocyclic, bicyclic, or tricyclic, respectively). Any ring atom can be substituted (e.g., with one or more substituents). Heterocyclyl groups can contain fused rings, which are rings that share one or more common atoms. Examples of heterocyclyl groups include, but are not limited to, radicals of tetrahydrofuran, tetrahydrothiophene, tetrahydropyran, piperidine, piperazine, morpholine, pyrroline, pyrimidine, pyrrolidine, indoline, tetrahydropyridine, dihydropyran, thianthrene, pyran, benzopyran, xanthene, phenoxathiin, phenothiazine, furazan, lactones, lactams such as azetidinones and pyrrolidinones, sultams, sultones, and the like.

[0043] The term "hydroxy" refers to an –OH radical. The term "alkoxy" refers to an –O-alkyl radical. The term "aryloxy" refers to an –O-aryl radical. The term "haloalkoxy" refers to an –O-haloalkyl radical.

[0044] The term "substituent" refers to a group "substituted" on an alkyl, alkenyl, alkynyl, cycloalkyl, heterocyclyl, aryl, arylalkyl or heteroaryl group at any atom of that group. Suitable substituents include, without limitation: acyl, acylamido, acyloxy, alkoxy, alkyl, alkenyl, alkynyl, amido, amino, carboxy, cyano, ester, halo, hydroxy, imino, nitro, oxo (e.g., C=O), phosphonate, sulfinyl, sulfonyl, sulfonate, sulfonamino, sulfonamido, thioamido, thiol, thioxo (e.g., C=S), and ureido. In embodiments, substituents on a group are independently any one single, or any combination of the aforementioned substituents. In embodiments, a substituent may itself be substituted with any one of the above substituents.

[0045] The above substituents may be abbreviated herein, for example, the abbreviations Me, Et and Ph represent methyl, ethyl and phenyl, respectively. A more comprehensive list of the abbreviations used by organic chemists appears in the first issue of each volume of the Journal of Organic Chemistry; this list is typically presented in a table entitled Standard List of Abbreviations. The abbreviations contained in said list, and all abbreviations used by organic chemists of ordinary skill in the art, are hereby incorporated by reference.

[0046] For compounds, groups and substituents thereof may be selected in accordance with permitted valence of the atoms and the substituents, such that the selections and substitutions result in a stable compound, e.g., which does not spontaneously undergo transformation such as by rearrangement, cyclization, elimination, etc.

[0047] Where substituent groups are specified by their conventional chemical formulae, written from left to right, they optionally encompass substituents resulting from writing the structure from right to left, e.g., $-CH_2O-$ optionally also recites $-OCH_2-$.

[0048] In accordance with a convention used in the art, the group:

is used in structural formulas herein to depict the bond that is the point of attachment of the moiety or substituent to the core or backbone structure.

[0049] In the context of treating a disorder, the term "effective amount" as used herein refers to an amount of the compound or a composition comprising the compound which is effective, upon single or multiple dose administrations to a subject, in treating a cell, or curing, alleviating, relieving or improving a symptom of the disorder in a subject. An effective amount of the compound or composition may vary according to the application. In the context of treating a disorder, an effective amount may depend on factors such as the disease state, age, sex, and weight of the individual, and the ability of the compound to elicit a desired response in the individual. In an example, an effective amount of a compound is an amount that produces a pharmacologically useful change in a given parameter as compared to a control, such as in cells (e.g., a culture of cells) or a subject not treated with the compound.

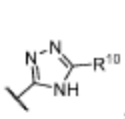
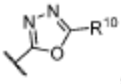
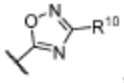
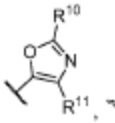
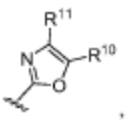
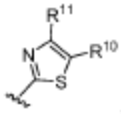
[0050] A therapeutic window over benzodiazepine-type CNS effects refers to having a desired therapeutic effect at a target organ (e.g., lung) at a dose or range of doses where benzodiazepine-type CNS effects (e.g., sedation) are at an acceptable level in the context of the particular therapeutic treatment. For example, in the context of asthma treatment acceptable levels of CNS effects include no CNS effects or mild CNS effects. For example, in some embodiments, the therapeutic index is 10 or more. In some embodiments, the therapeutic index is 20 or more. In some embodiments, the therapeutic index is 24 or more. Reduced benzodiazepine-type CNS effects includes reduced benzodiazepine-type CNS effects in a subject compared to diazepam at therapeutic doses. For example, in some embodiments, benzodiazepine-type CNS effects are reduced by 10-fold or more compared to diazepam at therapeutic doses. In some embodiments, benzodiazepine-type CNS effects are reduced by 20-fold or more compared to diazepam at therapeutic doses. In some embodiments,

benzodiazepine-type CNS effects are reduced by 24-fold or more compared to diazepam at therapeutic doses.

[0051] It is specifically understood that any numerical value recited herein (e.g., ranges) includes all values from the lower value to the upper value, i.e., all possible combinations of numerical values between the lowest value and the highest value enumerated are to be considered to be expressly stated in this application. For example, if a concentration range is stated as 1% to 50%, it is intended that values such as 2% to 40%, 10% to 30%, or 1% to 3%, etc., are expressly enumerated in this specification. These are only examples of what is specifically intended.

Compounds

[0052] In a first aspect are provided compounds of formula (I), or a pharmaceutically acceptable salt thereof. Embodiments of formula (I) include the following descriptions of X, R^1, R^2, $R^{2'}$, and R^3, and any combinations thereof.

[0053] In some embodiments of formula (I), R^3 is OH when R^1 is a carboxylic ester or a carboxylic ester isostere; and/or R^1 is not a carboxylic ester or a carboxylic ester isostere when R^3 is H, F, Cl, Br, $-OC_{1-4}$alkyl, –C≡CH, or cyclopropyl; and/or R^1 is not a carboxylic amide, a carboxylic thioester,  ,  ,  ,  ,  , or  , wherein R^{10} and R^{11} are independently H or C_{1-6}alkyl, when R^3 is –C≡CH; and/or R^1 is not COOH when R^3 is –C≡CH; and/or R^1 is not COOH, a carboxylic ester, a carboxylic amide, or a carboxylic thioester when R^2 and $R^{2'}$ are both H; X is C–H, C–F, C–Br, or C–I; and R^3 is H, F, Cl, or Br. In some embodiments, the compound of formula (I) is not (R)-8-ethynyl-6-(2-fluorophenyl)-4-methyl-4H-benzo[f]imidazo[1,5-a][1,4]diazepine-3-carboxylic acid. In some embodiments, R^1 is not COOH when R^3 is –C≡CH and R^2 or $R^{2'}$ are independently H or C_{1-4}alkyl.

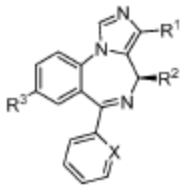
[0054] In embodiments of formula (I), as described herein, X is C–H, C–F, C–Cl, C–Br, C–I, C–CF_3, or N. In further embodiments, X is C–H, C–F, C–Cl, C–Br, C–I, or N. In further embodiments, X is C–H, C–F, C–Cl, C–Br, or N.

[0055] In embodiments of formula (I), as described herein, R^2 and $R^{2'}$ are each independently H, D, C_{1-4} alkyl, CD_3, F, Cl, CF_3, CCl_3, or cyclopropyl; or R^2 and $R^{2'}$ together form an optionally substituted ring. In further embodiments, R^2 and $R^{2'}$ are each independently H, C_{1-4} alkyl, F, Cl, CF_3, CCl_3, or cyclopropyl; or R^2 and $R^{2'}$ together form a ring. In further embodiments, R^2 and $R^{2'}$ are each independently H, C_{1-4} alkyl, F, Cl, CF_3, or CCl_3; or R^2 and $R^{2'}$ together form a ring. In still further embodiments, R^2 and $R^{2'}$ are each independently H, D, CH_3, CD_3, CF_3, or cyclopropyl; or R^2 and $R^{2'}$ together form a C_{3-6}cycloalkyl (e.g., cyclopropyl). In still further embodiments, R^2 and $R^{2'}$ together form a C_{3-6}cycloalkyl optionally substituted with 1-4 substituents independently selected from the group consisting of CH_3, F, OH, OCH_3, oxo, and CF_3.

[0056] In embodiments of formula (I), as described herein, R^3 is H, F, Cl, Br, CF_3, CHF_2, –OCF_3, –$OCHF_2$, CN, OH, –OC_{1-4}alkyl, –C≡CH, or cyclopropyl. In further embodiments, R^3 is H, F, Cl, Br, OH, OCH_3, –C≡CH, or cyclopropyl. In further embodiments, R^3 is H, F, Cl, OCH_3, or –C≡CH. In still further embodiments, R^3 is OH, wherein X, R^1, R^2, and $R^{2'}$, and combinations thereof, are as described herein. In some embodiments, R^3 is OH.

[0057] In further embodiments, R^3 is OH; X is C–H, C–F, C–Cl, C–Br, C–I, or N; and R^2 and $R^{2'}$ are each independently selected from C_{1-4}alkyl, F, Cl, CF_3, CCl_3, or cyclopropyl, or together form a ring; and R^1 is defined herein. In still further embodiments, R^2 and $R^{2'}$ together form a C_{3-6}cycloalkyl optionally substituted with 1-4 substituents independently selected from the group consisting of CH_3, F, OH, OCH_3, oxo, and CF_3. In some embodiments, one or more hydrogens may be replaced with a deuterium. Suitably, the compound may be the S-isomer. Alternatively, the compound may be the R-isomer.

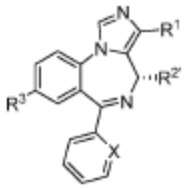
[0058] Embodiments of formula (I) include compounds of formula (I-A)



(I-A);

wherein R^2 is D, C_{1-4} alkyl, CD_3, F, Cl, CF_3, CCl_3, or cyclopropyl, and combinations with X, R^1, and R^3 are as described herein. In some of the embodiments of formula (I-A), R^2 is D, CH_3, CD_3, CF_3, or cyclopropyl. In some embodiments of formula (I-A) according to the foregoing, R^3 is OH.

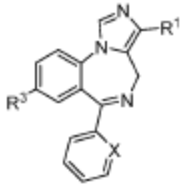
[0059] Embodiments of formula (I) include compounds of formula (I-B)



(I-B);

wherein $R^{2'}$ is D, C_{1-4} alkyl, CD_3, F, Cl, CF_3, CCl_3, or cyclopropyl, and combinations with X, R^1, and R^3 are as described herein. In some of the embodiments of formula (I-B), $R^{2'}$ is D, CH_3, CD_3, CF_3, or cyclopropyl. In some embodiments of formula (I-B) according to the foregoing, R^3 is OH.

[0060] Embodiments of formula (I) include compounds of formula (I-C)



(I-C)

wherein X, R^1, and R^3 and combinations thereof, are as described herein. In some embodiments of formula (I-C) according to the foregoing, R^3 is OH.

[0061] In some combinations of X, R^2, $R^{2'}$, and R^3, X is C–H, C–F, C–Cl, C–Br, C–I, or N; R^2 is C_{1-4} alkyl, CD_3, F, Cl, CF_3, CCl_3, or cyclopropyl; $R^{2'}$ is H or D; and R^3 is H, F, Cl, Br, OH, OCH_3, –C≡CH, or cyclopropyl. In some of the embodiments, R^2 is C_{1-4} alkyl (e.g., CH_3). In further embodiments, R^3 is H, F, Cl, Br, OH, OCH_3, or cyclopropyl, and R^2 is C_{1-4} alkyl. In further combinations with the foregoing, R^1 is COOH.

[0062] In some embodiments, the invention provides a compound according to formula (I) wherein R^1 is a carboxylic acid isostere; X is C–H, C–F, C–Cl, C–Br, C–I, or N; R^2 and $R^{2'}$ are independently selected from H, C_{1-4} alkyl, F, Cl, CF_3, CCl_3, or cyclopropyl, or together form a ring; and R^3 is selected from H, F, Cl, Br, OMe, –C≡CH, or cyclopropyl. In still further embodiments, R^2 and $R^{2'}$ together form a C_{3-6}cycloalkyl optionally substituted with 1-4 substituents independently selected from the group consisting of CH_3, F, OH, OCH_3, oxo, and CF_3. In embodiments, R^2 and $R^{2'}$ are H and (R)-Me, or H and (S)-Me, or R^2 and $R^{2'}$ are both H. In some embodiments, one or more hydrogens may be replaced with a deuterium. Suitably, the compound may be the S-isomer. Alternatively, the compound may be the R-isomer.

[0063] In another embodiment of formula (I), R^1 is COOH; X is C–H, C–F, C–Cl, C–Br, C–I, or N; R^2 and $R^{2'}$ are independently selected from C_{1-4} alkyl, F, Cl, CF_3, CCl_3, or cyclopropyl, or together form a ring; and R^3 is selected from H, F, Cl, Br, OMe, –C≡CH, Br, or cyclopropyl. In still further embodiments, R^2 and $R^{2'}$ together form a C_{3-6}cycloalkyl optionally substituted with 1-4 substituents independently selected from the group consisting of CH_3, F, OH, OCH_3, oxo, and CF_3. In some embodiments, one or more hydrogens may be replaced with a deuterium. Suitably, the compound may be the S-isomer. Alternatively, the compound may be the R-isomer.

[0064] In another aspect are provided compounds of formula (II), or a pharmaceutically acceptable salt thereof. Embodiments of formula (II) include the following descriptions of X, R^1, and R^3, and combinations thereof.

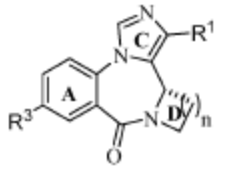
[0065] In some embodiments of formula (II), R^3 is OH when R^1 is COOH, a carboxylic ester, a carboxylic amide, or a carboxylic thioester. In other embodiments, R^3 is OH when R^1 is COOH. In other embodiments, R^1 is not a carboxylic ester, a carboxylic amide, or a carboxylic thioester. In other embodiments, R^1 is not a carboxylic ester, a carboxylic amide, or a carboxylic thioester when R^3 is $–OC_{1-4}$alkyl or OH. In some embodiments, the compound of formula (II) is

not ethyl (S)-7-hydroxy-9-oxo-11,12,13,13a-tetrahydro-9H-benzo[e]imidazo[5,1-c]pyrrolo[1,2-a][1,4]diazepine-1-carboxylate.

[0066] In embodiments of formula (II), as described herein, R^3 is H, F, Cl, Br, CF_3, CHF_2, $-OCF_3$, $-OCHF_2$, CN, OH, $-OC_{1-4}$alkyl, $-C\equiv CH$, or cyclopropyl. In further embodiments, R^3 is H, F, Cl, Br, OH, $-OCH_3$, $-C\equiv CH$, or cyclopropyl. In further embodiments, R^3 is H, F, Cl, Br, $-OCH_3$, or $-C\equiv CH$. In further embodiments, R^3 is H, F, Cl, $-OCH_3$, or $-C\equiv CH$. In still further embodiments, R^3 is OH. In further embodiments, R^3 is OH, wherein X and R^1, and combinations thereof, are as described herein.

[0067] In certain combinations, R^1 is a carboxylic acid isostere and R^3 is H, F, Cl, Br, CF_3, CHF_2, $-OCF_3$, $-OCHF_2$, CN, $-OC_{1-4}$alkyl, $-C\equiv CH$, or cyclopropyl. In other combinations, R^1 is COOH, a carboxylic ester, a carboxylic acid isostere, or a carboxylic ester isostere; and R^3 is OH.

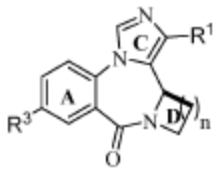
[0068] Embodiments of formula (II) include compounds of formula (II-A)



(II-A);

wherein X, R^1, and R^3 are as described herein. In some of the embodiments of formula (II-A) according to the foregoing, R^3 is OH. In certain combinations, R^1 is a carboxylic acid isostere and R^3 is H, F, Cl, Br, CF_3, CHF_2, $-OCF_3$, $-OCHF_2$, CN, $-OC_{1-4}$alkyl, $-C\equiv CH$, or cyclopropyl. In certain combinations, R^1 is a carboxylic acid isostere and R^3 is H, F, Cl, Br, OH, $-OCH_3$, $-C\equiv CH$, or cyclopropyl. In other combinations, R^1 is COOH, a carboxylic ester, a carboxylic acid isostere, or a carboxylic ester isostere; and R^3 is OH.

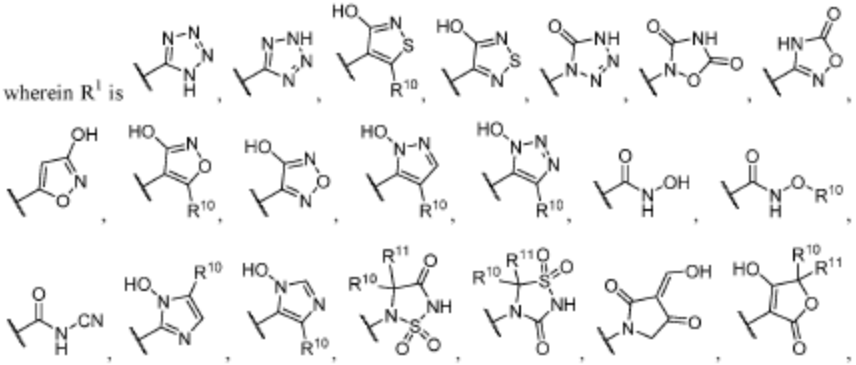
[0069] Embodiments of formula (II) include compounds of formula (II-B)

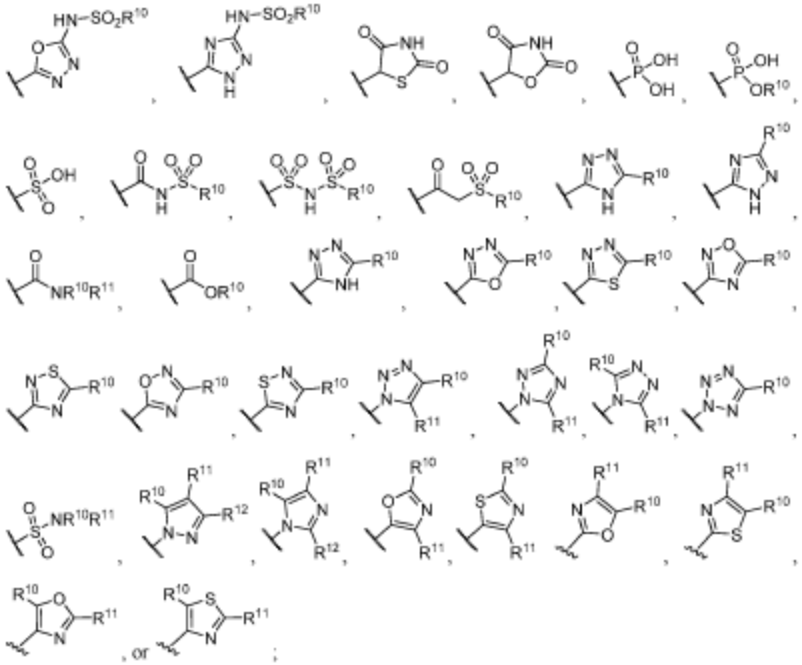


(II-B);

wherein X, R^1, and R^3 are as described herein. In some of the embodiments of formula (II-B) according to the foregoing, R^3 is OH. In certain combinations, R^1 is a carboxylic acid isostere and R^3 is H, F, Cl, Br, CF_3, CHF_2, $-OCF_3$, $-OCHF_2$, CN, $-OC_{1-4}$alkyl, $-C\equiv CH$, or cyclopropyl. In certain combinations, R^1 is a carboxylic acid isostere and R^3 is H, F, Cl, Br, OH, $-OCH_3$, $-C\equiv CH$, or cyclopropyl. In other combinations, R^1 is COOH, a carboxylic ester, a carboxylic acid isostere, or a carboxylic ester isostere; and R^3 is OH.

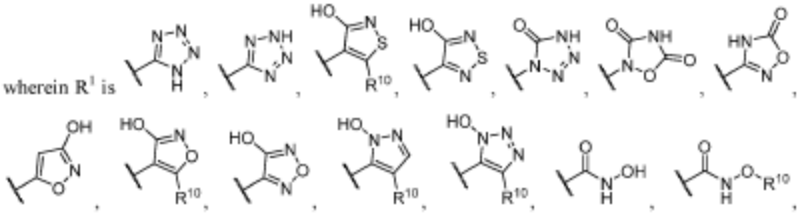
[0070] Unless otherwise stated, the embodiments described herein include further embodiments wherein R^1 is COOH. Unless otherwise stated, the embodiments described herein include further embodiments wherein R^1 is a carboxylic ester. In some embodiments, the carboxylic ester is $-C(O)OC_{1-6}$alkyl or $-C(O)OC_{3-6}$cycloalkyl. Unless otherwise stated, the embodiments described herein include further embodiments wherein R^1 is carboxylic acid isostere. Unless otherwise stated, the embodiments described herein include further embodiments wherein R^1 is a carboxylic ester isostere.

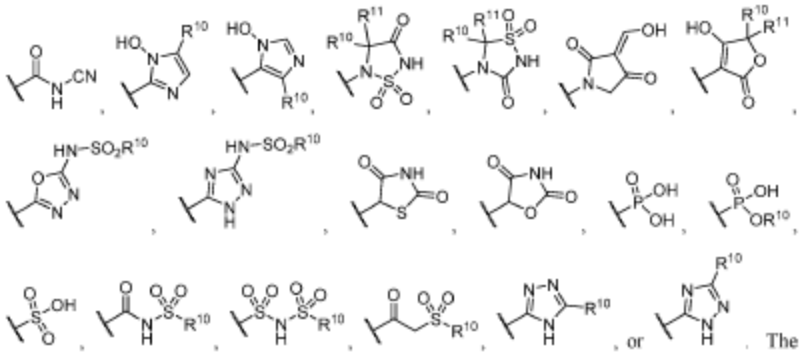
[0071] Included in the embodiments described herein, are still further embodiments wherein R^1 is 



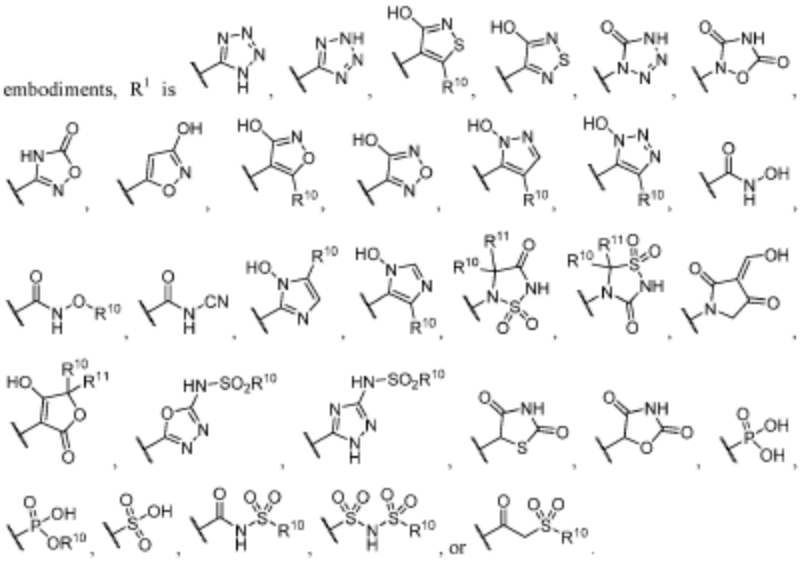
wherein R^{10}, R^{11}, and R^{12} are independently selected from H, D, or C_{1-6}straight or cyclic saturated or substituted alkyl group.

[0072] Included in the embodiments described herein, are still further embodiments wherein R^1 is



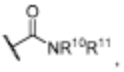
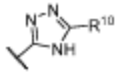
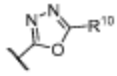
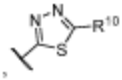
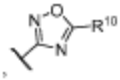
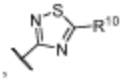
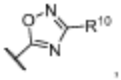
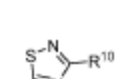
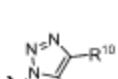
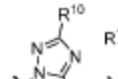
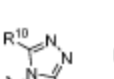
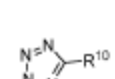
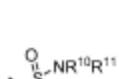
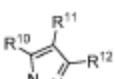
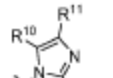
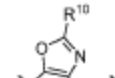
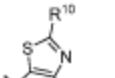
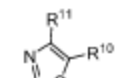
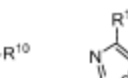
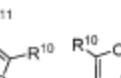
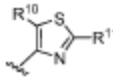
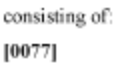


foregoing R^1 group members are included in the term "carboxylic acid isostere." In further embodiments, R^1 is



[0073] In still further embodiments, and combinations, R^{10}, R^{11}, and R^{12} are independently H, D, C_{1-6}alkyl, or C_{3-6}cycloalkyl.

[0074] In still further embodiments, R^1 is a tetrazole (e.g., ).

[0075] According to the foregoing, a carboxylic ester isostere includes  ,  ,  ,  ,  ,  ,  ,  ,  ,  ,  ,  ,  ,  ,  ,  ,  ,  ,  ,  ,  ,  , , , , , , , and  .

[0076] In another aspect, the invention provides a compound selected from the group consisting of:

[0077] (R)-8-ethynyl-6-(2-fluorophenyl)-4-methyl-4H-benzo[f]imidazo[1,5-a][1,4]diazepine-3-carboxylic acid (SH-053-2'F-R-CH_3 Acid);

[0078] (R)-8-bromo-6-(2-fluorophenyl)-4-methyl-4H-benzo[f]imidazo[1,5-a][1,4]diazepine-3-carboxylic acid (GL-II-93);

[0079] (R)-8-cyclopropyl-6-(2-fluorophenyl)-4-methyl-4H-benzo[f]imidazo[1,5-a][1,4]diazepine-3-carboxylic acid (GL-III-43);

[0080] (R)-8-chloro-6-(2-fluorophenyl)-4-methyl-4H-benzo[f]imidazo[1,5-a][1,4]diazepine-3-carboxylic acid (GL-III-54);

[0081] (R)-8-bromo-4-methyl-6-(pyridin-2-yl)-4H-benzo[f]imidazo[1,5-a][1,4]diazepine-3-carboxylic acid (GL-II-51);

[0082] (R)-8-ethynyl-4-methyl-6-(pyridin-2-yl)-4H-benzo[f]imidazo[1,5-a][1,4]diazepine-3-carboxylic acid (GL-II-30);

[0083] (S)-7-methoxy-1-(1H-tetrazol-5-yl)-11,12,13,13a-tetrahydro-9H-benzo[e]imidazo[5,1-c]pyrrolo[1,2-a][1,4]diazepin-9-one (RJ-03-57);

[0084] (S)-N,7-dimethoxy-9-oxo-11,12,13,13a-tetrahydro-9H-benzo[e]imidazo[5,1-c]pyrrolo[1,2-a][1,4]diazepine-1-carboxamide (MRS-III-87);

[0085] (S)-N-cyano-7-methoxy-9-oxo-11,12,13,13a-tetrahydro-9H-benzo[e]imidazo[5,1-c]pyrrolo[1,2-a][1,4]diazepine-1-carboxamide (MRS-III-90);

[0086] ethyl (S)-7-hydroxy-9-oxo-11,12,13,13a-tetrahydro-9H-benzo[e]imidazo[5,1-c]pyrrolo[1,2-a][1,4]diazepine-1-carboxylate (RJ-02-50);

[0087] (S)-7-hydroxy-9-oxo-11,12,13,13a-tetrahydro-9H-benzo[e]imidazo[5,1-c]pyrrolo[1,2-a][1,4]diazepine-1-carboxylic acid (RJ-03-90);

[0088] (S)-7-hydroxy-1-(oxazol-5-yl)-11,12,13,13a-tetrahydro-9H-benzo[e]imidazo[5,1-c]pyrrolo[1,2-a][1,4]diazepin-9-one (RJ-03-30); and

[0089] tert-butyl (S)-7-hydroxy-9-oxo-11,12,13,13a-tetrahydro-9H-benzo[e]imidazo[5,1-c]pyrrolo[1,2-a][1,4]diazepine-1-carboxylate (RJ-02-67);

[0090] or a pharmaceutically acceptable salt thereof.

[0091] In another aspect, the invention provides a compound selected from the group consisting of:

[0092] 5-(8-ethynyl-6-(pyridin-2-yl)-4H-benzo[f]imidazo[1,5-a][1,4]diazepin-3-yl)oxazole (KRM-II-81);

[0093] 5-(8-ethynyl-6-phenyl-4H-benzo[f]imidazo[1,5-a][1,4]diazepin-3-yl)oxazole (KRM-II-82);

[0094] 5-(8-ethynyl-6-(2-fluorophenyl)-4H-benzo[f]imidazo[1,5-a][1,4]diazepin-3-yl)oxazole (KRM-II-18B);

[0095] methyl (R)-8-ethynyl-6-(2-fluorophenyl)-4-methyl-4H-benzo[f]imidazo[1,5-a][1,4]diazepine-3-carboxylate (MP-III-004);

[0096] (R)-8-ethynyl-6-(2-fluorophenyl)-N,4-dimethyl-4H-benzo[f]imidazo[1,5-a][1,4]diazepine-3-carboxamide (MP-III-022);

[0097] ethyl-1,1-d_2 8-ethynyl-6-(pyridin-2-yl)-4H-benzo[f]imidazo[1,5-a][1,4]diazepine-3-carboxylate (MP-III-068);

[0098] 5-(8-ethynyl-6-(pyridin-2-yl)-4H-benzo[f]imidazo[1,5-a][1,4]diazepin-3-yl)-3-methyl-1,2,4-oxadiazole (MP-III-085);

[0099] 3-ethyl-5-(8-ethynyl-6-(pyridin-2-yl)-4H-benzo[f]imidazo[1,5-a][1,4]diazepin-3-yl)-1,2,4-oxadiazole (MP-III-080);

[00100] ethyl 8-ethynyl-6-phenyl-4H-benzo[f]imidazo[1,5-a][1,4]diazepine-3-carboxylate (XHe-II-053);

[00101] ethyl 8-ethynyl-6-(pyridin-2-yl)-4H-benzo[f]imidazo[1,5-a][1,4]diazepine-3-carboxylate (HZ-166); and

[00102] ethyl 8-ethynyl-6-(2-fluorophenyl)-4H-benzo[f]imidazo[1,5-a][1,4]diazepine-3-carboxylate (JY-XHe-053);

[00103] or a pharmaceutically acceptable salt thereof.

[00104] For compounds according to the present invention, groups and substituents thereof may be selected in accordance with permitted valence of the atoms and the substituents, such that the selections and substitutions result in a stable compound, e.g., which does not spontaneously undergo transformation such as by rearrangement, cyclization, elimination, etc.

[00105] Where substituent groups are specified by their conventional chemical formulae, written from left to right, they optionally encompass substituents resulting from writing the structure from right to left, e.g., $-CH_2O-$ optionally also recites $-OCH_2-$.

[00106] Compounds according to the present invention include compounds that differ only in the presence of one or more isotopically enriched atoms. For example, compounds may have the present structures except for the replacement of hydrogen by deuterium or tritium, or the replacement of a carbon by a $^{13}C-$ or ^{14}C-enriched carbon.

[00107] A compound according to the present invention can be in the form of a salt, e.g., a pharmaceutically acceptable salt. The term "pharmaceutically acceptable salt" includes salts of the active compounds that are prepared with relatively nontoxic acids or bases, depending on the particular substituents found on the compounds. Suitable pharmaceutically acceptable salts of the compounds of this invention include acid addition salts which may, for example, be formed by mixing a solution of the compound according to the invention with a solution of a pharmaceutically acceptable acid such as hydrochloric acid, sulfuric acid, methanesulfonic acid, fumaric acid, maleic acid, succinic acid, acetic acid, benzoic acid, oxalic acid, citric acid, tartaric acid, carbonic acid or phosphoric acid. Furthermore, where the compounds of the invention

carry an acidic moiety, suitable pharmaceutically acceptable salts thereof may include alkali metal salts, e.g. sodium or potassium salts, alkaline earth metal salts, e.g. calcium or magnesium salts; and salts formed with suitable organic ligands, e.g. quaternary ammonium salts.

[00108] Neutral forms of the compounds may be regenerated by contacting the salt with a base or acid and isolating the parent compound in a conventional manner. The parent form of the compound differs from the various salt forms in certain physical properties, such as solubility in polar solvents, but otherwise the salts are equivalent to the parent form of the compound for the purposes of this disclosure.

[00109] In addition to salt forms, the present invention may also provide compounds according to the present invention in a prodrug form. Prodrugs of the compounds are those compounds that readily undergo chemical changes under physiological conditions to provide the active compounds. Prodrugs can be converted to the compounds of the present invention by chemical or biochemical methods in an ex vivo environment. For example, prodrugs can be slowly converted to the compounds of the present invention when placed in a transdermal patch reservoir with a suitable enzyme or chemical reagent.

[00110] Compounds described herein may exist as stereoisomers wherein asymmetric (or chiral) centers are present. These stereoisomers are "R" or "S" depending on the configuration of substituents around the chiral carbon atom. The terms "R" and "S" used herein are configurations as defined in IUPAC 1974 Recommendations for Section E, Fundamental Stereochemistry, Pure Appl. Chem., 1976, 45: 13-30.

[00111] Compounds according to the present invention can be, for example, an enantiomerically enriched isomer of a stereoisomer described herein. Enantiomer, as used herein, refers to either of a pair of chemical compounds whose molecular structures have a mirror-image relationship to each other. For example, a compound may have an enantiomeric excess of at least about 10%, 15%, 20%, 25%, 30%, 35%, 40%, 45%, 50%, 55%, 60%, 65%, 70%, 75%, 80%, 85%, 90%, 95%, 96%, 97%, 98%, or 99%.

[00112] A preparation of a compound according to the present invention may be enriched for an isomer of the compound having a selected stereochemistry, e.g., R or S, corresponding to a selected stereocenter. For example, the compound may have a purity corresponding to a compound having a selected stereochemistry of a selected stereocenter of at least about 60%, 65%, 70%, 75%, 80%, 85%, 90%, 95%, 96%, 97%, 98%, or 99%. A compound can, for

example, include a preparation of a compound disclosed herein that is enriched for a structure or structures having a selected stereochemistry, e.g., R or S, at a selected stereocenter.

[00113] In some embodiments, a preparation of a compound according to the present invention may be enriched for isomers (subject isomers) which are diastereomers of the compound. Diastereomer, as used herein, refers to a stereoisomer of a compound having two or more chiral centers that is not a mirror image of another stereoisomer of the same compound. For example, the compound may have a purity corresponding to a compound having a selected diastereomer of at least about 60%, 65%, 70%, 75%, 80%, 85%, 90%, 95%, 96%, 97%, 98%, or 99%.

[00114] When no specific indication is made of the configuration at a given stereocenter in a compound, any one of the configurations or a mixture of configurations is intended. The formulae within this specification can represent only one of the possible tautomeric forms. It is to be understood that encompassed herein are any tautomeric form, and mixtures thereof, and is not to be limited merely to any one tautomeric form utilized within the naming of the compounds or formulae

[00115] Compounds may be prepared in racemic form or as individual enantiomers or diastereomers by either stereospecific synthesis or by resolution. The compounds may, for example, be resolved into their component enantiomers or diastereomers by standard techniques, such as the formation of stereoisomeric pairs by salt formation with an optically active base, followed by fractional crystallization and regeneration of the free acid. The compounds may also be resolved by formation of stereoisomeric esters or amides, followed by chromatographic separation and removal of the chiral auxiliary. Alternatively, the compounds may be resolved using a chiral HPLC column. The enantiomers also may be obtained from kinetic resolution of the racemate of corresponding esters using lipase enzymes.

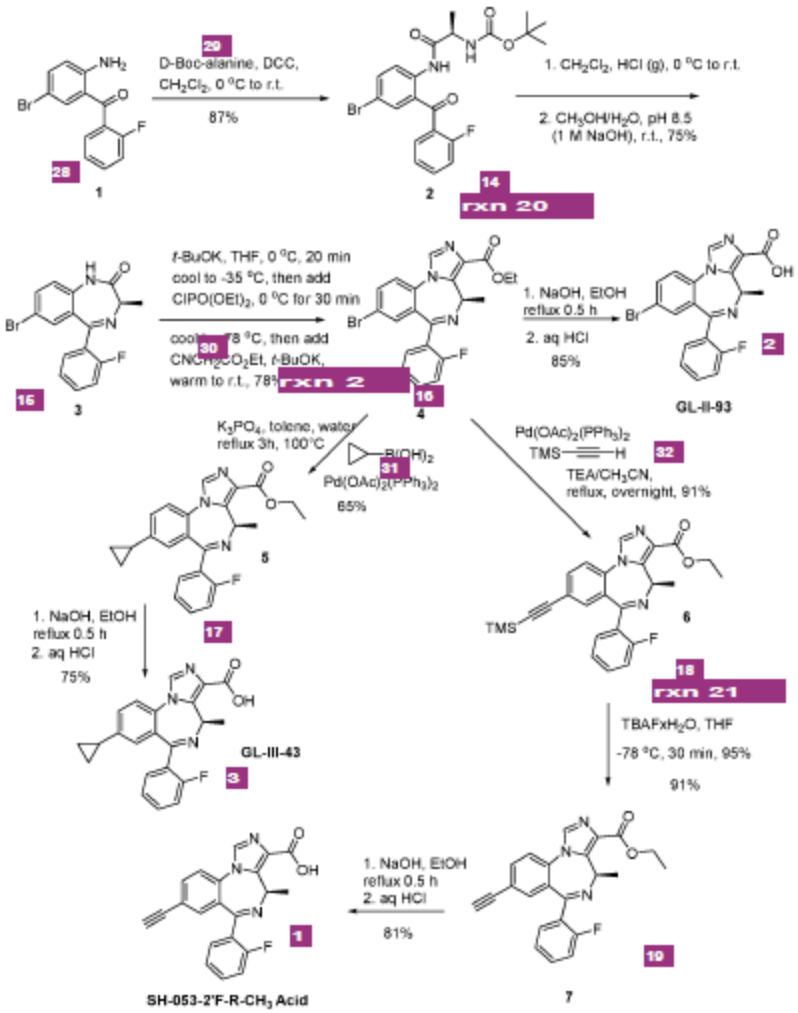
[00116] A compound according to the present invention can also be modified by appending appropriate functionalities to enhance selective biological properties. Such modifications are known in the art and include those that increase biological penetration into a given biological system (e.g., blood, lymphatic system, central nervous system), increase oral availability, increase solubility to allow administration by injection, alter metabolism, and/or alter rate of excretion. Examples of these modifications include, but are not limited to, esterification with polyethylene glycols, derivatization with pivolates or fatty acid substituents,

conversion to carbamates, hydroxylation of aromatic rings, and heteroatom substitution in aromatic rings.

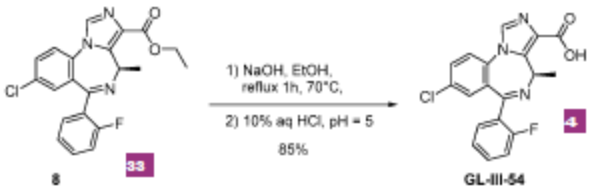
[00117] The compounds of the present invention may also be adapted as "soft drugs". A soft drug may be defined as a biologically active compound having predictable and controllable in vivo metabolism to inert species after it achieves its desired therapeutic effect. That is, the compounds of the present invention may contain a moiety which allows for rapid metabolism of the compounds in the lung or other target tissue. In lungs, several cytochrome isoforms are found, as well as other biotransformation enzymes such as sulfotransferases, UDP glucuronosyl transferases, glutathione S-transferases, esterases, peptidases, cyclo-oxygenases, and flavine mono-oxygenases . The wide range of biotransformation enzymes enables metabolism of a broad spectrum of chemically different substrates, for example compounds with a labile ester function. Soft drugs would have shorter systemic half-life than compounds without the moiety and may limit undesirable systemic effects (such a distribution to CNS tissues).

Synthesis of compounds

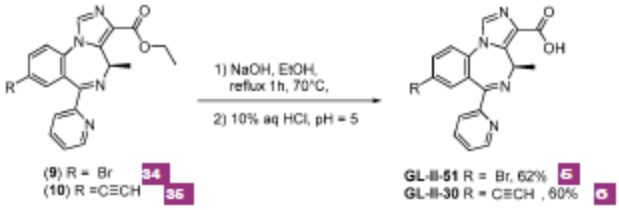
[00118] Compounds of formulae (I) and (II) may be synthesized using commercially available starting materials. Exemplary syntheses are summarized in Schemes 1-5 and in (*Cook, J.M., Zhou, H., Huang S., Sarma, P.V.V.S., Zhang, C., 2009. Stereospecific anxiolytic and anticonvulsant agents with reduced muscle-relaxant, sedative hypnotic and ataxic effects, PCTWO2006/004945A1, US Patent7,618,958*).



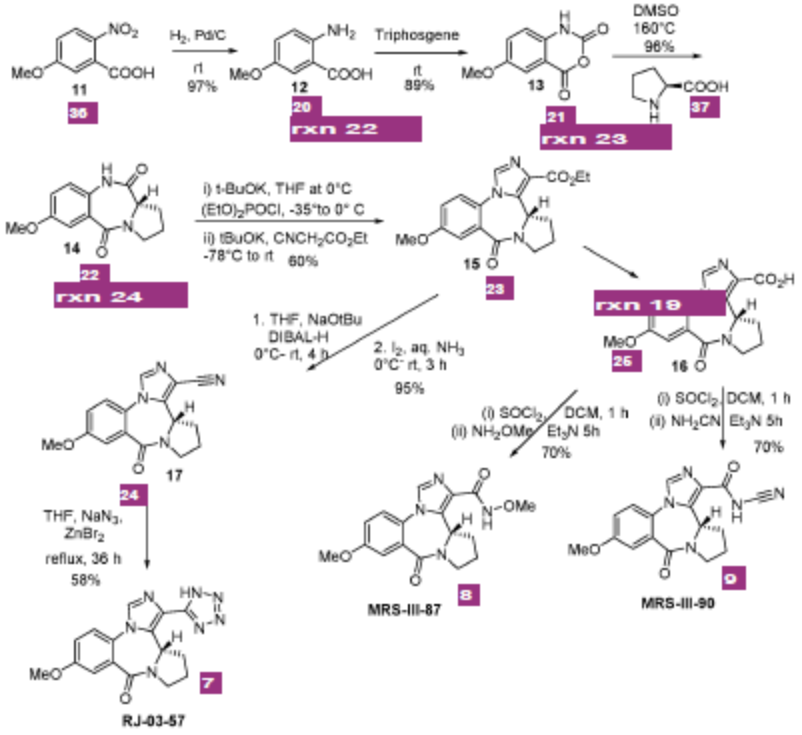
Scheme 1. Synthesis of compounds with formulae (I) part I.



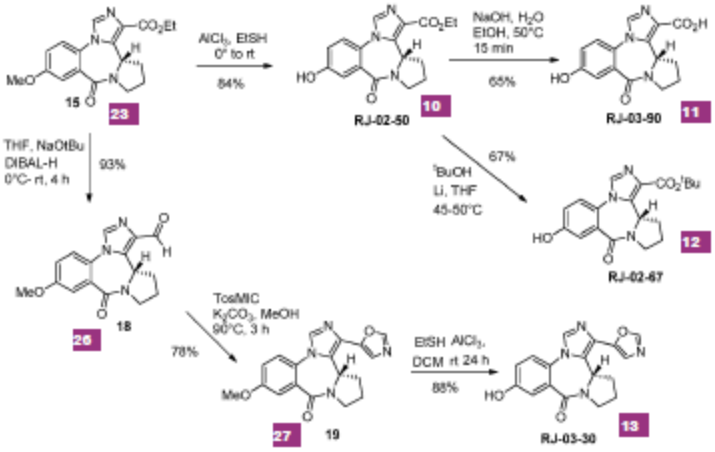
Scheme 2. Synthesis of compounds with formulae (I) part II.



Scheme 3. Synthesis of compounds with formulae (I) part III.



Scheme 4. Synthesis of compounds with formulae (II).



Scheme 5. Synthesis of compounds with formulae (II).

[00119] Compounds of formulae (II) may be synthesized using commercially available starting materials. Exemplary syntheses are illustrated in the Exhibits hereto and in (*Jahan et al. European J. Med Chem. 2017, 126, 550-560*).

[00120] Other methods of synthesizing the compounds of the formulae herein will be evident to those of ordinary skill in the art. Synthetic chemistry transformations and protecting group methodologies (protection and deprotection) useful in synthesizing the compounds are known in the art and include, for example, those such as described in R. Larock, *Comprehensive Organic Transformations*, VCH Publishers (1989); T.W. Greene and P.G.M. Wuts, *Protective Groups in Organic Synthesis*, 2d. Ed., John Wiley and Sons (1991); L. Fieser and M. Fieser, *Fieser and Fieser's Reagents for Organic Synthesis*, John Wiley and Sons (1994); and L. Paquette, ed., *Encyclopedia of Reagents for Organic Synthesis*, John Wiley and Sons (1995), and subsequent editions thereof.

Evaluation of compounds

[00121] Compounds may be analyzed using a number of methods, including receptor binding studies and in vivo methods.

[00122] For example, the $GABA_A$ subunit selectivity of compounds can be evaluated, for example, using competitive binding assays. Such assays have been described (Choudhary et al. *Mol Pharmacol.* 1992, *42*, 627-33; Savić et al. *Progress in Neuro-Psychopharmacology & Biological Psychiatry*, 2010, 34, 376–386). The assays involve the use of a radiolabeled compound known to bind to $GABA_A$ receptors, such as [^{3}H]flunitrazepam. Membrane proteins can be harvested and incubated with the radiolabeled compound, and non-specific binding can be evaluated by comparing binding of the radiolabeled compound to another, non-labeled compound (e.g., diazepam). Bound radioactivity can be quantified by liquid scintillation counting. Membrane protein concentrations can be determined using commercially available assay kits (e.g., from Bio-Rad, Hercules, CA).

[00123] Compounds can also be evaluated in electrophysiological assays in *Xenopus* oocytes or HEK293T cells that overexpress a particular $GABA_AR$ subtype. Compounds can be pre-applied to cells before the addition of GABA, which can then be co-applied with the compounds until a peak response is observed. Between applications, cells can be washed to ensure full recovery from desensitization. For current measurements, cells can be impaled with microelectrodes, and recordings performed using voltage clamps.

[00124] Compounds described herein may be $GABA_A$ receptor ligands which bind to endogenous airway smooth muscle $GABA_A$ receptors and potentiate relaxation of cholinergic airway smooth muscle contraction. This is due to increased targeting for the benzodiazepine allosteric modulatory sites at the α4 and α5 subunits. The compounds may possess at least 2-fold, suitably at least 5-fold, and advantageously at least a 10-fold, selective efficacy for the $GABA_A$/α4 and/or $GABA_A$/α5 allosteric modulatory sites relative to those $GABA_A$/α1, $GABA_A$/α2, and $GABA_A$/α3. However, compounds which are not selective for the benzodiazepine allosteric modulatory binding sites on $GABA_A$/α4 and/or $GABA_A$/α5 receptors are also encompassed within the scope of the present invention. Such compounds will desirably exhibit functional selectivity by demonstrating decreased efficacy at the benzodiazepine allosteric modulatory sites of other $GABA_A$ receptors.

[00125] A selective or preferential therapeutic agent has less binding affinity or efficacy to the other benzodiazepine allosteric modulatory sites on $GABA_A$ receptors as compared to the benzodiazepine allosteric modulatory sites on the $GABA_A$/α4 or $GABA_A$/α5 subunits. Alternatively, the agent targets benzodiazepine allosteric modulatory sites on all $GABA_A$

receptors with a comparable affinity but exerts preferential efficacy for the benzodiazepine allosteric modulatory sites on $GABA_A/\alpha_4$ and $GABA_A/\alpha_5$ receptors compared to those on other $GABA_A$ receptors. A selective agent of the present invention can also have a greater or lesser ability to bind benzodiazepine allosteric modulatory sites on other $GABA_A$ receptors relative to $GABA_A/\alpha_2$ and $GABA_A/\alpha_3$ receptors.

[00126] Other methods for evaluating compounds are known to those skilled in the art. To assess a compound's undesirable side effects (toxicity), animals may monitored for overt signs of impaired neurological or muscular function. In mice, the rotarod procedure (Dunham, M. S. et al. *J. Amer. Pharm. Ass. Sci. Ed.* 1957, 46, 208-209) is used to disclose minimal muscular or neurological impairment. When a mouse is placed on a rod that rotates at a speed of 6 revolutions-per-minute (rpm), the animal can maintain its equilibrium for long periods of time. The compound is considered toxic if it falls off this rotating rod three times during a 1-minute period. In rats, minimal motor deficit is indicated by ataxia, which is manifested by an abnormal, uncoordinated gait. Rats used for evaluating toxicity are examined before the test drug is administered, since individual animals may have peculiarities in gait, equilibrium, placing response, etc., which might be attributed erroneously to the test substance. Animals may exhibit a circular or zigzag gait, abnormal body posture and spread of the legs, tremors, hyperactivity, lack of exploratory behavior, somnolence, stupor, catalepsy, loss of placing response and changes in muscle tone.

[00127] Compounds described herein may reduce airway hyperresponsiveness in animal models of asthma. Therefore, mice may be sensitized three times with intra-peritoneal (i.p.) injections of 2 mg/ kg/ d of ovalbumin (Ova) emulsified in 2 mg on days 0, 7 and 14 in a total volume of 100 µL. In addition, mice may be challenged intra-nasally (i.n.) with 1 mg/ kg/ d Ova for 5 days from days 23–27. Control mice may be sensitized with Ova and challenged with saline. The airway hyperresponsiveness measurements may be carried out with DSI's Buxco® FinePointe Non-Invasive Airway Mechanics (NAM) instrument consisting of a nasal chamber in combination with the thoracic chamber that allows the computation of specific airway resistance (sRaw). Treated conscious, spontaneously breathing Ova S/C mice may be exposed to aerosolized phosphate buffered saline (PBS) (for the baseline measurement) or methacholine (1.5625-12.5 mg/mL) for 1 minute and readings (sRaw) may be taken and averaged for 3 minutes after each nebulization.

[00128] The change of the number of specific immune cells caused by compounds may be investigated in the bronchoalveolar lavage fluid (BALF) of Ova S/C mice. Therefore, a bronchoalveolar lavage may be carried out followed by the lysis of red blood cells. Incubation of cell-type specific antibodies with BALF may allow the quantification of leukocytes such as eosinophils and $CD4^+$ T-lymphocytes using flow cytometry.

[00129] Direct interaction between compounds and $CD4^+$ T cells may be investigated by electrophysiology. Therefore, $CD4^+$ T cells may be isolated from the spleen of asthmatic mice and treated with compounds during an automated patch clamp experiment.

[00130] The change of cytokine expression caused by compounds may be investigated in the lung of Ova S/C mice. Therefore, lungs of treated and non-treated asthmatic mice may be harvested, homogenized and cleared by centrifugation. Cytokines may be identified and quantified with specific antibodies and flow cytometry.

[00131] The pharmacokinetic properties of compounds may be investigated in animals. Therefore, animals may be exposed to compounds for different time intervals. Quantification of compounds concentrations may occur for blood, lung and brain using specific preparation protocols followed by quantification using mass spectrometry.

[00132] The cytotoxicity of compounds may be evaluated by treating HEK293 human embryonic kidney cells with increasing concentrations of compounds for 24-48 hours followed by the quantification of living cells using Cell-Titer Glo (Promega).

Compositions and Routes of Administration

[00133] In another aspect, the invention provides pharmaceutical compositions comprising one or more compounds of this invention in association with a pharmaceutically acceptable carrier. Such compositions may be in unit dosage forms such as tablets, pills, capsules, powders, granules, sterile parenteral solutions or suspensions, metered aerosol or liquid sprays, drops, ampoules, auto-injector devices or suppositories; for oral, parenteral, intranasal, sublingual or rectal administration, or for administration by inhalation or insufflation. It is also envisioned that compounds may be incorporated into transdermal patches designed to deliver the appropriate amount of the drug in a continuous fashion. For preparing solid compositions such as tablets, the principal active ingredient is mixed with a pharmaceutical carrier, e.g. conventional tableting ingredients such as corn starch, lactose, sucrose, sorbitol, talc, stearic acid, magnesium stearate,

dicalcium phosphate or gums, and other pharmaceutical diluents, e.g. water, to form a solid preformulation composition containing a homogeneous mixture for a compound of the present invention, or a pharmaceutically acceptable salt thereof. When referring to these preformulation compositions as homogeneous, it is meant that the active ingredient is dispersed evenly throughout the composition so that the composition may be easily subdivided into equally effective unit dosage forms such as tablets, pills and capsules. This solid preformulation composition is then subdivided into unit dosage forms of the type described above containing from 0.1 to about 500 mg of the active ingredient of the present invention. Typical unit dosage forms contain from 1 to 100 mg, for example, 1, 2, 5, 10, 25, 50 or 100 mg, of the active ingredient. The tablets or pills of the novel composition can be coated or otherwise compounded to provide a dosage form affording the advantage of prolonged action. For example, the tablet or pill can comprise an inner dosage and an outer dosage component, the latter being in the form of an envelope over the former. The two components can be separated by an enteric layer, which serves to resist disintegration in the stomach and permits the inner component to pass intact into the duodenum or to be delayed in release. A variety of materials can be used for such enteric layers or coatings, such materials including a number of polymeric acids and mixtures of polymeric acids with such materials as shellac, cetyl alcohol and cellulose acetate.

[00134] The liquid forms in which the compositions of the present invention may be incorporated for administration orally or by injection include aqueous solutions, suitably flavored syrups, aqueous or oil suspensions, and flavored emulsions with edible oils such as cottonseed oil, sesame oil, coconut oil or peanut oil, as well as elixirs and similar pharmaceutical vehicles. Suitable dispersing or suspending agents for aqueous suspensions include synthetic and natural gums such as tragacanth, acacia, alginate, dextran, sodium carboxymethylcellulose, methylcellulose, polyvinylpyrrolidone or gelatin.

[00135] Suitable dosage level is about 0.01 to 250 mg/kg per day, about 0.05 to 100 mg/kg per day, or about 0.05 to 5 mg/kg per day. The compounds may be administered on a regimen of 1 to 4 times per day, or on a continuous basis via, for example, the use of a transdermal patch.

[00136] Pharmaceutical compositions for enteral administration, such as nasal, buccal, rectal, sub-lingual or, especially, oral administration, and for parenteral administration, such as intravenous, intramuscular, subcutaneous, peridural, epidural or intrathecal administration, are

suitable. The pharmaceutical compositions comprise from approximately 1% to approximately 95% active ingredient, or from approximately 20% to approximately 90% active ingredient.

[00137] For parenteral administration including intracoronary, intracerebrovascular, or peripheral vascular injection/infusion preference is given to the use of solutions of the subunit selective GABAA receptor agonist, and also suspensions or dispersions, especially isotonic aqueous solutions, dispersions or suspensions which, for example, can be made up shortly before use. The pharmaceutical compositions may be sterilized and/or may comprise excipients, for example preservatives, stabilizers, wetting agents and/or emulsifiers, solubilizers, viscosity-increasing agents, salts for regulating osmotic pressure and/or buffers and are prepared in a manner known per se, for example by means of conventional dissolving and lyophilizing processes.

[00138] For oral pharmaceutical preparations suitable carriers are especially fillers, such as sugars, for example lactose, saccharose, mannitol or sorbitol, cellulose preparations and/or calcium phosphates, and also binders, such as starches, cellulose derivatives and/or polyvinylpyrrolidone, and/or, if desired, disintegrators, flow conditioners and lubricants, for example stearic acid or salts thereof and/or polyethylene glycol. Tablet cores can be provided with suitable, optionally enteric, coatings. Dyes or pigments may be added to the tablets or tablet coatings, for example for identification purposes or to indicate different doses of active ingredient. Pharmaceutical compositions for oral administration also include hard capsules consisting of gelatin, and also soft, sealed capsules consisting of gelatin and a plasticizer, such as glycerol or sorbitol. The capsules may contain the active ingredient in the form of granules, or dissolved or suspended in suitable liquid excipients, such as in oils.

[00139] Transdermal application is also considered, for example using a transdermal patch, which allows administration over an extended period of time, e.g. from one to twenty days.

Methods of Use

[00140] The present invention provides a method of reducing airway constriction comprising administering an effective amount of a compound or composition of formulae (I) or (II), or a salt thereof. In some embodiments, compounds of formula (I) or (II) have reduced

benzodiazepine-type CNS effects in a subject compared to diazepam at therapeutic doses. In some embodiments, airway constriction occurs during anesthesia.

[00141] The present invention further provides a method of reducing lung inflammation comprising administering an effective amount of a compound or composition of formula (I) or (II), or a pharmaceutically acceptable salt thereof to a subject in need thereof. In some embodiments, compounds of formula (I) or (II) have reduced benzodiazepine-type CNS effects in a subject compared to diazepam at therapeutic doses. In some embodiments, the lung inflammation is associated with asthma, chronic obstructive pulmonary disease, emphysema, cystic fibrosis, pulmonary fibrosis, bronchiectasis, fibrosing alveolitis, Wegener's granulomatosis, intrinsic alveolitis or infection. The infection is suitably caused by viral, bacterial and/or fungal agents.

[00142] Lung inflammation may be evidenced in a patient by impaired pulmonary function, shortness of breath, especially with exertion or exercise, coughing, or labored breathing. A wide variety of diagnostic tools, including chest x-rays, CT scans, and pulmonary function tests are used to diagnose inflammatory lung disease. Pulmonary function and exercise tests may be used to determine lung capacity impaired by inflammation. Tissue samples from the lungs can be obtained for more definite diagnosis of inflammation. This can be obtained with a bronchoscopy (transbronchial biopsy) or bronchoalveolar lavage or surgical lung biopsy. Histologically, inflammation may reveal increased numbers of macrophages, lymphocytes, or polymorphonuclear cells in sputum and bronchoalveolar lavage fluid or lung parenchema or airways. Migration and activation of immune/inflammatory cells to the lung is regulated by a variety of different mediators, including proteases, cytokines, and chemokines secreted by a variety of inflammatory and resident cells.

[00143] In another aspect, the present invention provides a method of reducing the development of disease in subjects having risk factors associated with lung inflammation comprising administering an effective amount of a compound or composition of formula (I) or (II), or a pharmaceutically acceptable salt thereof to a subject in need thereof. In some embodiments, compounds of formula (I) or (II) have reduced benzodiazepine-type CNS effects in a subject compared to diazepam at therapeutic doses.

[00144] A number of factors may increase the likelihood of developing inflammatory lung diseases: low birth weight, having a blood relative with a condition such as asthma (thus a

genetic predisposition), the presence of specific gene mutations (such as in cystic fibrosi transmembrane conductor regulator (CFTR) genes), obesity, smoking or exposure to smok (including in-utero exposure), exposure to exhaust fumes or other types of environmenta pollution, or exposure industrial or agricultural chemicals.

[00145] In some embodiments, the lung inflammation is associated with asthma, chroni obstructive pulmonary disease, emphysema, cystic fibrosis, pulmonary fibrosis, bronchiectasis fibrosing alveolitis, Wegener's granulomatosis, intrinsic alveolitis or infection. The infection i suitably caused by viral, bacterial and/or fungal agents.

[00146] The present invention further provides a method of reducing inflammation in subject having an autoimmune disease comprising administering an effective amount of compound or composition of formula (I) or (II), or a pharmaceutically acceptable salt thereof to subject in need thereof. In some embodiments, compounds of formula (I) or (II) have reduce benzodiazepine-type CNS effects in a subject compared to diazepam at therapeutic doses. I some embodiments, the autoimmune disease is selected from arthritis, diabetes, lupus, an Crohn's disease.

[00147] The following non-limiting examples are intended to be purely illustrative o some aspects and embodiments, and show specific experiments that were carried out i accordance with the disclosure.

EXAMPLES

Example 1. Synthesis of (R)-8-ethynyl-6-(2-fluorophenyl)-4-methyl-4H benzo[f]imidazo[1,5-a][1,4]diazepine-3-carboxylic acid (SH-053-2'F-R-CH3-Acid)

[00148] Compound 7 (2.0 g, 5.16 mmol) was stirred in ethanol (100 mL) and 3 M sodiun hydroxide (20 mL, 60 mmol) was added and the solution was heated and refluxed for 1 hou The reaction solution was then cooled to room temperature and diluted with water (100 mL). Th solution was placed under reduced pressure until half of the solvent remained. The remainin reaction mixture was stirred at room temperature and hydrochloric acid (1 M) was adde dropwise at room temperature until the product precipitated out. The product was filtered, rinse with water and dried to afford pure acid SH-053-2'F-R-CH3-Acid as a white solid (81% yield). ^{1}H NMR (300 MHz, DMSO-d_6) δ 8.42 (s, 1H), 7.94 (d, 1H, J = 8.4 Hz), 7.82 (d, 1H, J = 8.2 Hz)

7.56 (dt, 2H, J = 7.8, 6.5 Hz), 7.33 (t, 1H, J = 7.4 Hz), 7.22 (t, 2H, J = 9.3 Hz), 6.53 (d, 1H, J
7.1 Hz), 2.51 (s, 1H), 1.16 (d, 3H, J = 6.8 Hz); ^{13}C NMR (75 MHz, DMSO-d6) δ 164.76, 162.8
158.19, 140.57, 136.57, 135.54, 134.74, 133.18, 132.65, 131.88, 129.88, 129.35, 125.17, 123.9
121.09, 116.53, 116.25, 83.42, 82.01, 49.79, 15.08; HRMS (LCMS-IT-TOF) Calc. f
$C_{21}H_{14}FN_3O_2$ (M + H)+ 360.1143, found 360.1140.

Example 2. Synthesis of (R)-8-Bromo-6-(2-fluorophenyl)-4-methyl-4H-benzo[f]imidazo[1,5-a][1,4] diazepine-3-carboxylic acid (GL-II-93)

[00149] Compound **4** (5.1 g, 11.5 mmol) was dissolved in EtOH (150 mL), after whi solid NaOH (0.9 g, 23 mmol) was added to the solution. This reaction mixture was heated to °C for 1 hour and the EtOH was removed under reduced pressure. The remaining aquec solution was stirred at 0 °C for 10 minutes and then 10 % aqueous HCl was added dropwise the solution until the pH was 5 (pH paper). A pale white precipitate which formed, was left in t solution for 10 minutes and was then collected by filtration. The solid was washed with cc water and the aqueous layer also allowed to stand at room temperature for 10 hours to yie additional acid. The combined solids were dried in a vacuum oven at 80 °C for 7 hours provide pure GL-II-93 as a white powder (4 g, 9.7 mmol, 85.2%). ^{1}H NMR (500 MHz, CDCl δ 8.12 (s, 1H), 7.73 (d, J = 7.6 Hz, 1H), 7.63 (s, 1H), 7.55 (d, J = 8.3 Hz, 1H), 7.50 – 7.37 (2H), 7.25 (t, J = 7.3 Hz, 1H), 7.07 – 6.99 (m, 1H), 6.78 (q, J = 7.2 Hz, 1H), 1.27 (d, J = 6.3 H 3H); ^{13}C NMR (126 MHz, $CDCl_3$): δ 164.94, 162.87, 161.09, 159.09, 141.28, 135.04, 134.9 133.59, 133.08, 132.51, 132.12, 131.34, 131.11, 129.38, 128.16, 124.57, 123.91, 120.40, 116.3 116.13, 49.83, 14.91; HRMS (LCMS-IT-TOF) Calc. for $C_{19}H_{13}N_3O_2FBr$ (M + H)+ 414.024 found 414.0235.

Example 3. Synthesis of (R)-8-Cyclopropyl-6-(2-fluorophenyl)-4-methyl-4H-benzo[f]imidazo[1,5-a][1,4]diazepine-3-carboxylic acid (GL-III-43).

[00150] Compound **4** (2.1 g, 4.8 mmol) was dissolved in toluene (20 mL). T cyclopropylboronic acid (1.0 g, 12.0 mmol) and water (1.5 mL) were added to the mixture. reflux condenser was attached and the mixture was degassed under vacuum with argon; tl process was repeated four times. The bis(triphenylphosphine)-palladium (II) acetate (0.72 g, 0

for another four times. Then the reaction mixture was heated to reflux under argon and allowed to stir for 3 hours. The reaction mixture was quenched by addition of cold water and extracted with ethyl acetate. The organic layers were combined and washed with brine (2 x 150 mL), dried Na_2SO_4 and the solvent was removed under reduced pressure to afford a brown solid. The crude solid was purified by column chromatography (silica gel, ethyl acetate/hexanes 5:5) to provide pure compound **5** as an off-white solid (1.2 g, 3.0 mmol, 65%): ^{1}H NMR (500 MHz,$CDCl_3$) δ 7.88 (s, 1H), 7.55 (t, J = 7.1 Hz, 1H), 7.44 (d, J = 8.3 Hz, 1H), 7.39 (dd, J = 13.3, 5.8 Hz, 1H), 7.19 (dd, J = 12.9, 6.1 Hz, 2H), 6.98 (dd, J = 18.9, 9.9 Hz, 2H), 6.64 (q, J = 7.2 Hz, 1H), 4.45 – 4.25 (m, 2H), 1.91 – 1.78 (m, 1H), 1.38 (t, J = 7.1 Hz, 3H), 1.24 (d, J = 7.3 Hz, 3H), 1.04 – 0.88 (m, 2H), 0.59 (m, 2H); ^{13}C NMR (126 MHz, $CDCl_3$): δ 164.17, 163.12, 161.12, 159.12, 143.88, 141.58, 134.85, 132.09, 131.65, 131.21, 129.16, 129.04, 128.47, 127.87, 124.33, 121.95, 116.08, 115.91, 60.59, 50.05, 15.04, 14.64, 14.44, 9.91, 9.89; HRMS (LCMS-IT-TOF) Calc. for $C_{24}H_{22}N_3O_2F$ (M + H)+ 404.1769, found 404.1763.

[00151] GL-III-43 was prepared from compound **5** following the general procedure outlined for GL-II-93 in the previous procedure and obtained GL-III-43 as a white solid (0.62 g, 1.7 mmol, [illegible] NMR (500 MHz, DMSO-d6) δ 8.34 (s, 1H), 7.77 (d, J = 7.2 Hz, 1H), 7.58 – 7.49 (m, 2H), 7.32 (m, 2H), 7.21 (t, J = 8.8 Hz, 1H), 6.94 (s, 1H), 6.50 (q, J = 5.2 Hz, 1H), 1.93 (m, J = 4.1 Hz, 1H), 1.13 (d, J = 6.4 Hz, 3H), 0.95 (d, J = 7.7 Hz, 2H), 0.61 (m, 2H); HRMS (LCMS-IT-TOF) Calc. for $C_{22}H_{18}N_3O_2F$ (M + H)+ 376.1456, found 376.1453.

Example 4. Synthesis of (R)-8-Chloro-6-(2-fluorophenyl)-4-methyl-4H-benzo[f]imidazo[1,5-a][1,4]diazepine-3-carboxylic acid (GL-III-54)

[00152] GL-III-54 was prepared from compound **8** following the general procedure reported above and obtained as a white solid (0.93 g, 2.5 mmol, 85%). ^{1}H NMR (500 MHz, DMSO-d6) δ 8.41 (s, 1H), 7.97 (d, J = 8.4 Hz, 1H), 7.84 (t, J = 10.0 Hz, 1H), 7.65 – 7.52 (m, 2H), 7.34 (t, J = 7.4 Hz, 1H), 7.27 – 7.14 (m, 2H), 6.56 (q, J = 7.0 Hz, 1H), 1.17 (d, J = 6.9 Hz, 3H); HRMS (LCMS-IT-TOF) Calc. for $C_{19}H_{13}N_3O_2FCl$ (M + H)+ 370.0753, found 370.0752.

Example 5. Synthesis of (R)-8-Bromo-4-methyl-6-(pyridin-2-yl)-4H-benzo[f]imidazo[1,5-a][1,4]diazepine-3-carboxylic acid (GL-II-51)

[00153] GL-II-51 was prepared from compound **9** following the general procedure reported above and obtained as a white solid (0.87 g, 2.2 mmol, 88%). ^{1}H NMR (500 MHz, DMSO-d6) δ 8.51 (s, 1H), 8.38 (s, 1H), 8.01 (d, J = 7.5 Hz, 1H), 7.98 – 7.89 (m, 2H), 7.84 (d, J = 7.6 Hz, 1H), 7.47 (m, 2H), 6.54 (d, J = 5.3 Hz, 1H), 1.17 (d, J = 6.4 Hz, 3H).; HRMS (LCMS-IT-TOF) Calc. for $C_{18}H_{13}N_4O_2Br$ (M + H)+ 397.0295, found 397.0299.

Example 6. Synthesis of (R)-8-Ethynyl-4-methyl-6-(pyridin-2-yl)-4H-benzo[f]imidazo[1,5-a][1,4]diazepine-3-carboxylic acid (GL-II-30)

[00154] GL-II-30 was prepared from compound **10** following the general procedure reported above and obtained as a white solid (1.06 g, 3.1 mmol, 88%). ^{1}H NMR (500 MHz, DMSO-d6) δ 8.57 (d, J = 3.8 Hz, 1H), 8.02 (dd, J = 27.8, 13.9 Hz, 2H), 7.84 (t, J = 6.6 Hz, 1H), 7.69 (d, J = 8.0 Hz, 1H), 7.57 (d, J = 8.2 Hz, 1H), 7.42 (s, 1H), 7.40 – 7.31 (m, 1H), 6.72 (q, J = 7.0 Hz, 1H), 3.15 (s, 1H), 1.25 (d, J = 7.0 Hz, 3H); HRMS (LCMS-IT-TOF) Calc. for $C_{20}H_{14}N_4O_2$ (M + H)+ 343.1190, found 343.1188.

Example 7. Synthesis of (S)-7-methoxy-1-(1H-tetrazol-5-yl)-11,12,13,13a-tetrahydro-9H-benzo[e] imidazo[5,1-c]pyrrolo[1,2-a][1,4]diazepin-9-one (RJ-03-57)

[00155] DIBAL-H (1.2 M, 6.2 mL, 7.4 mmol) was added at 0°C to a solution of sodium tert-butoxide (0.76 g, 7.9 mmol) in 20 mL of dry tetrahydrofuran. The resulting mixture was stirred for 1 hour at room temperature under argon atmosphere. Compound **15** (1.5 g, 4.4 mmol) was then added to the above solution at 0°C and stirred for 3 hours (or until the complete consumption of **15**) at room temperature under argon atmosphere. After that, concentrated NH_4 (28%, 20 mL) and I_2 (4.57 g, 18.0 mmol) were added at 0°C and the resulting mixture was stirred at room temperature for 3 hours. After complete disappearance of the aldehyde intermediate, the reaction mixture was treated with a saturated solution of sodium thiosulfate (~10 mL) and extracted with ethyl acetate (3x 30 mL). The combined organic layers were washed with brine, dried over Na_2SO_4 and solvent was evaporated under reduced pressure. The residue was purified with silica gel flash column chromatography (70% ethyl acetate in hexanes) to furnish the nitrile **17** as white solid, 1.225 g, 95%. At this point, to a solution of the nitrile **17** (0.295 g, 1.0 mmol) in 30 mL of tetrahydrofuran, $ZnBr_2$ (0.34 g, 1.50 mmol) and NaN_3 (78 mg, 1.20 mmol) were added and the mixture was heated to reflux for 36 hours (or until the complete

consumption of **17**). The solution was treated with 1M HCl to dissolve the solid material and bring the pH of the solution to 1. The solution was extracted with ethyl acetate (4x 40 mL). The solvent was evaporated under reduced pressure and the residue was passed through a short pad of silica with 7% methanol in dichloromethane to furnish 196 mg of RJ-03-5[illegible]R (300 MHz, DMSO-d_6): δ 1.96-2.14 (m, 2H), 2.23-2.40 (m, 1H), 3.40-3.50 (m, 1H), 3.5-3.66 (m, 1H), 3.89 (s, 3H), 3.96-4.10 (m, 1H), 4.95 (d, 1H, J = 8.34 Hz), 7.31-7.38 (m, 1H), 7.43 (d, 1H, J = 2.8 Hz), 7.69 (d, 1H, J = 8.8 Hz), 8.60 (s, 1H); ^{13}C NMR (75 MHz, DMSO-d_6): δ 24.7, 27.9, 46.6, 52.3, 56.3, 115.1, 119.2, 123.5, 126.0, 126.5, 130.9, 137.7, 155.4, 159.3, 163.3; HRMS (ESI) (M-H), calcd for $C_{16}H_{16}N_7O_2$ 336.1360; found 336.1357.

Example 8. Synthesis of (S)-N,7-Dimethoxy-9-oxo-11,12,13,13a-tetrahydro-9H-benzo[e] imidazo[5,1-c]pyrrolo[1,2-a][1,4]diazepine-1-carboxamide (MRS-III-87)

[00156] A mixture of compound **16** (0.15 g), thionyl chloride (1 mL) and dry CH_2Cl_2 (8 mL) was added to an oven dried round bottomed flask under argon. This suspension was allowed to reflux at 52 ºC (the outside oil bath temperature was at 60 ºC) for 1 hour under an atmosphere of argon. The solution became a clear yellow color. The absence of the starting material was confirmed by the examination of the solution by thin-layer chromatography (TLC) (silica gel). The organic solvent and excess thionyl chloride were removed under reduced pressure. This flash evaporation with dry dichloromethane (5 mL) was repeated two times to remove excess thionyl chloride and any HCl. The yellow residue, which was obtained, was dissolved in dry CH_2Cl_2 (10 mL) and cooled to 0 ºC for 10 minutes under argon. Then methyl hydroxylamine hydrochloride (2.5 equivalents), followed by triethylamine (5 equivalents) was added to the reaction mixture at 0 ºC and the mixture was then allowed to warm to room temperature and stirred for 4 hours. After the completion of the reaction (TLC, silica gel), the solvent was removed under reduced pressure and acetone (4 mL) was added to the residue. The salt was removed by filtration and the solvent was removed under reduced pressure to provide MRS-III-87[illegible]H NMR (300 MHz, $CDCl_3$) δ 2.14-2.22 (m, 2H), 2.30-2.39 (m, 1H), 3.08-3.10 (m, 1H), 3.51-3.57 (m, 1H), 3.75-3.80 (m, 1H), 3.88 (s, 3H), 3.91 (s, 3H), 4.72 (d, 1H, J = 8.0 Hz), 7.14 (dd, 1H, J = 8.8 Hz, 2.7 Hz), 7.28 (d, 1H, J = 8.8 Hz), 7.58 (d, 1H, J = 2.7 Hz), 7.69 (s, 1H), 9.84 (bs, 1H); LCMS (ESI, m/z, relative intensity (ESI), calcd. for$C_{17}H_{17}N_4O_4$ $(M-H)^+$ 341.35; Found 341.00.

Example 9. Synthesis of (S)-N-Cyano-7-methoxy-9-oxo-11,12,13,13a-tetrahydro-9H-benzo[e]imidazo [5,1-c]pyrrolo[1,2-a][1,4]diazepine-1-carboxamide (MRS-III-90)

[00157] A mixture of compound **16** (0.15 g), thionyl chloride (1 mL) and dry CH_2Cl_2 (8 mL) were added to an oven dried round bottomed flask under argon. This suspension was allowed to reflux at 52 ℃ (the outside oil bath temperature was at 60 ℃) for 1 hour under an atmosphere of argon. The solution became a clear yellow color. The absence of the starting material was confirmed by the examination of the solution by TLC (silica gel). The organic solvent and excess thionyl chloride were removed under reduced pressure. This evaporation was repeated a couple of times with dry CH_2Cl_2 (5 mL) to remove excess thionyl chloride and any HCl. The yellow residue, which was obtained, was dissolved in dry CH_2Cl_2 (10 mL) and cooled to 0 ℃ for 10 minutes under argon. The methyl cyanamide (2.5 equivalents), followed by triethylamine (5 equivalents) were added to the reaction mixture at 0 ℃ and the mixture was then allowed to warm to room temperature and stirred for 5 hours. After the completion of the reaction (TLC, silica gel), the solvent was removed under reduced pressure and acetone (4 mL) was added to the residue. The salt was filtered off and the solvent was removed under reduced pressure to obtain MRS-III-90 in 7[illegible] yield. ^{1}H NMR (300 MHz, DMSO-d6) δ 2.10-2.13 (m, 2H), 3.34-3.58 (m, 3H), 3.88 (s, 3H), 3.91 (s, 3H), 4.73 (d, 1H, J = 7.5 Hz, major rotamer 83%), 4.84 (d, J = 7.5 Hz, minor rotamer, 17%), 7.27-7.29 (m, 1H, major rotamer), 7.31-7.33 (m, minor rotamer), 7.38 (d, 1H, J = 2.0 Hz, major rotamer), 7.41 (d, J = 2.5 Hz, minor rotamer), 7.57 (d, 1H, J = 8.5 Hz, major rotamer), 7.64 (d, J = 9.0 Hz, minor rotamer), 8.00 (s, 1H, major rotamer), 8.21 (s, minor rotamer), 9.49-10.11 (bs, 1H); LCMS (ESI, m/z, relative intensity (ESI), calcd. for $C_{17}H_{14}N_5O_3$ (M-H)+ 336.33; Found 336.00.

Example 10. Synthesis of (S)-Ethyl-7-hydroxy-9-oxo-11,12,13,13a-tetrahydro-9H-benzo[e]imidazo[5,1-c] pyrrolo[1,2-a][1,4]diazepine-1-carboxylate (RJ-02-50):

[00158] In an oven dried round bottom flask, dry CH_2Cl_2 (50 ml) was added and cooled to 0 °C. Then $AlCl_3$ (3 g, 22.8 mmol) and ethanethiol (4.5 ml, 60.8 mmol) were added to the above flask slowly at 0 °C. The ice bath was removed and the reaction was allowed to warm up to room temperature. After the $AlCl_3$ dissolved completely, ester **15** (2.6 g, 7.62 mmol) was added to the mixture at room temperature and it was stirred for 24-36 hours under Ar. After completion of the

reaction (TLC, silica gel), the solution was poured onto ice and was acidified using an aq 2N HCl solution. The solution was extracted 5-7 times with CH_2Cl_2 and 3-4 times with ethyl acetate separately. The combined organic layer was washed with brine and dried (Na_2SO_4). The solvent was removed under reduced pressure and the residue was purified by flash column chromatography on [silica gel, 4% methanol in CH_2Cl_2] to furnish RJ-02-50 as a solid (2.1 g) in 84% yield. M.p = >260 °C (decomp.); ^{1}H NMR (300 MHz, $CDCl_3$) δ 1.44 (t, 3H, J = 7.1 Hz), 2.19-2.42 (m, 3H), 3.55-3.64 (m, 2H), 3.81-3.89 (m, 1H), 4.42 (q, 2H, J = 7.1 Hz), 4.82 (d, 1H, J = 7.3 Hz), 7.13 (dd, 1H, J = 8.7 Hz, 2.6 Hz), 7.27-7.31 (m, 1H), 7.85 (s, 1H), 7.91 (d, 1H, J = 2.6 Hz), 9.22 (s, 1H); ^{13}C NMR (75 MHz, $CDCl_3$) δ 14.3, 24.4, 28.4, 46.9, 53.8, 61.2, 117.5, 120.8, 124.9, 125.2, 127.7, 129.5, 136.0, 137.2, 157.6, 162.8, 164.6; HRMS (ESI) (M+H)+, calcd. for $C_{17}H_{18}N_3O_4$ 328.1292; Found 328.1293.

Example 11. Synthesis of (S)-7-hydroxy-9-oxo-11,12,13,13a-tetrahydro-9H-benzo[e]imidazo[5,1-c] pyrrolo[1,2-a][1,4]diazepine-1-carboxylic acid (RJ-03-90)

[00159] RJ-02-50 (1.52 g, 4.6 mmol) was dissolved in a mixture of ethanol (4 mL) and H_2O (3 mL) after which solid NaOH (1.0 g, 25.0 mmol) was added to the solution. This reaction mixture was heated to 50°C for 15 minutes and the ethanol was removed under reduced pressure. The remaining aqueous solution was stirred at 0°C for 10 minutes and then concentrated HCl was added dropwise to the solution until the pH was 3-4 (pH paper). A pale yellow precipitate which formed was left in the solution and the mixture was allowed to stir at room temperature for 2 hours. The precipitate was collected by filtration, washed with cold water (2-5 mL) and the aqueous layer also was allowed to stand at room temperature for 10 hours to obtain additional RJ-03-90. The combined solids were dried in a vacuum oven at 80°C for 7 hours to get pure RJ-03-90 in 85% yield. ^{1}H NMR (300 MHz, CD_3OD): δ 2.14-2.29 (m, 3H), 3.50-3.63 (m, 2H), 3.70-3.78 (m, 1H), 4.95 (d, 1H, merged with solvent peak), 7.15 (d, 1H, J = 8.7 Hz, 3.0 Hz), 7.38-7.43 (m, 1H), 7.53 (d, 1H, J = 8.76 Hz), 8.48 (m, 1H); ^{13}C NMR (75 MHz, CD_3OD) δ 24.0, 27.7, 46.2, 53.4, 116.2, 119.8, 124.5, 125.4, 128.4, 130.2, 136.2, 137.5, 158.2, 162.5, 164.4; HRMS (ESI) (M+H)+, calcd. for $C_{15}H_{14}N_3O_4$ 300.0979; Found 300.0990.

Example 12. Synthesis of (S)-tert-Butyl-7-hydroxy-9-oxo-11,12,13,13a-tetrahydro-9H-

[00160] A flame dried round bottom flask was charged with dry tetrahydrofuran (30 mL) and lithium rod (excess, cut into small pieces) was added. Dry tert-butanol (2.6 mL, 27.1 mmol) was added to the above flask at room temperature and the mixture which resulted was heated to 45-50 °C under Ar until the tert-butanol reacted completely. This freshly prepared lithium tert-butoxide solution was transferred carefully with a cannula to another flame dried round bottom flask charged with RJ-02-50 (1.0 g, 2.71 mmol) and stirred at 50 °C under Ar for 30 minutes. After the completion of the reaction (TLC, silica gel), the flask was cooled to room temperature and the tetrahydrofuran removed under reduced pressure. Ice water (10 mL) was added to the residue and it was then extracted with ethyl acetate. The organic layer was washed with water (2 X 10 mL) and brine (15 mL). The solvent was removed under reduced pressure and the residue was purified by flash column chromatography [silica gel, ethyl acetate/hexane (7:3)] to yield RJ-02-67 as a solid (0.72 g) in 65% yield. M.p = 174-175 °C; ^{1}H NMR (300 MHz, $CDCl_3$) δ 1.63 (s, 9H), 2.09-2.34 (m, 3H), 3.50-3.62 (m, 2H), 3.77-3.85 (m, 1H), 4.79 (d, 1H, J = 7.1 Hz), 7.10 (dd, 1H, J = 8.6 Hz, 2.2 Hz), 7.23-7.28 (m, 1H), 7.77 (bs, 1H), 7.85 (s, 1H), 9.75 (bs, 1H); ^{13}C NMR (75 MHz, $CDCl_3$) δ 24.4, 28.2, 28.3, 46.9, 53.7, 82.0, 117.4, 120.7, 124.9, 125.1, 129.1, 129.6, 135.8, 136.2, 157.7, 162.3, 164.6; HRMS (ESI) $(M+H)^+$, calcd. for $C_{19}H_{22}N_3O_4$ 356.1605; Found 356.1615.

Example 13. Synthesis of (S)-7-hydroxy-1-(oxazol-5-yl)-11,12,13,13a-tetrahydro-9H-benzo[e]imidazo[5,1-c]pyrrolo[1,2-a][1,4]diazepin-9-one (RJ-03-30):

[00161] DIBAL-H (1M, 20.4 mL, 20.4 mmol) was added at 0°C to a solution of sodium tert-butoxide (2.02 g, 21.02 mmol) in 30 mL of dry tetrahydrofuran. The resulting mixture was stirred for 1 hour at room temperature under argon atmosphere. Compound **15** (4 g, 11.72 mmol) was then added to the above solution at 0°C and stirred for 3 hours (or until the complete consumption of 15) at room temperature under argon atmosphere. After completion of the reaction, excess DIBAL-H was quenched by careful addition of methanol (~ 15 mL), followed by 5% aqueous HCl (20-30 mL) at 0 °C. After this the resulting mixture was allowed to warm to room temperature. The aqueous layer was extracted with CH_2Cl_2 (2x 50 mL). The combined organic layers were washed with brine and dried (Na_2SO_4). The solvent was removed under reduced pressure to afford the crude aldehyde. This residue was purified by flash

chromatography (2:1 ethyl acetate/hexane) to afford the pure diazepine aldehyde **18** as a white solid, (3.32

[00162] Toluenesulfonylmethyl isocyanide, TosMIC (3.28 g, 16.8 mmol) was placed in a dry two neck round bottom flask and dissolved in dry methanol (40 mL) under an argon atmosphere. At room temperature, K_2CO_3 (4.64 g, 33.57 mmol) was added as well as aldehyde 18 (3.325 g, 11.18 mmol) to the reaction mixture, which was heated to reflux for 3 hours. After completion of the reaction as indicated by TLC (silica gel ethyl acetate), the reaction mixture was quenched with cold water. After this, 1/3 of the solvent was removed under reduced pressure and extracted with ethyl acetate (3x 20 mL). The combined organic layers were washed with water and brine successively and dried (Na_2SO_4). The solvent was then removed under reduced pressure and the residue was purified by silica gel flash chromatography to give the pure oxazole **19** as white solid (2.83

[00163] In an oven dried round bottom flask, dry CH_2Cl_2 (50 mL) was taken and cooled to 0 °C. Then $AlCl_3$ (3.33 g, 24.97 mmol) and ethanethiol (5.0 ml, 67.52 mmol) were added to the above flask slowly at 0 °C. The ice bath was removed and the reaction was allowed to warm up to room temperature. After $AlCl_3$ dissolved completely, **19** (2.8 g, 8.32 mmol) was added to the mixture at room temperature and stirred for 24-36 hours under Ar. After completion of the reaction (TLC, silica gel), the solution was poured to ice and was acidified using 2N HCl solution. The solution was extracted 5-7 times with CH_2Cl_2 and 3-4 times with ethyl acetate separately. The combined organic layers were washed with brine and dried over Na_2SO_4. The solvent was removed under reduced pressure and the residue was purified by flash column chromatography on [silica gel, 4% methanol in CH_2Cl_2] to furnish RJ-03-30 as a solid (2.36 g) in 88% yield. ^1H NMR (500 MHz, $CDCl_3$): δ 1.97-2.08 (m, 2H), 2.25-2.35 (m, 1H), 2.65-2.73 (m, 1H), 3.63-3.71 (m, 1H), 3.76-3.84 (m, 1H), 4.84-4.88 (m, 1H), 7.10 (dd, 1H, J = 8.6, 2.2 Hz), 7.30 (d, 1H, J = 5.3 Hz), 7.40 (s, 1H), 7.75 (d, 1H, J = 1.9 Hz), 7.95 (s, 1H), 8.02 (s, 1H), 9.85 (s, 1H); ^{13}C NMR (125 MHz, $CDCl_3$): δ 23.9, 27.8, 47.2, 52.8, 117.6, 120.8, 123.5, 124.7, 125.3, 126.2, 129.3, 131.9, 136.5, 145.4, 150.9, 157.5, 164.8; HRMS (ESI) $(M+H)^+$, calcd. for $C_{17}H_{15}N_4O_3$ 323.1139; Found 323.1130.

Example 14. Determination of $GABA_AR$ subtypes selectivity

[00164] Compounds having selective activity bias for α4 and α5-$GABA_AR$ can be identified. Patch clamp assays are used to quantify chloride flux induced inward currents resulting from agonism of $GABA_AR$ containing single α-subunits. These results can demonstrate the ability to finely discriminate functional activity of $GABA_AR$ receptor-ligand interactions. For electrophysiological experiments with Xenopus oocytes (Ramerstorfer et al. *European journal of pharmacology* 2010, 636, 8-27) mature female Xenopus laevis (Nasco, Fort Atkinson, WI, USA) were anaesthetized in a bath of ice-cold 0.17% Tricain (Ethyl-m-aminobenzoate) before decapitation and transfer of the frog's ovary to ND96 medium (96 mM NaCl, 2 mM KCl, 1 mM MgCl2, 5 mM HEPES; pH 7.5). Following incubation in 1mg/ml collagenase (Sigma-Aldrich, St. Louis, MO, USA) for 30 minutes, stage 5 to 6 oocytes were singled out of the ovary and defolliculated using a platinum wire loop. Oocytes were stored and incubated at 18°C in NDE medium (96 mM NaCl, 2 mM KCl, 1 mM MgCl2, 5 mM HEPES, 1.8 mM CaCl2; pH 7.5) that was supplemented with 100 U·mL-1 penicillin, 100 µg·mL-1 streptomycin and 2.5 mM pyruvate. Oocytes were injected with an aqueous solution of mRNA. A total of 2.5 ng of mRNA per oocyte was injected. Subunit ratio was 1:1:5 for αxβ3γ2 (x = 1,2,3,5) and 3:1:5 for α4β3γ2 receptors. Injected oocytes were incubated for at least 36 hours before electrophysiological recordings. Oocytes were placed on a nylon-grid in a bath of NDE medium. For current measurements, the oocytes were impaled with two microelectrodes (2–3MΩ), which were filled with 2M KCl. The oocytes were constantly washed by a flow of 6 mL·min-1 NDE that could be switched to NDE containing GABA and/or drugs. Drugs were diluted into NDE from dimethylsulfoxide (DMSO) solutions resulting in a final concentration of 0.1% DMSO. Maximum currents measured in mRNA injected oocytes were in the microampere range for all receptor subtypes. To test for modulation of GABA induced currents by compounds, a GABA concentration that was titrated to trigger 3-5% of the respective maximum GABA-elicited current of the individual oocyte (EC3-5) was applied to the cell together with various concentrations of tested compounds. All recordings were performed at room temperature at a holding potential of -60 mV using a Warner OC-725C TEV (Warner Instrument, Hamden, CT, USA) or a Dagan CA-1B Oocyte Clamp or a Dagan TEV-200A TEV (Dagan Corporation, Minneapolis, MN, USA). Data were digitized using a Digidata 1322A or 1550 data acquisition

system (Axon Instruments, Union City, CA, USA), recorded using Clampex 10.5 software (Molecular Devices, Sunnyvale, CA, USA), and analyzed using Clampfit 10.5 and GraphPad Prism 6.0 (La Jolla, CA, USA) software. Concentration-response data were fitted using the Hill equation. Data are given as mean ± SEM from at least three oocytes of two batches. Alternatively, compound selectivity for α4 and α5-$GABA_A$R can be identified by automated patch clamp assay. Therefore, Patch clamp assay: HEK293T stably expressing α1β3γ2 GABAAR or α4β3γ2 were maintained RPMI 1640 medium with L-glutamine supplemented with 10% (v/v) fetal bovine serum and 1% penicillin/streptomycin (Forkuo et al., *Molecular Pharmaceutics* 2016, 13, 2026-38). Briefly, the IonFlux plate layout consists of units of 12 wells: two wells contain intracellular solution (ICS containing 140 mM CsCl, 1 mM $CaCl_2$, 1 mM $MgCl_2$, 11 mM EGTA, 10 mM HEPES, pH 7.2 with CsOH), one contains cells diluted in extracellular solution (ECS containing 140 mM NaCl, 5.4 mM KCl, 1 mM $CaCl_2$, 10 mM D-glucose monohydrate, and 10 mM HEPES, pH 7.4 with NaOH), eight contain different concentration of 1 in the presence of GABA (EC_{20} concentration) at 0.1% DMSO. Well 1 is for waste collection. Cells are captured from suspension by applying suction to microscopic channels in ensemble recording arrays. Once the array is fully occupied, the applied suction breaks the membranes of captured cells, which establishes whole cell voltage clamp. For compound applications, pressure is applied to the appropriate compound wells, which introduces the compound into the extracellular solution rapidly flowing over the cells. For recording $GABA_A$R induced currents, cell arrays were voltage clamped at a hyperpolarizing holding potential of −80 mV. Prior to use on the automated patch clamp, cells were centrifuged at 380g for 5 minutes and resuspended gently in ECS. This was repeated two more times before the cells were dispensed into the plate. All compound application were carried out for 3 seconds followed by a 5 second washout.

[00165] FIGs. 1A and 1B show $GABA_A$ receptor subtype selectivity. In FIG. 1A, dose dependent modulation of GABA (EC3-5 concentration) elicited currents by SH-053-2'F-R-CH_3-Acid on Xenopus oocytes expressing $GABA_A$ receptor subtypes α1β3γ2, α2β3γ2, α3β3γ2, α4β3γ2 and α5β3γ2. Data points represent means ± SEM from 2-8 oocytes from 2 batches, normalized to control currents (100%) in the absence of compound. SH-053-2'F-R-CH_3-Acid is a positive α5β3γ2-selective $GABA_A$ receptor modulator. FIG. 1B shows automated patch clamp

with RJ-02-50. Concentration-dependent negative current responses in the presence of EC_{20} concentration of GABA and increasing concentration of compound 1 applied together for 3 seconds using α1β3γ2 or α4β3γ2 GABAAR expressing HEK293T cells. Negative current readings were normalized to EC_{20} concentration of GABA response set as 100% (n = 16). RJ-02-50 is a positive α4β3γ2-selective $GABA_A$ receptor modulator.

Example 15. Determination of cytotoxicity of compounds.

[00166] Compounds with increased cytotoxicity can be identified using an in vitro cytotoxicity assay. Therefore, human embryonic kidney 293T (HEK293T) cell lines were purchased (ATCC) and cultured in 75 cm2 flasks (CellStar). Cells were grown in DMEM/High Glucose (Hyclone, #SH3024301) media to which non-essential amino acids (Hyclone, #SH30238.01), 10 mM HEPES (Hyclone, #SH302237.01), 5 x 106 units of penicillin and streptomycin (Hyclone, #SV30010), and 10% of heat inactivated fetal bovine serum (Gibco, #10082147) were added. Cells were harvested using 0.05% Trypsin (Hyclone, #SH3023601). The cell viability assay was evaluated using CellTiter-Glo™ Luminescent Cell Viability Assay Kit (Promega, Madison, WI), which contains luciferase and all its substrate except ATP. The controls for the cytotoxicity assay used were (E)-10-(bromotriphenylphosphoranyl)decyl 4-(4-(tert-butyl)phenyl)-4-oxobut-2-enoate (400 μM in DMSO, positive control) and DMSO (negative control). All luminescence readings were performed on a Tecan Infinite M1000 plate reader. Small volume transfers were performed on the Tecan Freedom EVO liquid handling system with a 100 nL pin tool transfer (V&P Scientific). Serial dilutions were done in 96-well polypropylene plates (Corning, #3365) and assays were conducted in 384-well white optical bottom plates. The assays were carried out in quadruplet in three independent runs. The data were normalized to the controls and if possible analyzed by nonlinear regression (GraphPad Prism).

Table 1. Cytotoxicity of compounds determined in the presence of human kidney and liver cells. None of the investigated compounds induced cytotoxicity up to a concentration of 100 μM. For the majority of compounds, no toxicity was observed at a concentration of 400 μM.

Compound	LD_{50} HEK293 (μM)	LD_{50} HEPG2 (μM)

	(Kidney)	(Liver)
RJ-03-57	>200	>200
SH-053-2'F-R-CH$_3$-acid	>400	>400
GL-II-93	>400	>400
RJ-02-50	>400	>400
RJ-02-67	>400	>400
RJ-03-30	>400	>400

Example 16. Rotarod assay, to determine induced CNS effects by compounds

[00167] Compounds with the ability to cross the blood brain barrier and induce CNS effects modulating the sensorimotor skills of mice can be identified with the rotarod. Female Swiss Webster mice were trained to maintain balance at a constant speed of 15 rpm on the rotarod apparatus (Omnitech Electronics Inc., Nova Scotia, Canada) until mice could perform for three minutes at three consecutive time points. Separate groups of mice received intraperitoneal (i.p.) injections of compounds in vehicle (10% DMSO, 40% propylene glycol and 50% PBS) or oral gavage (p.o.) in vehicle (2 % hydroxypropyl methylcellulose and 2.5% polyethylene glycol) in an approximate volume of 100 µl. Ten, thirty, and sixty minutes after each injection, mice were placed on the rotarod for three minutes. In case that mice fell from the rotarod prior to 3 minutes the time was noted and averaged for the group of mice. An unpaired t-test (GraphPad Prism) was used to determine significance for *$p < 0.05$, **$p < 0.01$, and ***$p < 0.001$. FIG. 2 shows the effect of compounds on sensorimotor coordination. Swiss Webster mice were tested on a rotarod at 15 rpm for 3 minutes at 10, 30, and 60 min following compound exposure. Mice ($N = 10$) received a single injection (i.p. or p.o.) of test compound. The time of fall was recorded if it occurred prior to 3 minutes. Data are expressed as mean ± SEM ($N = 10$). Student's t-test was used to calculate significance: *($p < 0.05$), ** ($p < 0.01$) or *** ($p < 0.001$) significance compared to vehicle-treated mice. None of the investigated compounds induced any sensorimotor impairments at the concentration tested.

Example 17. Microsomal Stability of compounds

[00168] The metabolic stability of compounds in vivo can be estimated with the stability of compounds in the presence of liver microsomes. Therefore, 4 µL of 1 mM DMSO solution of test compound at a final concentration of 10 µM were preincubated at 37°C for 5 minutes on a digital heating shaking dry bath (Fischer scientific, Pittsburgh, PA) in a mixture containing 282 µL of water, 80 µL of phosphate buffer (0.5 M, pH 7.4) 20 µL of NADPH Regenerating System Solution A (BD Bioscience, San Jose, CA) and 4 µL of NADPH Regenerating System Solution B (BD Bioscience, San Jose, CA) in a total volume of 391.2 µL. Following preincubation, the reaction was initiated by addition of 8.8 µL of either human liver microsomes (BD Gentest, San Jose, CA) or mouse liver microsomes (Life technologies, Rockford, IL) at a protein concentration of 0.5 mg/mL. Aliquots of 50 µL were taken at time intervals of 0 (without microsomes), 10, 20, 30, 40, 50 and 60 minutes. Each aliquot was added to 100 µL of cold acetonitrile solution containing 1 µM of verapamil HCL as internal standard. This was followed by sonication for 10 seconds and centrifugation at 10,000 rpm for 5 minutes. 100 µL of the supernatant was transferred into Spin-X HPLC filter tubes (Corning Incorporated, NY) and centrifuged at 13,000 rpm for 5 minutes. The filtrate was diluted 100-fold and subsequently analyzed by LC-MS/MS with Shimadzu LCMS 8040, (Shimadzu Scientific Instruments, Columbia, MD). The ratio of the peak areas of the internal standard and test compound was calculated for every time point and the natural log of the ratio were plotted against time to determine the linear slope (k). The metabolic rate (k*C0/C), half-life (0.693/k), and internal clearance (V*k) were calculated, where k is the slope, C0 is the initial concentration of test compound, C is the concentration of microsomes, and V is the volume of incubation in µL per microsomal protein in mg. All experiments were repeated two time in triplicates.

Table 2. Microsomal stability of compounds was tested with human and mouse liver microsomes. The majority of compounds exhibited a similar stability in the presence of human and mouse liver microsomes except compound RJ-02-67. More than 90% of all other compounds was observed after 60 minutes, when incubated with human and mouse liver microsomes.

Compound	HLM % remaining after 60 min	MLM % remaining after 60 min
RJ-03-57	94.3 ± 0.1	98.3 ± 0.2
SH-053-2'F-R-CH_3-Acid	92.0 ± 0.2	89.0 ± 0.3
RJ-02-50	91.7 ± 0.2	91.1 ± 0.1
RJ-02-67	90.6 ± 0.2	46.6 ± 0.3
RJ-03-30	91.8 ± 0.2	80.0 ± 0.3

Example 18. Relaxation of Guinea pig Airway Smooth Muscle by compounds.

[00169] All studies were conducted after approval of the Columbia University IACUC. Adult male Hartley guinea pigs were euthanized by intraperitoneal pentobarbital (100 mg/kg). The tracheas were surgically removed and transected into cross-sections containing two cartilaginous rings. The rings are washed for one hour with at least five buffer exchanges to remove any pentobarbital. After the epithelium was removed with a cotton swab, the rings were suspended from two silk threads in a 4 mL jacketed organ bath (Radnoti Glass Technology), with one thread attached to a Grass FT03 force transducer (Grass-Telefactor) coupled to a computer via Biopac hardware and Acknowledge 7.3.3 software (Biopac Systems) for continuous digital recording of muscle tension. The rings were bathed in 4 ml of KH buffer solution (composition in mM: 118 NaCl, 5.6 KCl, 0.5 $CaCl_2$, 0.2 $MgSO_4$, 25 $NaHCO_3$, 1.3 NaH_2PO_4, 5.6 D-glucose) with 10 μM indomethacin (DMSO vehicle final concentration of 0.01%), which was continuously bubbled with 95% O_2 and 5% CO_2 at pH 7.4, 37 °C. The rings were equilibrated at 1 g of isotonic tension for 1 hour with new KH buffer added every 15 minutes. All rings were precontracted with 10 μM N-vanillylnonanamide (capsaicin analog) and then two cycles of cumulatively increasing concentrations of acetylcholine (0.1−100 μM) with extensive buffer washes between and after those two cycles with resetting of the resting tension to 1.0 g. Tetrodotoxin (1 μM) and pyrilamine (10 μM) were added to the buffer in the baths to eliminate

the confounding effects of airway nerves and histamine receptors. After a stable baseline at 1.0 g resting tension was established, tracheal rings were contracted with 1 μM of substance P. After the peak contraction was reached, indicated concentrations of compounds or vehicle (0.1% DMSO) was added to the bath. The percentage of initial contraction remaining at indicated time points after compound exposure was expressed as a percentage of the remaining contractile force in vehicle-treated tissues and compared between groups. FIGs 3A-3C show airway smooth muscle contractile force in guinea pig tracheal rings. Tracheal rings were contracted with 1 mM substance P and then treated with 50 mM of compounds or vehicle control (0.1% DMSO). The percent of remaining contractile force was measured at various time points and expressed as a percent of the initial substance P induced contractile force. ($N > 6$) A 2way ANOVA was used to calculate significance with *($p < 0.05$), ** ($p < 0.01$) or *** ($p < 0.001$) p-values are given for each condition. All investigated compounds except RJ-03-57 reduced the constriction of airway smooth muscle after 15 minutes for a period of at least 60 minutes.

Example 19. Relaxation of human airway smooth muscle by compounds.

[00170] Human airway smooth muscle strips were dissected from human trachea obtained from healthy donor lungs incidental to lung transplantations. Studies were reviewed by the Columbia University Institutional Review Board (IRB) and deemed not to be human subject research. Strips were suspended as above in organ baths in oxygenated KH buffer at 37 °C at 1.5 g of resting tension. Following equilibration for 1 hour with buffer exchanges every 15 minutes, strips were contracted with 3 cycles of increasing concentrations of acetylcholine (100 nM - 1 mM) will extensive buffer exchanges between and after these pre-contractile challenges. MK571 (10 μM), pyrilamine (10 μM) and tetrodotoxin (1 μM) were added to the buffer before each strip was contracted to its individually calculated EC_{50} concentration of acetylcholine. When a plateau in the increase in contractile force was achieved (typically 15 minutes) 100 μM of compound or its vehicle (0.2% ethanol) was added to the buffer and the maintenance of contractile force was continuously measured over 1 hour. The remaining contractile force at 15, 30, 45 and 60 minutes was expressed as a percentage of the initial acetylcholine-induced contractile force. FIG 4 shows airway smooth muscle contractile force in human airway smooth muscle. Human tracheal airway smooth muscle strips were contracted with an EC_{50}

concentration of acetylcholine (Ach) and then treated with 100 μM of SH-053-2F'F-R-CH3-Acid or the vehicle 0.2% ethanol. Muscle force was measured at 15, 30, 45, and 60 minutes after addition of compound. Data are expressed as the percent of the initial Ach-induced contractile force. Individual muscle strips from at least seven humans were used. A 2way ANOVA was used to calculate significance with *($p < 0.05$), ** ($p < 0.01$) or *** ($p < 0.001$) p-values are given for each condition. SH-053-2F'F-R-CH3-Acid reduced the constriction of human airway smooth muscle after 15 minutes for a period of at least 60 minutes.

Example 20. Compound effects on allergen-induced mouse asthma model.

[00171] Drug treatment protocol: Sterile solutions of compounds were prepared in 2% hydroxypropyl methylcellulose solution (Sigma-Aldrich, St. Louis, MO) and 2.5% polyethylene glycol (Sigma Aldrich, St. Louis, MO) for oral administration in a biological safety cabinet. A fine suspension was obtained by grinding the mixture with a mortar and pestle. Drugs were administered individually at 100 mg/kg by oral gavage (200 ul) with 20G gavage needles (Kent Scientific Corporation, Torrington CT) to groups of ova s/c BALB/c twice daily for 5 days during the ova challenge period. Mice received a single p.o. dose of the compounds just before airway parameter measurements. Compounds for i.p. injection were prepared in 10% DMSO, 40% propylene glycol, and 50% PBS and given as 100 ul injection. Mice were monitored daily after drug administration. Assessment of Airway hyper-responsiveness: Airway hyper-responsiveness to methacholine in conscious, spontaneously breathing animals was measured by DSI's Buxco® FinePointe Non-Invasive Airway Mechanics (NAM) instrument. Before measurements were taken, mice were acclimated to the chambers 15 minutes daily for 5 days. In addition, an ovalbumin sensitization and challenge protocol consists of randomized male BALB/c mice that were sensitized three times with intra-peritoneal (i.p.) injections of 2 mg/ kg/ d of ovalbumin (Ova) (Sigma-Aldrich, St. Louis, MO) emulsified in 2 mg of Alum (Imject Alum; Thermo Scientific, Pierce, Rockford, IL) on days 0, 7 and 14 in a total volume of 100 μL. The mice were then challenged intra-nasally (i.n.) with 1 mg/ kg/ d Ova for 5 days from days 23–27. Control mice were sensitized with Ova and challenged with saline. The chambers were also calibrated each time before data collection. Briefly, the nasal chamber in combination with the thoracic chamber allows the computation of specific airway resistance (sRaw). The FinePointe

software computes specific airway resistance (sRaw) with all other ventilatory parameters derived by the NAM analyzer. Mice were exposed to aerosolized PBS (for the baseline measurement) or methacholine (1.5625-12.5 mg/mL) for 1 minute and readings were taken and averaged for 3 minutes after each nebulization. Data obtained were presented as sRaw versus the methacholine concentration (mg/mL) used to generate the aerosol. FIG. 5A-5F show compound effects on airway hyperresponsiveness. Specific airway resistance (sRaw) was measured at increasing dosages of methacholine by a DSI's Buxco FinePointe non-invasive airway mechanics instrument. Ova s/c BALB/c mice were administered all compounds via oral gavage, 100 mg/kg twice daily for 5 days. Data represent mean ± SEM from 10 mice in each group. *, **, and *** indicate $p < 0.05$, $p < 0.01$, $p < 0.001$ significance, respectively, compared to vehicle treated ova s/c BALB/c mice. Compounds RJ-03-57, RJ-03-30 and GL-III-43 were not able to alleviate airway hyperresponsiveness. However, compounds SH-053-2F'F-R-CH3-Acid, GL-II-93 and RJ-02-50 reduced airway hyperresponsiveness at one or multiple concentrations of methacholine.

Example 21. Pharmacokinetic analysis of compounds.

[00172] Determination of pharmacokinetic parameters in mice. Female Swiss Webster mice received intra-gastric gavage of vehicle or compound formulated in 2% hydroxypropyl methylcellulose solution and 2.5% polyethylene glycol at a dose of 25 mg/kg. At 10, 20, 40 60,120, 240, 480 and 1440 minutes, the blood (collected into heparinized tubes), lungs and brain were harvested and samples stored in liquid nitrogen until analysis. Sample preparation and LC/MS: Blood samples were thawed on ice, vortexed for 10 seconds, and a 100 µL aliquot was taken and added to 400 µL cold acetonitrile containing [100 nM 4,5-diphenyl imidazole, 100 nM HZ-166, RJ-02-50 or SH-053-2'RCH3-Acid] internal standard (I.S.). Samples were vortexed for 30 seconds and centrifuged at 10,000 RPM for 10 minutes. The supernatant layer was then transferred to clean tubes and evaporated using Speedvac concentrator. The residue was reconstituted with 400 µL of mobile phase and spin-filtered through 0.22 µm nylon centrifugal filter units (Costar). After reconstitution, the samples are properly diluted, verapamil or 4,5-diphenyl imidazole was added and 5 µL of the sample was injected to the LC–MS/MS. Brain and lung tissue samples were thawed, weighed, and homogenized directly into 400 µL acetonitrile

containing I.S. using a Cole Palmer LabGen 7B Homogenizer. Samples were centrifuged for 10 minutes at 10,000 RPM. The supernatant was then retrieved, and prepared in the same manner as the blood samples for LC-MS/MS analysis. High performance liquid chromatography (HPLC) was performed with Shimadzu Nexera X2 LC30AD series pumps (Shimadzu, Kyoto, Japan). Analytes were separated by a Restek Pinnacle II C18 column (2.1 mm × 100 mm, 5 µm particle size, Restek, California, US) under gradient elution at a flow rate of 0.5 mL/minute (SH-053-2'R-CH3-Acid), 0.4 mL/minute (RJ-02-50), and 0.6 mL/min (RJ-03-57 and GL-II-93). The mobile phase was acetonitrile or methanol and water (both containing 0.1% formic acid). Time program: 20% B → 70% B (3 minutes) →99% B (5 minutes), hold at 99% B (8 minutes), return to 10% B (9 minutes), hold (9.5 minutes) (SH-053-2'R-acid), 70% B → 70% B (6 minutes) (Isocratic for SH-053-2'F-R-CH3-Acid), 20% B → 70% B (2 min) →99% B (4 min), hold at 99% B (4.5 min), return to 20% B (4.75 min), hold (5 min) (RJ-03-57) and 20% B → 70% B (2 min) →99% B (5 min), hold at 99% B (5.5 min), return to 20% B (5.75 min), hold (6 min) (GL-II-93) at a column temperature: 40 °C. Analytes were monitored under positive mode by Shimadzu 8040 triple quadrupole mass analyzer (Shimadzu, Kyoto, Japan) electrospray and atmospheric pressure ionization run in dual (DUIS) mode. The following transitions are monitored in multiple reaction monitoring (MRM) mode. Ion pairs for RJ-02-50 are m/z 327.85 > 281.95, m/z 327.85 >264.05, m/z 327.85 > 254.10, m/z 327.85 > 236.80 and m/z 327.85 > 212.75. Transition ion pairs for SH-053-2'F-R-CH3-Acid are m/z 360.0 > 342.10, m/z 360.0 > 316.00, m/z 360.0 > 301.10, m/z 360.0 > 249.05 and m/z 360.0 > 219.90. Transition pairs for HZ-166 are m/z 356.90 > 311.15, m/z 356.90 > 283.15, and m/z 356.90 > 282.15. Transition pairs for 4,5-diphenyl imidazole are m/z 220.80 > 193, m/z 220.80 > 167, m/z 220.80 >151.95 and m/z 220.80 > 115 transition pairs for verapamil (internal standard) are m/z 454.70 > 165.05, m/z 454.70 > 150 and m/z 454.70 > 303.0. Transition pairs for RJ-03-57 are m/z 337.85 > 265.95, m/z 337.85 > 252.05, m/z 337.85 > 238.0, 337.83 > 224.95 and m/z 337.85 > 209.85. Transition pairs for GL-II-93 are m/z 413.90 > 396, m/z 413.90 > 368, m/z 413.90 > 355.05, m/z 413.90 > 302.95, m/z 413.90 > 326.80, m/z 413.90 > 276.05, and m/z 413.90 > 248.20. Collision energy is optimized for each transition to obtain optimal sensitivity. The mass spectrometer was operated with the heat block temperature of 400°C, drying gas flow of 15 L/minute, desolvation line temperature of 250°C, nebulizing gas flow of 1.5 L/minute, and both needle and interface voltages of 4.5 kV. The response acquisition was performed using LabSolutions software.

Standard curves were fitted by a linear regression and the validation samples were calculated back by the calibration curve of that day. The mean and the coefficient of variance (CV) were calculated accordingly. Accuracy was calculated by comparing calculated concentrations to corresponding nominal. Pharmacokinetic parameters were calculated with PK solutions software 2.0 and fitted to the following equation: $c = A \cdot e^{-\alpha t} + B \cdot e^{-\beta t} + C \cdot e^{-\gamma t}$. FIGs 6A-6D show pharmacokinetic profiles of compounds in mice blood, lungs, and brain. Time-dependent systemic distribution of compounds administered at 25 mg/kg via oral gavage. RJ-02-50, SH-053-2F'F-R-CH3-Acid, and GL-II-93 exhibit excellent bioavailability in mouse, whereas RJ-03-57 has a moderate absorption and fast clearance.

Example 22. Changes of inflammatory cell numbers in mouse BALF by compounds.

[00173] Determination of anti-inflammatory properties of compounds were investigated in an allergen induced mouse model of asthma. At the day of analysis, bronchoalveolar lavage (BAL) was performed with 1 mL of Ca2+ and Mg2+ free PBS. Red blood cells (RBCs) were lysed using BD red blood cell lysis buffer (BD Pharmingen, San Jose, CA). BALF was split into four different tubes and non-specific binding to Fc receptors was blocked for 5 minutes using 6 µg/mL of 2.4G2 mouse BD Fc BlockTM (BD Pharmingen, San Jose, CA). BALF cells were stained for 30 minutes at 4°C in the dark with 100 µL BSA stain buffer (BD Pharmingen, San Jose, CA) containing the final concentrations of the following antibodies: anti-mouse CD45 APC (1:1000, 30-F11, Affymetrix eBiosciences, San Diego, CA), FITC rat anti-mouse CD4 (1:500, RM4-5, BD Pharmingen, San Jose, CA), PE Rat Anti-Mouse Siglec F (1:500, E50-2440, BD Pharmingen, San Jose, CA) and mouse CCR3 PE-conjugated antibody(1:40, 83101, R&D systems Inc, Minneapolis, MN). Flow cytometric studies were done using the BD FACS Calibur (BD Pharmingen, San Jose, CA) and data analyzed subsequently using Cell Quest pro software (BD Pharmingen, San Jose, CA). General gating for immune cells were followed. Total inflammatory cell count was obtained by running all samples on high (60 µL/min) for 180 seconds. The gated anti-mouse CD45 positive events in the fourth channel (FL4) were used to calculate the total inflammatory cell count as cells /mL. The frequencies of CCR3+/Siglec F were used for quantification of eosinophils and CD4+ for CD4+ T cell populations in their respective gates were multiplied by the total inflammatory cell count (cells/mL) to obtain the

differential cell population. Statistical analysis: Data were analyzed using GraphPad Prism 4 (GraphPad Software, San Diego, CA) and expressed as mean ± SEM. One-way analysis of variance (ANOVA) with Dunnet post hoc test or two-way ANOVA with Bonferroni post hoc test were performed for statistical difference for multiple groups. FIGs 7A-7C show effects of compounds on inflammatory cells. Groups of 10 ova s/c BALB/c mice were administered compounds at 100 mg/kg twice daily for 5 days. BALF was harvested from each animal and used for (A) quantification of total inflammatory cells; (B) eosinophils; (C) $CD4^+$ T cells. Cells were stained with mouse $CD45^+$ APC antibody, and samples were analyzed with BD FACS Calibur on high flow rate (60 µl/minute) for 180 seconds. The gated positive events in the fourth channel (FL4) were used to calculate the total inflammatory cell count as cells/ml. Quantification of specific leukocyte population (B) eosinophils (C) $CD4^+$ T cell populations were stained with specific antibodies and detected by flow cytometry. Data represent mean ± SEM from 10 mice in each group. *, **, and *** indicate $p < 0.05$, $p < 0.01$, and $p < 0.001$ significance, respectively, compared to vehicle treated ova s/c BALB/c mice. Compounds GL-II-43, RJ-03-30, RJ-03-90 did not modulate the numbers of inflammatory cells. However, RJ-02-50 and GL-II-93 did reduce the numbers of eosinophils and $CD4^+$ T cells in the asthmatic mouse lung. SH-053-2F'F-R-CH3-Acid reduced the numbers of eosinophils but not $CD4^+$ T cells.

Example 23. Electrophysiological measurement of $CD4^+$ T lymphocytes in the presence of compounds

[00174] To determine the effect of compounds on lymphocytes, $CD4^+$ T cells from Ova S/C mice were isolated and their interaction with compounds was measured by automated patch clamp. Splenocytes from ova s/c BALB/c mice were prepared following BD Biosciences instructions for preparation of murine splenocytes and red blood cell lysed using BD Pharm LyseTM lysing solution (BD Biosciences, San Jose, CA). Cells were maintained in suspension in RPMI 1640 medium with L-glutamine (Thermo Fisher Scientific Inc., Rockford, IL) supplemented with 10% (v/v) fetal bovine serum, 10 µM 2-mercaptoethanol and 1% penicillin/streptomycin in the presence or absence of 100 µg/mL ovalbumin. The cells were maintained in 5% CO_2, 95% humidified air at 37 °C for 48 hours. The IonFlux plate layout consists of units of 12 wells: two wells contain intracellular solution (ICS containing 346 mM

CsCl, 1 mM $CaCl_2$, 1 mM $MgCl_2$, 11 mM EGTA, 10 mM HEPES, pH 7.2 with CsOH), one contains cells diluted in extracellular solution (ECS containing 140 mM NaCl, 5 mM 349 KCl, 2 mM $CaCl_2$, 1 mM $MgCl_2$, 5 mM D-glucose monohydrate, and 10 mM HEPES, pH 7.4 with NaOH), eight contain the compounds of interest diluted in ECS, and one well is for waste collection. Cells are captured from suspension by applying suction to microscopic channels in ensemble recording arrays. Once the array is fully occupied, the applied suction breaks the membranes of captured cells, which establishes whole cell voltage clamp. For compound applications, pressure is applied to the appropriate compound wells, which introduces the compound into the extracellular solution rapidly flowing over the cells. For recording $GABA_AR$ induced currents, cell arrays were voltage clamped at a hyperpolarizing holding potential of −50 mV. Prior to use on the automated patch clamp, cells were centrifuged at 380g for 5 minutes and resuspended gently in ECS. This was repeated two more times before the cells were dispensed into the plate. GABA and muscimol were diluted to appropriate concentrations in ECS to appropriate concentrations before application and data recorded. FIG. 8 shows current recordings in the presence of 600 nM GABA and increasing concentrations of compounds applied together for 3 seconds using CD4+ T-cells isolated from ova s/c BALB/c mice spleen. The concentration-dependent current responses of CD4+ T-cells in the presence of 600 nM GABA and increasing concentration of compounds were carried out with an N of 16 and normalized to the current response of 600 nM GABA. Compound RJ-02-50 potentiated the GABA-induced membrane current more than SH-053-2F'F-R-CH3-Acid. Importantly, GL-II-93 and RJ-03-30 evoked a very pronounced GABA-induced transmembrane current.

Example 24. In vivo modulation of lung cytokine expression by compounds

[00175] Anti-inflammatory properties of compounds in respect to cytokine production were investigated after the AHR measurement by harvesting the lungs of treated and non-treated Ova S/C mice (N = 10). Whole lungs were homogenized in 200 µL of T-PER® tissue protein extraction reagent (Thermo Fisher Scientific Inc., Rockford, IL) containing 1X protease inhibitor cocktail using a hand-held tissue homogenizer. Homogenized lung samples were centrifuged at 10,000 RPM for 5 minutes to pellet cell/tissue debris. Tissue supernatant was collected for cytokine analysis using BD cytometric bead array mouse Th1/Th2/Th17 cytokine kit (BD

Biosciences, San Jose, CA) following manufacturer's instruction. Data were analyzed using GraphPad Prism 4 (GraphPad Software, San Diego, CA) and expressed as mean ± SEM. One-way analysis of variance (ANOVA) with Dunnet post hoc test was performed for statistical difference for multiple groups. FIG. 9 shows quantification of cytokine levels in the mouse lung. Among the cytokines tested IL-10, IL-17A, TNF-α and IL-4 were expressed significantly higher in the lungs of ova s/c mice in comparison to normal BALB/c mice. Data represent mean ± SEM from 10 mice in each group. *, **, and *** indicate $p < 0.05$, $p < 0.01$, and $p < 0.001$ significance. The ova s/c mice expressed higher levels of IFN-γ, IL-6, and IL-2 but the change was not significant in comparison to normal mice. Ova s/c mice treated with GL-II-93 exhibited reduced the levels of IL-17, TNFα, and IL-4 in the mouse lung.

Example 25. Absence of mucus hypersecretion modulation by compounds

[00176] Pharmacodynamic effects of compounds in respect to mucus production were investigated after the AHR measurement by harvesting the lungs of treated and non-treated Ova S/C mice followed by formalin fixation and paraffin embedding. Sections were prepared from one lobe (including large and small airways) and processed for standard H&E (for general histopathology and inflammation) and PAS (for mucous cell; as cells/mm of basement membrane) staining. FIGs 10A-10B show compound effects on mucin production: (A) Morphometric quantification of mucin volume density and (B) representative images of mucin (red) in the airway epithelium (green) with periodic acid fluorescent Schiff's stain. Balb/c mice were administered compounds at 100 mg/kg twice for five days. Data represent mean ± SEM from 5-7 mice in each group. Scale bar represents 100 μm. GL-II-93, RJ-02-50 and SH-053-2'F-R-CH3 Acid did not change the production of mucin.

Example 26. Inhibition of lung cell proliferation by compounds

[00177] ASM hyperplasia was determined by incooperation of EdU into the DNA of newly formed cells. Herein, at the end of the ovalbumin sensitization and challenge protocol, mice received a single i.p. injection of EdU (Invitrogen, Carlsbad, CA) at a dose of 100 mg/kg. Mice were euthanized 4 hours after injection and the lungs formalin fixed, harvested and paraffin embedded. 6 μm sections of formalin fixed and paraffin embedded lung sections were mounted

onto Fisher Superfrost Plus Slides. EdU staining was conducted using Click-iT™ EdU imaging kit (Invitrogen, Carlsbad, CA) according to manufacturer's instructions. Briefly lungs were deparaffinized in histoclear and rehydrated in graded ethanol. Tissue sections were washed twice with 3% bovine serum albumin (BSA) in PBS and permeablized with 0.5% Triton X-100 in PBS for 20 minutes. The sections were again washed twice with 3% BSA in PBS and then incubated with a Click-iT™ reaction cocktail containing Click-iT™ reaction buffer, CuSO4, Alexa Fluor® 488 Azide, and reaction buffer additive for 30 minutes in the dark. The sections were washed once more with 3% BSA in PBS. For DNA staining, sections were washed once with PBS and then incubated with 5 μg/mL Hoechst 33342 for 30 minutes. The slides were then washed twice with PBS and coverslipped with Permount mounting media. All steps were carried out at room temperature. FIG. 11 shows proliferation of lung cells. Lung sections of non-treated and GL-II-93 treated Ova s/c mice were analyzed for the incooperation of EdU, a thymidine analog that can be visualized after click chemistry with a fluorescent azide. For the negative control EdU was not injected resulting in no visible fluorescence. Non-treated Ova S/C mice showed a high proliferation rate in comparison to GL-II-93 treated animals. Nuclei specific Hoechst 33342 stain ensure similar cell density between the two sections that are compared in Figure 11.

Example 27. Virus-induced asthma model.

[00178] Efficacy of $GABA_AR$ compounds in chronic lung disease will be studied in a virus induced asthma model. C57BL/6 mice (at 6-20 weeks of age; groups of 10) will be inoculated intranasally with 2x105 pfu SeV (Strain 52; ATCC) or UV-inactivated SeV (UV-SeV) (69), at day 0. Mice are monitored daily for weight and activity; with chronic disease being well established by day 49 post-inoculation (P-I). Four experimental groups will be arranged, with test compound (or vehicle) administered i.p. during days 49-56 P-I. For prophylactic studies, treatment would be administered during days 13-21, followed by disease measurement at days 49-56; to model a dosing regimen that corresponds to childhood treatment following RSV exposure (thus, investigating if immune modulation early after viral infection or during the acute post-infection phase can influence development of later inflammatory lung disease). Serial non-invasive AHR measurements (sRAW) in response to methacholine will be measured in all Groups on days 13, 49, and 56 PI. Following AHR measurements on day 56, animals will be euthanized and BALF, blood, and tissue samples will obtained. BALF will be collected in 1 ml

PBS, centrifuged, and the cell supernatants collected for cytokine analysis as above. The cell pellet will be resuspended in RPMI and samples taken for differential cell counts (Diff-Quik) and flow cytometry. For flow cytometry, cell preparations will be stained with fluorophore labeled monoclonal antibodies to mouse CD1d (Invitrogen) and Mac-3 (BD) for M2 macrophages or CD3 and NK1.1 (both Invitrogen) for NKT cells. Antibody labeled cells will be examined with a FACS Calibur instrument (BD Biosciences) and data analyzed with FlowJo software (Tree Star, Ashland, OR) (69, 70, 84). All other lung tissue and biochemical testing will be performed and data analyzed as in the OVA model.

Example 28. Chronic Obstructive Pulmonary Disease (COPD) Model.

[00179] Efficacy of $GABA_AR$ compounds will be studied by lipopolysaccharide (LPS) lung challenge in mice as a model of human COPD. LPS is a proinflammatory stimulant that is present as a contaminant in cigarette smoke, air pollution, and organic dusts. In humans, chronic exposure to LPS-laden dusts results in decreased lung function. In the acute model, LPS induces a mixed inflammatory reaction with increases in neutrophils and increased tumor necrosis factor (TNF), IL-1, and other mediators in brochoalveolar fluid. Prior to administration, each test compound is diluted in a buffer solution vehicle (phosphate buffered saline, pH 7.4) and filter sterilized. Test compound is administered i.p. in a total volume of 100 ul, in each of the indicated days (thus 3 doses). Approximately one hour after the final i.p. compound administration, mice receive LPS intratracheally using a non-surgical procedure. Mice are first anesthetized by subcutaneous (s.c.) injection with ketamine hydrochloride and xylazine hydrochloride solution (Cat. no. K113; Sigma; 50 mg/kg ketamine HCl). LPS (Cat. no. L2880; Sigma, type O55:B5), dissolved in 50 µL sterile 0.9% NaCl, is instilled intratracheally (i.t.) (20 µg LPS/mouse) via a cannula and syringe (2×25 µl), followed by 100 µl air. Sham-treated mice are instilled i.t. with 50 µL sterile 0.9% NaCl. After i.t. treatment, mice are kept in an upright position for 10 minutes to allow the fluid to spread throughout the lungs. Mice are allowed to recover from anesthesia and the sacrificed 24 hours after using cervical CO_2 asphyxiation. Blood is collected via heart puncture in EDTA-containing tubes, immediately centrifuged (2000×g, 10 minutes, 4°C) and plasma was stored at −80°C. Lungs tissue is removed and snap-frozen for RNA-isolation and MPO analysis. For immunohistochemical analyses lung tissue is placed in 10% phosphate-buffered formalin (pH 7.4).

Example 29. Immune Arthritis Model.

[00180] Groups of 8-10 male DBA/1j mice (Jackson Laboratories, Bar Harbor, ME, USA) 8–10 weeks of age are immunized with 200 mg bovine collagen II (bCII, Chondrex, Redmond, WA, USA) in 50% complete Freund's adjuvant intradermally at the base of the tail. Mice are similarly boosted 21 days later with 100 mg of bCII in incomplete Freund's adjuvant. Groups of control mice are treated with sham immunizations without bCII. Food and water consumption, body weights, as well as clinically observable joint inflammation are measured throughout the treatment course. Beginning after the initial immunization, mice are administered $GABA_A$ receptor agents of the instant invention 3 times per week for 8 weeks. Compound dosing will be determined as described in Example 22. Serum collagen-specific IgG, IgG1, and IgG2a antibodies in individual control and experimental mice 8 weeks after the final immunization are characterized by microtiter plate ELISA. In the ELISA bCII is used as antigen for coating the plate wells and isotype-specific, fluorophore-conjugated rabbit anti-mouse antibodies are used to quantify primary antibody binding. Wells in the ELISA plates are read using a standard fluorescent plate reader. Compound efficacy will be evidenced by reduction of clinical joint inflammation and/or reduction in IgG antibody titers to bCII in the treated in comparison to control mice.

Example 30. Autoimmune Diabetes Model

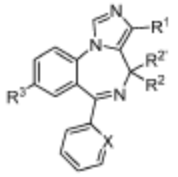
[00181] Non-obese diabetic (NOD) mice have been used for 30 years in the study of diabetes. NOD mice are characterized by insulitis, a leukocytic infiltrate of the pancreatic islets. Decreases in pancreatic insulin content occur spontaneously in females at about 12 weeks of age and several weeks later in males. Diabetic mice are hypoinsulinemic and hyperglucagonemic, indicating a selective destruction of pancreatic islet beta cells. Compounds of the instant invention are dosed QD or BID for 28 days via one of the route of administration (PO, IP, IM, SC); control animals are similarly given vehicle doses. Doses are determined as described in Example 22. 8-10 mice are assigned per group. Animals are monitored twice per week for body weight, food consumption, water intake, and blood or urine glucose, are measured. Urine glucose can be determined using commonly available test strips (Bayer Diastix). Efficacy of compounds

is evidenced by reduction in one or more of these clinical markers in the treated versus the control groups.

[00182] All patents, publications and references cited herein are hereby fully incorporated by reference. In case of conflict between the present disclosure and incorporated patents, publications and references, the present disclosure should control.

We claim:

1. A compound of formula (I), or a pharmaceutically acceptable salt thereof,



(I)

wherein:

R^1 is COOH, a carboxylic ester, a carboxylic acid isostere, or a carboxylic ester isostere;

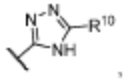
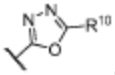
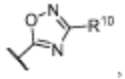
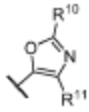
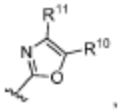
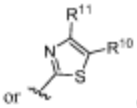
X is C–H, C–F, C–Cl, C–Br, C–I, C–CF_3, or N;

R^2 and $R^{2'}$ are each independently H, D, C_{1-4} alkyl, CD_3, F, Cl, CF_3, CCl_3, or cyclopropyl; or R^2 and $R^{2'}$ together form an optionally substituted ring; and

R^3 is H, F, Cl, Br, CF_3, CHF_2, –OCF_3, –$OCHF_2$, CN, OH, –OC_{1-4}alkyl, –C≡CH, or cyclopropyl;

provided that

R^3 is OH when R^1 is a carboxylic ester or a carboxylic ester isostere;

R^1 is not a carboxylic amide, a carboxylic thioester,  ,  ,  ,  ,  , or  , wherein R^{10} and R^{11} are independently H or C_{1-6}alkyl, when R^3 is –C≡CH;

R^1 is not COOH when R^3 is –C≡CH; and

R^1 is not COOH, a carboxylic ester, a carboxylic amide, or a carboxylic thioester when R^2 and $R^{2'}$ are both H; X is C–H, C–F, C–Br, or C–I; and R^3 is H, F, Cl, or Br.

2. The compound of claim 1, or a pharmaceutically acceptable salt thereof, wherein X is C–H, C–F, C–Cl, C–Br, C–I, or N.

3. The compound of claim 2, or a pharmaceutically acceptable salt thereof, wherein X is C–H, C–F, C–Cl, C–Br, or N.

4. The compound of any of claims 1-3, or a pharmaceutically acceptable salt thereof, wherein:
R^2 and $R^{2'}$ are each independently H, C_{1-4} alkyl, F, Cl, CF_3, CCl_3, or cyclopropyl; or R^2 and $R^{2'}$ together form a ring.

5. The compound of any of claims 1-3, or a pharmaceutically acceptable salt thereof, wherein:
R^2 and $R^{2'}$ are each independently H, C_{1-4} alkyl, F, Cl, CF_3, or CCl_3; or R^2 and $R^{2'}$ together form a ring.

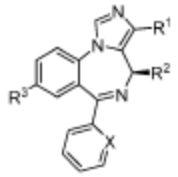
6. The compound of any of claims 1-3, or a pharmaceutically acceptable salt thereof, wherein:
R^2 and $R^{2'}$ are each independently H, D, CH_3, CD_3, CF_3, or cyclopropyl; or R^2 and $R^{2'}$ together form a C_{3-6}cycloalkyl.

7. The compound of any of claims 1-6, or a pharmaceutically acceptable salt thereof, wherein R^3 is H, F, Cl, Br, OH, OCH_3, –C≡CH, or cyclopropyl.

8. The compound of any of claims 1-7, or a pharmaceutically acceptable salt thereof, wherein R^3 is OH.

9. The compound of any of claims 1-7, or a pharmaceutically acceptable salt thereof, wherein R^3 is H, F, Cl, OCH_3, or –C≡CH.

10. The compound of any of claims 1-9 of formula (I-A), or a pharmaceutically acceptable salt thereof,

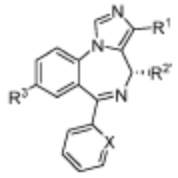


(I-A);

wherein R^2 is D, C_{1-4} alkyl, CD_3, F, Cl, CF_3, CCl_3, or cyclopropyl.

11. The compound of claim 10, or a pharmaceutically acceptable salt thereof, wherein R^2 is D, CH_3, CD_3, CF_3, or cyclopropyl.

12. The compound of any of claims 1-9 of formula (I-B), or a pharmaceutically acceptable salt thereof,

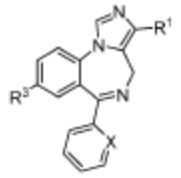


(I-B);

wherein $R^{2'}$ is D, C_{1-4} alkyl, CD_3, F, Cl, CF_3, CCl_3, or cyclopropyl.

13. The compound of claim 12, or a pharmaceutically acceptable salt thereof, wherein $R^{2'}$ is D, CH_3, CD_3, CF_3, or cyclopropyl.

14. The compound of any of claims 1-9 of formula (I-C), or a pharmaceutically acceptable salt thereof,



(I-C).

15. The compound of claim 1, or a pharmaceutically acceptable salt thereof, wherein:

X is C–H, C–F, C–Cl, C–Br, C–I, or N;

R^2 is C_{1-4} alkyl, CD_3, F, Cl, CF_3, CCl_3, or cyclopropyl;

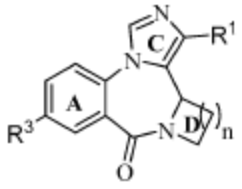
$R^{2'}$ is H or D; and

R^3 is H, F, Cl, Br, OH, OCH_3, –C≡CH, or cyclopropyl.

16 The compound of claim 15, or a pharmaceutically acceptable salt thereof, wherein

R^2 is C_{1-4} alkyl.

17. A compound of formula (II), or a pharmaceutically acceptable salt thereof,



(II)

wherein:

R^1 is COOH, a carboxylic ester, a carboxylic acid isostere, or a carboxylic ester isostere;

n is 1 or 2; and

R^3 is H, F, Cl, Br, CF_3, CHF_2, $–OCF_3$, $–OCHF_2$, CN, OH, $–OC_{1-4}$alkyl, –C≡CH, or cyclopropyl;

provided that R^3 is OH when R^1 is COOH, a carboxylic ester, a carboxylic amide, or a carboxylic thioester.

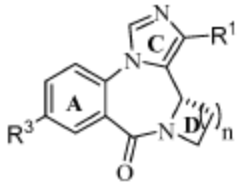
18. The compound of claim 17, or a pharmaceutically acceptable salt thereof, wherein R^3 is H, F, Cl, Br, OH, $-OCH_3$, $-C\equiv CH$, or cyclopropyl.

19. The compound of claim 17, or a pharmaceutically acceptable salt thereof, wherein R^3 is H, F, Cl, Br, OCH_3, $-C\equiv CH$, or cyclopropyl.

20. The compound of claim 17, or a pharmaceutically acceptable salt thereof, wherein R^3 is H, F, Cl, OCH_3, or $-C\equiv CH$.

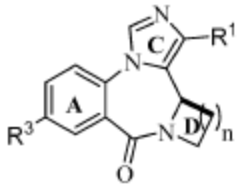
21. The compound of claim 17, or a pharmaceutically acceptable salt thereof, wherein R^3 is OH.

22. The compound of any of claims 17-21 of formula (II-A), or a pharmaceutically acceptable salt thereof



(II-A).

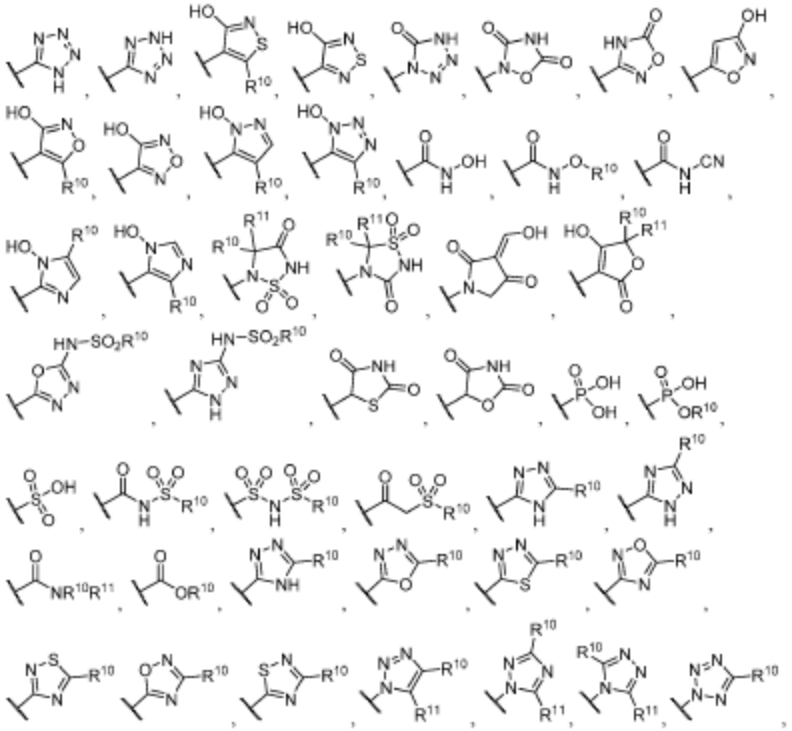
23. The compound of any of claims 17-21 of formula (II-B), or a pharmaceutically acceptable salt thereof

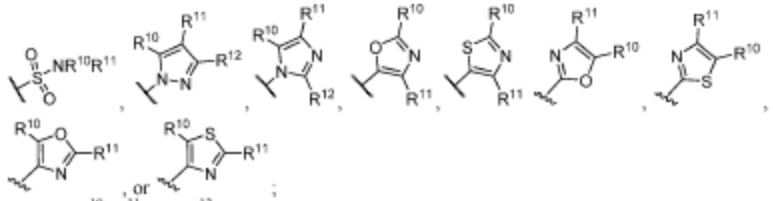


(II-B).

24. The compound of any of claims 1-23, or a pharmaceutically acceptable salt thereof, wherein R^1 is a carboxylic acid isostere.

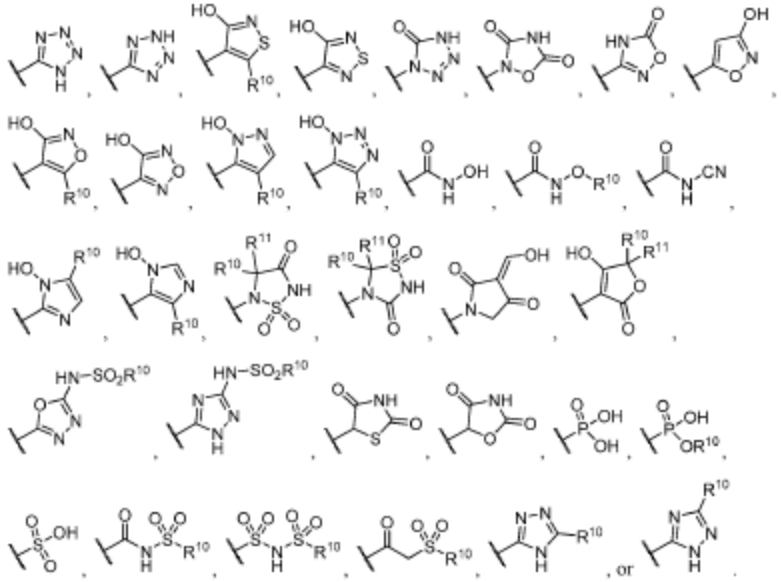
25. The compound of any of claims 1-23, or a pharmaceutically acceptable salt thereof, wherein R^1 is



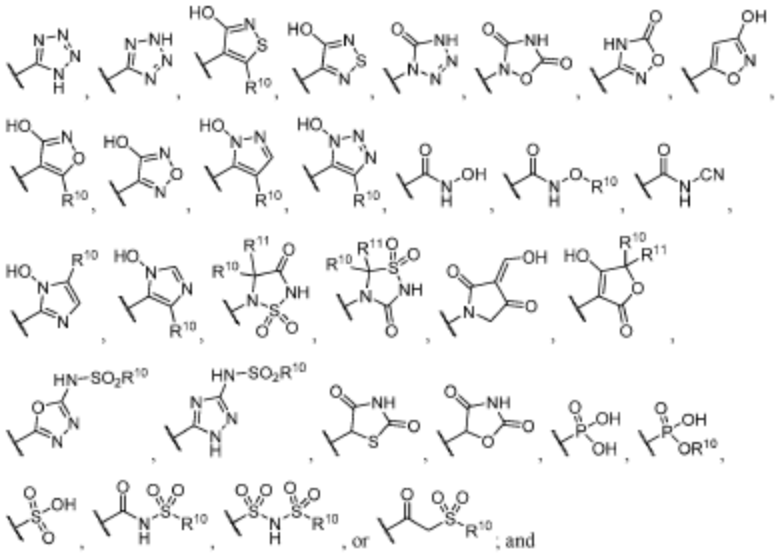


wherein R^{10}, R^{11}, and R^{12} are independently selected from –H, -D or C_{1-6}straight or cyclic saturated or substituted alkyl group.

26. The compound of claim 25, or a pharmaceutically acceptable salt thereof, wherein R^1 is



27. The compound of claim 25, or a pharmaceutically acceptable salt thereof, wherein R^1 is



R^{10} and R^{11} are independently selected from H, C_{1-6}alkyl, or C_{1-6}cycloalkyl.

28. A compound selected from the group consisting of

(R)-8-ethynyl-6-(2-fluorophenyl)-4-methyl-4H-benzo[f]imidazo[1,5-a][1,4]diazepine-3-carboxylic acid; 1

(R)-8-bromo-6-(2-fluorophenyl)-4-methyl-4H-benzo[f]imidazo[1,5-a][1,4]diazepine-3-carboxylic acid; 2

(R)-8-cyclopropyl-6-(2-fluorophenyl)-4-methyl-4H-benzo[f]imidazo[1,5-a][1,4]diazepine-3-carboxylic acid; 3

(R)-8-chloro-6-(2-fluorophenyl)-4-methyl-4H-benzo[f]imidazo[1,5-a][1,4]diazepine-3-carboxylic acid; 4

(R)-8-bromo-4-methyl-6-(pyridin-2-yl)-4H-benzo[f]imidazo[1,5-a][1,4]diazepine-3-carboxylic acid; 6

(R)-8-ethynyl-4-methyl-6-(pyridin-2-yl)-4H-benzo[f]imidazo[1,5-a][1,4]diazepine-3-carboxylic acid; 6

(S)-7-methoxy-1-(1H-tetrazol-5-yl)-11,12,13,13a-tetrahydro-9H-benzo[e]imidazo[5,1-c]pyrrolo[1,2-a][1,4]diazepin-9-one; 7

(S)-N,7-dimethoxy-9-oxo-11,12,13,13a-tetrahydro-9H-benzo[e]imidazo[5,1-c]pyrrolo[1,2-a][1,4]diazepine-1-carboxamide; 8

(S)-N-cyano-7-methoxy-9-oxo-11,12,13,13a-tetrahydro-9H-benzo[e]imidazo[5,1-c]pyrrolo[1,2-a][1,4]diazepine-1-carboxamide; 9

ethyl (S)-7-hydroxy-9-oxo-11,12,13,13a-tetrahydro-9H-benzo[e]imidazo[5,1-c]pyrrolo[1,2-a][1,4]diazepine-1-carboxylate; 10

(S)-7-hydroxy-9-oxo-11,12,13,13a-tetrahydro-9H-benzo[e]imidazo[5,1-c]pyrrolo[1,2-a][1,4]diazepine-1-carboxylic acid; 11

(S)-7-hydroxy-1-(oxazol-5-yl)-11,12,13,13a-tetrahydro-9H-benzo[e]imidazo[5,1-c]pyrrolo[1,2-a][1,4]diazepin-9-one; and 13

tert-butyl (S)-7-hydroxy-9-oxo-11,12,13,13a-tetrahydro-9H-benzo[e]imidazo[5,1-c]pyrrolo[1,2-a][1,4]diazepine-1-carboxylate; 12

or a pharmaceutically acceptable salt thereof.

29. A pharmaceutical composition comprising the compound of any of claims 1-28, or a pharmaceutically acceptable salt thereof, and a pharmaceutically acceptable carrier.

30. A method of reducing airway constriction comprising administering an effective amount of the compound of any of claims 1-28, or a pharmaceutically acceptable salt thereof, or the pharmaceutical composition of claim 29 to a subject in need thereof.

31. A method of reducing lung inflammation comprising administering an effective amount of the compound of any of claims 1-28, or a pharmaceutically acceptable salt thereof, or the pharmaceutical composition of claim 29 to a subject in need thereof.

32. A method of reducing development of disease in a subject having risk factors associated with lung inflammation comprising administering an effective amount of the compound of any of claims 1-28, or a pharmaceutically acceptable salt thereof, or the pharmaceutical composition of claim 29 to a subject in need thereof.

33. A method of treating lung disease comprising administering an effective amount of the compound of any of claims 1-28, or a pharmaceutically acceptable salt thereof, or the pharmaceutical composition of claim 29 to a patient in need thereof.

34. A compound or pharmaceutical composition of any of claims 1-29, or a pharmaceutically acceptable salt thereof, for use in the manufacture of a medicament for reducing airway constriction, reducing lung inflammation, reducing development of risk factors associated with lung inflammation, or treating lung disease.

35. A compound or pharmaceutical composition of any of claims 1-29, or a pharmaceutically acceptable salt thereof, for use in reducing airway constriction, reducing lung inflammation, reducing development of risk factors associated with lung inflammation, or treating lung disease.

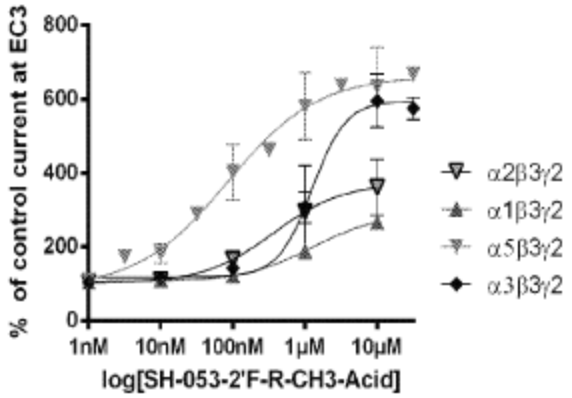

% of control current at EC3
800
600
400
200
0
1nM
10nM
100nM
1μM
10μM
log[SH-053-2'F-R-CH3-Acid]
α2β3γ2
α1β3γ2
α5β3γ2
α3β3γ2

FIG. 1A

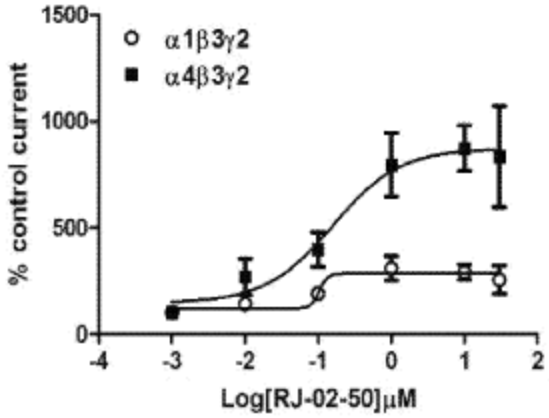

% control current
1500
1000
500
0
-4
-3
-2
-1
0
1
2
Log[RJ-02-50]μM
α1β3γ2
α4β3γ2

FIG. 1B

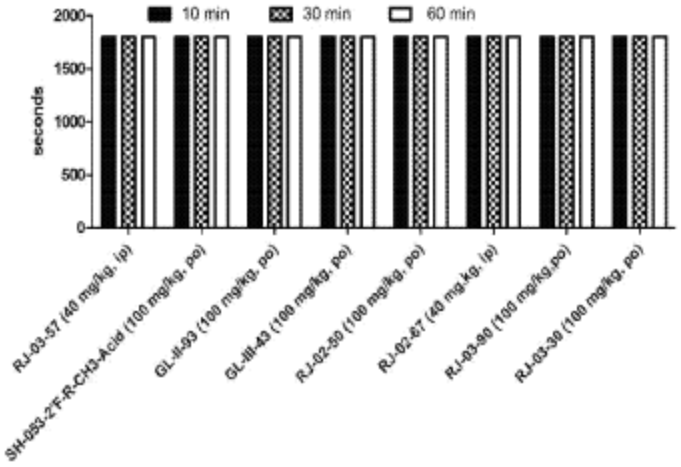

10 min
30 min
60 min
seconds
2000
1500
1000
500
0
RJ-03-57 (40 mg/kg, ip)
SH-053-2'F-R-CH3-Acid (100 mg/kg, po)
GL-II-93 (100 mg/kg, po)
GL-III-43 (100 mg/kg, po)
RJ-02-59 (100 mg/kg, po)
RJ-02-67 (40 mg/kg, ip)
RJ-03-90 (100 mg/kg,po)
RJ-03-38 (100 mg/kg, po)

FIG. 2

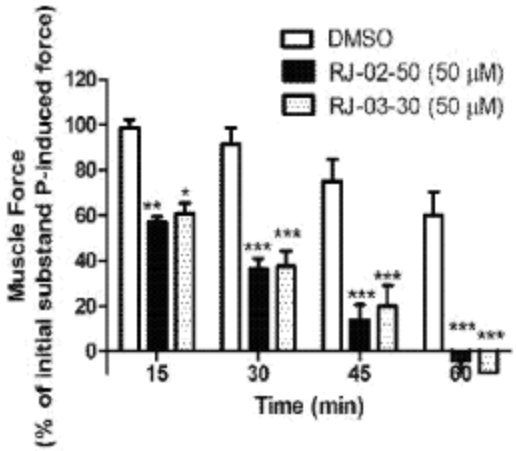

DMSO
RJ-02-50 (50 μM)
RJ-03-30 (50 μM)
Muscle Force
(% of initial substand P-induced force)
120
100
80
60
40
20
0
**
*
***
***
***
***
***
***
15
30
45
60
Time (min)

FIG. 3A

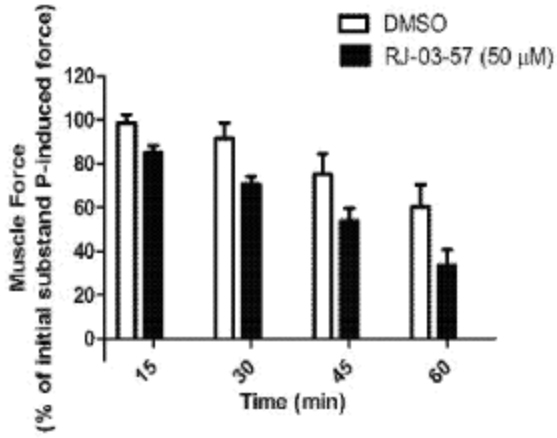

DMSO
RJ-03-57 (50 μM)
Muscle Force
(% of initial substand P-induced force)
120
100
80
60
40
20
0
15
30
45
60
Time (min)

FIG. 3B

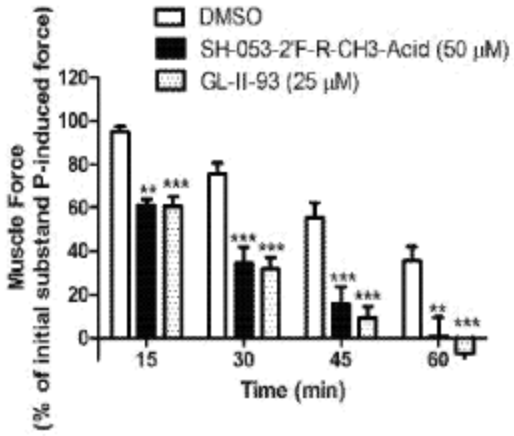

DMSO
SH-053-2'F-R-CH3-Acid (50 μM)
GL-II-93 (25 μM)
Muscle Force
(% of initial substand P-induced force)
120
100
80
60
40
20
0
**
***
***
***
***
***
**
***
15
30
45
60
Time (min)

FIG. 3C

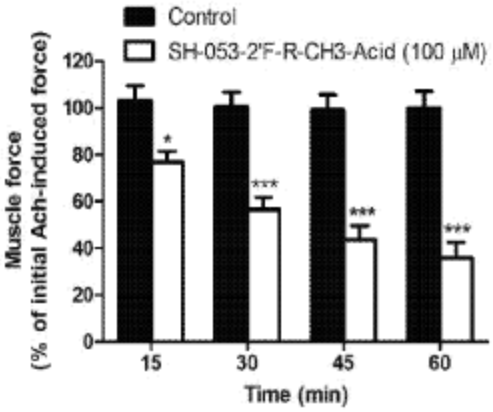

Control
SH-053-2'F-R-CH3-Acid (100 μM)
Muscle force
(% of initial Ach-induced force)
120
100
80
60
40
20
0
*
***
***
***
15
30
45
60
Time (min)

FIG. 4

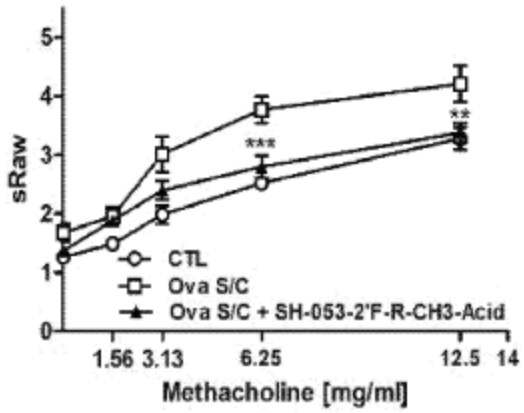

sRaw
Methacholine [mg/ml]
CTL
Ova S/C
Ova S/C + SH-053-2'F-R-CH3-Acid
***
**
1.56 3.13 6.25 12.5 14

FIG. 5A

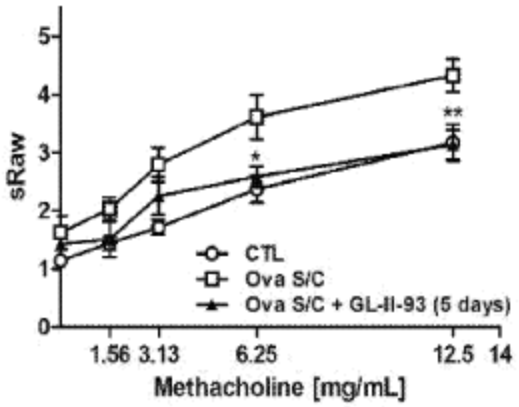

sRaw
Methacholine [mg/mL]
CTL
Ova S/C
Ova S/C + GL-II-93 (5 days)
*
**
1.56 3.13 6.25 12.5 14

FIG. 5B

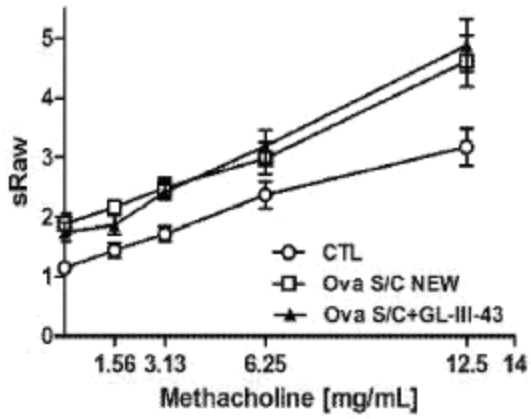

sRaw
0
1
2
3
4
5
1.56 3.13 6.25 12.5 14
Methacholine [mg/mL]
CTL
Ova S/C NEW
Ova S/C+GL-III-43

FIG. 5C

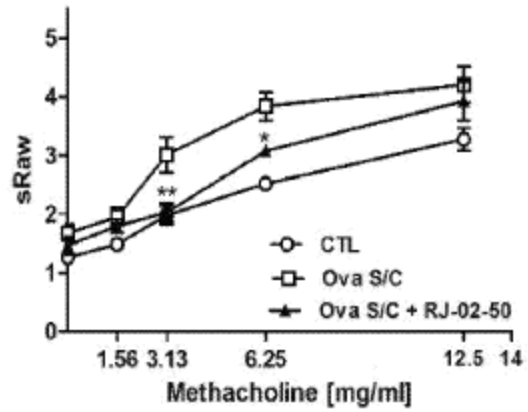

sRaw
0
1
2
3
4
5
**
*
1.56 3.13 6.25 12.5 14
Methacholine [mg/ml]
CTL
Ova S/C
Ova S/C + RJ-02-50

FIG. 5D

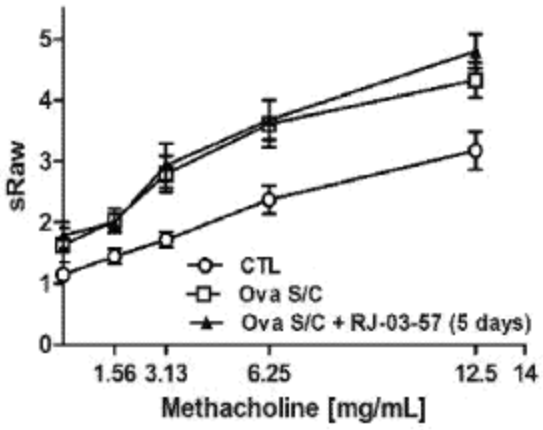

sRaw
5
4
3
2
1
0
CTL
Ova S/C
Ova S/C + RJ-03-57 (5 days)
1.56 3.13
6.25
12.5 14
Methacholine [mg/mL]

FIG. 5E

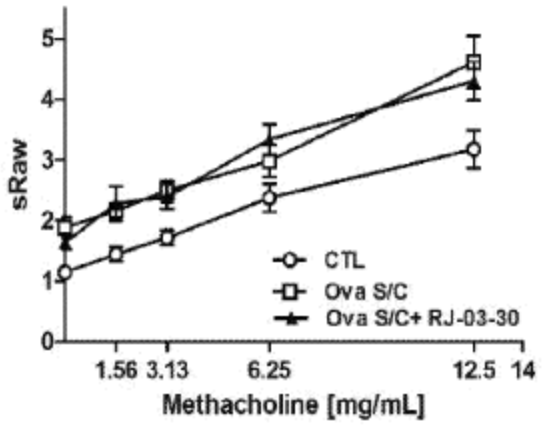
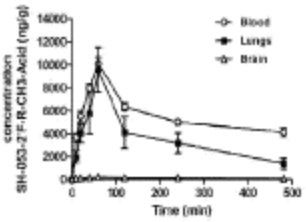

sRaw
5
4
3
2
1
0
CTL
Ova S/C
Ova S/C+ RJ-03-30
1.56 3.13
6.25
12.5 14
Methacholine [mg/mL]

FIG. 5F

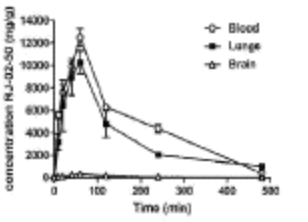
A



	Blood	Lung	Brain
t_{max} (min)	60	60	60
C_{max} (gg'g)	10.13	9.55	0.23
E_{xtz} (min^{-1})	0.0007	0.0034	0.0022
$t_{1/2}$ (min)	905	203	313
A_{exp} (min^{-1})	0.043	0.035	0.024
AUC_{0-t} (gg*min/g)	2648.9	1687.7	66.7

FIG. 6A

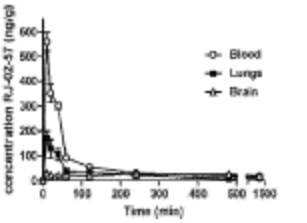
B



	Blood	Lung	Brain
t_{max} (min)	60	60	60
C_{max} (gg'g)	12.51	10.23	0.33
E_{xtz} (min^{-1})	0.010	0.003	0.004
$t_{1/2}$ (min)	70	238	159
A_{exp} (min^{-1})	0.014	0.046	0.039
AUC_{0-t} (gg*min/g)	2270.2	1640.4	56.3

FIG. 6B

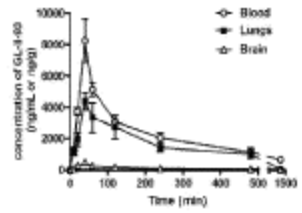
C



	Blood	Lung	Brain
t_{max} (min)	10	10	-
C_{max} (ng/g)	559.8	171.6	-
E_{xtz} (min^{-1})	0.019	0.012	-
$t_{1/2}$ (min)	37.4	59.0	-
A_{exp} (min^{-1})	0.147	0.063	-
AUC_{0-t} (ng*min/g)	47344	24584	-

FIG. 6C

D



	Blood	Lung	Brain
t_{max} (min)	40	40	40
C_{max} (μg/g)	8.24	4.39	0.48
E_{max} (min^{-1})	0.001	0.003	0.001
$t_{1/2}$ (min)	836	234	601
A_{TAS} (min^{-1})	0.027	0.035	0.030
AUC_{0-1} (μg*min/g)	2087.1	1390.5	107.7

FIG. 6D

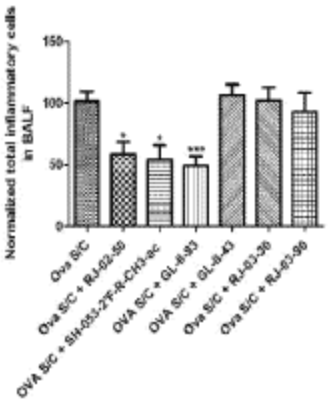


FIG. 7A

SUBSTITUTE SHEET (RULE 26)

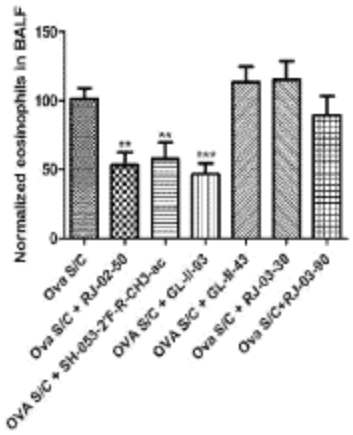

Normalized eosinophils in BALF
150
100
50
0
**
**
***
Ova S/C
Ova S/C + RJ-02-50
OVA S/C + SH-053-2'F-R-CH3-ac
OVA S/C + GL-II-93
OVA S/C + GL-II-43
Ova S/C + RJ-03-30
Ova S/C+RJ-03-90

FIG. 7B

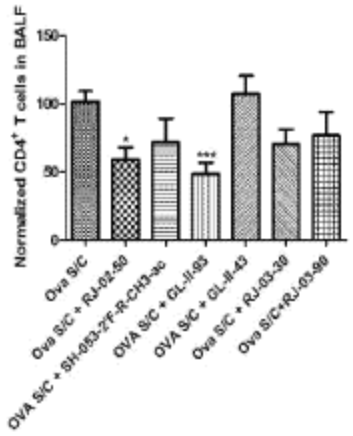

Normalized CD4+ T cells in BALF
150
100
50
0
*
***
Ova S/C
Ova S/C + RJ-02-50
OVA S/C + SH-053-2'F-R-CH3-ac
OVA S/C + GL-II-93
OVA S/C + GL-II-43
Ova S/C + RJ-03-30
Ova S/C+RJ-03-90

FIG. 7C

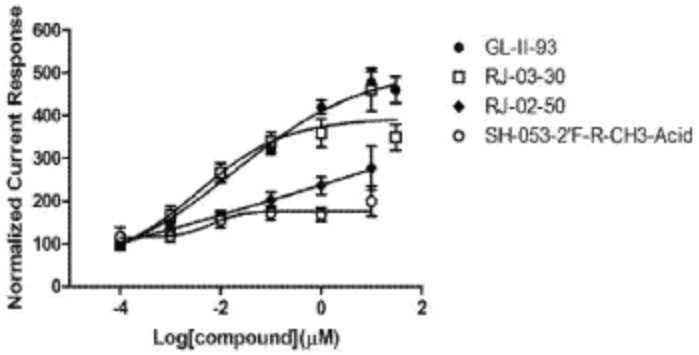

Normalized Current Response
600
500
400
300
200
100
0
-4
-2
0
2
Log[compound](μM)
GL-II-93
RJ-03-30
RJ-02-50
SH-053-2'F-R-CH3-Acid

FIG. 8

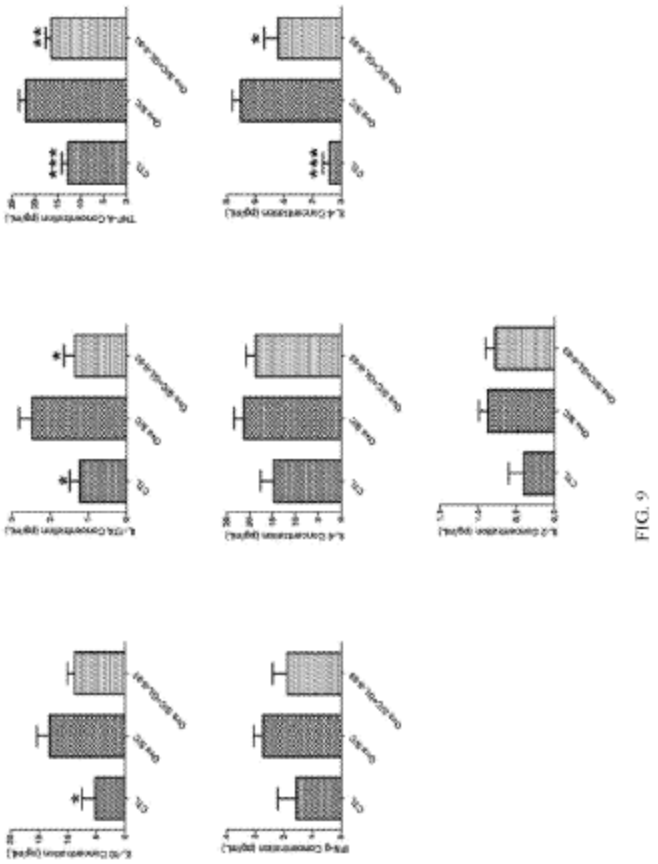


FIG. 9

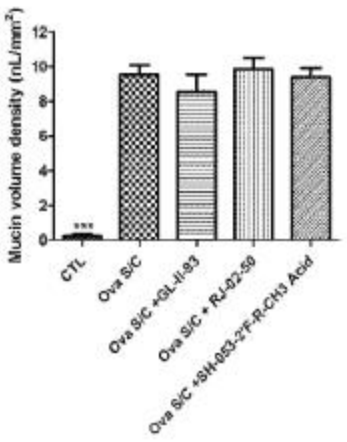


FIG. 10A

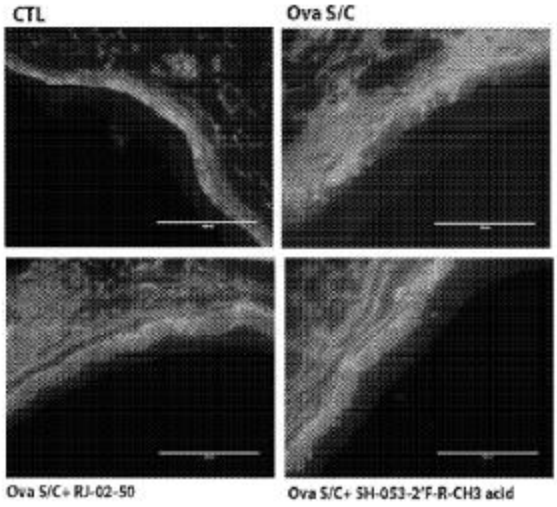


FIG. 10B

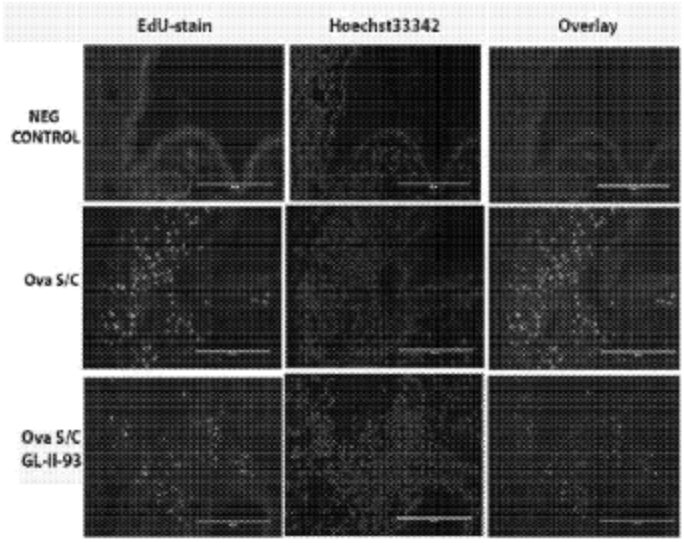

EdU-stain
Hoechst33342
Overlay
NEG CONTROL
Ova S/C
Ova S/C GL-II-93

FIG. 11

INTERNATIONAL SEARCH REPORT

International application No
PCT/US2017/047185

A. CLASSIFICATION OF SUBJECT MATTER
INV. C07D487/04 C07D487/14 A61K31/5517 A61P11/00
ADD.

According to International Patent Classification (IPC) or to both national classification and IPC

B. FIELDS SEARCHED

Minimum documentation searched (classification system followed by classification symbols)
C07D A61K A61P

Documentation searched other than minimum documentation to the extent that such documents are included in the fields searched

Electronic data base consulted during the international search (name of data base and, where practicable, search terms used)
EPO-Internal, EMBASE, WPI Data

C. DOCUMENTS CONSIDERED TO BE RELEVANT

Category*	Citation of document, with indication, where appropriate, of the relevant passages	Relevant to claim No.
A	WO 2014/047413 A1 (UWM RES FOUNDATION INC [US]) 27 March 2014 (2014-03-27) claims 1, 23, 27; figure 12	1-16, 24-35
X	US 4 226 768 A (WALSER ARMIN) 7 October 1980 (1980-10-07) examples 23, 25	1-7,9,14
X	US 2006/003995 A1 (COOK JAMES M [US] ET AL) 5 January 2006 (2006-01-05) compound 49 (PS-1-27); page 39	1-7,14

-/--

[X] Further documents are listed in the continuation of Box C. [X] See patent family annex.

* Special categories of cited documents :

"A" document defining the general state of the art which is not considered to be of particular relevance
"E" earlier application or patent but published on or after the international filing date
"L" document which may throw doubts on priority claim(s) or which is cited to establish the publication date of another citation or other special reason (as specified)
"O" document referring to an oral disclosure, use, exhibition or other means
"P" document published prior to the international filing date but later than the priority date claimed
"T" later document published after the international filing date or priority date and not in conflict with the application but cited to understand the principle or theory underlying the invention
"X" document of particular relevance; the claimed invention cannot be considered novel or cannot be considered to involve an inventive step when the document is taken alone
"Y" document of particular relevance; the claimed invention cannot be considered to involve an inventive step when the document is combined with one or more other such documents, such combination being obvious to a person skilled in the art
"&" document member of the same patent family

Date of the actual completion of the international search	Date of mailing of the international search report
20 September 2017	11/12/2017

Name and mailing address of the ISA/	Authorized officer
European Patent Office, P.B. 5818 Patentlaan 2 NL - 2280 HV Rijswijk Tel. (+31-70) 340-2040, Fax: (+31-70) 340-3016	Moriggi, J

Form PCT/ISA/210 (second sheet) (April 2005)

INTERNATIONAL SEARCH REPORT

International application No
PCT/US2017/047185

C(Continuation). DOCUMENTS CONSIDERED TO BE RELEVANT

Category*	Citation of document, with indication, where appropriate, of the relevant passages	Relevant to claim No.
X	WALSER A ET AL: "Quinazolines and 1,4-Benzodiazepines. CCV (1). Synthesis of 1,4-Benzodiazepines by Ring Expansion of 2-Chloromethylquinazolines with Carbanions", JOURNAL OF HETEROCYCLIC CHEMISTRY, WILEY-BLACKWELL PUBLISHING, INC, US, vol. 23, no. 4, 1 September 1986 (1986-09-01), pages 1303-1314, XP002901312, ISSN: 0022-152X, DOI: 10.1002/JHET.5570230509 compounds 41-43, 63, 65	1-7,9, 14,29
X	WATJEN F ET AL: "NOVEL BENZODIAZEPINE RECEPTOR PARTIAL AGONISTS: OXADIAZOLYLIMIDAZOBENZODIAZEPINES", JOURNAL OF MEDICINAL CHEMISTRY, AMERICAN CHEMICAL SOCIETY, vol. 32, no. 10, 1 January 1989 (1989-01-01), pages 2282-2291, XP002050070, ISSN: 0022-2623, DOI: 10.1021/JM00130A010 compounds 11e-11l, 11q, 11r, 12d-12k, 12p-12s	1-7,9, 14,29
X	CARLOS DEL POZO ET AL: "Reactions of 1,4-Benzodiazepinic N -Nitrosoamidines with Tosylmethyl Isocyanide: A Novel Synthesis of Midazolam", SYNTHESIS, vol. 2004, no. 16, 1 January 2004 (2004-01-01), pages 2697-2703, XP055408305, STUTTGART, DE. ISSN: 0039-7881, DOI: 10.1055/s-2004-831243 compounds 4a, 4b, 4d, 4e	1-7,9,14
X	US 2012/295892 A1 (COOK JAMES M [US] ET AL) 22 November 2012 (2012-11-22) the compounds of examples 4-6 and the synthetic intermediates 23, 25-27, 29-33 and 35; compound SH-053-2'F-RCH3	1-7,9, 14,29

2

Form PCT/ISA/210 (continuation of second sheet) (April 2005)

INTERNATIONAL SEARCH REPORT

International application No.
PCT/US2017/047185

Box No. II Observations where certain claims were found unsearchable (Continuation of item 2 of first sheet)

This international search report has not been established in respect of certain claims under Article 17(2)(a) for the following reasons:

1. ☐ Claims Nos.:
because they relate to subject matter not required to be searched by this Authority, namely:

2. ☐ Claims Nos.:
because they relate to parts of the international application that do not comply with the prescribed requirements to such an extent that no meaningful international search can be carried out, specifically:

3. ☐ Claims Nos.:
because they are dependent claims and are not drafted in accordance with the second and third sentences of Rule 6.4(a).

Box No. III Observations where unity of invention is lacking (Continuation of item 3 of first sheet)

This International Searching Authority found multiple inventions in this international application, as follows:

see additional sheet

1. ☐ As all required additional search fees were timely paid by the applicant, this international search report covers all searchable claims.

2. ☐ As all searchable claims could be searched without effort justifying an additional fees, this Authority did not invite payment of additional fees.

3. ☐ As only some of the required additional search fees were timely paid by the applicant, this international search report covers only those claims for which fees were paid, specifically claims Nos.:

4. ☒ No required additional search fees were timely paid by the applicant. Consequently, this international search report is restricted to the invention first mentioned in the claims; it is covered by claims Nos.:

1-16(completely); 24-35(partially)

Remark on Protest

☐ The additional search fees were accompanied by the applicant's protest and, where applicable, the payment of a protest fee.

☐ The additional search fees were accompanied by the applicant's protest but the applicable protest fee was not paid within the time limit specified in the invitation.

☐ No protest accompanied the payment of additional search fees.

Form PCT/ISA/210 (continuation of first sheet (2)) (April 2005)

FURTHER INFORMATION CONTINUED FROM PCT/ISA/ 210

This International Searching Authority found multiple (groups of) inventions in this international application, as follows:

1. claims: 1-16(completely); 24-35(partially)

The compounds of formulas (I), (I-A), (I-B) and (I-C), their compositions and their uses

---

2. claims: 17-23(completely); 24-35(partially)

The compounds of formula (II), (II-A) and (II-B), their compositions and their uses

---

INTERNATIONAL SEARCH REPORT

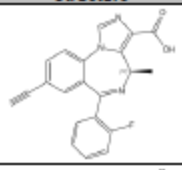
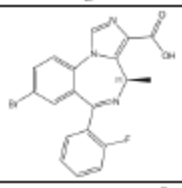
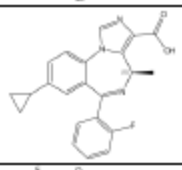
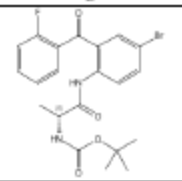
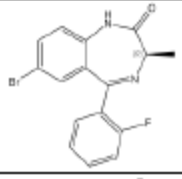
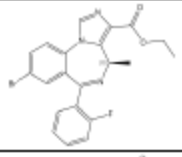
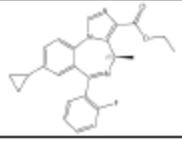
Information on patent family members

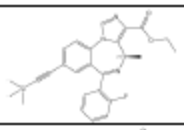
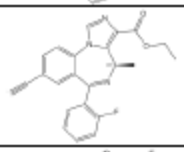
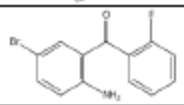
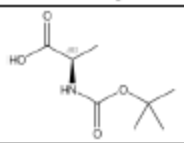
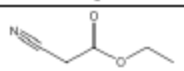
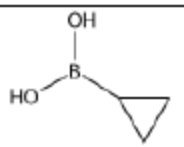
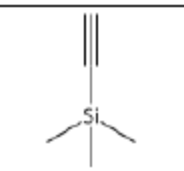
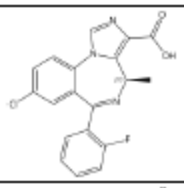
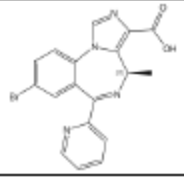
International application No
PCT/US2017/047185

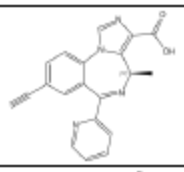
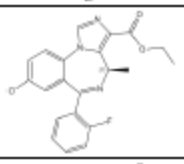
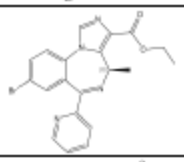
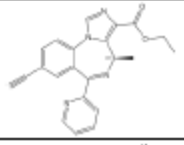
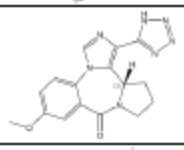
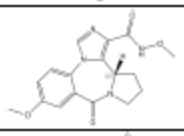
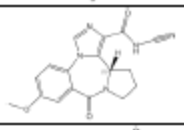
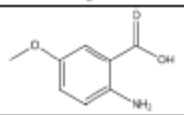
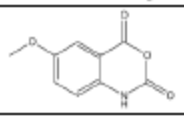
Patent document cited in search report	Publication date	Patent family member(s)	Publication date
WO 2014047413 A1	27-03-2014	CA 2885148 A1	27-03-2014
		EP 2897963 A1	29-07-2015
		JP 2015529254 A	05-10-2015
		US 2015232473 A1	20-08-2015
		WO 2014047413 A1	27-03-2014
US 4226768 A	07-10-1980	CH 644380 A5	31-07-1984
		DE 3020267 A1	11-12-1980
		FR 2457868 A1	26-12-1980
		GB 2052493 A	28-01-1981
		IT 1131195 B	18-06-1986
		JP S55160778 A	13-12-1980
		US 4226768 A	07-10-1980
US 2006003995 A1	05-01-2006	AU 2005260650 A1	12-01-2006
		CA 2570185 A1	12-01-2006
		EP 1761508 A1	14-03-2007
		US 2006003995 A1	05-01-2006
		US 2010004226 A1	07-01-2010
		WO 2006004945 A1	12-01-2006
US 2012295892 A1	22-11-2012	US 2012295892 A1	22-11-2012
		US 2015258128 A1	17-09-2015

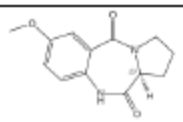
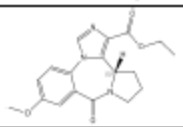
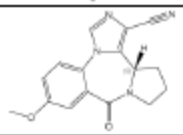
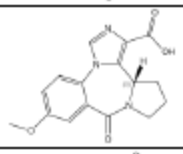
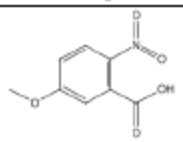
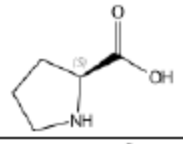
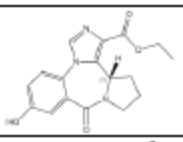
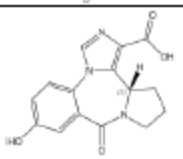
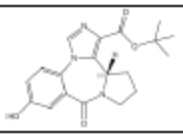
Form PCT/ISA/210 (patent family annex) (April 2005)

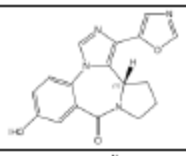
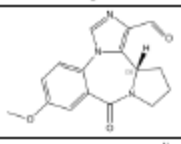
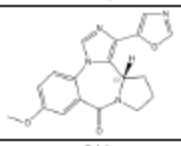
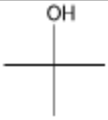
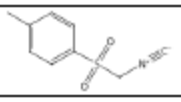
Key Substances In Patent

Mark	Page #	CAS RN	Name	Structure
1	p.25 p.35 p.69	2095608-41-4	4*H*-Imidazo[1,5-*a*][1,4]benzodiazepine-3-carboxylic acid, 8-ethynyl-6-(2-fluorophenyl)-4-methyl-, (4*R*)-	
2	p.25 p.36 p.69	2187489-08-1	4*H*-Imidazo[1,5-*a*][1,4]benzodiazepine-3-carboxylic acid, 8-bromo-6-(2-fluorophenyl)-4-methyl-, (4*R*)-	
3	p.25 p.36 p.69	2187489-09-2	4*H*-Imidazo[1,5-*a*][1,4]benzodiazepine-3-carboxylic acid, 8-cyclopropyl-6-(2-fluorophenyl)-4-methyl-, (4*R*)-	
14	p.25	872874-10-7	Carbamic acid, *N*-[(1*R*)-2-[[4-bromo-2-(2-fluorobenzoyl)phenyl]amino]-1-methyl-2-oxoethyl]-, 1,1-dimethylethyl ester	
15	p.25	872874-11-8	2*H*-1,4-Benzodiazepin-2-one, 7-bromo-5-(2-fluorophenyl)-1,3-dihydro-3-methyl-, (3*R*)-	
16	p.25 p.36	872874-12-9	4*H*-Imidazo[1,5-*a*][1,4]benzodiazepine-3-carboxylic acid, 8-bromo-6-(2-fluorophenyl)-4-methyl-, ethyl ester, (4*R*)-	
17	p.25 p.37	2187380-28-3	4*H*-Imidazo[1,5-*a*][1,4]benzodiazepine-3-carboxylic acid, 8-cyclopropyl-6-(2-fluorophenyl)-4-methyl-, ethyl ester, (4*R*)-	

18	p.25	872874-13-0	4*H*-Imidazo[1,5-*a*][1,4]benzodiazepine-3-carboxylic acid, 6-(2-fluorophenyl)-4-methyl-8-[2-(trimethylsilyl)ethynyl]-, ethyl ester, (4*R*)-	
19	p.25	872874-14-1	4*H*-Imidazo[1,5-*a*][1,4]benzodiazepine-3-carboxylic acid, 8-ethynyl-6-(2-fluorophenyl)-4-methyl-, ethyl ester, (4*R*)-	
28	p.25	1479-58-9	Methanone, (2-amino-5-bromophenyl)(2-fluorophenyl)-	
29	p.25	7764-95-6	D-Alanine, *N*-[(1,1-dimethylethoxy)carbonyl]-	
30	p.25	105-56-6	Acetic acid, 2-cyano-, ethyl ester	
31	p.25 p.36	411235-57-9	Boronic acid, *B*-cyclopropyl-	
32	p.25	1066-54-2	Silane, ethynyltrimethyl-	
4	p.26 p.37 p.69	2187489-10-5	4*H*-Imidazo[1,5-*a*][1,4]benzodiazepine-3-carboxylic acid, 8-chloro-6-(2-fluorophenyl)-4-methyl-, (4*R*)-	
5	p.26 p.37 p.70	2187489-11-6	4*H*-Imidazo[1,5-*a*][1,4]benzodiazepine-3-carboxylic acid, 8-bromo-4-methyl-6-(2-pyridinyl)-, (4*R*)-	

6	p.26 p.38 p.70	2187489-12-7	4*H*-Imidazo[1,5-*a*][1,4]benzodiazepine-3-carboxylic acid, 8-ethynyl-4-methyl-6-(2-pyridinyl)-, (4*R*)-	
33	p.26 p.37	2187380-32-9	4*H*-Imidazo[1,5-*a*][1,4]benzodiazepine-3-carboxylic acid, 8-chloro-6-(2-fluorophenyl)-4-methyl-, ethyl ester, (4*R*)-	
34	p.26 p.38	2133458-19-0	4*H*-Imidazo[1,5-*a*][1,4]benzodiazepine-3-carboxylic acid, 8-bromo-4-methyl-6-(2-pyridinyl)-, ethyl ester, (4*R*)-	
35	p.26 p.38	1258278-12-4	4*H*-Imidazo[1,5-*a*][1,4]benzodiazepine-3-carboxylic acid, 8-ethynyl-4-methyl-6-(2-pyridinyl)-, ethyl ester, (4*R*)-	
7	p.27 p.38 p.70	2187489-13-8	9*H*-Imidazo[1,5-*a*]pyrrolo[2,1-*c*][1,4]benzodiazepin-9-one, 11,12,13,13a-tetrahydro-7-methoxy-1-(2*H*-tetrazol-5-yl)-, (13a*S*)-	
8	p.27 p.39 p.70	2187489-14-9	9*H*-Imidazo[1,5-*a*]pyrrolo[2,1-*c*][1,4]benzodiazepine-1-carboxamide, 11,12,13,13a-tetrahydro-*N*,7-dimethoxy-9-oxo-, (13a*S*)-	
9	p.27 p.40 p.70	2187489-15-0	9*H*-Imidazo[1,5-*a*]pyrrolo[2,1-*c*][1,4]benzodiazepine-1-carboxamide, *N*-cyano-11,12,13,13a-tetrahydro-7-methoxy-9-oxo-, (13a*S*)-	
20	p.27	6705-03-9	Benzoic acid, 2-amino-5-methoxy-	
21	p.27	37795-77-0	2*H*-3,1-Benzoxazine-2,4(1*H*)-dione, 6-methoxy-	

22	p.27	130477-46-2	1*H*-Pyrrolo[2,1-*c*][1,4]benzodiazepine-5,11(10*H*,11a*H*)-dione, 2,3-dihydro-7-methoxy-, (11a*S*)-	
23	p.27 p.28 p.38 p.42	130477-52-0	9*H*-Imidazo[1,5-*a*]pyrrolo[2,1-*c*][1,4]benzodiazepine-1-carboxylic acid, 11,12,13,13a-tetrahydro-7-methoxy-9-oxo-, ethyl ester, (13a*S*)-	
24	p.27 p.38	2187380-29-4	9*H*-Imidazo[1,5-*a*]pyrrolo[2,1-*c*][1,4]benzodiazepine-1-carbonitrile, 11,12,13,13a-tetrahydro-7-methoxy-9-oxo-, (13a*S*)-	
25	p.27 p.39 p.40	663620-78-8	9*H*-Imidazo[1,5-*a*]pyrrolo[2,1-*c*][1,4]benzodiazepine-1-carboxylic acid, 11,12,13,13a-tetrahydro-7-methoxy-9-oxo-, (13a*S*)-	
36	p.27	1882-69-5	Benzoic acid, 5-methoxy-2-nitro-	
37	p.27	147-85-3	L-Proline	
10	p.28 p.40 p.70	2055157-81-6	9*H*-Imidazo[1,5-*a*]pyrrolo[2,1-*c*][1,4]benzodiazepine-1-carboxylic acid, 11,12,13,13a-tetrahydro-7-hydroxy-9-oxo-, ethyl ester, (13a*S*)-	
11	p.28 p.41 p.70	2187489-16-1	9*H*-Imidazo[1,5-*a*]pyrrolo[2,1-*c*][1,4]benzodiazepine-1-carboxylic acid, 11,12,13,13a-tetrahydro-7-hydroxy-9-oxo-, (13a*S*)-	
12	p.28 p.41 p.70	2055157-84-9	9*H*-Imidazo[1,5-*a*]pyrrolo[2,1-*c*][1,4]benzodiazepine-1-carboxylic acid, 11,12,13,13a-tetrahydro-7-hydroxy-9-oxo-, 1,1-dimethylethyl ester, (13a*S*)-	

13	p.28 p.42 p.70	2187489-17-2	9*H*-Imidazo[1,5-*a*]pyrrolo[2,1-*c*][1,4]benzodiazepin-9-one, 11,12,13,13a-tetrahydro-7-hydroxy-1-(5-oxazolyl)-, (13a*S*)-	
26	p.28 p.43	2187380-30-7	9*H*-Imidazo[1,5-*a*]pyrrolo[2,1-*c*][1,4]benzodiazepine-1-carboxaldehyde, 11,12,13,13a-tetrahydro-7-methoxy-9-oxo-, (13a*S*)-	
27	p.28 p.43	2187380-31-8	9*H*-Imidazo[1,5-*a*]pyrrolo[2,1-*c*][1,4]benzodiazepin-9-one, 11,12,13,13a-tetrahydro-7-methoxy-1-(5-oxazolyl)-, (13a*S*)-	
38	p.42	75-65-0	2-Propanol, 2-methyl-	
39	p.43	36635-61-7	Benzene, 1-[(isocyanomethyl)sulfonyl]-4-methyl-	

Copyright © 2019 American Chemical Society (ACS). All Rights Reserved.

Published papers (please click DOI to get full manuscript)

1. **Pandey, K.P.**; Rahman, M.T.; and Cook, J.M. 'Bisindole Alkaloids from the *Alstonia* Species: Recent Isolation, Bioactivity, Biosynthesis, and Synthesis' *Molecules* **2021**, *26*, 3459. https://doi.org/10.3390/molecules26113459.

molecules

MDPI

Review

Bisindole Alkaloids from the *Alstonia* Species: Recent Isolation, Bioactivity, Biosynthesis, and Synthesis †

Kamal P. Pandey [1], Md Toufiqur Rahman [2] and James M. Cook [1,*]

[1] Department of Chemistry and Biochemistry, University of Wisconsin Milwaukee, Milwaukee, WI 53211, USA; kppandey@uwm.edu
[2] RTI International, Center for Drug Discovery, Research Triangle Park, Durham, NC 27709, USA; mrahman@rti.org
* Correspondence: capncook@uwm.edu; Tel.: +1-414-614-0919
† This review is dedicated to Professor Samuel J. Danishefsky for his outstanding contributions to total synthesis and organic chemistry as a whole.

Abstract: Bisindoles are structurally complex dimers and are intriguing targets for partial and total synthesis. They exhibit stronger biological activity than their corresponding monomeric units. Alkaloids, including those containing C-19 methyl-substitution in their monomeric units, their synthetic derivatives, and their mismatched pairs can be attractive targets for synthesis and may unlock better drug targets. We herein discuss the isolation of bisindoles from various *Alstonia* species, their bioactivity, putative biosynthesis, and synthesis. The total synthesis of macralstonidine, macralstonine, *O*-acetylmacralstonine, and dispegatrine, as well as the partial synthesis of alstonisidine, villalstonine, and macrocarpamine are also discussed in this review. The completion of the total synthesis of pleiocarpamine by Sato et al. completes the formal synthesis of the latter two bisindoles.

Keywords: bisindole synthesis; biosynthesis; bioactivity; *Alstonia*; Apocynaceae; sarpagine; macroline; ajmaline; pleiocarpamine; partial; biomimetic or total synthesis

check for updates

Citation: Pandey, K.P.; Rahman, M.T.; Cook, J.M. Bisindole Alkaloids from the *Alstonia* Species: Recent Isolation, Bioactivity, Biosynthesis, and Synthesis. *Molecules* **2021**, *26*, 3459. https://doi.org/10.3390/molecules26113459

Academic Editor: Maria José U. Ferreira

Received: 29 April 2021
Accepted: 27 May 2021
Published: 7 June 2021

Publisher's Note: MDPI stays neutral with regard to jurisdictional claims in published maps and institutional affiliations.

Copyright © 2021 by the authors. Licensee MDPI, Basel, Switzerland. This article is an open access article distributed under the terms and conditions of the Creative Commons Attribution (CC BY) license (https://creativecommons.org/licenses/by/4.0/).

1. Introduction

Nature has been a substantial and sustainable pool of biologically active compounds. Since ancient times natural product extracts (in crude form) have been used in traditional and folk medicines in many countries. In modern times pure (isolated) natural products and their derivatives play an important role in drug discovery, as indicated by their prevalence in approved drugs for clinical use. Out of the 1881 newly FDA-approved drugs over the last four decades (1 January 1981 to 30 September 2019), a significant portion comprising 506 (26.9%) were either natural products or derived from or inspired by natural products [1]. It is expected that the advent of modern and innovative technologies such as computational software, cheminformatics, artificial intelligence, automation, and quantum computing will further boost natural product-based drug discovery. A synergy among these technological milestones would accelerate *hit to lead to clinic* pathways of drug discovery, and natural products are expected to remain an important source [2]. Moreover, pharmacophores and their unique stereochemical interactions with natural products may stimulate more demanding targets such as protein–protein interactions in the near future and open up a new avenue in modern drug discovery [3]. The majority of biologically active natural products are produced in plants, known traditionally as medicinal plants.

Alstonia, a major genus in the Apocynaceae family of plants, has nearly 155 species and is found all over the world [4]. Robert Brown named it in 1811 in honor of Charles Alston (1685–1760), an eminent botanist at the University of Edinburgh [4]. The *Alstonia* genus' trees and shrubs are prevalent in the tropical and subtropical parts of Africa, Asia, and Australia [5]. They contribute significant pharmacological activity, including anticancer, antileishmanial, antimalarial, antitussive, antiviral, antiarthritic, and antibacterial

2. **Pandey, K. P.**, Khan, Z. A., Golani. L. K.; Mondal, P.; Mian, Y.; Rashid, F.; Tiruveedhula, V.V.N.; Knutson, D.; Sharmin, D.; Ahmed, T.; Rezvanian, S.; Zahn, N. M.; Arnold, L. A.; Witkin, J. M.; and Cook, J. M. Design, synthesis and characterization of novel gamma-aminobutyric acid type A receptor ligands. *Arkovic*, **2020**, 242–256. https://doi.org/10.24820/ark.5550190.p011.398.

Arkivoc

Archive for Organic Chemistry

The Free Internet Journal for Organic Chemistry

Paper

Arkivoc 2020, part vii, 242-256

Design, synthesis and characterization of novel gamma-aminobutyric acid type A receptor ligands

Kamal P. Pandey,[#] Md Zubair Ahmed Khan,[#] Lalit K. Golani,[#] Prithu Mondal, Md Yeunus Mian, Farjana Rashid, V. V. N. Phani Babu Tiruveedhula, Daniel E. Knutson, Dishary Sharmin, Taukir Ahmed, Sepideh Rezvanian, Nicolas M. Zahn, Leggy A. Arnold, Jeffrey M. Witkin, and James M. Cook[*]

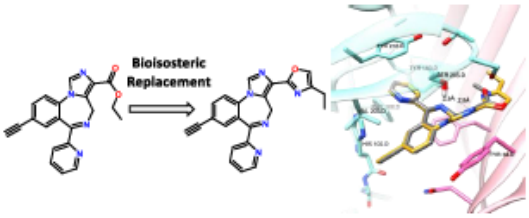
Department of Chemistry and Biochemistry, Milwaukee Institute for Drug Discovery, University of Wisconsin-Milwaukee, Milwaukee, Wisconsin 53211, USA
E-mail: capncook@uwm.edu

We dedicate this work to Professor Jan Bergman for his outstanding contributions to heterocyclic and organic chemistry as a whole

Received 10-15-2020 Accepted 11-11-2020 Published on line 12-02-2020

Abstract

Antinociceptive ligand HZ-166 is a $GABA_A$ α2/α3 receptor subtype-selective potentiator. It has been shown to exhibit anxiolytic-like effects in rodent and rhesus monkeys, as well as reduced sedative/ataxic liabilities. In order to improve the metabolic stability of HZ-166, the ethyl ester moiety was bioisosterically replaced with 2,4-disubstituted oxazoles and oxazolines. The new analogs of HZ-166 were synthesized, characterized, and evalutated for their biological activity and docked in the human full-length heteromeric α1β3γ2L $GABA_A$ receptor subtype CyroEM structure (6HUO). Importantly no sedation nor ataxia was observed on the rotorod for LKG-I-70 (**6**) or KPP-III-51 (**6c**) at 100 and 120 mg/kg, respectively. There was also no loss of righting response for either ligand.



Keywords: $GABA_A$ receptor, bioisosteres, subtype selectivity, metabolism, docking

DOI: https://doi.org/10.24820/ark.5550190.p011.398 ©AUTHOR(S)

3. Witkin, J. M., **Pandey, K. P.,** Smith J. L. 'Clinical investigations of compounds targeting metabotropic glutamate receptors' *Pharmacology Biochemistry and Behavior*, **2022**, 173446. https://doi.org/10.1016/j.pbb.2022.173446.

Pharmacology, Biochemistry and Behavior 219 (2022) 173446

Contents lists available at ScienceDirect

Pharmacology, Biochemistry and Behavior

journal homepage: www.elsevier.com/locate/pharmbiochembeh

Clinical investigations of compounds targeting metabotropic glutamate receptors

Jeffrey M. Witkin [a,b,c,*], Kamal P. Pandey [b], Jodi L. Smith [a]

[a] Laboratory of Antiepileptic Drug Discovery, Ascension St. Vincent, Indianapolis, IN, USA
[b] Department of Chemistry & Biochemistry, Milwaukee Institute of Drug Discovery, University of Wisconsin-Milwaukee, Milwaukee, WI, USA
[c] Respirerx Pharmaceuticals Inc, Glen Rock, NJ, USA

ARTICLE INFO

Keywords:
mGlu receptors
Anxiety
Depression
Neurological disorders
Psychiatric disorders

ABSTRACT

Pharmacological modulation of glutamate has long been considered to be of immense therapeutic utility. The metabotropic glutamate receptors (mGluRs) are potential targets for safely altering glutamate-driven excitation. Data support the potential therapeutic use of mGluR modulators in the treatment of anxiety, depression, schizophrenia, and other psychiatric disorders, pain, epilepsy, as well as neurodegenerative and neurodevelopmental disorders. For each of the three mGluR groups, compounds have been constructed that produce either potentiation or functional blockade. PET ligands for mGlu5Rs have been studied in a range of patient populations and several mGlu5R antagonists have been tested for potential efficacy in patients including mavoglurant, diploglurant, basimglurant, GET 73, and ADX10059. Efficacy with mGlu5R antagonists has been reported in trials with patients with gastroesophageal reflux disease; data from patients with Parkinson's disease or Fragile X syndrome have not been as robust as hoped. Fenobam was approved for use as an anxiolytic prior to its recognition as an mGlu5R antagonist. mGlu2/3R agonists (pomaglumated methionil) and mGlu2R agonists (JNJ-40411813, AZD 8529, and LY2979165) have been studied in patients with schizophrenia with promising but mixed results. Antagonists of mGlu2/3Rs (decoglurant and TS-161) have been studied in depression where TS-161 has advanced into a planned Phase 2 study in treatment-resistant depression. The Group III mGluRs are the least developed of the mGluR receptor targets. The mGlu4R potentiator, foliglurax, did not meet its primary endpoint in patients with Parkinson's disease. Ongoing efforts to develop mGluR-targeted compounds continue to promise these glutamate modulators as medicines for psychiatric and neurological disorders.

1. Introduction

Creating a medicine requires the combining of two arts for which precise recipes for either are not available. The first is the art of achieving efficacy in the therapeutic domain, the second art is used to sculpt a compound with tolerability and safety. Glutamate is the primary excitatory neurotransmitter in the mammalian nervous system and thereby controls pathophysiological processes of immense therapeutic need (Curtis and Johnston, 1974; Graham et al., 1967; Krnjević, 1970). Therefore, the desire to target glutamate receptors and associated machinery has been and continues to be immense. However, because of its elite status as a dominant regulator of excitatory processing, tolerability and safety issues from the pharmacological manipulation of this system have been and continue to be an obstacle.

One example of this drug development problem comes from the efforts to make antagonists of the *N*-methyl-D-aspartate (NMDA) receptor (see Witkin et al., 2022 for a brief overview). Since direct block of the NMDA receptor ion channel produces side effects that are either patient intolerable or undesirable, work over decades was directed toward the identification of compounds that produced the ideal interplay of efficacy and side effects. Although the NMDA receptor has multiple allosteric domains, increasing the probability of finding the right combination, and despite the number of compounds introduced into clinical development, there was little success in finding a medicine. Memantine (Namenda®), a low affinity channel blocker is the success story of this long exploration, with its approved use in dementias (Arvanitakis et al., 2019; Czarnecka et al., 2021). As an antidepressant, meta-analysis of controlled trials with memantine has also recently shown its efficacy (Hsu et al., 2022). The 2019 approval of the NMDA receptor antagonist, (*S*)-ketamine (Spravato®), as an adjunct therapy for treatment-resistant

* Corresponding author at: Laboratory of Antiepileptic Drug Discovery, Ascension St. Vincent, Indianapolis, IN, USA.
E-mail address: witkinconsult@gmail.com (J.M. Witkin).

https://doi.org/10.1016/j.pbb.2022.173446
Received 28 April 2022; Received in revised form 22 June 2022; Accepted 8 August 2022
Available online 17 August 2022
0091-3057/© 2022 Elsevier Inc. All rights reserved.

4. Golani, L. K.; Mian, M. Y., Ahmed, T. **Pandey, K. P**., Mondal, P., Sharmin, D., Rezvanian, S., Witkin, J. M., and Cook, J. M. 'Rationalizing the binding and α subtype selectivity of synthesized imidazodiazepines and benzodiazepines at GABAA receptors by using molecular docking studies' *Bioorganic and medicinal chemistry letters*, **2022**, 62. https://doi.org/10.1016/j.bmcl.2022.128637.

Bioorg. Med. Chem. Lett. 62 (2022) 128637

Contents lists available at ScienceDirect

Bioorganic & Medicinal Chemistry Letters

journal homepage: www.elsevier.com/locate/bmcl



Rationalizing the binding and α subtype selectivity of synthesized imidazodiazepines and benzodiazepines at GABAA receptors by using molecular docking studies

Lalit K Golani [a,1], Md Yeunus Mian [a,1], Taukir Ahmed [a], Kamal P Pandey [a], Prithu Mondal [a], Dishary Sharmin [a], Sepideh Rezvanian [a], Jeffrey M Witkin [a,b], James M Cook [a,*]

[a] Department of Chemistry and Biochemistry, Milwaukee Institute of Drug Discovery, University of Wisconsin-Milwaukee, Milwaukee, WI, USA
[b] Laboratory of Antiepileptic Drug Discovery, St. Vincent's Hospital, Indianapolis, IN USA

ARTICLE INFO

Keywords:
γ-Aminobutyric acid type A receptor
Benzodiazepines
Halogen bond
Bioisostere
Molecular docking
Protein ligand interactions

ABSTRACT

The pharmacological actions exerted by benzodiazepines are dependent on the discrete α protein subunits of the γ-aminobutyric acid type A receptor ($GABA_A$ R). Recent developments via a cryo-EM structure of the α1β3γ2L $GABA_A$ R ion channel provide crucial insights into ligand efficacy and binding affinity at this subtype. We investigated the molecular interactions of diazepam and alprazolam bound $GABA_A$ R structures (6HUP and 6HUO) to determine key binding interaction domains. A halogen bond between the chlorine atoms of diazepam and alprazolam with the group on the backbone of the α1 histidine amino acid 102 is important to the positive allosteric modulatory actions of diazepam and alprazolam in the α1β3γ2L $GABA_A$ R ion channel. In order to gain insight into α subtype selectivity we designed and synthesized close structural analogs of diazepam and alprazolam. These compounds were then docked into the recently publish cryo-EM structures of $GABA_A$ Rs (6HUP and 6HUO). This modeling along with radio-ligand binding data resulted in the conclusion that the non-classical bioisosteric replacement of the chlorine atom at C7 with an ethinyl group (compound **5**) resulted in an 11-fold gain in α5 binding selectivity over the α1 subtype. Moreover, the potency of compound **5** resulted in a ligand with less sedation than diazepam, while still maintaining the same anxiolytic potency. These modeling data extend our understanding of the structural requirements for α-subtype-selective compounds that can be utilized to achieve improved medical treatments. It is clear that the ethinyl group in place of a halogen atom decreases the affinity and efficacy of benzodiazepines and imidazodiazepines at α1 subtypes, which results in less sedation and ataxia.

The γ-aminobutyric acid type A receptor ($GABA_A$ R) is an ionotropic receptor and ligand-gated chloride ion channel that is regulated by the endogenous ligand γ-aminobutyric acid (GABA). [1–2] Activation of $GABA_A$ Rs leads to the inhibition of neurotransmission by hyperpolarization of the neuron. $GABA_A$ Rs are heteropentameric ligand-gated membrane bound ion channels and are composed of different subunits (six α, three β, three γ, one δ, one ε, one θ, one π, and three ρ subunits). [3] The majority of $GABA_A$ Rs, however, are composed of two α, two β, and one γ2 subunits. The subunit composition of $GABA_A$ R is thought to control the different pharmacological and biological effects of GABA and exogenous ligands. Benzodiazepines (BZDs) are a general class of drugs known to bind to the $GABA_A$ R at an allosteric site. A large set of data has been assembled indicating that α and γ subunits are necessary for the pharmacological actions of BZDs. Classical 1,4-BZDs, such as diazepam (DZP), bind non-selectively to α1-3 and 5βγ2 $GABA_A$ Rs at the well-documented BZD binding site located at the $\alpha^+\gamma^-$ interface. [4–5] The pharmacological actions exerted by a BZD are dependent on the discrete subunits of the $GABA_A$ R complex. The BZDs exert sedative, hypnotic, anxiolytic, antinociceptive muscle relaxant and anticonvulsant actions. From a therapeutic perspective, it has been the goal of drug discovery efforts to design compounds that can specifically modulate selective biological actions that can translate into directed therapeutic effects. Precise knowledge of the structure of the binding site of action enables rational approaches to chemical design for this purpose. Much effort has

* Corresponding author.
E-mail address: capncook@uwm.edu (J.M. Cook).
[1] Both authors contributed equally.

https://doi.org/10.1016/j.bmcl.2022.128637
Received 15 July 2021; Received in revised form 18 February 2022; Accepted 20 February 2022
Available online 23 February 2022
0960-894X/© 2022 Elsevier Ltd. All rights reserved.

5. Rahman, M. D., Tiruveedhula, V.V.N.P. Stephen, M. R., Rallapalli, S. K., **Pandey, K. P.**, and Cook, J. M. 'Completion of the Total Synthesis of Several Bioactive Sarpagine/Macroline Alkaloids including the Important NF-κB Inhibitor N_4-Methyltalpinine' *Molecules*, **2022**, 27, 1738. https://doi.org/10.3390/molecules27051738.

molecules

MDPI

Article

Completion of the Total Synthesis of Several Bioactive Sarpagine/Macroline Alkaloids including the Important NF-κB Inhibitor N_4-Methyltalpinine

Md Toufiqur Rahman, Veera Venkata Naga Phani Babu Tiruveedhula, Michael Rajesh Stephen, Sundari K. Rallapalli, Kamal P. Pandey and James M. Cook *

Department of Chemistry and Biochemistry, University of Wisconsin Milwaukee, Milwaukee, WI 53211, USA; mdrahman@uwm.edu (M.T.R.); ttiruvee2@uwm.edu (V.V.N.P.B.T.); smichaelrajesh@gmail.com (M.R.S.); rallapallisk@gmail.com (S.K.R.); kppandey@uwm.edu (K.P.P.)
* Correspondence: capncook@uwm.edu; Tel.: +1-414-614-0919

Abstract: The unification of the general synthetic strategy regarding the important and emerging group of C-19 methyl-substituted sarpagine/macroline alkaloids has culminated in the completion of the total synthesis of several bioactive alkaloids. Key transformations include an ACE-Cl mediated late-stage N(4)-demethylation and an anhydrous acid-mediated intramolecular quaternary hemiaminal formation between a tertiary amine and an aldehyde function to allow efficient access to several biologically important alkaloids from this group. Herein, the enantiospecific total synthesis of the first known sarpagine/macroline alkaloid with NF-κB inhibitory activity, N(4)-methyltalpinine (as a chloride salt), as well as the anticancer alkaloids talpinine, *O*-acetyltalpinine, and macrocarpines F-G, are described.

Keywords: sarpagine alkaloids; macroline alkaloids; macrocarpine F; macrocarpine G; talpinine; *O*-acetyltalpinine; N(4)-methyltalpinine; NF-κB inhibitor; anticancer alkaloids; N-dealkylation; bioactive alkaloids

check for updates

Citation: Rahman, M.T.; Tiruveedhula, V.V.N.P.B.; Stephen, M.R.; Rallapalli, S.K.; Pandey, K.P.; Cook, J.M. Completion of the Total Synthesis of Several Bioactive Sarpagine/Macroline Alkaloids including the Important NF-κB Inhibitor N_4-Methyltalpinine. *Molecules* **2022**, *27*, 1738. https://doi.org/10.3390/molecules27051738

Academic Editor: Gianpiero Cera

Received: 31 January 2022
Accepted: 1 March 2022
Published: 7 March 2022

Publisher's Note: MDPI stays neutral with regard to jurisdictional claims in published maps and institutional affiliations.

Copyright: © 2022 by the authors. Licensee MDPI, Basel, Switzerland. This article is an open access article distributed under the terms and conditions of the Creative Commons Attribution (CC BY) license (https://creativecommons.org/licenses/by/4.0/).

1. Introduction

The sarpagine/macroline/ajmaline family represents an important class of biosynthetically related monoterpene indole alkaloids [1–3]. Sarpagine, ajmaline, and macroline individually are eponymous with respect to their corresponding subclass of alkaloids. To date, this family comprises more than 300 monomeric and about 100 bisindole alkaloids [2,4–6]. A number of alkaloids from this family have been reported to possess important biological properties, such as anticancer, antileishmanial, antiarrhythmic, and antimalarial activities, which is not surprising since these alkaloids occur primarily in various plant species of the *Apocynaceae* family that have been used in traditional or folk medicines for centuries [4,7–11].

The C-19 methyl-substituted sarpagine/ajmaline sub-family of alkaloids is a growing ensemble of alkaloids with a common structural feature, i.e., alkaloids having a stereogenic methyl group at the C-19 position of their biogenetic architecture. To date, this group has been populated with more than seventy alkaloids [8,12]. Despite this common structural feature, notable diversity in substitution patterns, and oxidation states, very few syntheses have been reported for this sub-group [13–15]. In addition, as usual, the paucity of isolated material has impeded the study of medicinal properties.

A general and unified synthetic approach regarding this emerging group has been of interest due to the important biological activities as well as the interesting structures of a number of alkaloids from the *Apocynaceae* [8]. One of the important outcomes of the general strategy developed in Milwaukee is the improved and readier access to the core sarpagine/ajmaline architecture via an ambidextrous Pictet–Spengler/Dieckmann protocol,

6. Golani, L.K., Divoc, B., Sharmin, D., **Pandey, K. P**., Mian, M. Y., Cerne, R., Zahn, N. M., Meyer, M. J., Tiruveedhula, V. V. N. P., Smith, J.L., Pin, X., Jin, X, Lippa, A., Schkeryantz, J. M., Arnold, L. A., Cook, J. M., Savic, M. M., and Witkin, J. M. 'Metabolism, pharmacokinetics, and anticonvulsant activity of a deuterated analog of the α2/3-selective GABAkine KRM-II-81', *Biopharmaceutics & Drug Disposition*, **2022.** https://doi.org/10.1002/bdd.2313.

Received: 14 December 2021 | Revised: 14 February 2022 | Accepted: 16 February 2022

DOI: 10.1002/bdd.2313

WILEY

ORIGINAL ARTICLE

Metabolism, pharmacokinetics, and anticonvulsant activity of a deuterated analog of the α2/3-selective GABAkine KRM-II-81

Lalit K. Golani[1] | Branka Divović[2] | Dishary Sharmin[1] | Kamal P. Pandey[1] | Md Yeunus Mian[1] | Rok Cerne[3,4,5,6] | Nicolas M. Zahn[1] | Michelle J. Meyer[1] | Veera V. N. P. B. Tiruveedhula[1] | Jodi L. Smith[3] | Xingjie Ping[4] | Xiaoming Jin[4] | Arnold Lippa[6] | Jeffrey M. Schkeryantz[7] | Leggy A. Arnold[1] | James M. Cook[1,6] | Miroslav M. Savić[2] | Jeffrey M. Witkin[1,3,6]

[1]Department of Chemistry & Biochemistry, Milwaukee Institute of Drug Discovery, University of Wisconsin-Milwaukee, Milwaukee, Wisconsin, USA

[2]Department of Pharmacology, Faculty of Pharmacy, University of Belgrade, Belgrade, Serbia

[3]Laboratory of Antiepileptic Drug Discovery, Ascencion St. Vincent, Indianapolis, Indiana, USA

[4]Department of Anatomy and Cell Biology, Indiana University/Purdue University, Indianapolis, Indiana, USA

[5]Faculty of Medicine, University of Ljubljana, Ljubljana, Slovenia

[6]RespireRx Pharmaceuticals Inc, Glen Rock, New Jersey, USA

[7]Bristol Myers Squibb, Cambridge, Massachusetts, USA

Correspondence
Jeffrey M. Witkin, Laboratory of Antiepileptic Drug Discovery, Ascencion St. Vincent, Indianapolis, IN, USA.
Email: witkinconsult@gmail.com

Funding information
NSF, Grant/Award Number: CHE-1625735; NIH, Grant/Award Numbers: DA-043204, NS-076517

Abstract

The imidazodiazepine, (5-(8-ethynyl-6-(pyridin-2-yl)-4H-benzo [*f*]imidazole[1,5-α] [1,4]diazepin-3-yl) oxazole or KRM-II-81) is a new α2/3-selective GABAkine (gamma aminobutyric acid A receptor potentiator) with anticonvulsant, anxiolytic, and antinociceptive activity in preclinical models. Reducing metabolism was utilized as a means of potentially extending the half-life of KRM-II-81. *In vitro* and *in vivo* studies were conducted to evaluate metabolic liabilities. Incubation of KRM-II-81 in hepatocytes revealed sites of potential metabolism on the oxazole and the diazepine rings. These sites were targeted in the design of a deuterated analog (D5-KRM-II-81) that could be evaluated as a potentially longer-acting analog. In contrast to computer predictions, peak plasma concentrations of D5-KRM-II-81 in rats were not significantly greater than those produced by KRM-II-81 after oral administration. Furthermore, brain disposition of KRM-II-81 was higher than that of D5-KRM-II-81. The half-life of the two compounds in either plasma or brain did not statistically differ from one another but the t_{max} for D5-KRM-II-81 occurred slightly earlier than for KRM-II-81. Non-metabolic considerations might be relevant to the lack of increases in exposure by D5-KRM-II-81. Alternative sites of metabolism on KRM-II-81, not targeted by the current deuteration process, are also possible. Despite its lack of augmented exposure, D5-KRM-II-81, like KRM-II-81, significantly prevented seizures induced by pentylenetetrazol when given orally. The present findings introduce a new orally active anticonvulsant GABAkine, D5-KRM-II-81.

KEYWORDS
epilepsy, GABA, KRM-II-81, metabolism, pharmacokinetics

Lalit K. Golani, Branka Divović, and Dishary Sharmin contributed equally to this work.

 © 2022 John Wiley & Sons Ltd.

7. Mian, M.Y., Mondal, P., Sharmin, D., **Pandey, K.P.**, Rashid, F., Rezvanian, S., Golani, L.K., Tiruveedhula, V.P.B., Rajaratnam, V., Mirza, S.P., Chan, J.D., Witkin, J. M., and Cook, J. M. 'An efficient debromination technique using PMHS with a number of ligands containing different functional groups' *Arkivoc*, **2021**, (part v), pp.0-0. https://doi.org/10.24820/ark.5550190.p011.712.

Arkivoc

A Platinum Open Access Journal for Organic Chemistry

Paper

Free to Authors and Readers

DOAJ Seal

Arkivoc 2021, part v, 0-0

to be inserted by editorial office

An efficient debromination technique using PMHS with a number of ligands containing different functional groups

Md Yeunus Mian,[a] Prithu Mondal,[a] Dishary Sharmin,[a] Kamal P. Pandey,[a] Farjana Rashid,[a] Sepideh Rezvanian,[a] Lalit K. Golani,[a] V.V.N. Phani Babu Tiruveedhula,[a] Vilashini Rajaratnam[1], Shama P. Mirza[1], John D. Chan[2], Jeffrey M. Witkin[1], and James M. Cook*[1]

[1]*Department of Chemistry and Biochemistry, Milwaukee Institute of Drug Discovery, University of Wisconsin-Milwaukee, Milwaukee, WI-53211*

[2]*Department of Chemistry, University of Wisconsin-Oshkosh, Oshkosh, WI-54901*

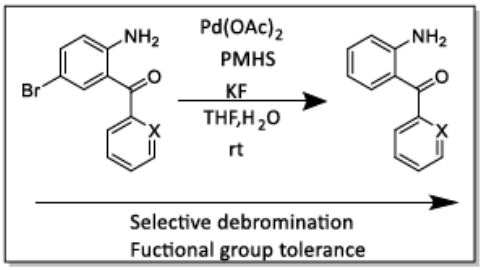
E-mail: capncook@uwm.edu

This paper is dedicated to Professor Peter Alan Jacobi for his many important contributions to Organic Chemistry

Received 12-22-2021 Accepted Manuscript 03-21-2022 Published on line 04-07-2022

Abstract

Herein is described the strategy to debrominate different aryl bromides selectively, using polymethylhydrosiloxane (PMHS) which tolerates a variety of functional groups. Key elements of this approach include the use of catalytic $Pd(OAc)_2$ and the correct equivalents of polymethylhydrosiloxane (PMHS), in conjunction with aqueous KF. The present reaction process provides a strategic tool for the synthesis of a number of medicinally important molecules.



Keywords: debromination, polymethylhydrosiloxane, benzodiazepines, palladium acetate

DOI: https://doi.org/10.24820/ark.5550190.p011.712 ©AUTHOR(S)

8. Mian, Md Y., Divovic, B., Sharmin, D., **Pandey, K. P.,** Golani, L. K. Tiruveedhula, V.V.N. P. B., Cerne, R., Smith, J. L., Ping, X., Jin, X., Imler, G. H., Deschamps, J. R., Lippa, A., Cook, J.M., Savic, M. M., Rowlett, J., Witkin, J. M 'Hydrochloride Salt of the GABAkine KRM-II-81' *ACS Omega* **2022**. https://doi/org/10.1021/acsomega.2c03029.

ACS OMEGA

http://pubs.acs.org/journal/acsodf

Article

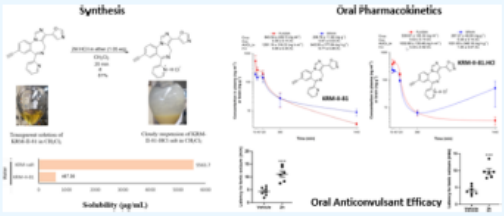
Hydrochloride Salt of the GABAkine KRM-II-81

Md Yeunus Mian,* Branka Divović, Dishary Sharmin, Kamal P. Pandey, Lalit K. Golani, V. V. N. Phani Babu Tiruveedhula, Rok Cerne, Jodi L. Smith, Xingjie Ping, Xiaoming Jin, Gregory H. Imler, Jeffrey R. Deschamps, Arnold Lippa, James M. Cook, Miroslav M. Savić, James Rowlett, and Jeffrey M. Witkin

Cite This: https://doi.org/10.1021/acsomega.2c03029

Read Online

ACCESS | Metrics & More | Article Recommendations | Supporting Information



ABSTRACT: Imidazodiazepine (*S*-(8-ethynyl-6-(pyridin-2-yl)-4*H*-benzo[*f*]imidazole[1,5-α][1,4]diazepin-3-yl) oxazole or KRM-II-81) is a potentiator of $GABA_A$ receptors (a GABAkine) undergoing preparation for clinical development. KRM-II-81 is active against many seizure and pain models in rodents, where it exhibits improved pharmacological properties over standard-of-care agents. Since salts can be utilized to create opportunities for increased solubility, enhanced absorption, and distribution, as well as for efficient methods of bulk synthesis, a hydrochloride salt of KRM-II-81 was prepared. KRM-II-81-HCl was produced from the free base with anhydrous hydrochloric acid. The formation of the monohydrochloride salt was confirmed by X-ray crystallography, as well as ^{1}H NMR and ^{13}C NMR analyses. High water solubility and a lower partition coefficient (octanol/water) were exhibited by KRM-II-81-HCl as compared to the free base. Oral administration of either KRM-II-81-HCl or the free base resulted in high concentrations in the brain and plasma of rats. Oral dosing in mice significantly increased the latency to both clonic and tonic convulsions and decreased pentylenetetrazol-induced lethality. The increased water solubility of the HCl salt enables intravenous dosing and the potential for higher concentration formulations compared with the free base without impacting anticonvulsant potency. Thus, KRM-II-81-HCl adds an important new compound to facilitate the development of these imidazodiazepines for clinical evaluation.

Downloaded via 47.227.233.83 on July 27, 2022 at 14:49:53 (UTC).
See https://pubs.acs.org/sharingguidelines for options on how to legitimately share published articles.

INTRODUCTION

KRM-II-81 is the latest in a series of imidazodiazepine potentiators of $GABA_A$ receptors (GABAARs) or GABAkines that is under development.[1,2] KRM-II-81 produces anxiolytic effects,[3,4] antidepressant-like activity,[5] anticonvulsant activity,[6−9] and efficacy in a host of acute and chronic pain models in rodents.[10] The efficacy of KRM-II-81 is associated with a low sedative and motor-impairing profile, lack of tolerance development, and abuse liability.[2,10] Further, KRM-II-81 is efficacious in models of pharmacoresistant epilepsy[7] and did not produce tolerance.[7,11] In animal models used to predict drug abuse liability, KRM-II-81 differentiated from classical GABAkines like midazolam or diazepam.[2]

Salt formation has been considered as an important step during the preformulation stage of drug development.[12,13] Preparing a salt form can overcome the nonoptimal physicochemical and/or biopharmaceutical properties of an ionizable molecule.[14] The key salt form selection early in the development process can improve the bioavailability of a compound. Proper salt form selection is facilitated by an efficient salt screening strategy that involves the evaluation of crystallinity, hygroscopicity, solubility, stability, purity, polymorphism/hydrate formation, and powder flowability, in addition to the practical importance of cost and reaction yield.[15,16] In addition to enhancing physiochemical and biopharmaceutical properties of compounds,[17] creation of salts has also been shown to improve compound druggability.[18]

Received: May 15, 2022
Accepted: July 14, 2022

ACS Publications

© XXXX The Authors. Published by American Chemical Society

9. Manuscript (accepted in *JPET*) as it is (in original form)

JPET-AR-2022-001362

Structural analogs of the GABAkine (5-(8-ethynyl-6-(pyridin-2-yl)-4H -benzo[*f*]imidazole[1,5-α][1,4]diazepin-3-yl) oxazole) (**KRM-II-81) are orally bioavailable anticonvulsants without sedation[1]**

Kamal P. Pandey[1#], Branka Divović[2#], Farjana Rashid[1#], Lalit K. Golani[1#], Rok Cerne[3,4,5], Nicolas M. Zahn[1], Michelle Jean Meyer[1], Leggy A. Arnold[1], Dishary Sharmin[1], Md Yeunus Mian[1], Jodi L. Smith[3], Xingjie Ping[4], Xiaoming Jin[4], Arnold Lippa[6], V. V. N. Phani Babu Tiruveedhula[1], James M. Cook[1,6], Miroslav M. Savić[2], and Jeffrey M. Witkin[1,3,6]

[1]Department of Chemistry & Biochemistry

University of Wisconsin-Milwaukee, Milwaukee, WI, USA

[2]Department of Pharmacology, Faculty of Pharmacy, University of Belgrade, Belgrade, Serbia

[3]Laboratory of Antiepileptic Drug Discovery

St. Vincent's Hospital, Indianapolis, IN USA

[4]Department of Anatomy and Cell Biology

Indiana University/Purdue University, Indianapolis, IN, USA

[5]Faculty of Medicine, University of Ljubljana, Založka cesta 4, Ljubljana, Slovenia.

[6]RespireRx Pharmaceuticals Inc, Glen Rock, NJ, USA

# These authors contributed equally to the manuscript

Running Title Page

Running Title: KRM-II-81 Analogs

Correspondence:

Kamal P. Pandey

kppandey@uwm.edu

or

Jeff Witkin

witkinconsult@gmail.com

Document Statistics

Tables	9
Figures	9
Abstract	239 words

Abstract

In order to provide back-up compounds to support the development of the $GABA_A$ receptor potentiator, KRM-II-81, three novel analogs were designed: replacement of the pyridinyl with Cl-phenyl (FR-II-60), changing the positions of the N and O atoms in the oxazole ring with addition of an ethyl group (KPP-III-34 and 51), or substitution of a Br atom for the ethinyl of KRM-II-81 (KPP-III-34). The compounds bound to brain $GABA_A$ receptors. Intraperitoneal administration of FR-II-60 and KPP-III-34 produced anticonvulsant activity in mice (maximal electroshock (MES)-induced seizures or 6Hz-induced seizures) whereas KPP-III-51 did not. Although all compounds were orally bioavailable, structural changes reduced the plasma and brain exposure relative to KRM-II-81. Oral administration of each compound produced dose-dependent increases in the latency for both clonic and tonic seizures and the lethality induced by pentylenetetrazol (PTZ) in mice. Since KPP-III-34 produced the highest oral exposures, it was selected for further profiling. Oral administration of KPP-III-34 suppressed seizures in corneal-kindled mice, hippocampal paroxysmal discharges in mesial temporal lobe epileptic mice, and PTZ-induced convulsions in rats. Only transient sensorimotor impairment was observed in mice and doses of KPP-III-34 up to 500 mg/kg did not produce impairment in rats. Molecular docking studies demonstrated that all compounds displayed a reduced propensity for binding to the α1His102 compared to the sedating compound alprazolam; the bromine-substituted KPP-III-34 achieved the least interaction. Overall, these findings document the oral bioavailability and anticonvulsant efficacy of three novel analogs of KRM-II-81 with reduced sedative effects.

Significance Statement

Sedation and tolerance development are obstacles to the development of improved antiepileptic drugs. A new non-sedating compound, KRM-II-81, with a reduced propensity for toleranceis currently moving into clinical development. All three compounds were orally bioavailable, produced anticonvulsant effects in rodents, and displayed low cytotoxicity and sensorimotor impairment. An advanced compound, KPP-III-34, demonstrated efficacy in models of pharmacoresistant epilepsy. Molecular docking studies demonstrated a low propensity for compound binding to the α1His102 residue implicated in sedation. Thus, three additional structures have thus been added to the list of non-sedating imidazodiazepine anticonvulsants that could serve as backups in the clinical development of KRM-II-81.

Introduction

Potentiators of $GABA_A$ receptors (GABAARs) or GABAkines have tremendous value in the therapeutics of neurological (e.g., epilepsy) and psychiatric (e.g., anxiety) disorders. For example, diazepam (Valium®) is on the World Health Organization's List of Essential Medicines. However, GABAkines can come with a risk of tolerance development, abuse, and dependence liability, along with sedative and motor-impairing effects (see Cerne et al., 2021). The search for GABAkines without these safety and side-effect issues has been ongoing in earnest since the discovery of receptor subtypes (Klepner et al., 1979; Lippa et al., 1982, 1981, 1978). The recent U.S. FDA approval of brexanolone (Zulresso®) has led to a resurgence of new GABAkines entering clinical development (Cerne et al., 2021; Witkin et al., 2022). As recently as March 2022, another GABAkine (ganaxolone or Ztalmy®) was approved for seizure control in patients with CDKL5 deficiency disorder (FDA-CDER, 2022).

An imidazodiazepine GABAkine, KRM-II-81 (Witkin et al., 2022), is currently being readied for IND-enabling safety studies. In rodent models, KRM-II-81 has demonstrated anxiolytic-like efficacy (Poe et al., 2016; Witkin et al., 2017), antidepressant-like activity (Methuku et al., 2018), anticonvulsant activity (Knutson et al., 2020; Witkin et al., 2020, 2018), and efficacy in a host of acute and chronic pain models in rodents (Cerne et al., 2022). The efficacy of KRM-II-81 is coupled with an intriguing side-effect profile that includes low sedative and motor-impairing

effects, lack of tolerance development, and abuse liability (Cerne et al., 2021; Witkin et al., 2022). KRM-II-81 is active in models predicting efficacy in pharmacoresistant epilepsy (Witkin et al., 2020). In cortical slices from patients with pharmacoresistant epilepsy, KRM-II-81 has demonstrated suppression of hyperactivity across the neuronal network (Witkin et al., 2018). As an anticonvulsant, KRM-II-81 does not develop tolerance (Witkin et al., 2020). In a murine model of neuropathic pain, no analgesic tolerance was observed (Biggerstaff et al., 2020). In the intracranial self-stimulation model that detects drugs of abuse, KRM-II-81 did not show activity (Moerke et al., 2019). And, when studied as a discriminative stimulus, another model used to predict abuse liability, KRM-II-81 did not fully reproduce the effects of midazolam (Lewter, 2019).

Given the pharmacological profile of KRM-II-81, chemistry in the imidazodiazepine structural series has continued (e.g., (Knutson et al., 2020; Pandey et al., 2020). In the present manuscript, the oral bioavailability, anticonvulsant activity, and sedative side-effect profile of three structural analogs of KRM-II-81 (**Fig. 1**) will be disclosed. A structural basis for the reduced sedative profile of these imidazodiazepine was also elucidated. The compounds were constructed to determine changes in bioavailability and *in vivo* efficacy (anticonvulsant activity) with specific structural variation of the KRM-II-81 compound as shown in **figure 1**. FR-II-60 replaced the pyridine with a 2'-Cl phenyl group. Both KPP-III-34 and KPP-III-51 substituted the 1, 3 oxazole, with a 1,4 oxazole, known also to produce a non-sedating molecule like KRM-II-81 (compound 6 in Pandey et al., 2020). Ethyl substituents were added to the oxazoles as another structural change. In addition, the ethinyl of KPP-III-51 was replaced by a bromine atom to create KPP-III-34 allowing direct comparisons of this structural element. Since KPP-III-34 demonstrated the best oral exposure in rats, this compound was selected for additional more detailed anticonvulsant profiling.

Materials and Methods

Compounds.

FR-II-60, KPP-III-34, and KPP-III-51 were synthesized by us (JM Cook laboratory, University of Wisconsin-Milwaukee) as previously described (Knutson et al., 2020; Li et al., 2018; Pandey et al., 2020; Poe et al., 2016; Rashid, 2021). The other compounds were obtained from Sigma-Aldrich (St. Louis, MO, USA).

The test compounds were suspended in 1% carboxymethylcellulose unless otherwise noted; PTZ was dissolved in 0.9%NaCl. Compounds were dosed at 10 ml/kg in mice and 1 ml/kg in rats.

Cytotoxicity.

These studies were conducted at the University of Wisconsin-Milwaukee. The methods used with cultured human embryonic kidney HEK293T cells were reported (Supplementary Information of Poe et al., 2016). 3-dibutylamino-1-(4- hexyl-phenyl)-propan-1-one (150 µM in DMSO) was used as a positive control and DMSO alone as a negative control. After 18 h incubation, cell levels were assayed.

Receptor binding.

Radioligand binding studies at the primary (benzodiazepine binding site of the $GABA_A$ receptor) and at secondary protein binding sites were conducted by the National Institute of Mental Health Psychoactive Drug Screening Program (NIMH PDSP) with 4 replicates using the methods described (Roth, 2018)(see Besnard et al. 2012 for overview of assay systems). Binding in rat brain tissue using [^{3}H]flunitrazepam was used as the primary screen as described (Chang and Snyder, 1978; Sieghart et al., 1983).

Rodent assays.

All studies were performed in accordance with guidelines of the national government and by local Animal Care and Use Committees. All animals had free access to food and water except

when they were removed from their cages for the experimental procedure. All animals were group-housed in approved density housing in a temperature-, humidity-, and light-controlled vivarium prior to experimental study.

Intraperitoneal dosing - Seizure models and rotarod.

These studies were conducted by the U.S. National Institutes of Health Epilepsy Therapy Screening Program (formerly Anticonvulsant Screening Program). The assay methods used have been reported ("PANAChE current screening," n.d.; Witkin et al., 2020, 2018). The male, CF1 mice and Male, Sprague-Dawely rats, both sourced from Charles River Breeders, used in these experiments were group housed prior to experimental treatments.

In the 6 Hz (44 mA) model, the eyes of mice were treated with a drop of 0.5% tetracaine hydrochloride in 0.9% NaCl. 44 mA stimulation to induce seizures was delivered by corneal electrodes for 3s (Witkin et al., 2018). A seizure was defined as occurring if there was an initial momentary stun followed by jaw clonus, forelimb clonus, twitching of the vibrissae, and Straub tail.

In the Maximal Electroshock (MES) test, mice were given 50 mA, 60 Hz, for 0.2 s via corneal electrodes after eye treatment with 0.5% tetracaine hydrochloride.

Behavioral assessment of the mice was made after dosing with the test compound by placing them on a 1-inch knurled rod rotating at 6 r.p.m. A mouse was scored as impaired if it fell off three times during a 1 min period.

Additionally, 36 specific signs were monitored by the observers blinded to treatments (e.g., salivation, hyperactivity, loss of righting, lethality).

Data are presented as the number of mice affected (protected in seizure assays or failing the rotorod test for motor-impairment assay). Fisher's Exact Probability test (one-tail) assessed statistical significance with the priori prediction of increases in number of mice protected compared to the no drug treatment condition ($p<0.05$). The N value for control (no drug) condition was 12 (three dose conditions x 4 mice/dose condition). Historical controls were employed where under vehicle conditions there was neither any protection from seizures nor

impairment of rotarod performances (C, Metcalf, University of Utah, personal communication). Probit analysis was used to calculate ED_{50} and the 95% confidence interval.

Oral dose pharmacokinetics.

These experiments were conducted at the University of Belgrade, Serbia. To determine pharmacokinetic parameters and concentration-time profiles of the selected ligands, a standard pharmacokinetic study was conducted using adult male Sprague Dawley rats (University of Belgrade, Belgrade, Serbia). Rats were housed in groups of five (21±2 °C, 40–45% relative humidity). They had free access to standard rat chow and water under a 12:12 h light/dark cycle (lights on at 06.00 h). All animal handling and testing occurred in the light phase.

The study was conducted as approved by the Ethical Council for the Protection of Experimental Animals of the Ministry of Agriculture, Forestry and Water Management of the Republic of Serbia.

The rats (n = 45, 280-320 g) were divided into three cohorts of five groups of animals; each group contained three animals corresponding to predetermined time sampling intervals (15 min, 40 min, 2 h, 6 h and 24 h). Rats received a cassette of three compounds (2.0 mg/kg) from 0.4 mg/ml suspension in 0.25% methyl cellulose in distilled water.

At the designated time intervals, animals were anesthetized with ketamine HCl (90 mg/kg, i.p.) (Ketamidor, Richter Pharma AG, Wels, Austria) and xylazine HCl (10 mg/kg, i.p.) (Xylased, Bioveta, A. S., Ivanovice na Hane, Czech Republic), and samples of blood (collected via cardiac puncture in heparinized syringes) and brain were taken. Plasma was obtained after centrifugation for 10 min at 1000 x g (MiniSpin® plus centrifuge, Eppendorf, Germany). Brain tissue samples were weighted and homogenized in 1 ml of methanol via ultrasonic probe sonication (70% amplitude 2 x 20 s). Supernatants were separated after centrifugation for 20 min at 3400 × g (MiniSpin® plus centrifuge). Plasma and supernatants were further processed with solid phase extraction using Oasis HLB cartridges (Waters Corporation, Milford, MA). Sample preparation and concentration determination were performed by ultraperformance liquid chromatography–tandem mass spectrometry (UPLC–MS/MS) with Thermo Scientific Accela 600 UPLC system connected to a Thermo Scientific TSQ Quantum Access MAX triple quadrupole mass spectrometer (Thermo Fisher Scientific, San Jose, California), equipped with an electrospray ionization source, as described in detail (Obradović et al., 2014). Non-compartmental pharmacokinetic analysis was performed using PK Functions for Microsoft Excel

software developed by J. Usansky and colleagues (see www.pharmpk.com/xcel/pkf/pkf.doc for details and software download) Graph construction was by Sigma Plot 12 (Systat Software Inc., USA).

Oral dose – anticonvulsant effects.

Pentylenetetrazol (PTZ)-induced seizures in mice.

These studies were conducted at Indiana University, Indianapolis, IN. Male, C57BL/6N mice (Charles River, Indianapolis, IN) were used. Experimental compounds were suspended in 1% carboxymethylcellulose and PTZ was dissolved in 0.9% NaCl. Compounds were dosed at 10 ml/kg. The mice were given test compound (p.o) and placed back into their home cages. After 60 min, these mice were given PTZ (75 mg/kg, s.c.) as described (Knutson et al. (2020). The latency to produce clonic or tonic seizures was measured by a stopwatch to the second by a trained observed. The number of mice that died within the 60 min observation period was also recorded.

Latency to clonus and tonus were analyzed separately by one-way ANOVA, followed by Dunnett's test (a priori probabilities of 0.05 were set for statistical significance). Lethality was statistically evaluated by Fisher's Exact Probability test at 0.05.

Pentylenetetrazol (PTZ)-induced seizures in rats.

KPP-III-34 was studied in rats as a protector against clonic convulsions induced by PTZ. Following the oral administration of KPP-III-34, PTZ was given to male, CD Sprague-Dawley IGSrats at 68 mg/kg, s.c.. An episode of approximately 3 to 5 s of clonic spasms of the fore and/or hind limbs, jaws, or vibrissae was taken as the endpoint. Animals not displaying fore and/or hind limb clonus, jaw chomping, or vibrissae twitching were considered protected. Both time course and dose-response data were collected.

Corneal kindling in mice.

In these experiments (University of Utah, Salt Lake City, UT), KPP-III-34 was evaluated for its ability to block seizures in fully-kindled mice using methods as described previously (Witkin et al., 2020). Adult, male CF1 mice (n = 8 per group, 18-25 g) were kindled to a criterion of 5

consecutive secondarily generalized seizures of stage 5 by exposure to twice daily corneal stimulation (3 mA at 60 Hz for 3 s). After reaching the first stage 5 seizure (generally after about two weeks), the twice daily stimulation regimen was continued until each mouse achieved the criteria of 5 consecutive stage 5 seizures, at which point the mouse was considered to be fully seizure kindled. Fully kindled mice continued to be stimulated every 2 to 3 days until all mice become fully kindled.

Testing of KPP-III-34 began at least 5 days after the last corneal stimulation. Compounds were dosed 1 h prior to stimulation for the assessment of anticonvulsant efficacy. Doses of 1-30 mg/kg, p.o. were tested in groups of 8 mice. The percentage of mice protected, and the seizure severity score were measured.

The effects of KPP-III-34 on seizure protection were assessed by Fisher's exact probability test and the ED_{50} and 95% confidence limits were determined by probit analysis. Effects of the compounds on seizure severity scores were analyzed by one-way ANOVA followed by Dunnett's test. Probabilities of < 0.05 were set a priori as the accepted level of statistical significance.

Mesial temporal lobe model.

Seven, male C57/Bl6 mice (10 wk old from Janvier Labs, Le-Genest-St-Isle, France) were used in these experiments conducted by Synapcell (Saint Ismier, France). Seizures are generated by unilateral application of kainic acid into the dorsal hippocampus according to standard protocol (https:/panache.ninds.nih.gov) as previously described (Witkin et al., 2020). Two to three weeks after the kainate injection, spontaneous recurrent hippocampal paroxysmal discharges were recorded in the epileptic hippocampus. The mice were allowed to recover for 4 wk prior to drug testing. Each mouse was used as its own control. Digital EEG recordings were performed on freely moving mice for 20 min prior to drug testing and then for 90 min post dosing.

KPP-III-34 (30 mg/kg) was given orally, 60 min prior to EEG recording. The number of hippocampal paroxysmal discharges were counted during baseline and drug conditions and compared by Student's t-test for paired observations. Probabilities of < 0.05 were set a priori as the accepted level of statistical significance.

Oral dose side-effect profiling.

Motor-impairment: Rotarod in mice.

Methods were generally as previously reported (Pandey et al., 2020) and were carried out at the University of Wisconsin-Milwaukee, WI. Female, Swiss Webster mice were trained to maintain balance at a constant speed of 15 rpm on the rotarod apparatus (Omnitech Electronics Inc., Nova Scotia, Canada) until they reached a behavioral criterion of successful balance for 3 min across three consecutive trials. Separate groups of nine mice received oral gavage of vehicle (2% hydroxypropyl methylcellulose and 2.5% polyethylene glycol) or compounds in a volume of 200 µL. Diazepam in 10% DMSO, 40% propylene glycol, and 50% phosphate-buffered saline was used as a positive control at 5 mg/kg, p.o. The mice were placed on the rotarod at three separate time points of 10, 30, and 60 minutes after administration. A 'fail' was defined for each mouse falling twice prior to 3 min.

Data were analyzed separately for each compound tested by two-way repeated-measures ANOVA with time, dose, and animals as factors. Post-hoc analyses were made by Bonferroni's multiple comparison test ($p<0.05$ set as the a priori rate for statistical significance).

Modified Irwin test in rats. KPP-III-34 that was chosen for profiling was given orally and assessed for untoward effects by previously published methods (Mathiasen and Moser, 2018). The studies were conducted at the University of Utah, Salt Lake City, UT. Before testing, animals are handled over two days to familiarize them with handling. Rats were visually evaluated by two independent observers for impaired autonomic (e.g., salivation, porphyrin), neuromuscular (e.g., ataxia, tremors), sensorimotor (e.g., hyperesthesia, loss of righting reflex), and behavioral (e.g., vocalizations, grooming) function at 0.25, 0.5, 1, 2, and 4 h post oral dosing (50-500 mg/kg) (N=8/dose). The rats were also observed 24 h after compound dosing to assess recovery from any impairment seen the previous day. A numerical score is assigned for the severity, from normal to extreme, for each functional parameter.

Molecular docking studies.

Studies were conducted as previously described (Golani et al., 2022b; Pandey et al., 2020; Witkin et al., 2020) at the University of Wisconsin-Milwaukee. In brief, molecular docking was performed using AutoDock Vina 1.5.6.22 using the CryoEM structure of the human full-length α1β3γ2L $GABA_A$ receptor ion complex with alprazolam (PDB: 6HUO) (Masiulis et al., 2019). FR-

II-60 and KPP-III-34 were so modeled. The docking analysis of KPP-III-51 was reported previously (Pandey et al., 2020).

Results

Cytotoxicity. 3-dibutylamino-1-(4- hexyl-phenyl)-propan-1-one was run as a positive control at 150 μM; all cells were killed at this concentration. For FR-II-60, the IC_{50} was >150 μM and for KPP-III-34 and KPP-III-51, the IC_{50} was > 300 μM for cytotoxicity in HEK 293 cells.

Receptor Binding. The inhibition of radioligand binding is shown in **Table 1**. Only the receptor proteins for which binding was inhibited by >50% at 10 μM across 47 receptor targets (including hERG for potential cardiovascular liability) in the primary screen; the values for 5-HT_{1A} and peripheral benzodiazepine receptor (PBR) are shown for purposes of comparison to the other analogs.

Table 1. Primary and secondary binding data for the three compounds studied.

Compound	**Receptor**	**Primary (mean % inhibition)**	**Secondary (K_i in nM)**	**Fold Selectivity**
FR-II-60	BZP	99.1	34.0	NA
	5-HT_{1A}	26.7	NA	NA
	KOR	53.4	1847	54.3
	PBR	40.1	NA	NA
	Sigma2	60.5	4396	129

KPP-III-34	BZP	92.2	47.4	NA
	5-HT_{1A}	50.2	1835	38.7
	KOR	90.6	380	5.9
	PBR	63.9	591	12.5
KPP-III-51	BZP	92.0	182	NA
	5-HT_{1A}	51.5	2108	11.6
	KOR	65.6	1292	7.10
	PBR	74.3	1263	6.94

BZP: Benzodiazepine binding site assessed by inhibition of [^{3}H]-flunitrazepam binding in rat brain homogenates

5-HT_{1A}: Serotonin 1A receptor was assessed by inhibition of [^{3}H]-WAY100635 binding

KOR: Kappa opioid receptor was assessed by inhibition of [^{3}H]-U69593 binding

PBR: Peripheral benzodiazepine receptor sites were assessed by inhibition of [^{3}H]-PK11195 in rat brain homogenates

NA: not applicable

Intraperitoneal Dosing – Seizure models and rotarod.

Intraperitoneal dosing with FR-II-60, KPP-III-34, and KPP-III-51 was studied in two seizure models in mice at 0.5 h and 2 h post dosing. The mice were also tested for motor impairment as measured on a rotarod to ascertain the impact of the compounds on the ability of the mice to maintain balance. The data are summarized in **Table 2**. Dose-dependent increases in the number of mice protected from seizures were observed for FR-II-60 and for KPP-III-34 but was

much less evident for KPP-III-51 where no dose produced significant protection. The doses that produced seizure protection were also generally motorically impairing as assessed on the rotarod for FR-II-60 and KPP-III-51. In contrast KPP-III-34 protected against seizures induced by 6Hz stimulation at 100 mg/kg without significantly impairing rotarod performance.

All mice were observed for atypical body signs including sedation, ataxia, parasympathetic activity, seizures, tremor, and death. No adverse reactions were noted at either the 0.5 or 2 h time points except for KPP-III-51 where mice had difficulty grasping the rotarod at 300 mg/kg at 0.5 h post dosing. There was no mortality at 72 h post dosing in any of the mice dosed with the exception of one mouse in the 100 mg/kg group for KPP-III-51 that died during the MES test (**Table 2**).

Table 2. Effects of the test compounds given i.p. in two acute seizure provocation models and on rotarod performance of male, CF1 mice[1].

FR-II-60

Assay	**Dose (mg/kg, IP)**	**Number Affected/ Number Tested @ 0.5 h**	**Number Affected/ Number Tested @ 2 h**
6Hz	30	3/4*	1/4
	100	3/4*	3/4*
	300	3/4*	4/4*
MES	30	2/4	1/4
	100	4/4*	4/4*
	300	4/4*	4/4*

Rotorod	30	4/8	0/8
	100	6/8*	5/8
	300	8/8*	7/8*

KPP-III-34

6Hz	30	0/4	0/4
	100	3/4*	0/4
	300	3/4*	2/4
MES	30	0/4	0/4
	100	2/4	0/4*
	300	2/4	3/4*
Rotorod	30	0/8	0/8
	100	2/8	0/8
	300	8/8*	2/8

KPP-III-51

6Hz	30	0/4	0/4
	100	0/4	0/4
	300	0/4	2/4
MES	30	0/4	0/4
	100	0/4	0/4[&]

	300	0/4	0/4
Rotorod	30	0/8	0/8
	100	2/8	0/8
	300	8/8*#	3/8

[1] Historical controls were employed where under vehicle conditions there was neither any protection from seizures nor impairment of rotarod performances (C, Metcalf, University of Utah, personal communication).

*P < 0.05: &Death associated with tonic seizure; #Unable to grasp rotarod.

A further study of the anticonvulsant effects of KPP-III-34 was conducted in rats with i.p. doses of 10-25 mg/kg KPP-III-34 with 8 rats/dose (0.25 h post dosing with KPP-III-34). Using s.c. pentylenetetrazol as a chemoconvulsant, the ED_{50} of KPP-III-34 was 16.6 mg/kg (95% Cl: 13.6-19.0 mg/kg). In the rotarod assay in rats conducted at 0.5 h post dosing in 8 rats each at doses of 50-100 mg/kg, i.p., the ED_{50} for disruption of performances was 77.4 mg/kg (95% Cl: 62.6 – 91.0 mg/kg).

Oral Dose Pharmacokinetics.

Pharmacokinetic studies were performed in order to evaluate the *in vivo* fate, after oral gavage, of the three structural analogs of KRM-II-81 (KPP-III-51, KPP-III-34 and FR-II-60). Kinetic profiles in plasma and brain for FR-II-60 (**Fig. 2**), KPP-III-34 (**Fig. 3**), and KPP-III-51 (**Fig. 4**) show similarities and some striking differences. Using the compound concentration summary parameters of C_{max} and AUC (**Table 3**), the plasma levels achieved by KPP-III-34 are greater than that of the two other analogs (~ 10x). Likewise, the brain levels achieved by KPP-III-34 (AUC) are 2x higher than the other analogs. The C_{max} for brain levels of KPP-II-51 is much lower than

that of the other two analogs. However, given the sustained increases in brain levels of KPP-III-51 (**Fig. 4**) compared to the other two analogs, the AUC differences are not as great.

It is also noted that whereas FR-II-60 displays relatively linear kinetics (**Fig. 2**), KPP-III-34 (**Fig. 3**) and KPP-III-51 (**Fig. 4**) show higher levels of compound in brain than plasma at 24h than that of FR-II-60). Compound concentrations from these studies in nM are shown in **Table 3** for direct comparison. Brain to plasma ratios of compound concentration document the larger brain to plasma uptake of FR-II-60 compared to the other compounds (**Table 3**). The large brain/plasma ratio for FR-II-60 is accounted for by the high brain levels achieved compared to plasma (with variability) at 2-6 h post dosing (**Fig. 2**).

Table 3. Concentrations of compounds in plasma and brains of rats after oral dosing.

Compound	**C_{max} (Plasma)**	**C_{max} (Brain)**	**C_{max} (Brain/Plasma)**	**AUC 24h (Plasma)**	**AUC 24 h (Brain)**	**AUC 24 h (Brain/Plasma)**
FR-II-60	22.4	391.2	17.5	63.5	1047	16.5
KPP-III-34	228.2	259.2	1.14	1064.2	2336.2	2.20
KPP-III-51	39.3	69.6	1.77	253.4	1134	4.48

Concentrations are in nM.

Oral Dosing – PTZ seizures in mice

FR-II-60 significantly increased the latency of PTZ to produce clonic seizures in mice ($F_{2,16} = 33.6$, $P < 0.0001$). Post-hoc Dunnett's test revealed that doses of 10 and 30 mg/kg both significantly increased clonic seizure latency (**Fig. 5, left panels**). Tonic seizure latency was also significantly increased by FR-II-60 ($F_{2,13} = 35.7$, $P < 0.0001$). Post-hoc Dunnett's tested revealed that both 10 and 30 mg/kg significantly increased tonic seizure latency (**Fig. 5, right panels**).

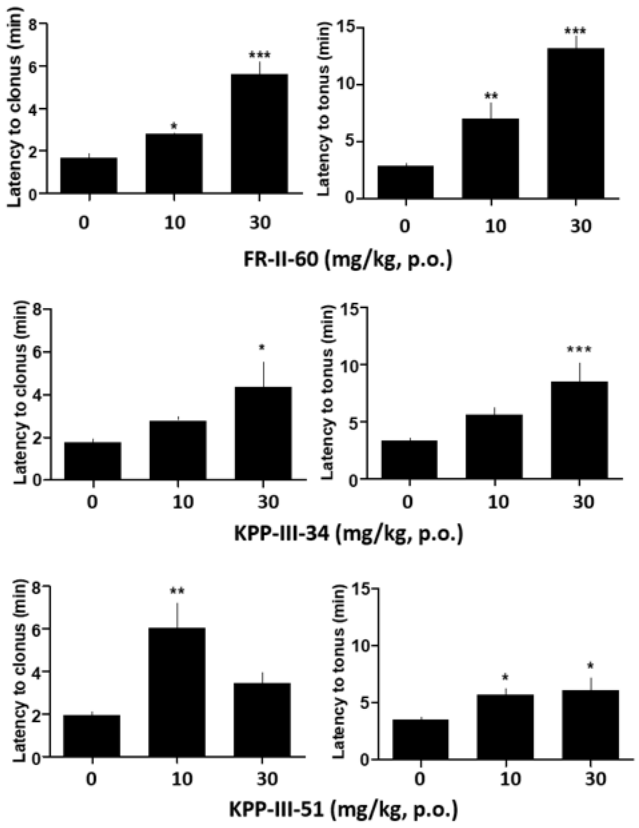


Figure 5. Effects of orally administered FR-II-60, KPP-III-34, or KPP-III-51 on the latency to produce clonic (left panels) or tonic (right panels) seizures after 75 mg/kg PTZ, s.c. in male, C57BL/6N mice. *, **, *** P <0.05, 0.01, and 0.001 compared to respective vehicle control value. N=6-9 mice per group.

KPP-III-34 also significantly increased the latency to clonus ($F_{2,20}$ = 4.68; P = 0.023) and tonus ($F_{2,21}$ = 9.13; P = 0.002). Only the 30 mg/kg dose of KPP-III-34 significantly increased seizure latencies (**Fig. 5**).

KPP-III-51 significantly increased the latency for PTZ to induce clonic seizures ($F_{2,20}$ = 14.4; P = 0.0002) and tonic seizures ($F_{2,21}$ = 6.54; P = 0.007). Whereas only 10 mg/kg significantly increased the latency to produce clonus, both 10 and 30 mg/kg significantly increased the latency for PTZ to induce tonus (**Fig. 5**). The increases in latency to produce tonus by KPP-III-51 were also generally less than those increases produced by FR-II-60 and KPP-III-34.

All three compounds significantly prevented or exhibited trends toward preventing PTZ-induced lethality (**Table 4**). This effect was not always dose dependent. In contrast to FR-II-60 and KPP-III-34, KPP-III-51 was less efficacious on this measure.

Table 4. Protection against lethality induced by 75 mg/kg PTZ (s.c.) after oral administration (60 min prior) of test compounds in male, C57BL/6N mice.

Compound	**Lethality/ Number Tested**	
Vehicle	12/15	
FR-II-60 (10 mg/kg)	0/6*	
FR-II-60 (30 mg/kg)	1/6*	
KPP-III-34 (10 mg/kg)	0/6*	
KPP-III-34 (30 mg/kg)	2/6	
KPP-III-51 (10 mg/kg)	1/6*	
KPP-III-51 (30 mg/kg)	4/6	

Shown are the number of mice that died/number of mice tested.

*$P < 0.05$

KPP-III-34: Oral anticonvulsant activity in rats.

Based upon the preceding findings, KPP-III-34 was chosen as a compound for further anticonvulsant screening. In these studies with rats, there were no signs of impairment by KPP-III-34 and no deaths. Blockade of pentylenetetrazol-induced convulsions was dose- and time-dependent (**Table 5**). Dose-response data for orally administered KPP-III-34 are shown in **Table 6** (testing at 0.5 h post dosing of KPP-III-34). The data from the dose-response curve when dosed 0.5 h prior to PTZ yielded an ED_{50} of 15.5 mg/kg with 95% confidence limits of 8.75-25.0.

High oral doses of KPP-III-34 (50, 100, 300, 500 mg/kg) was given to rats (N = 8/group) under observation in a modified Irwin test. There were no observed signs of untoward effects at any of the time points evaluated (0.25, 0.5, 1, 2, 4, and 8 h) and no observations at 24 h post dosing of KPP-III-34 (data not shown). Further, no adverse events or lethality were observed in the rats in a functional test battery that observed autonomic, neuromuscular, sensorimotor, and behavioral functions (data not shown).

Table 5. Time course of the anticonvulsant effects of orally administered KPP-III-34 on PTZ-induced convulsions in rats.

Dose (mg/kg)	0.25 h	0.5 h	1 h	2 h	4 h
5	1/4	1/4	0/4	1/4	0/4
20	3/4*	4/4*	3/4*	3/4*	2/4
50	6/8*	8/8*	6/8*	7/8*	7/8*

Male, Sprague-Dawley rats were tested for seizure induction by PTZ at different times after dosing of KPP-III-34

Data are shown as number of rats protected/number of rats tested

* p < 0.05 compared to vehicle control

Table 6. Dose-response of orally administered KPP-III-34 on PTZ-induced convulsions in rats

Dose (mg/kg)	Number Protected /Number Tested	Adverse Events
5	1/4	0/8
10	1/8	0/8
20	5/8	0/8
50	8/8*	0/8

Male, Sprague-Dawley rats were tested at 0.5 h post dosing of KPP-III-34

Data are shown as number of rats protected/number of rats tested

* p < 0.05 compared to vehicle control

KPP-III-34: Oral dose anticonvulsant activity in the 6Hz (44mA) assay in mice.

Effects of KPP-III-34 were studied in mice using 6Hz (44mA) electrical stimulation to induced seizures. A second experiment was conducted with doses of 50-300 mg/kg (N=8 mice/dose) given 1 h prior to 6Hz stimulation. The ED_{50} for blocking seizures was 115.5 mg/kg with 95% confidence limits of 62.0 -177 mg/kg. In contrast, the ED_{50} for rotarod impairment was calculated to be > 300 mg/kg with the mice affected only at 300 mg/kg (2 of 8).

KPP-III-34: Oral dose anticonvulsant activity in corneal-kindled mice.

Mice that were seizure kindled by daily electrical corneal stimulation, were tested with KPP-III-34 (**Table 7**). Oral doses of KPP-III-34 dose-dependently reduced the incidence of seizures in

these mice ($F_{4,39}$ = 7.17, p < 0.001) with an ED_{50} of 12.7 mg/kg (95% confidence limits: 4.35-21.9).

KPP-III-34: Oral dose anticonvulsant activity in the mesial temporal lobe model in mice.

In the mesial temporal lobe epilepsy model, KPP-III-34 significantly reduced the number of the baseline level of spontaneous recurrent hippocampal paroxysmal discharges when given at 30 mg/kg, p.o. (t_6 = 2.74, p = 0.034) (**Fig. 6**).

18.86 ± 2.09 9.86 + 3.83 after 30 mg/kg KPP-III-34, p.o.

Table 7. Effects of KPP-III-34 on orally administered KPP-III-34 on corneal kindling in male, CF1 mice.

Dose (mg/kg)	Number Protected /Number Tested	Individual Seizure Scores	Mean Seizure Score (S.E.M)
3.5	1/8	0,4,5,4,4,5,5,4	3.88 (0.58)
15	6/8*	0,0,0,4,0,5,0,0	1.12 (0.74)**
30	5/8	0,0,3,0,4,4,0,0	1.38 (0.68)*
60	6/8*	0,0,0,0,0,2,0,3	0.62 (0.42)***
120	8/8*	0,0,0,0,0,0,0,0	0.00 (0.00)***

KPP-III-34 was given orally, 1 h prior to corneal stimulation and given a seizure severity score from 0 to 5 as describe in Methods.

A mouse was considered protected from seizures when they did not exhibit any seizure signs (Methods); such mice were given a score of 0 for their seizure score.

*P < 0.05; **P < 0.01; ***P < 0.001 compared to effects at 3.5 mg/kg

Oral dose motor-impairment: rotarod.

Mice trained over days to balance on the rotarod for 3 min were given diazepam, FR-II-60, or KPP-III-34. Rotarod data for KPP-III-51 has been disclosed recently where an oral dose of 120 mg/kg did not significantly disrupt motor performance (Pandey et al., 2020).

FR-II-60 (p.o.) was studied alongside 5 mg/kg diazepam, p.o (**Fig. 7**). In this experiment there was a significant effect of drug treatment ($F_{4,80}$ = 6.91; P = 0.0003), of time ($F_{2,80}$ = 4.75; P = 0.011), subjects ($F_{40,80}$ = 3.63; P < 0.0001) but not an overall significant treatment x time interaction ($F_{8,80}$ = 1.72; P = 0.11). Post-hoc analyses documented a significant effect of diazepam at 10- and 30-min post dosing. Significant impairment at 80 mg/kg FR-II-60 was also observed at 10 and 30 min post dosing. (**Fig. 7**).

Effects of KPP-III-34 (**Fig. 7**) showed a toward a trend toward an effect of dose ($F_{3,64}$ = 2.29; P = 0.097), an effect of time ($F_{2,64}$ = 4.38; P = 0.017), and a significant dose x time interaction ($F_{6,64}$ = 2.29; P = 0.046), but not a significant effect of subjects ($F_{32,64}$ = 1.00; P = 0.49). The effect of 120 mg/kg KPP-III-34 showed a significant effect of dose only at the 10 min time point. Effects of no other doses significantly separated from vehicle (**Fig. 7**).

Molecular docking studies.

The minimal effects of the three test compounds on rotorod performances encouraged molecular docking studies to help to define a structural basis. Docking experiments with KPP-III-51 have been reported (Pandey et al., 2020). Comparison of the docking of FR-II-60 and the sedating compound alprazolam are shown in **Figure 8**. Docking results from the modeling experiments indicated that replacing the C8 chlorine atom in alprazolam, with the ethinyl group in FR-II-60 leads to a loss in this key halogen bond interaction with α1His102. The docking score of FR-II-60 (**Table 8**) also indicates that the binding affinity of FR-II-60 should be less as compared to alprazolam at the α1subtype $GABA_A$ receptor.

The alprazolam forms a crucial halogen bond interaction between the carbonyl oxygen atom of the α1His102 backbone and the chlorine atom. The angle between the oxygen, chlorine, and carbon atoms is 167º. KPP-III-34 was docked into the CryoEM structure (**Figure 9 A and B**). The docking pose shows that the angle between the oxygen, bromine and carbon atoms is 122.75º. The docking score of KPP-III-34 (**Table 8**) also indicates that the binding affinity of KPP-III-34 should be less ascompared to alprazolam at the α1subtype $GABA_A$ receptor. This was found to be the case (see **Table 8**).

With the exception of the halogen bond interaction, other interactions with the α1 subunit were maintained by the predicted binding poses of FR-II-60 and KPP-III-34. Here we show that the predicted binding pose of FR-II-60 overlapped with that of alprazolam better than the predicted binding pose of KPP-III-34 (**Fig. 8B, 9B**). This predicted interaction is consistent with the greater impairment in rotarod performance observed with FR-II-60 (**Fig. 7**). Indeed, KPP-III-34 was not sedating in rats up to 500 mg/kg, p.o. (data presented here). The disorientation of the diazepine ring, which occurs in the predicted binding pose of KPP-III-34, is probably due to compensation for the binding of the ethyl substituted oxazole ring that allows the ligand to fit in the binding pocket (**Fig. 9**). Also, the Br atom of KPP-III-34 in place of the ethinyl moiety of KPP-III-51 (**Table 8**) enables reducedbinding interaction due to length differences of these two substituents.

Table 8. Docking scores of alprazolam, FR-II-60, and KPP-III-34, and KPP-III-51.

Compound	**Docking score (Binding affinity in kcal/mol)**
alprazolam	-10.8
FR-II-60	-9.5
KPP-III-34	-9.1

KPP-III-51	-9.6

Data on KPP-III-51 are from Pandey et al. (2020)

Discussion

The imidazodiazepine, or KRM-II-81 is undergoing preparations for clinical development (Witkin et al., 2022) In the present set of experiments, three novel analogs were synthesized to broadly test effects of specific structural features on pharmacokinetics and *in vivo* activity.

All compounds bound to brain receptors labeled by [^{3}H]-flunitrazepam (benzodiazepine binding site on the $GABA_A$ receptor). Non-GABA binding was observed at only a few of the 47 other receptors evaluated and, with one exception, binding at these non-GABA sites was with much weakerpotency than at $GABA_A$ receptors. The three analogs also presented low potency cytotoxicity with selectivity over [^{3}H]-flunitrazepam binding. Binding to hERG channels, another potential marked of in vivo toxicity was also weak with binding for all compounds greater than 10 μM.

The most striking findings observed with structural modifications of KRM-II-81 were the reduced biological exposures after oral administration for FR-II-60 and KPP-III-51. One factor affecting pharmacokinetics is compound lipophilicity (Lipinski, 2004). The CLogP values for the compounds were 1.58 (KRM-II-81), 3.05 (FR-II-60), 2.38 (KPP-III-51), and 2.97 (KPP-III-34). The increase in CLogP in FR-II-60, and in KPP-III-51, might therefore be one factor responsible for the reduction in plasma and brain exposures relative to KRM-II-81. Theoretically, such a difference is expected to deteriorate the absorption at the level of intestinal barrier, while enhancing at the same time its capability to pass the blood-brain barrier. Changes in lipophilicity do appear to have some impact on the oral pharmacokinetics of these compounds. However, the substitution of a Br atom in KPP-III-34 for the ethinyl group in KPP-III-51, re-instated plasma exposures to near the levels of KRM-II-81 (**Table 9**). The dynamics regulating this difference in the two compounds will require detailed study of drug disposition, in particular, the role of metabolism.

A second peak of exposure at 24 h was also observed with KPP-III-34 suggesting a potential depot effect. This might have resulted from unpredicted precipitation in the gastrointestinal tract, even though a standard vehicle for oral dosing in preclinical animal models was chosen. enterohepatic recirculation (Zhang et al., 2021) for KPP-III-34

The brain exposures of the compounds in rats after oral administration were compared to their affinities for binding to rat brain benzodiazepine receptors. The C_{max} level of exposure was greater than the IC_{50} for FR-II-60 (11.5 times) but not the other two compounds. However, the AUC over 24 h was 31 (FR-II-60), 3.2 (KPP-III-34), and 6.2 (KPP-III-51) times greater than the potency for benzodiazepine site binding.

Intraperitoneal administration of FR-II-60 and KPP-III-34, but not that of KPP-III-51, produced anticonvulsant activity (6Hz model and maximal electroshock) at doses lower than those required to disrupt rotarod performance of mice. Further investigation of KPP-III-34 showed that it was also an effective anticonvulsant (vs. PTZ) in rats by the intraperitoneal route. Oral administration of all three compounds was anticonvulsant in mice against PTZ-induced seizures and lethality, an effect also shared by KRM-II-81 (Witkin et al., 2018). However, KPP-III-51 was the weakest anticonvulsant in this assay with a lack of dose-dependence and a reduced efficacy against tonic seizures. However, that the relatively low plasma and brain exposure of KPP-III-51 was sufficient to drive oral anticonvulsant activity is consistent with the ability of other imidazodiazepines, like HZ-166, to be anticonvulsant despite low exposure levels (Rivas et al., 2009). HZ-166 is the precursor molecule for KRM-II-81. An ester group in the position of the oxazole of KRM-II-81 was a target for metabolism that resulted in low bioavailability (Poe et al., 2016) and in some cases, a lack of anticonvulsant activity (Witkin et al., 2018).

Although FR-II-60 and KPP-III-51 showed marked reductions in plasma and brain exposure after oral administration compared to KRM-II-81, they were still able to produce anticonvulsant effects. This suggests potentially important features of these compounds as antiepileptics since lower plasma exposures generating therapeutic efficacy should be associated with larger margins of safety. In this vein, the pharmacokinetic behavior of KPP-III-51 and FR-II-60 cannot be seen as inadequate for their possible further development as brain targeting treatments.

We suggest that the anticonvulsant activity of the compounds is due to their ability to act as GABAkines (potentiators) of $GABA_A$ receptors. However, ancillary activity (**Table 1**) might be responsible or contribute though we view this as unlikely. Kappa opioid receptor agonists have been shown to be anticonvulsant (Loacker et al., 2007; Manocha et al., 2003; Zangrandi and Schwarzer, 2022). Peripheral benzodiazepine receptor ligands have also shown potential relationships toward seizure control (Ferrarese et al., 1997; Shiotani et al., 2000) as have 5-HT_{1A}

receptors (Gharib et al., 2018; Pelz et al., 2017; Sapa et al., 2014; Waszkielewicz et al., 2015)(Gharib et al., 2018; Pelz et al., 2017; Sapa et al., 2014; Waszkielewicz et al., 2015). However, the selectivity of these compounds over these targets is one piece of evidence that these ancillary actions are not necessary for the anticonvulsant activity of these compounds. Nonetheless, the possibility that multiple actions contribute to anticonvulsant efficacy cannot be excluded with these data alone.

KPP-III-34 was selected for additional anticonvulsant profiling based upon its excellent oral exposure and anticonvulsant data. In addition to protecting against PTZ-induced seizures and lethality in mice, KPP-III-34, like KRM-II-81 (Witkin et al., 2020, 2018), was an efficacious anticonvulsant against PTZ in rats, and against fully kindled seizures (corneal kindled seizures in mice), as well in a kainate-induced mouse model of mesial temporal lobe epilepsy. The 6Hz (44mA), corneal kindling, and mesial temporal lobe models are all used to help identify improved anticonvulsants and those that might function against pharmacoresistant epilepsy (Barton et al., 2001; Bouilleret et al., 1999; Leclercq et al., 2014; Rowley and White, 2010; Wilcox et al., 2013).

The three analogs of KRM-II-81 did not show appreciable sensorimotor impairment in mice when measured on the rotarod; in contrast diazepam disrupted performances. The ability of benzodiazepine GABAkines to produce sedative effects and decreases in locomotion in rodents is well documented (c.f., Knutson et al., 2021; Witkin et al., 2018). In comparison, when tested up to 500 mg/kg in rats, p.o., KPP-III-34 did not exhibit any signs indicative of untoward effects. These findings are congruent with the reduced impact of imidazodiazepines of this series on sensorimotor function including HZ-166 and KRM-II-81 (c.f., (Cerne et al., 2022; Witkin et al., 2020;2022). As with KPP-II-51 which also demonstrated low sensorimotor impairing effects (Pandey et al., 2020), FR-II-60 and KPP-III-34 showed weaker halogen bonding with the backbone of α1His102. The ideal bond angle for a halogen bond is 180º; the halogen bond becomes weaker if the angle deviates from linear (Shinada et al., 2019). Consequently, KPP-III-34 forms a weaker halogen bond with the backbone of α1His102. This could be the reason for the decreased affinity towards α1, which results in non-sedation of KPP-III-34 up to 120 mg/kg in mice. KPP-III-34 was also devoid of notable side-effects when given up to 500 mg/kg. The ethyl oxazole, KPP-III-34, was less sedating and ataxic than FR-II-60 and related oxazoles because the former ethyl oxazole fits into the binding pocket with a slightly different alignment, which decreased the strength of the halogen bond of the C-8 bromine atom with the histidine backbone of the C-loop (see Golani et al., 2022b).

That these three novel imidazodiazepine GABAkines displayed oral bioavailability and anticonvulsant efficacy with low propensity to disrupt sensorimotor function or produce other untoward side-effects is encouraging of further development. The comparative pharmacology of KPP-III-34 relative to the parent molecule KRM-II-81 is summarized in **Table 9**. Small decreases in bioavailability were observed with KPP-III-34 but the brain levels and brain to plasma ratio of this analog was generally unharmed. Although equally efficacious to KRM-II-81, the oral anticonvulsant potency of KPP-III-34 was slightly less than that of KRM-II-81. Both compounds demonstrated good tolerability in mice and rats that corresponded to their molecular modelling docking scores with the Brominated KPP-III-34 molecule showing the least interaction with the critical α1 residue. The potency of KPP-III-34 at GABAA receptors was more potent than that of KRM-II-81 but KPP-III-34 also incurred additional off-target activity than KRM-II-81. Thus, KPP-III-34 presents as a novel compound with overlapping as well as unique pharmacological properties that continues to carry anticonvulsant activity with low sedative liability.

Table 9. Comparative Effects of KPP-III-34 and KRM-II-81*

Assay	**KPP-III-34**	**KRM-II-81**	**KRM-II-81 Reference**
C_{max} Plasma - rat	228 nM	395 -1832 nM	Golani et al., 2021; Mian et al., 2022
C_{max} Brain - rat	259 nM	594 - 678 nM	Golani et al., 2021; Mian et al., 2022
C_{max} – Brain/Plasma	1.14	0.32 – 1.7	Golani et al., 2021; Mian et al., 2022
AUC_{0-24} Plasma – rat	1064 nM	2161 - 3589 nM	Golani et al., 2021; Mian et al., 2022
AUC_{0-24} Brain - rat	2336 nM	2343 – 2690 nM	Golani et al., 2021; Mian et al., 2022d
PTZ clonus - mouse	30 mg/kg	10 mg/kg	Golani et al., 2021; Mian et al., 2022
PTZ tonus - mouse	30 mg/kg	10 mg/kg	Golani et al., 2021; Mian et al., 2022
PTZ lethality - mouse	10 mg/kg	10 mg/kg	Golani et al., 2021; Mian et al., 2022

6Hz (44 mA) – mouse	200 mg/kg	50 mg/kg	Witkin et al., 2018
Corneal kindling - mouse	13 mg/kg	8 mg/kg	Witkin et al., 2020
Mesial temporal lobe seizures – mouse	30 mg/kg	15 mg/kg	Witkin et al., 2020
Rotarod – mouse	120 mg/kg	100 mg/kg	Ping et al., unpublished
Molecular modeling docking score	-9.1 kcal/mol	-9.4 kcal/mol	Witkin et al., 2020
Adverse events – rat	> 500 mg/kg	> 300 mg/kg	Witkin et al., 2020
Cytotoxicity	> 300 μM	> 100 μM	Poe et al., 2016
hERG binding	> 10 μM	> 100 μM	Poe et al., 2016 suppl.
BZP binding	47.4	294-554	From NIMH PDSP
5-HT1A binding	1835	29.5% inhibition	From NIMH PDSP
KOR binding	380	45.9% inhibition	From NIMH PDSP
PBR	591	435-723	From NIMH PDSP

*Data for KPP-III-34 are from the present study. In vivo data are with oral dosing.
Anticonvulsant data are minimum effective doses.
For the mesial temporal lobe seizure assay, only one dose was tested.
For the cytotoxicity assay, only 100 μM was tested for KRM-II-81.
Binding data are shown for the receptors identified in a primary screen for KPP-III-34 where >50% inhibition was observed at 10 μM. Data are expressed as K_i in nM or as % inhibition in the primary screen.

Acknowledgements

We are grateful to John and Nancy Peterson for their support of this research. We thank the following granting agencies for support: DA-043204 and NS-076517 and the National Science Foundation, Division of Chemistry [Grant CHE-1625735]. We also acknowledge the UW-Milwaukee Shimadzu Laboratory for Advanced and Applied Analytical Chemistry and support from the Milwaukee Institute of Drug Discovery and the University of Wisconsin-Milwaukee Research Foundation.

Part of this work was funded by the Ministry of Education, Science and Technological Development, Republic of Serbia through Grant Agreement with University of Belgrade-Faculty of Pharmacy No: 451-03-9/2021-14/200161.

We thank the NIH Epilepsy Therapy Screening Program for some of the data collection.

Authorship Contributions

Participated in research design and conceptualization: all authors

Conducted experiments: Pandey, Rashid, Divović, Golani, Ping

Contributed new reagents or analytic tools: Pandey, Rashid, Golani

Performed data analysis: Divović, Golani, Ping, Witkin

Wrote or contributed to the writing of the manuscript: all authors

REFERENCES

Barton ME, Klein BD, Wolf HH, and White HS (2001) Pharmacological characterization of the 6 Hz psychomotor seizure model of partial epilepsy. Epilepsy Res 47: 217–227.

Besnard J, Ruda GF, Setola V, Abecassis K, Rodriguiz RM, Huang XP, Norval S, Sassano MF, Shin AI, Webster LA, Simeons FR, Stojanovski L, Prat A, Seidah NG, Constam DB, Bickerton GR, Read KD, Wetsel WC, Gilbert IH, Roth BL, Hopkins AL. Automated design of ligands to polypharmacological profiles. Nature. 2012 Dec 13;492(7428):215-20. doi: 10.1038/nature11691. PMID: 23235874; PMCID: PMC3653568.

Biggerstaff, A., Kivell, B., Smith, J.L., Mian, M.Y., Golani, L.K., Rashid, F., Sharmin, D., Knutson, D.E., Cerne, R., Cook, J.M., Witkin, J.M., 2020. The α2,3-selective potentiators of GABAA receptors, KRM-II-81 and MP-III-80, produce anxiolytic-like effects and block chemotherapy-induced hyperalgesia in mice without tolerance development. Pharmacol Biochem Behav 196, 172996. https://doi.org/10.1016/j.pbb.2020.172996

Bouilleret V, Ridoux V, Depaulis A, Marescaux C, Nehlig A, and Le Gal La Salle G (1999) Recurrent seizures and hippocampal sclerosis following intrahippocampal kainate injection in adult mice: electroencephalography, histopathology and synaptic reorganization similar to mesial temporal lobe epilepsy. Neuroscience 89: 717–729.

Cerne, R., Lippa, A., Poe, M.M., Smith, J.L., Jin, X., Ping, X., Golani, L.K., Cook, J.M., Witkin, J.M., 2021. GABAkines - Advances in the discovery, development, and commercialization of positive allosteric modulators of GABAA receptors. Pharmacol Ther 108035. https://doi.org/10.1016/j.pharmthera.2021.108035

Cerne, R., Smith, J.L., Fisher, J.L., Golani, L.K., Knutson, D.E., Cook, J.M., Witkin, J.M., 2022. Chapter 11 - The orally bioavailable imidazodiazepine, KRM-II-81, is a novel potentiator of α2/3-containing GABAA receptors with analgesic efficacy, in: Rajendram, R., Patel, V.B., Preedy, V.R., Martin, C.R. (Eds.), The Neurobiology, Physiology, and Psychology of Pain. Academic Press, pp. 117–127. https://doi.org/10.1016/B978-0-12-820589-1.00011-7

Chang, R.S., Snyder, S.H., 1978. Benzodiazepine receptors: labeling in intact animals with [3H] flunitrazepam. Eur J Pharmacol 48, 213–218. https://doi.org/10.1016/0014-2999(78)90330-8

FDA-CDER, 2022. FDA approves drug for treatment of seizures associated with rare disease in patients two years of age and older [WWW Document]. FDA. URL https://www.fda.gov/drugs/news-events-human-drugs/fda-approves-drug-treatment-seizures-associated-rare-disease-patients-two-years-age-and-older (accessed 3.28.22).

Ferrarese, C., Tortorella, R., Bogliun, G., Beghi, E., Cogliati, T., Zoia, C., Passoni, D., Frattola, L., 1997. Decreased density of lymphocyte benzodiazepine receptors in drug-resistant epileptic patients. Epilepsy Res 27, 181–185. https://doi.org/10.1016/s0920-1211(97)01035-8

Gharib, A., Sayyahi, Z., Komaki, A., Barkley, V., Sarihi, A., Mirnajafi-Zadeh, J., 2018. The role of 5-HT1A receptors of hippocampal CA1 region in anticonvulsant effects of low-frequency stimulation in amygdala kindled rats. Physiol Behav 196, 119–125. https://doi.org/10.1016/j.physbeh.2018.08.025

Golani, L. K., Yeunus Mian, M., Ahmed, T., Pandey, K. P., Mondal, P., Sharmin, D., Rezvanian, S., Witkin, J. M., & Cook, J. M. (2022). Rationalizing the binding and α subtype selectivity of synthesized imidazodiazepines and benzodiazepines at GABAA receptors by using molecular docking studies. *Bioorganic & medicinal chemistry letters*, *62*, 128637. https://doi.org/10.1016/j.bmcl.2022.128637

Klepner, C.A., Lippa, A.S., Benson, D.I., Sano, M.C., Beer, B., 1979. Resolution of two biochemically and pharmacologically distinct benzodiazepine receptors. Pharmacol. Biochem. Behav. 11, 457–462. https://doi.org/10.1016/0091-3057(79)90125-4

Knutson, D.E., Smith, J.L., Ping, X., Jin, X., Golani, L.K., Li, G., Tiruveedhula, V.V.N.P.B., Rashid, F., Mian, M.Y., Jahan, R., Sharmin, D., Cerne, R., Cook, J.M., Witkin, J.M., 2020. Imidazodiazepine Anticonvulsant, KRM-II-81, Produces Novel, Non-diazepam-like Antiseizure Effects. ACS Chem Neurosci 11, 2624–2637. https://doi.org/10.1021/acschemneuro.0c00295

Mian MY, Divović B, Sharmin D, Pandey KP, Golani LK, Tiruveedhula VVNPB, Cerne R, Smith JL, Ping X, Jin X, Imler GH, Deschamps JR, Lippa A, Cook JM, Savić MM, Rowlett J, Witkin JM. Hydrochloride Salt of the GABAkine KRM-II-81. ACS Omega. 2022 Jul 27;7(31):27550-27559. doi: 10.1021/acsomega.2c03029. PMID: 35967038; PMCID: PMC9366947.

Leclercq K, Matagne A, and Kaminski RM (2014) Low potency and limited efficacy of antiepileptic drugs in the mouse 6 Hz corneal kindling model. Epilepsy Res 108: 675–683.

Lewter, L.A., 2019. Characterization of novel α2/α3 subtype-selective GABAA receptor positive allosteric modulators. A dissertation submitted to the faculty of the Graduate School of the University at Buffalo, The State University of New York, Buffalo, NY.

Li, G., Golani, L.K., Jahan, R., Rashid, F., Cook, J.M., 2018. Improved Synthesis of Anxiolytic, Anticonvulsant, and Antinociceptive α2/α3-GABA(A)-ergic Receptor Subtype Selective Ligands as Promising Agents to Treat Anxiety, Epilepsy, and Neuropathic Pain. Synthesis 50, 4124–4132. https://doi.org/10.1055/s-0037-1610211

Lipinski C. A. (2004). Lead- and drug-like compounds: the rule-of-five revolution. *Drug discovery today. Technologies*, *1*(4), 337–341. https://doi.org/10.1016/j.ddtec.2004.11.007

Lippa, A.S., Beer, B., Sano, M.C., Vogel, R.A., Meyerson, L.R., 1981. Differential ontogeny of type 1 and type 2 benzodiazepine receptors. Life Sci 28, 2343–2347. https://doi.org/10.1016/0024-3205(81)90498-7

Lippa, A.S., Klepner, C.A., Yunger, L., Sano, M.C., Smith, W.V., Beer, B., 1978. Relationship between benzodiazepine receptors and experimental anxiety in rats. Pharmacol Biochem Behav 9, 853–856. https://doi.org/10.1016/0091-3057(78)90368-4

Lippa, A.S., Meyerson, L.R., Beer, B., 1982. Molecular substrates of anxiety: clues from the heterogeneity of benzodiazepine receptors. Life Sci 31, 1409–1417. https://doi.org/10.1016/0024-3205(82)90001-7

Loacker, S., Sayyah, M., Wittmann, W., Herzog, H., Schwarzer, C., 2007. Endogenous dynorphin in epileptogenesis and epilepsy: anticonvulsant net effect via kappa opioid receptors. Brain 130, 1017–1028. https://doi.org/10.1093/brain/awl384

Manocha, A., Mediratta, P.K., Sharma, K.K., 2003. Studies on the anticonvulsant effect of U50488H on maximal electroshock seizure in mice. Pharmacol Biochem Behav 76, 111–117. https://doi.org/10.1016/s0091-3057(03)00218-1

Masiulis, S., Desai, R., Uchański, T., Martin, I.S., Laverty, D., Karia, D., Malinauskas, T., Zivanov, J., Pardon, E., Kotecha, A., Steyaert, J., Miller, K.W., Aricescu, A.R., 2019. GABA A receptor signalling mechanisms revealed by structural pharmacology. Nature 565, 454. https://doi.org/10.1038/s41586-018-0832-5

Mathiasen, J.R., Moser, V.C., 2018. The Irwin Test and Functional Observational Battery (FOB) for Assessing the Effects of Compounds on Behavior, Physiology, and Safety Pharmacology in Rodents. Curr Protoc Pharmacol 83, e43. https://doi.org/10.1002/cpph.43

Methuku, K.R., Li, X., Cerne, R., Gleason, S.D., Schkeryantz, J.M., Tiruveedhula, V.V.N.P.B., Golani, L.K., Li, G., Poe, M.M., Rahman, Md.T., Cook, J.M., Fisher, J.L., Witkin, J.M., 2018. An antidepressant-related pharmacological signature for positive allosteric modulators of α2/3-containing GABAA receptors. Pharmacology Biochemistry and Behavior 170, 9–13. https://doi.org/10.1016/j.pbb.2018.04.009

Moerke, M.J., Li, G., Golani, L.K., Cook, J., Negus, S.S., 2019. Effects of the α2/α3-subtype-selective GABAA receptor positive allosteric modulator KRM-II-81 on pain-depressed behavior in rats: comparison with ketorolac and diazepam. Behav Pharmacol 30, 452–461. https://doi.org/10.1097/FBP.0000000000000464

Obradović, A.L., Joksimović, S., Poe, M.M., Ramerstorfer, J., Varagic, Z., Namjoshi, O., Batinić, B., Radulović, T., Marković, B., Roth, B.L., Sieghart, W., Cook, J.M., Savić, M.M., 2014. Sh-I-048A, an in vitro non-selective super-agonist at the benzodiazepine site of GABAA receptors: the approximated activation of receptor subtypes may explain behavioral effects. Brain Res 1554, 36–48. https://doi.org/10.1016/j.brainres.2014.01.036

PANAChE current screening [WWW Document], n.d. URL https://panache.ninds.nih.gov/Home/CurrentModels (accessed 3.25.22).

Pandey, K.P., Khan, Z.A., Golani, L.K., Mondal, P., Mian, Y., Rashid, F., Tiruveedhula, V.V.N.P.B., Knutson, D.E., Sharmin, D., Ahmed, T., Rezvanian, S., Zahn, N.M., Arnold,

L.A., Witkin, J.M., Cook, J.M., 2020. Design, synthesis and characterization of novel gamma-aminobutyric acid type A receptor ligands. ARKIVOC 2020, 242–256. https://doi.org/10.24820/ark.5550190.p011.398

Pelz, M.C., Schoolcraft, K.D., Larson, C., Spring, M.G., López, H.H., 2017. Assessing the role of serotonergic receptors in cannabidiol's anticonvulsant efficacy. Epilepsy Behav 73, 111–118. https://doi.org/10.1016/j.yebeh.2017.04.045

Poe, M.M., Methuku, K.R., Li, G., Verma, A.R., Teske, K.A., Stafford, D.C., Arnold, L.A., Cramer, J.W., Jones, T.M., Cerne, R., Krambis, M.J., Witkin, J.M., Jambrina, E., Rehman, S., Ernst, M., Cook, J.M., Schkeryantz, J.M., 2016. Synthesis and characterization of a novel gamma-aminobutyric acid type A (GABAA) receptor ligand that combines outstanding metabolic stability, pharmacokinetics, and anxiolytic efficacy. J Med Chem 59, 10800–10806. https://doi.org/10.1021/acs.jmedchem.6b01332

Rashid, F., 2021. Design and Synthesis of Achiral and Chiral Benzodiazepines and Imidazodiazepine to Modulate the Activity of GABAA Receptors for the Treatment of Cancer, CNS disorders and Pain., PhD dissertation. ed. University of Wisconsin-Milwaukee, Milwaukee, WI.

Rivas, F.M., Stables, J.P., Murphree, L., Edwankar, R.V., Edwankar, C.R., Huang, S., Jain, H.D., Zhou, H., Majumder, S., Sankar, S., Roth, B.L., Ramerstorfer, J., Furtmüller, R., Sieghart, W., Cook, J.M., 2009. Antiseizure activity of novel gamma-aminobutyric acid (A) receptor subtype-selective benzodiazepine analogues in mice and rat models. J. Med. Chem. 52, 1795–1798. https://doi.org/10.1021/jm801652d

Roth, B.L., 2018. ASSAY PROTOCOL BOOK - Version III [WWW Document]. National Institute of Mental Health Psychoactive Drug Screening Program (NIMH PDSP). URL https://pdsp.unc.edu/pdspweb/content/PDSP%20Protocols%20II%202013-03-28.pdf (accessed 3.26.22).

Sapa, J., Zygmunt, M., Kulig, K., Malawska, B., Dudek, M., Filipek, B., Bednarski, M., Kusak, A., Nowak, G., 2014. Evaluation of anticonvulsant activity of novel pyrrolidin-2-one derivatives. Pharmacol Rep 66, 708–711. https://doi.org/10.1016/j.pharep.2014.02.014

Shinada, N.K., de Brevern, A.G., Schmidtke, P., 2019. Halogens in Protein-Ligand Binding Mechanism: A Structural Perspective. J Med Chem 62, 9341–9356. https://doi.org/10.1021/acs.jmedchem.8b01453

Shiotani, T., Nakamoto, Y., Watabe, S., Yoshii, M., Nabeshima, T., 2000. Anticonvulsant actions of nefiracetam on epileptic EL mice and their relation to peripheral-type benzodiazepine receptors. Brain Res 859, 255–261. https://doi.org/10.1016/s0006-8993(00)01971-5

Sieghart, W., Mayer, A., Drexler, G., 1983. Properties of [3H]flunitrazepam binding to different benzodiazepine binding proteins. Eur J Pharmacol 88, 291–299. https://doi.org/10.1016/0014-2999(83)90579-4

Waszkielewicz, A.M., Cegła, M., Żesławska, E., Nitek, W., Słoczyńska, K., Marona, H., 2015. N-[(2,6-Dimethylphenoxy)alkyl]aminoalkanols-their physicochemical and anticonvulsant properties. Bioorg Med Chem 23, 4197–4217. https://doi.org/10.1016/j.bmc.2015.06.045

Wilcox KS, Dixon-Salazar T, Sills GJ, Ben-Menachem E, White HS, Porter RJ,

Dichter MA, Moshé SL, Noebels JL, Privitera MD, et al. (2013) Issues related to

development of new antiseizure treatments. Epilepsia 54 (Suppl 4):24–34.

Witkin, J.M., Cerne, R., Wakulchik, M., S, J., Gleason, S.D., Jones, T.M., Li, G., Arnold, L.A., Li, J.-X., Schkeryantz, J.M., Methuku, K.R., Cook, J.M., Poe, M.M., 2017. Further evaluation of the potential anxiolytic activity of imidazo[1,5-a][1,4]diazepin agents selective for α2/3-containing GABAA receptors. Pharmacol Biochem Behav 157, 35–40. https://doi.org/10.1016/j.pbb.2017.04.009

Witkin, J.M., Li, G., Golani, L.K., Xiong, W., Smith, J.L., Ping, X., Rashid, F., Jahan, R., Cerne, R., Cook, J.M., Jin, X., 2020. The Positive Allosteric Modulator of α2/3-Containing GABAA Receptors, KRM-II-81, Is Active in Pharmaco-Resistant Models of Epilepsy and Reduces Hyperexcitability after Traumatic Brain Injury. J. Pharmacol. Exp. Ther. 372, 83–94. https://doi.org/10.1124/jpet.119.260968

Witkin, J.M., Lippa, A., Smith, J.L., Jin, X., Ping, X., Biggerstaff, A., Kivell, B.M., Knutson, D.E., Sharmin, D., Pandey, K.P., Mian, M.Y., Cook, J.M., Cerne, R., 2022. The imidazodiazepine, KRM-II-81: An example of a newly emerging generation of GABAkines for neurological and psychiatric disorders. Pharmacol Biochem Behav 173321. https://doi.org/10.1016/j.pbb.2021.173321

Witkin, J.M., Smith, J.L., Ping, X., Gleason, S.D., Poe, M.M., Li, G., Jin, X., Hobbs, J., Schkeryantz, J.M., McDermott, J.S., Alatorre, A.I., Siemian, J.N., Cramer, J.W., Airey, D.C., Methuku, K.R., Tiruveedhula, V.V.N.P.B., Jones, T.M., Crawford, J., Krambis, M.J., Fisher, J.L., Cook, J.M., Cerne, R., 2018. Bioisosteres of ethyl 8-ethynyl-6-(pyridin-2-yl)-4H-benzo[f]imidazo [1,5-a][1,4]diazepine-3-carboxylate (HZ-166) as novel alpha 2,3 selective potentiators of GABAA receptors: Improved bioavailability enhances anticonvulsant efficacy. Neuropharmacology 137, 332–343. https://doi.org/10.1016/j.neuropharm.2018.05.006

Woodbury, L.A., Davenport, V.D., 1952. Design and use of a new electroshock seizure apparatus, and analysis of factors altering seizure threshold and pattern. Arch Int Pharmacodyn Ther 92, 97–107.

Zangrandi, L., Schwarzer, C., 2022. The Kappa Opioid Receptor System in Temporal Lobe Epilepsy. Handb Exp Pharmacol 271, 379–400. https://doi.org/10.1007/164_2021_444

Zhang, D., Wei, C., Hop, C., Wright, M. R., Hu, M., Lai, Y., Khojasteh, S. C., & Humphreys, W. G. (2021). Intestinal Excretion, Intestinal Recirculation, and Renal Tubule Reabsorption Are Underappreciated Mechanisms That Drive the Distribution and Pharmacokinetic Behavior of Small Molecule Drugs. *Journal of medicinal chemistry*, *64*(11), 7045–7059. https://doi.org/10.1021/acs.jmedchem.0c01720

Figure Legends

Figure 1. Structures of KRM-II-81 and the structural analogs reported in this manuscript.

Figure 2. Pharmacokinetic profiles and calculated parameters of FR-II-60 in plasma and brain after oral gavage in adult male, Sprague Dawley rats (n = 3 per time point) at dose of 2 mg/kg. C_{max} – maximum concentration; t_{max} – time of maximum concentration; $AUC_{0–24}$ – area under the concentration versus time curve from zero to last measurable time point; $t_{1/2}$ - terminal elimination half-life.

Figure 3. Pharmacokinetic profiles and calculated parameters of KPP-III-34 in plasma and brain after oral gavage in adult male, Sprague Dawley rats (n = 3 per time point) at dose of 2 mg/kg. C_{max} – maximum concentration; t_{max} – time of maximum concentration; $AUC_{0–24}$ – area under the concentration versus time curve from zero to last measurable time point; $t_{1/2}$ - terminal elimination half-life.

Figure 4. Pharmacokinetic profiles and calculated parameters of KPP-III-51 in plasma and brain after oral gavage in adult male, Sprague Dawley rats (n = 3 per time point) at dose of 2 mg/kg. C_{max} – maximum concentration; t_{max} – time of maximum concentration; $AUC_{0–24}$ – area under the concentration versus time curve from zero to last measurable time point; $t_{1/2}$ - terminal elimination half-life.

Figure 5. Effects of orally administered FR-II-60, KPP-III-34, or KPP-III-51 on the latency to produce clonic (left panels) or tonic (right panels) seizures after 75 mg/kg PTZ, s.c. in male, C57BL/6N mice. *, **, *** P <0.05, 0.01, and 0.001 compared to respective vehicle control value. N=6-9 mice per group.

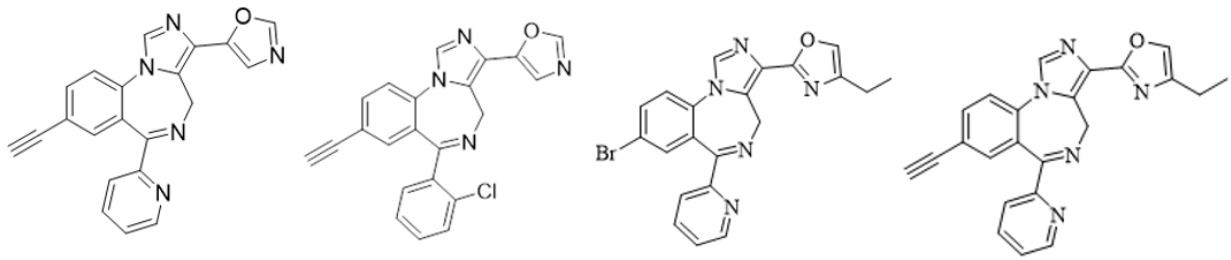
Figure 6. Effects of KPP-III-34 in male, C57/Bl6 mice that were created to exhibit spontaneous recurrent hippocampal discharges. N=8 mice/group.

Figure 7. Effect of orally administered diazepam (5 mg/kg), FR-II-60, and KPP-III-34 on sensorimotor coordination in female, Swiss Webster mice as assessed by rotarod performance. Data are means ± SEM (N = 10/group). ∗ ($p<0.05$) or ∗∗∗ ($p <0.001$) compared to vehicle-treated mice at the same time point.

Figure 8. A: Showing best pose of compound FR-II-60 (goldenrod) docked in 6HUO. **B**: Showing best pose of compound FR-II-60 (goldenrod) docked in 6HUO, overlay with bound alprazolam (grey) in 6HUO. α1 (aquamarine) and γ2 (orchid) subunits of α1β3γ2L $GABA_A$ receptor 6HUO. Dashed lines indicate π–π, hydrogen bond and halogen bond interactions.

Figure 9. A: Showing best pose of compound KPP-III-34 (purple) docked in 6HUO. **B**: Showing best pose of compound KPP-III-34 (purple) docked in 6HUO, overlay with bound alprazolam (grey) in 6HUO. α1 (aquamarine) and γ2 (orchid) subunits of α1β3γ2L $GABA_A$ receptor 6HUO. Dashed lines indicate π–π, hydrogen bond and halogen bond interactions.

Figure 1.



KRM-II-81 FR-II-60 KPP-III-34 KPP-III-51

Figure 2.

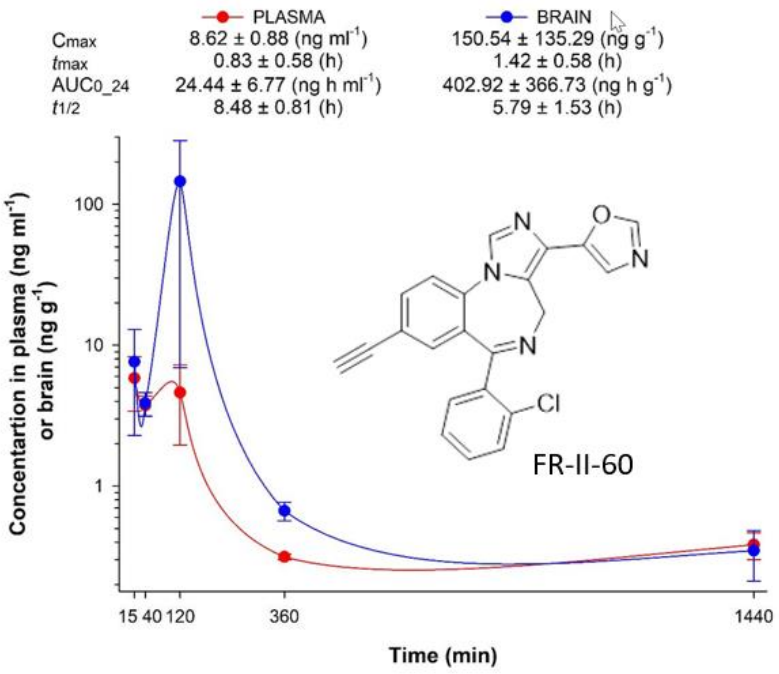


Figure 3.

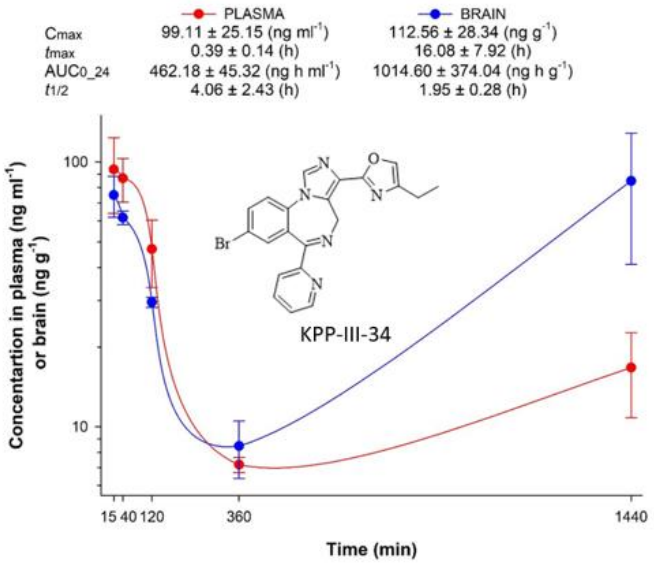


Figure 4.

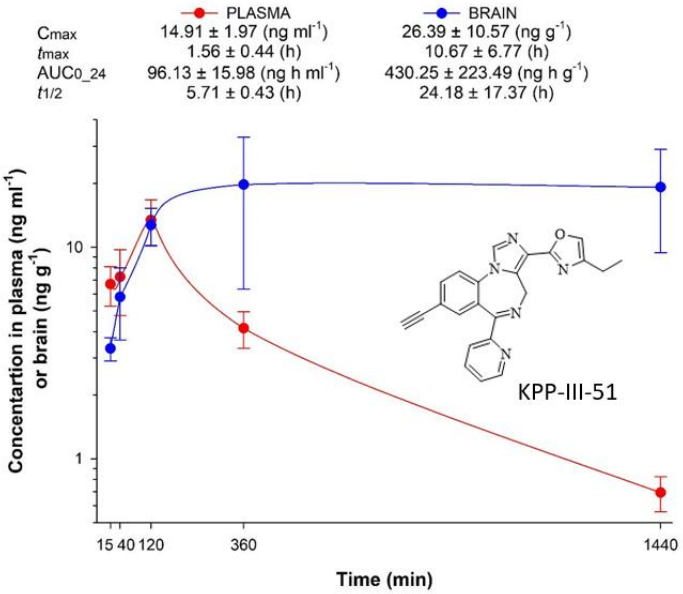


Figure 5.

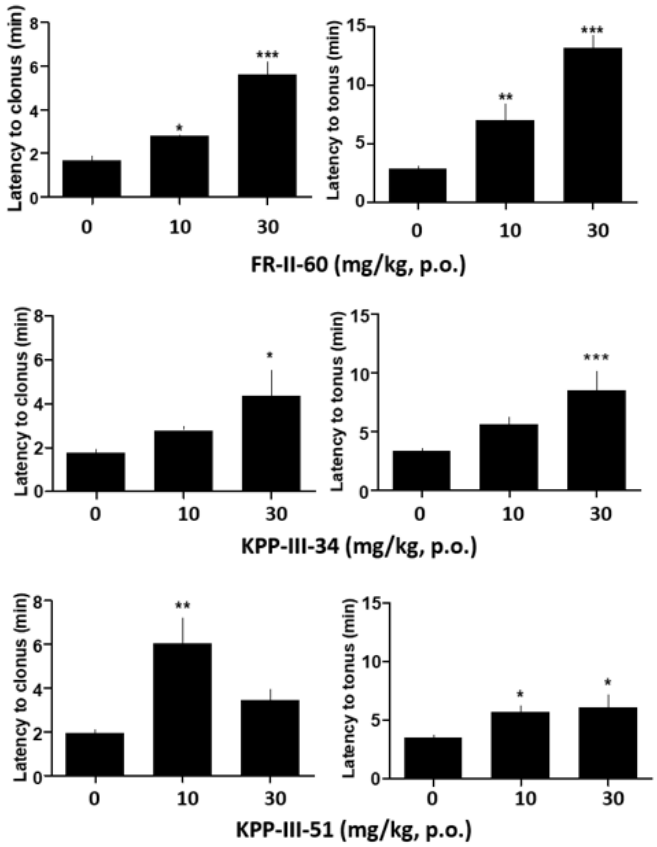

Latency to clonus (min)
Latency to tonus (min)
0
10
30
FR-II-60 (mg/kg, p.o.)
KPP-III-34 (mg/kg, p.o.)
KPP-III-51 (mg/kg, p.o.)

Figure 6.

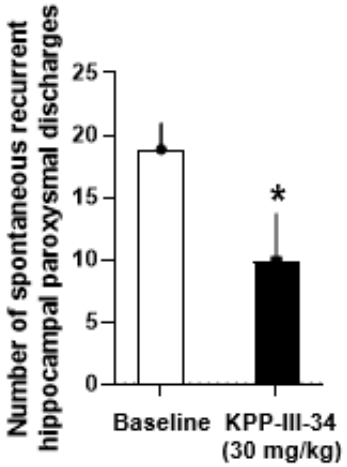


Figure 7.

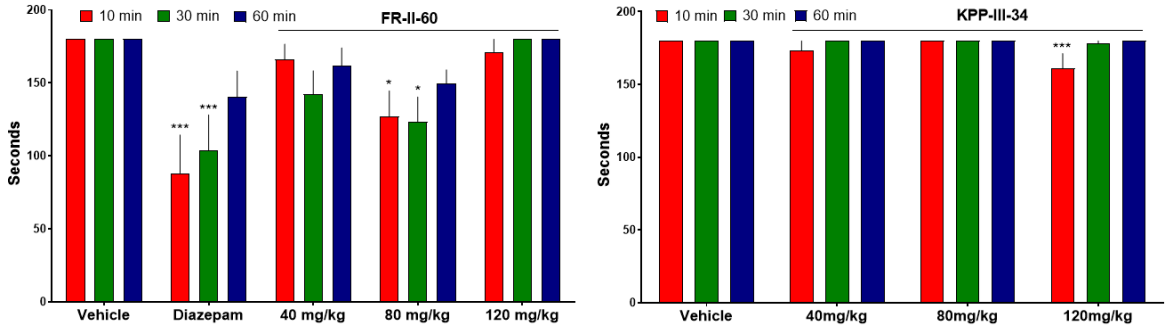


Figure 8.

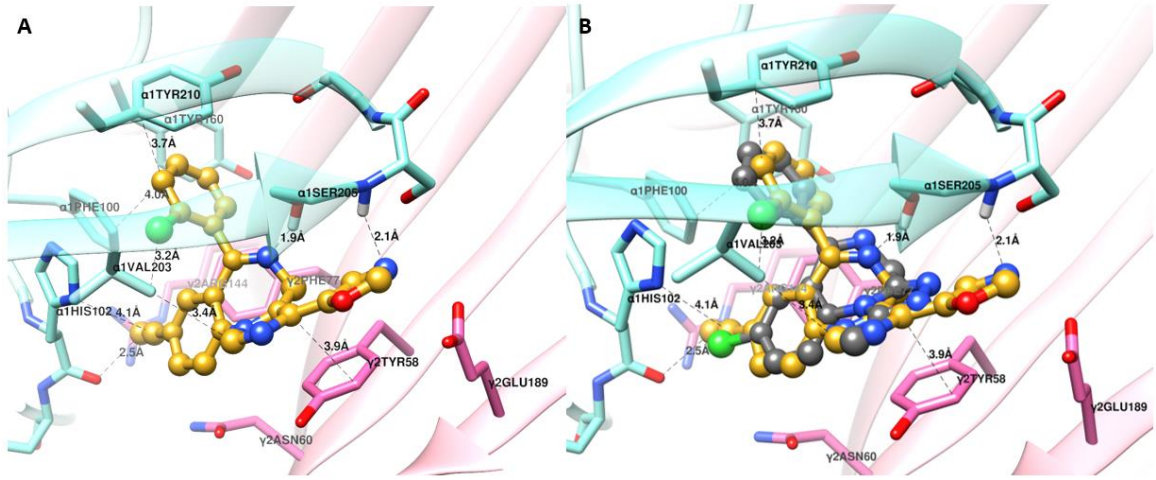
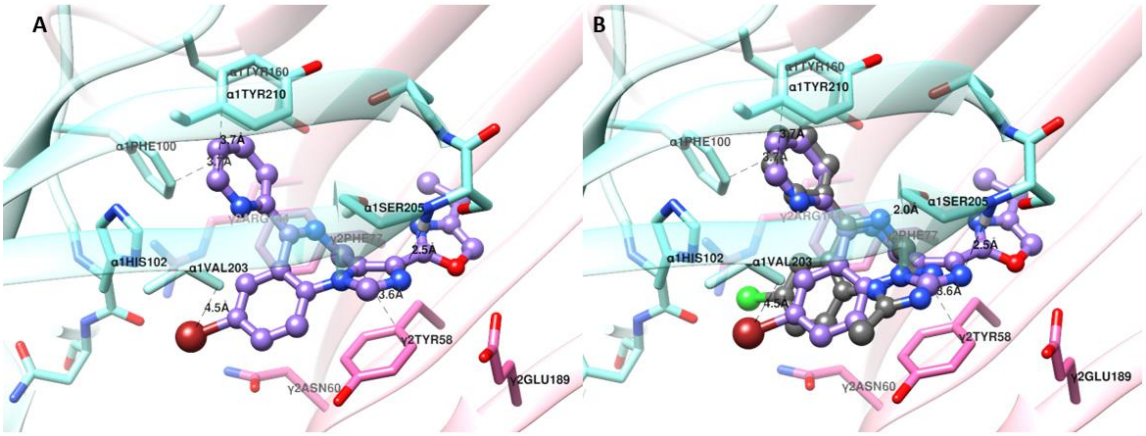


Figure 9.



10. Witkin, J.M.; Lippa, A.; Smith, J. L.; Jin, X.; Ping, X.; Biggerstaff, A.; Kivell, B. M.; Knutson, D. E.; Sharmin, D.; **Pandey, K. P**.; Mian, M. Y.; Cook, J. M., and Cerne, R. 'The imidazodiazepine, KRM-II-81: An example of newly emerging generation of GABAkines for neurological and psychiatric disorders' *Pharmacology, Biochemistry and Behavior*. **2022**, 213. https://doi.org/10.1016/j.pbb.2021.173321.

Pharmacology, Biochemistry and Behavior 213 (2022) 173321

Contents lists available at ScienceDirect

Pharmacology, Biochemistry and Behavior

journal homepage: www.elsevier.com/locate/pharmbiochembeh

Review

The imidazodiazepine, KRM-II-81: An example of a newly emerging generation of GABAkines for neurological and psychiatric disorders☆,☆☆

Jeffrey M. Witkin[a,b,c,*], Arnold Lippa[b], Jodi L. Smith[a], Xiaoming Jin[d], Xingjie Ping[d], Andrew Biggerstaff[e], Bronwyn M. Kivell[e], Daniel E. Knutson[c], Dishary Sharmin[c], Kamal P. Pandey[c], Md Yeunus Mian[c], James M. Cook[b,c], Rok Cerne[a,b,d,f,*]

[a] Laboratory of Antiepileptic Drug Discovery, Ascension St. Vincent, Indianapolis, IN, USA
[b] Respirerix Pharmaceuticals Inc., Glen Rock, NJ, USA
[c] Department of Chemistry and Biochemistry, Milwaukee Institute of Drug Discovery, University of Wisconsin-Milwaukee, Milwaukee, WI, USA
[d] Department of Anatomy and Cell Biology, Indiana University/Purdue University, Indianapolis, IN, USA
[e] School of Biological Sciences, Centre for Biodiscovery, Victoria University of Wellington, Wellington, New Zealand
[f] Faculty of Medicine, University of Ljubljana, Zaloška cesta 4, Ljubljana, Slovenia

ARTICLE INFO

Keywords:
GABAkines
Neuroactive steroids
KRM-II-81
Epilepsy
Anxiety
Depression
Pain

ABSTRACT

GABAkines, or positive allosteric modulators of γ-aminobutyric acid-A ($GABA_A$) receptors, are used for the treatment of anxiety, epilepsy, sleep, and other disorders.

The search for improved GABAkines, with reduced safety liabilities (e.g., dependence) or side-effect profiles (e.g., sedation) constituted multiple discovery and development campaigns that involved a multitude of strategies over the past century. Due to the general lack of success in the development of new GABAkines, there had been a decades-long draught in bringing new GABAkines to market. Recently, however, there has been a resurgence of efforts to bring GABAkines to patients, the FDA approval of the neuroactive steroid brexanolone for post-partum depression in 2019 being the first. Other neuroactive steroids are in various stages of clinical development (ganaxolone, zuranolone, LYT-300, Sage-324, PRAX 114, and ETX-155). These GABAkines and non-steroid compounds (GRX-917, a TSPO binding site ligand), darigabat (CVL-865), an α2/3/5-preferring GABAkine, SAN711, an α3-preferring GABAkine, and the α2/3-preferring GABAkine, KRM-II-81, bring new therapeutic promise to this highly utilized medicinal target in neurology and psychiatry. Herein, we also discuss possible conditions that have enabled the transition to a new age of GABAkines.

We highlight the pharmacology of KRM-II-81 that has the most preclinical data reported. KRM-II-81 is the lead compound in a new series of orally bioavailable imidazodiazepines entering IND-enabling safety studies. KRM-II-81 has a preclinical profile predicting efficacy against pharmacoresistant epilepsies, traumatic brain injury, and neuropathic pain. KRM-II-81 also produces anxiolytic- and antidepressant-like effects in rodent models. Other key features of the pharmacology of this compound are its low sedation rate, lack of tolerance development, and the ability to prevent the development of seizure sensitization.

1. Introduction

GABAkines or positive allosteric modulators of $GABA_A$ receptors (GABAARs) have been highly used medicines for many decades in a host of neuropsychiatric disorders starting with the barbiturates (Fig. 1) (see Sieghart and Savić, 2018; Ghit et al., 2021). They have been prescribed to millions of patients around the world and are generally safe and highly efficacious against their disease targets of insomnia, anxiety, and seizures. The efficacy and general safety of these early compounds beginning with meprobamate in the 1950s created a wide-spread use of these drugs. They were used by so many people in the United States that they were endemic to the culture and iconic (Tone, 2009). Such

☆ This manuscript is dedicated to Dr. James E. Barrett who introduced one of the authors (JMW) to the world of GABAkines and for his long-term friendship and collegial relationship with us (AL, JMW, and JMC).☆☆ It is with great regret that we report the passing of a dear friend and colleague, Dr. Richard B. Carter, in November 2021. Richard was a major advocate of ganaxolone as he headed the biology efforts on neuroactive steroids at CoCensys Pharmaceuticals.

* Corresponding authors at: Laboratory of Antiepileptic Drug Discovery, Ascension St. Vincent, Indianapolis, IN, USA.
E-mail addresses: witkinconsult@gmail.com (J.M. Witkin), rok.cerne@yahoo.com (R. Cerne).

https://doi.org/10.1016/j.pbb.2021.173321
Received 31 October 2021; Received in revised form 21 December 2021; Accepted 30 December 2021
Available online 15 January 2022
0091-3057/© 2022 Elsevier Inc. All rights reserved.

11. M. Witkin, Hana Shafique, Arnold Lippa, **Kamal P. Pandey**, Jodi L. Smith, James M. Cook and Rok Cerne, a book chapter titled '*better than Xanax'* (chapter 5*).* Book name: Advances in health and diseases, volume 61. Publisher name: Nova Science publisher Inc. Newyork. Editor name: Lowell T. Dunken. ISBN: 979-8-88697-464-5 (ebook) ISSN: 2770-7385. Publication Date: Dec 8, 2022.

Chapter

Better than Xanax

Jeffrey M. Witkin[1,3,4,*], Hana Shafique[2], Arnold Lippa[1], Kamal P. Pandey[4], Jodi L. Smith[3], James M. Cook[1,4] and Rok Cerne[1,3,5,6]

[1]RespireRx Pharmaceuticals Inc, Glen Rock, NJ, USA
[2]Duke University School of Medicine, Durham, NC, USA
[3]Laboratory of Antiepileptic Drug Discovery, Ascension St. Vincent, Indianapolis, IN USA
[4]Department of Chemistry and Biochemistry, Milwaukee Institute of Drug Discovery, University of Wisconsin-Milwaukee, Milwaukee, WI, USA
[5]Department of Anatomy and Cell Biology, Indiana University/Purdue University, Indianapolis, IN, USA
[6]Faculty of Medicine, University of Ljubljana, Zaloška cesta 4, Ljubljana, Slovenia

Abstract

Alprazolam (Xanax®) is the major medicine in an evolutionary lineage dating back to the 1950s with meprobamate. Alprazolam is a highly used drug with multiple uses including generalized anxiety disorder, one of the most prevalent psychiatric disorders. Like its predecessors, Librium® and Valium®, alprazolam suffers from major health liabilities and safety concerns. These include the development of tolerance, physical dependence, addiction, sedation, cognitive impairment, and respiratory depression, which in conjunction with other drugs has been lethal. Scientific data beginning in the 1970s demonstrated the ability to identify compounds that displayed valuable exposure margins over these adverse effects. Although dedicated discovery efforts over many decades had been less successful than predicted at bringing such improved medicines to patients, 2019 heralded a new era in research on compounds with the general mechanism of action of alprazolam. These are potentiators of $GABA_A$ receptor function or GABAkines. The current chapter outlines

* Corresponding Author's Email: witkinconsult@gmail.com.

CURRICULUM VITAE

Kamal Pandey, Ph.D. candidate.

kppandey@uwm.edu Google Scholar profile: click here Milwaukee, WI, 53211 414-366-8569

EDUCATION

Ph.D. candidate in Organic Chemistry (Medicinal and Natural Product Chemistry), University of Wisconsin-Milwaukee (UWM). Prof. James M Cook research group. Expected year of graduation: May 2023.

Master's Degree in Chemistry, (US equivalent), graduated with distinction (>79%) and a batch topper (award winner from the president and prime minister of Nepal), Tribhuvan University (TU), Kathmandu, Nepal. Dec 2015.

Bachelor's degree in Science (Chemistry major), TU, Nepal. April 2011.

PH.D. THESIS TITLE

Project I: Total Synthesis of Unnatural Enantiomers of C-19 Methylated Sarpagine/Macroline/Ajmaline-Type Biologically Active Indole Alkaloids Via the Pictet-Spengler Reaction/Dieckmann Cyclization Process.

Project II: Design, Synthesis, and Characterization of Novel Gamma-Aminobutyric Acid Type A ($GABA_A$) Receptor Ligands for the Treatment of Neurological Disorders Including Epilepsy, Depression, Anxiety, Pain and the Synthesis of Back up Compounds for the Clinically Progressing KRM-II-81 for the Treatment of Pharmaco-Resistant Epilepsy and Dravet Syndrome.

PUBLICATIONS (PEER-REVIEWED, TOTAL 10)

Witkin, J. M., **Pandey, K. P**., Smith J. L. 'Clinical investigations of compounds targeting metabotropic glutamate receptors' Pharmacology Biochemistry and Behavior, 2022, 173446. https://doi.org/10.1016/j.pbb.2022.173446.

Mian, Md Y., Divovic, B., Sharmin, D., **Pandey, K. P**., Golani, L. K. Tiruveedhula, V.V.N. P. B., Cerne, R., Smith, J. L., Ping, X., Jin, X., Imler, G. H., Deschamps, J. R., Lippa, A., Cook, J.M., Savic, M. M., Rowlett, J., Witkin, J. M 'Hydrochloride Salt of the GABAkine KRM-II-81' ACS Omega 2022. https://doi/org/10.1021/acsomega.2c03029.

Rahman, M. D., Tiruveedhula, V.V.N.P. Stephen, M. R., Rallapalli, S. K., **Pandey, K. P**., and Cook, J. M. 'Completion of the Total Synthesis of Several Bioactive Sarpagine/Macroline Alkaloids including the Important NF-κB Inhibitor N4-Methyltalpinine' Molecules, 2022, 27, 1738. https://doi.org/10.3390/molecules27051738.

Golani, L.K., Divoc, B., Sharmin, D., **Pandey, K. P**., Mian, M. Y., Cerne, R., Zahn, N. M., Meyer, M. J., Tiruveedhula, V. V. N. P., Smith, J.L., Pin, X., Jin, X, Lippa, A., Schkeryantz, J. M., Arnold, L. A., Cook, J. M., Savic, M. M., and Witkin, J. M. 'Metabolism, pharmacokinetics, and anticonvulsant activity of a deuterated analog of the α2/3-selective GABAkine KRM-II-81', Biopharmaceutics & Drug Disposition, 2022. https://doi.org/10.1002/bdd.2313.

Mian, M.Y., Mondal, P., Sharmin, D., **Pandey, K.P**., Rashid, F., Rezvanian, S., Golani, L.K., Tiruveedhula, V.P.B., Rajaratnam, V., Mirza, S.P., Chan, J.D., Witkin, J. M., and Cook, J. M. 'An efficient debromination technique using PMHS with a number of ligands containing different functional groups' Arkivoc, 2021, (part v), pp.0-0. https://doi.org/10.24820/ark.5550190.p011.712.

Golani, L. K.; Mian, M. Y., Ahmed, T. **Pandey, K. P**., Mondal, P., Sharmin, D., Rezvanian, S., Witkin, J. M., and Cook, J. M. 'Rationalizing the binding and α subtype selectivity of synthesized imidazodiazepines and benzodiazepines at GABAA receptors by using molecular docking studies' Bioorganic and medicinal chemistry letters, 2022, 62. https://doi.org/10.1016/j.bmcl.2022.128637.

Witkin, J.M.; Lippa, A.; Smith, J. L.; Jin, X.; Ping, X.; Biggerstaff, A.; Kivell, B. M.; Knutson, D. E.; Sharmin, D.; **Pandey, K. P**.; Mian, M. Y.; Cook, J. M., and Cerne, R. 'The imidazodiazepine, KRM-II-81: An example of newly emerging generation of GABAkines for neurological and psychiatric disorders' Pharmacology, Biochemistry and Behavior. 2022, 213. https://doi.org/10.1016/j.pbb.2021.173321.

Pandey, K.P.; Rahman, M.T.; and Cook, J.M. 'Bisindole Alkaloids from the Alstonia Species: Recent Isolation, Bioactivity, Biosynthesis, and Synthesis' Molecules 2021, 26, 3459. https://doi.org/10.3390/molecules26113459.

Pandey, K. P., Khan, Z. A., Golani. L. K.; Mondal, P.; Mian, Y.; Rashid, F.; Tiruveedhula, V.V.N.; Knutson, D.; Sharmin, D.; Ahmed, T.; Rezvanian, S.; Zahn, N. M.; Arnold, L. A.; Witkin, J. M.; and Cook, J. M. Design, synthesis and characterization of novel gamma-aminobutyric acid type A receptor ligands. Arkovic, 2020, 242–256. https://doi.org/10.24820/ark.5550190.p011.398.

(*Note: Some manuscripts are under review or preparation*)

RESEARCH PRESENTATIONS (>10)

Pandey *et* al. Synthesis of analogs of KRM-II-81, Gamma Aminobutyric Acid Type A (GABAA) Receptor α2/α3 Subtype-selective Ligand, for Epilepsy Treatment without any adverse effects. ACS - National Meeting and Exposition-Fall, 2022, Chicago, IL, August 2022.

Pandey *et* al. Approach Towards the Total Synthesis of Enantiomers of Biologically Active C-19 Methyl- Substituted Sarpagine/Macroline Type Indole Alkaloids Using Ambidextrous Pictet-Splenger/Dieckmann Cyclization Protocol. Chemistry and Biochemistry Department, Graduate Student council, UWM, WI, April 2022.

Pandey *et* al. Design, Synthesis, and Characterization of Novel Analogs of Clinically Progressing Gamma Aminobutyric Acid Type A (GABAA) Receptor α2/α3 Subtype-selective Ligand KRM-II-81 for Treatment of Epilepsy. ACS-National Meeting and Exposition-Spring, 2022, San Diego, CA, March 2022.

Pandey *et* al. The Total Synthesis Studies of Unnatural Enantiomers of Biologically Active C – 19 Methyl Substituted Macroline, Sarpagine, And Ajmaline-Type Indole Alkaloids. Presented a research talk on research symposium and Sosnovsky lecture hosted by chemistry and Biochemistry Department Graduate Student council, UWM, ACS-Milwaukee, Sep 2021. (Award winner presentation)

Pandey *et* al. Progress Towards the Total Synthesis Studies of Unnatural Enantiomers of Bioactive C – 19 Methyl Substituted Sarpagine/Macroline/Ajmaline Indole Alkaloids. Research poster presented on Research Symposium and Sosnovsky Lecture hosted by chemistry and Biochemistry Department Graduate Student council, UWM, WI. April 2019.

Pandey *et* al. Total Synthesis Studies of Unnatural Enantiomers of Bioactive C-19 Methyl Substituted Sarpagine/Macroline/Ajmaline Indole Alkaloids. Herbert C. Brown Lectures in Organic Chemistry, Purdue University, IN, April 2019.

Pandey *et* al. Total Synthesis Studies of Unnatural Enantiomers of Bioactive C – 19 Methyl Substituted Sarpagine/Macroline/Ajmaline Indole Alkaloids. ACS National Meeting, FL, March 2019.

Pandey *et* al. Total Synthesis Studies of Unnatural Enantiomers of Bioactive C – 19 Methyl Substituted Sarpagine/Macroline/Ajmaline Indole Alkaloids. Chemistry and Biochemistry Departmental Symposium, UWM, WI, May 2018.

Note: not all presentations are included here.

ENCYCLOPEDIA ENTRY

Bisindoles from *Alstonia* (link: Bisindole Alkaloids from *Alstonia* Species | Encyclopedia.
Authors: Pandey, K. P., Rahman, M. T., and Cook, J. M.

LANGUAGES

Fluent in 3 languages: English, Hindi, and Nepali

AWARDS

'Poster award'-ACS-Milwaukee 2021, USA.

'UWM Chemistry graduate student council travel award-2019 and 2021'.

'UWM graduate student travel award-2019 and 2021' and 'UWM chancellor's award, 2017-2022'.

'Outstanding Teaching Assistant Award-lab, 2018' UWM, USA.

'Nepal Bidhyabhusan Kha- 2016'. Ministry of Education, Government of Nepal. It was awarded by the President of Nepal.

‘Amrit Medal-2015’ and ‘P. M. Singh Medal-2015’; awarded by Prime Minister of Nepal.

VOLUNTEERING

April 7, 2018, Wisconsin Science Olympiad.

August 8, 2021, UWM day at Wisconsin State Fairgrounds.

MEMBERSHIPS

American Chemical Society. 2018-present.

Nepal Chemical Society-life member since 2016.